Illuminating the Life of the Adenosine Receptors:

Development and Application of Subtype-Selective Fluorescent Probes for the Study of the human A_1 and A_{2A} Adenosine Receptors in Living Cells

Eleonora Comeo, MSc

Thesis submitted to the University of Nottingham and Monash University for the degree of Doctor of Philosophy

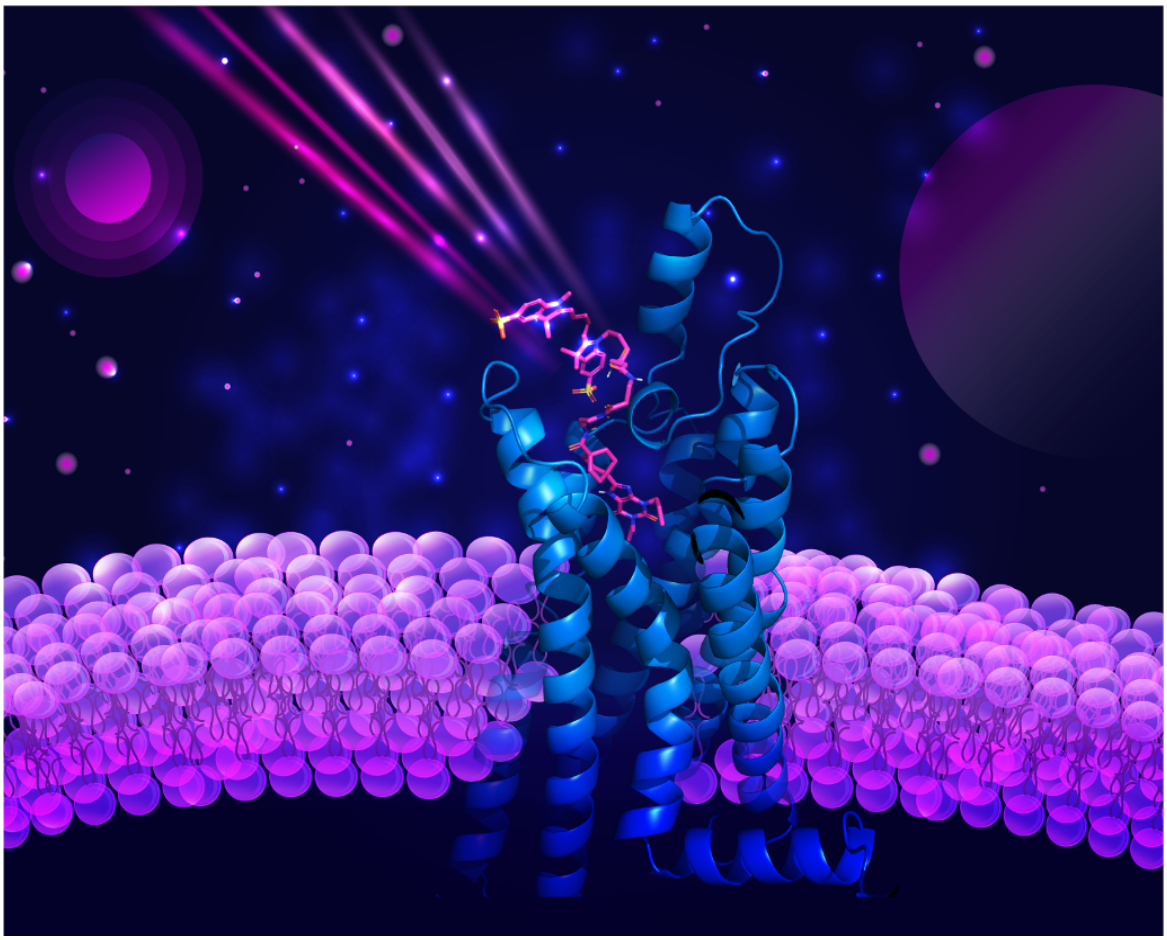
September 2021

This thesis is entirely the candidate's own work. The candidate was enrolled in a joint PhD Programme with both University of Nottingham, at the Division of Biomolecular Sciences and Medicinal Chemistry, in Nottingham, UK, and with Monash University, at the Monash Institute of Pharmaceutical Sciences (MIPS), Medicinal Chemistry Department, Melbourne, Australia. The experiments described in this Thesis were performed by the author between October 2017 and August 2021. Experiments performed between September 2019 and September 2020 were conducted at Monash University (MIPS). No part of the material has been submitted previously for a degree or any other qualification at any university.

Publications arising from this Thesis

- **Comeo, E.**, Trinh, P.; Nguyen, A.N.; Kindon, N.D., Soave, M., Stoddart, L.A; Hill, S.J., Kellam, B., Halls, M.L., May, L.T. and Scammells, P.J., Development and Application of Subtype-Selective Fluorescent Ligands for the Study of the Human Adenosine A_1AR Receptor in Living Cells. *J. Med. Chem.* **2021**, 64, 10, 6670-6695 (**Awarded journal's front cover of which I personally designed the artwork**). Reused in Chapter 4 with permission from https://doi.org/10.1021/acs.jmedchem.0c02067. Copyright ® 2021 The Authors. Published by American Chemical Society.
- **Comeo, E.**, Kindon, N.D., Soave, M., Stoddart, L.A, Kilpatrick, L.E., Scammells, P.J., Hill, S.J., Kellam, B. Subtype-Selective Fluorescent Ligands as Pharmacological Research Tools for the Human Adenosine A_{2A}AR Receptor. *J. Med. Chem.* **2020**, 63, 5, 2656-2672. Reused in Chapter 2 with permission from https://doi.org/10.1021/acs.jmedchem.9b01856. Copyright ® 2019 American Chemical Society.

Notice to readers: further permission related to the material excerpted of DOI: 10.1021/acs.jmedchem.0c02067 and DOI: 10.1021/acs.jmedchem.9b01856 should be directed to the ACS.



"In the darkness of the cell surface, the novel subtype-selective fluorescent antagonists developed in this study illuminate the pathways to a better understanding of the molecular pharmacology of the adenosine A_1 and A_{2A} receptors in living cells"

Abstract

Adenosine is an important regulatory endogenous molecule which can modulate all aspects of tissue functions upon engagement with four adenosine receptor (AR) subtypes namely A_1AR, A_{2A}AR, A_{2B}AR and A_3AR, respectively. These membrane proteins are distributed throughout the human body and, owing to their prominent role in modulating many physiological and pathological processes, they provide important therapeutic opportunities for a number of conditions including cardiovascular, inflammatory diseases, neuropathic pain, CNS disorders and cancer. Yet, translation of adenosine ligands from the bench to the clinic proved challenging. This suggests that better understanding of the molecular and cellular mechanisms of action underlying specific AR pharmacology in different tissues, cell types and subcellular compartments is required for the development of new AR therapeutics. Accordingly, subtype-selective fluorescent probes represent valuable tools to provide this knowledge as they allow real-time monitoring of receptor-specific pharmacology at the single-cell level, in its native, non-genetically modified environment.

This Thesis describes the rational design, synthesis and pharmacological validation of novel subtype-selective fluorescent antagonists targeting two AR subtypes, namely the A_1AR and A_{2A}AR, respectively. These probes allowed quantification of equilibrium and kinetic ligand binding parameters using biophysical methods such as NanoBRET and TR-FRET, in addition to allow visualisation of specific receptor localisation and distribution patterns in living cells by confocal microscopy and total internal reflection microscopy (TIRF-M). Moreover, to the best of our knowledge, probes **4.44b** and **4.46a** represent the first examples of subtype-selective fluorescent hA_1AR antagonists reported to date.

As an extension of the fluorescent ligand technology, this Thesis also reports the rational design of a Ligand-Directed (LD) chemistry approach, combined with an Inverse-Electron Demand Diels-Alder (IEDDA) click

reaction, which enabled fluorescent labelling of hA_1ARs expressed in living cells. This method offers a novel, non-invasive, bioorthogonal approach to study A_1AR function and dynamics in its native cellular environment.

Together, the tools developed in this Thesis may support the discovery of new sites and mechanisms for therapeutic intervention within the adenosine receptors research field, as well as facilitate the design of AR ligands with improved selectivity and safer mechanism of action.

Acknowledgments

First and foremost, I would like to show my deepest and sincere gratitude to my main supervisors at the University of Nottingham, Prof. Barrie Kellam and Prof. Stephen J. Hill, first for having taken the risk, four years ago, of allowing me to stay in Nottingham and pursue this amazing PhD journey in your labs; second, for all the guidance, support and help showed throughout the years. Thank you for pushing me to become a better scientist by questioning every observation made and data analysed as well as for encouraging me to develop and explore my own scientific creativity and leadership.

I also want to show my most sincere gratitude to my supervisors at the Monash Institute of Pharmaceutical Sciences (MIPS) in Melbourne, Australia, Prof. Peter J. Scammells, Dr. Lauren T. May and Associate Professor Michelle L. Halls for warmly welcoming me in your labs on my third year of PhD and for all the insightful and joyful discussions at project meetings, guidance, mentorship, help and support provided during my time at MIPS. This year was memorable.

Dr. Nicholas Kindon, Dr Aimie E. Garces and Dr. Sarah J. Mistry, you have been there since I walked my very first steps in C-floor during my Erasmus project. I soon felt welcomed and included in the big C-floor family. I cannot thank you all enough for all your wisdom, help, guidance, teaching and, above all, friendship which have never missed.

Nick, you really deserve a special mention and I give you my personal *laurea honoris causa* (honorary degree) in Chemistry of Eleonora's sanity. I cannot thank you enough for all the precious and invaluable teachings and brainstorming sessions every morning at 7 am at the white board as well as at the hood or simply while walking by the lake pointing at your favourite pikes! I am indeed very lucky for having been your young Italian padawan.

My sincere gratitude also goes to Dr. Mark Soave, Dr. Leigh Stoddart, Dr. Laura Kilpatrick and Dr Joëlle Goulding for the countless patience, support, supervision and friendship throughout my PhD.

All the friends, colleagues and members of staff in the chemistry labs in BDI and Cell Signalling Research Group at the University of Nottingham, as well as all Scammells, May and Halls' labs members really deserve special mention for all their support, help, guidance and for the countless laughs over the years. I feel extremely lucky for having worked with such great minds and human beings. Everyone I met along the way in this extraordinary PhD journey has surely contributed to making me become a better scientist.

I would like to thank my mum for having always supported me in my decisions and always been there for me, despite the long distances. Thank you for having taught me to be resilient and pushed me to always reach my goals and objectives with respect, great dedication and passion.

I would like to thank Leonardo, the love of my life. You are the very reason why I moved to the UK. Upon my graduation in Italy in 2016 I did not know who I wanted to become. Moving to the UK with you put the pieces together, allowing me to finally find my place in this planet. Thank you for your unconditional love, for having supported me over these tough years and for having moved to Australia with me in a very difficult period of your life.

I want to thank the Nottingham-Monash Joint Doctoral training Centre program and the University of Nottingham for funding my PhD. Finally, I would like to acknowledge BioRender.com for allowing me to generate great pictures for this thesis.

List of Abbreviations

ADA Adenosine Deaminase

ADO Adenosine

AMP Adenosine monophosphate

AR Adenosine Receptors

ATP Adenosine 5'-triphosphate

β-Ala β-Alanine

B_{max} receptor maximum occupancy

BEP 2-Bromo-1-ethyl pyridinium tetrafluoroborate

Boc *tert*-Butyloxylcarbonyl

BODIPY 4,4-difluoro-4-bora-3*a*,4*a*-diaza-*s*-indacene

BOP (benzotriazol-1-yloxy)tris- (dimethylamino)phosphonium hexafluorophosphate

BRET Bioluminescence Resonance Energy Transfer

cAMP cyclic adenosine monophosphate

Cbz Benzyloxy carbonyl group

CHO chinese hamster ovary

COMU (1-cyano-2-ethoxy-2- oxoethylidenaminooxy)dimethylamino-morpholino-carbenium hexafluorophosphate

CRE cAMP Response Element

Cy5, cyanine5

cDNA complementary DNA

DCC *N*,*N*-Dicyclohexylcarbodiimide

DIPEA diisopropylethylamine

DPCPX 8-Cyclopentyl-1,3-dipropylxanthine

DMAP 4-Dimethyl Amino Pyridine

DMEM Dulbecco's Modified Eagle Medium

ERK Extracellular-Signal-Regulated Kinase

ESI electrospray ionization

FACS Fluorescence Activated Cell Sorting

FCS Fluorescence Correlation Spectroscopy

GPCR G Protein-Coupled Receptor

GRKs G Protein-coupled Receptor Kinases

HATU O-(7-azabenzotriazol-1-yl)-1,1,3,3-tetramethyluronium hexa-fluorophosphate

HBSS HEPES or Hank's buffered saline solution

HEK293 Human Embryonic Kidney 293 cells

HPLC High-Performance Liquid Chromatography

HRMS High-Resolution Mass Spectrometry

IC_{50} half-maximal inhibitory concentration

IEDDA Inverse-Electron Demand Diels-Alder

K_D dissociation constant, concentration at which half the receptors are occupied

LC-MS Liquid Chromatography Mass Spectrometry

LDL Ligand-Directed Labelling

NLuc NanoLuciferase

NECA 5'-*N*-ethylcarboxamide adenosine

NMR Nuclear Magnetic Resonance

PyBrop Bromotripyrrolidinophosphonium hexafluorophosphate

RP Reverse Phase

SAR Structure-Activity Relationship

SPAP Secreted Placental Alkaline Phosphatase

TR-FRET Time Resolved Fluorescence Resonance Energy Transfer

XAC Xanthine Amine Congener

Table of Contents

Abstract ..... **iv**

Acknowledgments ..... **vi**

List of Abbreviations ..... **viii**

Chapter 1. General Introduction **1**

1.1 G Protein-Coupled Receptors (GPCRs) 1

1.2 Adenosine Receptors as Drug Discovery Targets 2

1.2.1 Adenosine production and metabolism 4

1.3 Structural and Dynamical Determinants of Subtype-Selectivity between the A_1 and the A_{2A} Receptors 6

1.4 Adenosine A_{2A} Receptor 9

1.4.1 Adenosine A_{2A} Receptor: Pharmacology and Therapeutic Application 10

1.4.1.1 Role of the A_{2A}AR in Cancer Immunotherapy 11

1.5 Adenosine A_1 Receptor 14

1.5.1 Adenosine A_1 Receptor: Pharmacology and Therapeutic Application 16

1.6 The use of Fluorescent Ligands for studying A_1AR and A_{2A}AR biology 18

1.6.1 Fluorescent Ligands Design 21

1.6.2 Fluorescent Ligands Properties and Recent Applications 22

1.6.3 Fluorescent Ligands Developed for the A_1AR and A_{2A}AR. 27

1.7 Ligand-Directed Labelling of Membrane Proteins 28

1.8 Thesis Aims 33

Chapter 2. Subtype-Selective Fluorescent Ligands as Pharmacological Research Tools for the Human Adenosine A_{2A}AR Receptor **34**

2.1 Brief Introduction 34

2.2 Rational Design of the Novel Fluorescent A_{2A}AR Antagonists 36

2.3 Results and Discussion 39
2.3.1 Chemistry 39
2.3.1.1 Synthesis of the Fluorescent $hA_{2A}AR$ antagonists 39
2.3.2 Pharmacology 42
2.4 Conclusions and Future Work 58
Chapter 3. Design, Synthesis and Pharmacological Evaluation of Novel Fluorescent A_1AR Antagonists Based on the 2,6,8-Trisubstituted 1-Deazapurine Scaffold 60
3.1 Brief Introduction 60
3.2 Design Strategy 62
3.3 Results and Discussion 64
3.3.1 Chemistry 64
3.3.2 Pharmacology 69
3.4 Conclusions and Future Work 75
Chapter 4. Development and Application of Subtype-Selective Fluorescent Antagonists for the Study of the Human Adenosine A_1 Receptor in Living Cells 78
4.1 Brief Introduction 78
4.2 Fluorescent Ligand Design 80
4.3 Results and Discussion 84
4.3.1 Chemistry 84
4.3.1.1 Synthesis of the 8-bicyclo[2.2.2]octylxanthine based congeners 84
4.3.1.2 Synthesis of the 1-propyl-3-(3-benzamidopropyl)-8-(3-adamantyl) xanthine-based congeners 88
4.3.1.3 Synthesis of fluorescent A_1AR antagonists 89
4.3.2 Pharmacology 90
4.4 Conclusions and Future Work 115

Chapter 5. Ligand-directed Labelling of the Human Adenosine A_1AR Receptors with Fluorescent Probes in Living Cells 117

5.1 Brief Introduction 117

5.2 Rational Design of A_1AR Ligand-directed Labels 119

5.3 Results and Discussions 124

5.3.1 Chemistry 124

5.3.1.1 Synthesis of 1-propyl-8-(3-adamantyl) xanthine-based ligand-directed probes 125

5.3.1.2 Synthesis of 8-(4-(hydroxymethyl)-bicyclo[2.2.2]octyl) xanthine-based ligand-directed probes 127

5.3.1.3 Synthesis of 4-(xanthine)bicyclo[2.2.2]octane-1-carboxilyc acid-based ligand-directed probes 129

5.3.2 Pharmacology 132

5.4 Conclusions and Future Work 150

Chapter 6. General Conclusions and Outlook 155

Chapter 7. General Methods 161

7.1 Chemistry 161

7.1.1 Materials and General Methods 161

7.1.2 Methods Chapter 2 164

7.1.3 Methods Chapter 3 174

7.1.4 Methods Chapter 4 192

7.1.5 Methods Chapter 5 238

7.1.6 Molecular Modelling Studies 280

7.2 Pharmacology 281

7.2.1 General Cell Culture 281

7.2.1.1 Passaging of Cells 281

7.2.1.2 Cell Freezing 282

7.2.1.3 Defrosting Cells 283

7.2.1.4 Cell lines used in the experiments 283

7.2.1 Cell Culture Chapter 4 285

7.2.3 Experiments 285
7.2.3.1 NanoBRET-based binding assays 285
7.2.3.2 NanoBRET Saturation Assay to Investigate A_1-A_{2A} Interactions (Chapter 4) 287
7.2.3.3 *CRE-SPAP* gene transcription functional assay (performed in Chapter 2) 288
7.2.3.4 HTRF Binding Kinetic of BODIPY-630/650-X conjugate *2.12* (performed in Chapter 2) 288
7.2.3.5 *[^{3}H] DPCPX* Radioligand binding assay (performed in Chapter 4) 289
7.2.3.6 cAMP functional assay 289
7.2.3.7 Confocal Imaging studies using Zeiss LSM710 290
7.2.3.8 Confocal Imaging studies using Leica TCS SP8X (Chapter 4) 292
7.2.3.9 Total Internal Reflection Fluorescence Microscopy *(TIRF-M,* Chapter 4*)* 293
7.2.3.10 Data Analysis 294
7.3 Appendix 297
7.3.1 Supplementary Information 297
References 306

Chapter 1. General Introduction

1.1 G Protein-Coupled Receptors (GPCRs).

G Protein-Coupled Receptors (GPCRs) are membrane receptors that recognise and respond to a variety of external stimuli (small molecules, photons, ions, hormones, peptides) and transduce this information to the intracellular environment of the cell through an interaction with a heterotrimeric guanine nucleotide-binding (G) protein.[1] GPCRs encompass the largest family of protein targets of currently marketed drugs, whereby approximately 35 % of approved drugs target a GPCR.[2] This is because they are involved in modulating many different aspects of human physiology and pathology e.g. cardiovascular diseases, central nervous system (CNS) disorders and cancer. Thus, understanding the molecular mechanisms underlying GPCR biology is pivotal for advancing more effective therapeutics targeting these important membrane receptors.

Based on sequence homology between the seven transmembrane (TM) domains and functional similarities, GPCR can be classified into five main families : class A (or *rhodopsin*-like family), class B (or *secretin* family), class C (or *metabotropic glutamate/pheromone* family), class F (or *frizzled/smoothened* family) and the adhesion family of GPCRs.[3,4] Nonetheless, all GPCRs share common structural features which are conserved across all families: this includes seven-membrane spanning α-helices embedded in the plasma membrane which are connected by three extracellular loops (ECL1-ECL3) and three intracellular loops (ICL1-ICL3), with an extracellular amino *N*-terminus and an intracellular carboxyl *C*-terminus of different lengths.[5]

Binding of an agonist molecule to a GPCR elicits conformational changes in the intracellular domains, which in turn initiates a cascade of signalling events as result of the activation of intracellular coupling partners, such as heterotrimeric G proteins, G protein-coupled receptor kinase (GRK) and arrestins.[6,7] G protein-engagement and activation represent the classical signalling pathway by which GPCR function. In particular, G proteins are a heterotrimer composed of three subunits, namely Gα, Gβ and Gγ

respectively. Receptor activation results in an exchange of guanosine diphosphate (GDP) with guanosine triphosphate (GTP). This leads to the dissociation of Gα and Gβγ subunits, which can then modulate various downstream effector proteins.[7]

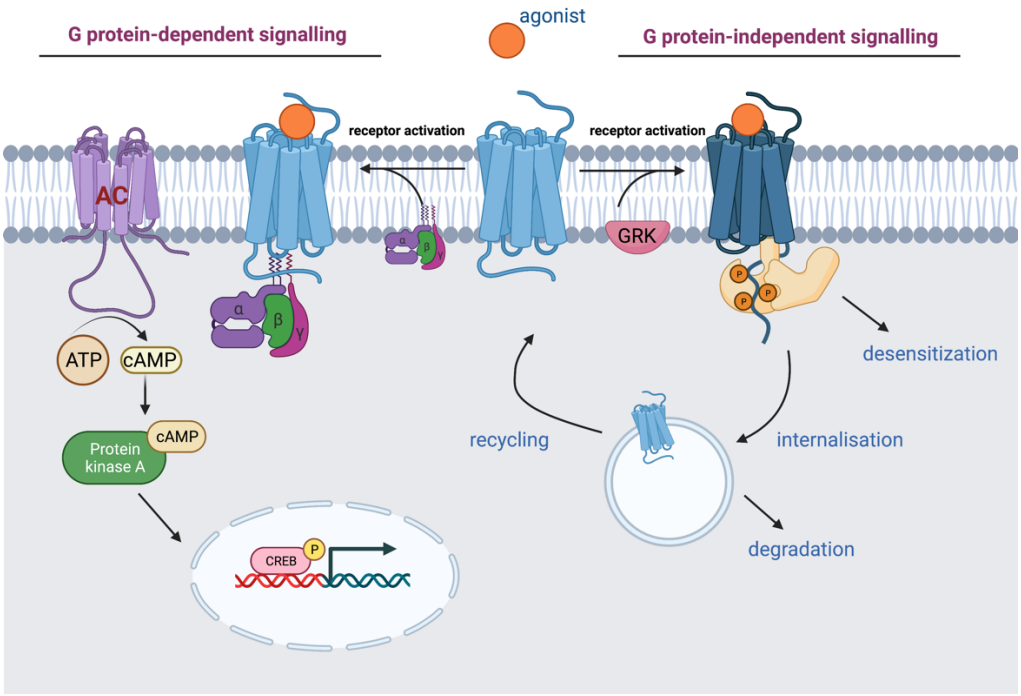


Figure 1.1 Schematic representation of the signalling cascade triggered by G protein coupled receptor activation. GPCR activation can trigger G protein-dependent or G protein independent pathways. Image modified after Hilger, D. et al.[7] Image created with Biorender.com

Recent advances in the field of structural biology, as well as innovations in molecular pharmacology and chemical biology are leveraging our understanding of the complexity of GPCR function and dynamics, providing new avenues for targeting with new drugs for a particular therapeutic indication.[8,9]

1.2 Adenosine Receptors as Drug Discovery Targets.

The role of adenosine, a naturally occurring nucleoside, in modulating heart functions was firstly described by Drury and Szent-Györgyi in 1929.[10] Forty years later, studies on the role of caffeine in mammalian atrial muscles,[11] as well as studies reporting the effects of adenosine and adenine

nucleotides in enhancing cyclic adenosine monophosphate (cAMP) accumulation on mammalian cerebral cortex slices[12] suggested the existence of specific adenosine receptors (ARs) at which methylxanthines caffeine and theophylline were acting as antagonists.[13–15] Observations that adenosine and adenosine analogues were able either to stimulate or inhibit the accumulation of cAMP led to the conclusion that these opposite effects were mediated by two different adenosine receptor subtypes. The adenosine receptors responsible for inhibiting cAMP accumulation were classified as A_1AR subtypes, whilst those with a stimulating effect towards cAMP accumulation were classified as A_2AR subtypes.[16] In later studies Daly and colleagues documented that the A_2AR could be additionally divided into two subfamilies: a high affinity A_{2A}AR and low affinity A_{2B}AR receptor subtypes as a result of the different affinities of adenosine exhibited at the two distinct receptors.[17]

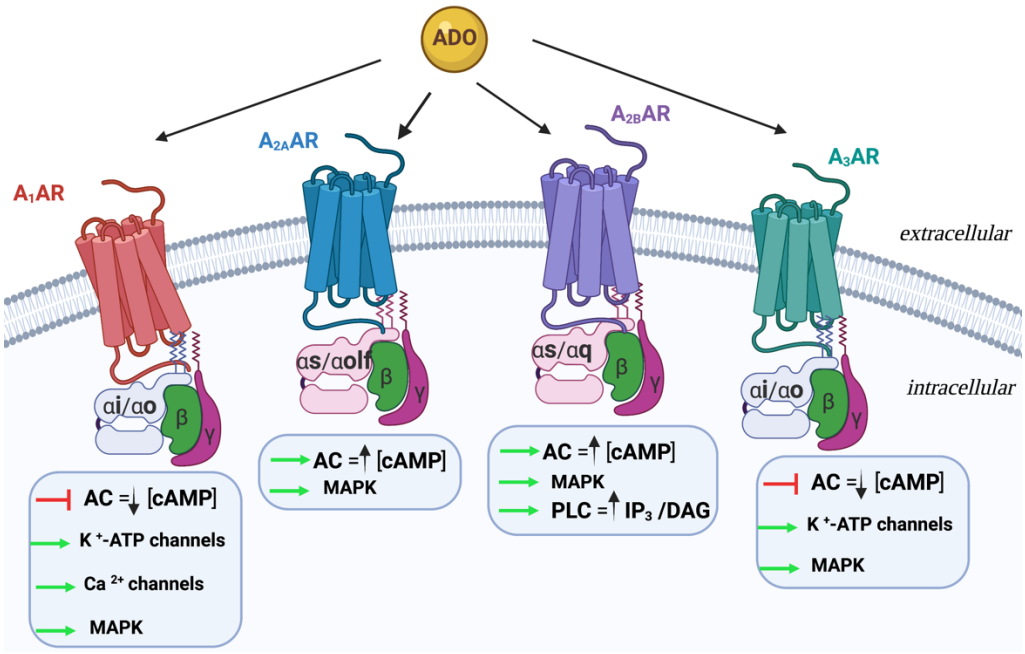


Figure 1.2 Adenosine receptors subtypes and downstream effectors activated following AR-stimulation by an agonist ligand such as adenosine, ADO. A_{2A}AR and A_{2B}AR stimulate adenylyl cyclase (AC), resulting in an increase of cyclic adenosine monophosphate (cAMP) production from ATP. Conversely, A_1AR and A_3AR inhibit AC, resulting in a decrease of cAMP production. The activation of A_1AR and A_3AR can also stimulate Ca^{2+} accumulation and activation of potassium K^+-ATP channels mediated by the Gβγ subunit.[18,19] All four receptor subtypes stimulate MAPK signalling pathways, which can lead to activation of ERK ½, JNK and p38 MAPK.[20]

After decades of research, it is now widely acknowledged that the endogenous ligand adenosine mediates many central and peripheral effects upon activation of four adenosine receptor subtypes, namely the A_1-, A_{2A}-, A_{2B}- and A_3AR, respectively (**Figure 1.2**). The adenosine receptors belong to the class A GPCR superfamily and display a structural architecture common to other GPCRs. Each AR subtype, however, display a unique pharmacological profile owing to the coupling to different effector proteins and tissue distribution.[21]

Adenosine A_1AR and A_3AR receptors mainly couple to Gαi proteins, resulting in adenylyl cyclase inhibition and subsequent reduction of cAMP accumulation. Conversely, the A_{2A}AR and A_{2B}AR subtypes primarily engage Gαs proteins promoting the accumulation of cAMP due to the activation of adenylyl cyclase.[5,15] ARs activation can also initiate other downstream signalling pathways, such as phospholipase C (PLC) and the subsequent mobilisation of intracellular calcium [Ca^{2+}].[22] Additionally, ARs also regulate the mitogen-activated protein kinase (MAPK) signalling responses, including extracellular regulated kinase 1/2 (ERK1/2), p38-MAPK and Jun-NH_2 terminal kinase (JNK), which are involved in cell growth, survival and differentiation.[18]

1.2.1 Adenosine production and metabolism

Adenosine is a modulatory molecule, which constitutes a fundamental structural unit for nucleic acids and partakes in energy metabolism. Specifically, adenosine is released by most cells following hypoxia, inflammation and cell damage to promote tissue protection and repair.[23,24]

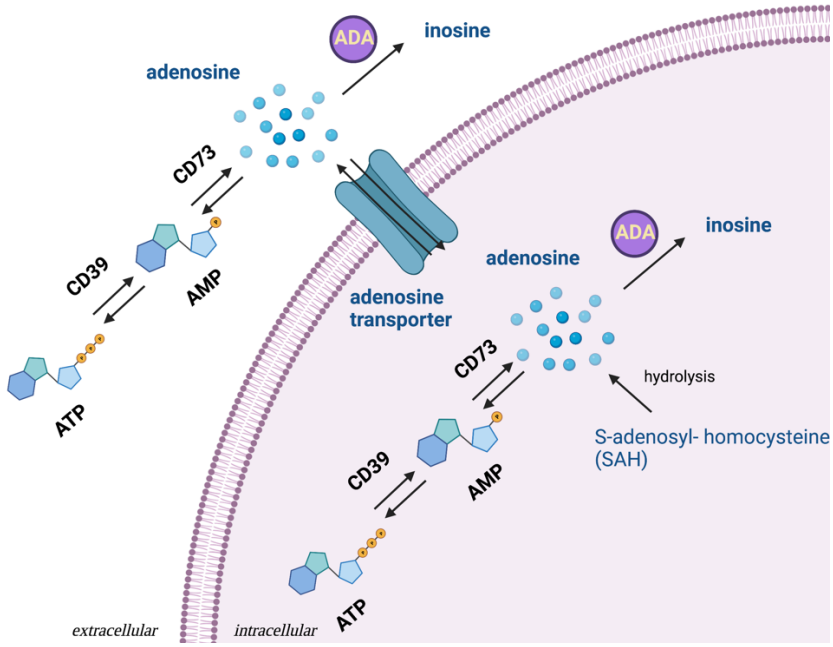


Figure 1.3 Schematic representation of the main pathways involved in adenosine production and metabolism. Abbreviations: ADA, adenosine deaminase; ATP, adenosine triphosphate; AMP, adenosine monophosphate; CD39, nucleoside triphosphate diphosphohydrolase; CD73, 5' nucleotidase. Image modified from Antonioli, L. et al.[25]

Under physiological conditions, intracellular and extracellular levels of adenosine are continuously produced and sustained by many biological processes (**Figure 1.3**). For example, the main source of extracellular adenosine derives from the breakdown of ATP by the activity of specific ectoenzymes: ectonucleoside triphosphate diphosphohydrolase (CD39) and ecto-5' nucleotidase (CD73). Intracellular adenosine mainly arises from the hydrolysis of S-adenosylhomocysteine (SAH) and from the dephosphorylation of AMP, catalysed by the endo-5' nucleotidase (CD73).[20] Adenosine concentration is maintained under equilibrium by the activity of specific nucleoside transporters (NTs) which are expressed in most cells. Additionally, adenosine is quickly metabolised to inosine through the activity of adenosine deaminase (ADA) or can be phosphorylated to AMP by adenosine kinase (ADK).

Under normal physiological conditions, the concentration of adenosine varies between 30-200 nM. This concentration can increase to micromolar

(μM) levels depending on the onset of pathologies or on the metabolic demand of the cell.[25]

1.3 Structural and Dynamical Determinants of Subtype-Selectivity between the A_1 and the A_{2A} Receptors

Recent advances in the field of structural biology are leveraging our understanding of the molecular determinants involved in GPCR pharmacology. With the availability of detailed structural data, derived from X-ray crystallography and cryoelectron microscopy (Cryo-EM), drug discovery programs can now leverage this information for the design and development of specific ligands for the targeted receptor.

The adenosine A_{2A} receptor subtype has been the third GPCR, after rhodopsin[26] and β_2-AR,[27,28] of which the three-dimensional structure has been elucidated. [29] Since then, the Protein Data Bank (PDB) depository houses more than 50 A_{2A} crystal structures in either agonist[30] or antagonist-bound[31] states and fully active state in which the A_{2A}AR is coupled with its intracellular binding partner, an engineered heterotrimeric G_S protein.[32,33] Additionally, structures of the A_1AR subtype in either active (agonist-bound)[34,35] and inactive (antagonist-bound)[36,37] states have been recently solved. Therefore, mutagenesis studies[38,39], molecular modelling simulations[40,41] and SARs studies[42–44], relative to the A_1AR and A_{2A}AR subtypes, can now be analysed in the context of structural information and, together, provide a compiled map for the rational design of selective ligands for the these specific adenosine receptors.

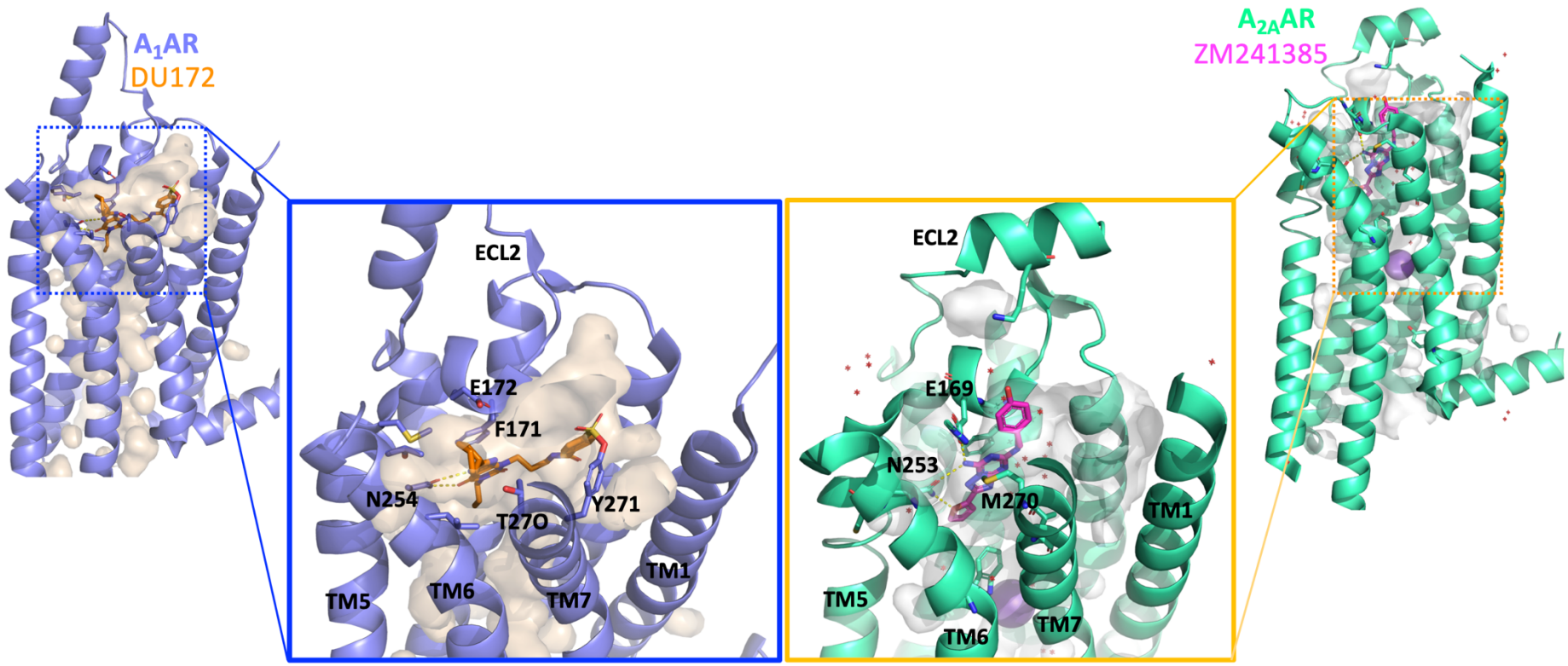


Figure 1.4 Comparison of the crystal structures of the adenosine A_1AR (left hand images) and A_{2A}AR (right hand images) receptors in their inactive states. The A_1AR in complex with the irreversible antagonist DU172 (PDB : 5UEN)[36] is shown in ribbon coloured lightblue . DU172 is depicted as sticks coloured orange. The broad binding pocket cavity is shown as surface coloured wheat. The A_{2A}AR in complex with the inverse agonist ZM241385 (PDB : 4EIY)[45] is shown in ribbon coloured greencyan. ZM241385 is shown as sticks coloured magenta. The binding pocket cavity is depicted as white surface. For both A_1AR and A_{2A}AR structures, hydrogen bonds are shown as dashed lines. The key residues (shown in sticks), transmembrane (TM) domains and Extra Cellular Loop 2 (ECL2) are labelled for clarity. With both structures' representations, a zoomed view of co-crystalised ligand (DU172 for A_1AR and ZM241385 A_{2A}AR) in the binding pocket is depicted in the box (blue for A_1AR and orange for A_{2A}AR). Images were generated in PyMol (version 2.2.0) using the crystal structures deposited in the Protein Data Bank with the corresponding codes provided.

A principal drawback in developing selective adenosine ligands is the high sequence similarity displayed between the four adenosine receptor subtypes,[46] in particular at the level of the orthosteric binding pocket, which results in only limited structural differences among these purinergic receptors that are particularly challenging to address from a medicinal chemistry point of view. First of all, comparing the structures of the A_1AR and A_{2A}AR in their inactive states (**Figure 1.4**), a striking difference between the two receptors is represented by the binding pocket cavity, which is particularly open and wide in the A_1 subtype. Conversely, the A_{2A} displays a much narrower and elongated pocket. Interestingly, a key structural determinant for subtype selectivity between the two adenosine receptors is represented by the residue at position 7.35 , $T270^{7.35}$ in A_1AR and $M270^{7.35}$ in A_{2A}AR (the superscript number refers to the Ballesteros-Weinstein numbering scheme in which the first value represents the transmembrane helix and the second the position of the residue with respect to the most conserved residue of the helix, which is conventionally set to 50).[47] The role of this single amino acid in shaping ligand binding selectivity has been supported by site-directed mutagenesis studies and molecular modelling simulations. It is widely accepted that bulky substituents at 8-position of the prototypical xanthine scaffold as well as alkyl chains at the N^1 and N^3 positions are the principal drivers for affinity and selectivity for the A_1 subtype. These features of ligand recognition can be rationalised with the available crystal structures:[36,37,45] owing to the smaller side chain of threonine $270^{7.35}$ in A_1, bulkier groups at C8 position are allowed to engage with the hydrophobic pocket shaped by residues $M177^{5.35}$, $L253^{6.54}$ and $T257^{6.57}$. Conversely, the access to the same pocket in the A_{2A} is hindered by the much bulkier methionine residue ($M270^{7.35}$) which is thought to act as *"gatekeeper"* as reported by Glukhova *et al.*[36] Interestingly, while this residue in the A_{2A} is well conserved across different species, in the A_1 there is more variability, resulting in significant differences of ligand binding affinities for A_1 ligands.[48,49] In the A_{2A} crystal structure residue 270 points towards the binding pocket, thereby restricting the pose of the co-crystalized ligand ZM241385. This feature is a result of a more inward movement of TM7 towards the core of A_{2A} compared to the A_1. Indeed, the steric clash with M270 in A_{2A} can account for the reduced

affinity displayed by xanthine-based ligands substituted with bulky groups at C8 position.

Marked differences between the A_{2A} and A_1 have been observed in the extracellular region of the receptors. ECL2 in A_1 adopts a conformation perpendicular to the plane of the membrane. In contrast, the corresponding ECL2 in A_{2A} folds towards the top of TM3 adopting a conformation almost parallel to plane of the membrane. This structural feature is a result of two additional disulphide bonds (C74-C146 and C71-C159) joint between ECL 2 and ECL1[29] displayed by the A_{2A} but not the A_1, which restrict the conformation of the ECL2 and narrow the entrance to the binding pocket.
An interesting study by Mattedi *et al.*[50], conducted through unbiased molecular dynamic (MD) simulations, complemented the available structural information for the A_1 and A_{2A}, demonstrating the importance of the salt bridge at the entrance of the orthosteric binding cavity[51] and the network of water molecules[52] in modulating the dynamics of adenosine ligands, ultimately affecting their selectivity properties. This study has enabled further understanding of the dynamic aspects of ligand recognition exhibited by the two adenosine receptors, thereby elucidating the structural and dynamical determinants of selectivity.

1.4 Adenosine A_{2A} Receptor

The adenosine A_{2A}AR receptor exerts prominent functions in the immune and cardiovascular systems as well as in the brain. Along with the other AR subtypes, the A_{2A}AR has been cloned from several mammalian species, including dog, human, rat, mouse and guinea pig.[53] A_{2A}ARs are highly expressed in the striatum, olfactory bulb, immune cells, blood platelets and spleen. To a lesser extent A_{2A}ARs are expressed in cardiac tissue, blood vessels and lungs.[15,54]

Of note, the A_{2A}AR is considered a high affinity receptor because it is activated by nanomolar (*circa* 316 nM, hA_{2A}AR) concentrations of adenosine. Conversely, the A_{2B}AR is activated by micromolar (*circa* 15 μM, hA_{2B}AR) adenosine concentrations.[55] As mentioned in section **1.2**, A_{2A}ARs signal mainly through $G\alpha_s$ proteins in the periphery,[56] but can also signal through

$G\alpha_{olf}$ in the striatum.[57] Engagement of both Gα proteins stimulate adenylyl cyclase, leading to an increase in cAMP accumulation and subsequent activation of a series of effector signalling proteins. A_{2A}AR activation can also stimulate the phospholipid C (PLC) pathway, leading to activation of protein kinase C (PKC) and mobilisation of intracellular Ca^{2+}. The signalling pathway engaged by the A_{2A}AR can differ depending on the cell type and tissue in which the receptor is expressed. For example, it has been observed that A_{2A}ARs either stimulates or inhibits ERK phosphorylation depending on the cellular background (HEK 293 cells vs CHO cells).[56]

1.4.1 Adenosine A_{2A} Receptor: Pharmacology and Therapeutic Application

The application of ARs radioligands and microscopy techniques coupled with studies using genetically ARs-deleted mice have allowed mapping of the occupancy, as well as understanding of the distribution and physio-pathological roles of the different adenosine receptor subtypes.[58,59]

The activation of A_{2A}ARs expressed in coronary arteries and other blood vessels produces vasodilating effects, leading to an increase of blood flow through a mechanism that can be ascribed to nitric oxide (NO)-mediated activation of guanylyl ciclase.[60] Indeed, the A_{2A}AR agonist Regadenoson (Lexiscan, Astellas Pharma) is currently used in the clinic as pharmacological stress agent for myocardial perfusion imaging (MPI).[61]

Moreover, A_{2A}ARs are highly expressed in striato-pallidal GABA neurons in the striatum and regulate neurotransmission. Here, it was found that A_{2A}ARs form heterodimeric complexes with dopaminergic D_2 receptors,[62,63] whereby activation of A_{2A}ARs allosterically inhibit D_2 signalling, leading to inhibition of motor activity. This inhibitory function mediated by the A_{2A}AR signalling prompted scientists to investigate the therapeutic role of A_{2A}AR antagonists for relieving motor deficits in Parkinson's Disease (PD) patients.[64] In 2019, the therapeutic role of A_{2A}AR in PD was validated by the U.S. Food and Drug Administration (FDA) with the approval of the A_{2A}AR antagonist istradefylline (Nourianz, Kyowa Kirin Inc.) as co-therapy with levodopa/carbidopa to treat the "off" episodes of PD.[65] Owing to the

protective role played by A_{2A}AR blockade in the CNS, it was suggested that A_{2A}AR antagonists could also offer a therapeutic benefit for many other neurological disorders including Huntington's Disease (HD),[21,66] schizophrenia,[67] depression,[68] drug addiction[69] and neuropathic pain.[21,59]

Signalling mediated by the activation of the A_{2A}AR plays an important role in inflammation and cancer biology.[25] Activation of A_{2A}AR following tissue stress or damage, suppress inflammation by downregulating pro-inflammatory molecules such as cytokines or oxygen free radicals with the aim to restore cellular homeostasis and stimulate healing processes.[70] However, when episodes of tissue stress or damage exceed the acute-injury phase, activation of A_{2A}AR can instead trigger pro-inflammatory and immunosuppressive responses.[71]

1.4.1.1 Role of the A_{2A}AR in Cancer Immunotherapy

Within the tumour microenvironment (TME) micromolar levels of adenosine are continuously produced and sustained. Here, adenosine can engage and activate the A_{2A}ARs which are expressed on the surface of immune cells including T-lymphocytes, macrophages, dendritic cells (DCs) and natural killer (NK) cells. These cells are found to populate the TME and the activation of A_{2A}AR signalling in these cells has been identified as the mechanism by which cancer can hijack the immune response in the host, thereby promoting its further development and progression. In this regard, small-molecule A_{2A}AR antagonists are being explored as novel therapeutic agents in cancer immunotherapy owing to the promising preclinical outcomes observed with blocking the A_{2A}AR pathway.[72,73]

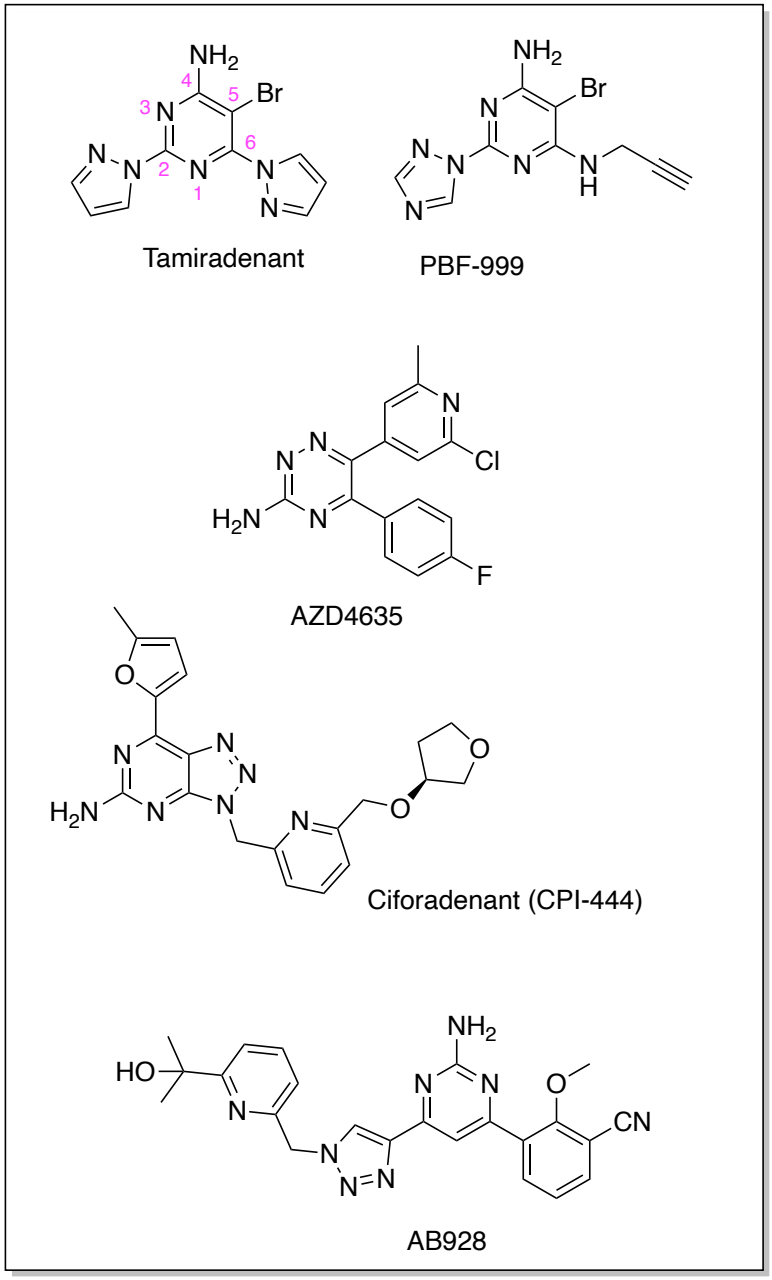


Figure 1.5 Structures of representative $A_{2A}AR$ antagonists or dual $A_{2A}AR/A_{2B}AR$ antagonist (AB928), which are undergoing clinical trials in patients with solid malignancies.[74]

Several $A_{2A}AR$ antagonists have now entered clinical trials to explore their efficacy profiles in patients with solid tumours (**Figure 1.5**). Sosei Heptares/ Astra Zeneca's AZD4635 (HTL1071)[75] is 1,3,4 triazine-based $A_{2A}AR$ antagonist, which was developed following Structure-Based Drug Discovery (SBDD) approach, exhibited promising *in vitro* pharmacodynamics in preclinical studies (K_i = 1.7 nM, with 30-fold $A_{2A}AR$ selectivity compared to binding the other adenosine receptor subtypes).[76] Subsequent *in vivo* studies

demonstrated that inhibition of A_{2A}AR signalling in syngeneic mouse tumour models by AZD4635 caused a reduction in tumour growth alone and in combination with anti-PD-L1 Ab.[77] This molecule is currently under investigation in Phase II clinical trial in combination with durvalumamb or with durvalumab and cabazitaxel in patients with advanced solid malignancies (NCT04495179). A collaboration between Palobiofarma SL and Novartis led to the development of a series of 2,6-Bis-(heteroaryl)-4-amino pyrimidines as novel A_{2A}AR antagonist for immune-oncology applications. Amongst these, Taminadenant (also known as PF-509/NIR178) showed high hA_{2A}AR affinity (K_i = 12 nM), selectivity (A_1AR K_i = 2500 nM, A_{2B}AR K_i = 1000 nM and A_3AR K_i = 5000 nM) and antitumour activity in *in vivo* models.[78] Taminadenant (NCT03549000) along with the 2-triazole, 6-propargyl pyrimidine analogue (PBF-999) are currently in Phase I clinical trial in patients with solid tumours (NCT03786484).

Notably, several studies have shown that the A_{2B}AR subtypes also mediates immunosuppression, as its activation leads to tumour growth and metastasis.[79] Owing to the promise that A_{2B}AR inhibition holds for cancer treatments, several antagonist molecules are undergoing clinical trials for this application.[80] Among these, Etrumadenant (AB928) a dual A_{2A}AR/A_{2B}AR inhibitor (K_B = 1.5 nM and K_B = 2 nM, respectively) developed by Arcus Bioscience, which showed significant antitumour effects in cancer models. Following the positive results obtained in Phase I,[81] AB928 has entered Phase II clinical trial for the evaluation as monotherapy and combination with immunotherapies in patients with advanced solid tumours (ClinicalTrials.gov identifier NCT04262856). The simultaneous targeting of A_{2A}AR/A_{2B}AR signalling in immuno-oncology could provide superior therapeutic activity compared to the inhibition of the A_{2A}AR subtype alone. Although preclinical data supporting this hypothesis are still lacking, AB928 proved to be well tolerated in addition to demonstrate good antitumour activity in mouse models of cancer.[82]

Remarkably, the studies reported herein support the evidence that blocking adenosine signalling or production in combination with chemotherapy or immune checkpoint blockade inhibitors promotes

beneficial outcomes in cancer treatments, offering a new avenue for the design and development of novel anticancer drugs.

1.5 Adenosine A_1 Receptor

The adenosine A_1AR receptor subtype is predominantly expressed in the CNS, cardiovascular system, immune system, airway smooth muscles, kidney, eye and adipose tissue. Owing to the abundance and wide-spread distribution throughout the human body, A_1ARs exert many modulatory effects, including bradycardia, neuroprotection, inhibition of neurotransmitter release and neural firing.[43] A_1AR mainly signal upon coupling with $G\alpha_{i/o}$ proteins, which cause reduction of cAMP accumulation, following inhibition of adenylyl cyclase activity. Additionally, A_1AR activation stimulates phospholipase C (PLC) pathway, thereby leading to an incrase of intracellular [Ca^{2+}] levels. Importantly, in myocardial and neural tissues A_1AR stimulates K_{ATP} channels, thereby exerting prominent functions in tissue preconditioning.[20,21]

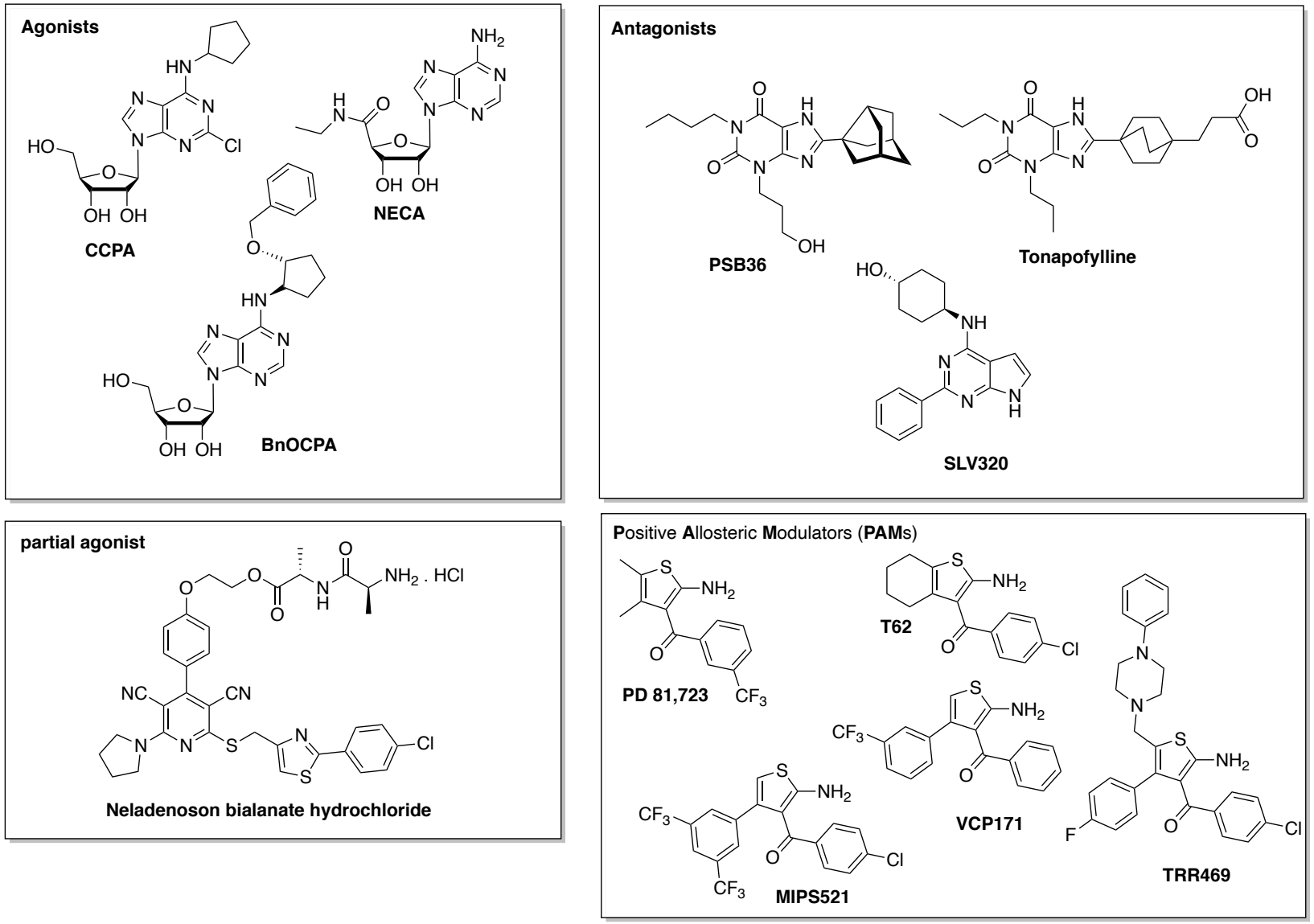


Figure 1.6 Structures of representative A_1AR ligands that progressed into clinical trials and/or are currently employed as chemical probe

1.5.1 Adenosine A_1 Receptor: Pharmacology and Therapeutic Application

Owing to the prominent role in the heart, where activation of A_1AR exerts negative inotropic, chronotropic and dromotropic effects, small-molecule A_1AR agonists have been explored as therapeutics for cardiovascular indications including angina pectoris, paroxysmal supraventricular tachycardia (PSVT) and atrial fibrillation.[20] Adenosine itself is currently used in the clinic for these specific therapeutic applications and as a diagnostic tool. Furthermore, although adenosine-mediated anti-inflammatory and protective effects have been reported for all the four AR subtypes, these effects appeared to be primarily mediated following A_1AR-engagement, in particular, during ischemia and reperfusion injury.[23] Preclinical data showed that inhibition of A_1AR signalling offered potential for the development of potassium sparing diuretics[83,84] owing to improved glomerular filtration rate (GFR) and natriuresis responses under congestive heart failure (HF) conditions.[85] Furthermore, blocking A_1AR activity may offer an avenue for the development of cognitive enhancers.[86]

Many medicinal chemistry efforts have been undertaken to improve the pharmacology of canonical orthosteric A_1AR agonists and antagonists (**Figure 1.6**).[43,44] Yet the clinical success of these ligands is still hampered by limited efficacy and/or the difficulties of separating central and hemodynamic therapeutic effects (e.g. cytoprotection) from undesired effects (e.g. bradycardia, atrioventricular (AV) block and seizures)[87,88] which are mediated by engagement of the same protein receptor.[89] The therapeutic limitations of canonical orthosteric A_1AR ligands might be overcome through the application of emerging pharmacological paradigms. These comprise of the development of biased ligands[90,91] - ligands that stabilise different receptor conformations, thereby leading to the selective activation (bias) of one signalling pathway over another. In a recent study, the A_1AR subtype-selective full agonist **BnOCPA**[92] (**Figure 1.6**) showed to discriminate between G_o subtypes, by selectively coupling with the G_{ob}

isoform. Notably, when dosed in a rat model of chronic neuropathic pain, **BnOCPA** produced analgesia without the occurrence of commonly associated adverse effects such as bradycardia or respiratory depression. As such, this novel mechanism of selective A_1AR-engagement could provide a new opportunity for the development of non-opioids analgesic.[93]

Another approach that could exploited for improving more efficacious and selective therapeutic A_1AR-targeting relies on the application of allosteric modulators.[94,95] That is, ligands which bind to a spatially and topologically distinct (allosteric) site on their target receptor, whereby they can enhance (positive allosteric modulator, PAM) or inhibit (negative allosteric modulators, NAM) the binding of endogenous or synthetic ligands to their receptor binding site and/or alter the resulting functional effect.[96–98] In principle, the major advantage of using such molecules is that greater target, tissue and functional selectivity could be achieved, whilst minimizing non-specific interactions and/or unwanted side effects.[90,94]

Since the discovery of the first A_1AR PAM **PD 81,723** by Bruns and colleagues,[99,100] medicinal chemistry endeavours have been undertaken by several research groups to probe the structure-activity relationships (SARs)[43,101–104] underlying compounds' specific pharmacology and physicochemical properties (**Figure 1.6**). Overall, these studies highlighted that only limited structural diversification from the reference PD compound was allowed, with the core 2-amino-3-benzoylthiophen (2A3BT) scaffold required as minimal pharmacophore to maintain reasonable PAM activity and the 4- and 5- positions of the thiophene ring allowing greater structural modifications. While the potential of allosterically modulate A_1AR activity has been described in many *in vitro* studies, the number of A_1AR PAM molecules explored in more physiologically relevant models is limited to few examples. 3-trifluorophrenyl 2A3BT analogue **VCP171**[102] could inhibit primary afferent synaptic transmission in rat models of neuropathic pain,[105] where the adenosine tone in the dorsal horn of the spinal cord was enhanced following injury. Furthermore, benzoylthiophene analogues **TRR469**[103,106] and **T62**[107] were able to produce anti-nociceptive effects in neuropathic pain models *in vivo*, with **T62** being further advanced to Phase II clinical trials to be evaluated in patients with postherpetic neuralgia applications.[108] This

study was however terminated owing to patients experiencing transient elevations in liver transaminases and lack in demonstrating efficacy (NCT00809679).[109] Recently, PAM 3,5-bis(trifluoromethyl) 2A3BT analogue **MIPS521** (cmpd **13o** in Aurelio, L. et al.)[102] exhibited analgesic efficacy in rat models of neuropathic pain through the on-target modulation of elevated adenosine tone that arises in the spinal cord following neuropathic pain.[35]

In a recent Phase II clinical trial, the partial A_1AR agonist **neladenoson bialanate**[110] (**Figure 1.6**) has been evaluated as potential treatment in patients with chronic heart failure. However, failures in demonstrating the primary efficacy endpoints led to discontinue the study.[111]

Despite the breadth of preclinical data supporting the development of adenosine ligands for many therapeutic indications, the number of adenosine ligands used in the clinic is limited to three molecules including synthetic adenosine, regadenoson and istradefylline (section 1.3.1). Although the reasons for the inability to translate *in vitro* data into clinical benefit may not be completely understood, it could be hypothesised that, failures in demonstrating therapeutic efficacy of a particular drug candidate in patients could be ascribed to many potential factors.[112] These include, but are not limited to, 1) the limited predictive power of translational animal models for therapeutic efficacy in humans,[113,114] owing to possible interspecies differences;[49,115] 2) in the patient population studied, some AR ligands might be incapable of exerting on-target beneficial effects in the absence of on-target adverse effects;[116,117] 3) difficulties in confirming robust AR-engagement in a particular disease states *in vivo* and its link to the disease studied.[118] Notably, these hypotheses suggest that improved understanding of AR biology is therefore needed for advancing AR ligands with superior therapeutic action and selectivity.

1.6 The use of Fluorescent Ligands for studying A_1AR and A_{2A}AR biology

The limited translation of AR ligands from the bench to the clinic, suggested that a better understanding of the molecular and cellular

mechanism of action underlying specific AR pharmacology is required for the improvement of new AR therapeutics.[119] Specifically, before ARs can be exploited as therapeutic targets, it is essential to gain better and thorough knowledge on the real-time receptor cellular and/or subcellular location, organisation and signalling as well as how different cellular and/or subcellular locations may influence specific AR signalling and how these events may eventually contribute to the particular physiology or pathology studied.[120,121] Accordingly, imaging tools represents a useful avenue to further this knowledge and help with the clinical advancement of more selective and efficacious AR therapeutics.

Traditionally, radioligands - ligands whereby a radioisotope, such as [^{3}H], [^{11}C], [^{19}F] or [^{125}I], is introduced in the core structure of the molecule and the specific radioactivity can be detected and monitored (emission of β-particle, positrons) - have been extensively used to measure ligand binding affinities and kinetic rate parameters of unlabelled ligands. In addition, some radioligands can be combined with Positron Emission Tomography (PET) to quantify receptor expression, distribution and occupancy in patients with a particular disease studied.[122,123] Owing to the hazards and costs associated to the handling, licensing and disposal of such ligands,[124] coupled with insufficient sensitivity, specificity and/or metabolic stability of some reported probes applied in *in vivo* studies,[122,125] many research endeavours have been undertaken to improve the methods which allow specific visualisation of ARs. Among these, fluorescence-based techniques offer the opportunity to interrogate and understand the molecular pharmacology of these membrane proteins in their native, unmodified cellular environment, in real-time and at single cell level with great spatial and temporal resolution.[126–128]

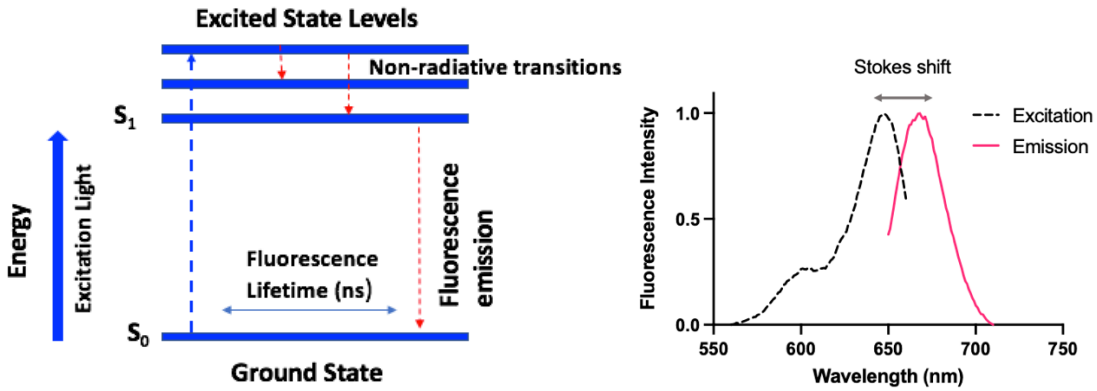


Figure 1.7. Schematic representation of the fluorescence principle as described by the Jablonski energy diagram. Upon exposure of light the electrons are promoted to a higher energy state. After a transient excited state with minimal energy loss, the fluorescent molecule returns to its ground state by emitting light. [129]

Fluorescence is a physical process that consists of the emission of light by a molecule (fluorophore) which has absorbed light energy. After a transient excited state with minimal loss of energy the molecule returns to its ground state triggering light emission at longer wavelengths than the excitation light. The difference in the excitation wavelength and the emission wavelength is called the Stokes shift of the fluorophore (**Figure 1.7**)

Examples of fluorescence techniques which allow imaging and monitoring of receptor functions and dynamics include confocal laser scanning microscopy (CLSM), Fluorescence Correlation Spectroscopy (FCS),[130] Fluorescence Polarization (FP),[131] specialised flow cytometry techniques such Fluorescence-Activated Cell Sorting (FACS),[132] fluorescence-resonance energy transfer (FRET)[133,134] and super resolution microscopy, which overcomes the diffraction limit of standard light microscopy.[135,136] These approaches rely on the possibility of fluorescently label the protein studied and this can be primarily achieved in three different ways: 1) through the use of fluorescent proteins[137] or self-labelling protein tags (e.g SNAP-tag, CLIP-tag), fluorescently labelled antibodies[138] and/or small-molecules fluorescent ligands.[139] Notably, compared with the above mentioned labelling approaches, the fluorescent ligand technology has the greater advantage of being readily applicable for the study of protein receptors in their native,

unmodified expressing system, which in a drug discovery program should be more disease-relavant.[140,141]

Fluorescent ligands are designed and synthesised by tethering an organic fluorescent dye to a known agonist or antagonist ligand for the receptor studied *via* a linker.[127,128,142] Notably, the development and application of small-molecule fluorescent probes for ARs, and for GPCR in general, has rapidly increased in the past 20 years; this has been achieved owing to advancements in imaging approaches coupled with increased availability of structural information, from both X-ray crystallography[29,30,36] and cryoelectron microscopy (Cryo-Em),[33,34] which can allow the rational design of ligands with improved affinity and selectivity for the target protein.[40,143]

1.6.1 Fluorescent Ligands Design

Some considerations must be addressed when designing fluorescent ligands. Fluorescently-labelled ligands are composed by three independent units: the parent pharmacophore, the fluorophore and the linker which connects the former two parts together (**Figure 1.8**). It is important to understand that the pharmacological profile of the resulting fluorescent ligand is critically influenced by each of these components. Indeed, every time a new design approach is carried out, it essential to consider the novel fluorescent ligands as new pharmacological entities. The addition of a quite bulky fluorophore as well as the linker are likely to alter the pharmacological profile of the parent pharmacophore.[144–146]

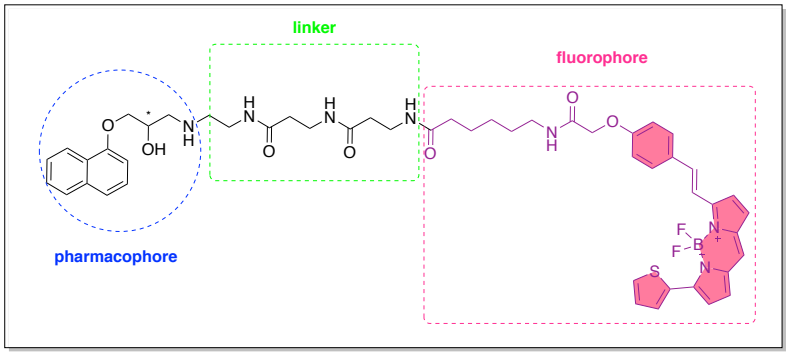


Figure 1.8 Fluorescent ligand components. Specifically depicted is a fluorescent analogue of propranolol (BODIPY 630/650-X- β-Ala- β-Ala propranolol) designed by Alcobia et al.,[147]

Firstly, it is important to elucidate the structure-activity relationship (SAR) of the parent pharmacophore at the receptors of interest. This process is extremely fundamental because it suggests the most suitable position which tolerates the addition of the fluorophore or the linker, therefore without possibly affecting the binding affinity or efficacy of the final ligand. An ideal fluorescently-labelled compound would retain the pharmacological properties of the parent ligand. When available, structural knowledge of the target protein can be leveraged for the rational design of these ligands. Secondly, the choice of the fluorophore heavily depends on the application of the fluorescent probe as different imaging approaches require fluorophores with specific spectral properties, such as excitation and emission wavelength, quantum yield, exciton coefficient and fluorescence lifetime. Additionally, it has been demonstrated that the chemical composition and the length of the linker may affect the binding affinity and efficacy of the fluorescent ligand.[144,148] For example, this theory has been investigated by our research group on the adenosine receptor A_1 and A_3 subtypes.[144,149] More precisely, Vernall et al.,[150] have shown that the non-selective xanthine amine congener (XAC) linked to BODIPY 630/650-X through a dipeptide linker was converted into a ligand selective towards the adenosine A_3 receptor subtypes. The introduction of amino acids as part of the linker contributed in enhancing ligand binding affinity compared to the parent ligand as well as generating a selective compound.[149,150]

1.6.2 Fluorescent Ligands Properties and Recent Applications

The first examples of fluorescent ligands used in bioimaging studies encompassed molecules conjugated with dansyl, pyrene and fluorescein isothiocyanate (FITC) fluorophores. These dyes, however, exhibited some drawbacks such as reduced photostability and sensitivity to environmental pH, short excitation and emission wavelengths (<450 nm). Nowadays, numerous fluorophores are commercially available, covering the full range of the visible /electromagnetic spectrum. Interestingly, the vast collection of available fluorophores derives from a handful of "core" scaffolds belonging to the

families of coumarins, rhodamines, boron dipyrromethene (BODIPY), fluoresceins and cyanines dyes.[151,152] Furthermore, recent synthetic chemistry endeavours have shown the possibility of accessing a wider palette of fluorescent dyes, whereby the spectral and physicochemical properties of the latter can be easily tuned and improved for their application in more advanced biological techniques.[153–155] For broader biological applications such as *in vivo*, fluorophores that absorb and emit in the near-IR region (such as Cyanine5 or BODIPY-630/650 dyes) of the electromagnetic spectrum (> 600 nm) are preferred owing to the significant reduction, in this optical window, of light scattering and background autofluorescence originating from endogenous molecules (e.g reduced nicotinamide cofactors NADH, aromatic amino acids, flavoproteins, collagen)[156], resulting in enhanced tissue penetration, in addition to applying wavelengths that, at this lower energy, are less harmful and toxic to tissues.[147,157,158] BODIPY 630/650 dyes are amongst the preferred choice for fluorophore conjugation as they display great stability and spectral properties, such as high fluorescence quantum yield (Φ) and high absorption coefficient (ε).[159–161] Moreover, these dyes are shown to be heavily quenched in aqueous environment, whilst, in marked contrast, are brighter when located in a more lipophilic environments, such as the plasma membrane.[144] Accordingly, this fluorogenic property of BODPY dyes is particularly advantageous for imaging studies as it reduces the background fluorescence from unbound ligand. The inherent lipophilicity of these dyes may however limit their application in more physiological relevant models such as *in vivo*. In this regard, more water-soluble dyes such as those belonging to the Cyanine (e.g Sulfo-Cyanine5) and Alexafluor (e.g. Alexafluor647)[157,158] may overcome some of the limitations discussed above.

Advancement in fluorescent ligands design and imaging techniques have broadened the application of such tools, whereby novel facet of ARs pharmacology , and GPCRs in general, could be also investigated not only in model systems but also in native, unmodified environments.[126,140] For example, pan-selective fluorescent analogues (BODIPY-630/650-X-lablled) of adenosine (ABA-X-BY630/650) and NECA(ABEA-BY630/650)[148] and CA200645[162] (Figure X) have been successfully used in conjunction with Nanoluciferase Bioluminescence Resonance Energy Transfer (NanoBRET)[163–

[165] ligand binding assays to quantify the effect of positive allosteric modulation at human and rat NanoLuc-A_1AR (**Figure 1.9**).[49] Moreover, fluorescent ligands offer the opportunity to study allosteric interactions following oligomeric complexes formation. Indeed, fluorescent agonist ABA-X-BY630/650 was applied in confocal microscopy studies coupled with continuous perfusion of buffer to visualise and quantify negative cooperativity across the A_3AR-A_3AR homodimeric interface at single cell level.[166] The application of specific fluorescent D_2R (N-(p-aminophenthyl)spiperone NPS-Lumi4-Tb)[167] and A_{2A}AR (SCH-red, Figure 1)[168] antagonists in FRET studies allowed to monitor allosteric interactions across D_2R-A_{2A}AR complexes in healthy and disease striatal tissues, thus providing mechanistic insights into the functional effect of D_2R-A_{2A}AR dimerization in a native environment.[168,169]

Another exciting opportunity for investigating ligand binding and receptor functions under endogenous promotion is through the application of genome-editing approaches in combination with fluorescent ligands. White et al[170]were able to use CRISPR/Cas9[171] technology to insert the bright NanoLuc protein into endogenous genome and thus to monitor NanoBRET ligand binding at native adenosine hA_{2B}AR[172] and chemokine CXCR4[173] receptors, respectively.

In a more recent study subtype-selective fluorescent β_2-AR antagonists have also been successfully combined with CRISPR/Cas9 genome-edited HEK293 cells to quantify and visualise ligand binding in a more physiologically relevant environment using NanoBRET luminescence imaging.[141]

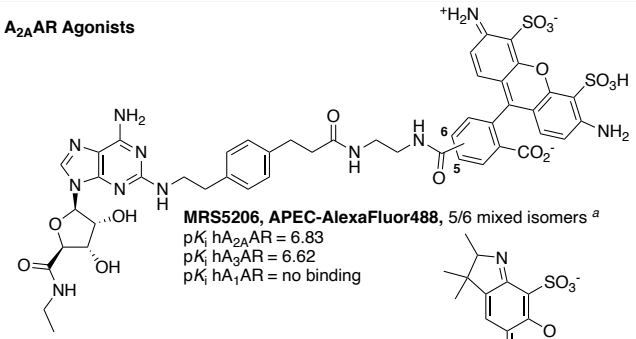
Notably, a specific fluorescent TSH ligand enabled monitoring of endogenous TSH internalisation and signalling from intracellular compartments (endosomes and Trans Golgi Network, TGN)[174] in primary cells, thus providing better understanding of the signalling events triggered by receptor activation in native settings. Recently, a pan-selective fluorescent β_1-AR and β_2-AR ligand based on carazolol was combined with FCS to study the localisations and dynamics of both adrenoreceptors in adult murine cardiomyocytes, thereby shedding new light into the influence of receptor specific localisation on its functional effects.[120]

The few examples discussed herein demonstrate the power of the combination of fluorescent ligands with more advanced fluorescence-based

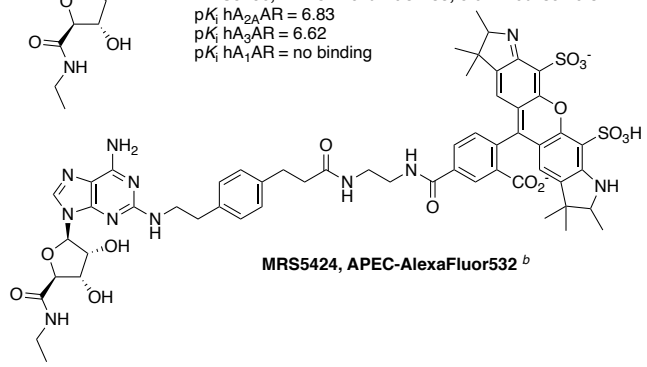
techniques to study receptors functions and dynamics not only in model systems, but also in more physiologically relevant settings.

For a more detailed analysis of fluorescent ligands design and applications, examples of excellent reviews on the subject are provided.[123,126–128,146,175,176]

A_{2A}AR Agonists

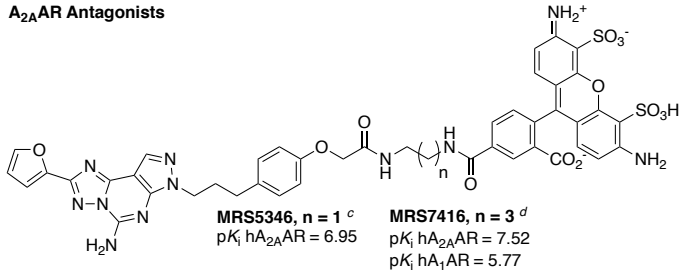


MRS5206, APEC-AlexaFluor488, 5/6 mixed isomers [a]
pK_i hA_{2A}AR = 6.83
pK_i hA_3AR = 6.62
pK_i hA_1AR = no binding



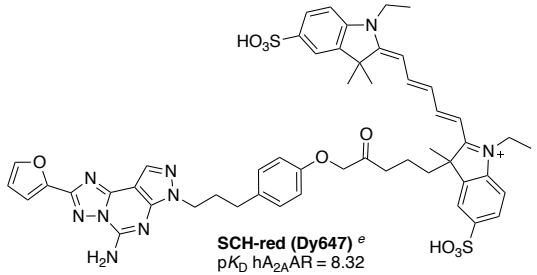
MRS5424, APEC-AlexaFluor532 [b]

A_{2A}AR Antagonists



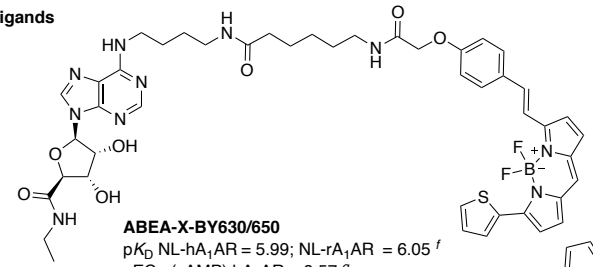
MRS5346, n = 1 [c]
pK_i hA_{2A}AR = 6.95

MRS7416, n = 3 [d]
pK_i hA_{2A}AR = 7.52
pK_i hA_1AR = 5.77

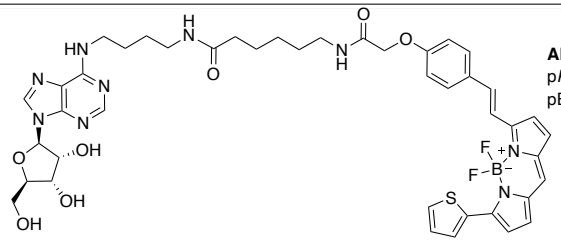


SCH-red (Dy647) [e]
pK_D hA_{2A}AR = 8.32

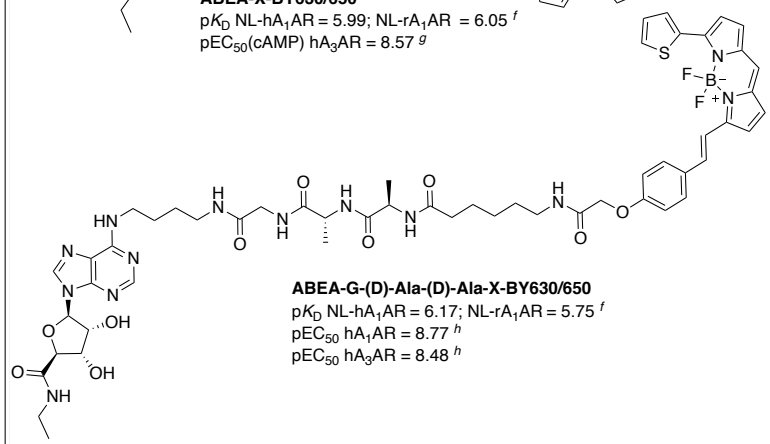
A_1AR ligands



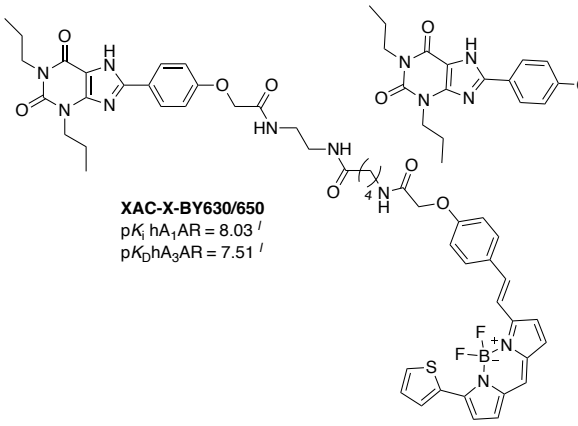
ABEA-X-BY630/650
pK_D NL-hA_1AR = 5.99; NL-rA_1AR = 6.05 [f]
pEC$_{50}$(cAMP) hA_3AR = 8.57 [g]



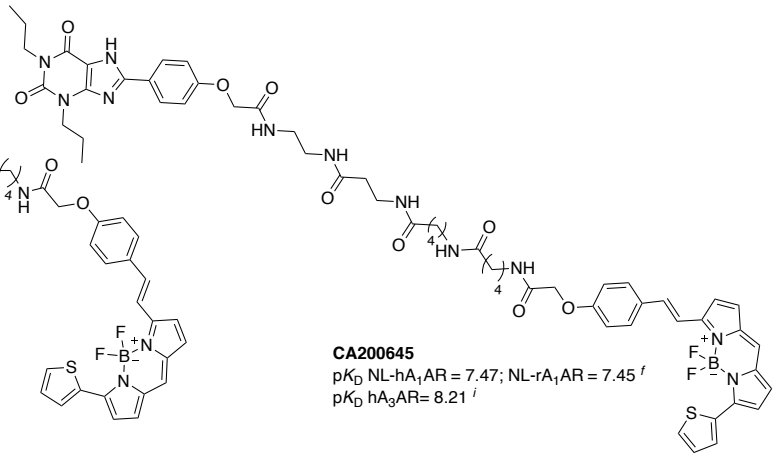
ABA-X-BY630/650
pK_D NL-hA_1AR = 6.23; NL-rA_1 = 6.05 [f]
pEC$_{50}$(Ca^{2+}) hA_3AR = 5.9 pEC$_{50}$(ERK1/2) hA_3AR = 7.3 [g]



ABEA-G-(D)-Ala-(D)-Ala-X-BY630/650
pK_D NL-hA_1AR = 6.17; NL-rA_1AR = 5.75 [f]
pEC$_{50}$ hA_1AR = 8.77 [h]
pEC$_{50}$ hA_3AR = 8.48 [h]



XAC-X-BY630/650
pK_i hA_1AR = 8.03 [l]
pK_DhA_3AR = 7.51 [l]



CA200645
pK_D NL-hA_1AR = 7.47; NL-rA_1AR = 7.45 [f]
pK_D hA_3AR= 8.21 [i]

Figure 1.9 Structures of representative fluorescent ligands available for studying the A_{2A}AR and A_1AR. Fluorescent ligand binding affinity [a, b, c, d, e, f, i, l] (pK_D and pK_i)[131,149,162,168,177–179] and potency [g, b] (pEC_{50})[180–182] quantified in cell lines stably expressing the human A_1AR (hA_1AR), rat A_1AR (rA_1AR) or human A_3AR (hA_3AR). NL denotes the presence of an N-terminal NLuc tag.

1.6.3 Fluorescent Ligands Developed for the A_1AR and A_{2A}AR

In 1987 Jacobson and co-workers pioneered the development of fluorescent ligands for the adenosine receptors as they applied the functionalised congener approach to design fluorescent analogues of adenosine,[183] NECA[184] and xanthine amine congener (XAC)[185], which encompassed fluorophores such as nitrobenzoxadiazole (NBD) and fluorescein isothiocyanate (FITC).[186] The utility of the A_{2A}AR-selective FITC-labelled analogue of NECA has been also recently showed in fluorescence polarisation studies to measure binding kinetic paraments of unlabelled A_{2A}AR ligands.[187] Synthetic efforts oriented towards enhancing ligand binding and photochemical properties of available fluorescent A_{2A}AR ligands, led to the discovery of the first examples of subtype-selective fluorescent A_{2A}AR antagonists based on the subtype-selective A_{2A}AR antagonist SCH4424416: AlexaFluor-488 conjugated ligands MRS5346[131,188] and MRS7416, [179] respectively (**Figure 1.9**). These fluorescent conjugated were successfully employed in fluorescence polarisation and flow cytometry experiments. In addition, molecular modelling studies suggested that these ligands exhibited a bitopic character, owing to the ability of the probe to simultaneously engage two distinctive sites within the same receptor.[179] More recently, functional characterisation of MRS7416 acting at the hA_{2A}AR has been performed in stable cell lines, thereby showing that the bitopic fluorescent analogue displayed an allosteric mode of action.[189]

Fluorescent agonist and antagonists developed for the human A_1AR have been developed by many research groups, including ligands prepared from the endogenous A_1AR agonist, adenosine, tethered with fluorescein isothiocyanate (FITC) and nitrobenzoxadiazole (NBD) (FITC-ADAC and NBD-ADAC)[186] or BODIPY-X-630/650 (ABA-X-BY630).[148] Moreover, fluorescent ligands

synthesised from the full agonist NECA (dansyl-NECA,[190] ABEA-BY630[148] and ABEA-G-(*D*)-Ala-(*D*)-Ala-X-BY630[181]) and antagonists based on xanthine amine congener (XAC)[185] (XAC-X-BY630)[191] and its analogue with a polyamide linker (CA200645) are also available (**Figure 1.9**).[162,192] Importantly, these fluorescent ligands have allowed researchers to gain important insights into A_1AR localisation, spatio-temporal organization[148,191,193] and functional activity in living cells.[49] Nonetheless, many of these ligands suffer from poor selectivity of binding as they equally engage with other adenosine receptor subtypes. Therefore, this feature limits their application to recombinant expression systems and suggests the need for additional fluorescent ligands with improved A_1AR subtype-selectivity.

1.7 Ligand-Directed Labelling of Membrane Proteins

In previous sections the utility of fluorescent ligands to study membrane proteins in model systems and/or native settings, with a particular focus to ARs, has been described. The main advantage of using fluorescent ligands is that genetic manipulation of the protein of interest with a tag or fluorescent protein is not required. Thus, this minimises possible alterations of the biological functions and expression of the protein studied that could arise from such modifications. However, as for any technique, fluorescent ligands also display some limitations. For example, the size and the nature of the reporter fluorophore could alter receptor affinity and/or selectivity, [144,150,194] and could accumulate inside the cell, leading to non-specific binding.[149,195]

Another limitation of fluorescent ligands is that their inherent reversible nature of ligand binding with the receptor could hinder the extent by which many aspects of receptor pharmacology can be visualised and interrogated real-time, in endogenous expressing systems. In this regard, ligand-directed chemistry has emerged as complementary, biorthogonal approach for labelling membrane proteins in their unmodified, native environment.[196,197]

The Hamachi group in Japan has pioneered the ligand-directed (LD) chemistry technology, a traceless[198] affinity-based labelling approach which

uses a cleavable electrophilic group incorporated into the labelling reagent (**Figure 1.10 A**). The labelling reagent is composed of an "affinity" ligand (agonist or antagonist) which binds to the protein under study with good affinity and selectivity, and a reactive cleavable moiety conjugated with a reporter functional group. In principle, the affinity ligand moiety "directs" ligand binding to the protein. Upon ligand binding, close proximity of the electrophilic cleavable group with a nucleophilic amino acid side chain in the ligand binding site promotes efficient transfer of the reporter functional group to the residue, through formation of a covalent bond.[199] Once the reporter group is covalently transferred to the receptor, the rest of the molecule should be able to act as a leaving group and freely dissociate from the binding site, leaving it intact and available for additional ligands to engage with the receptor.[200] Therefore, the key advantage of this technology is that once the protein is labelled, its functionality should be preserved.[199]

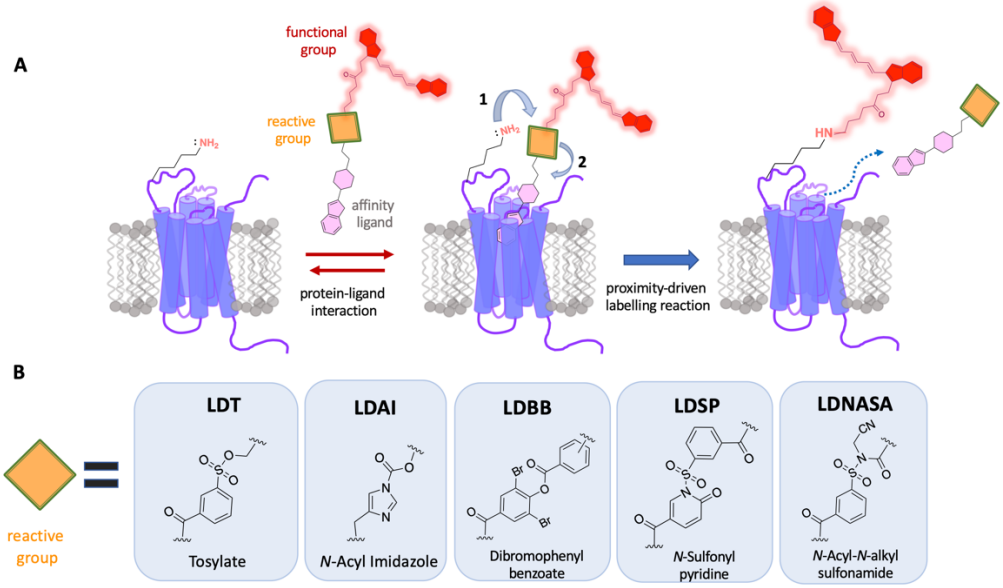


Figure 1.10 A) General schematic representation of the Ligand-Directed (LD) labelling reaction. The affinity ligand moiety of the labelling reagent "directs" ligand-protein engagement. The reactive group undergoes proximity-driven nucleophilic substitution/addition (depending on the nature of the electrophilic centre), thus resulting in covalent transfer of the functional group to the nucleophilic residue side chain. The affinity ligand may behave as a leaving group and freely dissociate from the binding site leaving it intact. **B**) Examples of reported reactive group structures, ordered chronologically from the first reagent reported in 2009 (LDT, Tosylate)[196], to the best of our knowledge, up to the most recent reagent described by the Hamachi group in 2018 (LDNASA).[201]

Many ligand-directed labelling reagents have been developed and applied by the Hamachi laboratory as well as other research groups to study a variety of proteins, such as enzymes[196,202], intracellular proteins[201] and membrane-associated proteins in their native environment, such as ligand-gated ion channel proteins ($GABA_AR$[203], *N*-methyl-*D*-Aspartate, NMDA[204] and AMPA[205,206] receptors) and the GPCR bradykinin B_2 receptor.[204] In addition to enable the study of protein functions, this technology can be also applied for drug screening purposes[203] and for the development of targeted covalent inhibitors (TCIs)[201] and covalent drugs.[207]

Different electrophilic cleavable moieties have been designed and used for ligand-directed chemistries, with each group displaying distinctive features such as reactivity, stability and amino acid selectivity for protein labelling.[200,208]

The first generation of traceless affinity labels encompasses Ligand-Directed Tosyl (LDT)[196,202] chemistry (**Figure 1.10 B**). This approach exploits a phenylsulfonate (tosyl) ester group as cleavable electrophile which undergoes S_N2 to transfer the reporter functional group to a specific residue. Notwithstanding its ability to label endogenous FKBP12, the low labelling yield as well as the slow kinetics of labelling, prompted the authors to explore alternative reactive groups. This led to Ligand-Directed Acyl Imidazole (LDAI)[197] chemistry, which uses a moderately reactive alkyloxy acyl imidazole as cleavable reactive group, with improved labelling efficiency and kinetics. To expand the scope of the method to also enable labelling of intracellular proteins, new reactive groups were explored, owing to the reduced stability of the acyl imidazole moiety inside the cells, as the group represented a good enzyme (e.g. esterases, proteases) substrate and could be easily degraded. It was envisaged that application of reactive groups which did not occur in nature and, therefore, could minimise enzymatic degradation, could achieve more specific and faster labelling kinetics. This led to the design and application of Ligand-Directed Dibromophenyl Benzoate (LDBB)[209], Ligand-Directed *N*-Sulfonyl Pyridione (LDSP)[210] and Ligand-Directed *N*-Acyl-*N*-Alkyl Sulfonamide (LDNASA)[201] chemistries (**Figure 1.10 B**). These approaches can be applied for labelling both intracellular and membrane-bound proteins. Moreover, these methods display greater stability and

improved kinetics of labelling, with the LDNASA method showing the fastest labelling kinetics among all the LD approaches reported. Notably, an in vitro study of this reaction kinetics yielded a second-order rate constant k_2 = ~10^4 M^{-1} s^{-1}, a value which, for instance, is very similar to the kinetic parameters measured with the fastest biorthogonal click reaction, such as IEDDA reaction between a tetrazine and a *trans*-cyclooctene.[200,211]

In the context of GPCR research, ligand-directed chemistry has been applied for labelling three GPCRs such as the bradykinin B_2 receptor with biotin[204] and, more recently, the μ-Opioid[212] and the A_{2A}AR[213] receptors with a fluorescent dye. Directed covalent modification of the A_{2A}AR with a reporter has been also achieved in an earlier study.[214] it was shown, however, that the number of binding sites available for subsequent radioligand engagement was significantly reduced, suggesting that the binding pocket was effectively blocked following covalent labelling.[214] This result highlights the importance of confirming the unaltered functionality of the labelled receptor for the implementation of a ligand-directed chemistry approach.

As mentioned above, the LD approach has been applied for studying the expression pattern, function and organisation of endogenously expressed μ opioid receptors and A_{2A}AR receptors. The ligand-directed label described for the A_{2A}AR encompassed a novel electrophilic cleavable group based on a 3-fluoro-phenyl ester moiety. A Structure-Based Drug Discovery (SBDD) approach was used to guide reagent design and close proximity with the nucleophilic K153 side chain. This new reagent enabled visualisation of endogenously expressed A_{2A}AR on a human breast cancer cell line SK-BR-3 by confocal microscopy and detection of endogenously expressed A_{2A}AR on human monocyte-derived macrophages by FACS analysis.[213]

The labelling reagent described for the μ opioid receptors was based on the LD Acyl Imidazole (LDAI) chemistry, which allowed detection of neurons expressing opioid receptors in various brain regions in rats and mice. Furthermore, the ability to monitor agonist-induced receptor internalisation, following labelling with the LDAI reagent, confirmed that the function of the receptor was preserved.[212]

In addition to complement the successful methods reported for labelling a GPCR such as SNAP-tag[139] and NanoLuc[215], ligand-directed chemistry provides the opportunity of labelling endogenously expressed proteins without affecting their natural functions. Indeed, ligand-directed chemistry is a non-invasive approach which allows to visualise and monitor many aspects of receptor pharmacology in unmodified and more clinically relevant systems.

1.8 Thesis Aims

The complexity of adenosine signalling under normal health conditions as well as at different stages of disease has played a crucial role for limiting the development of efficacious and safe AR therapeutics. As such, superior fundamental understanding of the molecular mechanisms underlying specific AR pharmacology in health and disease is required for improving AR therapeutic targeting. Importantly, novel subtype-selective fluorescent AR ligands should be developed and combined with more advanced fluorescence-based techniques for better understanding adenosine receptors function and signalling in different cellular or subcellular elements.[216]

The primary aim of this thesis was to expand upon the current pharmacological toolkit available to study the adenosine A_{2A}AR and A_1AR receptors subtypes, through the development of additional subtype-selective fluorescent ligands, labelled with a broader range of fluorescent dyes and which could be amenable for applications in multiple fluorescent-based techniques.

- Subtype-selective fluorescent A_{2A}AR antagonists have been reported and successfully applied for flow cytometry and fluorescence polarisation studies. However, the utility of these probes for bioimaging studies has not yet been reported. Accordingly, the first project explored in this thesis involved the design, development and application of subtype-selective fluorescent A_{2A}AR antagonists, labelled with a broad range of fluorophores and that could be coupled with multiple fluorescent-based techniques for the study of A_{2A}AR in living cells.
- The second aim of the thesis was to design and develop the first examples of subtype-selective fluorescent A_1AR antagonists, since, to the best of our knowledge, there haven't been yet reports in the available literature.
- Finally, as an extension of the fluorescent ligands technology, it was explored the design, development and application of a ligand-directed chemistry approach for labelling the A_1AR in living cells.

Chapter 2. Subtype-Selective Fluorescent Ligands as Pharmacological Research Tools for the Human Adenosine A_{2A}AR Receptor

2.1 Brief Introduction

Among the G Protein-Coupled Receptor (GPCR) superfamily of membrane receptors, the adenosine A_{2A}AR is one of the four adenosine receptors (AR) subtypes (A_1AR, A_{2B}AR and A_3AR) which respond to extracellular adenosine as their natural agonist and modulator of many physiological processes.[15,74] A_{2A}AR primarily operates by coupling with $G\alpha_s$ proteins[56] but, in the striatum, can also signal through engagement of $G\alpha_{olf}$ protein.[57] Upon A_{2A}AR activation, both $G\alpha_s$ and $G\alpha_{olf}$-coupled A_{2A}AR receptors stimulate adenylyl cyclase resulting into an increase of intracellular levels of cAMP, with subsequent activation of a series of downstream signalling pathways.[21] With the protein data bank (PDB) and GPCR database (GPCRdb)[217] repositories housing over fifty crystal structures, the A_{2A}AR is possibly one the most structurally resolved membrane proteins.[29,30,32,33,45,218,219] This structural knowledge could be leveraged by researchers for the rational design and development of selective A_{2A}AR ligands[9,42,74,220] whereby agonists could be used for cardiovascular disorders, inflammation, wound healing and respiratory diseases.[54,109,221] A_{2A}AR antagonists offer therapeutic opportunities for CNS disorders including Parkinson's (PD), Alzheimer's (AD) diseases and attention deficit hyperactivity disorder (ADHD).[21,74] Moreover, owing to the role of the A_{2A}AR pathway in the immune system, A_{2A}AR antagonists could be used in cancer immunotherapy.[222] A number of preclinical studies using murine models of cancer have shown that pharmacological inhibition of A_{2A}AR signalling[71,72] or genetic A_{2A}AR deletion[223] produced antitumor effects owing to the activity of immune cells that could be restored.[73] Indeed, as explained in more detailed in Chapter 1 (section 1.4.1.1), a number of small-molecule A_{2A}AR antagonists are currently undergoing evaluation in clinical trials for their ability to inhibit the adenosine-mediated suppression of the immune response in patients with

solid tumours such breast cancer, prostate carcinoma and non-small cell lung cancer.[73]

At the current time, only two A_{2A}AR ligands have been approved for clinic use: Regadenoson (Lexiscan, Astellas Pharma) a pharmacological stress agent for myocardial perfusion injury[21,61] and Istradefylline (NOURIANZ®, Kyowa Kirin Inc.),[224] a xanthine-based hA_{2A}AR antagonist which has reached the market in Japan for treating the symptoms of Parkinson's Disease (PD).[225,65] However, despite the many therapeutic opportunities associated with the A_{2A}AR, translation of adenosine ligands from the bench into the clinic has been hampered by the difficulties in deciphering distinct receptor effects dependent on the tissue, cell-type and disease states leading to on-target side effects. The successful development of more selective and efficacious therapeutics targeting the A_{2A}AR heavily relies on the ability to monitor real-time the localisation and function of the receptor at native expression levels in different kind of human cells in both health and disease states.[216] Accordingly, fluorescent ligands represent valuable pharmacological tools to achieve this aim as they allow to interrogate the target receptor with high spatiotemporal resolution at endogenous expression levels and in unmodified living cells.[226]

Jacobson and co-workers developed the first examples of subtype-selective fluorescent A_{2A}AR antagonists, which comprised of fluorescent analogues of the A_{2A}AR selective antagonist SCH442416[227] conjugated with an AlexaFluor488 dye (**MRS5346** and **MRS7416**, **Figure 1.9** in **Chapter 1**) that have been successfully applied for fluorescence polarization[131] and flow cytometry[179] experiments. However, the utility of these fluorescent conjugates for bioimaging studies was not explored, suggesting that there still remains the scope for the development of additional selective fluorescent A_{2A}AR probes optimised for imaging studies, that would allow visualisation of specific A_{2A}AR distribution and localisation patterns at single cell level in healthy and diseased systems. In the work presented in this chapter we expand the current pharmacological toolkit for the A_{2A}AR by developing a more versatile suite of fluorescent probes with regard to their photochemical properties and areas of potential application.

2.2 Rational Design of the Novel Fluorescent A_{2A}AR Antagonists

Preladenant (SCH 420814/MK-3814; Merck) is a pyrazolo[4,3-e]-1,2,4-triazolo-[1,5-c]pyrimidine (PTP) based A_{2A}AR antagonist, displaying high affinity ($hA_{2A}AR$ K_i = 1.0 nM)[228] and high $hA_{2A}AR$ selectivity (hA_1, hA_{2B} and hA_3 K_i > 1000 nM), which entered Phase III clinical trial for PD. Yet, failures in demonstrating efficacy versus placebo led to discontinue the study.[229,230] Notably, preladenant has been recently repurposed in immune-oncology (NCT03099161), but the clinical trial was terminated early as the data failed to support the study end points.[73]

Owing to the great pharmacodynamic properties displayed, preladenant indeed represented an excellent template from which to start designing and developing the novel series of fluorescently-labelled $hA_{2A}AR$ antagonists. The synthetic strategy began by surveying the existing structure-activity relationships (SAR)[42,220,231–235] of the selected parent drug preladenant in binding to the $hA_{2A}AR$ to identify the optimal position of the molecule that would be relatively insensitive to structural changes and allow linker and fluorophore conjugation without significantly impairing the original pharmacology of the ligand. This preliminary assessment was complemented with molecular docking studies which were undertaken to rationalize the possible molecular interactions governing preladenant-$hA_{2A}AR$ binding (**Figure 2.1**).

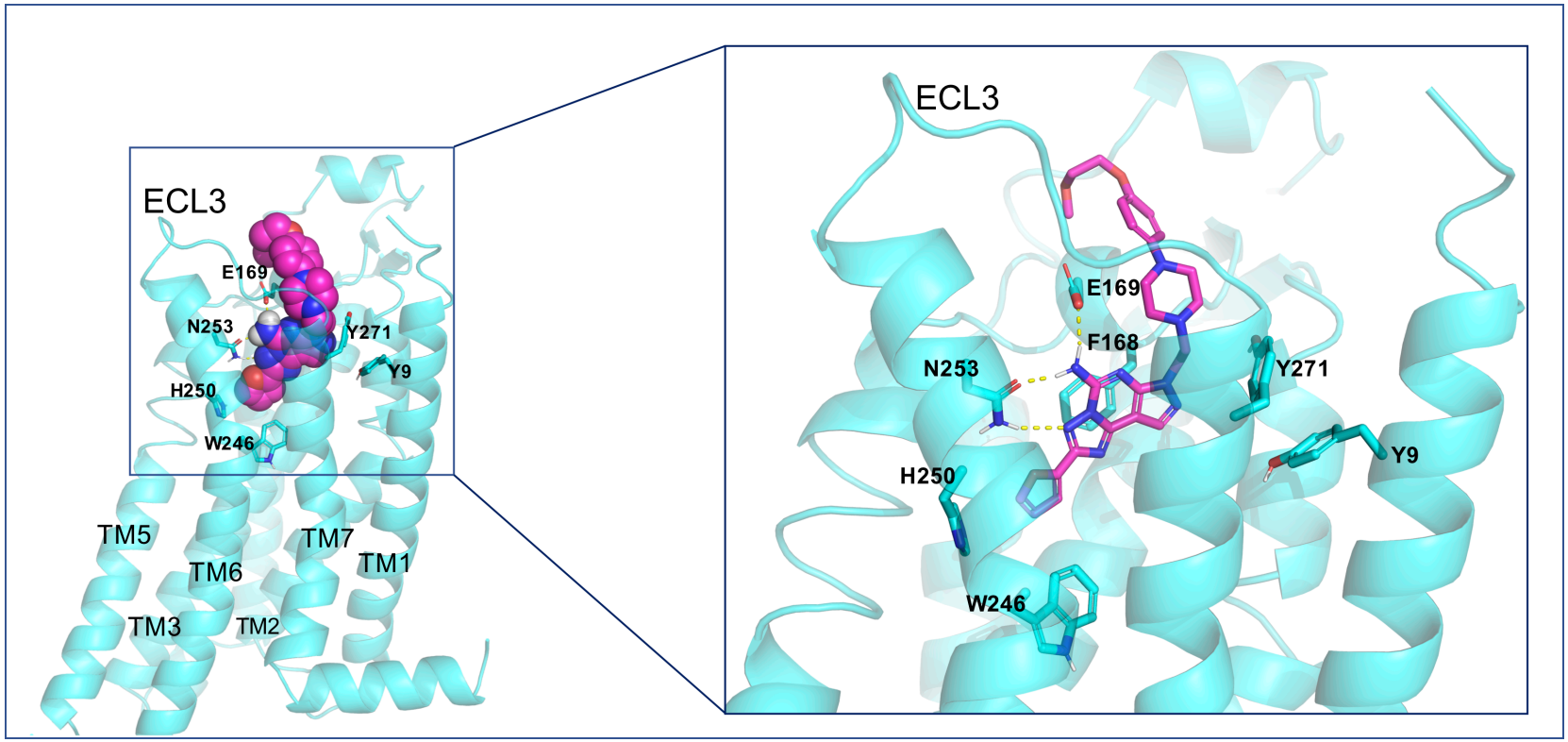


Figure 2.1 Molecular Docking of preladenant to the crystal structure of the $hA_{2a}AR$ (PDB=4EIY) executed with Schrödinger's Glide (Schrödinger release 2018-3). The images were generated with PyMOL (version 2.2.0). Preladenant is shown in spheres colored magenta. The GPCR is shown in ribbon colored cyan. The key residues are labelled and shown in sticks. A zoomed view of preladenant (shown in licorice) in the binding pocket is depicted in the box with hydrogen bonding interactions depicted as dashed lines.

Docking studies of preladenant (**Figure 2.1**) to the 1.8 Å resolution crystal structure of the $hA_{2A}AR$[45] showed the core pyrazolo[4,3-*e*][1,2,3]triazolo[1,5-*c*]pyrimidin-5-amine (PTP) scaffold interacts with key receptor residues in an equivalent fashion to the co-crystalised inverse agonist ZM241385, including polar contacts with Asn253 and Glu169 and a π-π stacking interaction with Phe168.[29,45] The distal region of preladenant adopted a conformation extending towards extracellular loop 3 (ECL3) and, thus, to a more solvent-exposed region of the membrane protein. These results were further corroborated by previously reported SAR studies which indicated that chemical modifications at the extended methoxyethylether moiety were well tolerated.[42,231,233,234] Therefore, it appeared logical to use this side chain of preladenant as a flexible conjugation point. Based on the docking results, it was envisaged that an amino alkyl spacer would provide sufficient spatial separation between the fluorescent dye and the orthosteric binding core. Fluorescent ligand design often involves the introduction of a spacer between the parent pharmacophore and the fluorophore moieties, whereby the chemical composition and length of the linker, as well as the fluorophore itself, can significantly influence the final pharmacological profile of the fluorescent ligand.[144,146,150,236] Structural changes must be performed at precise positions of the parent drug which can be well tolerated without significantly impairing the original pharmacological activity. Therefore, the methoxy tail in the distal region of preladenant was modified with an amino alkyl spacer yielding the corresponding amino functionalised congener which could be conjugated with a different range of commercially available fluorescent dyes (**Scheme 2.1**).

The novel series of fluorescent ligands described in this chapter encompassed fluorophores of different physico- and photochemical properties such as the 4,4-difluoro-4-bora-3*a*,4*a*-diaza-*s*-indacene (BODIPY) dyes together with water-soluble dyes such as sulfonated cyanine-5 (sulfo-Cy5) and AlexaFluor647 fluorophores. The choice of these fluorophores was determined by their specific physico- and photochemical properties displayed. For instance, the use of fluorescent dyes with long-wavelength excitation/emission spectra is preferred as it minimizes the degree of overlap

with background autofluorescence in living cells.[150,237–239] BODIPY derivatives represent the first choice for fluorescent derivatization owing to their excellent phtochemical properties and stability.[161] The 6-(((4,4-difluoro-5-(2-thienyl)-4-bora-3*a*,4*a*-diaza-*s*-indacene-3-yl)styryloxy)acetyl)aminohexanoic acid (BODIPY630/650) is often the favoured among this family of fluorophores due to its advantageous spectral profile (excitation 630 nm, emission 650 nm). Previous studies have suggested that, owing to its lipophilic nature, the BODIPY 630/650 fluorophore likely resides within the membrane bilayer. Indeed, this fluorescent dye has been shown to be heavily quenched in aqueous solution, while its quantum yield significantly increased in proximity to the plasma membrane, suggesting its optimal location would be in a lipid environment.[144,237] This property is particularly advantageous for imaging studies as it minimises background fluorescence from non-bound florescent ligand. However, the intrinsic lipophilic nature of the BODIPY fluorophores may limit their applicability in more complex systems such as in a *in vivo* setting due to the reduced stability in the bloodstream as well as limited detection after IV administration.[147] One possible strategy to overcome these issues is by employing more water-soluble fluorophores such as those belonging to the Cy5 and AlexaFluor families of dyes. These water-soluble dyes also possess excellent photochemical properties and have therefore been particularly advantageous for the development of *in vivo* probes to visualise endogenous GPCRs.[157,158]

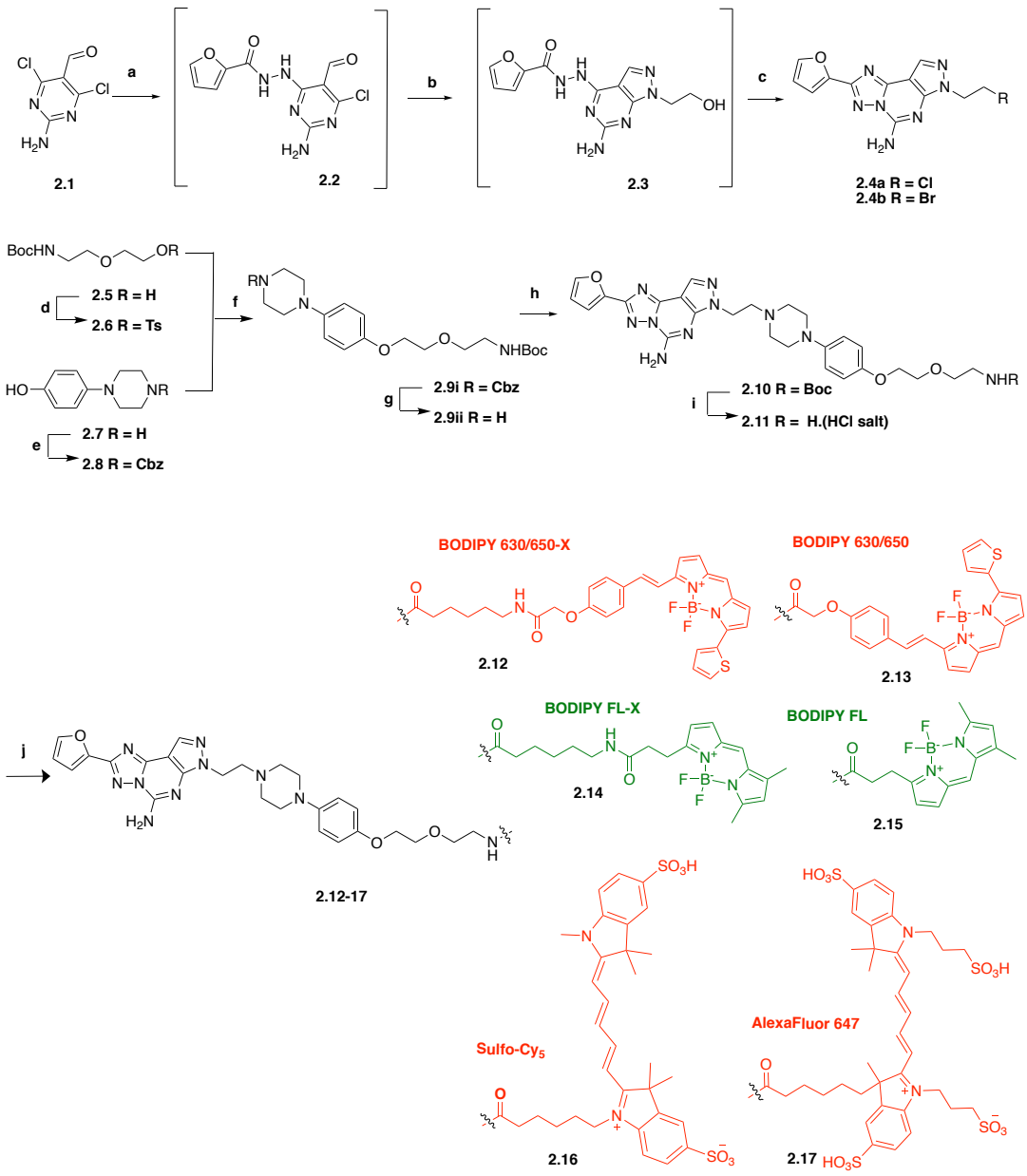
2.3 Results and Discussion

2.3.1 Chemistry

2.3.1.1 Synthesis of the Fluorescent $hA_{2A}AR$ antagonists

Based on the knowledge obtained from molecular modelling studies, a novel series of fluorescent analogues of preladenant were synthesised encompassing BODIPY, SulfoCy5 and AF647-conjugated probes. The synthetic route to the desired fluorescent probes is outlined in **Scheme 2.1**

Scheme 2.1 Synthesis of the Fluorescent $A_{2A}AR$ Antagonists [a]



[a] Reagents and conditions a) 2-furoic hydrazide, NEt_3, dry THF, reflux b) 2-hydroxyethylhydrazine, CH_3CN/H_2O, reflux c) $POCl_3$, $ZnBr_2$, 80°C for 5h, 11% over three steps d) TsCl, DIPEA, DMAP 5%mol, DCM, 86% e) CbzCl, K_2CO_3, DMF, 66% f) K_2CO_3, CH_3CN, 100°C for 6h, 40% g) H_2, Pd/C, EtOH, 82% h) 4, DIPEA, DMF, 80°C, 20% i) 4N HCl in dioxane, RT, 100% -quantitative j) 12-14-15-16-17 Fluorophore-NHS, DIPEA, DMF, RT,97% -quantitative; 13 BODIPY carboxylic acid, HATU, DIPEA, DMF, 96%.

The synthesis involved ten steps to a common precursor from which six fluorescently-labelled compounds were generated. First, the core tricycle **2.4** was prepared following a one pot procedure reported by Kuo et al.[240] This involved reaction of commercially available 2-amino-4,6-dichloropyrimidine-5-carbaldehyde **2.1**[241] with 2-furoic hydrazide in anhydrous THF in the presence of Et_3N under reflux for 2 h yielding 2.2 via nucleophilic aromatic substitution (S_NAr).Once the desired product was formed, the solvent was evaporated under reduced pressure and a solution of hydroxyethylhydrazine in a mixture of CH_3CN/H_2O was added to the crude product to displace the chlorine at 2-position through S_NAr, affording intermediate 2.3 after ring rearrangement. Subsequently, **2.3** was reacted in the presence of a catalytic amount of $ZnBr_2$ and an excess of $POCl_3$. A dehydrative cyclization occurred with concomitant Dimroth rearrangement[242] to afford intermediate **2.4** in a disappointing poor yield (11 %). Mass spectroscopy and ^{1}HNMR showed that the desired product afforded was a 2:1 mixture of chloride and bromide derivatives: one single peak at t_R=2.50, $M+H^+$ = 304 (**4**$_a$) and $M+H^+$ = 348 (**4**$_b$); ^{1}HNMR spectra showed the peaks characteristic of the aromatic region of the spectra were in common to both. Conversely, the peaks characteristic of the alkyl halide tail appeared in the spectra with different chemical shift for both bromide and chloride derivatives: peaks at 4.66 ppm (t, *J*=6.2 Hz, 1H, -C<u>H</u>$_2$Br), 4.60 ppm (t, *J*=5.9 Hz, 2H, -C<u>H</u>$_2$Cl), 4.09 ppm (t, *J*=5.9 Hz, 2H, -C<u>H</u>$_2$CH$_2$Cl), 3.94 ppm (t, *J*=6.2 Hz, 1H, -C<u>H</u>$_2$CH$_2$Br).

In parallel, the amino functionalized tail of the final congener was prepared starting from activating the hydroxyl group of commercially available **2.5** with tosyl chloride in DCM to furnish **2.6**. Under basic conditions, commercially available 1-(4-hydroxyphenyl) piperazine **2.7** was protected at the free secondary amine group with benzyl chloroformate to yield the corresponding benzylcarbamate-protected piperazine intermediate **2.8** with reasonable yield (66%). Under basic conditions, the tosyl group of **2.6** underwent nucleophile displacement by the phenolic hydroxyl of **2.8** to afford the di-protected derivative **2.9**. This enabled selective removal of the two protecting groups under different experimental conditions: hydrogenation of the benzylcarbamate group using H_2 and 10% palladium-on-carbon (Pd/C) afforded the free secondary amine in quantitative yield. Under basic

conditions, the primary ethyl halide tail of **2.4** underwent S_N2 by the nucleophilic piperazine nitrogen of **2.9** to afford compound **2.10.** Acid-mediated Boc deprotection of the latter afforded the corresponding amine **2.11** as its HCl salt. Finally, **2.11** was coupled with the appropriate commercially available fluorophore (e.g. BODIPY, SulfoCy5 and AF647) and to a BODIPY 630/650 carboxylic acid synthesized in our laboratory as previously reported[243] to afford a focused library of six fluorescent conjugates (**2.12**-**2.17**).

The novel fluorescent analogues were isolated and purified by reverse-phase performance liquid chromatography (RP-HPLC). The final purity of the fluorescent ligands was confirmed by analytical RP-HPLC with dual wavelength detection and were determined as being >96% homogeneous. Furthermore, the chemical identity of the probes (**2.12**-**2.17**) was confirmed by High Resolution Mass Spectrometry (HRMS) (TOF ES+ and ES-).

2.3.2 Pharmacology

The novel series of fluorescently-labelled analogues of preladenant were subjected to pharmacological profiling in a variety of *in vitro* assays. First, fluorescent analogues **2.12**-**2.17** were validated through Nanoluciferase Bioluminescence Energy Transfer Resonance (NanoBRET) ligand binding assay.[165,215] NanoBRET is a quantitative, proximity (< 10 nm) method that allows to monitor protein-ligand binding interactions in real-time and in living cells. This method exploits the non-radiative energy transfer between the donor bioluminescent protein nanoluciferase (NanoLuc)[163] tagged to the receptor of interest at its *N*-terminus (NanoLuc-A_{2A}AR) and an acceptor fluorophore (**Figure 2.2**)

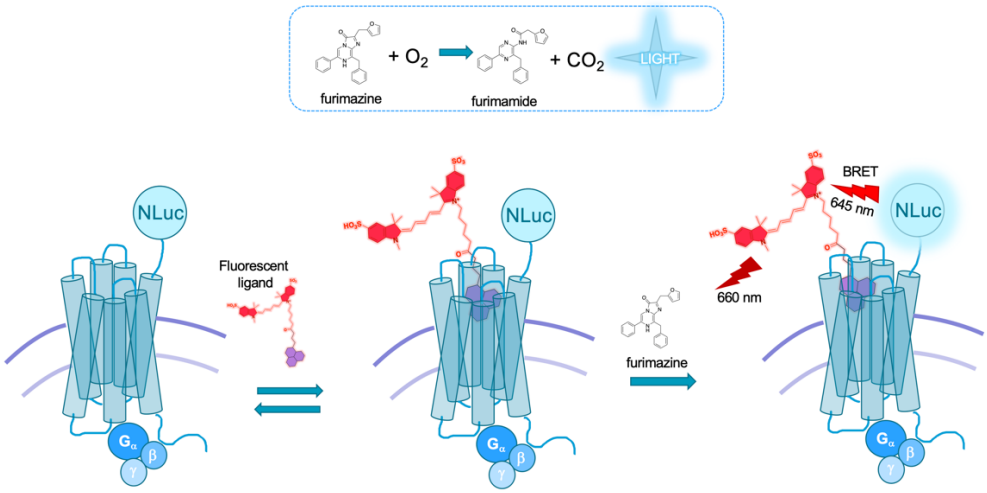


Figure 2.2. Schematic representation of NanoBRET to monitor receptor-fluorescent ligand dynamic interactions. The Nanoluc (NLuc)[163] luciferase is fused on the *N*-terminus of the receptor of interest. Cells are treated with the desired fluorescent ligand for the time required and the substrate furimazine is directly added to the assay buffer. Upon furimazine oxidation to furimamide, the NanoLuc produces a glow type of luminescence (max emission peak λ = 460 nm). Close proximity of the donor NanoLuc tag with the acceptor fluorescent ligand bound, promotes the non-radiative transfer of this energy (light) to the acceptor fluorophore employed. Both donor NanoLuc and acceptor fluorophore emissions can be measured using a plate reader and BRET ratio are calculated dividing the acceptor fluorophore emission by the donor luminescence emission measures.[215]

When profiled in NanoBRET saturation ligand binding assays, all the fluorescent conjugates tested (**2.12**-**2.17**) in this study produced a clear saturable and concentration-dependent BRET signal, consistent with specific binding to the NanoLuc-hA_{2A}AR (**Figure 2.3** and **Table 2.1**), which was associated with low levels of non-specific binding detected across all the concentrations of fluorescent ligands measured.

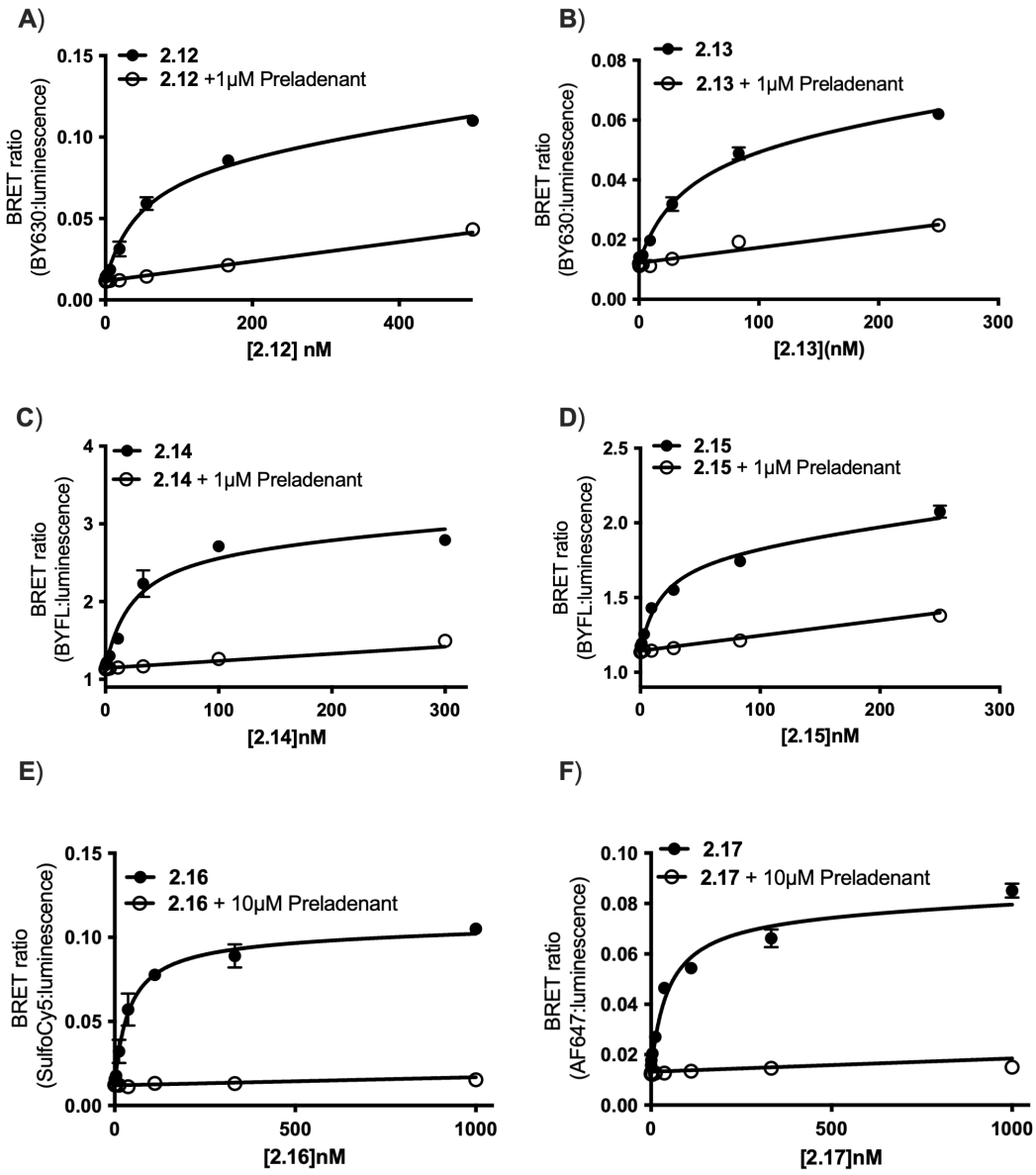


Figure 2.3 NanoBRET saturation binding curves quantified in HEK293G cells transiently expressing the NanoLuc-hA_{2A}AR for **a**) **2.12**, **b**) **2.13**, **c**) **2.14**, **d**) **2.15**, **e**) **2.16** and **f**) **2.17** in the presence (open circles) or absence (closed circles) of high concentration of competitive antagonist preladenant as indicated. The graph shown are representative of $n = 5$ (a, d, e and f) or $n = 4$ (b and c) separate experiments. Each data point represents the mean value ± SEM performed in triplicate in a single experiment.

All the novel synthesised fluorescent ligands were able to engage the NanoLuc-hA_{2A}AR with reasonable affinity (**Table 2.1**). Interestingly, compared to what has been previously observed with other adenosine receptor subtypes (e.g A_1AR[144,149] and A_3AR[150]), there were only small differences in affinities depending on nature of the fluorophore component

tethered to the molecule, with the affinity values measured with water-soluble dyes (SulfoCy5 and AF647) being slightly lower than the values measured with the BODIPY-labelled conjugates (Table 2.1). As the fluorophore constituted the only structural difference between the compounds synthesised, it is possible that the boron dipyrromethene scaffold of the BODIPY-conjugated probes engages in a cooperative fashion with key residues in an additional pocket of the receptor, thereby contributing to increase the binding affinity of the ligands.[179] In contrast, owing to the more hydrophilic character of the SulfoCy5 and AF647-labelled ligands it is possible that these dyes are likely extending towards the extracellular medium without establishing specific interactions with amino acid residues. This hypothesis would be consistent with the work reported by Duroux et al.[179], whereby molecular modelling of a BODIPY 630/650-labelled analogue of SCH4416 (named MRS7396) to the crystal structure of $hA_{2A}AR$ (PDB = 4EIY) showed the interaction of the BODIPY moiety with an accessory hydrophobic pocket located between TM7, TM1 and TM2 of the $hA_{2A}AR$. Interestingly, this pocket has been suggested as potential novel allosteric binding site.[219]

Moreover, differences in the BRET ratio measured could be ascribed to a variety of reasons (**Figure 2.3**). For instance, for BRET to occur, as with all the resonance energy transfer approaches, there must be a spectral overlap between the emission spectra of the donor (NanoLuc) and the emission spectra of the acceptor (fluorophore). When using green-emitting fluorophores (excitation 503 nm, emission 512 nm) a greater contribution from the NanoLuc background emission spectra (bandpass 475-530 nm) is recorded in the acceptor emission channel, leading to an increase in BRET ratio. In contrast, with red-shifted fluorophores (610-longpass) the contribution of the NanoLuc emission is markedly reduced in the red emission channel, which results into a reduction in the background BRET ratio.[215] Furthermore, the distance and the specific orientation of the acceptor fluorophore with respect to the donor NanoLuc can also affect the efficiency of the energy transfer between the two species and contribute to the abosulte differences in the BRET ratio observed.[164]

Table 2.1. Binding Affinities of the novel Fluorescent Ligands determined in whole HEK293G cells transiently expressing the NanoLuc-*h*A_{2A}AR.

Compound	pK_D (LogM)[a]	*n*
2.12 (BY630/650-X)	7.39 ± 0.05	5
2.13 (BY630/650)	7.39 ± 0.02	4
2.14 (BY-FL-X)	7.77 ± 0.06	4
2.15 (BY-FL)	7.65 ± 0.10	5
2.16 (Sulfo-Cy5)	7.08 ± 0.09	5
2.17 (AF647)	7.22 ± 0.05	5

[a]pK_D value was calculated from the negative logarithm of the equilibrium dissociation constant (K_D) determined from saturation ligand binding assay using increasing concentration of labelled ligand in the absence or presence (to determine non-specific binding) of unlabeled ligand preladenant (1 μM). Data are expressed as mean ± SEM of *n* experiments, where each experiment was performed in triplicate.

A major objective of this study was to achieve A_{2A}AR selectivity as this novel series of fluorescent A_{2A}AR antagonists are being developed with the purpose of being applied to a variety of fluorescence-based techniques in different tissues and cellular systems endogenously expressing other adenosine receptors subtypes. Here, NanoBRET saturation binding assays were used to quantify the binding affinity of each fluorescent A_{2A}AR antagonist in HEK293 cells stably expressing either the NanoLuc-hA_1, NanoLuc-hA_{2B} or the NanoLuc-hA_3ARs. Pleasingly, the results revealed that no specific binding of the fluorescent conjugates (**2.12**-**2.17**) was detectable at A_1, A_{2B} and A_3 subtypes at the concentrations tested (**Figure 2.4**).

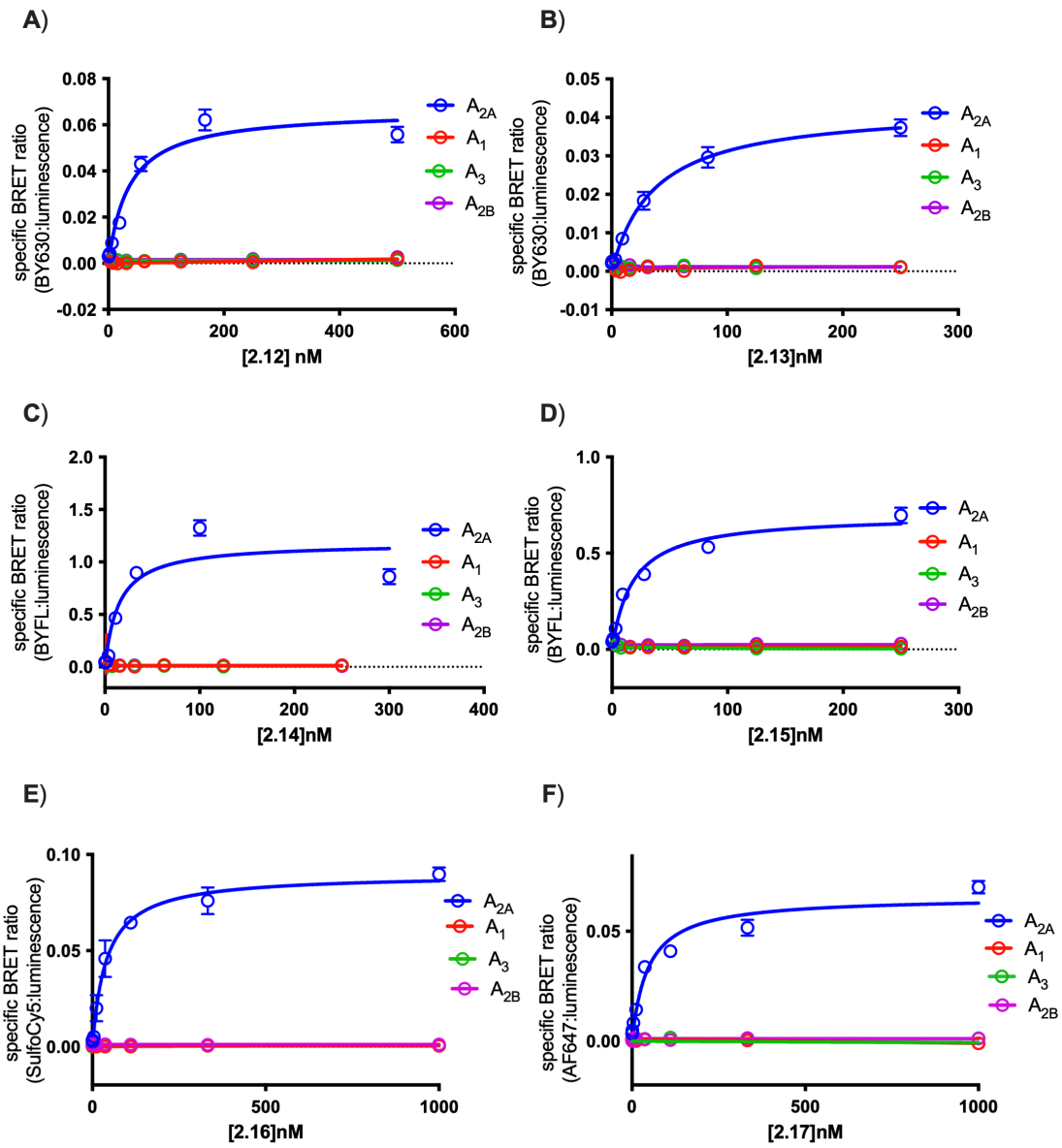


Figure 2.4 Specific binding of the novel synthesised hA$_{2A}$AR antagonists at each adenosine receptor subtype. For each compound tested **2.12 A**), **2.13 B**), **2.14 C**), **2.15 D**), **2.16 E**), **2.17 F**), the selectivity profiling is represented by showing only the specific binding at the each of the A_1, A_{2A}, A_{2B} and A_3, respectively. The specific binding at each adenosine receptor was quantified by subtracting the non-specific binding from the total binding component measured in the saturation binding assays (Figure 2.3 and Table 2.1). Non-specific binding was measured in the presence of a high concentration of unlabelled competitive antagonist specific for the receptor investigated: 1 μM preladenant for NanoLuc-hA$_{2A}$AR, 10 μM DPCPX for NanoLuc-hA$_1$AR, 10 μM PSB603 for NanoLuc-hA$_{2B}$AR and 10 μM MRS1220 for NanoLuc-hA$_3$AR, respectively. The graphs presented above are representative of n = 4 (**C** and **D**) and n = 5 (**A**, **B**, **E** and **F**) experiments and the data are mean ± SEM of triplicate determinations in a single representative experiment.

Owing to the better affinity exhibited at the $hA_{2A}AR$, the BODIPY-labelled fluorescent analogues were profiled for their ability to retain functional antagonism at the $hA_{2A}AR$ compared to the parent compound preladenant. This was achieved using a previously described CRE-SPAP reporter gene assay[244] in CHO cells stably expressing the human adenosine $hA_{2A}AR$ receptor. cAMP responsive element (CRE) is a transcription factor which is activated upon binding of the phosphorylated cAMP responsive element binding protein (CREB). Thus, activation of CRE initiates gene transcription, resulting to the translation of secreted placental alkaline phosphatase (SPAP). Once secreted outside the cell, SPAP can hydrolyse colourless *p*-nitrophenolphosphate (PNPP) into yellow *p*-nitrophenol (PNP). This hydrolysis reaction can be quantified on a plate reader by measuring the optical density at a wavelength of 405 nm, thus allowing to measure Gs-mediated receptor activation as a response of downstream activation of the SPAP gene (**Figure 2.5**).

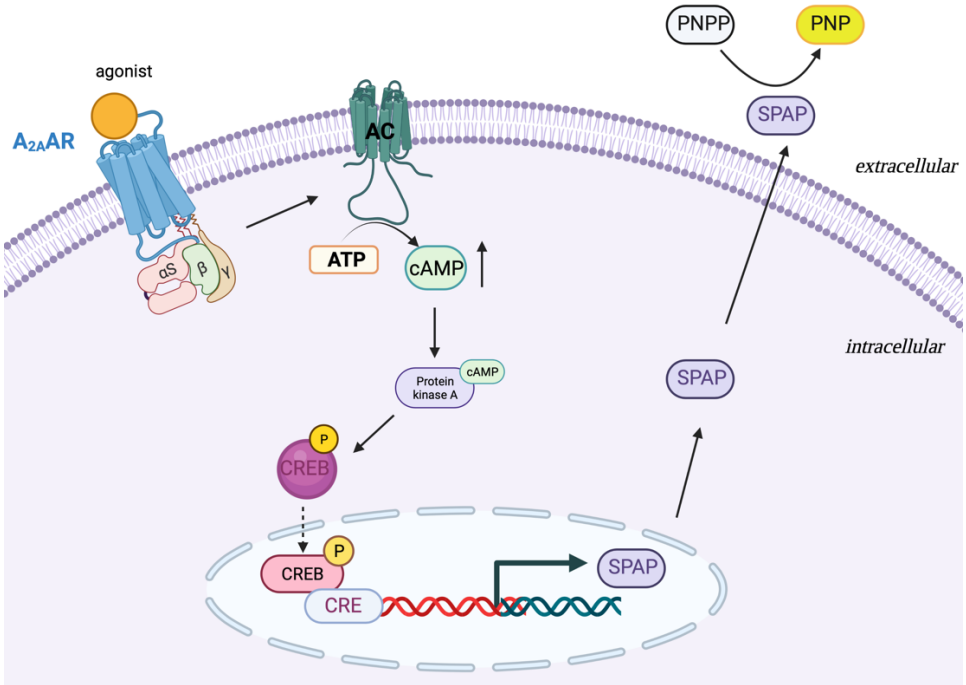


Figure 2.5 Secreted placental alkaline phosphatase (SPAP) mechanism of action. Agonist induces the activation of the A_{2A}-AR-Gs complex, which stimulates adenylate cyclase to produce cAMP from ATP. cAMP then binds to protein kinase A (PKA) which leads to the phosphorylation of cAMP response element binding protein (CREB). Once CREB has been phosphorylated, it binds to cAMP response element (CRE) leading to the translation of secreted placental alkaline phosphatase (SPAP), which is finally secreted outside the cell. The level of SPAP produced can be measured *via* a colorimetric assay.

More precisely, SPAP enzyme dephosphorylates *p*-nitrophenol (PNPP). This causes a colour change which is quantified by measuring the optical density at 450 nm using a plate reader.

When profiled in the CRE-SPAP gene reporter assay, all the BODIPY-labelled probes (**2.12**-**2.15**) could inhibit adenosine-5-*N*-ethylcarboxamide (NECA)-mediated increase in SPAP production in a competitive fashion, producing a rightward shift of the NECA response curve as represented in **Figure 2.6**. Moreover, from this data the affinity of each compound was estimated following Schild regression analysis (Table 2.2).

Table 2.2 pA_2 values of the BODIPY-labeled Fluorescent Ligands.

compound	h**A_{2A}AR pA_2** [a]	n
2.12 (BY630/650-X)	9.31± 0.38*†	7
2.13 (BY630/650)	8.61± 0.30	6
2.14 (BY-FL-X)	7.91± 0.26*	5
2.15 (BY-FL)	8.40± 0.26†	6

[a] Affinity of the BODIPY-labelled Fluorescent Ligands. Ability for these ligands to inhibit the NECA-stimulated CRE-SPAP response in CHO cells expressing the $h$$A_{2A}$AR. Data are mean ± SEM for *n* separate experiments performed in triplicate (statistical significance was defined as *$p < 0.05$ unpaired t-test comparing **2.12** and **2.14.** † $p < 0.05$ unpaired t-test comparing the binding affinity of **2.12** and **2.15** measured in CRE-SPAP assay and the NanoBRET assay).

The BODIPY-labelled probes largely retained their functional antagonism as compared to the parent compound preladenant. Moreover, when comparing fluorescent ligands labelled with BODIPY dyes without the integrated linker no significant difference in the measured functional affinity was observed ($p > 0.05$, comparing compounds **2.13** and **2.15**, unpaired *t*-test). Conversely, when comparing fluorescent ligands labelled with BODIPY dyes integrating an aminohexanoyl linker, the BODIPY 630/650 conferred 20-fold increase in affinity to the congener ($p < 0.05$, comparing compounds **2.12** and **2.14**, unpaired *t*-test). In this pharmacological assessment, fluorescent analogue

2.12 was the most potent of the series (pA_2 = 9.31± 0.38, **Figure 2.6 A**) and **Table 2.2**).

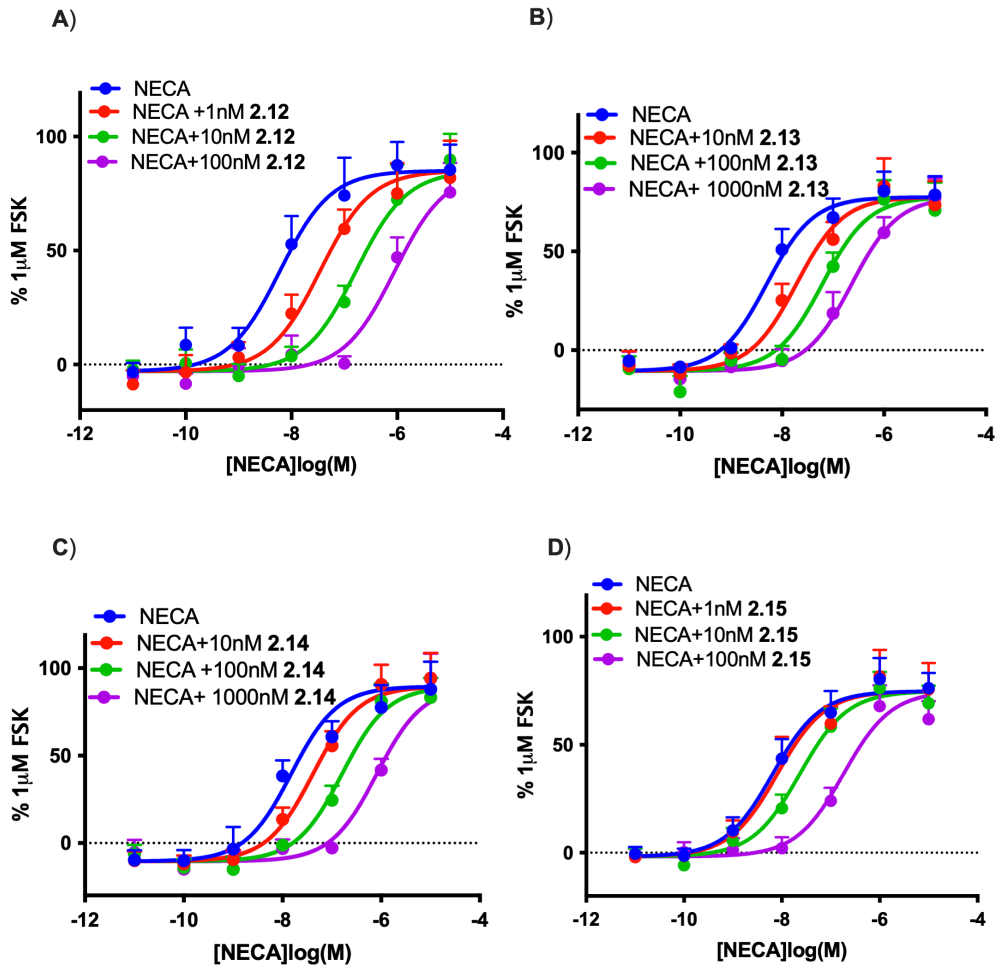


Figure 2.6 Inhibition of NECA-stimulated SPAP-secretion by the antagonists **2.12** (**A**), **2.13** (**B**), **2.14** (**C**) and **2.15** (**D**). CHO CRE-SPAP cells expressing the human A_{2A} receptor were stimulated with a concentration range of the agonist NECA in the absence and presence of the fluorescent antagonist of interest (1 nM, 10 nM, 100 nM for **2.12** and **2.15**; 10 nM, 100 nM, 1000 nM for **2.13** and **2.14).** Data have been expressed as a percentage of the SPAP production in response to serum-free media (0%) and to 1 μM forskolin (FSK, 100%). The data shown represent the combined mean ± SEM of n = 7 (**A**), n = 6 (**B** and **D**) and n = 5 (**C**) experiments, where each experiment was performed in triplicate.

Interestingly, the affinity values measured through the NanoBRET saturation ligand binding assay (**Table 2.1**) were significantly lower compared to the affinity values obtained in CRE-SPAP gene reporter assay (**Table 2.2**). The discrepancy in the affinity values is most likely due to the different host cell type and species (hamster versus human) employed in the two assays (CHO cells for CRE-SPAP and HEK293G cells for NanoBRET), the assay

configuration (e.g. the influence of the furimazine substrate for NanoLuc) as well as the influence of the tag used in the NanoBRET experiments (transiently expressed NanoLuc-hA_{2A}AR for NanoBRET and stably expressed wild-type hA_{2A}AR for CRE-SPAP).[245] However, it is important to note that a small reduction in binding affinity of the fluorescent probe is not necessarily detrimental as long as the probe binds to the targeted receptor with sufficient specificity.[246]

The incorporation of ligand-binding kinetic parameters into drug discovery endeavours is becoming extremely relevant considering the emerging concept that the rates at which a drug engages with its target receptor (k_{on}) and dissociates from it (k_{off}) may be considered more valuable parameters for predicting the effectiveness of a drug candidate in vivo.[246–249] Accordingly, BODIPY 630/650-X-labelled probe **2.12** was selected to be evaluated for its kinetic profile through time-resolved fluorescence energy transfer (TR-FRET)[133,250] assay in membrane preparations from SNAP-tagged hA_{2A}AR HEK293 cells (**Figure 2.7 A**). TR-FRET is a methodology which exploits proteins labelled with lanthanides (e.g. terbium) as donor fluorophores. Lanthanides display a long emission lifetime which allows for a time delay of the measurements between the excitation and the fluorescence of the acceptor fluorophore. This increases the sensitivity of the assay due to a reduction of the short-lived background fluorescence.[127,246,250] The TR-FRET technology allowed us to monitor the binding kinetics of **2.12** by measuring the observed association constant (k_{obs}) at four different concentrations of fluorescent ligand over a period of 1 h. The specific FRET signal was obtained by subtracting the non-specific signal (determined in the presence of 10 μM ZM241385) from the total signal at each time point. The kinetic parameters k_{on} = 2.4 ± 0.3 x 10^6 M^{-1} min^{-1}, k_{off} = 0.029 ± 0.004 min^{-1}, pK_D = 7.91 ± 0.06 and the residence time (1/ k_{off}) Tr = 35.36 ± 4.11 min, n = 5 were then calculated by globally fitting the resulting FRET data. This study revealed that fluorescent conjugate **2.12** has a relatively rapid on-rate but once bound dissociates slowly. In addition, from the 60 min time point we were also able to plot an equilibrium saturation curve of **2.12** and directly measure the equilibrium dissociation constant (K_D =

15.47 ± 1.92, **Figure 2.7 B**) which was comparable to the value obtained from the kinetic analysis fit.

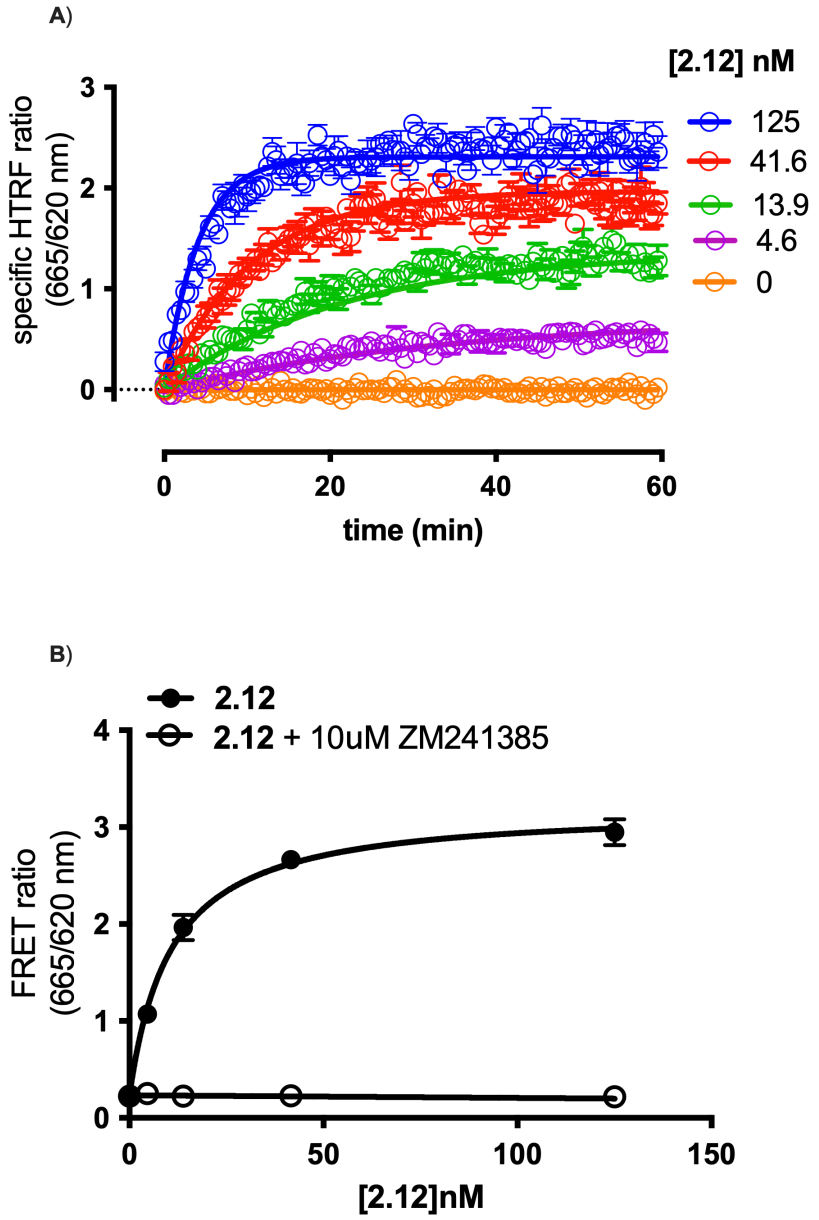


Figure 2.7 **A**) TR-FRET association kinetic curve of specific **12** binding to terbium-labelled SNAP-tagged-hA_{2A}AR-HEK293 cell membranes at 37 °C. Cell membranes were treated with the indicated concentration of fluorescent ligand and the FRET signal was monitored every 30 s for 1 h. Non-specific binding was determined in the presence of 10 μM ZM241385. The graph presented is a representative of n = 5 experiments performed in triplicate. **B**) Combined saturation binding curve measured at 60 min time point from FRET association kinetic curve of **2.12**. The graph shown is from a single experiment performed in triplicate and it is a representative of n = 5 experiments. Closed circles represent total binding of **2.12**, open circles represent non-specific binding of **2.12**

measured in the continuous presence of 10 μM ZM241385. Data are mean ± SEM of triplicate determinations in a single representative experiment.

Notably, it was found that the binding affinity (pK_D = 7.91± 0.06) of **2.12** measured through the TR-FRET kinetic study in HEK293G membrane preparations was similar to the binding affinity (pK_D = 7.39 ± 0.05) measured in the same cells in NanoBRET experiments. Thus, this data suggests that the large difference in measured binding affinity for fluorescent analogue 2.12 between NanoBRET experiments in HEK293G cells and CRE-SPAP gene reporter functional assays in CHO-K1 cells is largely due to the host cellular environment.

Having confirmed that the novel fluorescent ligands retain functional activity, binding affinity and selectivity at the target $hA_{2A}AR$, next it was explored if the novel probes could be suitable tools to allow visualisation of specific $hA_{2A}AR$ localisation and distribution patterns in imaging studies. Ideally, the novel fluorescent antagonists should bind specifically to the $hA_{2A}AR$ receptors on the cell surface and show both low levels of non specific binding and/or diffusion into the cell cytosol. From the BODIPY-labelled probes, fluorescent ligands **2.12** (BODIPY-630/650-X) and **2.15** (BODIPY-FL) (**Scheme 2.1**) were selected to determine wheter these probes were suitable for visualisation of receptors in living cells. To this end confocal microscopy was performed on HEK293 cells stably expressing the SNAP-$hA_{2A}AR$ (**Figure 2.8**). The images acquired with the confocal microscope revealed that both fluorescent derivatives **2.12** and **2.15** bound specifically to the SNAP-tagged $hA_{2A}AR$ as demonstrated by the high level of fluorescence localised at the cell membrane. Moreover, pre incubation with a high concentration (1 μM) of unlabelled competitive ligand ZM241385 caused a significant reduction of fluorescence intensity, with very little intracellular fluorescence observed. This demonstrated that binding of both probes was specific at the SNAP-$hA_{2A}AR$ as it was surmounted by high concentration of unlabelled $hA_{2A}AR$ antagonist.

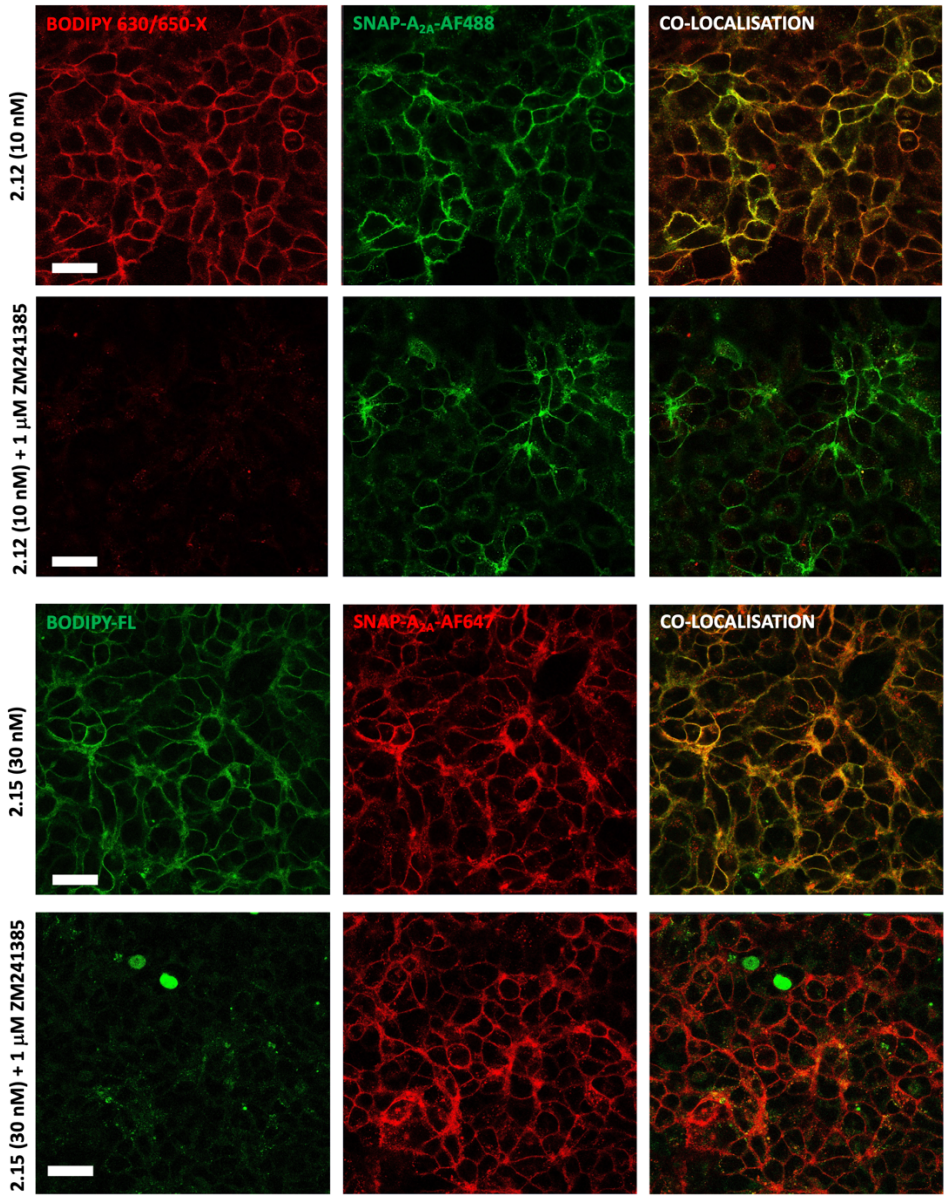


Figure 2.8 Live cell confocal imaging of **2.12** (10 nM) and **2.15** (30 nM) binding to SNAP-tagged *h*A_{2A}AR HEK293 cells in the absence or presence of 1 μM of unlabelled antagonist ZM241385. Cells were incubated at 37 °C with BG-AlexaFluor488 when imaging red-shifted ligands (**2.12**) or BG-AlexaFluor647 to label the SNAP-tag on the N-terminus of the receptor when imaging green-shifted ligands (**2.15**) (middle frames). Images are representative of images captured in three separate experiments (scale bar 20 μm).

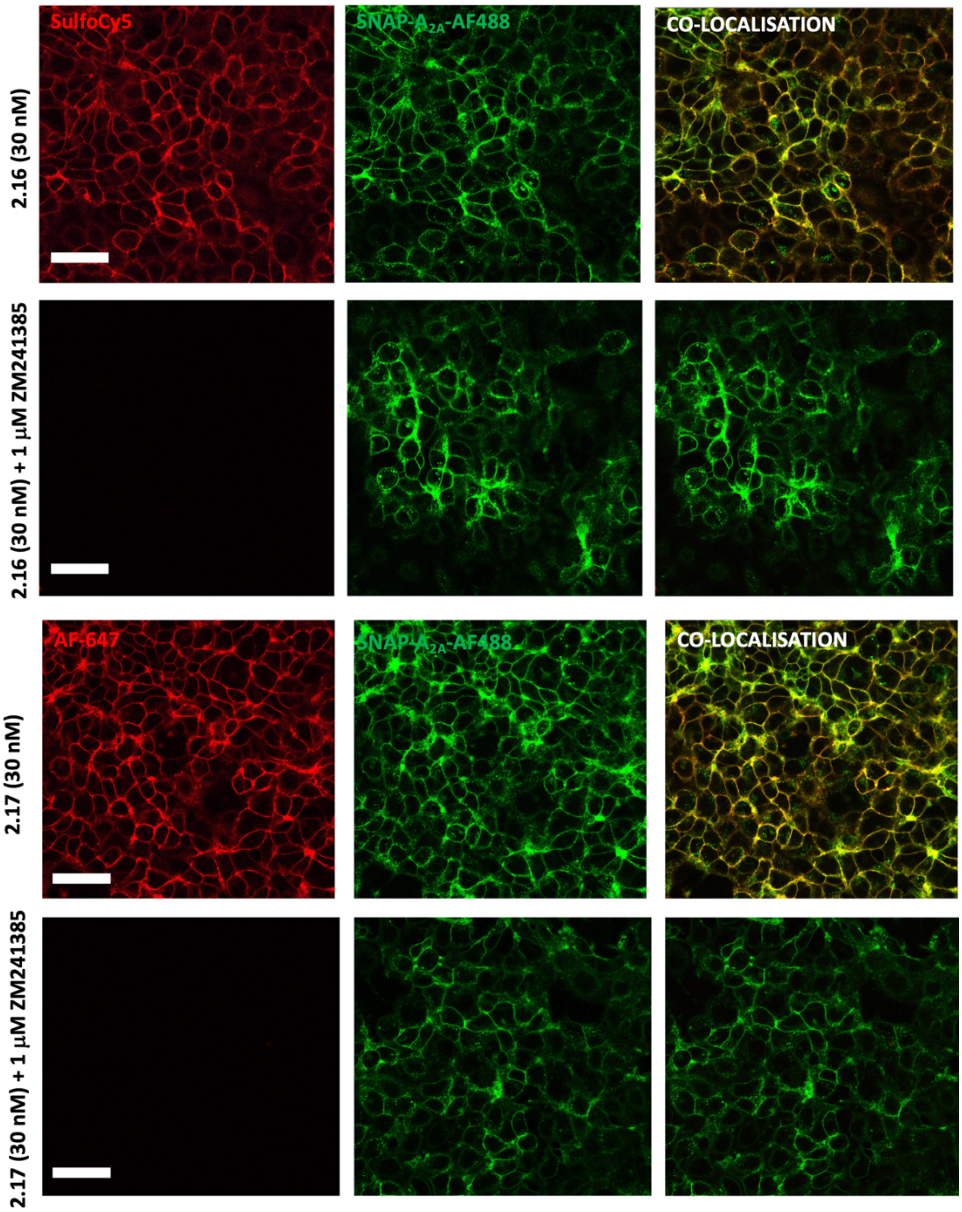


Figure 2.9 Live cell confocal imaging of **2.16** (30 nM) and **2.17** (30 nM) binding to SNAP-tagged $hA_{2A}AR$ expressed in HEK293 cells. Cells were incubated 30 min at 37°C with BG-AlexaFluor488 prior incubation in the absence or presence of 1 µM ZM241385. Subsequently, cells were incubated with 30 nM fluorescent ligand for 30 min at 37°C prior to imaging. The images generated are from one single experiment and are representative of three different experiments. The images were all captured using the same settings for laser power and detector gain. Scale bars are 50 µm,

Water-soluble fluorescent analogues **2.16** and **2.17** were also evaluated for their ability to allow the study of receptor localization and distribution in living cells through confocal microscopy. The results showed that probes **2.16** and **2.17** could label SNAP-hA_{2A}AR as demonstrated by the high degree of fluorescence intensity observed at the plasma membrane of living cells (**Figure 2.9**). Notably, the binding of the probes was specific to the target receptor as pre incubation with 1 μM cZM241385 ould prevent the binding of each fluorescent compound. Very little non-specific binding was detected, with no measurable uptake of these probes into the cell cytosol observed. These results further validated the utility of these novel probes synthesized for imaging studies.

AF647-labelled probe **2.17** was selected for additional studies. For instance, fluorescent antagonist **2.17** was applied in NanoBRET competition ligand binding assays to quantify the binding affinities of unlabelled hA_{2A}AR antagonists. To this end, HEK293 cells transiently expressing the NanoLuc-A_{2A}AR were treated with probe **2.17** (50 nM) and increasing concentrations of the hA_{2A}AR antagonists ZM241385, SCH58261, SCH442416 and MRS1334 a selective adenosine A_3AR antagonist which was used as negative control. A concentration dependent decrease of the BRET signal was observed for the A_{2A}AR selective compounds, allowing the binding affinities of the unlabelled antagonists to be measured (**Figure 2.10 A** and **Table 2.3**). The values obtained through fluorescent binding assays were comparable to the reported literature values (R^2 = 0.97, **Figure 2.10 B**) measured in radioligand binding experiments.[44,55] No concentration-dependent decrease of the BRET signal was observed in the presence of the selective A_3AR antagonist MRS1224 confirming the specificity of the binding of the probe **2.17** to the A_{2A}AR.

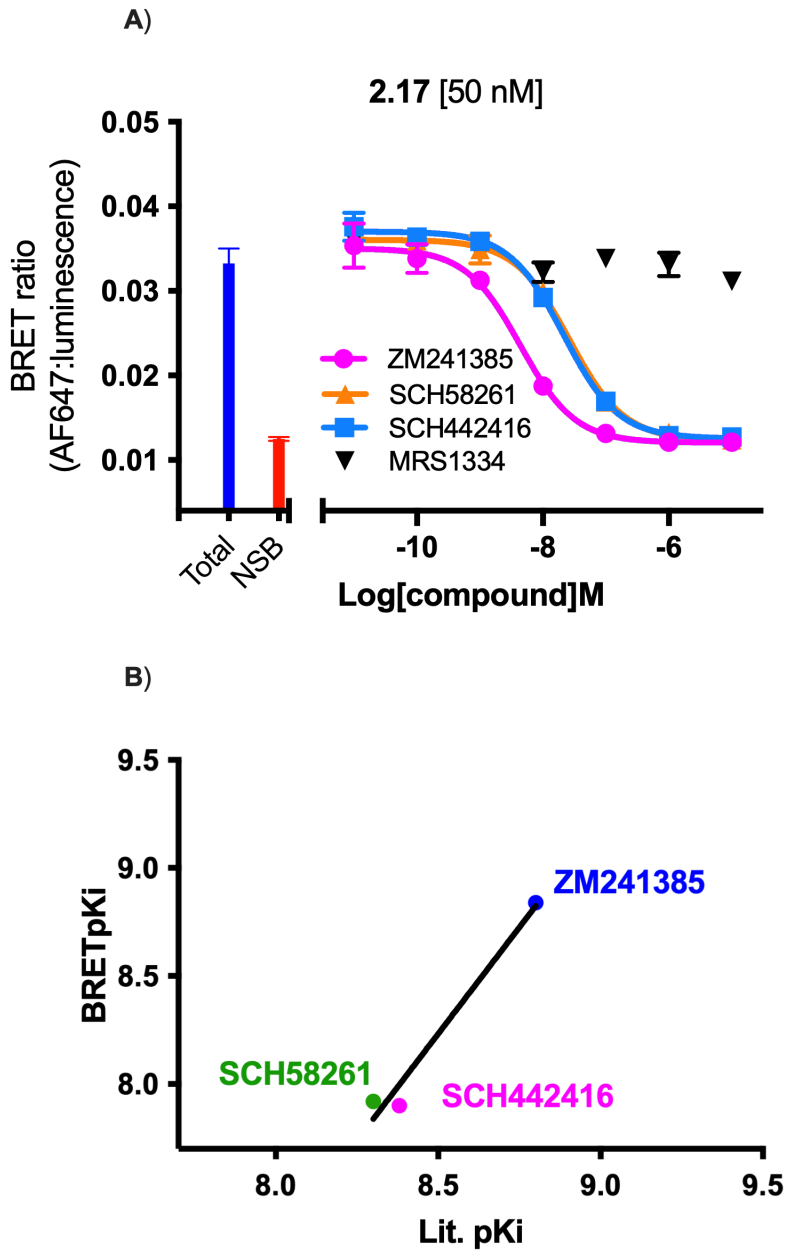


Figure 2.10 **A**) Displacement of **2.17** (50 nM) by unlabelled $hA_{2A}AR$ antagonists ZM241385, SCH58261, SCH442416 and hA_3AR antagonist MRS1334 in HEK293G cells transiently expressing the Nanoluc-$hA_{2A}AR$. Blue and red bars represent the total BRET signal of **2.17** in absence or presence of ZM241385 (10 μM), respectively. The decrease in BRET ratio was monitored as a function of increasing concentration of unlabelled antagonist. Each data point represents mean value ± SEM of triplicate determinations in a single representative experiment of n = 4 experiments. **B**) Plot of literature pK_i values measured in radioligand binding experiments against the pK_i values measured in NanoBRET competition binding experiments R^2 = 0.97.

Table 3. Binding affinities (pK_i) of target $hA_{2A}AR$ antagonists calculated from Cheng-Prusoff analysis of the data displayed in Figure 2.10 A.

Compound	pK_i (BRET binding assay)	pK_i (literature) [a]
ZM241385	8.84 ± 0.09	8.80 [b]
SCH58261	7.92 ± 0.10	8.30 [c]
SCH442416	7.90 ± 0.10	8.38 [d]

[a] Reported binding affinities of target $hA_{2A}AR$ antagonists. [b, c] Values determined in radioligand binding experiments in CHO-hA_{2A} and HEK293-hA_{2A} cells using [^{3}H] SCH58261.[55,251] [d] Values determined in HEK293-hA_{2A} using the radiolabelled agonist [^{3}H] CGS 21680.[233] The data measured through NanoBRET competition ligand binding assay are means ± SEM of n = 4 experiments performed in triplicate.

2.4 Conclusions and Future Work

The work presented in this chapter discussed the successful design, development and pharmacological evaluation of a novel series of fluorescent $hA_{2A}AR$ antagonists encompassing the BODIPY-bearing probes and water soluble SulfoCy5-labelled and AF647-labelled probes, which were based on the high affinity and selective preladenant scaffold. Notably, derivatization of the amino functionalized congener **2.11** with three families of fluorescent tags led to six $hA_{2A}AR$ fluorescent antagonists with retained affinity and, most importantly, selectivity at the $A_{2A}AR$ subtype. All families of compounds allowed visualization of $A_{2A}ARs$ expressed in live cells as demonstrated by the high fluorescence intensity at the cell membranes. The binding of these fluorescent ligands could be surmounted by a high concentration of ZM241385 confirming that the binding of the probes was specific. Very little non-specific binding was observed for the water-soluble fluorescent antagonists (**Figure 2.9**). Within the water-soluble family of probes, fluorescent conjugate **2.17** was selected to successfully monitor ligand binding of reported $hA_{2A}AR$ antagonists (**Figure 2.10** and **Table 2.3**).

Future studies will be aimed at applying the probes developed here in more physiologically relevant systems, such as native cells and/or tissues which endogenously express the $hA_{2A}AR$. For instance, owing to the crucial role played by the $A_{2A}AR$ in cancer immunotherapy, it would be interesting to apply these newly synthesized fluorescent $A_{2A}AR$ probes to study the functions and dynamics of the $hA_{2A}AR$ expressed in immune cells, such as in T-cells and macrophages,[252] under both normal and pathological condition at single molecule resolution. Specifically, these novel fluorescent $hA_{2A}AR$ probes could be combined with more advanced microcopy techniques such as FCS[253] or super resolution microscopy[254] to unravel the differential distribution and localization of the $hA_{2A}AR$ in diverse native cellular and subcellular compartments and better understand how and to what extent $A_{2A}AR$-specific spatiotemporal characteristics may influence and control the physiological response observed.[120,255] Moreover, CRISPR/Cas9 genome-editing technique could be applied to insert the NanoLuc bioluminescent protein into the *N*-terminus of $A_{2A}AR$ expressed under endogenous promotion in both healthy[15,21] or cancerous (e.g. SK-BR-3)[256] cell lines, and combined with the highly selective fluorescent $hA_{2A}AR$ antagonists described here to enable real-time NanoBRET ligand binding studies to be performed in systems which closely embodies a more "natural" cellular environment.[141,172,173,257]

All novel $hA_{2A}AR$ fluorescent ligands developed and described in this chapter exhibited comparable and optimal pharmacology, thereby allowing the opportunity of ligand choice in a broad series of fluorescence-based techniques, thus expanding the pharmacological toolbox to study the signaling and dynamics of unmodified adenosine $A_{2A}AR$ receptors in living cells.

Remarkably, the combination of these newly developed fluorescent $A_{2A}AR$ probes with the NanoBRET approach and bioimaging studies may help to shed light on the complexity of the $A_{2A}AR$ signaling in different biological elements and during disease progression. This ultimately should provide useful insights concerning specific $A_{2A}AR$-engagement in several disease phenotypes, including cancer.[118,216,258]

Chapter 3. Design, Synthesis and Pharmacological Evaluation of Novel Fluorescent A_1AR Antagonists Based on the 2,6,8-Trisubstituted 1-Deazapurine Scaffold.

3.1 Brief Introduction

The adenosine A_1AR receptor is one of the four specific GPCRs termed adenosine receptors (AR) -A_{2A}AR, A_{2B}AR and A_3AR- of which functions are stimulated by the endogenous nucleoside adenosine and inhibited by purine alkaloids methylxanthines such as 1,3,7-trimethylxanthine (caffeine) and 1,3-dimethylxanthine (theophylline),[20,43,74] with caffeine being the most widely consumed psychoactive substance worldwide.[74,259] Owing to the cardioprotective actions of the A_1AR in the heart, several A_1AR agonists have previously undergone evaluation for the treatment of cardiovascular diseases, including atrial fibrillation, angina pectoris and paroxysmal supraventricular tachycardia (PSVT).[43,44,109] Moreover, the partial agonist neladenoson bialanate[110] (**Chapter 1**) has been also evaluated as a potential treatment for heart failure, but did not meet the primary endpoints for efficacy, as well producing on-target side effects, such as a dose-dependent decrease in heart rate and glomerular filtration rate; this led to discontinue the study in Phase IIb.[111,116] A_1AR antagonists offer therapeutic opportunities for the development of cognitive enhancers,[43,260] potassium sparing diuretics[83,261] and anti-asthmatic agents.[262] Nonetheless, the number of A_1AR ligands that are being used as approved therapeutic agents is limited to adenosine itself, which is applied for arrhythmias and for diagnostic purposes as a myocardial perfusion imaging tool.[43] The principal reason for the limited number of A_1AR drugs approved in the market for a particular therapeutic indication is that adenosine signalling is widespread throughout the human body, which often results in traditional orthosteric ligands producing on-target side effects.[89] This suggests that a better understating of A_1AR-specific pharmacology in different tissues and cell types is still needed for the

development of more selective and efficacious A_1AR-targeting therapeutics.

Numerous selective agonist and antagonists A_1AR ligands have been developed and are currently applied as chemical probes for studying this receptor.[44,220,263] Yet, advancements in microscopy techniques coupled with the increased availability of methods for monitoring GPCR functions in real-time and unmodified living cells[140,264] warrant the development of new A_1AR-specific probes. Accordingly, fluorescent ligands represent extremely useful tools for improving the understanding of A_1AR expression patterns, functions and dynamics in different tissues and cell types with the aim to developping A_1AR ligands with superior therapeutic activity.

Macchia et al., developed the first subtype-selective fluorescent A_1AR probe, a fluorescent analogue of NECA conjugated with a dansyl dye through an aminohexyl spacer linked to the N^6 of the adenine moiety (rA_1AR K_i = 27 nM).[190] Owing to the short excitation spectra exhibited by dansyl dyes (340 nm), which lies in the region of the spectrum characterised by high background fluorescence arising from biological molecules, the same research group synthesized fluorescent analogues of NECA labelled with a fluorophore with longer excitation wavelength, a 7-nitrobenzoxadiazole (NBD) fluorophore (λexc = 465 nm and λem = 535 nm). This fluorophore switch, however, completely abolished A_1AR binding affinity, resulting in probes with high A_3AR affinity and selectivity.[194] This suggests the need still remains for fluorescent A_1AR ligands with superior subtype-selectivity, conjugated with a broader range of fluorophores, thereby allowing their application in multiple fluorescence-based techniques.

Although alkylxanthines embody the prototypical scaffold for the design of AR antagonists, xanthine-based probes exhibit some limitations, including poor solubility and AR selectivity as demonstrated by a range of xanthine amine conger (XAC)-fluorescent conjugates.[149] Accordingly, ligands displaying an alternative pharmacophore moiety were explored for the design of the novel fluorescent A_1AR ligands with the aim of achieving

improved A_1AR affinity and selectivity. To this end, LUF5981 (cmpd 10),[265] a 2,6,8-trisubstituted 1-deazapurine A_1AR antagonist with reported high A_1AR binding affinity (hA_1AR K_i = 0.90 nM) and selectivity ($hA_{2A}AR$ K_i = 194 nM and hA_3AR K_i = 637 nM), was selected as parent drug molecule for the design and synthesis of the novel series of fluorescent A_1AR antagonists.

3.2 Design Strategy

Previously reported structure-activity relationships (SAR) studies by Chang, L. et al., indicated that substitution at both 2,6-diphenyl rings was not well tolerated and both rings were essential for retaining high A_1 binding affinity and selectivity.[265,266] Moreover, *N*3 (H-bond acceptor) and *N*9 (H-bond donor) are also essential for binding as they are reported to establish important polar contacts with $N254^{6.55}$ residue (superscripts refers to the Ballesteros-Weinstein numbering scheme).[47] Therefore, it appeared logical to explore the cyclohexyl group on the C8 position for linker attachment and subsequent fluorophore conjugation. This hypothesis was further strengthened by molecular modelling studies, investigating the molecular interactions of LUF5981 when binding to the hA_1AR (**Figure 3.1**)

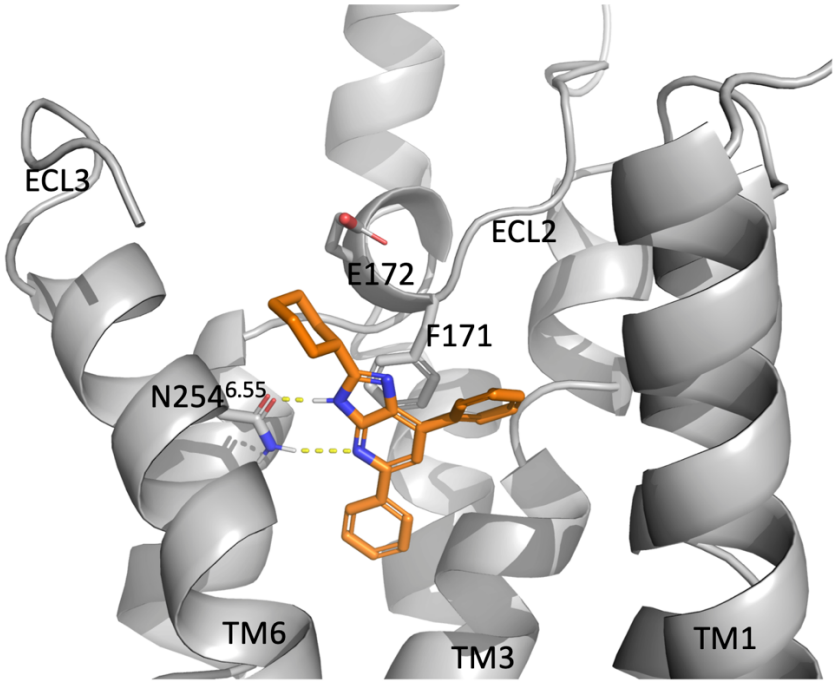


Figure 3.1 Molecular modelling of LUF5981 to the crystal structure of the hA$_1$AR (PDB=5UEN) executed with Schrödinger's Glide (Schrödinger release 2018-3). The images were generated with PyMOL (version 2.2.0). LUF5981 is shown in sticks coloured orange with hydrogen bonding interactions depicted as dashed lines. The transmembrane (TM) helices TM1, TM6 and TM3 are labelled alongside extracellular loop (ECL) 2 and ECL3, and TM7 was removed for clarity. The GPCR is shown in ribbon coloured grey. The key residues are labelled and shown in sticks.

Docking studies of LUF5981 (**Figure 3.1**) to the 3.2 Å resolution crystal structure of the hA$_1$AR[36] revealed that the core 1-deazapurine scaffold interacts with key receptor residues in an comparable manner to the co-crystalised irreversible antagonist DU172, including H-bonding contacts with Asn254$^{6.55}$ and a π-π stacking interaction with Phe171. The C6-phenyl ring appears to explore the hydrophobic pocket near T270$^{7.35}$, also referred as "secondary pocket" of the hA$_1$AR. The C8 cyclohexyl group is oriented towards the extracellular face of the receptor, facing ECL3.

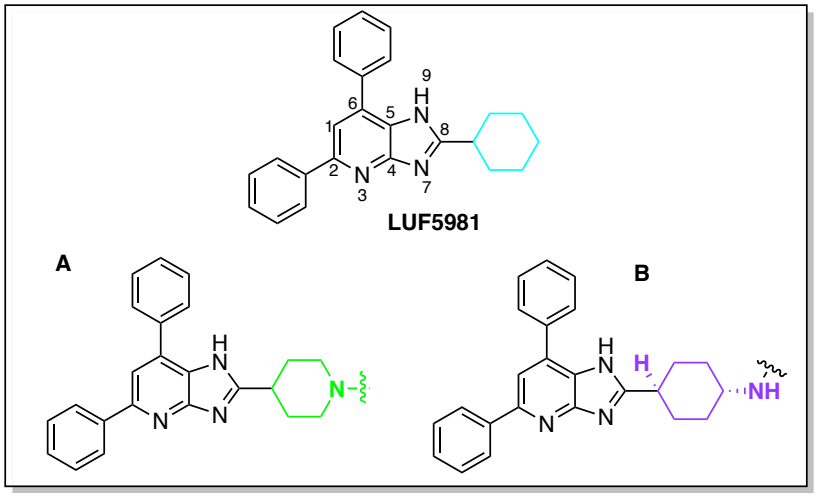


Figure 3.2 High affinity and selective A_1AR antagonist LUF5981 and the deazapurine numbering system (top structure). Structures of designed functionalised deazapurines, encompassing a piperidine (A) or a *trans*-4-amino cyclohexyl (B) moieties, respectively.

As LUF5981 lacks a reactive functional group to achieve the required linker/fluorophore derivatization, two analogues of LUF5981 were designed encompassing a piperidine and a *trans*-4-amino cyclohexyl group, respectively, on the C8 position of the deazapurine moiety to provide the anchor points for subsequent functionalisation (**Figure 3.2**). Moreover, to enhance the overall polarity of the final fluorescent ligands, it was envisaged that a polyethylene glycol (PEG)-based linker would be introduced between the pharmacophore and the fluorophore moieties.

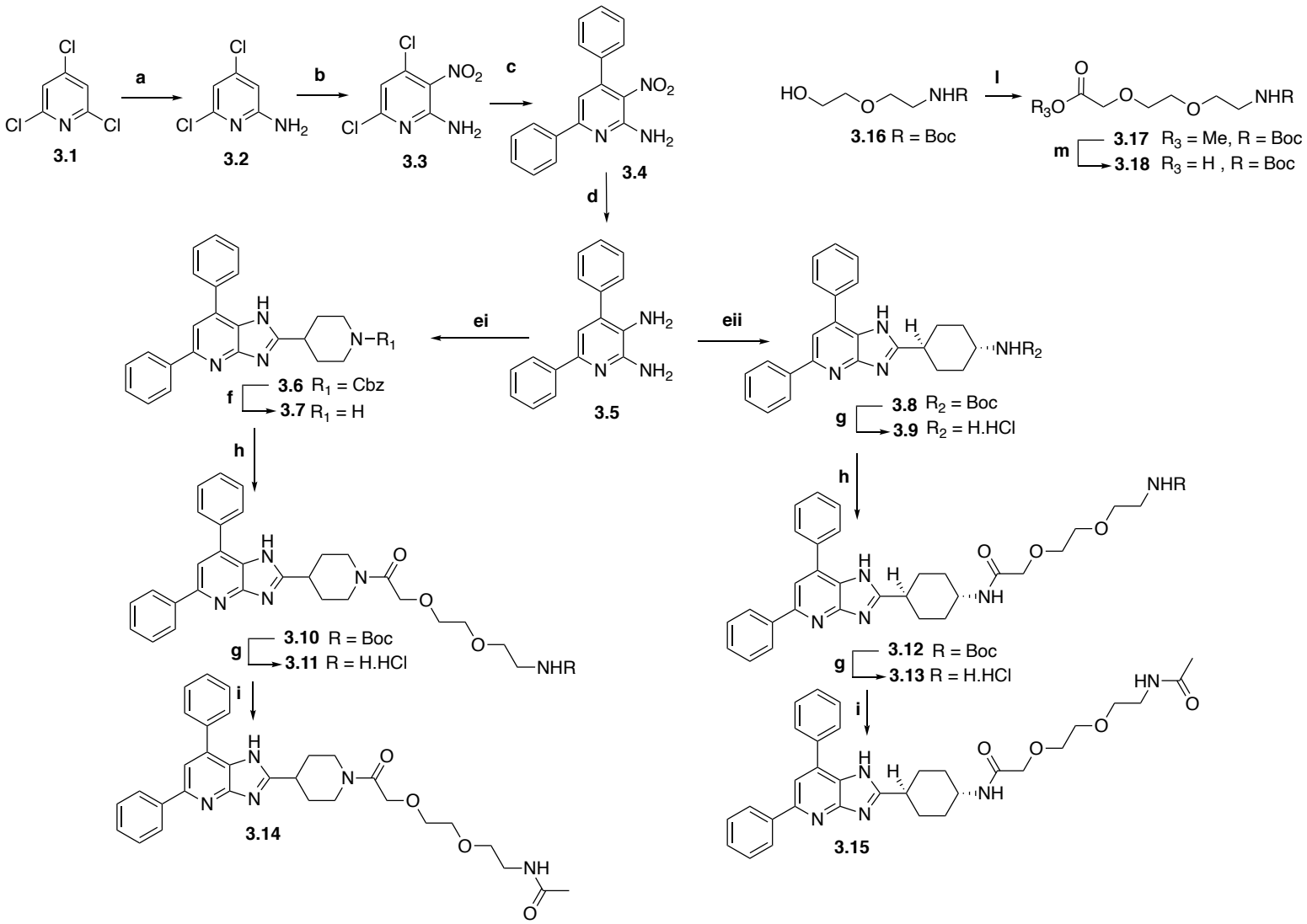
3.3 Results and Discussion

3.3.1 Chemistry

The synthetic route to the target congeners is outlined in **Scheme 3.1**. The synthesis involved four steps to a common precursor from which two series of congeners were generated. The target congeners were prepared starting from commercially available 2,4,6-trichloropyridine (**3.1**). Nucleophilic substitution of **3.1** with ammonia in a sealed vessel at 155 °C yielded 2-amino 4,6-dichloropyridine (**3.2**) as major product, which was

easily separated from the more polar 4-amino analogue by flash column chromatography. Subsequent introduction of a nitro (-NO_2) group at the 3- position of the pyridine ring was achieved through electrophilic aromatic substitution (S_EAr) employing a mixture of HNO_3 and H_2SO_4, thereby affording 4,6-dichloro-3-nitropyridin-2-amine (**3.3**) in good yield (76%). Suzuki-Miyaura cross-coupling conditions, which were facilitated by microwave heating, allowed the introduction of aryl substituents on pyridine **3.3** to furnish 3-nitro-4,6-diphenylpyridin-2-amine (**3.4**) in good yield (71%). Subsequent reduction of **3.4** under H_2 atmosphere in the presence of 11 % palladium on carbon (Pd/C) afforded the corresponding 2,3-diamine pyridine intermediate **3.5**. The ring closure step was less than straightforward. Different attempts were performed using reported methods for similar fused bi-cyclic compounds, which used polyphosphoric acid (PPA) as reaction solvent and could not afford any traces of desired product.[265,267] Therefore , a two-step procedure involving reaction of the diamino pyridine intermediate **3.5** with the corresponding freshly prepared acyl chloride, followed by cyclisation under basic conditions was envisaged.[268] However, reaction of diamino pyridine **3.5** with 1-[(benzyloxy)carbonyl]piperidine 4-carbonyl chloride, could only afford traces of the corresponding carboxamide products even after several days, without evidence of increase of product formation over time.

Scheme 3.1 Synthesis of the 2,6,8-Trisubstitued 1-Deazapurine-Based Congeners.[a]



[a] Reagents and conditions: **a**)NH_3 sol, 155 °C, sealed vessel, 24 h, 45%; **b**) HNO_3, H_2SO_4, 0 to 5 °C, 10 h, 76%; **c**) $PhB(OH)_2$, $Pd(PPh_3)_4$, K_2CO_3, toluene/H2O, mw 30 min, 150 °C, 71%; **d**) H_2, Pd/C, EtOH, rt, 5 h, 97%; **e$_i$**) 1-((benzyloxy)carbonyl)piperidine-4-carboxylic acid, PyBrop, NEt3, DMF, rt, o/v, then 90 °C, 24 h min, 38 %; **e$_{ii}$**) *trans*-4-(Boc-amino) cyclohexane carboxylic acid, BEP, *N*-methyl imidazole(NMI), CH_3CN, 97 °C, o/v, 35 %; **f**) H_2, Pd/C, MeOH, H_2O, rt, 1 h, 75 %; **g**) 4 M HCl in dioxane, rt, 45 min- 1 h, quantitative; **h**) **3.18**, PyBrop, DIPEA, DCM, rt, 3-4 h, 43-70 %; **i**) Acetic acid *N*-hydroxysuccinimide (NHS), DIPEA, DMF, 1 h, 33-95%; **l**) *tert*-Butyl (2-(2-hydroxyethoxy)ethyl)carbamate, NaH 60 %, Methyl bromoacetate, NaI, rt, o/v, 42 %; **m**) LiOH, H_2O, rt, 5 h, 69 %

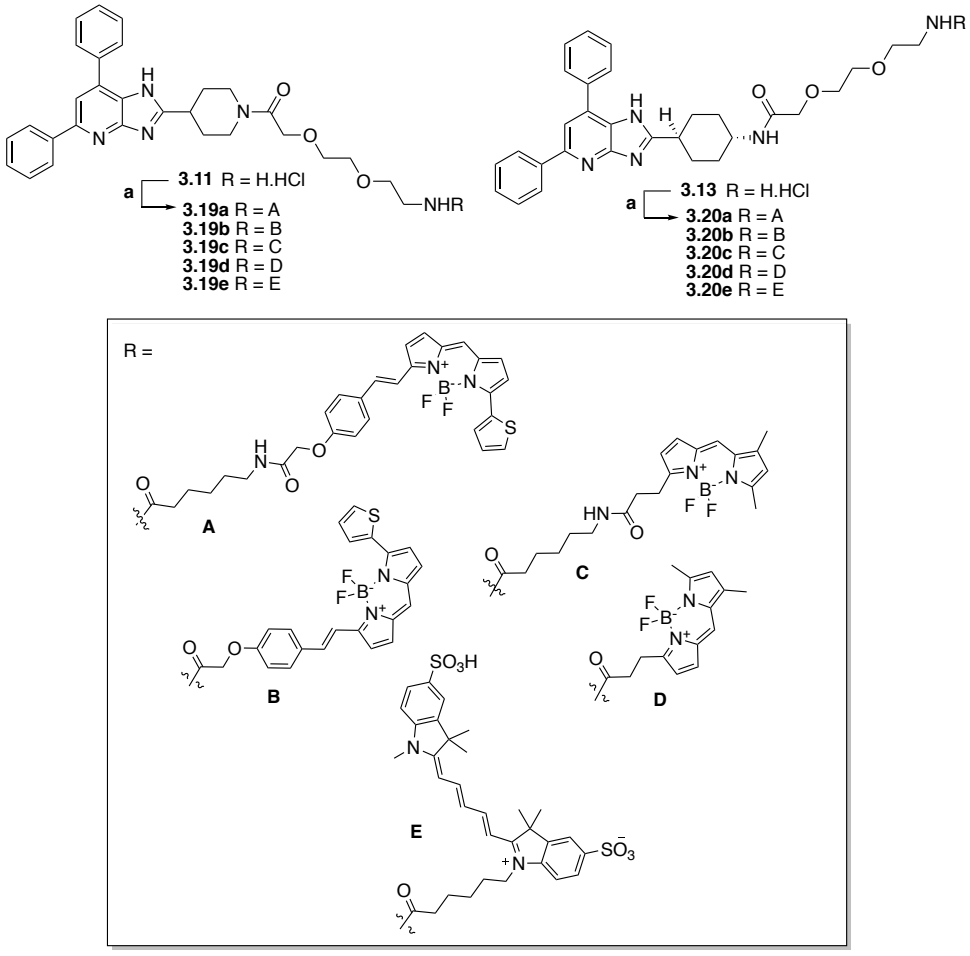
Thus, different coupling reagents and conditions were explored for the preparation of the desired carboxamide products. Standard coupling conditions using 1-ethyl-3-(3-dimethylaminopropyl)carbodiimide hydrochloride (EDC-HCl)[269,270] and 1-[bis(dimethylamino)methylene]-1*H*-1,2,3-triazolo[4,5-*b*]pyridinium 3-oxid hexafluorophosphate (HATU)[84] only gave poor yields of desired amides. Longer reaction times or heating (40 °C to 70 °C) could not improve the yields, leaving the majority of the pyridine **3.5** starting material unreacted. Condensation of electron-deficient 2,3-diamino pyridine **3.5** with the corresponding carboxylic acids proved indeed challenging, with the electronic influence of the 4,6-diphenyl substituents most likely further decreasing the overall reactivity of **3.5**. A combination of 2-bromo-1-ethyl pyridinium tetrafluoroborate (BEP) and *N*-methyl imidazole (NMI) in CH_3CN from a method reported by Beutner G. and colleagues [271] proved much more effective for the formation of the desired amide bond, albeit 50 % of amine remained unreacted as observed by LCMS. Combination of bromo-tripyrrolidino-phosphonium hexafluorophosphate (PyBrop) and NEt_3 in DMF was also found effective for the formation of the desired amide bond. The resulting amide was subsequently cyclised by heating the reaction mixtures to 90-97 °C overnight. Purification of both piperidine (**3.6**) and *trans*-4-amino-cyclohexyl (**3.8**) intermediates was problematic, leading to the isolation of the corresponding deazapurine analogues in low yield (38 % for **3.6** and 35% for **3.8**, respectively). Nonetheless, the material was found adequate for the remaining synthetic steps.

In parallel, linker moiety 2,2-dimethyl-4-oxo-3,8,11-trioxa-5-azatridecan-13-oic acid (**3.18**) was synthesised in two steps, thereby reacting *tert*-Butyl (2-(2-hydroxyethoxy)ethyl)carbamate (**3.16**) with methyl bromoacetate in the presence of NaH (60 %) to form the desired ester **3.17**. The latter easily underwent hydrolysis upon reaction with LiOH to furnish carboxylic acid **3.18**.

Removal of benzyl carbamate protecting group of **3.6** under normal hydrogenation conditions afforded the corresponding free piperidine **3.7**, which was readily coupled with PEG linker 2,2-dimethyl-4-oxo-3,8,11-trioxa-5-azatridecan-13-oic acid (**3.18**), thereby affording Boc-protected

intermediate **3.10**. In parallel, Boc-deprotection of *trans*-4-amino-cyclohexyl intermediate (**3.8**) was achieved upon treatment with 4 M HCl in dioxane to afford amine **3.9** as its HCl salt. Amine 3.9 was liberated in the presence of DIPEA and converted to the corresponding amide **3.12** upon coupling of carboxylic acid **3.18** in the presence of PyBrop. Acidolytic removal of both **3.10** and **3.12** Boc protecting group afforded amines **3.11** and **3.13** as their HCl salt, which were subsequently acylated with acetic acid *N*-hydroxysuccinimide (NHS) to yield the desired functionalised congeners **3.14** and **3.15** as acetyl derivatives.

Scheme 3.2 Synthesis of the 2,6,8-Trisubstitued 1-Deazapurine-based Fluorescent A_1AR ligands.[a]



[a] Reagents and conditions: **a**) **3.19a**, **3.19c**-**3.19e**, fluorophore NHS, DIPEA, DMF, rt, exclusion of light, 86 %-quantitative; **3.19b** BODIPY 630/650 carboxylic acid, HATU, DIPEA, DMF, exclusion of light, 77-83 %;

The desired 2,6,8-trisubstitued1-deazapurine-based fluorescent ligands were accessed upon treatment of amines **3.11** and **3.13** with DIPEA and subsequent reaction with the appropriate commercially available fluorophore (e.g BODIPY 630/650-X, BODIPY-FL and SulfoCy5) and to a BODIPY 630/650 carboxylic acid previously synthesised in our laboratory as previously described,[243]thereby affording a focused library of ten final fluorescent ligands (**3.19a-e** and **3.20a-e**, Scheme 3.2).

3.3.2 Pharmacology

Before embarking on the synthesis of the fluorescent A_1AR conjugates, functionalised congeners **3.14** and **3.15** were evaluated for their ability to retain reasonable A_1AR ligand binding. To this end, NanoBRET[165,215]competition ligand binding experiments (Chapter 2, **Figure 2.2**) were undertaken in HEK293 cell stably expressing the NanoLuc-A_1AR, whereby inhibition of 25 nM CA-XAC (CA200645)[162] binding by increasing concentrations of unlabelled congeners **3.14**, **3.15** and reported A_1AR antagonists LUF5981[265] and DPCPX was monitored at 37 ^{O}C in living cells. A concentration dependent decrease in the BRET signal was observed for unlabelled congeners **3.14** and **3.15** and for reported A_1AR selective compounds, allowing the binding affinities of all the compounds tested to be measured (**Figure 3.3 A** and **Table 3.1**). Interestingly, no differences in A_1AR ligand binding affinity between the two congeners was observed (pK_i = 6.52 ± 0.09 for **3.14** and pK_i = 6.52 ± 0.12 for **3.15**, n = 5, respectively), suggesting that incorporation of either piperidine or *trans*-4-amino-cyclohexyl ring into the C8 position of the deazapurine scaffold produced the same effect. The affinity measured for the congeners in this assay was however significantly lower than the affinity of the parent drug LUF5981 (**Table 3.1**), indicating that, overall, modification of the cyclohexyl group and subsequent linker coupling had a detrimental effect on A_1AR ligand binding. Moreover, the binding affinity of reported A_1AR selective antagonists LUF5981 and DPCPX were also lower compared to the reported measured values (**Table 3.1**). Hence, in a

control experiment, the binding affinity at the NanLuc-A_1AR of the previously characterised fluorescent derivative CA-XAC (CA200645) was also measured (**Figure 3.3 B**) in a NanoBRET saturation ligand binding assay. A clear saturable BRET signal was observed, which was indicative of CA-XAC specific binding to NanoLuc-A_1AR, which yielded a K_D = 92.1, 84.2 (n = 2) comparable to the K_D values measured for the same fluorescent antagonist at the NanoLuc-hA_1AR in previously reported studies.[49,272,273] This results confirmed that the pharmacology of the NanoLuc-A_1AR was unaltered. Thus, a possible reason for the lower binding affinity measured for LUF5981 and DPCPX may be ascribed to solubility issues arising when dosing the cells with the compounds prepared by serial dilutions.

Table 3.1. Binding affinities (pK_i) of synthesized congeners and target hA_1AR antagonists calculated from Cheng-Prusoff analysis of the data displayed in Figure 3.3 A.

Compound	pK_i (BRET binding assay)	pK_i (literature) [a]
3.14	6.52 ± 0.09	-
3.15	6.52 ± 0.13	-
LUF5981	7.80 ± 0.17	9.1[b]
DPCPX	7.31 ± 0.04	7.4-9.2[c]

[a] Reported binding affinities of target hA_{2A}AR antagonists. [b]Values determined in radioligand binding experiments in hA_1AR-CHO-K1 cell membranes using [^{3}H] DPCPX[265] [c]Values determined in radioligand binding experiments in A_1AR-COS-7[274] or hA_1AR-CHO-K1 cell membranes[275,276] or whole cells[277] using [^{3}H] DPCPX. Data are mean ± SEM for n = 5 separate experiments performed in triplicate

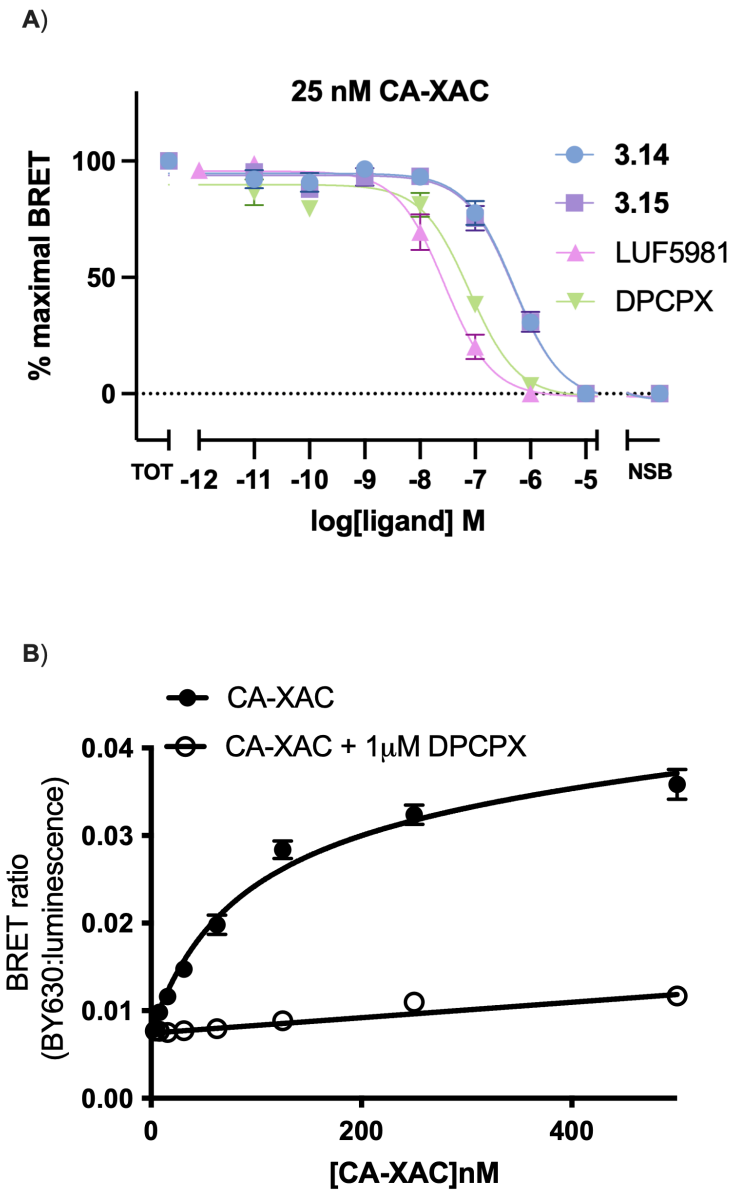


Figure 3.3 A) inhibition of CA-XAC(CA200645) specific binding (25 nM) in the presence of increasing concentration of competitive ligands (**3.14**, **3.15**, **LUF5981 and DPCPX**). TOT is total fluorescent ligand binding determined in the absence of competitor; NSB represents nonspecific binding determined in the presence of 10 μM DPCPX. Data points represent the combined mean ± SEM from n = 5 separate experiments performed in triplicate. **B**) NanoBRET saturation binding curve for CA-XAC (CA200645)[162] measured at 37 °C in HEK293 cells stably expressing the NanoLuc-hA_1AR in the presence (open circles) or absence (closed circles) of 1 μM A_1AR selective competitive antagonist DPCPX, where the latter was used to measure non-specific binding. Data are mean ± SEM of triplicate determinations in a single representative experiment of n = 2 separate experiments

Functionalised congeners **3.14** and **3.15** were also assessed for their ability to engage NanoLuc-hA_{2A}AR and NanoLuc-hA_3AR in parallel NanoBRET competition ligand binding assays. To this end, two subtype-selective fluorescent antagonists for each of adenosine A_{2A}AR and A_3AR receptors were used as fluorescent tracers. These were subtype-selective fluorescent A_{2A}AR antagonist **2.12** described and characterised in detailed in Chapter 2 and **AV039**, a highly potent and selective fluorescent A_3AR antagonist developed and successfully applied for live cells ligand binding and imaging studies.[150,278] From the NanoBRET competition ligand binding experiments it was found that compounds **3.14** and **3.15** could not displace specific A_{2A}AR fluorescent ligand binding (**2.12**, Chapter 2) when added (up to 10 μM) to HEK293 cells transiently expressing NanoLuc-A_{2A}AR. Conversely, over 95 % inhibition of specific **AV039** binding to NanoLuc-hA_3AR was only achieved at 10 μM concentration of both **3.14** and **3.15** (**Figure 3.4**). Thus, these results were indicative of poor NanoLuc-A_3AR and NanoLuc-hA_{2A}AR ligand binding abilities by the two congeners.

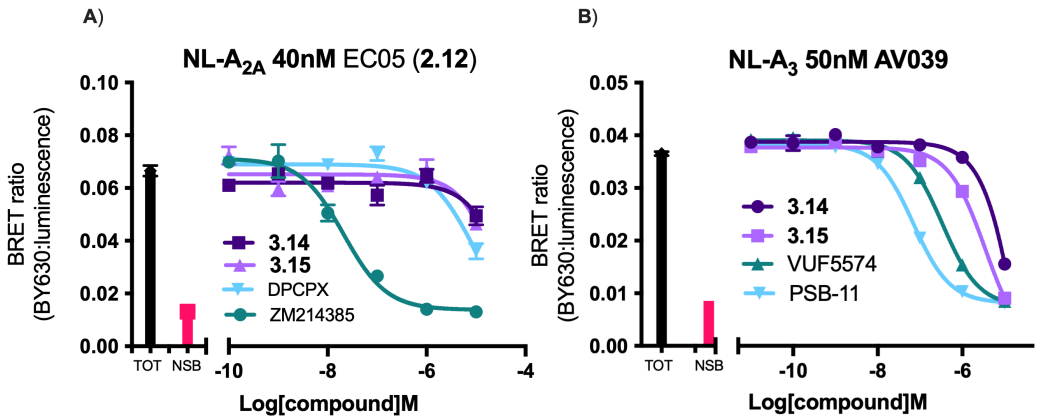


Figure 3.4 NanoBRET competition ligand binding characterisation of congeners **3.14** and **3.15** at transiently transfected NanoLuc-hA_{2A}AR (**A**) and stably expressing NanoLuc-hA_3AR (**B**) in HEK293 cells at 37 °C. **A**) Ability of increasing concentration of **3.14**, **3.15**, DPCPX and ZM241385 to inhibit A_{2A}AR-selective **2.12** binding (40 nM) NanoLuc-hA_{2A}AR and **B**) ability of increasing concentrations of **3.14**, **3.15**, VUF5574 and PSB-11 to inhibit A_3AR-selective **AV039** binding (50 nM) NanoLuc-hA_3AR. DPCPX is a A_1AR selective antagonist; ZM241385 is a A_{2A}AR selective inverse agonist; VUF5574 (measured pK_i = 7.35, n = 1)[279] and PSB-11(measured pK_i = 8.03, n = 1)[278,280] are A_3 selective and high affinity A_3 antagonists. TOT is total fluorescent ligand binding determined in the absence of competitor; NSB

represents nonspecific binding determined in the presence of 10 μM ZM241385 for NanoLuc-hA_{2A}AR and 10 μM PSB-11 for NanoLuc-hA_3AR. Data points are mean ± SEM of triplicate determinations in a single representative experiment of n = 3 separate experiments for **A**) and n = 1 for **B**).

Owing to the comparable ligand binding properties exhibited, both **3.14** and **3.15** were selected as model functionalised congeners for the development of the 1-deazapurine-based fluorescent A_1AR ligands (**Scheme 3.2**). NanoBRET saturation ligand binding assays were used to quantify the binding affinities of the ten newly synthesised fluorescent A_1AR ligands (**3.19a**-**e** and **3.20a**-**e**) at NanoLuc-hA_1AR HEK293 cells. The data revealed that, overall, conjugation with green-emitting fluorophores (BODIPY FL and BODIPY FL-X) and water-soluble red-emitting dye SulfoCy5 effectively abolished hA_1AR affinity as no specific BRET signal could be detected up to 1 μM concentration of fluorescent ligand tested (**Figure 3.5**). Although BODIPY 630/650- and BODIPY 630/650-X-labelled fluorescent probes **3.19a**, **3.19b**, **3.20a** and **3.20b** showed a small degree of binding to NanoLuc-hA_1AR, the specific binding window was small, with concomitant large values of standard error of the mean (SEM) of the measured equilibrium dissociation constants (K_D) for specific binding to NanoLuc-hA_1AR (**3.19a** K_D = 610.5 ± 183.4 nM, n = 3; **3.19b** K_D = 361.8 ± 221.9 nM, n = 3; **3.20a** K_D = 570.6 ± 305.3 nM, n = 4; **3.20b** K_D = 796.7 nM, n = 1, **Figure 3.6**).

Overall, this data indicated that conjugation with a fluorescent moiety was clearly detrimental with regard to retaining reasonable ligand binding abilities as A_1AR affinity was either completely abolished or significantly reduced compared to the parent congeners. Introduction of a linker (e.g PEG) and subsequent conjugation with a fluorescent moiety (e.g BODIPY 650/650-X) results in a significant increase of molecular weight (MW=1044.43 $gMol^{-1}$ for **3.19a** vs MW=353.20 $gMol^{-1}$ for LUF5981) and structural complexity compared to the original parent drug LUF5981, thereby resulting in a new molecule which could adopt different conformations with concomitant formation of unfavourable interactions or steric clashes within the receptor structure.[144,281]

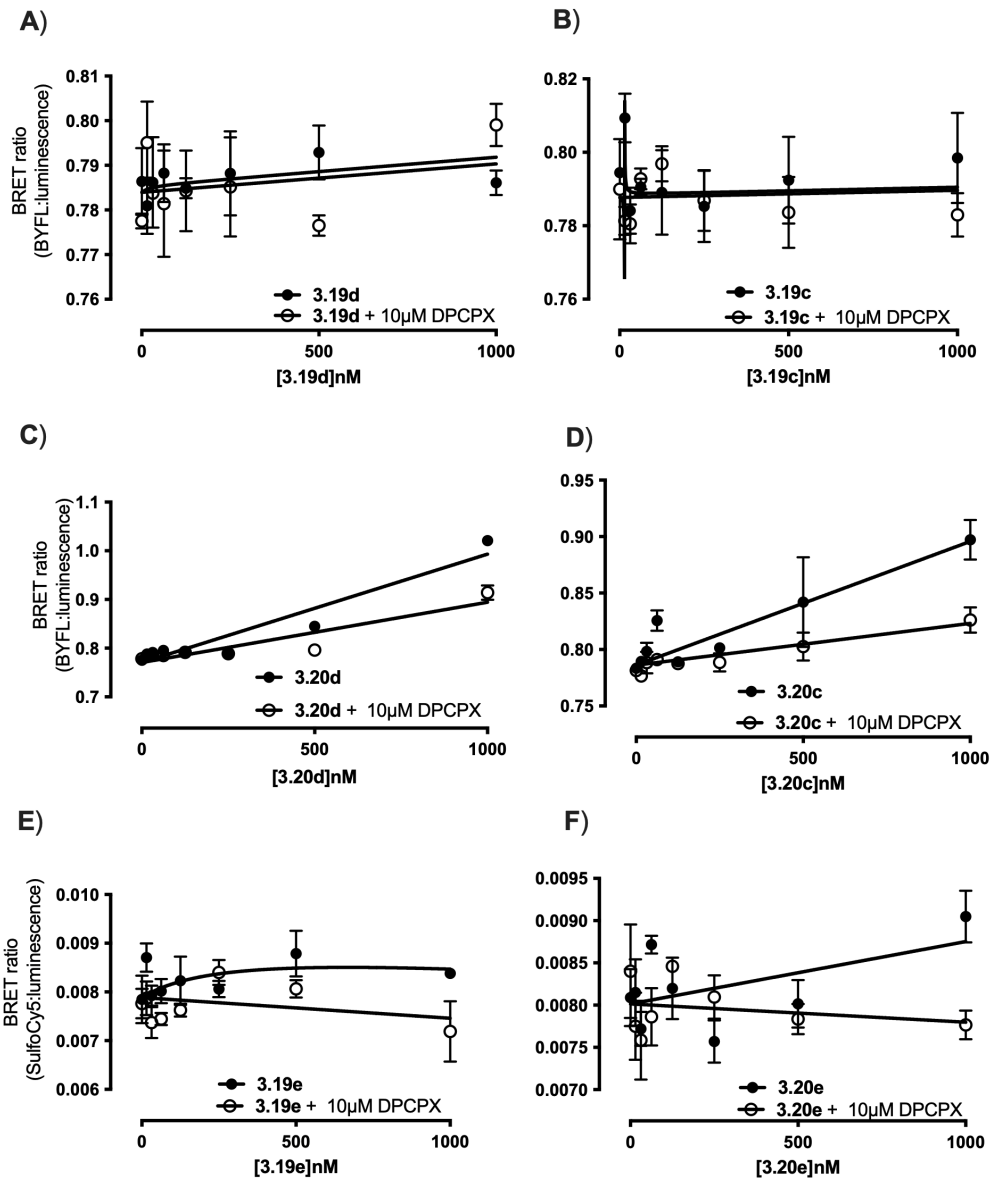


Figure 3.5 NanoBRET saturation binding curves measured in HEK293 cells stably expressing the NanoLuc-hA_1AR for **A**) **3.19d** (BY FL), **B**) **3.19c** (BY FL-X), **C**) **3.20d** (BY FL), **D**) **3.20c** (BY FL-X), **E**) **3.19e** (SulfoCy5) and **F**) **3.20e** (SulfoCy5) in the presence (open circles) or absence (closed circles) of high concentration (10 μM) of competitive antagonist DPCPX. The graph shown are from n = 1 and each data point represents the mean value ± SEM performed in triplicate.

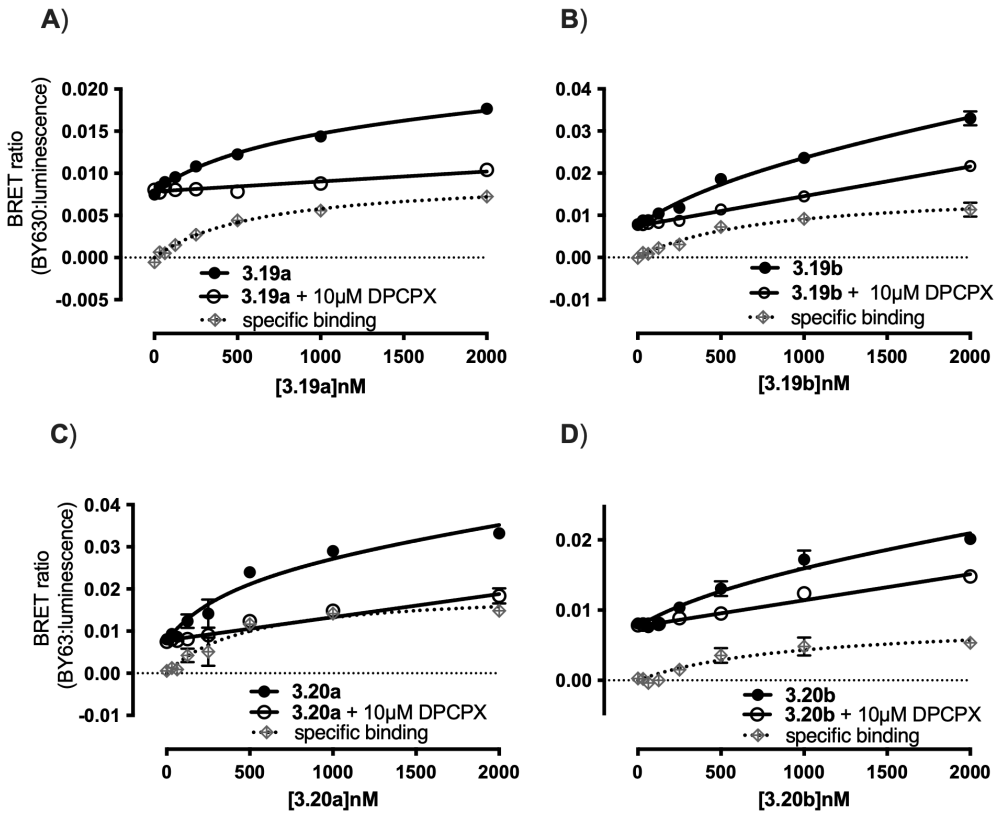


Figure 3.6 NanoBRET saturation binding curves measured in HEK293 cells stably expressing the NanoLuc-hA$_1$AR for **A**) **3.19a** (BY 630/650-X), **B**) **3.19b** (BY 630/650), **C**) **3.20a** (BY 630/650-X) and **D**) **3.20b** (BY 630/650) in the presence (open circles) or absence (closed circles) of high concentration (10 μM) of competitive antagonist DPCPX. Specific binding (diamonds, dashed line) was quantified by subtracting the non-specific binding from the total binding component. The graph shown are from n = 3 (A and B) and n = 4 (C and D), where each data point represents the mean value ± SEM performed in triplicate in a single experiment.

3.4 Conclusions and Future Work

The work presented in this Chapter described the synthetic endeavours and pharmacological assessments undertaken for the development of a novel series of fluorescent A$_1$AR ligands based on the 1-deazapurine scaffold. With the aim of providing fluorescent A$_1$AR antagonists displaying improved affinity and most importantly A$_1$AR selectivity, non-xanthine scaffolds were sort for the design of the orthosteric binding moiety of the final fluorescent ligand. To this end, LUF5981(**Figure 3.2**) a 2,6,8-trisubstitued 1-deazapurine based A$_1$AR was

selected as parent drug molecule owing to the great pharmacodynamic properties displayed. SAR studies were combined with molecular modelling to guide the rational design of functionalised congeners (**3.14** and **3.15**) as well as to inform on the most optimal position of the scaffold for linker and fluorophore conjugation (**Figure 3.1**).[265,266] A preliminary assessment of **3.14** and **3.15** A_1AR ligand binding abilities suggested that both congeners' scaffolds could be exploited for the subsequent conjugation with a series of commercially available fluorophores (**Figure 3.3 A**, **Figure 3.4** and **Table 3.1**). Accordingly, ten fluorescent A_1AR ligands were generated, five from each congener derivative, encompassing fluorophores of different spectral and physiochemical properties with the aim to be applied in a broad range of imaging or diverse fluorescence-based techniques. Unfortunately, when profiled in NanoBRET saturation ligand binding assays, the newly synthesised fluorescent ligands were found to either lack or possess only little A_1AR ligand binding ability. Thus, owing to the narrow specific binding window measured with fluorescent analogues **3.19a**, **3.19b**, **3.20a** and **3.20b** (**Scheme 3.2** and **Figure 3.6**) in the NanoBRET assay, it was reasoned to not progress the probes to further pharmacological assessments. In principle, the high signal-to-noise ratio displayed by the NanoBRET technology allows the application of higher concentrations of fluorescent tracers (hence, with much lower affinity e.g $K_D \geqq 500$ nM) compared to standard radioligand binding assays.[215] For instance, the fluorescent hP2Y_2R antagonists developed by Conroy et al., exhibited micromolar hP2Y_2R affinity values (e.g. p$K_D = 6.32 \pm 0.10$) and have been successfully applied in BRET-based ligand binding assay.[239]

Additional SAR studies could be undertaken with the aim of exploring a combination of different linker moieties as well as substituents on the C8 position of the deazapurine scaffold and generate ligands with potentially higher A_1AR affinity. Yet, the small specific binding window measured with this series of fluorescent analogues suggested that selection of a different high affinity and A_1AR selective pharmacophore moiety may be more advantageous compared to embarking in another SAR campaign using the same pharmacophore.

In the next chapter (**Chapter 4**) a new design approach will be presented for the development a new series of fluorescently-labelled A_1AR antagonists, the synthesis of which was based on the adenosine A_1AR antagonist Tonapofylline (BG9928).[83,88]

Chapter 4. Development and Application of Subtype-Selective Fluorescent Antagonists for the Study of the Human Adenosine A_1 Receptor in Living Cells.

4.1 Brief Introduction

Adenosine is an important endogenous nucleoside, which exerts its modulatory role upon binding to four adenosine receptors (AR) subtypes, namely A_1, A_{2A}, A_{2B} and A_3.[282] The adenosine A_1 receptor (A_1AR) operates mainly upon coupling with the $G_{i/o}$ family of heterotrimeric G-protein, resulting in adenylyl cyclase inhibition and a subsequent reduction of cAMP accumulation.[55] A_1ARs are highly expressed in the brain and, to a lesser extent, in peripheral tissues such as the heart, kidney and lungs,[15,56] and represent an attractive drug target for the development of therapeutic agents for CNS, cardiovascular, renal and respiratory disorders.[21,43,283] For instance, adenosine itself is administered to patients with paroxysmal supraventricular tachycardia (PSVT) to slow heart rate and contractility upon activation of the A_1AR.[21,284] A_1AR activation can also reduce ischemia-reperfusion injury and neuropathic pain.[20,21,23] On the other hand, inhibition of the A_1AR function may offer therapeutic opportunities for the development of potassium sparing diuretics,[20,21,44] anti-asthmatic agents[262] and cognitive enhancers.[43,260] However, a principal drawback in developing efficacious and safe A_1AR - selective therapeutics, is that this same biological target also mediates the onset of undesirable side effects including bradycardia, dyspnoea and seizures.[87,88,111] As such, the clinical application of A_1AR ligands has been hindered by the difficulty in separating on-target beneficial effects from adverse effects, coupled to the widespread expression of A_1AR in multiple tissues.[87,88,111] Alternative therapeutic approaches could be exploited to address the aforementioned issues, which include more selective targeting through A_1AR biased agonism and allosterism.[91,97,285] The development of more selective and efficacious therapies, however, heavily depends on our

understanding of how A_1AR pharmacology differs across tissues, cell types and subcellular compartments.[53,258,286,287] Fluorescent ligands represent valuable tools to enable real-time monitoring of receptor pharmacology, including ligand-receptor interactions, receptor signalling and trafficking in different cell types, in both health and disease.[162,165,181,191,238,239] Importantly fluorescent ligands are amenable to quantifying receptor pharmacology at the single cell level, in real-time and in unmodified, endogenously expressing systems.[126,147,226] In Chapter 1 a brief overview regarding reported and currently employed fluorescent A_1AR ligands has been provided (**Section 1.6.3** and **Figure 1.9**). Indeed, these probes have been successfully applied for studying A_1AR spatio-temporal organization[148,191,193] and signalling in living cells,[49] yet the ability of these probes to bind other adenosine receptors limits their use to recombinant expression systems. Interrogating A_1AR pharmacology in more physiologically relevant models necessitates that the fluorescent ligand binds to its receptor with high selectivity as other closely related adenosine receptors are often coexpressed.[56,118,126] Efforts to develop A_1AR-selective probes have been undertaken. For instance, Singh et al. designed fluorescent probes based on a (benzimidazolyl)isoquinolinol scaffold, which unfortunately did not show measurable binding affinity to the A_1AR.[272] In Chapter 3 synthetic endeavours towards the development of novel high affinity and selective fluorescent A_1AR antagonists based on reported deazapurine LUF5981[265] have been also discussed. However, this study could not generate fluorescent A_1AR antagonists with improved A_1AR affinity. Therefore there still remains a need for fluorescent probes with marked affinity and, most importantly, subtype selectivity for the A_1AR.

The study presented in this Chapter will discuss the design, synthesis and pharmacological evaluation of a novel series of subtype-selective fluorescent antagonists targeting the adenosine A_1AR receptor, which are amenable for use in a variety of fluorescence-based techniques. Two different positions of the prototypical xanthine scaffold were assessed for fluorophore/linker functionalization. To this end, the desired fluorescent antagonists were prepared by conjugating 8-bicylo[2.2.2]octylxanthine and 3-

functionalised 8-(adamant-1-yl)xanthine scaffolds with a series of commercially available far-red fluorophores.

4.2 Fluorescent Ligands Design

The available structural information for the hA_1AR[36,37] (in its inactive state) could be leveraged to rationalise the reported structure-activity relationships (SARs) relative to xanthine-based A_1AR antagonists,[43,44,232,276] thereby helping guide our design strategy. It was envisaged to explore two different positions of the prototypical xanthine scaffold, namely the 3- and 8-positions, for linker/fluorophore attachment as structural data suggested that functionalization of either of these positions could be harnessed for the development of chemical probes (Figure 4.1). Tonapofylline (BG9928)[83,88] and its synthetic precursor, compound **4.16** (from Kiesman et al.)[83] with a carboxylate handle directly attached to the bicyclo[2.2.2]octane group (**Figure 4.1 B** and **C**), were selected as parent molecules for the development of 8-position functionalized xanthine-based fluorescent ligands. These two ligands display high hA_1AR ligand binding affinities (K_i = 7.4 nM and K_i = 33 nM for Tonapofylline and compound **4.16**, respectively) and good selectivity profile with respect to binding other adenosine receptors subtypes ($hA_{2A}AR$ K_i = 6410 nM, $hA_{2B}AR$ K_i = 90 nM, hA_3AR K_i > 10000 nM for Tonapofylline and $hA_{2A}AR$ K_i = 1070 nM, $hA_{2B}AR$ (48%)[b], hA_3AR (100%)[b] ([b]% of specific radioligand binding) for compound **4.16**).[83] Moreover, the presence of a carboxylate group in both molecules represented an attractive functional handle for subsequent attachment of a linker and fluorophore.

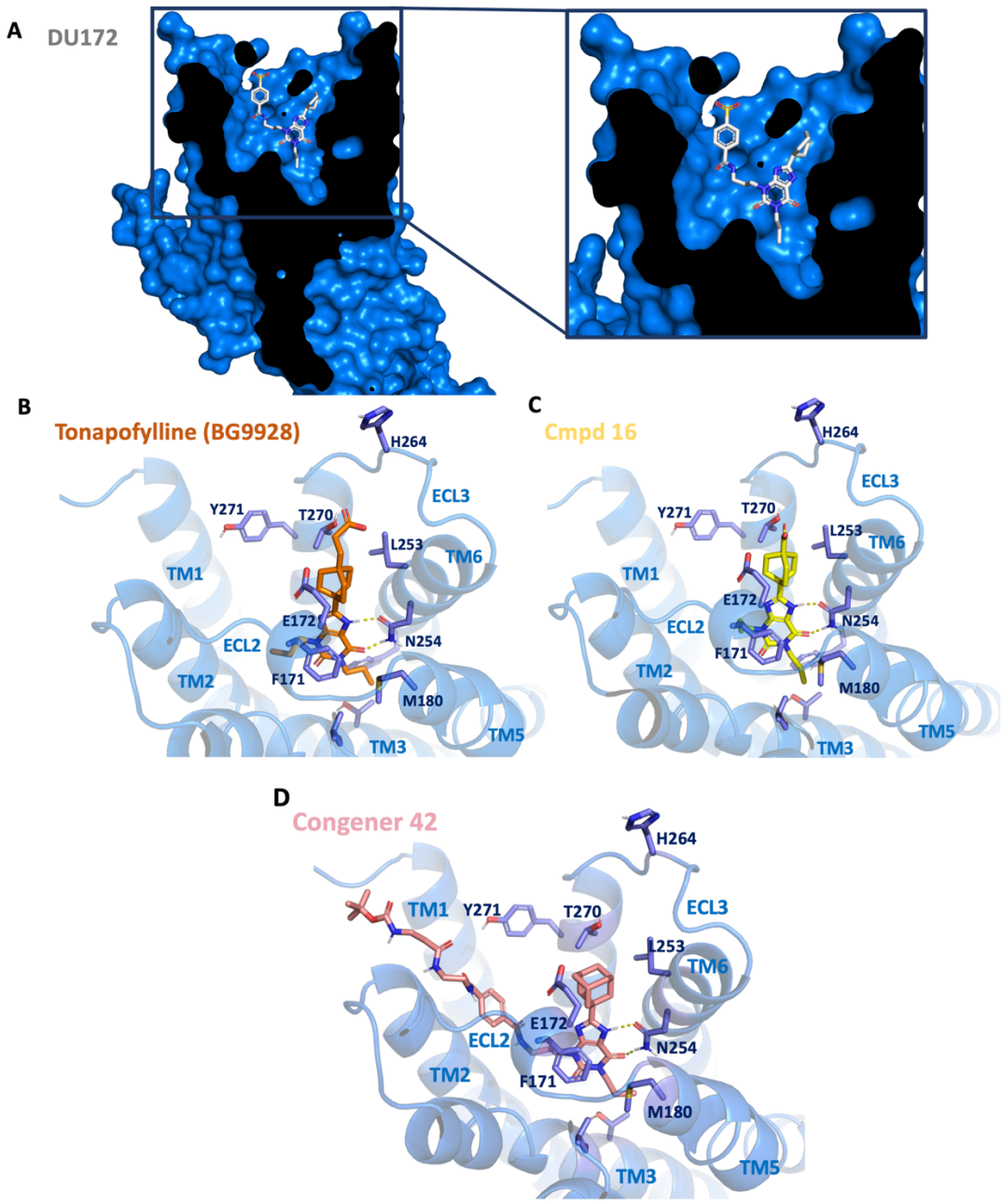


Figure 4.1 A) Sectional view of the hA$_1$AR Connolly surface to show the binding pose adopted by the co-crystallized irreversible ligand DU172 (Compound 23a in Beauglehole et al.)[288] (shown in grey sticks) with the 3-(4-fluorosulfonylbenzamido)propyl group directed towards the extracellular medium. Molecular docking of **B**) Tonapofylline (BG9928), **C**) compound 16 and **D**) congener **4.42** to the crystal structure of the hA$_1$AR (PDB:5UEN) performed with Schrödinger's Glide (Schrodinger release 2019-2). Tonapofylline is rendered in brick-red sticks, whilst compound **16** is shown in sticks coloured yellow and congener **4.42** is rendered in pink sticks. The hA$_1$AR is shown in ribbon coloured marine blue. The key residues are shown in sticks (violet) and are labelled. Hydrogen bonds are shown as yellow dashed lines and the transmembrane (TM) helices 1-3, 5 and 6 are labelled for clarity

alongside extracellular loop (ECL) 2 and ECL3. Images were generated using PyMOL (2.2.0).

Molecular modelling of Tonapofylline and compound **16** to the 3.2 Å resolution crystal structure (PDB: 5UEN)[36] of the hA_1AR revealed that both ligands exhibited comparable binding modes, with subtle differences in orientation of the 1- and 3-propyl groups for each ligand (**Figure 4.1B**, **C** and **D**). The pattern of key interactions established with the orthosteric site of the receptor was in keeping with those observed for A_1AR crystal structure co-bound with xanthine-based analogues, including hydrogen-bonding interactions with $N254^{6.55}$ and π-stacking interaction with $F171^{ECL2}$ (superscripts refer to the Ballesteros-Weinstein residues numbering system).[47,36,37] For both ligands, the carboxylate group was oriented towards the extracellular face of the A_1AR without making direct interactions with neighbouring residues. Structure-activity relationships (SAR) reported by Kiesman et al.,[83] indicated that A_1AR affinity was maintained when the carboxylate group was functionalized with amide linkers, thereby further supporting these docking results. Accordingly, it was sought to probe the area beyond the carboxylate group using linkers of different length and chemical compositions with the aim to find the optimal congener template upon which to append a series of commercially available fluorophores.

Furthermore, a second library of fluorescently-labelled compounds was generated featuring 3-functionalised xanthine-based fluorescent probes. This second library of probes, encompassed linkers with shorter length compared to the first library as structural data, complemented with docking studies, suggested that shorter linkers would provide sufficient spatial separation between the pharmacophore and the fluorophore (**Figure 4.1 D**). It was also of interest to explore probes lacking the linker, in which the fluorophores were directly conjugated to the orthosteric binding moiety as previous studies from our laboratories suggested that such modification was advantageous for the development of A_1AR fluorescent probes.[289]

The novel series of fluorescent ligands reported in this Chapter included far-red emitting probes tethered with the 6-(((4,4-difluoro-5-(2-thien-yl)-4-bora-3*a*,4*a*-diaza-*s*-indacene-3-yl)styryloxy)acetyl)aminohexanoic

acid (BODIPY630/650-X) dye and the water-soluble sulfonated cyanine5 (Sulfo-Cy5) dye. Overall, far-red emitting fluorophores were preferred as these fluorophores emit at wavelengths of 650-670 nm, where the degree of overlap with background autofluorescence from living cells is minimized.[156] In Chapter 3 derivatisation of congeners **3.14** and **3.15** with green-emitting BODIPY dyes (e.g. BODIPY FL and BODIPY FL-X) produced probes which effectively lack the ability to engage A_1AR. Moreover, previous studies have shown that conjugation of xanthine amine congener (XAC) with green-emitting fluorophores, such as BODIPY-FL dye, generated probes with markedly reduced affinity for the hA_1AR and disadvantageous imaging properties due to significant membrane penetration.[144] For these reasons, BODIPY-FL fluorophores were not included in the present study. Conversely, BODIPY 630/650 fluorophores are amongst the preferred candidates for fluorescence derivatization due to their advantageous spectral properties, including high fluorescence quantum yield (Φ) and photochemical stability.[160,161] The application of BODIPY dyes, however, may be limited by their intrinsic lipophilicity, which could lead to increased levels of nonspecific binding[195] and reduced stability in plasma. This would thereby limit their utility in more physiologically relevant models such as in vivo models.[147] Fluorescent dyes with improved water solubility, such as sulfonated cyanine 5 dyes, may overcome these limitations as demonstrated by the Cy5-labelled quinazoline-based probe developed by Ma et al., for the α_1-adrenoreceptor. [157] In addition, to the best of our knowledge, there are no reported examples of fluorescent hA_1AR antagonists integrating a Sulfo-Cy5 fluorophore that have been successfully utilised in studies of the hA_1AR in living cells.

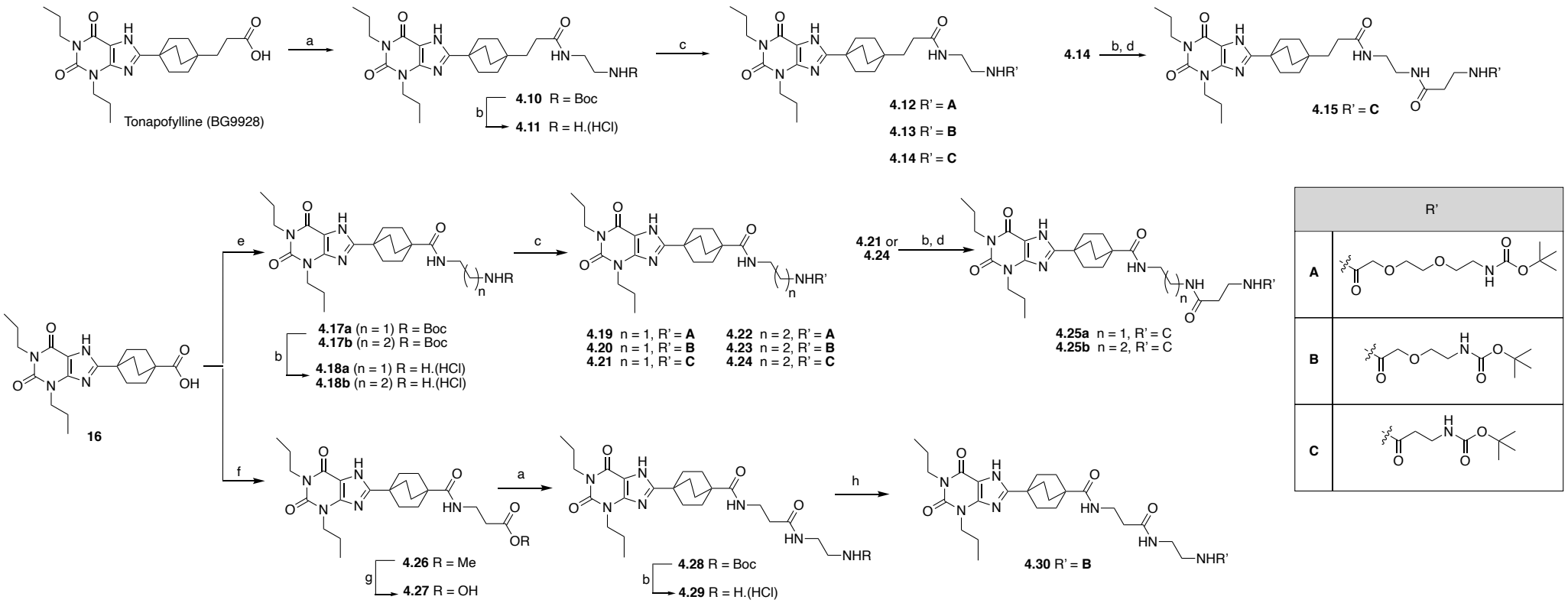
4.3 Results and Discussion

4.3.1 Chemistry

4.3.1.1 Synthesis of the 8-bicyclo[2.2.2]octylxanthine based congeners.

The chemical synthesis of the 8-bicyclo[2.2.2]octylxanthine based amino functionalized congeners is outlined in Scheme 1. Tonapofylline (BG9928) and **4.16** provided the framework for the development of the series of fluorescent ligands featuring linkers and fluorophores extending from the 8-position of the xanthine scaffold. Tonapofylline (BG9928) and **4.16** were synthesized as described in Keisman et al.[83] (detailed procedures are reported in Appendix I) and were further functionalized with a series of linker variants of different length and chemical composition to afford ten final *N*-Boc-protected amino functionalized congeners. Briefly, Tonapofylline (BG9928) was activated with (1-cyano-2-ethoxy-2-oxoethylidenaminooxy) dimethylamino-morpholino-carbenium hexafluorophosphate (COMU) in the presence of DIPEA and subsequently coupled with *N*-Boc-enthylenediamine in DMF to afford the corresponding mono-protected amine intermediate (**2.10**). Acidolytic removal of the Boc protecting group afforded the corresponding amine (**4.11**) as its HCl salt, which was subsequently functionalized in the presence of DIPEA and COMU with three linker variants of different length and chemical composition: Boc-8-amino-3,6-dioxaoctanoic acid, Boc-5-amino-3-oxapentanoic acid and Boc-β-alanine to afford **4.12**, **4.13** and **4.14** respectively (Scheme 4.1).

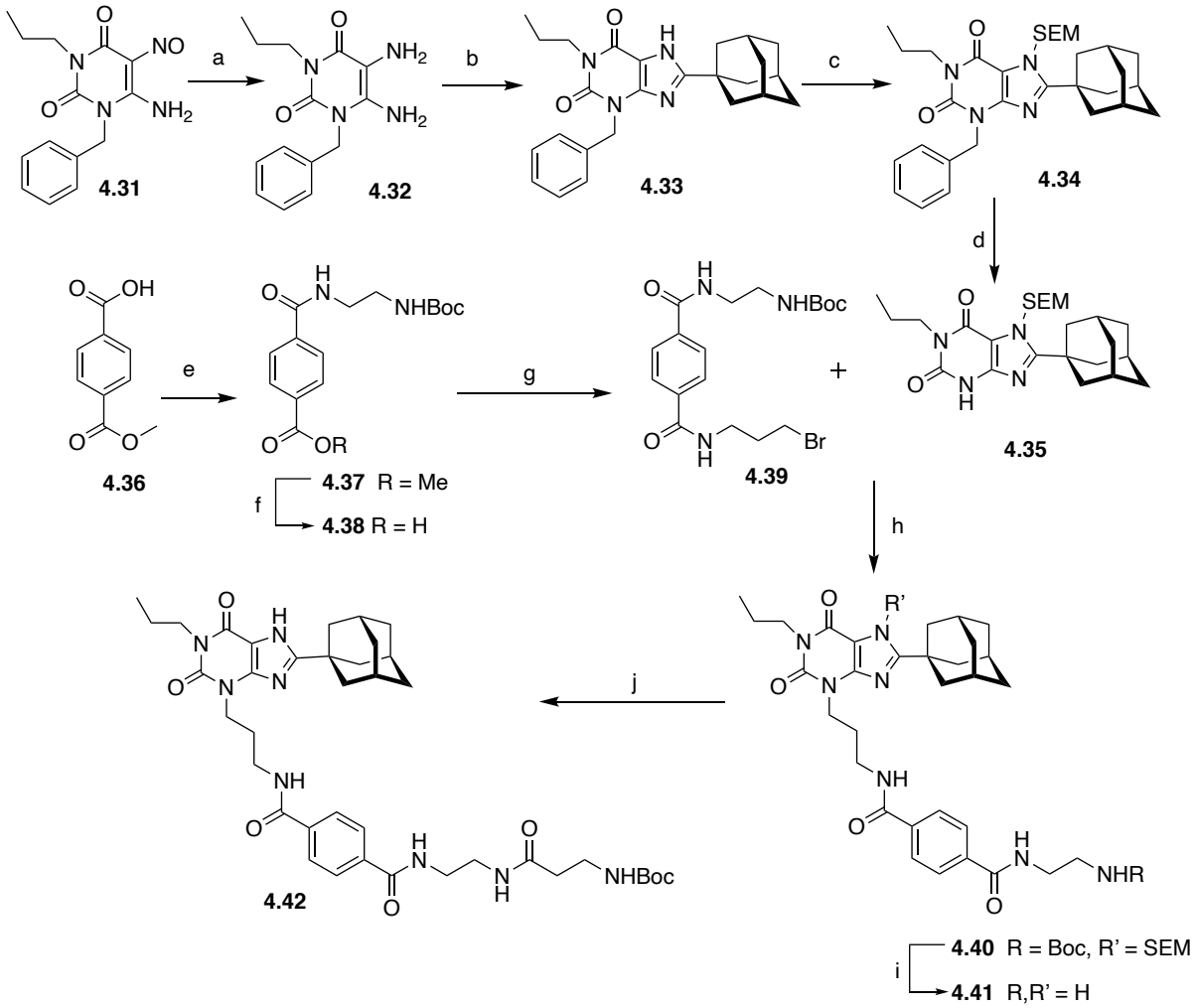
Scheme 4.1. Synthesis of the 8-Bicyclo[2.2.2]octylxanthine based Congeners.[a]



[a]Reagents and conditions: (a) *N*-Boc-ethylenediamine , COMU, DIPEA, DMF, rt, 1 h, 58%; (b) 4 N HCl in dioxane, rt, 30 min, quantitative; (c) *N*-Boc-8-amino-3,6-dioxaoctanoic acid or *N*-Boc-5-amino-3-oxapentanoic acid or *N*-Boc-β-alanine, COMU, DIPEA, rt, 1 h, 28-67%; (d) *N*-Boc-β-alanine, COMU, DIPEA, rt, 1 h; (e) N^1-Boc-ethylenediamine or *N*-Boc-1,3-propanediamine, BOP, DIPEA, DMF, rt, 1 h, 78-86%; (f) β-Alanine methyl ester, BOP, DIPEA, DMF, rt, 56%; (g) $LiOH.H_2O$, $MeOH/H_2O$ 1:1, rt, 40 min, 84%; (h) *N*-Boc-5-amino-3-oxapentanoic acid, COMU, DIPEA, rt,

Compound **4.16** was coupled with either *N*-Boc-ethylenediamine or *N*-Boc-1,3-propanediamine to afford the corresponding mono-protected intermediates **4.17a** and **4.17b** respectively. Following acidolysis, *N*-Boc deprotection gave the corresponding primary amines (**4.18a** and **4.18b**) as their HCl salts. COMU-mediated amide coupling of **4.18a** and **4.18b** with the *N*-protected linkers Boc-8-amino-3,6-dioxaoctanoic acid, Boc-5-amino-3-oxapentanoic acid or Boc-β-alanine afforded the Boc protected congeners **4.19-4.24**. An additional chain-extended congener was also synthesized, to investigate the effect of this longer linker variant in modulating A_1AR binding affinity. To this end, **4.16** was activated with (benzotriazol-1-yloxy)tris(dimethylamino)phosphonium hexafluorophosphate (BOP) and coupled with b-alanine methyl ester to afford **4.26**. Saponification of the latter and subsequent amide coupling with *N*-Boc-ethylenediamine yielded the corresponding Boc-protected intermediate (**4.28**). Treatment of **4.28** with 4 M HCl in dioxane afforded the corresponding amine (**4.29**) as its HCl salt, which was coupled with Boc-5-amino-3-oxapentanoic acid to afford the desired protected congener **4.30**.

Scheme 4.2. Synthesis of the 1-Propyl-3-(3-benzamidopropyl)-8-(3-adamantyl) xanthine based Congeners.[a]



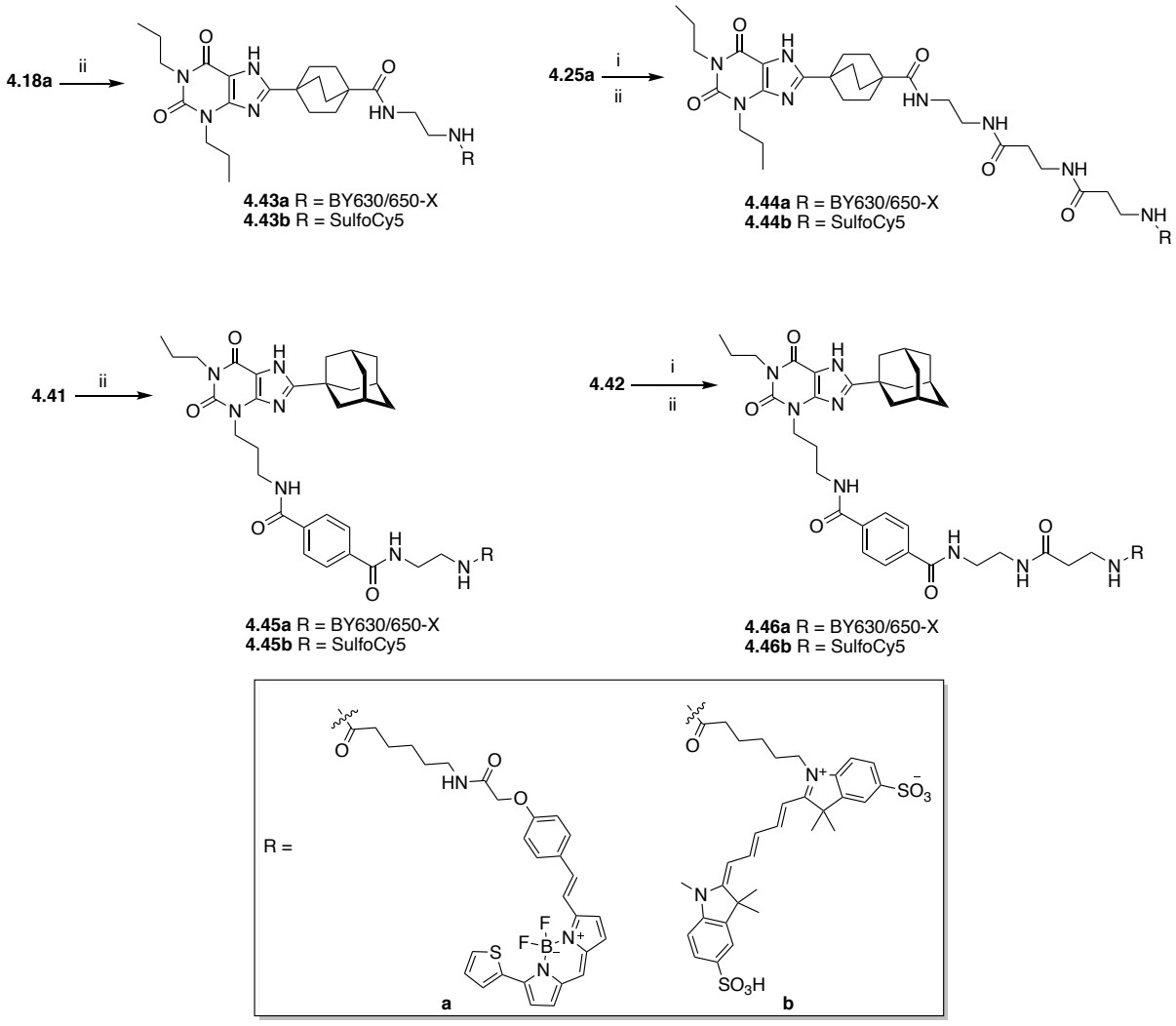
[a]Reagents and conditions: (a) $Na_2S_2O_4$, 30% NH_4OH in H_2O, 85 ^oC, 92%; (b) i) 1-Adamantane carboxylic acid, COMU, DIPEA, DMF, rt, 15 min, 87% ii) 1M KOH/ *n*-propanol 1:1, reflux, 1 h, 95%; (c) SEM-Cl, K_2CO_3, DMF, 4 h, 66%; (d) $NH_4^+HCO_2^-$, Pd/C, MeOH, 140 ^oC, 9 h, 67%; (e) *N'*-Boc ethylenediamine, COMU, DIPEA, DMF, rt, 20 min, 75%; (f) 1M NaOH, THF, rt, 3 h, 90%; (g) 3-bromopropylamine hydrobromide, COMU, DIPEA, DMF, rt, 15 min, 61%; h) **35** and **39**, K_2CO_3, DMF, 25-40 ^oC, 24 h, 49%; (i) 4 M HCl in dioxane, rt, 30 min, quantitative, then DIPEA; (j) Boc-β-Ala-OH, COMU, DIPEA, DMF, rt, 15 min, 47%.

4.3.1.2 Synthesis of the 1-propyl-3-(3-benzamidopropyl)-8-(3-adamantyl) xanthine-based congeners.

The synthetic approach for the preparation of 3-functionalized analogues is outlined in Scheme 4.2 and was adapted from procedures reported by Beauglehole et al.[288] 6-Amino-1-benzyl-5-nitroso-3-propylpyrimidine-2,4(1*H*,3*H*)-dione (**4.31**) was previously prepared in our laboratory following reported literature procedures.[290–292] Reduction of the nitroso group of **4.31** with sodium dithionite afforded the corresponding 5,6-diamino uracil product (**4.32**), which was subsequently acylated with 1-adamantane carboxylic acid in the presence of COMU[293] to afford the corresponding 6-amino-5-carboxamido uracil precursor. The latter then underwent cyclization in the presence of 1M KOH to the corresponding 8-adamantyl-substituted xanthine (**4.33**) in excellent yield (95%). To ultimately allow a selective alkylation of the unsubstituted 3-position of the xanthine ring following its debenzylation, a 2-(trimethylsilyl)ethoxymethyl (SEM) protecting group was introduced at the 7-position to afford the corresponding 7-*N*-SEM-protected intermediate (**4.34**) in good yield (66%). Subsequent debenzylation was achieved under transfer hydrogenation conditions using ammonium formate in the presence of 10% palladium on carbon (Pd/C) in methanol at high temperature,[294] affording the corresponding deprotected xanthine **4.35** in good yield (67%). The aryl amide linker variant was prepared starting from commercially available mono-methyl terephthalate (**4.31**), which was coupled with *N*-Boc ethyelenediamine by means of COMU, in the presence of DIPEA in DMF, affording intermediate **4.37**. The latter was then treated with 1 M NaOH to generate the corresponding carboxylic acid (**4.38**), which was subsequently coupled with 3-bromopropylamine hydrobromide in the presence of DIPEA, affording intermediate **4.39** with good yield (61%). Alkylation of the xanthine derivative **4.35** with **4.39** under basic conditions yielded the corresponding 3-*N*-propyl-3-benzamide intermediate (**4.40**) in reasonable yield (49%). Concomitant SEM- and Boc-removal was effected by reacting **4.40** with 4 M HCl in dioxane for 1 h, followed by treatment of the resulting HCl salt with DIPEA to liberate the corresponding amine (**4.41**), which was coupled with

Boc-β-Ala-OH using COMU in DMF to yield the final Boc-protected congener (**4.42**).

Scheme 4.3. Synthesis of the Fluorescent A_1AR Antagonists.



[a] Reagents and conditions: (i) 4 M HCl in dioxane, rt, 30 min, quantitative; (ii) BY630/650-X-NHS or SulfoCy5-NHS, DIPEA, DMF, rt, exclusion of light, 39-100%.

4.3.1.3 Synthesis of fluorescent A_1AR antagonists.

The 8-bicyclo[2.2.2]octylxanthine based congeners **4.18a** and **4.25a** and the 8-adamantyl-3-propyl-3-benzamide substituted congeners **4.41** and **4.42** were subsequently conjugated with a series of commercially available far-red emitting fluorophores (**Scheme 4.3**), namely BODIPY630/650-X (BY630/650-X) and sulfonated cyanine5 (Sulfo-Cy5) dyes, thereby yielding a

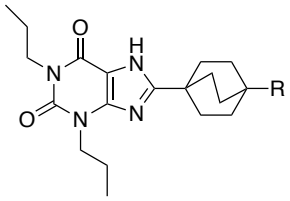
focused library of eight fluorescent analogues (**4.43a**-**b**-**4.46a**-**b**). The novel synthesized fluorescent probes were purified by reverse-phase high performance liquid chromatography (RP-HPLC) and the high purity of the final probes was confirmed by analytical RP-HPLC with dual wavelength detection and measured as ≥96% homogeneity. Furthermore, chemical identity of the final probes was confirmed by high resolution mass spectroscopy (HRMS) (TOF ES+ and ES-).

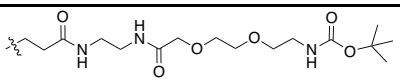
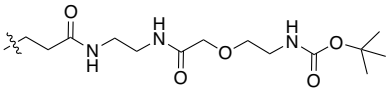
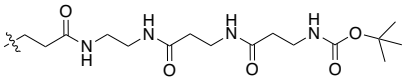
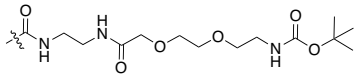
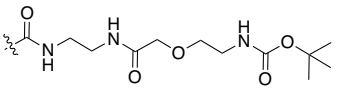
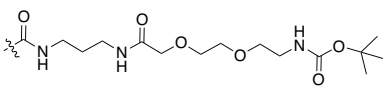
4.3.2 Pharmacology

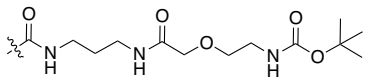
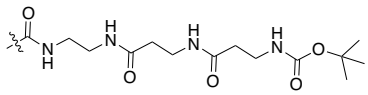
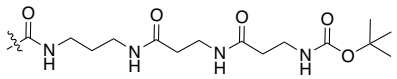
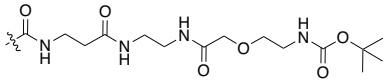
To evaluate which linker functionality could be harnessed for the development of the first library of fluorescent probes, the ten newly synthesized Boc-protected 8-bicyclo[2.2.2]octylxanthine congeners **4.12**, **4.13**, **4.15**, **4.19**, **4.20**, **4.22**, **4.23**, **4.25a**, **4.25b** and **4.30** (Scheme 4.1) were characterized using [^{3}H]DPCPX binding in FlpIn-CHO cells stably expressing the hA_1AR (A_1AR-FlpInCHO cells). All congeners displayed good hA_1AR ligand binding affinity (7.65-8.36 pK_i range, Table 4.1), demonstrating that all linker combinations were well tolerated. Comparison of the reported binding affinities[83] of Tonapofylline (BG9928) and **4.16** with the congeners synthesized in this Chapter corroborated the original observation whereby functionalization of the carboxylate handle of either Tonapofylline or **4.16** could be exploited for linker conjugation. Despite the similar affinity of these ligands, subtle differences in SARs were observed. There was a general trend for congeners incorporating the β-Ala-β-Ala linker moiety to possess higher hA_1AR affinities relative to congeners lacking the dipeptide linker (**4.15**, **4.25a** and **4.25b**, Table 1**.** ** $P < 0.01$ one-way ANOVA with Tukey's multiple comparison test). Likewise, congeners with an ethylenediamine spacer appeared to be better tolerated than those with a propane-1,3-diamine. Based on these initial results, compound **4.25a** (Table 4.1 and Scheme 4.1) was therefore chosen as model functionalized congener for the development of the 8-bicyclo[2.2.2]octylxanthine based fluorescent probes. Moreover, owing to the greater hA_1AR affinity observed with congeners conjugated with β-alanine, the β-alanine linker was also used for

the development of the 1-propyl-3-(3-benzamidopropyl)-8-(3-noradamantyl)xanthine based fluorescent ligands. Furthermore, structural data suggested that a single β-alanine moiety, coupled with an ethylenediamine spacer, should provide the optimal linker length for conjugating the 1-propyl-3-(3-benzamidopropyl)-8-(3-noradamantyl) xanthine-based scaffold with the desired fluorophore.

Table 4.1. Binding Affinities of the Novel 8-bicyclo[2.2.2]octylxanthine based amino Functionalized Congeners.



Cmpd	R	pK_i (LogM) ± SEM[a]
4.12		7.88 ± 0.06
4.13		7.83 ± 0.10
4.15		8.11 ± 0.09**
4.19		7.76 ± 0.06
4.20		7.86 ± 0.05
4.22		7.65 ± 0.05

4.23		7.79 ± 0.09
4.25a		8.36 ± 0.08**
4.25b		7.89 ± 0.05**
4.30		7.95 ± 0.04

[a] pK_i ± SEM values were calculated from the negative logarithm of the equilibrium inhibitory constant (K_i in nM) determined at 4 °C using [^{3}H] DPCPX competition binding experiments in FlpIn-CHO cells stably expressing the hA_1AR. Values represent the mean ± SEM from n = 3 experiments performed in duplicate. ** $P < 0.01$. compared to congeners lacking the dipeptide linker one-way ANOVA with Tukey's multiple comparison test.

Next, the newly synthesized 8-bicyclo[2.2.2]octylxanthine-based and 1-propyl-3-(3-benzamidopropyl)-8-(3-noradamantyl) xanthine-based fluorescent ligands (Scheme 3) were profiled in a variety of pharmacological assays. Initially, the fluorescent ligand binding was quantified using [^{3}H] DPCPX competition binding in A_1AR-FlpInCHO cells (**Figure 4.2** and **Table 4.2**).

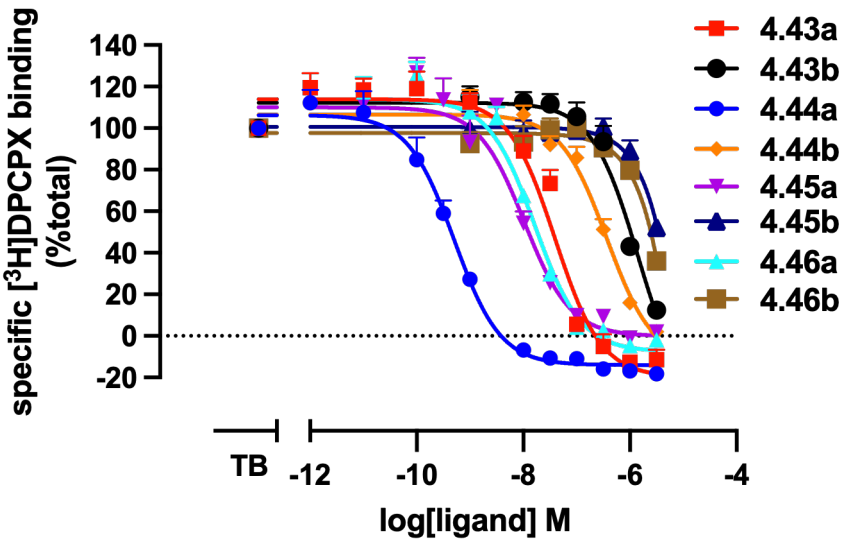
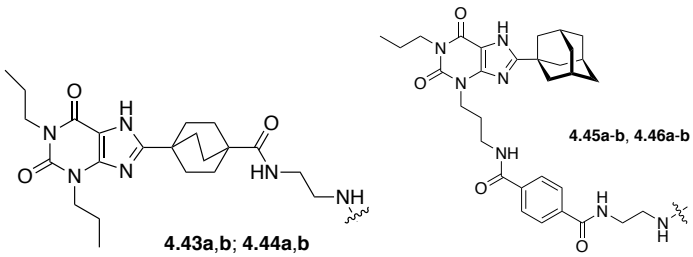


Figure 4.2 Inhibition of [^{3}H] DPCPX specific binding (1 nM) in the presence of increasing concentrations of fluorescent antagonist (**4.43a-b** to **4.46a-b**) at 37°C in hA$_1$AR-FlpInCHO cells. TB stands for total radioligand binding. Each data point represents the combined mean ± SEM from n = 5 experiments performed in triplicate.

Table 4.2. Binding Affinities of the Novel 8-bicyclo[2.2.2]octylxanthine based (4.43a-b, 4.44a-b) and 1-Propyl-3-(3-benzamidopropyl)-8-(3-noradamantyl) xanthine based (4.45a-b, 4.46a-b) Fluorescent Antagonists.



Cmpd	Linker	Fluorophore	pK_i (LogM) ± SEM[a]
SLV320	-	-	8.77± 0.05
4.43a	-	BY630/650-X	7.69 ± 0.06####
4.43b	-	Sulfo-Cy5	6.07 ± 0.09
4.44a	β-Ala-β-Ala	BY630/650-X	9.54 ± 0.05****

4.44b	β-Ala-β-Ala	Sulfo-Cy5	6.70 ± 0.06
4.45a	-	BY630/650-X	8.23 ± 0.07
4.45b	-	Sulfo-Cy5	< 5
4.46a	β-Ala	BY630/650-X	8.01 ± 0.03
4.46b	β-Ala	Sulfo-Cy5	<5

[a]pK_i values were calculated from the negative logarithm of the equilibrium inhibitory constant (K_i in nM) measured at 37 °C by radioligand competition binding employing [^{3}H] DPCPX as radiotracer in FlpIn-CHO cells stably expressing the hA$_1$AR. Values represent the mean ± SEM from n = 5 experiments performed in triplicate (statistical significance was defined as $^{****}p < 0.0001$ one-way ANOVA with Tukey's multiple comparison test comparing the pK_i of **4.44a** versus **4.44b.** $^{####}p < 0.0001$ one-way ANOVA with Tukey's multiple comparison test comparing the pK_i of **4.44a** versus **4.43a**).

Broad differences in hA$_1$AR ligand binding affinities could be measured across the novel fluorescent ligands synthesized (**Table 4.2**). These results are consistent with previous studies, which showed a significant contribution of the fluorophore in modulating the pharmacology of the final conjugates.[144,150,295] Indeed, there was a statistical difference for the BY630/650-X-labelled compounds (**4.43a-4.46a**) to display the highest affinities of the series compared to the corresponding SulfoCy5-labelled analogues (**4.43b-4.46b**) (Table 2). Overall, conjugation with the Sulfo-Cy5 probe was detrimental with regard to binding to the hA$_1$AR. Fluorescent analogue **4.44a** displayed the highest affinity of the series at the hA$_1$AR (pK_i = 9.54 ± 0.05). The addition of the BY630/650-X fluorophore resulted in a circa 16-fold increase of hA$_1$AR affinity compared to the Boc-protected congener **4.25a**. Replacement of the BY630/650-X fluorophore with Sulfo-Cy5 yielded fluorescent antagonist **4.44b** (pK_i = 6.70 ± 0.06) which resulted in a significant reduction in hA$_1$AR binding affinity (690-fold) compared to the BY630/650-X-labelled analogue. The fluorophore moiety alone, however, was not the only driver of hA$_1$AR affinity as demonstrated by ligands **4.43a** and **4.43b**, which had lower affinity compared to **4.44a** and

4.44b. These two fluorescent analogues lacked the dipeptide β-Ala-β-Ala linker and were synthesized to explore the effect of moving the fluorophore closer to the 8-bicyclo[2.2.2]octylxanthine scaffold. Despite the reasonable hA_1AR affinity displayed by compounds **4.43a** and **4.43b**, removal of the dipeptide β-Ala-β-Ala linker proved to be disadvantageous. This suggests that there may be a synergistic effect of both linker and fluorophore in influencing the binding affinity of the final fluorescent conjugates. The introduction of the Sulfo-Cy5 fluorophore to the 1-propyl-3-(3-benzamidopropyl)-8-(3-noradamantyl) xanthine scaffold (probes **4.45b** and **4.46b**) effectively abolished hA_1AR affinity ($pK_i < 5$). In contrast, conjugation with BY630/650-X fluorophore yielded fluorescent analogues **4.45a** and **4.46a** with good hA_1AR affinity ($pK_i = 8.23 \pm 0.07$ and $pK_i = 8.01 \pm 0.03$, respectively). These results supported the original hypothesis whereby fluorophore derivatization could be achieved at both the 8- and 3-position of the prototypical xanthine scaffold.

The SAR of these novel fluorescent ligands could be rationalized in the context of A_1AR structural information. For example, crystal structures for the hA_1AR[34,36,37] revealed the presence of a secondary hydrophobic pocket defined by residues $F171^{ECL2}$, $E170^{ECL2}$,$V83^{3.28}$, $I69^{2.64}$, $L65^{2.60}$. Molecular dynamics simulations (MD) studies suggest this pocket provides an important recognition mechanisms for ligand binding, with A_1AR ligands affinity and selectivity being influenced by their ability to engage with this accessory hydrophobic site.[50,296] The importance of hydrophobic pockets in influencing ligand binding has been suggested for various GPCRs, including the $A_{2A}AR$ and the C-C chemokine receptor type 5 (CCR5).[41,52] Accordingly, the lipophilic nature of the BODIPY probes may enable the boron dipyrromethene scaffold to establish favourable interactions with this accessory hydrophobic site with concomitant displacement of weakly associated water molecules from this pocket, thereby further enhancing the overall free energy of binding for the probe bound to the A_1AR. In contrast, molecular interactions of this type could not be established with the corresponding water-soluble SulfoCy5 analogues as, due to their hydrophilic nature, the interaction with the solvent could be more favourable.

One of the major objectives of this study was to synthesise and develop subtype-selective fluorescent ligands that can selectively engage with A_1AR in cells and tissues where other adenosine receptors are co-expressed. To this end, a nanoluc luciferase bioluminescence resonance energy transfer (NanoBRET)[164,165,215] ligand binding assay was used to quantify the selectivity profile of the novel fluorescent ligands synthesised. NanoBRET is a proximity assay (<10 nm) which relies upon the energy transfer between a donor bioluminescent protein (NanoLuc)[163] tagged on the *N*-terminus of the receptor of interest (NanoLuc-hA_1AR) and an acceptor fluorophore. The binding affinity of the most promising fluorescent ligands of both BODIPY- and Sulfo-Cy5-bearing probes (**4.44a-b** and **4.46a**, **Scheme 4.3**), selected based on [^{3}H] DPCPX binding results (**Table 4.2**), was quantified at each adenosine receptor subtypes using NanoBRET saturation ligand binding assay in HEK293A cells transiently expressing either the NanoLuc-A_1AR, NanoLuc-A_{2A}, NanoLuc-A_{2B} or the NanoLuc-A_3AR. A robust, specific and saturable BRET signal was detected at the NanoLuc-A_1AR for each fluorescent analogue investigated (**4.44a**, **4.44b** and **4.46a**), with low levels of nonspecific binding for all concentrations tested. Fluorescent analogue **4.44b** showed reasonable NanoLuc-hA_1AR affinity (pK_D = 7.35 ± 0.09, n = 3) and the most promising selectivity profile among the fluorescent probes tested in this NanoBRET assay (**Table 4.3** and **Figure 4.3 F**). Indeed, minimal BRET signal was detected at either NanoLuc-hA_{2A}AR, NanoLuc-hA_{2B}AR or NanoLuc-hA_3AR at 500nM-1 μM **4.44b** (**Figure 4.3 F**). A concentration-dependent BRET signal was observed for fluorescent analogues **4.44a** and **4.46a** at the NanoLuc-hA_{2A}AR, NanoLuc-hA_{2B}AR and NanoLuc-hA_3AR (**Figure 4.3 E**), allowing estimation of their equilibrium dissociation constant (K_D) (**Table 4.3**). **4.44a** exhibited high affinity for the NanoLuc-hA_1AR affinity (pK_D = 8.93 ± 0.02, n = 3) which was 25-fold, 7-fold and 117-fold greater than its affinity for the NanoLuc-hA_{2A}AR, NanoLuc-hA_{2B}AR and NanoLuc-hA_3AR, respectively. Fluorescent analogue **4.46a** also displayed high affinity at the NanoLuc-hA_1AR (pK_D = 8.50 ± 0.07, n = 3), whilst the affinities measured at the other adenosine receptors subtypes were appreciably lower, displaying approximately 20-fold greater affinity for the

NanoLuc-hA_1AR compared to the NanoLuc-hA_{2A}AR, NanoLuc-hA_{2B}AR and NanoLuc-hA_3AR.

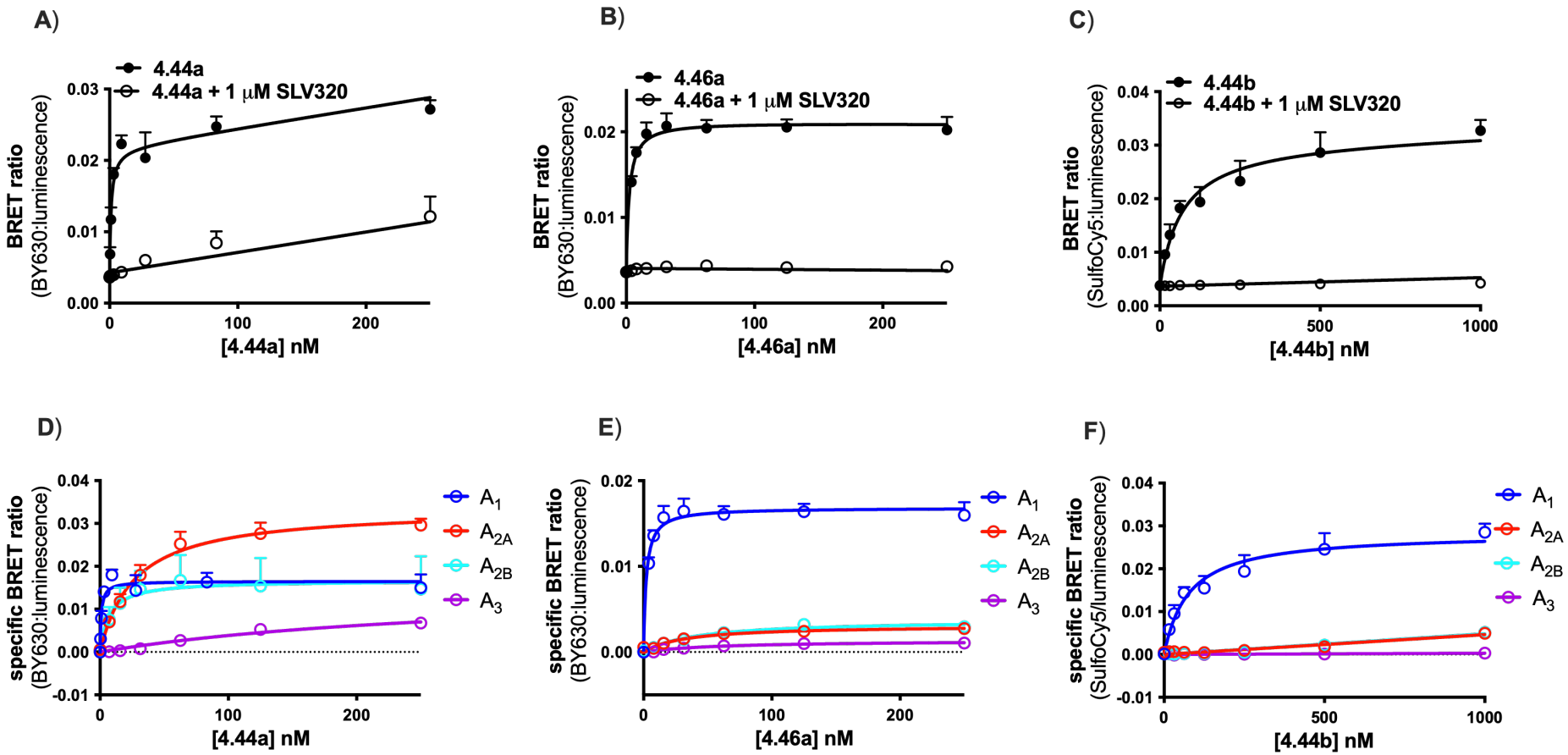


Figure 4.3 NanoBRET saturation ligand binding curves (A-C) measured in HEK293A cells transiently expressing the NanoLuc-hA$_1$AR for (A) **4.44a**, (B) **4.46a**, (C) **4.44b** in the presence (open circles) and absence (closed circles) of 1 μM SLV320. Graphs (D-F) depict the selectivity profile of the probes tested against each subtype of the adenosine receptors. Specific binding (D-F) of (D) **4.44a**, (E) **4.46a** and (F) **4.44b** at each subtype of adenosine receptors was measured from saturation binding curves (A-C) after subtraction of the nonspecific binding component from the total binding. Nonspecific binding was determined in the presence of 1 μM of ZM241385 for NanoLuc-hA$_{2A}$AR, 1 μM PSB603 for NanoLuc-hA$_{2B}$AR and 1 μM MRS1220 for NanoLuc-hA$_{2A}$AR. Data points represent the combined mean ± SEM from n = 3 experiments performed in duplicate.

Table 4.3 Binding Affinities of Fluorescent 8-Bicyclo[2.2.2]octylxanthine Based Conjugates 4.44a and 4.44b and Fluorescent 1-Propyl-3-(3-benzamidopropyl)-8-(3-noradamantyl) xanthine Based Conjugate 4.46a at NanoLuc-hA$_1$AR, NanoLuc-hA$_{2A}$AR, NanoLuc-hA$_{2B}$AR and NanoLuc-hA$_3$AR.

Cmpd		NLuc-hA$_1$AR	NLuc-hA$_{2A}$AR	NLuc-hA$_{2B}$AR	NLuc-hA$_3$AR
4.44a	pK_D **(LogM)**[a]	8.93 ± 0.02	7.55 ± 0.09	8.11 ± 0.08	6.87 ± 0.04
	B_{max}	0.018 ± 0.002	0.035 ± 0.001	0.016± 0.003	0.012 ± 0.001
4.46a	pK_D **(LogM)**	8.50 ± 0.07	7.30 ± 0.15	7.26 ± 0.08	7.23 ± 0.09
	B_{max}	0.019 ± 0.0005	0.003 ± 0.0003****	0.004 ± 0.0004****	0.001 ± 0.00007****
4.44b	pK_D **(LogM)**	7.35 ± 0.09	< 6	< 6	< 6
	B_{max}	0.030 ± 0.006	N.D.[b]	N.D.[b]	N.D.[b]

[a] pK_D values were calculated from the negative logarithm of the equilibrium dissociation constant (K_D) measured at 37°C by NanoBRET saturation binding using increasing concentration of fluorescent ligand in the absence or presence (to define nonspecific binding) of 1 μM of selective unlabelled AR antagonist (1 μM SLV320 for NanoLuc-A$_1$AR, 1 μM ZM241385 for NanoLuc-A$_{2A}$AR, 1 μM PSB603 for NanoLuc-A$_{2B}$AR and 1 μM MRS1220 for NanoLuc-A$_3$AR). Data are represented as mean ± SEM of n = 3 experiments, where each experiment was performed in duplicate. [b]N.D. = not determined. **** $P < 0.0001$. compared to NanoLucA$_1$ B_{max}, one-way ANOVA with Tukey's multiple comparison test.

Notably, the maximal binding capacity (B_{max}) value of probe **4.46a** was significantly higher at the NanoLuc-hA_1AR compared to binding to either of the NanoLuc-hA_{2A}AR, -hA_{2B}AR and -hA_3AR receptor subtypes (maximum BRET ratios of 0.003, 0.004, 0.001 respectively) (**Table 4.3**). They were also substantially different to the B_{max} values obtained at the NanoLuc-hA_{2A}AR, -hA_{2B}AR and -hA_3AR receptor subtypes with **4.44a** (0.035, 0.016, 0.012 respectively). These results are unlikely to reflect a lack of receptor expression for A_{2A}AR, A_{2B}AR and A_3AR when profiling **4.46a**, as these experiments were performed in parallel with **4.44a**, which exhibited robust expression for all adenosine receptor subtypes. It was therefore hypothesised that the BRET signal resulting from probe **4.46a** binding to the NanoLuc-hA_{2A}AR,-hA_{2B}AR and -hA_3AR could be a result of the so-called "bystander" BRET,[297–299] that is, non-specific enrichment of probe **4.46a** at the plasma membrane of cells expressing hA_{2A}AR, hA_{2B}AR or hA_3AR receptors could produce a measurable BRET signal owing to the close proximity between the probe and the bioluminescent protein NanoLuc. Alternatively, HEK293 cells are known to express hA_1AR at very low levels[300,301] and it is therefore possible the low BRET signal detected with **4.46a** at the NanoLuc-hA_{2A}AR and -hA_{2B}AR is a result of close proximity between the endogenous hA_1AR and the NanoLuc-hA_{2A}AR-receptors (such as might occur in oligomeric complexes). The ability of A_1AR and A_{2A}AR to form heterodimeric complexes has been previously described by Ciruela et al.[302] using BRET and FRET in membrane preparations of HEK293 cells co-transfected with A_{2A}AR-RLuc and A_1AR-YFP. In addition, formation of A_1AR-A_{2A}AR heterodimer complex was further confirmed in striatal glutamatergic nerve terminals by immunostaining and coimmunoprecipitation experiments.[302] In later studies Briddon et al. were able to visualise and quantify A_1AR-A_{2A}AR heterodimers expressed in living CHO cells by Bimolecular Fluorescence Complementation (BiFC).[303] Here, the NanoBRET technology was used to quantify direct A_1AR and A_{2A}AR heterodimerization in whole living HEK293T cells, whereby NanoLuc-tagged A_{2A}AR were used as resonance energy transfer (RET) donors and SNAP-tagged A_1AR receptors as RET acceptors. Indeed, the NanoBRET saturation assay represents a useful avenue to assess for specific protein-protein interactions as well as for non-

specific BRET signals that may potentially occur in cellular systems overexpressing the receptor of interest.[304] In these experiments, HEK293T cells were co-transfected with a fixed concentration (50 ng/well) of donor *N*-tagged NanoLuc-hA_{2A}AR and increasing concentrations (0.5-100 ng/well) of acceptor *N*-tagged SNAP-A_1AR. A significant saturable BRET signal could be measured (**Figure 4.4**) which was consistent with specific protein-protein interactions.[304,305]

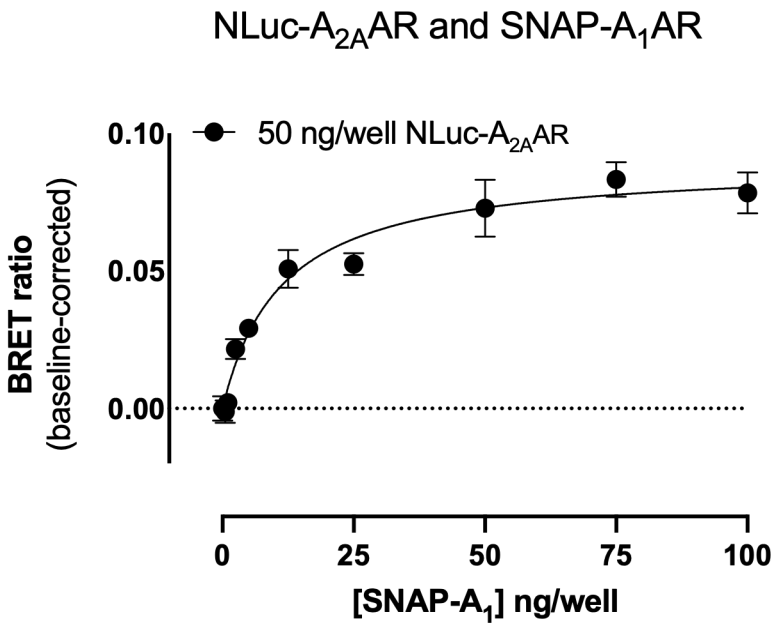


Figure 4.4 NanoBRET saturation assay investigating A_1AR-A_{2A}AR heterodimerization in whole living HEK293 cells. HEK293T cells were transiently co-transfected with 50 ng/well NanoLuc-hA_{2A}AR and increasing concentrations (0.5-100 ng/well) of SNAP-A_1AR cDNA, and empty vector (pcDNA3.1) was used to maintain the concentration of DNA constant in all wells. Saturation binding data presented was baseline-corrected by subtracting BRET values measured from cells treated with furimazine only. The data displayed represents mean ± SEM of one representative experiment from n = 4 experiments, which were performed in triplicate.

To further assess its subtype selectivity, fluorescent ligand **4.46a** was therefore assessed for its ability to antagonise the NECA-mediated cAMP accumulation in FlpIn-CHO cells expressing either of hA_{2A}AR, hA_{2B}AR and hA_3AR. It was reasoned that if the affinity of **4.46a** for the other AR subtypes measured in the NanoBRET saturation assay was "true affinity", one would expect to measure comparable affinity values in this functional assay. At the hA_{2A}AR and hA_{2B}AR **4.46a** caused a small but significant

rightward shift of NECA concentration response curve only at the highest concentration tested (1 μM) (**Figure 4.5**), with no detectable effect at the hA_3AR. Therefore, the estimated affinity of **4.46a** for each of the adenosine receptor subtypes, quantified using the Gaddum equation as previously described, was relatively low (pK_D $hA_{2A}AR$ = 6.11 ± 0.08, pK_D $hA_{2B}AR$ = 6.16 ± 0.07, pK_D hA_3AR < 6, n = 3)[150,306] compared to that observed from the NanoBRET assay (**Figure 4.3** and **Table 3.3**). Taken together, this functional data with the results obtained in the NanoBRET A_1AR-$A_{2A}AR$ dimerization study (**Figure 4.4**) suggested that the small BRET signal detected with **4.46a** in HEK293 cells expressing NanoLuc-$hA_{2A}AR$ and NanoLuc-$hA_{2B}AR$ may reflect BRET between **4.46a** bound to endogenous hA_1ARs and the transfected NanoLuc-tagged A_2AR receptors as a result of oligomerisation. The lower binding affinity obtained for **4.46a** in cells expressing NanoLuc-$hA_{2A}AR$ and NanoLuc-$hA_{2B}AR$, compared to NanoLuc-hA_1AR, would be consistent with negative allosterism across oligomeric receptor interfaces.[166]

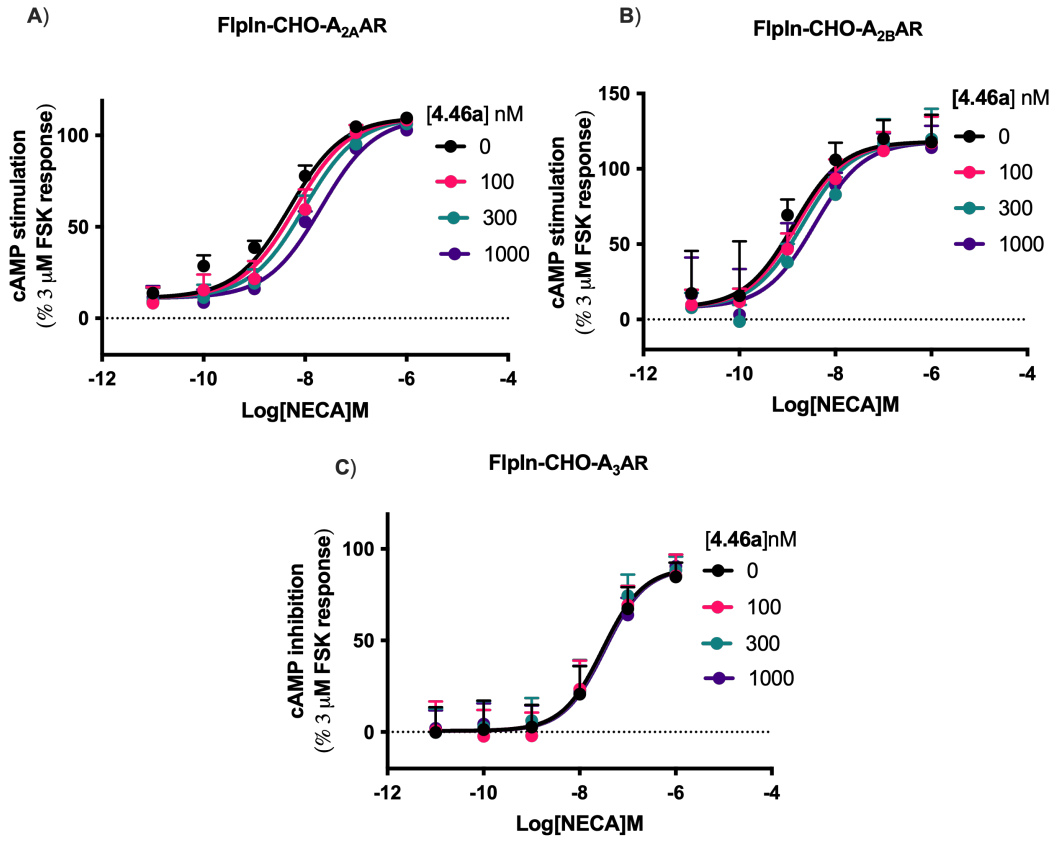


Figure 4.5 Stimulation of cAMP accumulation (**a** and **b**) or inhibition of forskolin-stimulated cAMP accumulation by NECA in the absence (0 nM) or presence of

increasing concentration of probe **46a**. Data are presented as percentage of cAMP accumulation normalized to the response mediated by 3 μM forskolin, (100%) or buffer (0%) alone (**a** and **b**) and (0%) or buffer (100%) alone (**c**). Each data point represents the combined mean value ± SEM of n = 3 separate experiments each of which was performed in triplicate.

The ability of fluorescent ligands **4.44a**, **4.46a** and **4.44b** (**Scheme 4.3**) to retain functional antagonism at the hA_1AR was also examined. This was performed in FlpIn-CHO cells stably expressing the hA_1AR. All three fluorescent probes demonstrated to be competitive antagonists at the A_1AR, causing a parallel rightward shift of the NECA response curve in a concentration dependent manner (**Figure 4.6**). From this data we performed Schild regression analysis and the pK_B value for each of the probe tested was calculated (Table 4.4). All three probes **4.44a**, **4.46a** and **4.44b** retained a functional antagonism activity at the hA_1AR comparable to the parent Tonapofylline[83] and DU172.[36] Moreover, the functional affinity (pK_B) measured for each of the fluorescent ligands was in agreement with the binding affinities measured in the same cell line (hA_1AR-FIpInCHO) by radioligand binding experiments.

Table 4.4 pK_B Values of Fluorescent Analogues 44a, 46a and 44b

cmpd	h**A$_1$AR pK_B**[a]	n
4.44a (BY630/650)	9.75 ± 0.11	3
4.46a (BY630/650)	8.72 ± 0.02	3
4.44b (SulfoCy5)	7.12 ± 0.12	4

[a]Affinity of the fluorescently-labelled antagonists 44a, 46a and 44b measured from the antagonism of the forskolin-stimulated inhibition of the cAMP accumulation in hA_1AR-FIpInCHO cells. Schild slopes were 1.14, 1.22 and 0.89 for 4.44a, 4.46a and 4.44b, respectively. Data represent mean value ± SEM of n separate experiments, where each experiment was performed in duplicate.

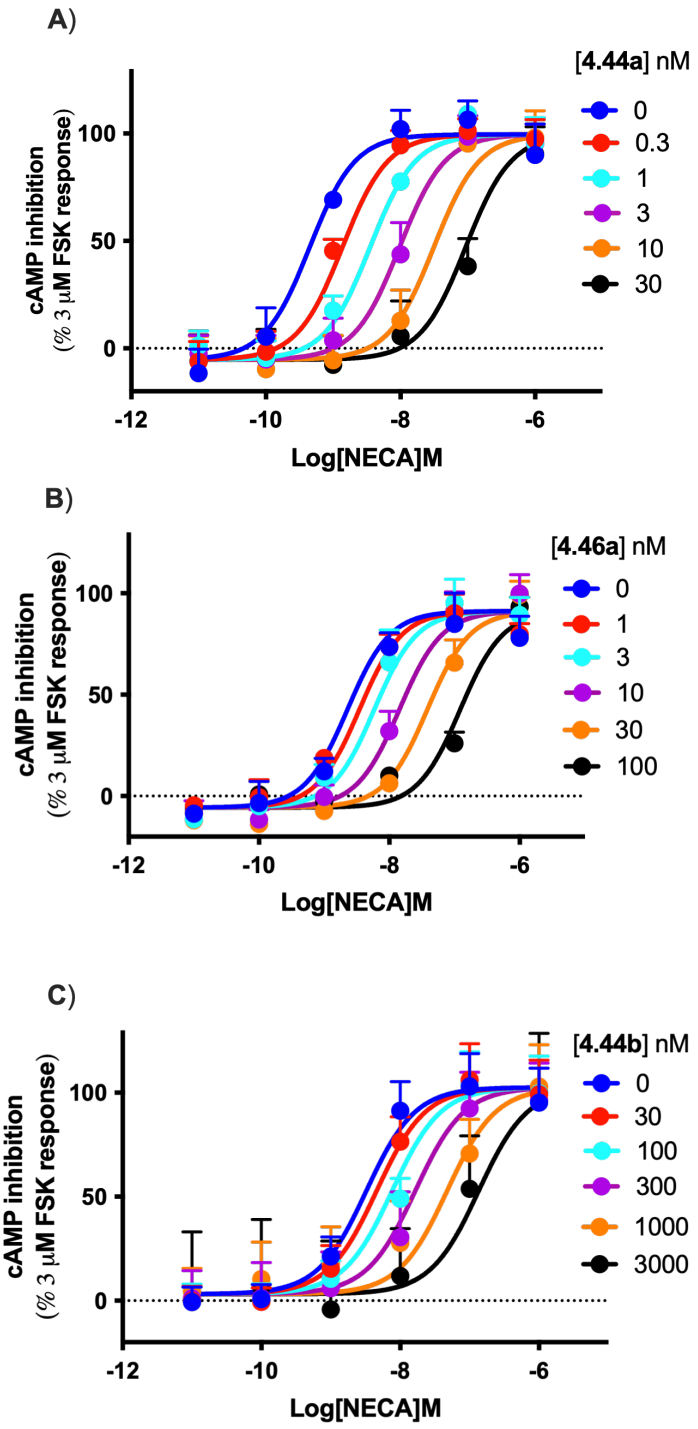


Figure 4.6 Effect of antagonists **4.44a** (A), **4.46a** (B) and **4.44b** (C) on the NECA-mediated inhibition of forskolin-stimulated cAMP accumulation. hA$_1$AR-FIpInCHO cells were stimulated with increasing concentrations of NECA in the absence and presence of increasing concentrations of the fluorescent antagonist Data have been presented as percentage of cAMP accumulation in response to 3 μM forskolin (0%) or buffer (100%) alone. Each data point represents the combined mean ± SEM from *n* separate experiments (*n* = 3 for **4.44a** and *n* = 3 for **4.46a**, *n* = 4 for **4.44b**) performed in duplicate.

The kinetics of ligand-receptor binding is emerging as powerful pharmacological paradigm for predicting the efficacy of drug candidates in vivo.[249,307] Accordingly, the availability of chemical probes and techniques which allow real-time monitoring of the rate at which a drug binds to its biological target (k_{on}) and dissociates from it (k_{off}) are therefore of great utility.[126,237,246] A recent study, which was focused on the real-time monitoring of ligand-binding kinetics at the hA_3AR expressed in living cells, has shown that the kinetics of the labelled probe can influence the kinetic parameters of the unlabelled ligands under investigation, suggesting that a labelled probe should be chosen with regard to its adequate kinetic profile for the given study.[278] In this regard, the ligand-binding kinetics of fluorescent ligands **4.44a**, **4.44b** and **4.46a** were monitored by NanoBRET ligand-binding kinetic assay in HEK293A cells transiently expressing the NanoLuc-hA_1AR. The kinetic parameters of each fluorescent probe were quantified by measuring the observed association constant (k_{obs}) at four concentrations of fluorescent probe over a time frame of 1 h. The specific BRET signal for each fluorescent probe was calculated after subtraction of the nonspecific binding, defined using 1 μM of unlabelled antagonist SLV320, from the total binding component at each time point (**Figure 4.7**). The kinetic parameters k_{on}, k_{off} and pK_D, along with the calculated residence time ($1/k_{off}$) were measured by globally fitting the resulting BRET data (**Table 4.5**).

Table 4.5. Kinetic Parameters of Fluorescent Analogues 4.44a, 4.44b and 4.46a Binding to the NanoLuc-hA$_1$AR.

Cmpd	k_{on} (x10^6 M^{-1}min^{-1})	k_{off} (min^{-1})	RT (1/ k_{off}) (min)	Kinetic pK_D (LogM)	Saturation pK_D (LogM)
4.44a	17.90 ± 3.69	0.054 ± 0.009	19.7 ± 3.7	8.51 ± 0.18	8.93 ± 0.02
4.44b	0.86 ± 0.13	0.117 ± 0.016	9.0 ± 1.0	6.86 ± 0.03*	7.35 ± 0.09
4.46a	3.60 ± 0.90	0.046 ± 0.008	23.8 ± 3.9	7.88 ± 0.04*	8.50 ± 0.07

The Kinetic parameters k_{on}, k_{off} and pK_D were calculated by monitoring the specific BRET signal of four concentrations of fluorescent ligand every 30 s for 1 h at 37 °C. The residence time (RT) was calculated from the reciprocal of the k_{off} value and the pK_D was derived from the negative logarithm of the kinetic K_D. The values listed represent the mean ± SEM of n = 3 performed in triplicate. *p < 0.05, kinetically derived pK_D versus equilibrium saturation derived pK_D value, Student's unpaired t-test.

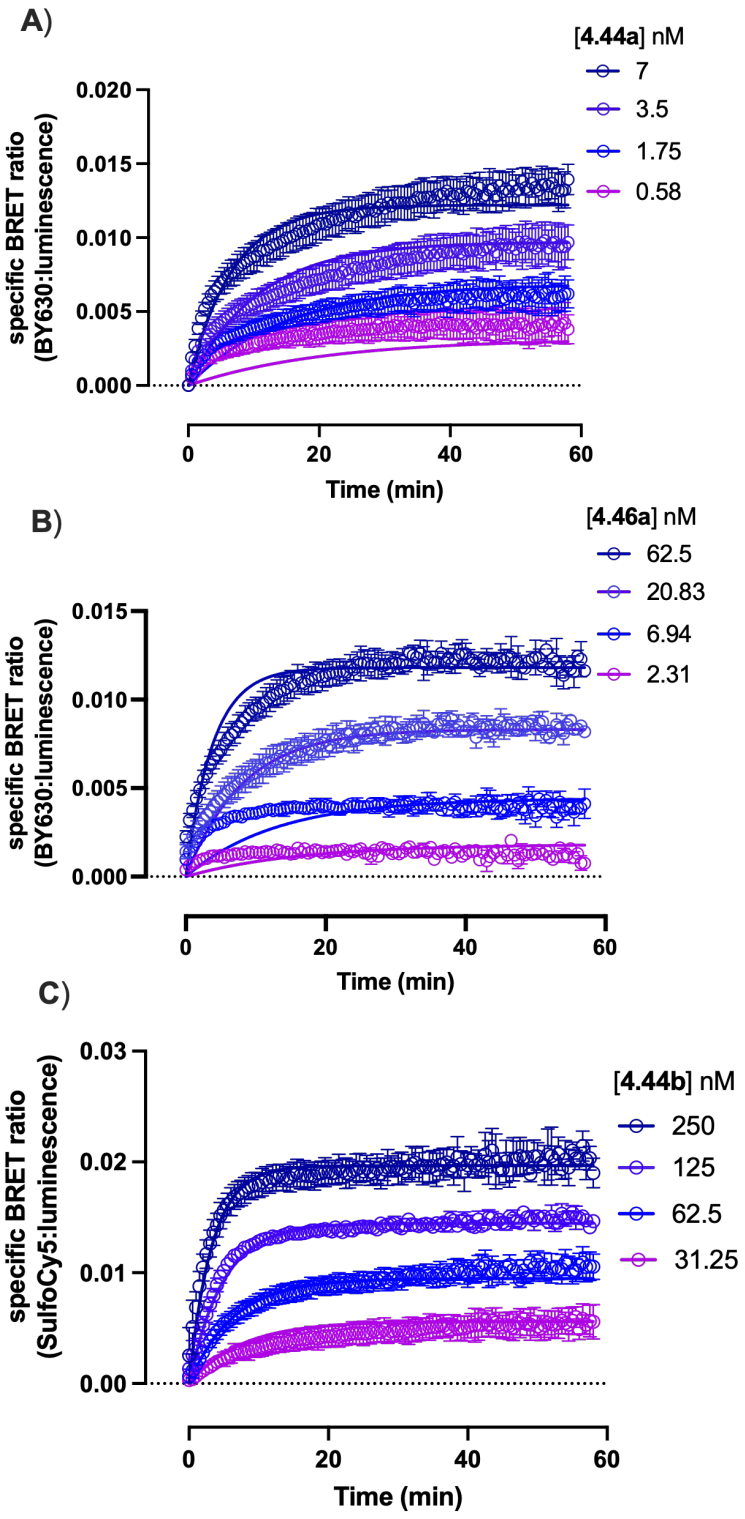


Figure 4.7 NanoBRET association binding kinetic curves of specific **4.44a** (A), **4.46a** (B) and **4.44b** (C) binding to NanoLuc-hA$_1$AR at 37°C. HEK293A cells transiently expressing the NanoLuc-hA$_1$AR were treated with the indicated concentration of fluorescent ligand and the NanoBRET signal was monitored every 30 s for 1 h. Nonspecific binding was determined in the presence of 1 μM SLV320. Each data point represents the combined mean value ± SEM of n = 3 separate experiments performed in triplicate.

These NanoBRET kinetic studies showed that all three fluorescent ligands displayed relatively fast kinetics. Additionally, for probe **4.44a** the pK_D values measured from the kinetic analyses was in agreement with that obtained from saturation ligand binding assays, whilst for **4.44b** and **4.46a** the kinetic pK_D values were significantly lower compared to the saturation pK_D. There were, however, large differences in the measured association rates (k_{on}) between the fluorescent ligands. Specifically, the BY630/650-X-labelled probe **4.44a** exhibited a k_{on} two orders of magnitude faster ($1.79 \pm 3.69 \times 10^7$ $M^{-1}min^{-1}$) than its SulfoCy5-labelled analogue **4.44b** ($8.6 \pm 0.13 \times 10^5$ $M^{-1}min^{-1}$). These two fluorescent analogues differ only by the attached fluorophore moiety, demonstrating the potential of the fluorescent pharmacophore to establish different interactions with the receptor and the nearby environment in a way that affect the observed binding kinetics. This would be consistent with observations described recently for the A_3AR, where in NanoBRET-based kinetic ligand binding studies it has been shown that the fluorophore moiety can not only influence the ligand binding affinity but also the ligand binding kinetics of the fluorescent ligand.[278] Moreover, in an elegant study with the β_2-adrenoreceptor, Sykes et al., showed that the lipophilic nature of some structural motifs in a molecule can influence the observed binding kinetics, dependent on direct interactions between these motifs and the plasma membrane.[308] This could therefore be the case for the BODIPY motif in the fluorescent analogues tested herein.

After having thoroughly characterised the pharmacology of the synthesized fluorescent A_1AR antagonists, it was subsequently investigated the utility of the probes in a broad range of fluorescence-based techniques. For instance, fluorescent analogues **4.44b** and **4.46a** were applied to monitor the ligand binding of unlabelled ligands to the hA_1AR. This was achieved through NanoBRET competition ligand binding assay in HEK293A cells transiently expressing the NanoLuc-hA_1AR. Cells were incubated with the indicated concentration of fluorescent ligand and increasing concentrations of hA_1AR antagonists SLV320, DPCPX and the non-selective agonist NECA. A clear concentration dependent inhibition of the BRET signal was observed for all the compounds tested (**Figure 4.8**), allowing for the relative

half-maximal inhibitory concentrations (IC_{50}) to be measured. These values were converted to the corresponding inhibitory constant (K_i) by means of the Cheng-Prusoff equation and are listed in **Table 4.6**.

Table 4.6 Binding Affinities of A_1AR ligands Measured by NanoBRET competition Ligand binding Assay and Affinities Reported in the Literature.

	4.44b (Sulfo-Cy5)	**4.46a (BY630/650)**	
	pK_i (LogM) ± SEM[d]		pK_i(literature)
SLV320	9.15 ± 0.07	8.85 ± 0.07	9 [a]
DPCPX	8.13 ± 0.05	7.68 ± 0.01	7.4-9.2 [b]
NECA	6.40 ± 0.10	5.96 ± 0.06	5.3-8.2 [c]

[a] Reported binding affinities.[55] Value determined in radioligand binding experiments in hA_1AR-CHO-K1 cells using [^{3}H] DPCPX.[309] [b]Values determined in radioligand binding experiments in A_1AR-COS-7[274] or hA_1AR-CHO-K1 cell membranes[275,276] or whole cells[277] using [^{3}H] DPCPX. [c] Values determined in radioligand binding experiments in cells expressing the wild type hA_1AR using [^{3}H] DPCPX[276,310,311] or [^{3}H]R-PIA[312]. [d]Measured pK_i in NanoBRET competition binding experiments in whole NanoLuc-hA_1ARHEK293A cells using the fluorescent ligand indicated. Values are mean ± SEM of n = 3 experiments performed in duplicate.

NanoBRET competition binding assays with fluorescent ligands **4.46a** and **4.44b** and the unlabelled competing A_1AR ligands yielded pK_i values that were comparable to the reported literature values measured by radioligand binding assays (R^2 = 0.95 using **4.46a**; R^2 = 0.94 using **4.44b;** (Figure S1 (Appendix I) (A) and (B)) and comparable to those measured in NanoBRET binding assays by Stoddart at al.,[165] and Cooper et al.[49] Overall, the pK_i values measured using both fluorescent probes were also comparable (R^2 = 0.99 **4.44b** vs. **4.46a**, Figure S1 (C)).

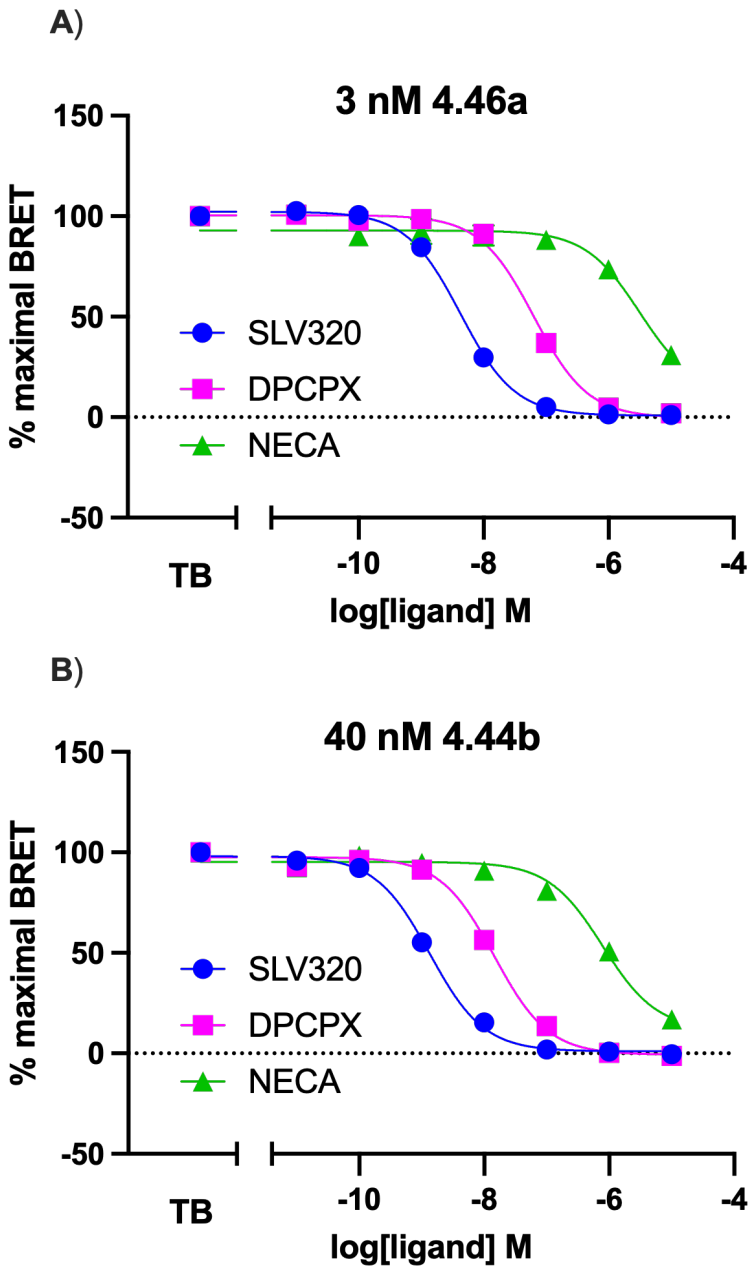


Figure 4.8 Displacement of 3 nM **4.46a** (A) and 40 nM **4.44b** (B) by unlabelled A_1AR antagonists SLV320 and DPCPX, and agonist NECA in HEK293A cells transiently expressing the NanoLuc-hA_1AR. The reduction of BRET signal was monitored as a function of increasing concentration of competing ligand. Data was normalized to maximal BRET signal in the absence of unlabelled competing ligand (total binding, TB). Each data point represents the combined mean ± SEM from n = 3 experiments performed in duplicate.

To further expand the utility of the novel synthesized probes, it was explored whether fluorescent probes **4.44a**, **4.46a** and **4.44b** would allow visualization of the hA_1AR expressed at the plasma membrane of living cells. To be suitable for imaging studies, a fluorescent ligand must possess adequate properties, showing specific binding of the target protein at the cell surface coupled with both low levels of non-specific membrane incorporation and diffusion into the cell cytosol. To this end, confocal microscopy studies of fluorescent analogues **4.44a**, **4.46a** and **4.44b** were performed in HEK293A cells transiently transfected with the engineered SNAP-tagged human A_1AR.

The equatorial images acquired with the confocal microscope (**Figure 4.9**) revealed high levels of fluorescent labelling of the SNAP-tagged-hA_1AR localized at the cell membrane for all the three red-shifted fluorescent probes tested. Moreover, preincubation of the cells with 10 μM of unlabelled A_1AR antagonist SLV320 prevented the binding of the fluorescent probes to the SNAP-tagged hA_1AR causing a reduction of fluorescence. This demonstrated that the binding of the probes was specific at the SNAP-tagged-hA_1AR localized at the cell membrane. Furthermore, when non-transfected (NT) HEK293 cells were treated with probes **4.44a**, **4.46a** and **4.44b**, under the same experimental conditions as the SNAP-tagged-hA_1AR HEK293 cells, no fluorescence signal was detected, further confirming the specificity of these fluorescent antagonists for binding to the hA_1AR and their low levels of non-specific binding (Figure S3, Appendix I)

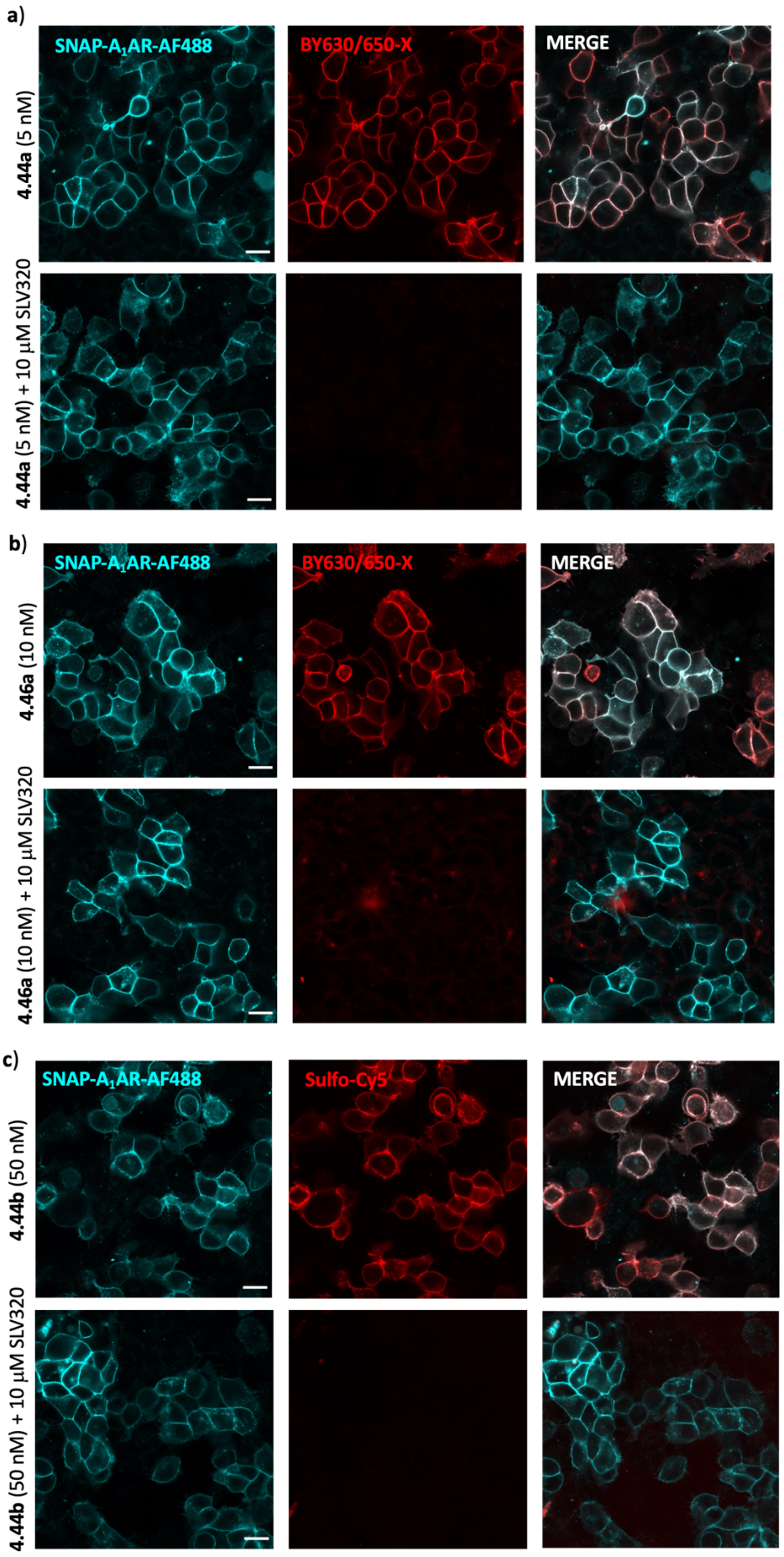

a)
SNAP-A1AR-AF488
BY630/650-X
MERGE
4.44a (5 nM)
4.44a (5 nM) + 10 µM SLV320
b)
SNAP-A1AR-AF488
BY630/650-X
MERGE
4.46a (10 nM)
4.46a (10 nM) + 10 µM SLV320
c)
SNAP-A1AR-AF488
Sulfo-Cy5
MERGE
4.44b (50 nM)
4.44b (50 nM) + 10 µM SLV320

Figure 4.9 Live cell confocal imaging studies of fluorescent analogues **4.44a** (5 nM) (**A**), **4.46a** (10 nM) (**B**) and **4.44b** (50 nM) (**C**) binding to SNAP-tagged human A_1AR expressed in HEK293 cells in the absence (top frames) or presence (bottom frames) of 10 μM unlabelled A_1AR antagonist SLV320. Cells were treated with BG-Alexa Fluor 488 for 30 min at 37 °C to label the SNAP-tag on the N-terminus of the A_1AR (left hand frames). Middle frames show fluorescent labelling of SNAP-tagged-hA_1AR by the red-shifted fluorescent analogues tested at the given concentration. The images presented here are representative of images captured in three independent experiments. Scale bar = 15 μm

Lastly, it was explored the suitability of the most hA_1AR selective probes reported here for single-molecule fluorescence microscopy. To this end, the Sulfo-Cy5-labelled ligand **4.44b** and the BODIPY-630/650-X-labelled ligand **4.46a** were used in Total Internal Reflection Fluorescence Microscopy (TIRF-M) to probe receptor distribution at the plasma membrane of living HEK293 cells transiently expressing the SNAP-tagged hA_1AR. TIRF-M is a wide-field imaging method that allows for the visualization of molecule localization and organisation on the surface of living cells with high spatial and temporal resolution.[121,313,314] Imaging living cells with fluorescent antagonist **4.44b** allowed for the detection of the SNAP-hA_1AR as single red fluorescent spots localized at the plasma membrane (**Figure 4.10a**). The location of the red fluorescent spots correlated with the green fluorescent spots of AF488-labelled SNAP-hA_1AR as shown in **Figure 4.10a**. Moreover, preincubation of the cells with 10 μM SLV320 prevented the visualization of SNAP-hA_1ARs by probe **4.44b**, further validating the specificity of probe **4.44b** (bottom frames, **Figure 4.10a**). While it was found that fluorescent antagonist **4.44b** had a high signal-to-noise ratio for single-molecule microscopy applications, fluorescent antagonist **4.46a** showed reduced performances. Indeed, when **4.46a** was used in TIRF-M experiments, it was not possible to distinguish the same localisation patterns as the AF488-labelled SNAP- hA_1AR (Figure S2, Appendix I). The BY630/650 moiety increases the lipophilicity of the fluorescent conjugate and might allow probe **4.46a** to stick either to the plasma membrane of the cell or to the glass coverslip surface, resulting in higher background signal in this particular microscopy approach.

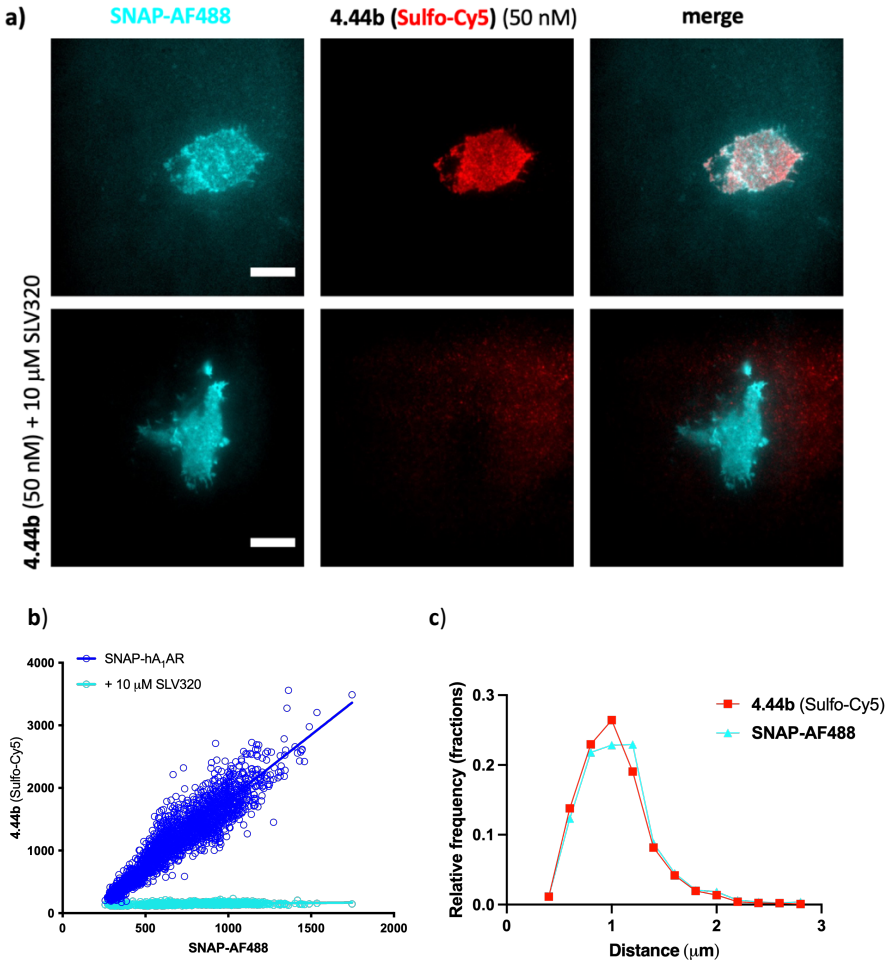


Figure 4.10 Fluorescent ligand **4.44b** (50 nM) allowed the visualization of the organisation of SNAP-tagged-hA$_1$AR localised at the plasma membrane of living HEK293 cells by Total Internal Reflection Fluorescence Microscopy (TIRF-M) in the absence (top frames) or presence (bottom frames) of 10 µM unlabelled A$_1$AR selective antagonist SLV320. **A)** Cells were labelled with 0.2 µM BG-Alexa Fluor 488 dye for 30 min at 37 °C (left hand frames). Top middle frame shows the labelling of SNAP-hA$_1$AR by probe **4.44b** (Sulfo-Cy5) at the given concentration. Bottom middle frame shows that pre-treatment of the cells with high concentration (10 mM) of A$_1$AR selective antagonist SLV320 prevents the binding of fluorescent ligand **4.44b** to the hA$_1$AR. Right hand frames represent merged green (AF488) and red (Sulfo-Cy5) channels **B)** Plot of fluorescence intensities of Sulfo-Cy5-labelled (**4.44b**) spots versus AF448-labelled spots, in the absence (blue) or presence (cyan) of 10 µM SLV320. **C)** Distribution of the nearest neighbour distances between single SNAP-hA$_1$ARs labelled with probe **4.44b** (red) and the BG-Alexa Fluor 488 (cyan). The images reported here are representative TIRF-M images from three independent experiments, each of which included the analysis of 14 to 18 cells. The data reported in graph **B)** and **C)** is the average of data analysed from 14 to 18 cells in a single representative experiment of three independent experiments. Scale bar = 12 µm.

4.4 Conclusions and Future Work

The study presented in this Chapter discussed the successful design, synthesis and pharmacological evaluation of a series of novel, high affinity and subtype-selective fluorescent probes for the study of human A_1AR in living cells. It has been demonstrated that both positions of the prototypical xanthine scaffold, namely the 3- and 8-positions could be harnessed for linker/fluorophore functionalisation. Additionally, modifications at both positions yielded fluorescent probes that retained binding affinity and functional activity at the hA_1AR. Overall, a good selectivity profile for the probes synthesized was observed, with the SulfoCy5-bearing probe **4.44b** and the BY630/650-X-bearing probe **4.46a** displaying the best selectivity profile for the hA_1AR compared to the other adenosine receptors. To the best of our knowledge, probes **4.44b** and **4.46a** represent the first examples of subtype-selective fluorescent hA_1AR antagonists reported to date.

Furthermore, fluorescent antagonists **4.44b** and **4.46a** were successfully applied to monitor ligand binding of known A_1AR ligands by the recently described NanoBRET ligand binding assay, demonstrating that these probes can be used as alternatives to radioligands. Confocal microscopy studies showed that fluorescent analogues **4.44a**, **4.46a** and **4.44b** could be applied to visualize the hA_1AR expressed at the membrane of living cells as demonstrated by the high degree of fluorescence intensity observed at the plasma membrane. The binding of the probes could be prevented by incubating the cells with a high concentration of non-fluorescent A_1AR antagonist, demonstrating the specificity of the binding of the probes to the SNAP-tagged-hA_1AR with very little non-specific cellular uptake detected across all the compounds tested.

Finally, the Sulfo-Cy5-labelled probe **4.44b** was successfully combined with TIRF microscopy to map hA_1AR distribution at the plasma membrane of HEK293 cells, suggesting that probe **4.44b** could be coupled with advanced microscopy techniques for the study of the spatial organization of A_1ARs at the plasma membrane of living cells. Remarkably, despite the introduction of the Sulfo-Cy5 fluorescent tag causing a reduced affinity for the hA_1AR compared to the corresponding BY630/650-labelled analogues,

it was found that the Sulfo-Cy5-labeleld probe (**4.44b**) proved as specific and effective as the BY630/650-labelled analogues (**4.44a** and **4.46a**) and possessed even superior physicochemical properties for single-molecule microscopy applications. These results highlight the importance of developing small-molecule probes labelled with dyes of different physicochemical properties and that the characterization and selection of these probes should not be merely based on their apparent binding affinity for the target protein under investigation, but, principally, for the specific biological application.

Future applications of the probes described in this Chapter, which have not been explored yet, include the study of the molecular pharmacology of A_1AR expressed in native cells and tissues, such as cardiomyocytes, cortical and/or spinal cord neurons.[315] For instance, owing to the therapeutic potential of targeting A_1AR in the treatment of neuropathic pain[35,105]it would be exciting to combine probes **4.44b** and/or **4.46a** with more advanced imaging techniques such as FCS[253] and super resolution microscopy to visualize specific localisation and organization of single A_1ARs expressed in native nociceptive neurons under normal health and pathological conditions (e.g. neuropathic pain) and study possible differences in receptor functions and dynamics between the two phenotypes. Thus, a better understanding of A_1AR-mediated analgesia, at molecular level, in these systems may provide new insights to facilitate the development of new non-opioid analgesic drugs.[35,316] Notwithstanding, to improve the translational potential of these fluorescent ligands, it would be also optimal to determine their equilibrium and kinetic parameters in rodents (mice and rats) A_1AR in order to account for possible interspecies differences.[49,115]

In summary, the work presented in this chapter expands the available fluorescent A_1AR ligand toolbox. The novel probes reported herein were thoroughly characterised, displayed improved A_1AR pharmacology and were amenable to a broad range of fluorescence-based techniques. We envisage that these novel A_1AR fluorescent probes will be valuable pharmacological tools to the wider scientific community to aid in understanding of the molecular mechanisms underlying A_1AR pharmacology in health and disease.

Chapter 5. Ligand-directed Labelling of the Human Adenosine A_1AR Receptors with Fluorescent Probes in Living Cells

5.1 Brief Introduction

The study of proteins function and dynamics in their native cellular environment is essential for progressing fundamental science, which can potentially benefit through advancement of a more selective and efficient therapeutic interventions. Over the past two decades scientists have made enormous progress in tackling the challenges associated with the complexity of cellular systems, by developing new technologies to allow the study of proteins in their native cellular settings, such as in live cells or *in vivo*.[200,317] In the context of GPCR research for example, the genetic fusion of a fluorescent protein tag such as green fluorescent protein (GFP) or self-labelling tag proteins such as SNAP-tag and Halo-tag as well as fluorescently-labelled antibodies have revolutionised the ways by which GPCR localisation, dynamics and functions can be monitored.[139] Although powerful, these techniques possess some limitations: the tag size and the need to genetically engineer the protein to express the tag moiety may disturb or alter the native functions of the protein, thereby introducing artefacts that can cause misinterpretation of biological data. Moreover, these methods cannot be readily applied for studies in endogenous expressing systems.[139,199] Fluorescent ligands offer an alternative and powerful avenue to investigate real-time function of receptors in their native cellular environments.[126] Yet, the inherent, reversible nature of ligand binding may still hamper the extent by which many temporal and spatial aspects of GPCR pharmacology can be investigated.[140] In this regard, Ligand-Directed (LD) chemistry[196,197] has most recently emerged as a complementary, bioorthogonal approach for labelling native proteins, whereby an affinity "guide" ligand for the protein of interest is conjugated to a reporter functional group via an electrophilic reactive linker; upon ligand binding, the close proximity of this electrophilic region with a nucleophilic amino acid side chain in the binding site effectively increases

the rate of the substitution reaction with the reactive group, resulting in covalent transfer of the chemical probe to the protein. The "guide" ligand therefore acts as a leaving group, which can then freely dissociate and leave the binding site of the protein intact. A schematic illustration of ligand-directed labelling of a GPCR is provided in **Figure 5.1**.

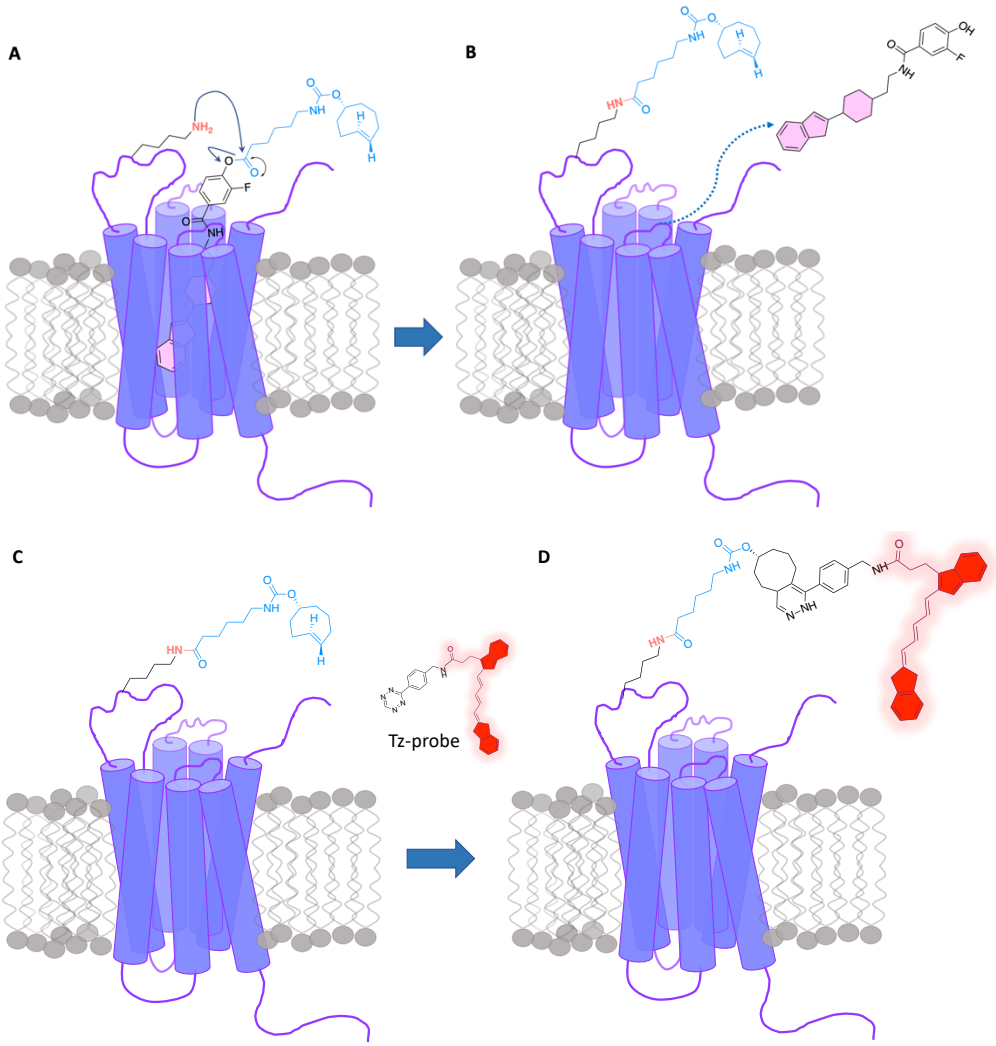


Figure 5.1 Schematic representation of ligand-directed labelling of a GPCR. **A**) Upon ligand binding, the electrophilic carbonyl group undergoes nucleophilic attack by a nucleophilic lysine side chain in proximity to the binding site; **B**) the functional probe (here represented by a strained alkene) is covalently attached to the receptor and the affinity "guide" ligand freely dissociates (dashed line) leaving the binding site available; **C**) Upon addition of a tetrazine-conjugated probe (Tz-probe), the labelled alkene group selectively undergoes an inverse electronic demand Diels-Alder (IEDDA) reaction forming the labelled cycloadduct **D**)

More recently, the utility of ligand-directed technology for labelling membrane receptors in living cells has been also described for three

GPCRs, the bradykinin B2 receptor,[204] the μ opiod[212] and the adenosine $A_{2A}AR$[213] receptors. In the study presented herein, we expand this method to another GPCR, by describing the rational design of chemical probes capable of covalently transferring a functional moiety to a nucleophilic residue on the hA_1AR in living cells by exploiting the ligand-directed chemistry approach.

5.2 Rational Design of A_1AR Ligand-directed Labels

To develop ligand-directed probes capable of labelling the A_1AR in living cells, we sought to perform a small and focused SAR study around known xanthine scaffolds (**Figure 5.2.2**), whereby different reactive groups as well as their introduction in different positions of the affinity ligand were evaluated to guide the efficient and selective transfer of a functional probe of choice into the targeted A_1AR, owing to the bound molecule's reactive centre's proximity to a nucleophilic amino acid side chain close to the ligand binding site.

From the available structural information,[34,36,37] it was possible to identify several nucleophilic amino acid residues located in the extracellular vestibules of the A_1 receptor; these comprised of lysine residues $K168^{ECL2}$, $K173^{ECL2}$, $K275^{ECL3}$ and tyrosine $Y271^{7.36}$ as potential targets for our ligand-directed chemistry approach (**Figure 5.2.1**). It is noteworthy that although the availability of structural information is of great advantage to guide the design of the targeted ligands, structural data only represents a static snapshot of one conformation of the receptor, which can only provide limited insights into the dynamics of binding, in particular when targeting residues located in a highly dynamic domain of the protein, such as the extracellular loop region.

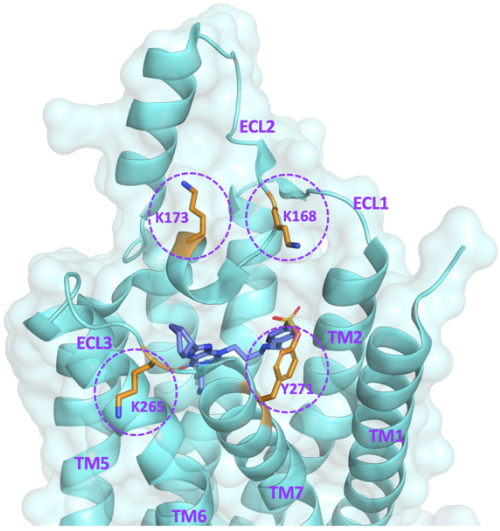


Figure 5.2.1 Crystal structure of the hA$_1$AR in complex with the orthosteric covalent antagonist DU172 coloured deep blue (PDB = 5UEN).[288] The structure is shown as combined ribbon and surface coloured aquamarine and is depicted focusing on the extracellular domains of the protein. The targeted surface-exposed nucleophilic amino acid residues are labelled and shown in sticks, coloured orange. The transmembrane (TM) helices TM1-TM7 are labelled for clarity alongside extracellular loop (ECL) 2, ECL1 and ECL3. Image was generated using PyMOL (2.2.0).

Based on this knowledge, and previous successes for the design of reversible subtype-selective fluorescent A$_1$AR ligands (**Chapter 4**),[318] we focused on exploring the *N*3 and C8 positions of the prototypical xanthine scaffold for linker and functional probe derivatization. Indeed, reported SAR studies suggested that modification of both positions could yield high affinity and selective A$_1$AR ligands and, most importantly, conjugation with a fluorescent moiety led to molecules with retained ligand binding abilities for the targeted receptor (**Chapter 4**).[295] Furthermore, selective high affinity irreversible A$_1$AR antagonists, designed upon modification of both *N3*[268,288] and C8[319,320] positions of the xanthine scaffold, have been also reported and successfully applied as pharmacological tools (**Figure 5.2.2**). For example, DU172, also reported as compound **23a**,[288] is a *N*3-substituted xanthine analogue bearing a 4-fluorosulfonyl reactive moiety, which establishes a covalent bond with Y271, as shown in its co-crystal structure with the human A$_1$AR.[36] *m* or *p*-DITC-XAC[319,320] are irreversible analogues of XAC[185] integrating an electrophilic isothiocyanate group in the aromatic ring distal to the xanthine core. When these latter molecules were

first described and characterised, neither structural information nor sequence analysis were available for the targeted A_1AR.[15] With the structural knowledge available today, one could identify $K168^{ECL2}$ or $K173^{ECL2}$ as potential nucleophilic residues engaged by these XAC-based irreversible analogues.

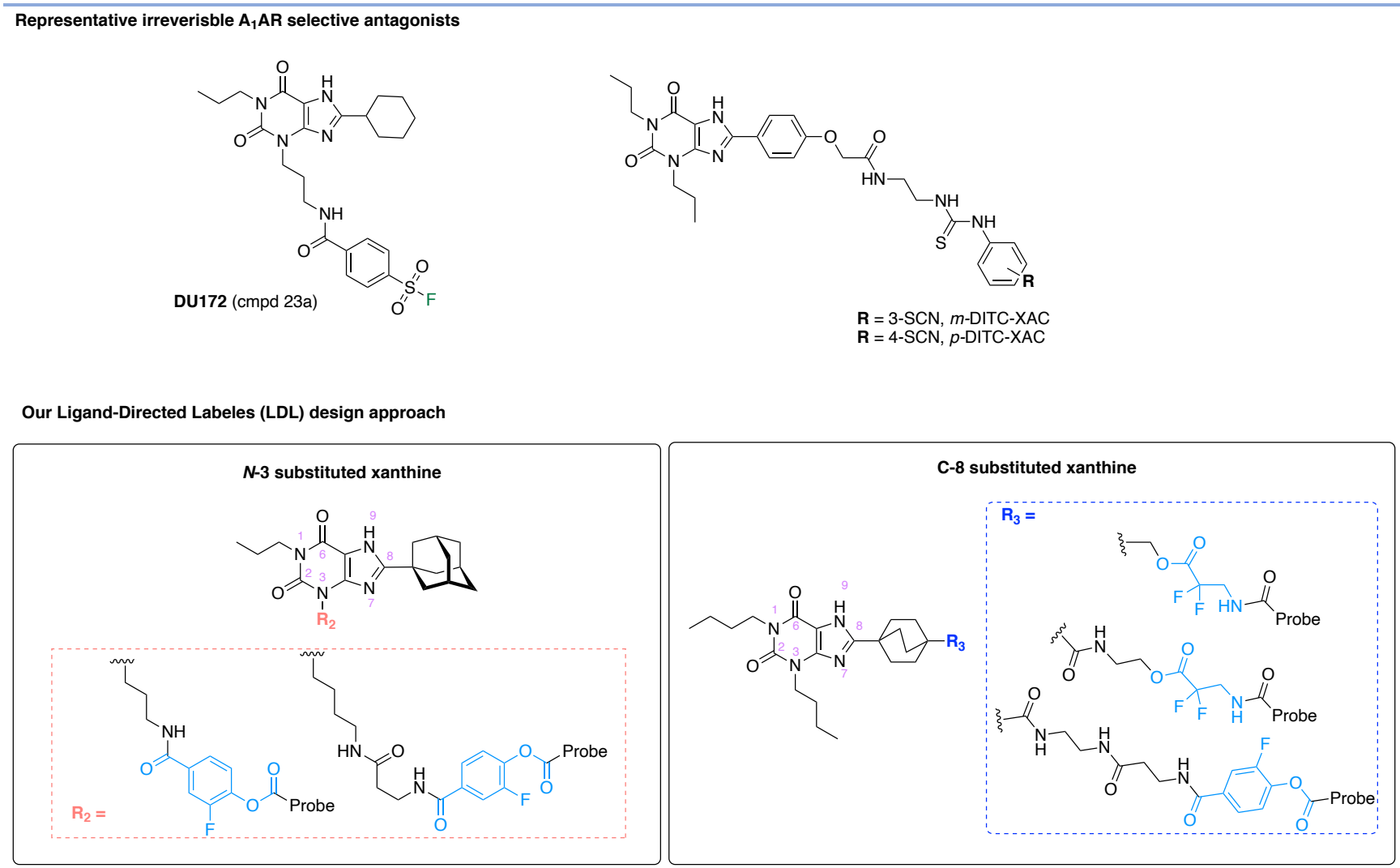


Figure 5.2.2 Examples of representative irreversible A_1AR antagonists and schematic summary of the design strategy adopted for the development of A_1AR ligand-directed probes. Reactive groups are drawn coloured blue.

A phenyl ester reactive group substituted with a fluorine atom, the most electronegative element, at the 3-position of the phenol ring (**Figure 5.2.2**) has been successfully employed for the development of subtype-selective ligand-directed labels for the $hA_{2A}AR$.[213] Moreover, the fluoro-substituted phenyl ester reactive group displays improved properties compared to reported ligand-directed labelling approaches.[207,321] These include smaller size, higher reactivity towards nucleophilic addition, with the possibility of tuning the reactivity of the ester by the removal or introduction of additional electron-withdrawing fluorine atoms into the phenyl ring, in addition to be a readily available building block which can be easily incorporated into specific ligands for a protein under investigation. Accordingly, the 3-fluorophenyl ester moiety was selected and introduced as chemoreactive group between the orthosteric moiety (guide ligand) and the functional probe of the A_1AR ligand-directed labels, with the phenyl ester constituting part of the orthosteric binding moiety.

Molecular modelling studies with C8 substituted xanthines showed that key interactions between $K265^{ECL3}$ and groups in close proximity to the bicyclic ring could be also established, indicating the potential of incorporating reactive groups also in this region of the binding pharmacophore. To retain the proximity effect with the targeted nucleophilic residue, this approach warranted the introduction of a smaller and more flexible reactive group compared to the phenyl ester moiety. It was envisaged that introduction of a β-alanine substituted with geminal α,α-fluorines would provide sufficient flexibility and reactivity for the labelling reaction to occur, in addition to being a structural modification that could be tolerated by the scaffold, according to reported SAR studies.[83] The utility of fluorinated amino acid residues has been extensively described and they have become increasingly prominent in peptide chemistry[322] and drug design applications.[323,324] In addition, it has been reported that α,α-difluoro-β-alanine esters easily undergo aminolysis with amines under neutral conditions at rt[325] and the estimated neutral hydrolysis of perfluorinated esters is 10^7 faster than the neutral hydrolysis of unsubstituted esters (e.g ethyl acetate).[326] Moreover, reported synthetic procedures demonstrated

that this ester moiety could be easily accessed[327,328] and integrated in the desired ligand-directed probe, without the occurrence of self-reactive intramolecular side reactions.[329]

Overall, a focused library of 15 ligand-directed probes for the A_1AR were designed and synthesised encompassing linkers of various lengths with the aim to identify the most optimal ligand-directed label to allow selective and efficient transfer of a functional small probe onto the receptor (**Figure 5.2.2**). Moreover, to expand the scope of their biological application, these novel labelling reagents were functionalised with chemical probes displaying different physico-chemical properties, including SulfoCy5 fluorophore, biotin and strained alkenes (*trans*-cyclooctene, TCO) and alkynes (bicyclooctyne, BCN).

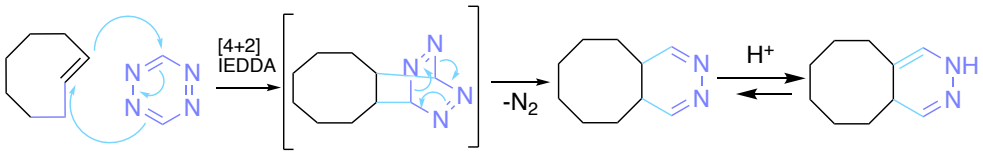


Figure 5.2.3 Schematic representation of the inverse-electron demand Diels-Alder [4+2] cycloaddition mechanism between a strained alkene (dienophile) and a 1,2,4,5-tetrazine (diene) to yield a 4,5-dihydropyridazine product upon loss of N_2. This isomerizes to the final 1,4-dihydropyridazine in protic solvents. Image reproduced from Lang, K. et al.[211]

Importantly, TCO and BCN reactive moieties encompass particularly versatile functional groups for ligand-directed chemistries as they undergo fast and selective click reactions with tetrazine-conjugated fluorophores *via* Inverse Electron Demand Diels-Alder (IEDDA) cycloaddition (**Figure 5.2.3**).[330,331] This methodology, in principle, offers the opportunity to use a single ligand-directed probe bearing a reactive handle that can be used for labelling the protein under study with a different range of organic dyes or probes as required.[199,211]

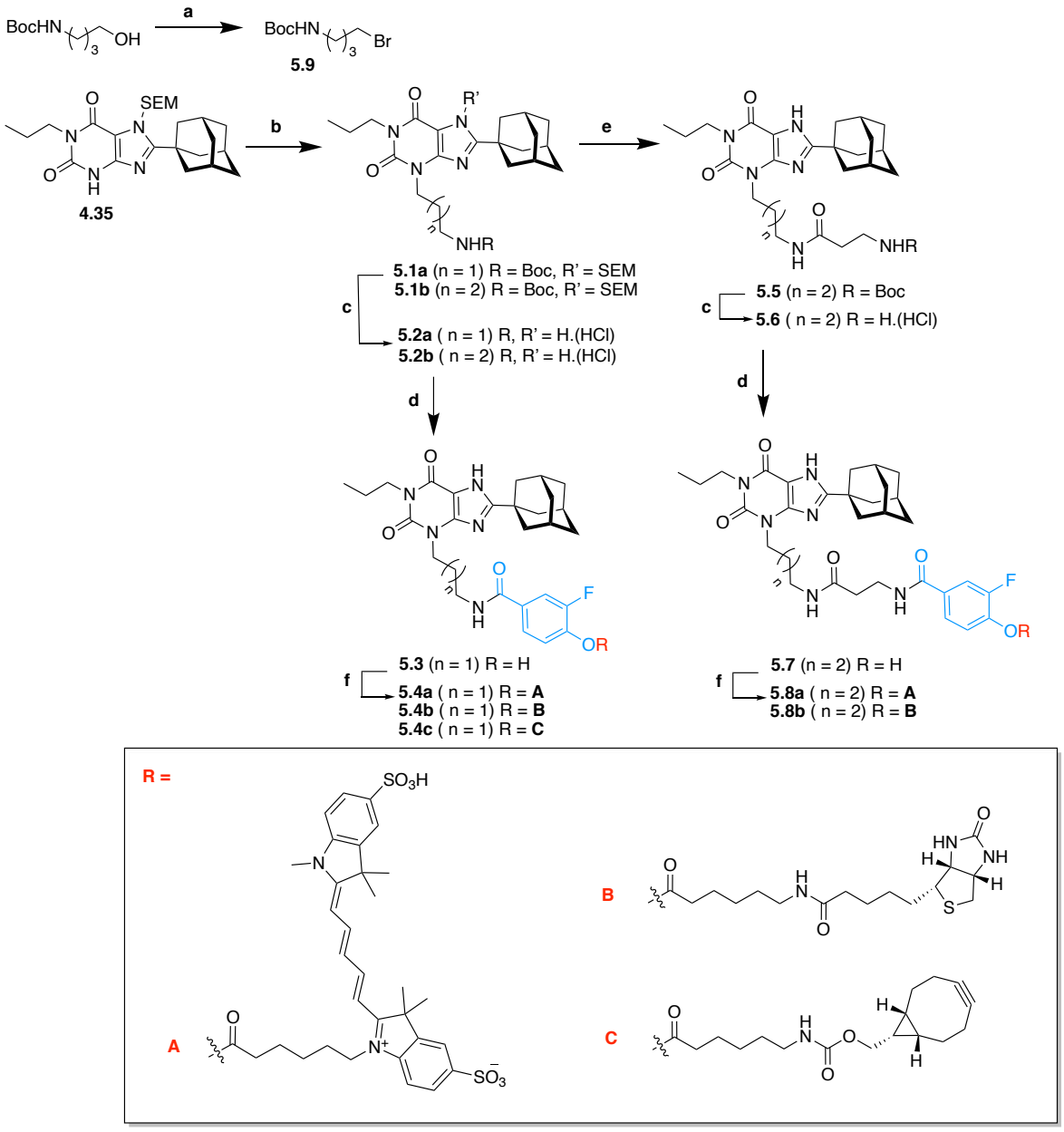
5.3 Results and Discussion

5.3.1 Chemistry

5.3.1.1 Synthesis of 1-propyl-8-(3-adamantyl) xanthine-based ligand-directed probes.

Chemical synthesis of the first series of ligand-directed probes, based on the 1-propyl-8-(3-adamantyl) xanthine scaffold, is outlined in **scheme 5.1**. Intermediate (**4.35**), the synthesis of which is detailed in Chapter 4, was alkylated under basic conditions with commercially available 3-(Boc-amino)propyl bromide or 4-(Boc-amino)butyl bromide (**5.9**) to furnish the corresponding *N*3 propyl (**5.1a**) and *N*3 butyl (**5.1b**) substituted xanthines. 4-(Boc-amino)butyl bromide (**5.9**) was previously prepared from the corresponding commercially available Boc-amino alcohol, following Appel-type reaction conditions.[332] Simultaneous SEM- and Boc-deprotection was achieved upon treatment with 4 M HCl in dioxane to afford amines **5.2a** and **5.2b** as their HCl salts. *N*3 substituted propyl amine **5.2a** was liberated in the presence of DIPEA and was converted to the 3-fluoro-4-hydroxyphenyl intermediate **5.3** upon coupling with commercially available 3-fluoro-4-hydroxybenzoic acid in the presence of COMU at high temperature (90 ^{O}C). Butyl amine **5.2b** was functionalised with Boc-β-alanine in the presence of DIPEA by means of COMU to afford Boc-protected intermediate **5.5**. Acidolytic removal of the Boc protecting group afforded amine **5.6** as its HCl salt, which was subsequently acylated with 3-fluoro-4-hydroxybenzoic acid to yield phenol intermediate **5.7** upon COMU-mediated activation. The desired *N*3-substituted xanthine-based ligand-directed probes were accessed following activation of the desired probe, namely Sulfo-cyanine5 (SulfoCy5, **A**), *N*-biotinyl-6-aminohexanoic acid (**B**) and bicyclooctyne (bicyclo[6.1.0]nonyne, BCN, **C**) respectively, with 2-bromo-1-ethylpyridinium tetrafluoroborate (BEP).[271] These underwent alcoholysis with the corresponding 3-fluoro-4-hydroxy-benzamido analogues **5.3** and **5.7**, thereby affording the title phenyl esters **5.4a**-**c** and **5.8a**-**b**

Scheme 5.1 Synthesis of *N*-3 substituted xanthine-based ligand-directed probes. [a]



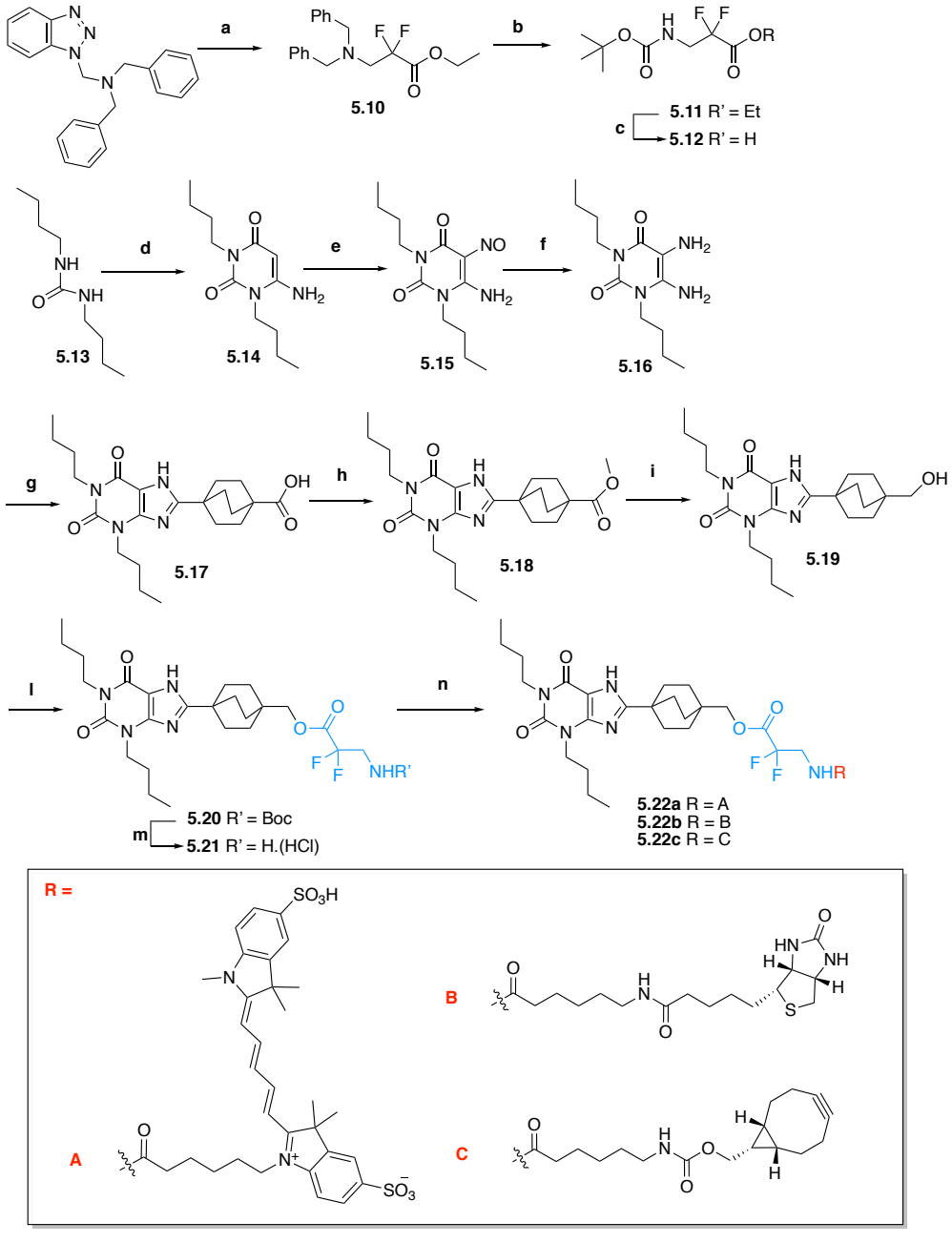
[a] Reagents and Conditions: **a**) *tert*-butyl(4-hydroxybutyl)carbamate, PPh_3, CBr_4, THF, rt, 3h, 98%; **b**) K_2CO_3, DMF, 2 h, rt then 3-(Boc-amino) propylbromide or 4-(Boc-amino)butyl bromide (**5.9**), 9h, rt 55-68%; **c**) 4 M HCl in dioxane, rt, 1 h, quantitative; **d**) 3-Fluoro-4-hydroxybenzoic acid, COMU, DIPEA, DMF, 1 h, 90 ^{O}C, 36-47 % **e**) **5.2b**, Boc-β-alanine, COMU, DIPEA, DMF, rt, 9 h, 77%; **f**) respective probe (R-OH), BEP, DIPEA, DMF, 15 min, rt, then amine, overnight 17-42%.

5.3.1.2 Synthesis of 8-(4-(hydroxymethyl)-bicyclo[2.2.2]octyl) xanthine-based ligand-directed probes.

A second series of ligand-directed probes was designed and synthesised based upon the 8-bicyclo[2.2.2]octylxanthine scaffold, of which the synthetic route is illustrated in **Scheme 5.2**. First, we embarked on the synthesis of the core xanthine scaffold following established procedures.[276,333,334]This involved reacting *N*-butylamine with butyl isocyanate to yield the corresponding 1,3-dibutylurea (**5.13**). This was readily reacted with cyanoacetic acid in the presence of acetic anhydride at 83 ^{O}C to afford intermediate 2-cyano-*N*-butyl-*N*-(butylcarbamoyl) acetamide, which was cyclized to the corresponding 1,3-dibutyl-6-amino uracil (**5.14**)[333] upon addition of few drops of 70% NaOH. A nitroso group was introduced *via* electrophilic substitution at the 5-position by means of sodium nitrite in aqueous acetic acid to afford the corresponding 6-amino-5-nitroso-1,3-dibutylpyrimidine-2,4(1*H*,3*H*)-dione (**5.15**) as pink solid.[334,335] Reduction of **5.15** with sodium dithionite in aqueous ammonia yielded the desired 5,6-diamino-1,3-dibuylpyrimidine-2,4(1*H*,3*H*)-dione (**5.16**).[334,335] This was immediately coupled with commercially available 4-(methoxycarbonyl) bicyclo[2.2.2]octane-1-carboxylic acid, employing COMU as coupling reagent in the presence of DIPEA at rt. Removal of water soluble by products by means of sequential acidic and basic work-ups, with 10% citric acid and sat. $NaHCO_3$ respectively, yielded the crude 6-amino-5-carboxamidouracil intermediate; subsequent dehydrative ring-closure to the corresponding 8-bicyclo[2.2.2]octylxanthine derivative (**5.17**) was achieved in a solution of 1 M KOH and propran-2-ol under reflux for 2 h. Intermediate **5.17** was subjected to Fischer-Speier[336] esterification with acidic MeOH to afford the corresponding methyl ester **5.18**. Reduction of methyl ester intermediate with 1.0 M $LiAlH_4$ in THF yielded the desired primary alcohol (**5.19**) in high yield (86%). The α,α-difluoro-β-alanine reactive linker (**5.12**) was accessed following reported literature procedures.[327,337] This involved treating commercially available ethyl bromodifluoroacetate with zinc dust in the presence of tetramethylsilyl chloride (TMSCl), which underwent Reformatsky-type condensation upon

reaction with commercially available *N*-((1*H*-benzo[*d*][1,2,3]triazol-1-yl)methyl)-*N*-benzyl-1-phenylmethanamine to afford α,α-difluoro-β-amino ester **5.10**.[328,337]

Scheme 5.2 Synthesis of the 8-(4-(hydroxymethyl)-bicyclo[2.2.2]octyl) xanthine based ligand-directed labels. [a]



[a]Reagents and conditions: **a**) ethyl bromodifluoroacetate, Zn dust, TMSCl, 1-(dibenzylaminomethyl)benzotriazole, THF, rt, 3 h, 86%; **b**) H_2, Pd/C, Boc_2O, EtOH, rt, overnight, 94%; **c**) LiOH, THF/H_2O (1:1), rt, 10 min, 75%; **d**) i. Cyanoacetic acid, Ac_2O, 83 ^{O}C, 2 h, ii. H_2O, 70% NaOH, rt, 64%; **e**) $NaNO_2$, 50% AcOH, 57 ^{O}C, 1 h, 41%; **f**)

$Na_2S_2O_4$, 12.5% NH_4OH, 60 ^{O}C, 30 min, 80%; **g**) i.4-(methoxycarbonyl)bicylo[2.2.2] octane-1-carboxylic acid, DIPEA, COMU, DMF, rt, 15 min. ii 1.0 M KOH, propan-2-ol, reflux, 2 h, 68% (over two steps); **h**) MeOH, conc. H_2SO_4, reflux, quantitative; **i**) $LiAlH_4$ (1.0 M in THF), anhydrous THF, 0 ^{O}C, 1 h, 86%; **l**) **5.12**, DCC, DMAP, dry DCM, 0 ^{O}C to rt, o/v 33%; **m**) 4 M HCl in dioxane/DCM (1:1), 20 min, rt, quantitative; **n**) respective probe (R-OH), BEP, DIPEA, DMF, 15 min, rt, then amine, overnight 17-42%

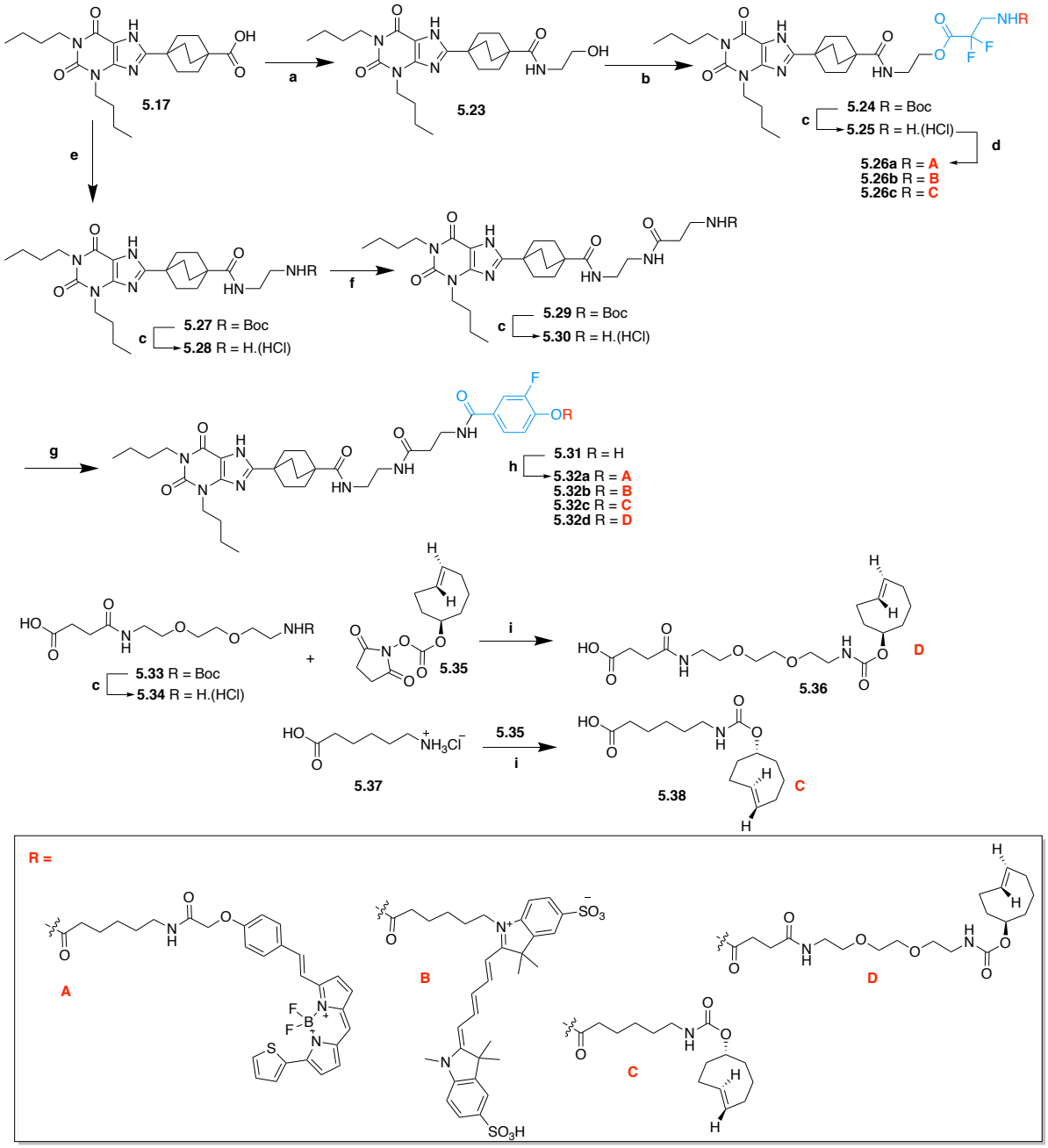
Concomitant *N*-debenzylation and *N*-Boc protection of the latter occurred upon hydrogenation of amino ester **5.10** in the presence of 10 % Pd/C catalyst with *tert*-butoxycarbonyl anhydride in EtOH to furnish the *N*-Boc protected α,α-difluoro-β-amino ester **5.11**.[338] This readily underwent hydrolysis upon treatment with LiOH to yield the title α,α-difluoro-β-alanine acid (**5.12**). Esterification of **5.12** with xanthine alcohol **5.19** under Steglich[339] conditions in the presence of *N*,*N*-dicyclohexylcarbodiimide (DCC) and 4-dimethylaminopyridine (DMAP) afforded the corresponding xanthine-based α,α-difluoro-β-alanine ester **5.20**. Acidolysis of the *N*-Boc group, followed by subsequent amidation of the resulting hydrochloride salt **5.21** with commercially available probes SulfoCy5 (**A**), *N*-biotinyl-6-aminohexanoic acid (**B**) and BCN(**C**) in the presence of BEP and DIPEA, furnished the title conjugates **5.22a** (SulfoCy5), **5.22b** (biotin) and **5.22c** (BCN), respectively.

5.3.1.3 Synthesis of 4-(xanthine)bicyclo[2.2.2]octane-1-carboxilyc acid-based ligand-directed probes.

More distal regions of carboxylic acid **5.17** were also explored for the introduction of the targeted α,α-difluoro-β-alanine and 3-fluoro phenyl reactive moieties, respectively. To this end, carboxylic acid **5.17** was either coupled with commercially available ethanolamine or *N*-Boc ethylenediamine to afford intermediates **5.23** and **5.27**, respectively. Alcohol **5.23** was subsequently reacted with **5.12** to afford α,α-difluoro-β-alanine ester **5.24**. Treatment of the latter with 4 M HCl in dioxane, followed by coupling of the resulting amine hydrochloride salt **5.25** with targeted functional probes by means of BEP, furnished the title functionalised α,α-difluoro-β-alanine esters **5.26a** (BY630/650-X), **5.26b** (SulfoCy5) and **5.26c** (*trans*-cyclooctene, TCO), respectively. Purification of the final reactive

probes by RP-HPLC, however, allowed for the sole isolation of compound **5.26a** (BY630/650-X), while analogues **5.26b** (SulfoCy5) and **5.26c** (TCO) partially or completely hydrolysed in the presence of H_2O. Although disappointing, this outcome also offered the opportunity to envisage the stability of this series of analogues in aqueous buffer during pharmacological assessment. The increased lability of this series of esters under neutral conditions, compared to the series described above (**5.22a**-**5.22c**), could be ascribed to the proximity of the electron-withdrawing amide group, which was only two methylene units away from the carbonylic carbon; this, coupled with the α,α-difluoro group could further increase the electrophilic character of the carbonyl, thereby facilitating a faster hydrolysis rate.

Scheme 5.3 Synthesis of the 4-(xanthine)bicyclo[2.2.2]octane-1-carboxilyc acid based ligand-directed labels.[a]



[a] Reagents and conditions: **a**) ethanolamine, COMU, DIPEA, DMF, rt 53%; **b**) 3-((*tert*-butoxycarbonyl)amino)-2,2-difluoropropanoic acid (**5.12**), DCC, DMAP, dry DCM, 71%; **c**) 4 M HCl in dioxane, rt, 1 h, quantitative; **d**) respective probe (-CO_2H), BEP, DIPEA, DMF, 15 min, rt, then amine, overnight 25%; **e**) *tert*-butyl (3- aminopropyl)carbamate, DIPEA, COMU, DMF, rt, 71 %; **f**) Boc-β-Ala-OH, COMU, DIPEA, DMF, rt, 88%; **g**) 3-Fluoro-4-hydroxybenzoic acid, COMU, DIPEA, DMF, 1 h, 90 ^{O}C, 53%; **h**) respective probe (R-OH), BEP, DIPEA, DMF,

15 min, rt, then amine, overnight 29-75%; **i**)TCO-NHS (**5.35**), NEt_3, DMF, rt, o/v 16-37%;

Meanwhile, intermediate **5.27** was subjected to acidolytic *N*-Boc-removal to afford the corresponding amine **5.28** as its HCl salt. This was coupled to Boc-β-Ala-OH in the presence of COMU to obtain carboxamide intermediate **5.29**. Following *N*-Boc deprotection, amine **5.30** was reacted with 3-fluoro-4-hydroxybenzoic acid to yield xanthine-based phenol **5.31**. Activation of the given functional probe, namely BY630/650-X (**A**), SulfoCy5 (**B**), TCO (**C**) and TCO-PEG (**D**), respectively, in the presence of BEP and DIPEA, followed by reaction with phenol **5.31**, furnished the title 3-fluorophenyl benzoate conjugates **5.32a**, **5.32b**, **5.32c** and **5.32d**. The novel synthesised ligand-directed labels were purified by RP-HPLC and the high purity of each final probe was assessed and confirmed by analytical RP-HPLC with a photodiode array detector and was confirmed as >98% homogeneity. Furthermore, the chemical identity of the final compounds was confirmed by NMR and high-resolution mass spectroscopy (HRMS).

5.3.2 Pharmacology

The ligand binding properties of the newly synthesised probes were assessed in a series of pharmacological assays. Initially, a NanoBRET saturation binding experiment was used to evaluate the binding affinity at the NanoLuc-hA_1AR of *N*3-substitued xanthine-based analogues fluorescently labelled with a SulfoCy5 fluorophore.

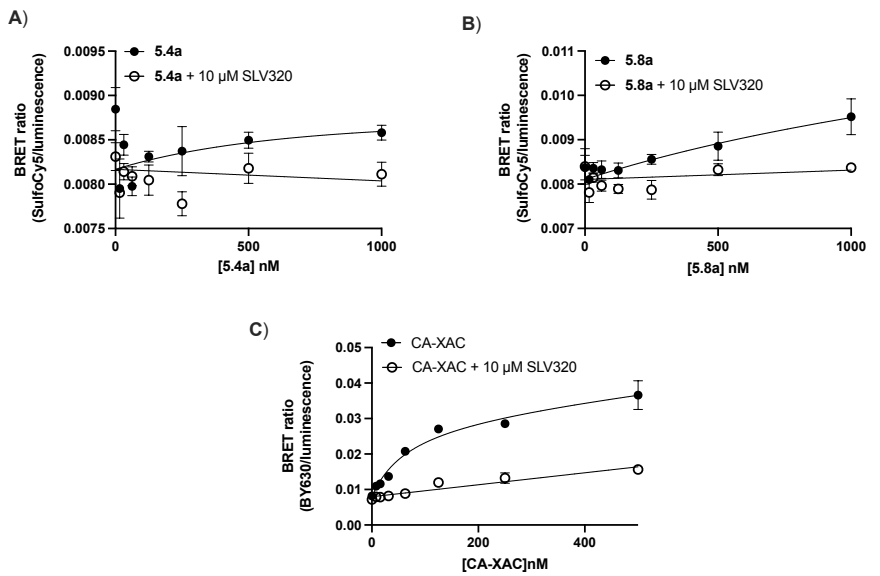


Figure 5.3.1 NanoBRET saturation binding curves for **5.4a** (**A**), **5.8a** (**B**) and CA-XAC (CA200645)[162] (**C**) measured at 37 °C in HEK293 cells stably expressing the NanoLuc-hA$_1$AR in the presence (open circles) or absence (closed circles) of 10 µM A$_1$AR selective competitive antagonist SLV320, where the latter was used to measure non-specific binding. Data are mean ± SEM of triplicate determinations in a single representative experiment of n = 2 separate experiments (**A** and **B**) and n = 1 (**C**).

Treatment of HEK293 cells stably expressing the NanoLuc-hA$_1$AR with increasing concentrations (0 - 1 µM) of analogues **5.4a** and **5.8a** produced a very weak BRET signal over the concentration range tested. This suggests that the probes effectively bind A$_1$AR with low affinity (**Figure 5.3.1 A** and **B**). In a control experiment, it was measured the binding affinity at the NanoLuc-A$_1$AR of a previously characterised fluorescent analogue of XAC, CA200645, which was shown to produce a specific saturable BRET signal in the same cell line, yielding a K_D = 33.9 nM.[49] Thus, in contrast to **5.4a** and **5.8a**, a clear specific binding of CA-XAC at the NanoLuc-A$_1$AR was observed (**Figure 5.3.1 C**), which yielded a K_D = 69 nM, n = 1. This was similar to the K_D values measured for the same fluorescent antagonist at the NanoLuc-hA$_1$AR in previously reported studies.[49,273]

Next, NanoBRET saturation ligand binding experiments were performed with SulfoCy5-labelled probe **5.22a**, which belonged to the C8-substitued xanthine-based series (**Figure 5.3.2**, **A**). Upon treatment of NanoLuc-hA$_1$AR HEK293 cells with compound **5.22a** for 1 h, a clear

saturable BRET signal was observed, allowing the measurement of its equilibrium dissociation constant, K_D = 201.8 ± 21.0, n = 3. To investigate the potential covalent labelling of NanoLuc-hA_1AR with **5.22a**, cells were treated with the compound for additional 3 h and 5 h periods. Albeit not conclusive, a time-dependent increase of binding affinity (K_D) could be indicative of an irreversible labelling character of **5.22a**, which could yield to higher labelling of available receptors with longer incubation time (**Figure 5.3.2**, **B** and **C**). However, it was found that with longer incubation time no specific BRET signal was observed, suggesting that the stability of the probe in HBSS was not optimal under longer incubation time conditions. In parallel, probes lacking a fluorescent group were characterised in a NanoBRET competition ligand binding assay using CA200645 (25 nM) as tracer. A concentration dependent reduction of BRET signal was observed for all the compounds tested, allowing for their binding affinity, as half-maximal inhibitory concentration (IC_{50}), to be quantified (**Figure 5.3.2**, **D**). This was converted to the corresponding inhibitory dissociation constant (K_i) value upon application of the Cheng-Prusoff equation.

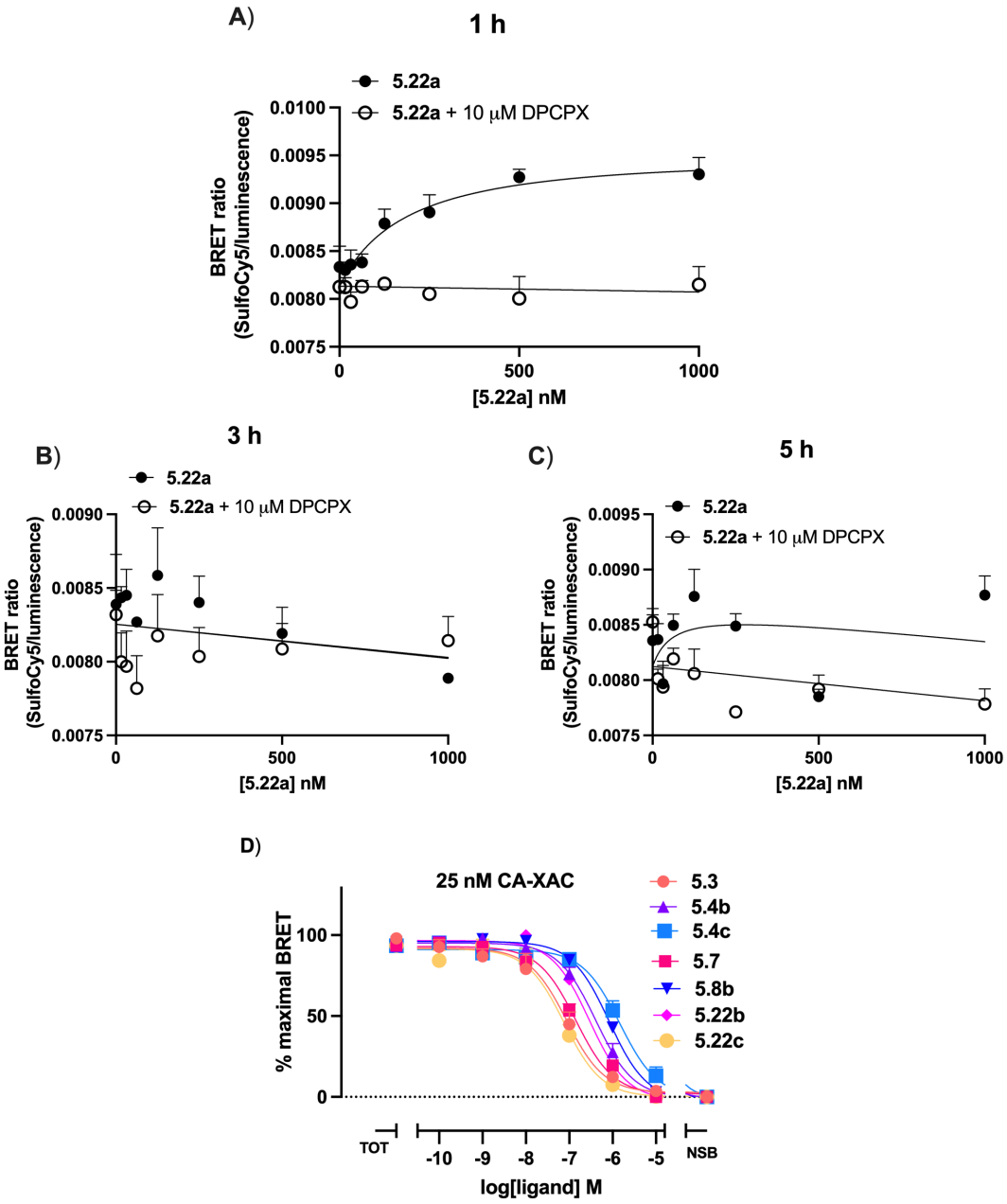
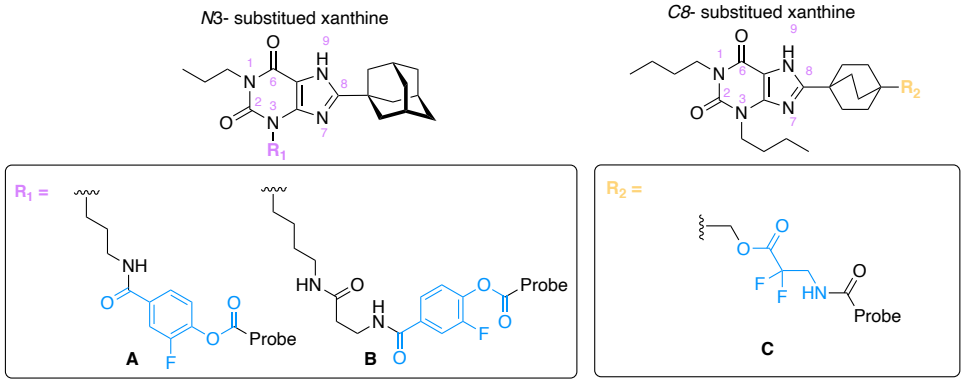


Figure 5.3.2 NanoBRET saturation (**A**-**C**) and competition (**D**) ligand binding curves measured in HEK293 cells stably expressing the NanoLuc-hA$_1$AR. In NanoBRET saturation ligand binding experiments, cells were treated with increasing concentration (0-1000 nM) **5.22a** for 1 h (**A**), 3 h (**B**) and 5 h (**C**) in the absence (closed circles) or presence (open circles) of 10 µM A$_1$AR selective competitive antagonist DPCPX, where the latter was used to determine non-specific binding. **D**) inhibition of CA-XAC(CA200645) specific binding (25 nM) in the presence of increasing concentration of competitive ligands (**5.3** to **5.22c**) at 37 °C for 1 h in NanoLuc-hA$_1$AR-HEK293 cells. TOT is total fluorescent ligand binding determined in the absence of competitor; NSB represents nonspecific binding determined in the presence of 10 µM DPCPX.

Data points represent the combined mean ± SEM from n = 3 (**A**), n = 4 (**D, 5.3**, **5.7 and 5.4b**), n = 2 (**D**, **5.8b** and **5.22b**), n = 5 (**D**, **5.4c** and **5.22c**) performed in triplicate.

Table 5.3.1 Binding Affinities of the Novel *N*3-substitued and C8-substitued xanthine-based ligand-directed labels.



cmpd	scaffold	R	probe	pK_i(LogM) ± SEM[a]
5.3	*N*3-substitued	A	-	7.29 ± 0.22 (4)
5.4b	*N*3-substitued	A	biotin	6.64 ± 0.02 (4)
5.4c	*N*3-substitued	A	BCN	6.10 ± 0.10 (5)*
5.7	*N*3-substitued	B	-	7.11 ± 0.09 (4)
5.8b	*N*3-substitued	B	biotin	6.20, 6.32
5.22b	C8-substitued	C	biotin	6.76, 6.98
5.22c	C8-substitued	C	BCN	7.35 ± 0.12 (5)

[a]pK_i values were calculated from the negative logarithm of the equilibrium inhibitory constant (K_i in nM) measured by NanoBRET competition ligand binding assay employing CA-XAC(CA200645) as fluorescent tracer in HEK293 cells stably expressing the NanoLuc-hA$_1$AR. Values represent the mean ± SEM from n separate experiments (value in parenthesis) performed in triplicate. * $p < 0.05$, compared to **5.4b**; one-way ANOVA with Tukey's multiple comparison test.

Overall, the introduction of functional groups to *N*3-substituted xanthine scaffolds yielded probes with markedly reduced hA$_1$AR affinity (*circa* 10-fold reduction) compared to the parent unlabelled phenol analogues **5.3** and **5.7**. Conjugation of phenol **5.3** with a BCN group proved to be disadvantageous with regard to hA$_1$AR binding, as probe **5.4c** exhibited the lowest hA$_1$AR affinity (pK_i = 6.10 ± 0.10, n = 5) measured amongst the synthesised compounds. This suggested that the nature of the functional group had a major impact on ligand binding when conjugated to *N*3-substitued

xanthines. In contrast, C8-substitued xanthine scaffolds appeared to better tolerate attachment of a functional group as the resulting **5.22b** and **5.22c** probes retained reasonable hA_1AR ligand binding affinity. Moreover, no significant difference ($p > 0.05$, one-way ANOVA with Tukey's multiple comparison test) in hA_1AR ligand binding affinity was observed between the two probes, indicating that biotin and BCN groups exerted minor influence on ligand binding when conjugated to C8-substitued xanthine scaffolds.

From this series of compounds, two representative biotin-labelled ligands, **5.4b** and **5.22b**, were used in a NanoBRET assay to quantify their ability to label hA_1AR in live cells. NanoLuc-hA_1AR HEK293 cells were treated with three concentrations (1 nM, 100 nM and 10 µM) of **5.4b** and **5.22b** in HBSS at 37 °C for 5 h. Reaction with streptadivin-AlexaFluor 633 conjugate (SAv-AF633), followed by the addition of the substrate furimazine, allowed to quantify the resulting BRET signal.

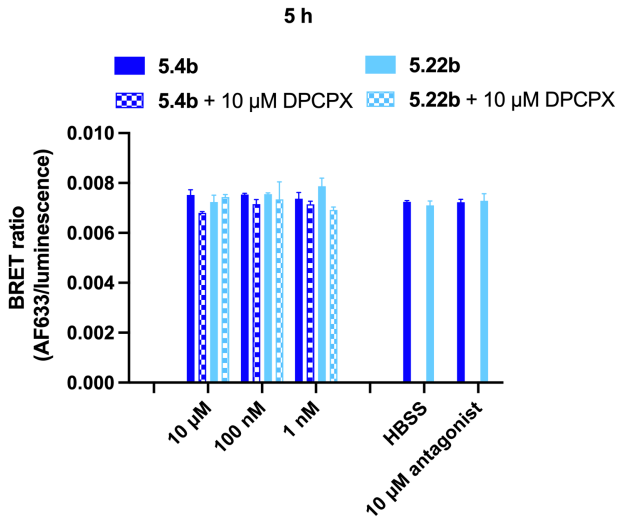


Figure 5.3.3 NanoLuc-hA_1AR HEK293 cells were treated with HBSS or 10 µM DPCPX alone, or biotin-labelled compound **5.4b** and **5.22b** added at the given concentrations for 5 h at 37 °C. Treatment of the cells with Streptadivin-AF633, followed by addition of furimazine allowed for the resulting BRET signal to be measured. For each compound, nonspecific binding was measured in the presence of 10 µM A_1AR antagonist DPCPX (squares pattern). Bars are mean ± SEM of triplicate determination in a single experiment.

The results from this experiment (**Figure 5.3.3**) showed that no significant labelling of the NanoLuc-hA_1AR was achieved upon treatment with **5.4b** and **5.22c** as, for each concentration of ligand, no significant increase in

BRET signal was observed compared to HBSS or 10 μM DPCPX alone ($p > 0.05$, two-way ANOVA with Dunnett's multiple comparison test). Overall, these preliminary data indicated that ligand-directed labelling of hA_1AR could not be achieved when using functionalised *N*3-substituted xanthines or when *C*8-subtitued alcohol **5.19** was acylated with α,α-difluoro-β-alanine reactive moiety.

Finally, the last series of functionalised analogues **5.32a**-**5.32d** (**Scheme 5.3**), based upon DITC-XAC ligands, were also evaluated for their ability to label hA_1AR in a series of pharmacological assays. First, we investigated the ability of the compounds to retain ligand binding at hA_1AR. This was achieved by performing NanoBRET saturation ligand binding experiments in NanoLuc-hA_1AR HEK293 cells with BY630/650-X-labelled **5.32a** and SulfoCy5-labelled **5.32b** analogues, respectively. Furthermore, NanoBRET competition ligand binding experiments were performed with ligands **5.32c**, which was functionalised with a *trans*-cyclooctene (TCO) group (**Figure 5.3.4**) and DPCPX, which was used as control.

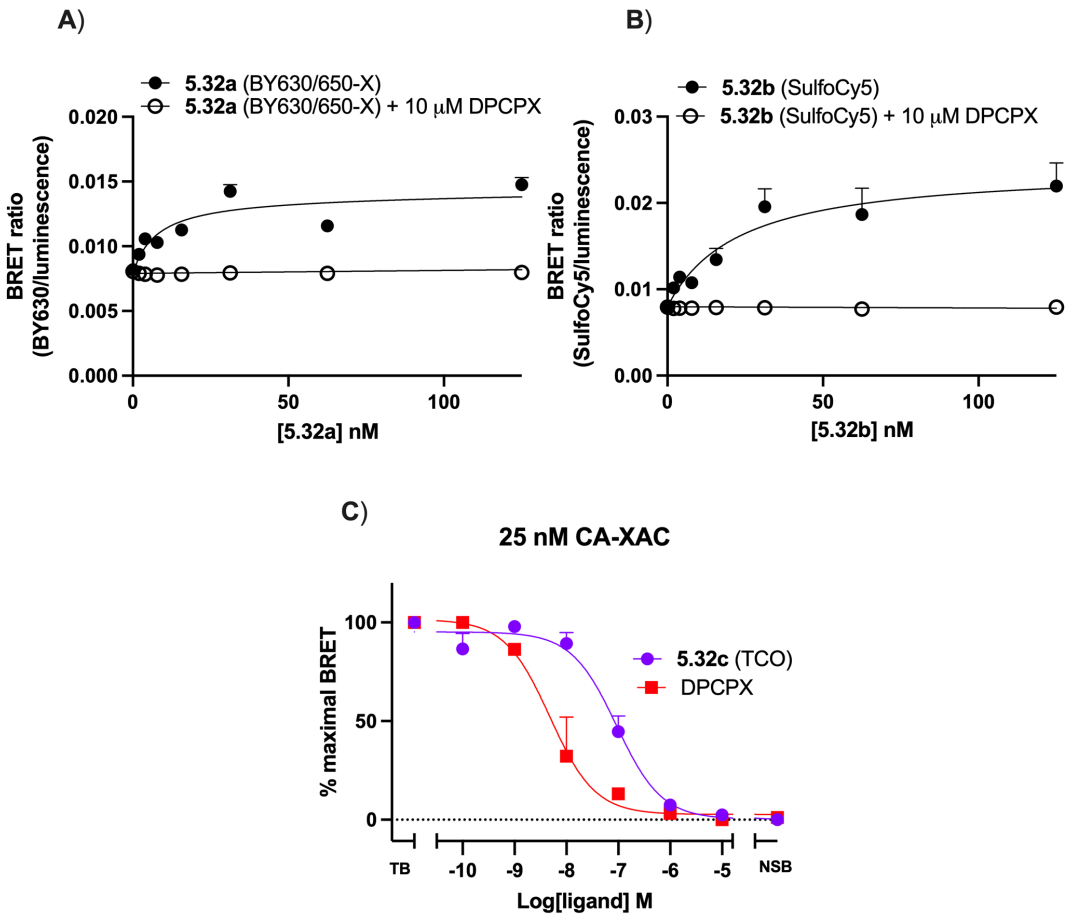


Figure 5.3.4 NanoBRET saturation (**A** and **B**) and competition (**C**) ligand binding curves measured in HEK293 cells stably expressing the NanoLuc-hA_1AR. In NanoBRET saturation ligand binding experiments, cells were treated with increasing concentration (0-125 nM) **5.32a** (**A**) and **5.32b** (**B**) for 1 h at 37 °C in the absence (closed circles) or presence (open circles) of 10 μM A_1AR selective competitive antagonist DPCPX, where the latter was used to determine non-specific binding. **C**) inhibition of CA-XAC(CA200645) specific binding (25 nM) in the presence of increasing concentration of competitive ligands (**5.32c** and **DPCPX**). Data was normalized to maximal BRET signal in the absence of unlabelled competing ligand (total binding, TB). Each data point represents the combined mean ± SEM from n = 4 (**A** and **B**) or n = 2 (**C**) experiments performed in triplicate.

Table 5.3.2 Binding Affinities of the 8-Bicyclo[2.2.2]octyl xanthine-based phenyl esters 5.32a-5.32c.

cmpd	probe	pK_D(LogM) ± SEM[a]
DPCPX	-	8.85, 8.11 [b,c]
5.32a	BY630/650-X	8.28 ± 0.12 (4)
5.32b	SulfoCy5	7.74 ± 0.05 (4)
5.32c	TCO	7.46, 7.03[b]

[a]pK_D values were calculated from the negative logarithm of the equilibrium dissociation constant (K_D in nM) measured by NanoBRET saturation ligand binding assay. [b]pK_i value calculated from the negative logarithm of the equilibrium inhibitory constant (K_i in nM) measured by NanoBRET competition ligand binding assay using CA-XAC (CA200645, 25 nM) as fluorescent tracer in HEK293 cells stably expressing the NanoLuc-hA_1AR. Values represent the mean ± SEM from *n* separate experiments (value in parenthesis) performed in triplicate. [c]pK_i value for DPCPX comparable to values measured by Cooper, S.[49] et al., and Stoddart, L. et al.,[165]

A concentration dependent increase in BRET signal was observed with fluorescently-labelled ligands **5.32a** (BY630/650-X) and **5.32b** (SulfoCy5)(**Figure 5.3.4**). This could be inhibited by co-treatment of the cells with 10 μM DPCPX, indicating that the binding was specific to NanoLuc-hA_1AR. From these curves was therefore possible to measure estimated equilibrium dissociation constants (K_D), subsequently converted to pK_D of 8.28 ± 0.12, n = 4 for **5.32a** and 7.74 ± 0.05, n = 4 for **5.32b**, respectively (**Table 5.3.2**). In parallel, non-fluorescent phenyl ester **5.32c** (TCO) produced a concentration-dependent inhibition of specific CA-XAC (25 nM) binding to NanoLuc-hA_1AR HEK293 cells, allowing for its binding affinity to be quantified as pK_i = 7.25 ± 0.22 (**Table 5.3.2**).

To assess the ability of **5.32a** (BY630/650-X) and **5.32b** (SulfoCy5) to covalently transfer the fluorophore to the hA_1AR, NanoBRET dissociation experiments were performed, whereby an excess (10 μM) of A_1AR-selective antagonist DPCPX was added to NanoLuc-hA_1AR HEK293 cells previously labelled with 100 nM **5.32a** and **5.32b** for 5 h. BRET was monitored over the subsequent 60 min and very little change in BRET ratio was observed compared to time 0. The small reduction in BRET signal observed towards the end of the reads could be most likely ascribed to

substrate (furimazine) consumption. These results indicated that, with both ligands, the fluorophores remained in close proximity to the NanoLuc-hA$_1$AR and could not be displaced by DPCPX, suggesting covalent transfer of the fluorophore to the receptor. In contrast, when the reversible fluorescent antagonist CA200645 was subjected to the same experimental conditions, upon addition of 10 µM DPCPX, the measured BRET signal returned to baseline within 4.7 minutes (**Figure 5.3.5**). A comparable fast $1/k_{off}$ for CA200645 was also measured in SNAP-A$_2$AR HEKG cells.[213]

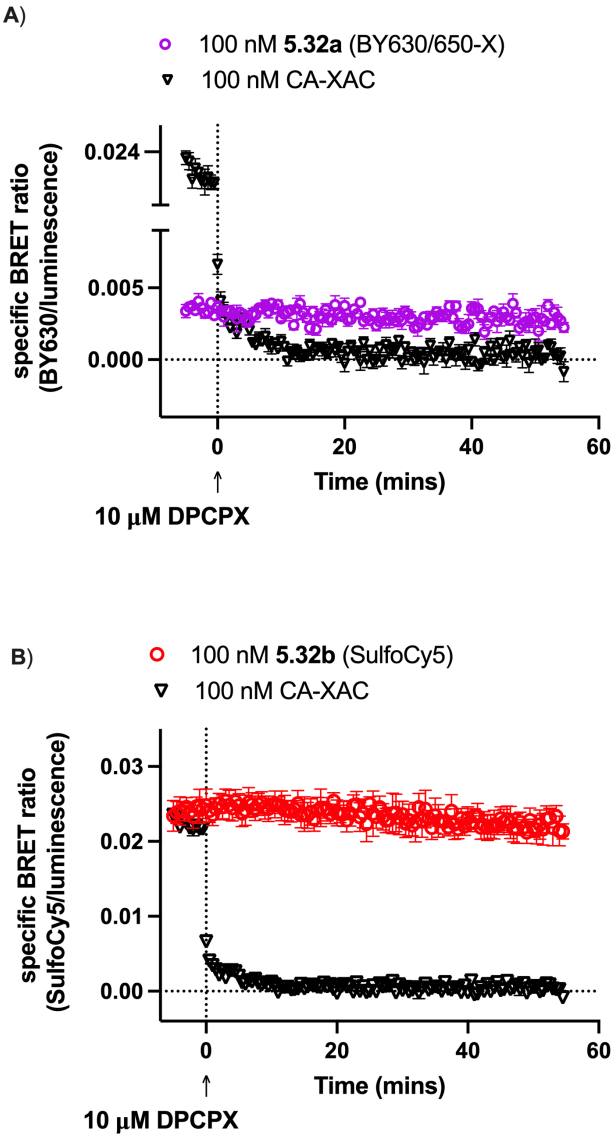


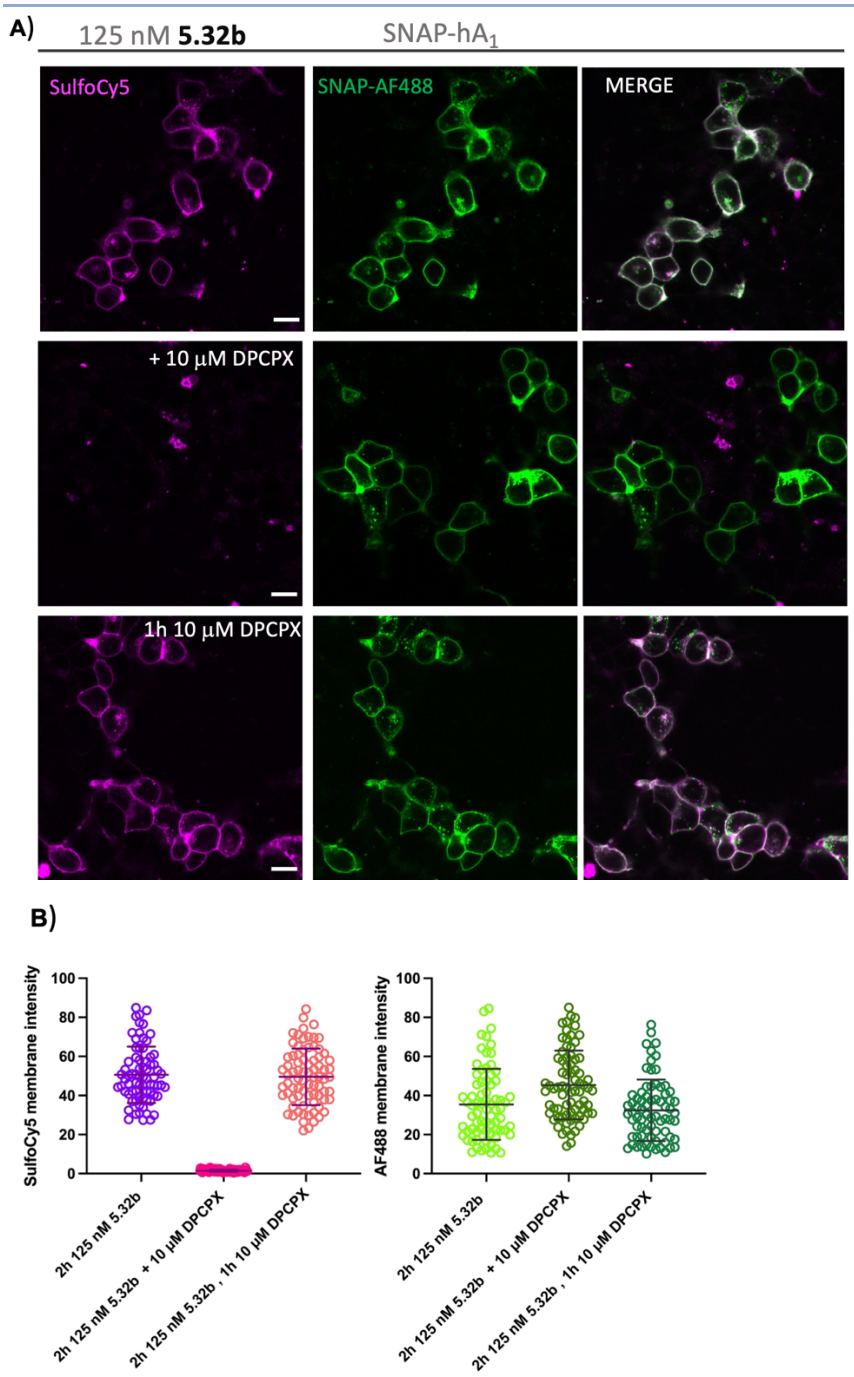
Figure 5.3.5 NanoBRET dissociation kinetics experiments with **A**) **5.32a** (BY630/650-X) and **B**) **5.32b** (SulfoCy5). NanoLuc-hA$_1$AR HEK293 cells were treated with 100 nM **5.32a** (purple open circles, **A**), 100 nM **5.32b** (red open circles, **B**) for 5 h and 100 nM CA-XAC (CA200645, black open circles) for 2 h. After baseline BRET was read every 30 sec for 5 min, 10 µM DPCPX was added and BRET measurements were taken every

30 sec over the subsequent 1 h. Specific BRET was calculated after subtraction of non-specific binding component, determined in the presence of 10 μM DPCPX, from the total binding. Each data point represents the mean ± SEM of triplicate determinations in a single experiment. This experiment is representative of a total of *n* = 5 experiments which showed similar effects.

Interestingly, BRET ratios measured when using BY630/650-X-labelled **5.32a** were significantly lower compared to the values measured with CA-XAC, which displayed the same BY630/650-X fluorophore (**Figure 5.3.5 A**). Moreover, the SulfoCy5 label in **5.32b** yielded similar BRET readings to CA-XAC which suggests that, as fluorescent conjugates **5.32a** and **CA-XAC** shared the same spectral properties, differences in BRET ratio observed could be therefore attributed to the specific orientation of the acceptor fluorophore in **5.32a** with respect to the donor NanoLuc on the receptor. These parameters have shown to contribute in influencing the efficiency of energy transfer between the NanoBRET acceptor/donor pairs.[164,299]

Next, SulfoCy5-labelled ester **5.32b** was used in confocal microscopy studies to test its ability to label and allow visualisation of SNAP-hA_1AR in living HEK293 cells. In these studies, **5.32b** was used at 125 nM as previously performed NanoBRET saturating binding experiments indicated that a 100 % of A_1AR labelling was achieved at this concentration (**Figure 5.3.4 B**). A clear fluorescent labelling of SNAP-hA_1AR localised at the plasma membrane was observed upon treatment with **5.32b** for 2 h. This fluorescence labelling was comparable to SNAP-hA_1AR labelled with AF488 (**Figure 5.3.6 A** top frames). Small levels of co-localised fluorescence signals were also observed in intracellular compartments, suggesting the possibility of a small population of receptors internalised within the timeframe of the experiments. Pre-treatment of the cells with 10 μM DPCPX prevented the labelling of SNAP-A_1AR, demonstrating that the labelling was specific for SNAP-hA_1AR and, therefore, **5.32b** necessitated to engage with the receptor to covalently transfer the SulfoCy5 fluorophore (**Figure 5.3.6 A** middle frames). The addition of 10 μM DPCPX to SNAP-hA_1AR HEK293 cells pre-labelled with **5.32b** for 2 h, could not change the level of fluorescence signal observed (**Figure 5.3.6 A** bottom frames, **B**). Moreover, treatment of

non-transfected HEK293 cells with **5.32b** could not produce any detectable fluorescent signal, further demonstrating the specificity of the probe for labelling hA_1AR and its low level of non-specific binding and non-specific fluorophore transfer to bystander proteins (**Figure 5.3.6 C**). Taken together, these results showed that **5.32b** allowed to covalently label and visualise specific SNAP-hA_1AR expressed in living cells.



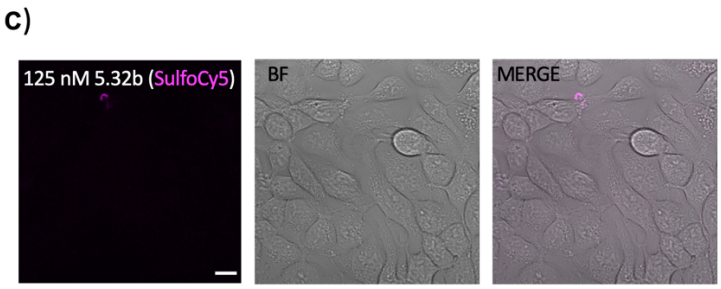


Figure 5.3.6 Live cell confocal microscopy studies of SulfoCy5-labelled **5.32b** (125 nM) labelling SNAP-hA_1AR HEK293 cells at 37 °C in the absence (**A** top frames) or following pre-treatment with (**A** middle frames) 10 μM DPCPX. Cells were treated with the compound for 2 h prior to the acquisition of the single equatorial images (**A**). Cells were treated for 1 h with 10 μM DPCPX after the binding of **5.32b** (125 nM) had reached equilibrium (2h incubation) (**A** bottom frames). Left hand frames represent SulfoCy5 channel, middle frames are AF488 channel and right-hand frames represent merged images of both channels. **B**) Fluorescence intensity plots (16-bit) were generated for both SulfoCy5 and AF488 channels by hand drawing membrane region of interests (ROI) in images obtained as indicated in **A** using Image J (FIJI). Each data point represents membrane fluorescence signal measured from one cell and error bar represent mean ± SD. Images were obtained from 3 independent experiments from which a total of 72 cells were analysed. **C**) Confocal imaging with Non-transfected (NT) HEK293 cells treated with **5.32b** (125 nM) for 2 h at 37 °C. Left hand frame represents SulfoCy5 channel, middle frame is brightfield (BF) channel and right-hand frame is merged image of the two channels. Images were obtained from 2 independent experiments Scale bars are = 13 μm.

A hallmark for the development and application of ligand-directed labels is that covalent labelling should be selectively achieved for the protein under study. Accordingly, to assess its selectivity profile, probe **5.32b** was added to HEK293 cells expressing one the three SNAP-tagged adenosine receptor subtypes, SNAP-hA_{2A}AR, SNAP-hA_{2B}AR and SNAP-hA_3AR, respectively (**Figure 5.3.7**). The levels of **5.23b**-directed fluorescent labelling at the cognate adenosine receptors were visualised by confocal microscopy. No specific SulfoCy5 labelling was observed in HEK293 cells expressing the SNAP-hA_{2B}AR and SNAP-hA_3AR when treated with **5.32b** (125 nM) for 2 h. In contrast, SulfoCy5 labelling localised at the plasma membrane was observed in cells expressing the SNAP-hA_{2A}AR.

SulfoCy5-conjugated **5.32b**, as well as all other xanthine analogues, were designed and synthesised to integrate structural motifs that are reported to enhance A_1AR affinity and, most importantly, imbue higher A_1AR subtype-selectivity with respect to binding other adenosine receptor subtypes. These include the introduction of butyl substituents on the *N*1 and *N*3 positions, as well as the presence of a bulky *C*8-bicyclo[2.2.2]octyl ring. Indeed, co-crystal structures of A_1AR in complex with irreversible antagonist DU172 (PDB:5UEN),[36] competitive antagonist PSB36 (PDB:5N2S)[37] and A_{2A}AR in complex with PSB36 (PDB:5N2R)[37], XAC (PDB:3REY)[218] showed that longer substituent at *N*1 and *N*3 positions cannot be easily accommodated in the narrower A_{2A}AR binding site and bulkier substituents at the C8 position may establish unfavourable steric clash with $M270^{7.35}$ residue side chain in A_{2A}AR (where the corresponding residue is $T270^{7.35}$ in A_1AR). Moreover, the previously discussed reversible SulfoCy5-labelled analogue (**4.44b** Chapter 4) proved to be highly A_1AR-selective and ligand-directed label **5.32b** differs from analogue (**4.44b** Chapter 4) by the introduction of the 3-fluorophenyl ester reactive group in place of the second β-alanine moiety. This suggests that the phenyl ester reactive group plays a major role in influencing **5.32b** labelling selectivity. As no A_{2A}AR ligand binding experiments were performed with **5.32b** to quantify its apparent A_{2A}AR affinity, it was hypothesised that the high concentration of fluorescent probe used (125 nM), coupled with the proximity effect with a nucleophilic lysine in the flexible ECL2 in A_{2A}AR and the highly efficient fluorophore transfer could be responsible for the resulting SulfoCy5 labelling of A_{2A}AR with **5.32b**.

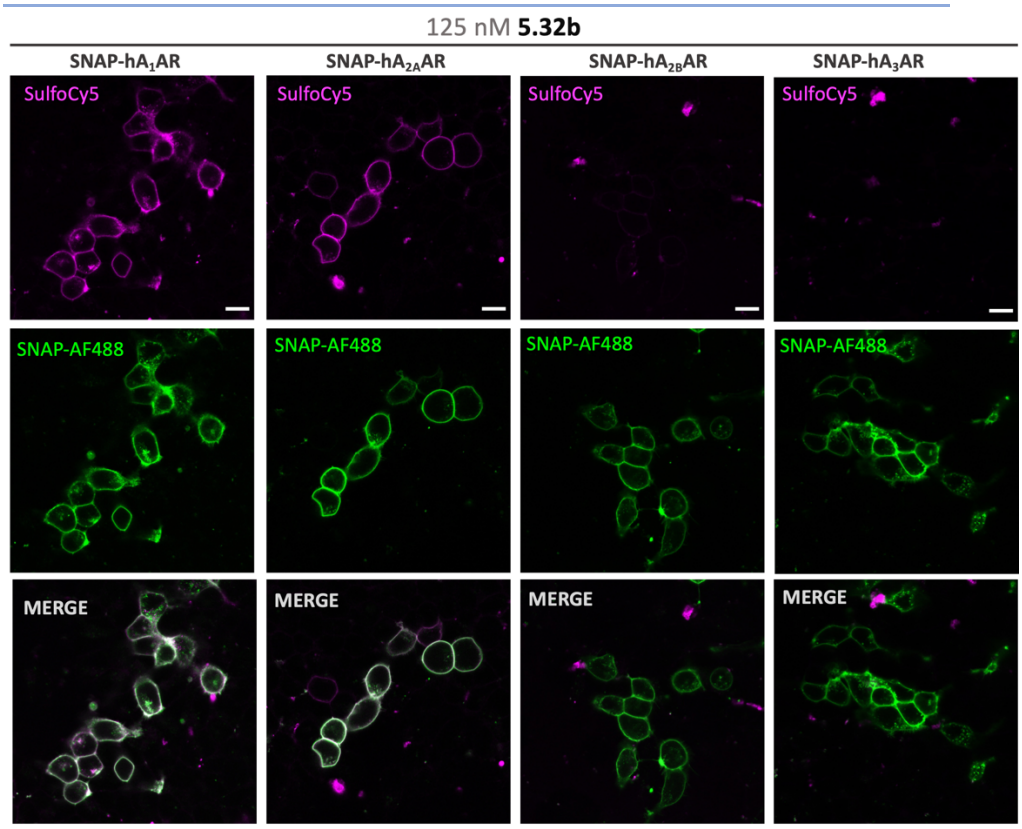


Figure 5.3.7 Live cell confocal microscopy studies of SulfoCy5-labelled **5.32b** (125 nM) labelling SNAP-hA$_1$AR, SNAP-hA$_{2A}$AR, SNAP-hA$_{2B}$AR and SNAP-hA$_3$AR HEK293 cells at 37 ^{o}C. Cells were labelled with SNAP-AF488 for 30 min prior treatment with **5.32b** for 2 h. Images were obtained from 3 independent experiments. Scale bar = 13 μm.

trans-Cyclooctene (TCO) analogue **5.32c** was subsequently evaluated for its ability to label A$_1$AR, following a two-step labelling approach, in confocal microscopy studies. First, SNAP-hA$_1$AR HEK293 cells were treated with **5.32c** (TCO) (2 μM) for 2 h in serum-free media. Second, membrane-impermeable SulfoCy5-methyltetrazine (MetTet-SulfoCy5, 1 μM) was added to the cells and allowed to react for 10 min prior imaging. As shown in **Figure 5.3.8 B**, no fluorescence labelling was observed upon addition of the tetrazine dye, indicating that the IEDDA reaction between the tetrazine and the TCO group of **5.32c** did not occur. This result was unexpected as substituted tetrazine are reported to undergo bioorthogonal reactions with *trans*-cyclooctenes with fast rates in aqueous media ($k_2 > 1x10^4$ $M^{-1}s^{-1}$).[340]

In a parallel experiment, the ability of TCO-functionalised ester **5.32c** to react with Met-TetSulfoCy5 in HBSS alone was evaluated. Indeed, tetrazines are reported to quench the fluorescence of the dyes with which they are conjugated to. Consequently, when tetrazines combine with the corresponding dienophile via IEDDA reactions, formation of the resulting six-member cycloadduct leads to an increase of fluorescence intensity observed. This "turn-on" system is particularly advantageous for imaging studies owing to the higher signal-to-noise (S/N) ratio. Therefore, as proof-of-concept study, the "turn-on" type fluorescence upon reaction of both unsubstituted tetrazine H-TetSulfoCy5 and substituted Methyl-TetSulfoCy5 with TCO-labelled **5.32c** was measured in solution in a Clariostar plate reader. As expected, when an excess of probe **5.32c** (10-fold, 1 μM) was added to a solution of HBSS and the tetrazine dye (100 nM), an increase of the measured fluorescence excitation and emissions spectra was observed compared to the measurements performed with the tetrazine dye alone (**Figure 5.3.7 A**), with the measured fold-increase values comparable to those reported in the literature with similar tetrazine-conjugated dyes.[206,341] These results suggested that the inability to detect fluorescence at the plasma membrane of SNAP-hA_1AR HEK293 cells, following reaction with **5.32c** (TCO) and tetrazineSulfoCy5, could be dependent on the cellular environment.

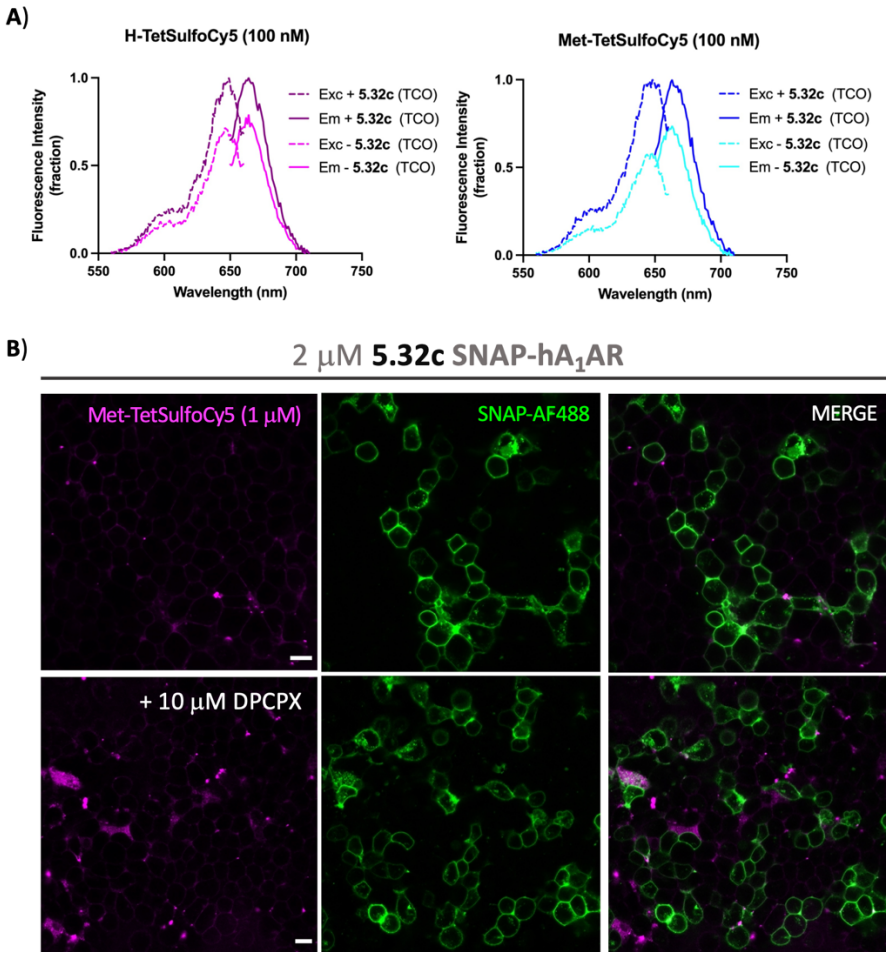


Figure 5.3.7 A) "Turn-on" type reaction of tetrazine-TCO (H-MetSulfoCy5, left graph magenta; Met-TetSulfoCy5, right hand graph, blue). Fluorescence excitation and emission spectra measured in HBSS with the corresponding tetrazineSulfoCy5 [100 nM] without, then with **5.32c** (TCO) [1 μM] (allowed to react for 10 min prior detection). Exc maxima (Met-TetSulfoCy5 + TCO) = 1.80-fold increase compared to Met-TetSulfoCy5 alone; Em maxima (Met-TetSulfoCy5 + TCO) = 1.40-fold; Exc maxima (H-TetSulfoCy5 + TCO) = 1.50-fold; Em maxima (H-TetSulfoCy5 + TCO) = 1.30-fold; **B**) Two-step labelling of SNAP-hA$_1$AR HEK293 cells with **5.32c** (TCO) at 37 °C. Cells were labelled with SNAP-AF488 (200 nM) for 30 min prior the addition of **5.32c** (2 μM) for 2 h, in the presence or absence of 10 μM DPCPX to determine non-specific binding. For the second step of the labelling, cells were treated with Met-TetrSulfoCy5 (1 μM) for 10 min at rt and imaged following 4 wash steps. Scale bar = 13 μm.

Several studies describing the biorthogonal labelling of proteins, following reaction of unnatural amino acids (UAAs) equipped with clickable handles with tetrazine dyes in living cells, reported that the precise location

of the UAA, hence the clickable moiety, in the receptor has a crucial impact on its ability to efficiently react with the corresponding tetrazine reporter.[342–345] For example, when labelled, the lipophilic TCO group may interact with the hydrophobic milieu at the plasma membrane and, as a result, cannot be accessed by the tetrazine reagent for the subsequent click reaction.[345] The reactivity of the TCO group could be enhanced by the introduction of a more hydrophilic linker, such as a poly(ethylene glycol) (PEG) between the TCO and the rest of the molecule. This strategy has been successfully applied for improving the fluorescence detection of TCO-conjugated antibodies.[344] In this regard, an additional TCO-conjugated probe integrating a PEG linker between the ester group and the *trans*-cyclooctene moiety was synthesised to investigate whether the new ligand possessed improved reactivity towards tetrazine dyes and subsequently allowed fluorescence detection of TCO-PEG-labelled SNAP-hA$_1$AR at the plasma membrane in living cells.

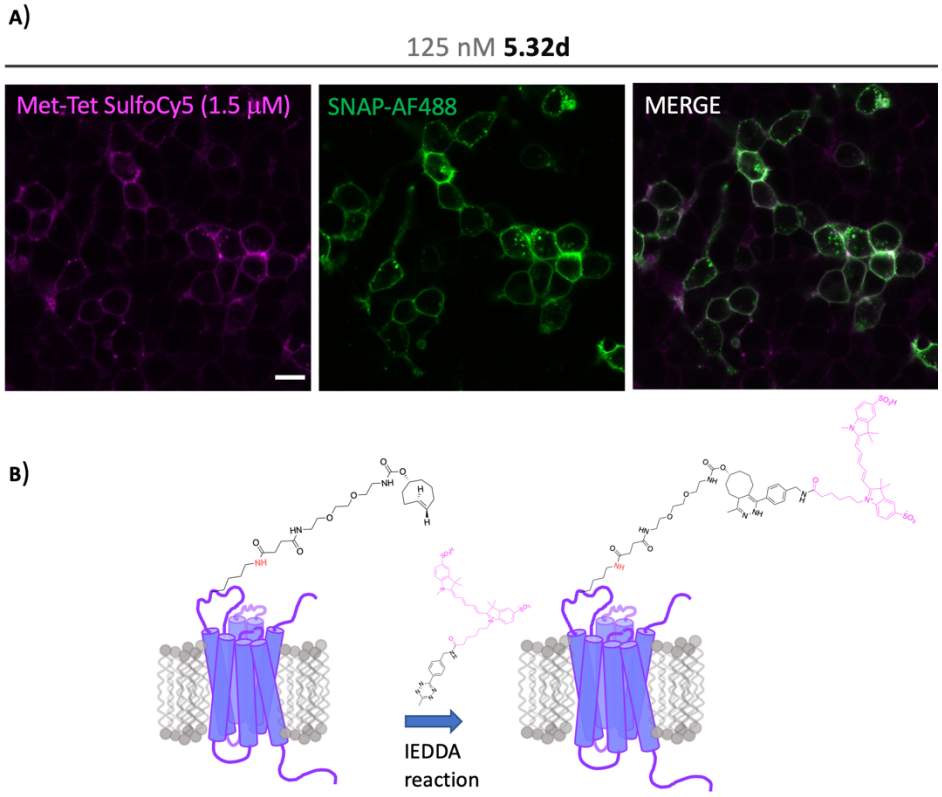


Figure 5.3.8 A) Two-step labelling of SNAP-hA$_1$AR HEK293 cells with **5.32d** (TCO-PEG) at 37 °C. Cells were labelled with SNAP-AF488 (200 nM) for 30 min prior the addition of **5.32d** (125 nM) for 2 h. For the second step of the labelling, cells were treated with Met-TetrSulfoCy5 (1.5 µM) for 10 min at rt and imaged following 4-wash steps. Scale bar = 13 µm. **B**) Schematic representation of hA$_1$AR two-step labelling with **5.32d** and Met-TetSulfoCy5.

Following a two-step labelling approach, SNAP-hA_1AR HEK293 cells were therefore treated with 125 nM **5.32d** (TCO-PEG) for 2 h and subsequently exposed to Met-TetSulfoCy5 (1.5 μM) for 10 min prior to imaging. Pleasingly, it was found that the new PEGylated TCO analogue **5.32d** effectively displayed higher reactivity towards the tetrazine-conjugated SulfoCy5, compared to **5.32c**, as demonstrated by the higher level of fluorescence intensity observed at the plasma membrane of SNAP-hA_1AR HEK293 cells (**Figure 5.3.8 A**). Indeed, this result confirmed the original hypothesis, whereby the possible location of reactive TCO group in a lipophilic environment may hinder its ability to react with the corresponding tetrazine-conjugated probe. Therefore, the introduction of more hydrophilic linkers or groups may physically preclude its interactions with lipophilic domains and could represent an useful strategy for improving the reactivity of TCO groups when required.[344,345]

5.4 Conclusions and Future Work

The work presented in this chapter discussed the rational design and development of a ligand-directed chemistry approach for labelling the human A_1AR in living cells. The combination of co-crystal structures of xanthines-A_1AR complexes with molecular modelling studies, as well as previously reported SAR profiles of xanthine-based A_1 ligands indicated the possibility of conjugating both *N*3 and *C*8 positions of the ligand scaffold with functional probes.[36,318] Furthermore, structural data provided valuable information on the population of nucleophilic amino acid residues harbouring the extracellular domains of A_1AR, whereby specific labelling of single residues could be achieved by the rational design of suitable reactive groups and their strategic introduction into the affinity ligand scaffold with linkers of optimal length, flexibility and/or rigidity.[199]

Interestingly, the co-crystal structure of irreversible antagonist DU172-A_1AR complex showed covalent engagement of DU172 sulfonyl group with $Y271^{7.36}$, thus representing an attractive functionalisation site that could be targeted with the LDL approach. Although fundamentally

compelling, replacement of the phenyl sulfonyl group with a 3-fluoro-phenyl ester, as for *N*3-subtitued xanthines, failed to achieve labelling of A_1AR with different functional groups. This result further emphasised the challenges and higher risks of accessing Tyr-targeting conjugations, compared to those involving Cys or Lys residues, with ligand-directed chemistries, owing to the weaker reactivity displayed by these aromatic amino acids.[200,346] Overall, derivatization of *N*3-subtitued xanthines proved ineffective for the targeted ligand-directed chemistries, as the newly synthesized ligands either lacked the ability to bind A_1AR or could not promote covalent transfer of a functional probe to a residue side chain in the receptor.

A novel electrophilic cleavable group, encompassing an α,α-difluoro-β-alanine moiety, was designed and incorporated into a 8-byciclo[2.2.2]octyl xanthine scaffold *via* hydroxymethyl or *N*-(2-hydroxyethyl)carboxamide linkers (**Scheme 5.2,** cmpd **5.22a-5.22c; Scheme 5.3,** cmpd **5.26a-5.26c**), on the basis of targetable amino acid residues in proximity to the binding site (**Figure 5.2**). Unfortunately, ligands **5.26a**-**5.26c** could not be isolated, owing to the reduced stability exhibited in aqueous environment as observed during RP-HPLC purifications. **5.22a**-**5.22c** could be isolated with high purity, yet the inability to measure specific BRET upon treatment of NanoLuc-hA_1AR HEK293 cells with the compounds for 5 h (**Figure 5.3.2** and **Figure 5.3.3**), demonstrated that α,α-difluoro-β-alanine esters **5.22a**-**5.22c** were unsuitable for labelling A_1ARs in living cells following LD chemistry approach. Although unsuccessful when incorporated into the ligands described herein, α,α-difluoro-β-alanine esters may still provide an useful avenue for the design of a novel series of reactive groups based on natural amino acids, whereby fine tuning of the reactivity and/or stability could be achieved by the strategic positioning of EWG atoms relative to the electrophilic carbonyl group.

Overall, the focused SAR study reported herein showed that ligand-directed labelling of A_1AR in living cells could only be achieved with the series of 8-bicyclo[2.2.2]octyl xanthine based 3-fluoro phenyl esters (**5.32a**-**5.32d**) which were inspired by features of *m*- or *p*-DITC-XAC.[319,320,347] Although structural knowledge can guide ligand design, this cannot readily translate into a functional labelling reagent as demonstrated by the results

presented in this chapter. Therefore, depending on the affinity ligand of choice, it may be recommended to undertake focused and detailed SAR studies to explore the positional effect of different reactive groups and linkers substitutions on the final labelling reagent to maximize the proximity effect for labelling nucleophilic amino acid residues close to the binding site.

Phenyl esters **5.32a**-**5.32c** displayed high A_1AR apparent ligand binding affinity as demonstrated in the NanoBRET ligand binding assays (**Figure 5.3.4** and **Table 5.3.2**). Furthermore, specific labelling of NanoLuc-hA_1AR with **5.32a** (BY630/650-X) and **5.32b** (SulfoCy5) could not be displaced following the addition of a high concentration (10 μM) of competitive A_1AR antagonist DPCPX, suggesting either covalent transfer of the fluorophore to a nucleophilic residue or very slow dissociation of the fluorescent analogues from the receptor. Moreover, ligand **5.32b** (SulfoCy5) was successfully applied in confocal imaging studies for labelling SNAP-A_1AR in living cells and the corresponding SulfoCy5 fluorescence signal remained unaffected upon treatment with 10 μM DPCPX for 1 h (**Figure 5.3.6 A** and **B**). Confocal microscopy studies also showed that **5.32b** (125 nM) could not label SNAP-A_{2B} and SNAP-A_3 expressed in living cells, demonstrating a good selectivity profile of the probe with respect to labelling these other adenosine receptor subtypes. Conversely, it was possible to visualise labelling of SNAP-A_{2A} following treatment with **5.32b** (125 nM) (**Figure 5.3.7**). Notably, 125 nM **5.32b** was used to perform these studies as it corresponded to the concentration whereby 100% of available A_1AR receptors were engaged after 1h treatment, as quantified in NanoBRET saturation binding experiments (**Figure 5.3.4 B**). Because of the high A_1AR apparent ligand binding affinity (pK_D = 7.74 ± 0.05), it is conceivable that lower concentrations of **5.23b** could yield 100% of specific receptor labelling with longer incubation time. The close proximity of the 3-fluoro phenyl reactive group to a nucleophilic amino acid side chain effectively increases the rate of the labelling reaction, thus allowing ligands of lower ligand binding affinity to promote efficient labelling of the protein under study[200,212]; for instance, such as it could occur with **5.32b** also labelling SNAP-A_{2A}AR. Optimisation of reaction conditions, such as

ligand concentration and incubation time, may result in a ligand exhibiting higher A_1AR-labelling selectivity with respect to also engaging A_{2A}AR. For instance, real-time monitoring of labelling kinetics could provide insights into the efficiency of the labelling reaction achieved over a specific time, as well as providing an opportunity to selectively label the A_1AR in a kinetically controlled process. Alternatively, change in linker length or replacing the 3-fluoro phenol with a 4-fluoro phenol, hence with a -OH on the meta position, could be explored for its effect on the selectivity profile (A_1AR vs A_{2A}AR).

To broaden the scope of the application of these new tools, a PEGylated *trans*-cyclooctene (TCO-PEG)-containing ligand-directed label was designed and synthesised (**5.32d**, **Scheme 5.3**). Upon the addition to SNAP-A_1AR HEK293 cells, **5.32d** reacted with substituted tetrazines (Met-Tet-SulfoCy5) following IEDDA reaction, allowing visualisation of SNAP-A_1AR expressed in living cells in confocal microscopy studies (**Figure 5.3.8**). In principle, a two-step labelling approach allows for a single ligand to direct covalent transfer of a small reactive clickable handle to the receptor (first step). This reactive handle can then specifically react with a different range of tetrazine-conjugated probes depending on the final application (second step). For example, when covalently bound to the receptor, reaction of a TCO group with tetrazine-functionalised lanthanides, such as terbium, could enable new RET-based studies of GPCR signalling and dynamics to be performed in unmodified, endogenous membrane proteins.[348]

Nonetheless, before this approach could be readily applied in more complicated tissues or cells expressing endogenous A_1AR (e.g. cortical neurons or cardiomyocytes), a complete validation and optimisation of the methodology is still required. For instance, it remains to be established whether the nature of the labelling of A_1AR is indeed covalent and the ligand-directed labels developed here do not exhibit a slow dissociation character instead. This could be achieved following purification of A_1AR pre-labelled with **5.32b** and subsequent visualisation of the corresponding labelled-protein band by in-gel fluorescence. Crucially, it would follow to assess that A_1ARs maintain their functionalities when labelled,

demonstrating that the probe, once covalently attached does not prevent additional ligands subsequently binding to the receptor. Establishment of a RET-based assay using TCO-tetrazine-functionalised pairs could allow the simultaneous assessment of covalent transfer of a reporter probe as well as demonstrating the ability of additional ligands (e.g. reversible fluorescent ligands) to access and engage the receptor, following departure of the affinity ligand moiety from the orthosteric binding site. Alternatively, Fluorescence-Cross Correlation Spectroscopy (FCCS) experiments could be also applied to assess the aforementioned hypothesis. FCCS allows for the simultaneous detection of two spectrally distinct fluorescent moieties interacting within the same detection volume at the same time, thus enabling to measure the diffusion coefficient and concentration of dual-labelled species.[349] For instance, A_1AR covalently labelled with **5.32b** (SulfoCy5) and subsequently occupied by a reversible BODIPY630/650-X-labelled ligands (such as EC067[318] or ABEA-X-630[148] or BY630-X-(D)-A(D)-A-G-ABEA[181]) could be specifically detected by FCCS.

Furthermore, site-directed mutagenesis studies could be performed to confirm the specific site for covalent attachment. Once established the site of attachment, for the most appropriate application of this technology in different model systems, it would be also required to assess whether the targeted residue is conserved across species (e.g. human, rat and mouse)[49,115] and covalent-labelling is maintained.

In summary, this chapter described the rational design and development of a ligand-directed approach for labelling hA_1AR in living cells. Although additional experiments are required for its complete validation, the method developed here hold promise for illuminating the functions and dynamics of non-genetically modified, native A_1AR in more physiologically relevant environments.

Chapter 6. General Conclusions and Outlook

Adenosine receptors (AR) signalling regulates almost all aspect of cell and tissues biology such as cardiovascular functions, neural firing, blood cells regulation, platelet aggregation, inflammation, immune response and hypoxia.[20,282] As such, for almost a century, these membrane proteins have gained intense research interest aimed at development of novel therapeutic strategies for treating a broad range of medical conditions.[15,21,55] Among these, medicinal chemistry endeavours have led to the discovery of many potent and selective agonists, partial agonists, antagonists, allosteric enhancers and enzyme modulators for these important receptors.[44,220,232,350] Yet, despite the many therapeutic opportunities offered by targeting adenosine receptors, the number of adenosine ligands that have reached the market is limited to only three molecules: adenosine itself,[54] Regadenoson (Lexiscan, Astellas Pharma)[351] and Istradefylline (Nourianz, Kyowa Kirin Inc.).[352] As discussed in **Chapter 1**, translation of adenosine ligands from the bench into the clinic has been hampered by the lack of understanding of distinct receptor pharmacology dependent on the tissue, cell-type and disease states, often leading to on-target side effects.[216,353] The successful development of AR agents with improved selectivity and therapeutic action heavily relies on the ability to monitor real-time the localisation and function of the receptors in its unmodified, native environment in different types of cells in both health and disease states.[215,354] As such, subtype-selective fluorescent probes embody valuable pharmacological tools to achieve this aim as they allow to probe the molecular mechanisms which govern specific receptor functions at single molecule level with great spatial and temporal resolution.[126,253]

The work presented in this thesis has focused on the design, synthesis and pharmacological characterisation of novel series of molecular probes which can be applied to study the molecular pharmacology of the hA_1AR and $hA_{2A}AR$ in living cells. This last Chapter summarises the main findings of this thesis work and provides possible future directions for the application

of these tools, which may facilitate the development of improved hA_1AR- and $hA_{2A}AR$-based therapeutics.

The primary aim of this thesis was to expand upon the current pharmacological toolkit available to study the adenosine $A_{2A}AR$ and A_1AR receptors subtypes, through the development of additional subtype-selective fluorescent ligands. Accordingly, **Chapter 2** reports on the design, synthesis and application of a novel series of subtype-selective fluorescent $hA_{2A}AR$ antagonists based on the high affinity and selective $hA_{2A}AR$ antagonist preladenant. These ligands were labelled with a broad range of fluorophores, encompassing both green- and red-emitting BODIPY-based dyes and more water-soluble dyes such as sulfonated cyanine-5 (SulfoCy5) and AlexaFluor647 (AF647) fluorophores. All fluorescent ligands synthesised retained $A_{2A}AR$ affinity, functional activity (antagonism of $A_{2A}AR$) and most importantly selectivity over all other adenosine receptor subtypes. Notably, the probes allowed clear visualisation of specific $A_{2A}AR$ localisation at the plasma membrane of living cells through confocal microscopy studies. Furthermore, AF647-labelled probe **2.17** enabled monitoring of ligand binding affinities of unlabelled $A_{2A}AR$ ligands using the nanoluciferase bioluminescence resonance energy transfer (NanoBRET) assay (**Figure 2.10**). All novel $hA_{2A}AR$ fluorescent ligands synthesised and described in **Chapter 2** exhibited comparable and optimal pharmacology, thereby allowing the opportunity of ligand choice in a broad series of fluorescence-based techniques. Finally, the work presented in **Chapter 2** significantly contributes to expanding the pharmacological toolbox to study the molecular pharmacology of $A_{2A}ARs$ and it may help to shed new light on the complexity of the $A_{2A}AR$ signalling in different biological elements and during disease progression.[295]

The work discussed in **Chapter 3** discussed the synthetic efforts and pharmacological assessment undertaken to develop novel fluorescent A_1AR ligands with improved A_1AR affinity and selectivity. The novel series of probes described in this Chapter encompassed ligands based on a 2,6,8-trisubstitued 1-deazapurine scaffold, which were inspired by features of a

reported high affinity and selective A_1AR antagonist LUF5981 (**Figure 3.2**). Previously reported structured-activity relationships (SARs) were combined with molecular modelling to guide the rational design of the desired probes. Two series of congeners were synthesised in rather challenging ten steps, from which, overall, ten fluorescent analogues were prepared (**Schemes 3.1** and **3.2**). Pharmacological assessment through NanoBRET ligand binding assays, unfortunately, revealed that the probes either lacked or possessed very weak A_1AR binding ability (**Figure 3.5** and **Figure 3.6**). Overall, the findings obtained from the work described in Chapter 3 indicated that the selection of a different high affinity and A_1AR selective pharmacophore moiety could be more advantageous, and this was subsequently explored in **Chapter 4**.

Chapter 4 described the development of a novel class of fluorescent ligands for the A_1AR exploring two different positions of the prototypical xanthine scaffold for linker/fluorophore elaboration. After a preliminary screening of a series of amino functionalized congeners equipped with linkers of different length and physiochemical composition, it was identified the best template upon which append a series of commercially available fluorophores. Our synthetic efforts, which involved over 15 steps synthesis, led to two families of fluorescent analogues (**Scheme 4.3**), including probes featuring the 4,4-difluoro-4-bora-3a,4a-diaza-s-indacene (BODIPY) dyes alongside water-soluble dyes such as sulfonated cyanine-5 (Sulfo-Cy5). This focused library of eight fluorescent ligands was thoroughly characterised pharmacologically, showing that these novel probes retained binding affinity to the target receptor, functional activity and most importantly, selectivity with respect to binding the other three adenosine receptor subtypes (A_{2A}AR, A_{2B}AR and A_3AR) (**Figure 4.3**). Subsequently, it was evaluated the utility of the novel probes as tracers in competition ligand binding assays, ultimately determining binding affinities of known unlabelled A_1AR ligands that are in very good agreement with literature values (**Table 4.6**). Lastly, three fluorescent A_1AR antagonists were used for visualizing specific fluorescent labelling of engineered A_1AR (SNAP-tagged) localized at the membrane of living cells by confocal imaging and Total Internal Reflection Fluorescence

Microscopy (TIRF-M) (**Figure 4.9** and **Figure 4.10**). To the best of our knowledge, probes **4.44b** and **4.46a** represent the first examples of subtype-selective fluorescent hA_1AR antagonists reported to date. **4.46a** and **4.44b** may provide new opportunities to study real-time A_1AR physiology and pathophysiology at cellular and subcellular level.

As an extension of the fluorescent ligands technology, **Chapter 5** discussed the design, development and application of a Ligand-Directed chemistry approach for labelling the hA_1AR in living cells. LD chemistry harnesses the specificity of ligand binding of a functionalised ligand to its target protein resulting in covalent transfer of the functional group through a proximity-driven reaction.[199] Structural data and molecular modelling guided the rational design of a focused structure-activity relationship (SAR) study around known xanthine scaffolds, whereby different reactive groups as well as their introduction in different positions of the affinity ligand were evaluated to guide the efficient and selective transfer of a functional probe of choice into the targeted A_1AR. These studies led to the discovery of phenyl esters **5.32a-5.32d** (**Scheme 5.3**), which were inspired by features of DITC-XAC ligands (**Figure 5.3**), as potential tools for "directing" covalent labelling of hA_1ARs expressed in living cells. **5.32a**-**5.32c** displayed high "apparent" hA_1AR affinity. Moreover, specific labelling of NanoLuc-hA_1AR and SNAP-A_1AR with **5.32b** (SulfoCy5) could not be displaced following the addition of 10 μM of competitive A_1AR antagonist DPCPX (**Figure 5.3.5** and **Figure 5.3.6**), which may be indicative of covalent transfer of the fluorophore to a nucleophilic residue in close proximity to the binding site. Furthermore, PEGylated *trans*-cyclooctene (TCO-PEG)-containing ligand **5.32d** enabled to perform a two-step labelling approach, which combined Ligand-directed chemistry with the Inverse Electronic Demand Diels-Alder (IEDDA) reaction (a type of fast click chemistry) to form a labelled cycloadduct (**Figure 5.1** and **Figure 5.3.8 B**). This two-step labelling approach allowed fluorescence detection of TCO-PEG-labelled SNAP-hA_1AR at the plasma membrane in living cells through confocal microscopy, following reaction with a corresponding sulfonated cyanine 5 (SulfoCy5)-conjugated tetrazine dye (**Figure 5.3.8**). Although additional experiments are

required for its complete validation, LD labelling of A_1AR described in this Chapter is a non-invasive approach which holds promise for illuminating ligand binding, receptor signalling and trafficking of unmodified, native A_1AR in more physiologically relevant environments.

Overall, the work presented in this Thesis has resulted in the development of novel high affinity and subtype-selective fluorescent A_{2A}AR (**Chapter 2**) and A_1AR (**Chapter 4**) antagonists which allowed quantification of equilibrium and kinetic ligand binding parameters using biophysical methods such as NanoBRET and TR-FRET, in addition to allow visualisation of specific receptor localisation and distribution patterns in living cells by confocal microscopy and total internal reflection microscopy (TIRF-M). Furthermore, this work has resulted in the development of both a ligand-directed (LD) approach and combined LD chemistry with IEDDA click reaction for labelling hA_1AR in living cells, which hold promise for labelling and studying endogenous A_1ARs (**Chapter 5**). It is envisaged that this work may provide the wider scientific community with a new set of pharmacological tools which may facilitate the understanding of the complexity of adenosine receptor signalling in its native environment, thereby providing new opportunities for the identification of new sites for therapeutic intervention as well as for the discovery and development of new A_{2A}AR and/or A_1AR ligands with fewer side effects.

The cellular context in which a receptor is localised can drastically affect its signalling propagation and physiological response, as well as formation of specific receptor-receptor complexes.[354–356] Accordingly, the availability of tools and techniques which allow detailed investigation of receptor specific molecular pharmacology in its native, non-genetically modified environment are of great utility. As overexpressing systems can lead to experimental artifacts,[173,356] it is becoming widely appreciated that there is a serious need to move the study of ARs' pharmacology, and GPCRs' in general, at single receptor resolution under more physiological expression levels.[140,253] Thus, the fluorescent ligands described here could be combined with advanced microscopy such as FCS or super resolution techniques to

probe the role of the A_1AR and A_{2A}AR organisation and distribution in native tissues and/or disease-relevant models. Moreover, CRISPR/Cas9 genome editing technology could be used to insert the NanoLuc[163] luciferase or its split 11-amino acid peptide derivative HiBiT[357] tags into endogenous genome of spinal cord neurons or breast cancer cells, and combined with the fluorescent ligands described in this Thesis to monitor AR-ligand engagement, kinetics of protein-protein interactions, changes in receptor expression and receptor internalisation via NanoBRET or NanoBiT-based assay. Finally, the application of the Ligand-Directed chemistry approach developed here for labelling A_1AR represents a complementary, biorthogonal technique for study the functions and dynamics of A_1ARs without the need of genetic manipulation of the protein of interest. This non-invasive approach opens up a broad spectrum of possibilities to investigate ligand binding, AR trafficking and signalling, as well as the role of AR oligomerisation in endogenous systems with greater spatial and temporal resolution.[201] Indeed, it may provide valuable and unique insights on the functions and dynamics of endogenously expressed ARs, which could not be explored using conventional genetic or overexpressing methods.[199]

We hope the results and tools arising from this Thesis work may help fellow researchers and colleagues within adenosine research field and beyond to shedding new light into the complexity of adenosine receptors signalling in more physiologically relevant models and thereby move a step closer towards the identification of new pharmacological agents with improved and safer mechanism of action.

Chapter 7: General Methods

7.1 Chemistry

7.1.1 Materials and General Methods

Chemicals and solvents of analytical and HPLC grade were purchased from commercial suppliers and used without further purification. BODIPY630/650-X-SE, BODIPY-FL-X-SE, and BODIPY-FL-SE were purchased from Molecular Probes (Thermo Fisher Scientific). AlexaFluor647 NHS ester was purchased from Thermo Fischer Scientific. SulfoCyanine5-CO_2H, Sulfo-Cyanine5 tetrazine (Met-TetCy5) and Sulfo-Cyanine5 NHS ester from Lumiprobe (Germany). (1*R*,8*S*,9*s*)-Bicyclo[6.1.0]non-4-yn-9-ylmethanol (BCN-OH) was from Sigma-Aldrich (UK) and *trans*-Cyclooctene-NHS (TCO-NHS) ester was from Jena Biosciences (Germany). All reactions were carried out at ambient temperature unless otherwise stated. Reactions were monitored by thin-layer chromatography on commercially available silica pre-coated aluminium-backed plates (Merck Kieselgel 60 F^{254}). Visualisation was under UV light (254 nm and 366 nm), followed by staining with iodine, ninhydrin or $KMnO_4$ dips. Flash column chromatography was performed using silica gel 60, 230-400 mesh particle size (Sigma Aldrich). Automated flash column chromatography was performed on a Interchim Puriflash 4100 system (PF4100-250) equipped with a dual wavelength DAD UV detector (200-600 nm) using either silica high performance (HP) 50 μm, or C18-HP (30 μm) cartridges. Methods were developed and run using Interchim Flash (ver:V5.1c.09) software. NMR spectra were recorded on a Bruker-AV 400. ^{1}H NMR spectra were recorded at 400.13 MHz and ^{13}C NMR spectra at 101.62 MHz. All ^{13}C NMR are ^{1}H broadband decoupled. Solvents used for NMR analysis (reference peaks listed) were $CDCl_3$ (δH = 7.26 ppm, δC = 77.16) supplied by Cambridge Isotope Laboratories Inc., $MeOD_4$ (δH = 3.34 ppm, δC = 49.86) and DMSO-d_6 (δH = 2.50 ppm, δC = 40.45) supplied by Sigma-Aldrich (UK). Chemical shifts (δ) are recorded in parts per million (ppm) and coupling constants are recorded in Hz. The following abbreviations are used to described signal shapes and multiplicities; singlet (s), doublet (d), triplet (t), quadruplet (q), broad (br), dd (doublet of doublets),

ddd (double doublet of doublets), dtd (double triplet of doublets) and multiplet (m). Processing of the NMR data was carried out using the NMR software Mnova 12.0.4. LC-MS spectra were recorded on a Shimadzu UFLCXR system coupled to an Applied Biosystems API2000 and visualised at 254 nm (channel 1) and 220 nm (channel 2). LC-MS was carried out using a Phenomenex Gemini-NX C18 110A, column (50 mm × 2 mm x 3 μm) at a flow rate 0.5 mL/min over a 5 min period (**Method A**) or on an Agilent 6100 series single quad coupled to an Agilent 1200 series HPLC instrument using the following buffers: buffer A, 0.1% formic acid in H2O; buffer B, 0.1% formic acid in CH3CN. The following gradient was used with a Poroshell 120 EC-C18 3.0 × 50mm, 2.7 μm column a flow rate of 0.5 mL/min and a total run time of 5 min: 0−1 min 95% buffer A and 5% buffer B, 1−2.5 min 0% buffer A and 100% buffer B, 2.5−3.8 min 0% buffer A and 100% buffer B, 3.8−4 min 95% buffer A and 5% buffer B, 4−5 min 95% buffer A and 5% buffer B (**Method B**)**.** High resolution mass spectra (HRMS) were recorded on a Bruker microTOF mass spectrometer using MS electrospray ionization operating in positive ion mode or on an Agilent 6624 TOF LC−MS spectrometer coupled to an Agilent 1290 Infinity system (Agilent, Palo Alto, CA). All data were acquired, and reference mass corrected via a dual-spray electrospray ionization (ESI) source. Acquisition was performed using Agilent Mass Hunter Data Acquisition software version B.05.00 Build 5.0.5042.2, and analysis was performed using Mass Hunter Qualitative Analysis version B.05.00 Build 5.0.519.13**.** RP-HPLC was performed on a Waters 515 LC system and monitored using a Waters 996 photodiode array detector at wavelengths between 190 and 800 nm. Spectra were analysed using Millenium 32 software. Semi-preparative HPLC was performed using YMC-Pack C8 column (150 mm × 10 mm × 5 μm) at a flow rate of 5.0 mL/min using a gradient method of 30-95% B over 24 minutes (Solvent A = 0.01% formic acid in H_2O, solvent B = 0.01% formic acid in CH_3CN (**Method C**). Preparative HPLC was performed on an Agilent 1260 infinity system coupled with a binary preparative pump and Agilent 1260 FC-PS fraction collector using an Altima C8, 250 × 22 mm, 5 μm column. The following conditions were used for this system: buffer A, H_2O and buffer B, CH_3CN with a gradient of 30− 100% buffer B over 11

min, with a flow rate of 20 mL/min. Spectra were analyzed using Agilent OpenLAB CDS software (**Method D**). Analytical RP-HPLC was performed using a YMC-Pack C8 column (150 mm × 4.6 mm × 5 μm) and a Phenomenex Gemini NX-C18 column (250 mm × 4.6 mm × 5 μm) at a flow rate of 1.0 mL/min. The retention time of the final product is reported using a gradient method of 10-90% solvent B in solvent A over 30 min. (Solvent A = 0.01% formic acid in H_2O, solvent B = 0.01% formic acid in CH_3CN (**Method E**). Purity was also verified on an analytical reverse-phase Agilent HPLC system coupled directly to a photodiode array detector and using a Zorbax Eclipse Plus C18 Rapid resolution 4.6 × 100 mm, 3.5 μm column using the following solvent system: buffer A, 0.1% TFA in H_2O; buffer B, 0.1% TFA in CH_3CN. The elution was performed on a gradient of 95% buffer A and 5% buffer A to 0% buffer A and 100% buffer B over 12 min at a flow rate of 1 mL/min (**Method F**). Final products were one single peak and >95% pure.

General Procedure A: Amide coupling. A solution of respective carboxylic acid (1.0 equiv) in anhydrous DMF (0.5 mL) was stirred with DIPEA (1.10 equiv) and COMU (1.10 equiv) for 5 min at rt. A solution of respective amine (1.10 equiv) was added to the reaction mixture and the resulting solution was stirred at rt for 15-60 min. Upon completion of the reaction, the solvent was evaporated to dryness. The residue was taken up in EtOAc and washed with 1 M aq. HCl, sat. NaHCO3, and brine. The organic layer was collected, dried over anhydrous MgSO4, filtered, and evaporated to dryness. The resulting residue was purified by flash column chromatography as indicated.

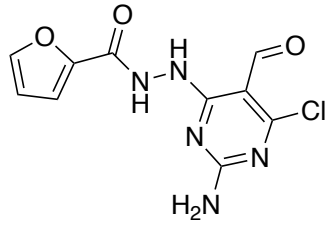
General Procedure B: Phenyl esters synthesis. To a solution of respective carboxylic acid (1.0 equiv) in anhydrous DMF (0.25 mL), was added a solution of 2-bromo-1-ethyl-pyridinium tetrafluoroborate (BEP) (0.8 equiv) and DIPEA (10 mg) in anhydrous DMF (0.25 mL). After stirring for 15 min in the dark, this solution was added to a solution of respective 3-fluoro-4-hydroxybenzamido congener (1.0 equiv) in anhydrous DMF (0.3 mL). After stirring under the exclusion of light for 16 h, the solvent was evaporated to dryness under high vacuum. Purification by semi-preparative RP-HPLC and subsequent lyophilization yielded the pure ligand-directed label as a bright

blue or off-white solid (for all evaporation steps the water bath was set to < 32 ^{O}C).

General Procedure C: Deprotection of tert-Butyl Carbamate (Boc-Group). To the respective Boc-protected amine (1 equiv) was added an excess of 4 M HCl in dioxane (1 mL). The resulting mixture was stirred at rt. for 30 min. Upon completion of the reaction, monitored by TLC and LC/MS, the solvent was evaporated to dryness to give the corresponding amine as its HCl salt, which was used for the subsequent step without further purification.

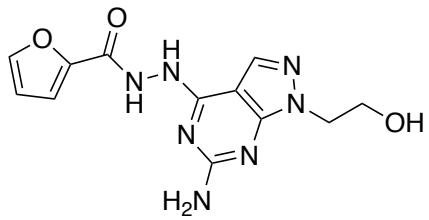
General Procedure D: Syntheses of the Fluorescent Ligands. The respective amine congener (as HCl salt) (1.1 equiv) was dissolved in DMF (0.5 mL), treated with DIPEA (3 equiv), and reacted with the desired fluorophore-NHS (0.5 mg, 1 equiv). The resulting mixture was stirred at rt. under the exclusion of light for 15−60 min. Upon completion of the reaction, monitored by TLC and LC/MS, the solvent was removed in vacuo and the residue was dissolved in a mixture of 1:1 CH_3CN/H_2O. Purification by reverse-phase preparative HPLC and subsequent lyophilization yielded the pure fluorescent ligand as a bright blue or orange solid.

7.1.2 Methods Chapter 2



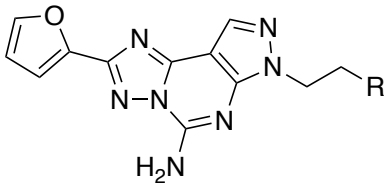
***N*-(2-Amino-6-chloro-5-formylpyrimidin-4-yl)furan-2-carbohydrazide (2.2).** 2-Amino-4,6-dichloropyrimidine-5-carbaldehyde (0.5 g, 2.6 mmol, 1 equiv.) was dissolved in anhydrous THF (20 mL). To the resulting mixture was added Et_3N (0.26 g, 2.86 mmol, 1.1 equiv.) followed by 2- furoic hydrazide (0.36 g, 2.86 mmol, 1.1 eq.). The above mixture was heated to 70°C for 3 h. The mixture was then evaporated *in vacuo* to give intermediate **2.2** as yellow solid which was used for the next reaction without further purification.

LC-MS ***m/z*** calc. for $C_{10}H_9ClN_5O_3$ $[MH]^+$ 282.04; found 282.10, t_R= 2.09min (Method A)



***N*-(6-Amino-1-(2-hydroxyethyl)-1*H*-pyrazolo[3,4-*d*]pyrimidin-4-yl)furan-2-carbohydrazide (2.3).** To a solution of *N*-(2-amino-6-chloro-5-formylpyrimidin-4-yl)furan-2-carbohydrazide (1 equiv.) in CH_3CN/water (10:2.5 mL) was added 2-hydrazinoethanol (0.35 mL, 5.2 mmol, 2 equiv.). The mixture was heated to reflux for 2.5 h. The solution was allowed to cool at RT. 0.1M HCl (5 mL) was added to the reaction mixture. Afterwards, the solution was evaporated *in vacuo* to 5mL and left overnight for a solid to appear. Water (10 mL) was added and the solid was collected by filtration. The solid was further washed with CH_3CN and Et_2O. The solid was dissolved in MeOH and the solution was evaporated azeotropically with toluene to give the desired compound **2.3** which was used for the next step without any further purification.

LC-MS ***m/z*** calc. for $C_{12}H_{14}N_7O_3$ $[MH]^+$ 304.12; found 304.10, t_R = 0.61 min (Method A).

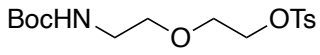


7-(2-Halooethyl)-2-(furan-2-yl)-7*H*-pyrazolo[4,3-*e*][1,2,4]triazolo[1,5-*c*]pyrimidin-5-amine (R = Cl and Br). Intermediate **2.3** *N*-(6-amino-1-(2-hydroxyethyl)-1*H*-pyrazolo[3,4-*d*]pyrimidin-4-yl)furan-2-carbohydrazide (0.550 g, 1.8 mmol, 1 equiv.) was dissolved in $POCl_3$ (4 mL). To the resulting mixture was added $ZnBr_2$ (0.1 g). The mixture was heated to 80°C for 5 h. Then, $POCl_3$ was evaporated, water (ice) was added and the resulting aqueous solution was extracted with EtOAc. Organic layers were collected, dried over Na_2SO_4 anhydrous, filtered and evaporated to dryness. Purification by flash column

chromatography on silica gel using 2:1 EtOAc/Pet. Spirits gave a mixture of intermediates **2.4a** and **2.4b** as a pale yellow solid (0.11 g, 11%).

LC-MS *m/z* calc. for $C_{12}H_{11}Cl^{35}N_7O$ $[MH]^+$ 304.07; found 304.10; calc. for $C_{12}H_{10}Br^{79}N_7O$ $[MH]^+$ 348.02; found 348.10, $C_{12}H_{10}Br^{81}N_7O$ $[MH]^+$ 350.02; found 350.10, t_R = 2.50 min (Method A).

^{1}H NMR (DMSO-d_6) δ 8.23 (s, *J* = 1.0 Hz, 1H, Ar-pyraz), 8.14 (br s, 2H, N<u>H</u>$_2$), 7.95 (d, *J* = 1.8 Hz, 1H, <u>H</u>-fur), 7.24 (d, *J* = 3.3 Hz, 1H, <u>H</u>-fur), 6.74 (dd, *J* = 3.4, 1.8 Hz, 1H, <u>H</u>-fur), 4.66 (t, *J* = 6.2 Hz, 1H, C<u>H</u>$_2$Br), 4.60 (t, *J* = 5.9 Hz, 2H, C<u>H</u>$_2$Cl), 4.09 (t, *J* = 5.9 Hz, 2H, C<u>H</u>$_2$CH$_2$Cl), 3.94 (t, *J* = 6.2 Hz, 1H, C<u>H</u>$_2$CH$_2$Br).

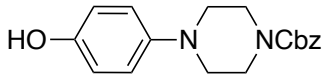


2-(2-((*tert*-Butoxycarbonyl)amino)ethoxy)ethyl 4-methylbenzenesulfonate *(2.5)*. *tert*-Butyl (2-(2-hydroxyethoxy) ethyl) carbamate (1 g, 4.87 mmol, 1 equiv.) was dissolved in DCM (20 mL). To the resulting mixture were added DIPEA (2.5 mL, 3 equiv.), DMAP (5%mol) and TsCl (1.85 g, 9.74 mmol, 1.3 equiv.). The mixture was stirred at RT overnight. The solution was concentrated under reduced pressure to a volume of 5mL. Purification by flash column chromatography on silica gel using a gradient of 0→4% MeOH/DCM gave the desired product as colourless oil (1.5 g, 86%).

LC-MS *m/z* calc. for $C_{16}H_{26}NO_6S$ $[MH]^+$360.15; found 360.10; t_R = 2.51min (Method A).

^{1}H NMR ($CDCl_3$) δ 7.80 (d, *J* = 8.0 Hz, 2H, Ar-<u>H</u>), 7.35 (d, *J* = 7.96 Hz, 2H, Ar-<u>H</u>), 4.80 (br s, 1H, N<u>H</u>), 4.16 (t, *J* = 4.1 Hz, 2H, -C<u>H</u>$_2$O), 3.63 (t, *J* = 4.3 Hz, 2H, -C<u>H</u>$_2$O), 3.45 (t, *J* = 4.4 Hz, 2H, -C<u>H</u>$_2$O), 3.24 (q, *J* = 5.4 Hz, 2H, -C<u>H</u>$_2$NH), 2.45 (s, 3H, Ar-C<u>H</u>$_3$), 1.45 (s, 9H, Boc).

^{13}C NMR ($CDCl_3$) δ 155.9 (NH<u>C</u>=O), 145.0 (C), 133.1 (C), 129.9 (Ar-H), 128.1 (Ar-H), 79.4 (C), 70.4 (<u>C</u>H$_2$O), 69.2 (<u>C</u>H$_2$O), 68.4 (<u>C</u>H$_2$O), 40.3 (<u>C</u>H$_2$NH), 28.5 (Boc), 21.7 (<u>C</u>H$_3$).

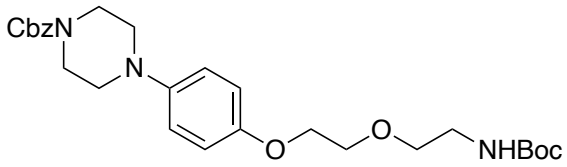


Benzyl 4-(4-hydroxyphenyl)piperazine-1-carboxylate (**2.8***).* Benzyl chloroformate (0.793 mL, 5.6 mmol, 1 equiv.) was added to a stirred suspension of 4-(piperazin-1-yl) phenol and K_2CO_3 in DMF (8 mL). Water was then added and the aqueous layer was extracted with EtOAc. The organic layer was further washed with water (x3), dried over anhydrous Na_2SO_4, filtered and evaporated to dryness. Purification by flash column chromatography on silica using 40% EtOAc/Pet. ether gave the desired product as pale beige pink solid. (1.2 g, 66%).

LC-MS *m/z* calc. for $C_{18}H_{21}N_2O_3$ $[MH]^+$ 313.15; found 313.10; t_R = 2.51 min (Method A).

^{1}H NMR ($CDCl_3$) δ 7.39 – 7.31 (m, 5H, Ar-H), 6.85 (d, *J* = 8.4 Hz, 2H, Ar-H), 6.77 (d, *J* = 7.6 Hz, 2H, Ar-H), 5.17 (br s, 1H, NH), 5.00 (s, 2H, -CH_2), 3.66 (t, *J* = 4.63 Hz 4H, CH_2piperaz), 3.01 (m, 4H, CH_2piperaz).

^{13}C NMR ($CDCl_3$) δ 155.1 (OC=O), 136.4 (Ar-C), 128.4 (Ar-CH), 127.9 (Ar-CH), 127.8 (Ar-CH), 119.1 (Ar-CH), 115.8 (Ar-CH), 67.1 (CH_2), 50.9 (CH_2-piperaz), 43.7 (CH_2-piperaz) (two quaternary carbons in the phenol ring not observed).



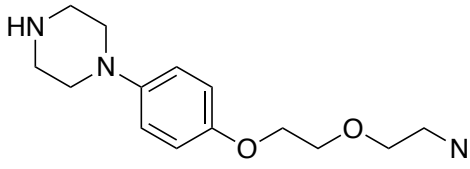
Benzyl 4-(4-(2-(2-((*tert*-butoxycarbonyl)amino)ethoxy)ethoxy)phenyl)piperazine-1-carboxylate (**2.9i**) Compound **2.8** (0.36 g, 1.16 mmol) was dissolved in CH_3CN (10 mL). K_2CO_3 (0.5 g) was subsequently added to the reaction mixture followed by compound **2.6** (0.416 g, 1.16 mmol, 1 equiv.). The resulting mixture was heated to 100°C and held at this temperature for 6 h. The reaction was allowed to cool, Et_2O was added and the mixture was washed with 1M NaOH (x3). The organic layer was collected and evaporated to dryness. Purification by flash column chromatography on

silica using 60% EtOAc/Pet. ether gave the final product as an off-white solid (0.2 g, 40%).

LC-MS *m/z* calc. for $C_{27}H_{38}N_3O_6$ $[MH]^+$ 500.28; found 500.10; t_R = 3.02 min (Method A).

^{1}H NMR ($CDCl_3$) δ 7.40 – 7.32 (m, 5H, Ar-H), 6.88 (s, 4H, Ar-H), 5.16 (s, 2H, Ar-H), 4.98 (br s, 1H, NH), 4.07 (t, *J* = 4.3Hz, 2H, -CH_2O), 3.79 (t, *J* = 4.5Hz, 2H, -CH_2O), 3.66 (t, *J* = 4.8 Hz, 4H, CH_2piperaz), 3.60 (t, *J* = 4.8Hz, 2H, -CH_2O), 3.34 (q, *J* = 4.6 Hz, 2H, -CH_2NH), 3.07 – 2.97 (m, 4H, CH_2piperaz), 1.44 (s, 9H, Boc).

^{13}C NMR ($CDCl_3$) δ 155.4 (NHC=O), 150.1 (OC=O), 141.3 (2xC), 136.4 (C-Ar), 128.4 (Ar-CH), 127.9 (Ar-CH), 127.79 (Ar-CH), 119.1 (Ar-CH), 115.3 (Ar-CH), 79.2 (C), 70.2 (CH_2O), 69.4 (CH_2O), 67.6 (CH_2O), 67.1 (CH_2), 50.7 (CH_2-piperaz), 43.7 (CH_2-piperaz), 40.2 (CH_2NH), 28.2 (Boc).

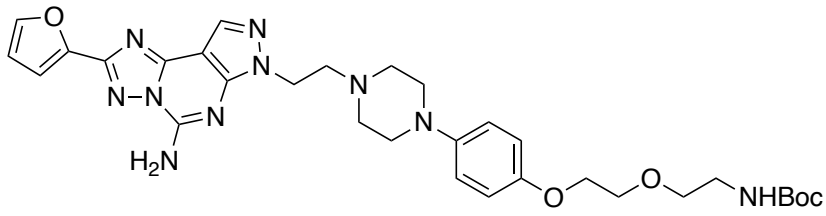


***tert*-Butyl (2-(2-(4-(piperazin-1-yl)phenoxy)ethoxy)ethyl)carbamate (2.9ii)** Compound **2.9i** (0.2 g, 1 equiv.) was dissolved in EtOH (4 mL) and the resulting mixture was stirred at RT under a nitrogen atmosphere. Pd/C 11% w/w was added to the reaction mixture and the flask was evacuated and replaced with a H_2 atmosphere. The reaction was stirred at RT for 3h. The completion of the reaction was confirmed by TLC. The mixture was then filtered through Celite™ and the pad was washed with EtOH (40 mL) and DCM (40 mL x 3). The filtrate was collected and concentrated under reduced pressure to give the pure product as an off-white solid (0.12 g, 82%).

LC-MS *m/z* calc. for $C_{19}H_{32}N_3O_4$ $[MH]^+$ 366.24; found 366.10; t_R = 2.12 min (Method A).

^{1}H NMR ($CDCl_3$) δ 6.92 – 6.84 (m, 4H, Ar-H), 5.00 (brs, 1H, -NH), 4.07 (t, *J* = 4.4 Hz, 2H, -CH_2O), 3.79 (t, *J* = 4.4 Hz, 2H, -CH_2O), 3.60 (t, *J* = 4.4 Hz, 2H, -CH_2O), 3.33 (q, *J* = 4.8 Hz, 2H, -CH_2NH), 3.05 (s, 6H, -CH_2piperaz), 2.14 (br s, 2H, CH_2piperaz)1.44 (s, 9H, Boc).

^{13}C NMR ($CDCl_3$) δ 156.1 (NHC=O), 153.1 (C), 146.5 (C), 118.4 (Ar-CH), 115.5 (Ar-CH), 79.4 (C-Boc), 70.5 (CH_2O), 69.7 (CH_2O), 67.9 (CH_2O), 51.7 (CH_2-piperaz), 46.2 (CH_2-piperaz), 40.5 (CH_2NH), 28.5 (Boc).



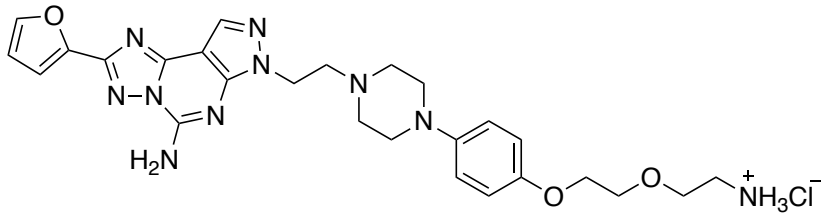
***tert*-Butyl (2-(2-(4-(4-(2-(5-amino-2-(furan-2-yl)-7*H*-pyrazolo[4,3-*e*][1,2,4]triazolo[1,5-*c*]pyrimidin-7-yl)ethyl)piperazin-1-yl)phenoxy)ethoxy)ethyl)carbamate** (**2.10**) *tert*-Butyl (2-(2-(4-(piperazin-1-yl)phenoxy)ethoxy)ethyl)carbamate (30 mg, 0.9 μmol, 1 equiv.) and **2.4a-b** (40 mg, $0.11x10^{-5}$ mol, 1 equiv.) were dissolved in DMF (0.5 mL) prior to the addition of DIPEA (4 equiv., 0.4 mL). The resulting mixture was heated and held at 100 °C overnight. Completion of the reaction was confirmed by TLC. The solution was further dissolved in EtOAc and washed with water (x3). The organic layer was collected and concentrated under reduced pressure. Purification by flash column chromatography on silica using DCM:MeOH (96:4) gave the pure compound as a pale yellow solid (12 mg, 19%).

LC-MS *m/z* calc. for $C_{31}H_{41}N_{10}O_5$ $[MH]^+$ 633.33; found 633.10; t_R = 2.12 min (Method A).

^{1}H NMR ($CDCl_3$) δ 8.18 (s, 1H, Ar-pyraz), 7.53 (d, *J* = 1.8 Hz, 1H, Ar-furan), 7.21 (d, *J* = 3.4 Hz, 1H, Ar-furan), 6.88 – 6.81 (m, 4H, Ar), 6.56 (dd, *J* = 3.5, 1.8 Hz, 1H, Ar-furan), 6.45 (brs, 2H, -NH_2), 5.01 (brs, 1H, -NH), 4.53 (t, *J* =

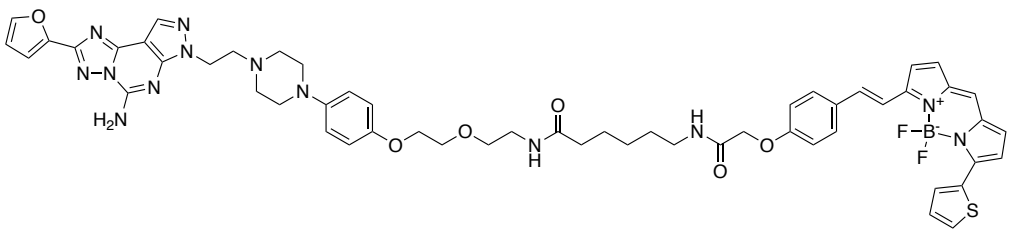
6.42 Hz, 2H, -C<u>H</u>$_2$), 4.05 (t, *J* = 3.72 Hz, 2H, -C<u>H</u>$_2$O), 3.78 (t, *J* = 4.2 Hz, 2H, -C<u>H</u>$_2$O), 3.59 (t, *J* = 4.1 Hz, 2H, -C<u>H</u>$_2$O), 3.33 (q, *J* = 5.1 Hz, 2H, -C<u>H</u>$_2$NH), 3.14 – 3.07 (m, 4H, <u>H</u>-piperaz), 2.98 (t, *J* = 6.00 Hz, 2H, -C<u>H</u>$_2$-piperaz), 2.78 – 2.69 (m, 4H, <u>H</u>-piperaz), 1.43 (s, 9H, Boc).

^{13}C NMR ($CDCl_3$) δ 156.7(<u>C</u>-NH_2), 156.1(NH<u>C</u>=O), 152.9 (C), 149.3(C), 148.3 (C), 145.9 (C), 145.5 (C), 145.5 (<u>C</u>H), 144.7 (<u>C</u>H), 132.3 (<u>C</u>H-pyraz), 118.1(Ar-<u>C</u>H), 115.5 (Ar-<u>C</u>H), 112.7 (C), 112.1 (C), 97.4 (<u>C</u>H), 79.4 (<u>C</u>-Boc), 70.5 (<u>C</u>H$_2$O), 69.7 (<u>C</u>H$_2$O), 67.9 (<u>C</u>H$_2$O), 57.0 (<u>C</u>H$_2$), 53.4 (<u>C</u>H$_2$-piperaz), 50.4 (<u>C</u>H$_2$-piperaz), 45.3 (<u>C</u>H$_2$), 40.5 (<u>C</u>H$_2$NH), 28.5 (Boc).



7-(2-(4-(4-(2-(2-Aminoethoxy) ethoxy) phenyl) piperazin-1-yl) ethyl)-2-(furan-2-yl)-7*H*-pyrazolo[4,3-*e*][1,2,4]triazolo[1,5-*c*]pyrimidin-5-amine (**2.11**) Compound **2.10** (12 mg, 1 eq.) was dissolved in 4 M HCl in dioxane (1 mL). The completion of the reaction was confirmed by TLC and LC-MS after 30min. The solvent was removed under reduced pressure and the compound was used in the next synthetic step without further purification. (10 mg, quantitative 100%).

LC-MS *m/z* calc. for $C_{26}H_{33}N_{10}O_3$ $[MH]^+$ 533.27; found 533.10; t_R = 1.85 min (Method A).

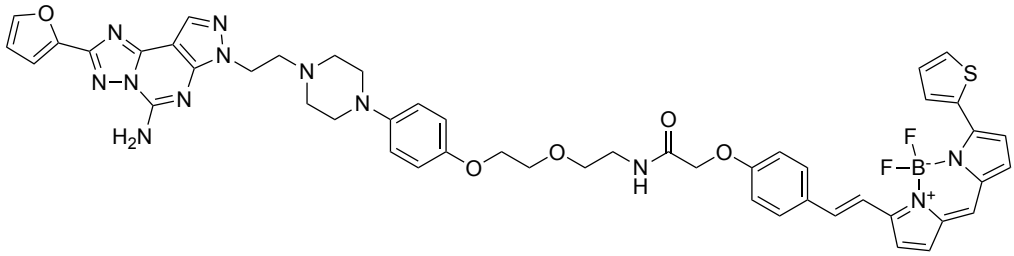


(*E*)-*N*-(2-(2-(4-(4-(2-(5-Amino-2-(furan-2-yl)-7*H*-pyrazolo[4,3-*e*][1,2,4]triazolo[1,5-*c*]pyrimidin-7-yl)ethyl)piperazin-1-yl)phenoxy)ethoxy)ethyl)-6-(2-(4-(2-(5,5-difluoro-7-(thiophen-2-yl)-

5*H*-5*l*^{4},6*l*^{4}-dipyrrolo[1,2-*c*:2',1'-*f*][1,3,2]diazaborinin-3-yl)vinyl)phenoxy)acetamido)hexanamide (**2.12**). Following general procedure D, amine congener **2.11** (0.5 mg, 1 equiv.) was converted to the BODIPY630/650–X conjugate **2.12**. Purification by RP-HPLC (Method C) gave, after lyophilization, the title compound as a blue solid (1.1 mg 98%).

Analytical RP-HPLC t_R =15.48 min (Method E), purity >98%.

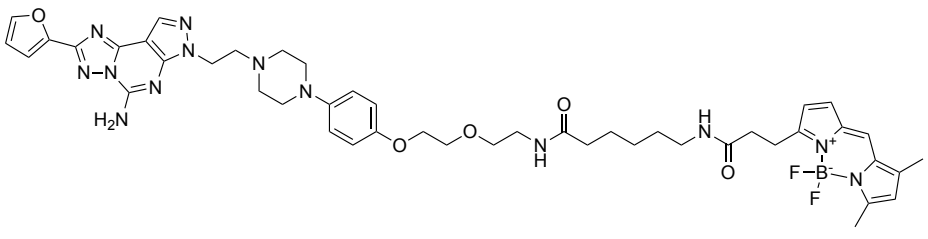
HRMS (ESI-TOF) calc. for $C_{55}H_{59}BF_2N_{13}O_6S$ $[M+H]^+$1078.4488; found 1078.4508 and 1100.4307 [M+Na].



(E)-*N*-(2-(2-(4-(4-(2-(5-Amino-2-(furan-2-yl)-7*H*-pyrazolo[4,3-*e*][1,2,4]triazolo[1,5-*c*]pyrimidin-7-yl)ethyl)piperazin-1-yl)phenoxy)ethoxy)ethyl)-2-(4-(2-(5,5-difluoro-7-(thiophen-2-yl)-5*H*-4*l*^{4},5*l*^{4}-dipyrrolo[1,2-*c*:2',1'-*f*][1,3,2]diazaborinin-3-yl)vinyl)phenoxy)acetamide (**2.13**)**.** Following general procedure D, amine congener **2.11** (1 equiv., 0.5 mg) was converted to the BODIPY630/650 conjugate **2.13**. Purification by RP-HPLC (Method C) gave, after lyophilization, the title compound as a blue solid (1 mg, 56%).

Analytical RP-HPLC t_R =15.30 min (Method E), purity >99%.

HRMS (TOF ES$^+$) calc. for $C_{49}H_{48}BF_2N_{12}O_5S$, $[M+H]^+$ 965.3574; found 965.3593.

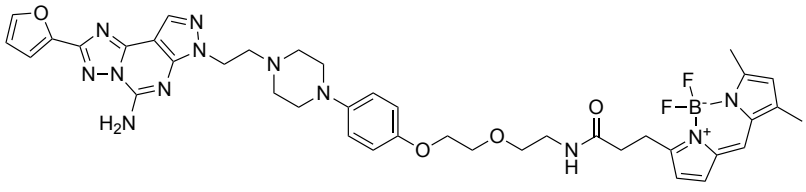


***N*-(2-(2-(4-(4-(2-(5-Amino-2-(furan-2-yl)-7*H*-pyrazolo[4,3-*e*][1,2,4]triazolo[1,5-*c*]pyrimidin-7-yl)ethyl)piperazin-1-**

yl)phenoxy)ethoxy)ethyl)-6-(3-(5,5-difluoro-7,9-dimethyl-5*H*-4l^4,5l^4-dipyrrolo[1,2-*c*:2',1'-*f*][1,3,2]diazaborinin-3-yl)propanamido)hexanamide (**2.14**). Following general procedure D, amine congener **2.11** (1 equiv., 0.5 mg) was converted to the BODIPY-FL–X conjugate **2.14**. Purification by RP-HPLC (Method C) gave, after lyophilization, the title compound as an orange solid, (1.2 mg, 70%).

Analytical RP-HPLC t_R =13.04 min (Method E) purity >99%.

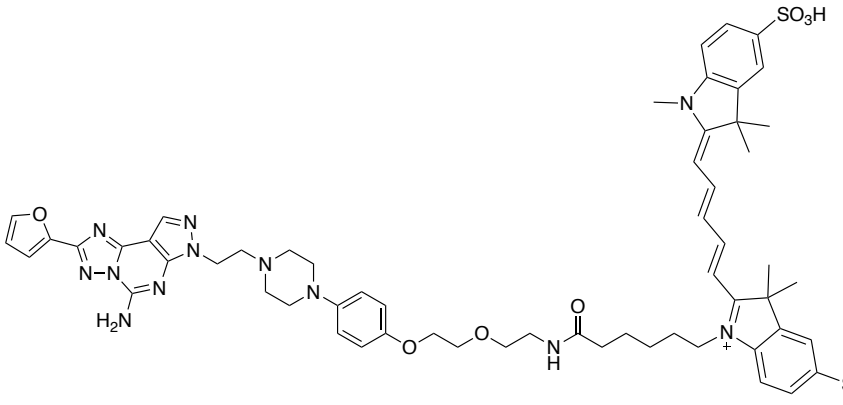
HRMS (TOF ES$^+$) calc. for $C_{46}H_{57}BF_2N_{13}O_5$, $[MH]^+$ 920.4588, found 920.4660.



***N*-(2-(2-(4-(4-(2-(5-Amino-2-(furan-2-yl)-7*H*-pyrazolo[4,3-*e*][1,2,4]triazolo[1,5-*c*]pyrimidin-7-yl)ethyl)piperazin-1-yl)phenoxy)ethoxy)ethyl)-3-(5,5-difluoro-7,9-dimethyl-5*H*-4l^4,5l^4-dipyrrolo[1,2-*c*:2',1'-*f*][1,3,2]diazaborinin-3-yl)propanamide** (**2.15**). Following general procedure D, amine congener **2.11** (1 equiv., 0.5 mg) was converted to the BODIPY–FL conjugate **2.15.** Purification by RP-HPLC (Method C) gave, after lyophilization, the title compound as an orange solid (0.7 mg, 100%).

Analytical RP-HPLC t_R =13.13 min (Method E), purity >99%.

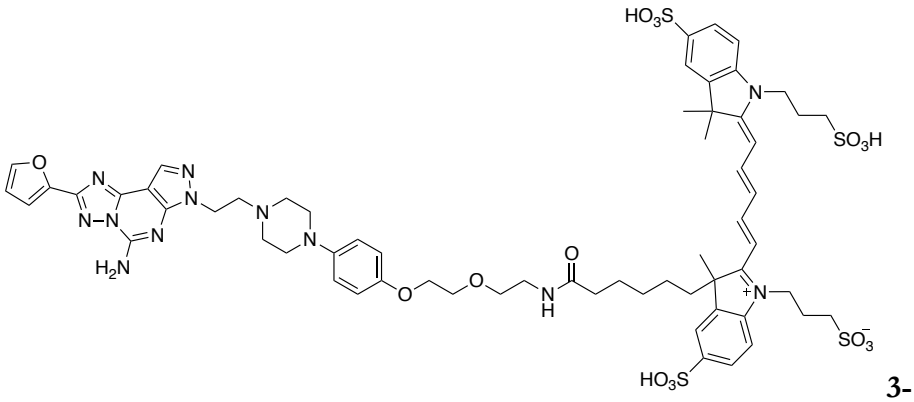
HRMS (TOF ES$^+$) calc. for $C_{40}H_{46}BF_2N_{12}O_4$, $[MH]^+$ 807.3821, found 807.3820 and calc. for $C_{40}H_{45}BF_2N_{12}O_4Na$ [M+Na] 829.3640, found 829.3627.



1-(6-((2-(2-(4-(4-(2-(5-Amino-2-(furan-2-yl)-7*H*-pyrazolo[4,3-*e*][1,2,4]triazolo[1,5-*c*]pyrimidin-7-yl)ethyl)piperazin-1-yl)phenoxy)ethoxy)ethyl)amino)-6-oxohexyl)-3,3-dimethyl-2-((1*E*,3*E*)-5-((*E*)-1,3,3-trimethyl-5-sulfoindolin-2-ylidene)penta-1,3-dien-1-yl)-3*H*-indol-1-ium-5-sulfonate (**2.16**). Following general procedure D, amine congener **2.11** (1 equiv., 0.5 mg) was converted to Sulfo-Cyanine-5 conjugate **2.16**. Purification by RP-HPLC (Method C) gave, after lyophilization, the title compound as bright blue solid (1.9 mg, 100%).

Analytical RP-HPLC t_R=12.41 min (Method E) purity >99%.

HRMS (TOF ES$^-$) $C_{58}H_{68}N_{12}O_{10}S_2$, $[MH]^-$ calculated 1155.4550, found 1155.4547



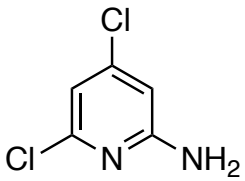
3-(6-((2-(2-(4-(4-(2-(5-Amino-2-(furan-2-yl)-7*H*-pyrazolo[4,3-*e*][1,2,4]triazolo[1,5-*c*]pyrimidin-7-yl)ethyl)piperazin-1-yl)phenoxy)ethoxy)ethyl)amino)-6-oxohexyl)-2-((1*E*,3*E*)-5-((*E*)-3,3-dimethyl-5-sulfo-1-(3-sulfopropyl)indolin-2-ylidene)penta-1,3-dien-1-yl)-3-methyl-5-sulfo-1-(3-sulfopropyl)-3*H*-indol-1-ium (**2.17**). Following general procedure D, amine congener **2.11** (1 equiv., 0.5 mg) was converted

to the AlexaFluor647 conjugate **2.17**. Purification by RP-HPLC (Method C) gave the title compound as bright blue solid (1.8 mg quantitative 100%).

Analytical RP-HPLC t_R =10.58 min (Method E) purity >99%.

HRMS (TOF ES$^-$) calc. for $C_{62}H_{76}N_{12}O_{16}S_4$, [MH]- 1372.4355; found 1372.4391 [M-2]$^-$ calculated 685.2120 found 685.2122.

7.1.3 Methods Chapter 3

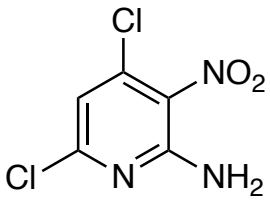


4,6-Dichloropyridin-2-amine (**3.2**).[358] In a pressure vessel, 2,4,6-trichloropyridine (1 g, 5.5 mmol) was dissolved in a solution of NH_3(15 mL). The vessel was sealed and heated for 24h at 155 ^{O}C. The reaction was then cooled at rt and the vessel was placed in an ice-bath and allow to vent slowly. The mixture was dissolved in H_2O and extracted with DCM (3x150 mL). The organics were collected, dried over anhydrous $MgSO_4$, filtered and concentrated *in vacuo*. Purification by flash chromatography with hexane/ethyl acetate 85:15 gave the desired product as off-white solid. (0.400 g, 45 %).

LC-MS ***m/z*** calcd for $C_5H_5Cl_2N_2[MH]^+$: 161.98, found 162.10 t_R = 2.56 min (Method A)

^{1}H NMR ($CDCl_3$) δ 6.68 (d, *J* = 1.4 Hz, 1H, Ar-H), 6.39 (d, *J* = 1.4 Hz, 1H, Ar-H), 4.74 (brs, 2H, NH_2).

^{13}C NMR ($CDCl_3$) δ 158.7 (CNH_2), 150.3(CCl), 146.3 (CCl), 113.5(CH), 106.2(CH).

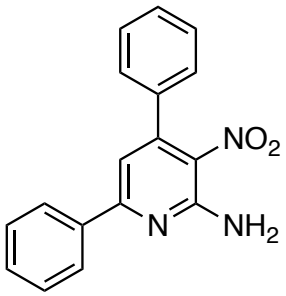


4,6-Dichloro-3-nitropyridin-2-amine (**3.3**).[359] At 0 ^{O}C, to 2-amino-4,6 dichloropyridine (0.200 g, 1.2 mmol) was added conc. H_2SO_4 (1.5 mL), followed by conc. HNO_3 (55 µL, 1.5 mmol, 1.2 equiv).The resulting mixture was stirred at 0 ^{O}C → 5 ^{O}C for 10h. Upon completion, the reaction was quenched in ice-water and neutralized with sat. $NaHCO_3$ (pH = 7). The yellow precipitate was filtered, collected, adsorbed on isolute and concentrated to dryness. Purification by flash column chromatography with Petroleum ether/EtOAc 70:30 gave the pure product as yellow solid (0.195 g, 76%).

LC-MS *m/z* calc. for $C_5H_4Cl_2N_3O_2$ $[MH]^+$ 208.10 found 208.10, t_R = 2.70 min

^{1}H NMR ($CDCl_3$) δ 6.83 (s, 1H, Ar-H), 6.24 (brs, 2H, NH_2).

^{13}C NMR ($CDCl_3$) δ 170.8 (C), 153.4 (C), 153.26 (C), 141.92 (C), 116.0 (CH).

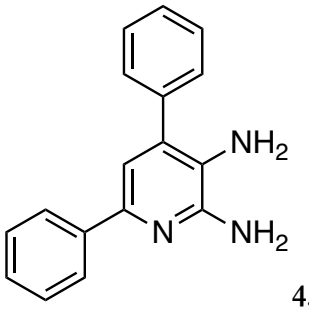


3-Nitro-4,6-diphenylpyridin-2-amine (**3.4**).[266] 4,6-Dichloro-3-nitropyridin-2-amine (0.100 g, 0.5 mmol, 1 equiv) was dissolved in toluene (2.5 mL). To the resulting mixture were added phenyl boronic acid (0.176 g, 1.4 mmol, 3 eq), tetrakis (triphenylphosphino) Pd (0) (29 mg, 25 µmol, 0.052 eq), K_2CO_3 (99 mg, 0.72 mmol, 1.5 eq) and H_20 (0.5 mL). The resulting mixture was heated in a MW reactor for 30 min at 150 ^{O} C. The solvent was evaporated and the residue adsorbed on isolute. Purification by flash column chromatography with Pet. Ether/EtOAc 9:1 afforded the pure product as yellow solid (0.100 g, 71%).

LC-MS *m/z* calc. for $C_{17}H_{14}N_3O_2$ $[MH]^+$ 292.00 found 291.9, t_R = 3.09 min

^{1}H NMR ($CDCl_3$) δ 8.04 – 7.98 (m, 2H, Ar-H), 7.50 – 7.42 (m, 6H, Ar-H), 7.39 – 7.34 (m, 2H, Ar-H), 7.10 (s, 1H, Ar-H), 6.17 (brs, 2H, NH_2).

^{13}C NMR ($CDCl_3$) δ 159.6 (C), 152.7 (C), 148.8 (C), 137.6 (C), 137.4 (C), 130.5 (C), 128.9 (CH), 128.8 (CH), 128.8 (CH), 127.5 (CH), 127.1 (CH), 113.8 (CH).

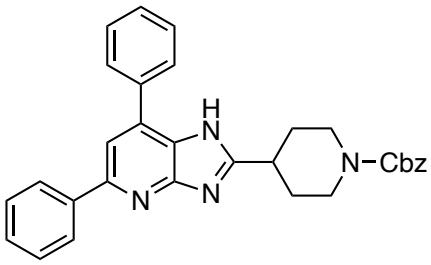


4,6-Diphenylpyridine-2,3-diamine (**3.5**)**.** To a solution of 3-nitro-4,6-diphenylpyridin-2-amine (0.100 g, 0.3 mmol, 1 equiv) in 30 mL of EtOH was added Pd/C 11% w/w. The reaction was stirred under N_2 at rt. The supply of N_2 was replaced with vacuum and this procedure was alternated three times. Ultimately the supply of N_2 was replaced with H_2 and the reaction was stirred at rt for 5h. Upon completion, the reaction mixture was filtered through celite and the pad was washed with EtOH and DCM. The filtrate was collected and concentrated in vacuo to give the pure product as yellow oil (yield 87 mg, 97%).

LC-MS *m/z* calc. for $C_{17}H_{16}N_3[MH]^+$ 262.00 found 261.8 t_R = 2.21 min

^{1}H NMR ($CDCl_3$) δ 7.93 – 7.88 (m, 2H, Ar-H), 7.54 – 7.46 (m, 4H, Ar-H), 7.45 – 7.37 (m, 3H, Ar-H), 7.34 – 7.28 (m, 1H, Ar-H), 7.10 (s, 1H, Ar-H), 4.39 (br s, 2H, NH_2), 3.50 (br s, 2H, NH_2).

^{13}C NMR ($CDCl_3$) δ 149.1(C), 146.3 (C), 139.8 (C), 137.7 (C), 135.4 (C), 129.1 (C), 128.6 (CH), 128.5 (CH), 128.2 (CH), 127.6 (CH), 126.2 (CH), 125.6 (CH), 113.9 (CH).



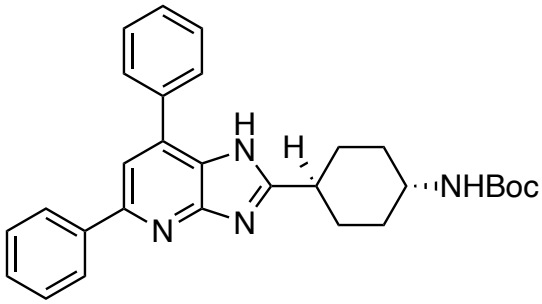
Benzyl 4-(5,7-diphenyl-1H-imidazo[4,5-b]pyridin-2-yl)piperidine-1-carboxylate (**3.6**)**.** A solution of 1-((benzyloxy)carbonyl)piperidine-4-carboxylic acid (56 mg, 0.2 mmol, 1 equiv) in dry DMF (0.3 mL) was treated with NEt_3 (80 mL, 0.57 mmol, 3 equiv), followed by PyBroP (89 mg, 0.2 mmol, 1 equiv). After 15 min the resulting mixture was added to a solution of 4,6-diphenylpyridine-2,3-diamine (**3.5**) (50 mg, 0.2 mmol, 1.1 equiv) in dry DMF (0.5 mL) and stirred under N_2 at rt overnight. Upon full conversion to the desired carboxamide product observed by LCMS (MH^+) 507.10, the resulting mixture was stirred at 90 °C for 24 h until complete conversion to the desired cyclised product. The reaction was cooled to rt, diluted with EtOAc (5 mL), washed with H_2O (2x10 mL), sat $NaHCO_3$ (2x5 mL) and brine (2x5 mL). The organic layers were combined, dried over anhydrous $MgSO_4$, filtered and concentrated to dryness. Purification by flash column chromatography on silica gel with DCM/MeOH 98:2 afforded the pure product as colourless film (35 mg, 38%).

LC-MS ***m/z*** calc. for $C_{31}H_{29}N_4O_2$ $[MH]^+$ 489.00 found 489.00 t_R = 3.11 min

^{1}H NMR ($CDCl_3$) δ 12.08 (brs, 1H, NH-imidazole), 8.24 (d, *J* = 6.7 Hz, 2H, Ar-H), 8.06 (d, *J* = 7.0 2H, Ar-H), 7.84 (s, 1H, Ar-H), 7.58 – 7.51 (m, 4H, Ar-H), 7.49 – 7.43 (m, 2H, Ar-H), 7.37 – 7.30 (m, 5H, Ar-H), 5.12 (s, 2H, benzyl-CH_2), 4.19 – 4.05 (m, 2H, CH_2 piperidine), 2.69 – 2.56 (m, 3H, CH + CH_2 piperidine), 1.89 – 1.80 (m, 2H, CH_2 piperidine), 1.79 – 1.66 (m, 2H, CH_2 piperidine).

^{13}C NMR ($CDCl_3$) δ 167.1(C), 159.0 (C), 155.1 (C=O), 152.1 (C), 140.3 (C), 139.8 (C), 136.8 (C), 136.0 (C), 129.3 (CH), 129.2 (CH), 128.8 (CH), 128.5

(CH), 128.0 (CH), 127.9 (CH), 127.6 (CH), 114.6 (CH), 67.1 (benzyl-CH_2), 43.4 (CH piperidine), 36.4 (CH_2 piperidine), 30.1 (CH_2 piperidine).



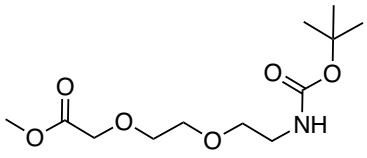
***tert*-Butyl ((1r,4r)-4-(5,7-diphenyl-1H-imidazo[4,5-b]pyridin-2-yl)cyclohexyl)carbamate** (**3.8**)**.** A solution of *trans*-4-(Boc-amino) cyclohexane carboxylic acid (20 mg, 82 mmol, 1 equiv) in CH_3CN (0.5 mL) was treated with N-methyl imidazole (23 mL, 0.29 mmol, 3.5 equiv), followed by 2-bromo-1-ethyl pyridinium tetrafluoroborate (BEP) (27 mg, 99 mmol, 1.2 equiv. To the resulting mixture was added a solution of 4,6-diphenylpyridine-2,3-diamine (**3.5**) in CH_3CN (0.5 mL) and the resulting solution was stirred at rt for 24 h. The solution was concentrated to dryness and the crude product was dissolved with toluene. The resulting mixture was heated to 97 °C overnight until complete conversion to the desired cyclised product was observed. The solvent was evaporated in *vacuo*. Purification by preparative TLC with DCM/MeOH 97:3 afforded the desired product as colourless film (15 mg, 35%).

LC-MS *m/z* calc. for $C_{29}H_{33}N_4O_2$ $[MH]^+$ 469.00 found 469.00 t_R =2.99 min

^{1}H NMR ($CDCl_3$) δ 12.70 (br s, 1H, NH-imidazole), 8.26 (d, *J* = 7.1 Hz, 2H, Ar-H), 8.09 (d, *J* = 7.2 Hz, 2H, Ar-H), 7.84 (s, 1H, Ar-H), 7.58 – 7.51 (m, 4H, Ar-H), 7.50 – 7.43 (m, 2H, Ar-H), 4.31 (d, *J* = 8.0 Hz, 1H, NHCO), 3.36 – 3.20 (m, 1H, CH cyclohexane), 2.43 – 2.29 (m, 1H, CH cyclohexane), 1.97 – 1.83 (m, 4H, CH_2 cyclohexane), 1.63 – 1.50 (m, 2H, CH_2 cyclohexane), 1.46 (s, 9H, Boc), 0.93 – 0.74 (m, 2H, CH_2 cyclohexane).

^{13}C NMR ($CDCl_3$) δ 160.2 (C), 155.1(C=O), 151.8 (C), 150.2 (C), 140.3 (C), 139.6 (C), 136.2 (C), 132.8(C), 129.3 (CH), 129.1 (CH), 129.0 (CH), 128.8 (CH), 128.7

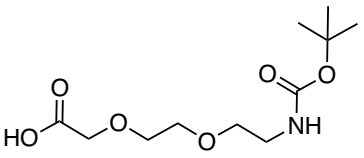
(CH), 127.7 (CH), 114.5 (CH), 79.0 (C), 48.9 (CH), 37.7 (CH), 32.8 (CH_2), 30.1 (CH_2), 28.5 (CH_3 Boc).



Methyl 2,2-dimethyl-4-oxo-3,8,11-trioxa-5-azatridecan-13-oate (**3.17**)**.** Under N_2, *tert*-Butyl (2-(2-hydroxyethoxy)ethyl)carbamate (0.500 g, 2.43 mmol, 1 equiv) was dissolved in anhydrous THF (30 mL) and cooled to 0 °C. To the solution was added NaH 60% mineral oil (0.146 g, 13.66 mmol, .5 equiv) portionwise and the mixture was stirred for 30 min. Methyl bromoacetate (0.447g, 2.92 mmol, 1.2 equiv) was added, followed by NaI (5% mol) and the resulting mixture was stirred overnight. The mixture was diluted with H_2O (30 mL) and extracted with DCM (30 mL). The organic layer was washed with brine, dried over anhydrous $MgSO_4$, filtered and concentrated to dryness. Purification by flash column chromatography with Petroleum ether/EtOAc 4:6 gave the pure product as colourless oil (0.300 g, 42%).

^{1}H NMR ($CDCl_3$) δ 5.02 (s, 1H, NH), 4.14 (s, 2H, CH_2), 3.74 (s, 3H, CH_3), 3.73 – 3.68 (m, 2H, CH_2), 3.66 – 3.61 (m, 2H, CH_2), 3.52 (t, J = 5.2 Hz, 2H, CH_2), 3.29 (q, J = 5.5 Hz, 2H, CH_2), 1.42 (s,9H, Boc).

^{13}C NMR ($CDCl_3$) δ 170.8 (C=O), 156.0 (C=O), 79.2 (C), 70.9(CH_2), 70.3 (CH_2), 70.3 (CH_2), 68.6 (CH_2), 51.8 (CH_2), 40.3 (CH_2), 28.4 ((CH_3)$_3$ Boc).

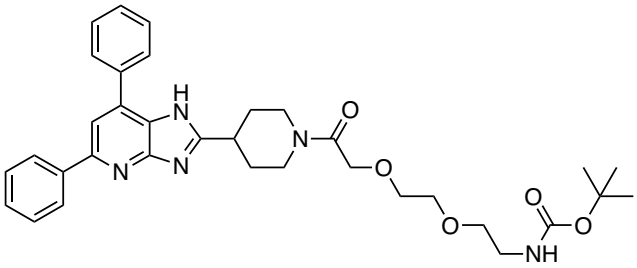


2,2-Dimethyl-4-oxo-3,8,11-trioxa-5-azatridecan-13-oic acid (**3.18**)**.** Methyl 2,2-dimethyl-4-oxo-3,8,11-trioxa-5-azatridecan-13-oate (0.300 g, 1.03 mmol, 1 equiv) was dissolved in THF (25 mL) and to the resulting mixture was added a solution of LiOH (0.216 g, 5.2 mmoL, 5 equiv) in H_2O (25 mL). The reaction mixture was stirred at rt for 3h. Upon completion of the reaction monitored by TLC, the organic layer was removed in vacuo and the water layer was extracted with EtOAc (2x 10 mL). The aqueous layer was separated and acidified with 2 M HCl until pH

= 3-4. The aqueous layer was extracted with EtOAc and the organic phase was separated, dried over anhydrous $MgSO_4$, filtered and evaporated to dryness to give the pure product as colourless oil (0.186 g, 69%).

^{1}H NMR ($CDCl_3$) δ 6.92 (br s, 1H, O<u>H</u>), 5.04 (s, 1H, N<u>H</u>), 4.16 (s, 2H, C<u>H</u>$_2$), 3.78 – 3.71 (m, 2H, C<u>H</u>$_2$), 3.69 – 3.63 (m, 2H, C<u>H</u>$_2$), 3.56 (t, *J* = 5.6 Hz, 2H, C<u>H</u>$_2$), 3.38 – 3.22 (m, 2H, C<u>H</u>$_2$), 1.43 (s, 9H, Boc).

^{13}C NMR ($CDCl_3$) δ 173.2 (<u>C</u>=O), 156.2 (<u>C</u>=O), 79.5 (<u>C</u>), 71.2 (<u>C</u>H$_2$), 70.5 (<u>C</u>H$_2$), 70.1 (<u>C</u>H$_2$), 68.6 (<u>C</u>H$_2$), 40.3 (<u>C</u>H$_2$), 28.4 ((<u>C</u>H$_3$)$_3$ Boc).



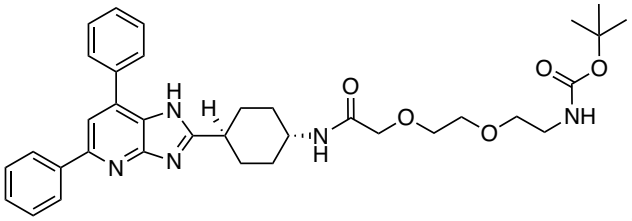
tert*-Butyl (2-(2-(2-(4-(5,7-diphenyl-1H-imidazo[4,5-b]pyridin-2-yl)piperidin-1-yl)-2-oxoethoxy)ethoxy)ethyl)carbamate** (**3.10**)**.** Benzyl 4-(5,7-diphenyl-1H-imidazo[4,5-b]pyridin-2-yl)piperidine-1-carboxylate (**3.6**)(66 mg, 135 μmol, 1 equiv) was dissolved in a mixture of MeOH (3 mL) and H_2O (0.3 mL). To the resulting solution, under N_2, was added Pd/C 11% w/w. The supply of N_2 was replaced with vacuum and this procedure was alternated three times. Ultimately the supply of N_2 was replaced with H_2 and the reaction was stirred at rt for 1h. Upon completion, the reaction mixture was filtered through celite and the pad was washed with EtOH and DCM. The filtrate was collected and concentrated in vacuo to give the desired 5,7-diphenyl-2-(piperidin-4-yl)-1H-imidazo[4,5-b]pyridine product as colourless oil (**3.7**) (yield 12 mg, 75%), which was used for the next step without further purification. **LC-MS *m/z calc. for $C_{23}H_{22}N_4$ $[MH]^+$ 355.2 found 355.2 t_R = 2.26 min. 5,7-diphenyl-2-(piperidin-4-yl)-1H-imidazo[4,5-b]pyridine product (**3.7**) (37 mg, 104 μmol, 1 equiv) was dissolved in anhydrous DCM (0.5 mL) and the resulting mixture was added to a previously reacted solution of 2,2-dimethyl-4-oxo-3,8,11-trioxa-5-azatridecan-13-oic acid (**3.18**) (30 mg, 104 mmol, 1 equiv), DIPEA (55 mL, 300 μmol, 3 equiv) and PyBroP (58 mg,

100 μmol, 1.2 equiv) in anhydrous DCM (0.5 mL).The resulting mixture was stirred at RT for 4h under N_2. Upon completion of the reaction, the solution was washed with sat. $NaHCO_3$ (2x5 mL) and brine (1x 10 mL). The organic layer was dried over anhydrous $MgSO_4$, filtered and concentrated to dryness. Purification by flash column chromatography with DCM/MeOH 98:2 yielded the pure product as colourless film (44 mg, 70%)

LC-MS *m/z* calc. for $C_{34}H_{42}N_5O_5$ $[MH]^+$ 600.00 found 599.9 t_R = 2.88min

^{1}H NMR ($CDCl_3$) δ 13.03 (brs, 1H, NH-imidazole), 8.24 (d, *J* = 7.0 Hz, 2H, Ar-H), 8.09 (d, *J* = 7.2 Hz, 2H, Ar-H), 7.84 (s, 1H, Ar-H), 7.60 – 7.52 (m, 4H, Ar-H), 7.52 – 7.44 (m, 2H, Ar-H), 5.15 (br s, 1H, NHCO), 4.50 – 4.36 (m, 1H, CH piperidine), 4.21 (d, *J* = 12.5 Hz, 1H, COHCHO), 4.15 (d, *J* = 12.4 Hz, 1H, COHCHO), 3.92 – 3.81 (m, 1H, CH_2 piperidine), 3.73 – 3.58 (m, 4H,CH_2), 3.52 (t, *J* = 4.9 Hz, 2H, CH_2), 3.31 – 3.19 (m, 2H, CH_2), 2.83 – 2.73 (m, 1H,CH_2 piperidine), 2.66 – 2.53 (m, 1H, CH_2 piperidine), 2.43 – 2.31 (m, 1H, CH_2 piperidine), 1.86 – 1.64 (m, 4H, CH_2 piperidine), 1.39 (s, 9H, Boc).

^{13}C NMR ($CDCl_3$) δ167.6 (C), 158.9 (C), 156.2 (C=O), 152.2 (C), 150.3 (C), 140.5 (C), 136.2 (C), 132.9 (C), 129.4 (CH), 129.3 (CH), 128.9 (CH), 127.8 (CH), 114.7 (CH), 79.2 (C), 70.7 (CH_2), 70.3 (CH_2), 44.7(CH_2), 41.6 (CH), 40.4 (CH_2), 36.6 (CH_2), 29.8 (CH_2), 28.5. (one carbonyl carbon not observed),



***tert*-Butyl (2-(2-(2-(((1r,4r)-4-(5,7-diphenyl-1H-imidazo[4,5-b]pyridin-2-yl)cyclohexyl)amino)-2-oxoethoxy)ethoxy)ethyl)carbamate** (**3.12**). *tert*-Butyl ((1r,4r)-4-(5,7-diphenyl-1H-imidazo[4,5-b]pyridin-2-yl)cyclohexyl)carbamate (**3.8**) (18 mg, 380 μmol, 1 equiv) was treated with 4 M HCl in dioxane for 45 min. Evaporation of the solvent in vacuo yielded the desired (1r,4r)-4-(5,7-diphenyl-1*H*-imidazo[4,5-b]pyridin-2-

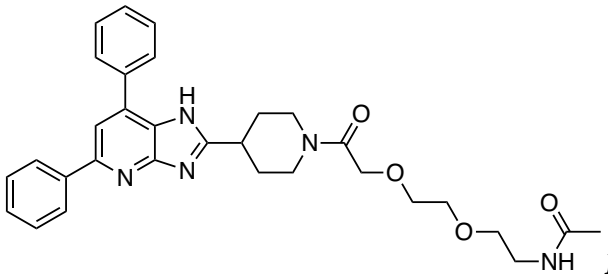
yl)cyclohexan-1-aminium chloride product (**3.9**) as off-white solid, which was used for the next step without further purification. **LC-MS *m/z*** calc. for $C_{24}H_{25}N_4$ $[MH]^+$ 369.20 found 369.00 t_R = 2.24 min.

2,2-dimethyl-4-oxo-3,8,11-trioxa-5-azatridecan-13-oic acid (**3.18**) (11 mg, 41 μmol, 1 equiv), DIPEA (55 mL, 40 μmol, 3 equiv) and PyBroP (19 mg, 40 μmol, 1.05 equiv) were reacted in anhydrous DCM (0.5 mL) for 15 min. Subsequently, a solution of (1r,4r)-4-(5,7-diphenyl-1*H*-imidazo[4,5-b]pyridin-2-yl)cyclohexan-1-aminium chloride product (**3.9**) (14 mg, 38 μmol, 1 equiv) in anhydrous DCM (0.5 mL) was added to the flask and the resulting mixture was stirred at rt, under N_2, for 3 h. Purification by preparative TLC with DCM/MeOH 96:4 afforded the desired product as colourless film (10 mg, 43%).

LC-MS *m/z* calc. for $C_{35}H_{44}N_5O_5$ $[MH]^+$ 614.00 found 614.00 t_R = 2.98min

^{1}H NMR ($CDCl_3$) δ 12.14 (br s, 1H, NH-imidazole), 8.20 (d, *J* = 7.0 Hz, 2H, Ar-H), 8.08 (d, *J* = 6.8 Hz, 2H, Ar-H), 7.82 (s, 1H, Ar-H), 7.57 – 7.40 (m, 6H, Ar-H), 6.79 (d, *J* = 7.0 Hz, 1H, NH), 4.93 – 4.84 (m, 1H, CH), 4.26 (s, 2H, $COCH_2O$), 4.05 – 3.91 (m, 1H, CH), 3.75 – 3.68 (m, 2H, CH_2), 3.68 – 3.61 (m, 2H, CH_2), 3.56 (t, *J* = 7.0 Hz, 2H, CH_2), 3.39 – 3.30 (m, 2H, CH_2), 2.90 – 2.80 (m, 1H, CH), 2.15 – 2.03 (m, 4H, CH_2 cyclohexane), 1.94 – 1.65 (m, 4H, CH_2 cyclohexane), 1.44 (s, 9H, Boc).

^{13}C NMR ($CDCl_3$) δ 169.7 (C), 160.1(C), 155.9 (C=O), 151.8 (C), 150.1 (C), 140.3 (C), 139.2 (C), 136.5 (C), 132.2 (C), 129.2 (CH), 128.8 (CH), 128.4 (CH), 127.2 (CH), 114.1 (CH), 79.6 (C), 70.9 (CH_2), 70.5 (CH_2), 70.4 (CH_2), 69.9 (CH_2), 47.5 (CH), 40.2 (CH_2), 38.5 (CH_2), 32.6 (CH_2), 30.2 (CH_2), 28.4 (CH_3 Boc).



N*-(2-(2-(2-(4-(5,7-Diphenyl-1*H*-imidazo[4,5-b]pyridin-2-yl)piperidin-1-yl)-2-oxoethoxy)ethoxy)ethyl)acetamide** (**3.14**)**.** *tert*-Butyl (2-(2-(2-(4-(5,7-diphenyl-1*H*-imidazo[4,5-b]pyridin-2-yl)piperidin-1-yl)-2-oxoethoxy)ethoxy)ethyl)carbamate (**3.10**) (3 mg, 5 μmol, 1 equiv) was treated with 4M HCl in dioxane (0.7 mL) for 1 h and 30 min. After the removal of the solvent in vacuo, the resulting product (x), as HCl salt, was used for the subsequent step without further purification. **LC-MS** ***m/z calc. for $C_{29}H_{34}N_5O_3$ $[MH]^+$ 500.0 found 500.00 t_R = 2.28 min. 2-(2-(2-(4-(5,7-Diphenyl-1*H*-imidazo[4,5-b]pyridin-2-yl)piperidin-1-yl)-2-oxoethoxy)ethoxy)ethan-1-aminium chloride product (**3.11**) (2 mg, 4 μmol, 1 equiv) was dissolved in DMF (0.5 mL) and treated with DIPEA (2 mL, 12 mmol, 3 equiv), followed by acetic acid *N*-hydroxysuccinimide ester (0.6 mg, 4 μmol, 1 equiv). The resulting mixture was stirred at rt for 1 h. Upon completion of the reaction, the solvent was removed in vacuo and the crude product was purified by preparative TLC with DCM/MeOH 96:4. Pure product obtained as white waxy solid (1.9 mg, 95%).

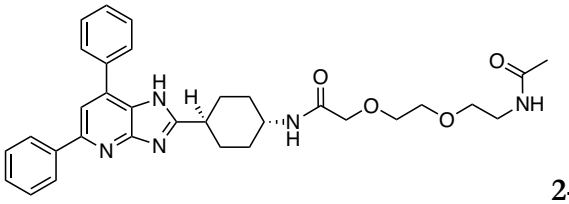
LC-MS ***m/z*** calc. for $C_{31}H_{36}N_5O_4$ $[MH]^+$ 542.30 found 542.00 t_R = 2.61 min

HRMS (TOF ES$^+$) calcd for $C_{31}H_{36}N_5O_4$ $[MH]^+$: 542.2762, found 542.2757; calcd for $C_{31}H_{35}NaN_5O_4$ $[MH]^+$: 564.2581, found 564.2591

^{1}H NMR ($CDCl_3$) δ 12.39 (br s, 1H, NH-imidazole), 8.22 (d, *J* = 7.0 Hz, 2H, Ar-H), 8.06 (d, *J* = 7.0 Hz, 2H, Ar-H), 7.84 (s, 1H, Ar-H), 7.59 – 7.51 (m, 4H, Ar-H), 7.50 – 7.43 (m, 2H, Ar-H), 6.68 (br s, 1H, NHCO), 4.54 – 4.45 (m, 1H, CH piperidine), 4.31 (d, *J* = 14.1 Hz, 1H, COHCHO), 4.14 (d, *J* = 13.2 Hz, 1H, COHCHO), 3.95 – 3.85 (m, 1H, CH_2 piperidine), 3.76 – 3.64 (m, 4H, CH_2), 3.62 – 3.55 (m, 2H, CH_2), 3.47 – 3.38 (m, 2H, CH_2), 2.95 –

2.76 (m, 2H, C$\underline{H}_2$ piperidine), 2.56 – 2.44 (m, 1H, C$\underline{H}_2$ piperidine), 1.95 (s, 5H, acetal -C$\underline{H}_3$ and cyclohexane-C$\underline{H}_2$ overlapping), 1.81 – 1.71 (m, 2H, cyclohexane-C$\underline{H}_2$ overlap with H_2O peak).

^{13}C NMR ($CDCl_3$) δ 170.9 (<u>C</u>=O), 167.8 (<u>C</u>), 158.6 (<u>C</u>), 152.4 (<u>C</u>), 150.1 (<u>C</u>), 140.4 (<u>C</u>), 139.9 (<u>C</u>), 136.2 (<u>C</u>), 132.6 (<u>C</u>), 129.4 (<u>C</u>H), 129.3 (<u>C</u>H), 129.2 (<u>C</u>H), 129.0 (<u>C</u>H), 128.9 (<u>C</u>H), 127.6 (<u>C</u>H), 114.8 (<u>C</u>H), 70.8 (<u>C</u>H_2), 70.6 (<u>C</u>H_2), 70.3 (<u>C</u>H_2), 69.9 (<u>C</u>H_2), 44.9 (<u>C</u>=O), 41.8 (<u>C</u>H), 39.4 (<u>C</u>H_2), 36.9 (<u>C</u>H_2), 30.6 (<u>C</u>H_2), 23.2 (<u>C</u>H_3).

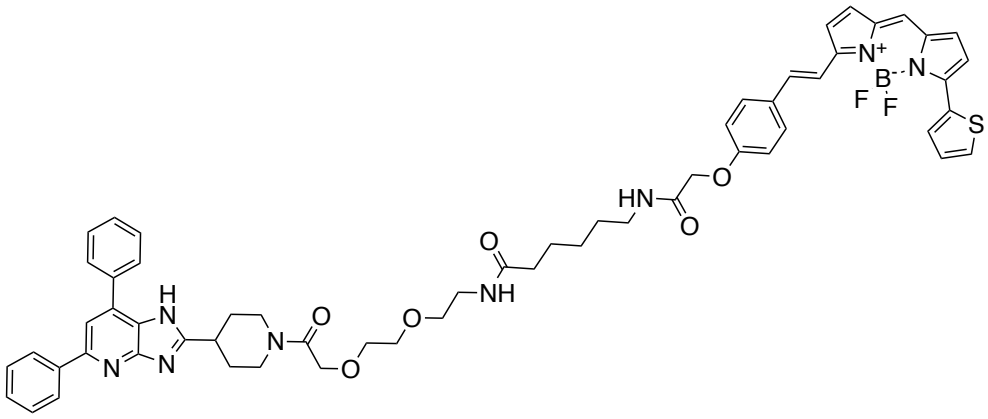


2-(2-(2-Acetamidoethoxy)ethoxy)-*N*-((1r,4r)-4-(5,7-diphenyl-1*H*-imidazo[4,5-b]pyridin-2-yl)cyclohexyl)acetamide (**3.15**)**.** *tert*-Butyl (2-(2-(2-(((1r,4r)-4-(5,7-diphenyl-1H-imidazo[4,5-b]pyridin-2-yl)cyclohexyl)amino)-2-oxoethoxy)ethoxy)ethyl)carbamate (**3.12**) (5 mg, 8 μmol, 1 equiv) was treated with 4M HCl in dioxane (0.7 mL) for 1 h and 30 min. After the removal of the solvent in vacuo, the resulting product (**3.13**), as HCl salt, was used for the subsequent step without further purification. **LC-MS *m/z*** calc. for $C_{30}H_{36}N_5O_3$ $[MH]^+$ 514.3 found 514.00 t_R = 2.27 min. 2-(2-(2-(((1r,4r)-4-(5,7-diphenyl-1H-imidazo[4,5-b]pyridin-2-yl)cyclohexyl)amino)-2-oxoethoxy)ethoxy)ethan-1-aminium chloride (**3.13**) (4 mg, 8 μmol, 1 equiv) was dissolved in DMF (0.5 mL) and treated with DIPEA (4 mL, 23 μmol, 3 equiv), followed by acetic acid *N*-hydroxysuccinimide ester (1.2 mg, 8 μmol, 1 equiv). The resulting mixture was stirred at rt for 1 h. Upon completion of the reaction, the solvent was removed in vacuo and the crude product was purified by preparative TLC with DCM/MeOH 96:4. Pure product obtained as white waxy solid (1.4 mg, 33%).

LC-MS *m/z* calc. for $C_{32}H_{38}N_5O_4$ $[MH]^+$ 556.30 found 555.8 t_R = 2.56min
HRMS (TOF ES$^-$) calcd for $C_{32}H_{36}N_5O_4$ $[MH]^-$: 554.2773, found 554.2765;

^{1}H NMR ($CDCl_3$) δ 11.14 (br s, 1H, NH-imidazole), 8.20 (d, *J* = 7.2 Hz, 2H, Ar-H), 8.09 (d, *J* = 7.2 Hz, 2H, Ar-H), 7.83 (s, 1H, Ar-H), 7.57 – 7.42 (m, 6H, Ar-H), 6.71 (d, *J* = 7.2 Hz, 1H, NH), 5.94 – 5.87 (m, 1H, CH), 4.21 (s, 2H, $COCH_2O$), 4.04 – 3.96 (m, 1H, CH), 3.76 – 3.72 (m, 2H, , CH_2), 3.68 – 3.64 (m, 2H, CH_2), 3.56 (d, *J* = 4.7 Hz, 2H, CH_2), 3.48 – 3.42 (m, 2H, CH_2), 2.96 – 2.87 (m, 1H, CH), 2.22 – 2.10 (m, 4H, CH_2 cyclohexane), 1.97 (s, 3H, CH_3), 1.91 – 1.80 (m, 2H, , CH_2 cyclohexane), 1.38 – 1.26 (m, 2H, , CH_2 cyclohexane).

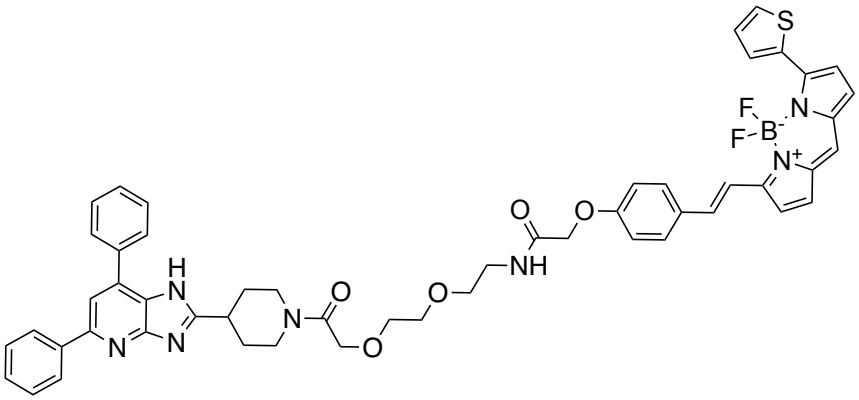
^{13}C NMR ($CDCl_3$) δ 170.3 (C=O), 169.6 (C), 159.6 (C), 152.0 (C), 149.8 (C), 140.1 (C), 139.3 (C), 136.4 (C), 132.2 (C), 129.3 (CH), 129.0 (CH), 129.0 (CH), 128.9 (CH), 128.6 (CH), 127.2 (CH), 114.2 (CH), 71.0 (CH_2), 70.8 (CH_2), 70.4 (CH_2), 70.2 (CH_2), 47.6 (C=O), 39.4 (CH), 38.5 (CH), 32.8 (CH_2), 30.4 (CH_2), 29.7 (CH_2), 23.4 (CH_3).



(*E*)-6-(2-(4-(2-(5,5-Difluoro-7-(thiophen-2-yl)-5*H*-4*l*^{4},5*l*^{4}-dipyrrolo[1,2-*c*:2',1'-*f*][1,3,2]diazaborinin-3-yl)vinyl)phenoxy)acetamido)-*N*-(2-(2-(2-(4-(5,7-diphenyl-1*H*-imidazo[4,5-b]pyridin-2-yl)piperidin-1-yl)-2-oxoethoxy)ethoxy)ethyl)hexanamide (**3.19a**)**.** Following general procedure D, amine congener **3.11** (0.6 mg, 1.2 μmoL, 1.1 equiv) was converted to the BODIPY 630/650-X conjugate **3.19a**. Purification by RP-HPLC (Method E) gave after lyophilisation the title compound as a blue solid (1.3 mg, quantitative)

HRMS (TOF ES$^+$) calcd for $C_{58}H_{60}BF_2N_8O_6S$ $[MH]^+$: 1045.4412, found 1045.4411;

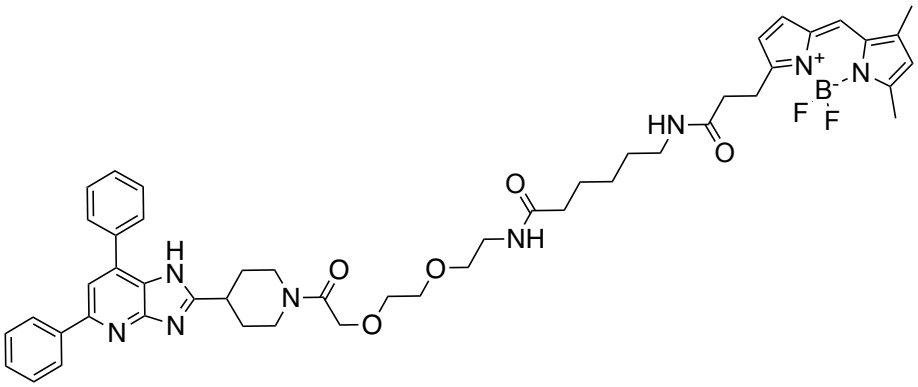
Analytical RP-HPLC t_R = 22.18 min, purity > 97% (Method C).



(*E*)-2-(4-(2-(5,5-Difluoro-7-(thiophen-2-yl)-5*H*-4*l*^{4},5*l*^{4}-dipyrrolo[1,2-*c*:2',1'-*f*][1,3,2]diazaborinin-3-yl)vinyl)phenoxy)-*N*-(2-(2-(2-(4-(5,7-diphenyl-1*H*-imidazo[4,5-b]pyridin-2-yl)piperidin-1-yl)-2-oxoethoxy)ethoxy)ethyl)acetamide (**3.19b**)**.** Following general procedure D, amine congener **3.11** (0.7 mg, 1.4 μmoL, 1.1 equiv) was converted to the BODIPY 630/650 conjugate **3.19b**, following pre activation of BODIPY 630/650 CO_2H (0.6 mg, 1.3 μmoL, 1 equiv) with HATU (0.6 mg, 1.5 μmoL, 1.2 equiv) in the presence of DIPEA (5 equiv). Purification by RP-HPLC (Method E) gave after lyophilisation the title compound as a blue solid (1 mg, 83%).

HRMS (TOF ES$^+$) calcd for $C_{52}H_{49}BF_2N_7O_5S$ $[MH]^+$: 932.3577, found 932.3642;

Analytical RP-HPLC t_R = 22.73 min, purity > 99% (Method C).

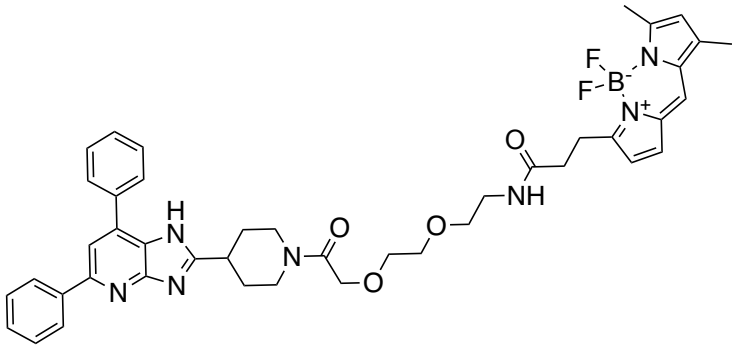


6-(3-(5,5-Difluoro-7,9-dimethyl-5*H*-4*l*^{4},5*l*^{4}-dipyrrolo[1,2-*c*:2',1'-*f*][1,3,2]diazaborinin-3-yl)propanamido)-*N*-(2-(2-(2-(4-(5,7-diphenyl-1*H*-imidazo[4,5-*b*]pyridin-2-yl)piperidin-1-yl)-2-oxoethoxy)ethoxy)ethyl)hexanamide (**3.19c**)**.** Following general

procedure D, amine congener **3.11** (0.7 mg, 1.4 μmoL, 1.1 equiv) was converted to the BODIPY FL-X conjugate **3.19c**. Purification by RP-HPLC (Method E) gave after lyophilisation the title compound as a blue solid (1.2 mg, quantitative)

HRMS (TOF ES$^+$) calcd for $C_{49}H_{58}BF_2N_8O_5$ $[MH]^+$: 887.4591, found 887.4586;

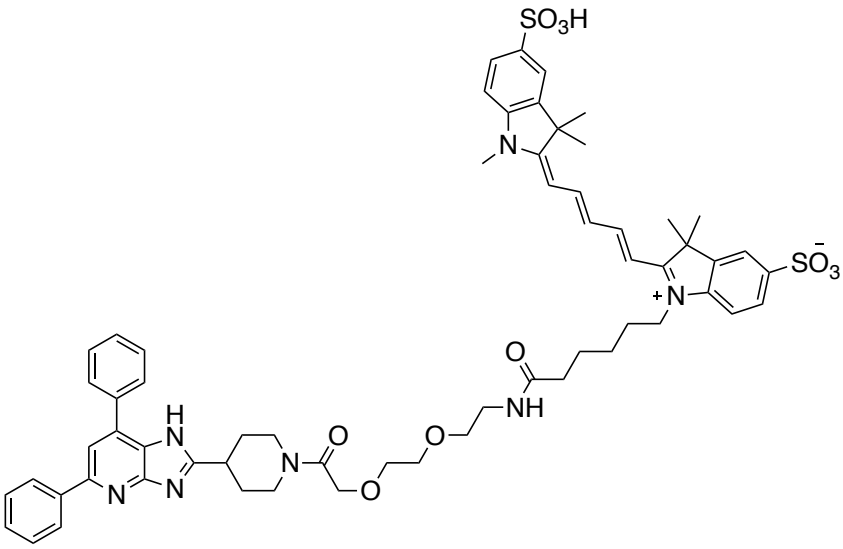
Analytical RP-HPLC t_R = 18.67 min, purity > 99% (Method C).



3-(5,5-Difluoro-7,9-dimethyl-5*H*-4*l*^{4},5*l*^{4}-dipyrrolo[1,2-*c*:2',1'-*f*][1,3,2]diazaborinin-3-yl)-*N*-(2-(2-(2-(4-(5,7-diphenyl-1*H*-imidazo[4,5-*b*]pyridin-2-yl)piperidin-1-yl)-2-oxoethoxy)ethoxy)ethyl)propenamide (**3.19d**)**.** Following general procedure D, amine congener **3.11** (0.5 mg, 1 μmoL, 1.1 equiv) was converted to the BODIPY FL conjugate **3.19d**. Purification by RP-HPLC (Method E) gave after lyophilisation the title compound as a blue solid (0.6 mg, 86%).

HRMS (TOF ES$^+$) calcd for $C_{43}H_{47}BF_2N_7O_4$ $[MH]^+$: 774.3745, found 774.3744; calcd for $C_{43}H_{46}NaBF_2N_7O_4$ $[MH]^+$: 796.3565, found 796.3550

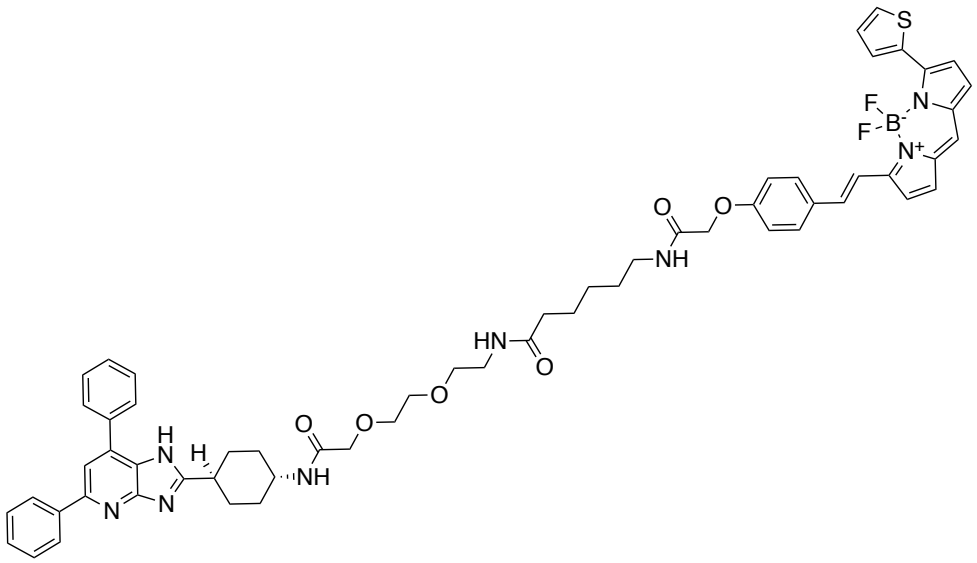
Analytical RP-HPLC t_R = 19.40 min, purity > 99% (Method C).



1-(6-((2-(2-(2-(4-(5,7-Diphenyl-1*H*-imidazo[4,5-*b*]pyridin-2-yl)piperidin-1-yl)-2-oxoethoxy)ethoxy)ethyl)amino)-6-oxohexyl)-3,3-dimethyl-2-((1*E*,3*E*)-5-((*E*)-1,3,3-trimethyl-5-sulfoindolin-2-ylidene)penta-1,3-dien-1-yl)-3*H*-indol-1-ium-5-sulfonate (**3.19e**)**.** Following general procedure D, amine congener **3.11** (0.5 mg, 1 μmoL, 1.1 equiv) was converted to the SulfoCy5 conjugate **3.19e**. Purification by RP-HPLC (Method E) gave after lyophilisation the title compound as a blue solid (1.6 mg, 89%).

HRMS (TOF ES$^+$) calcd for $C_{61}H_{70}N_7O_{10}S_2$ $[MH]^+$: 1124.4620, found 1124.4569;

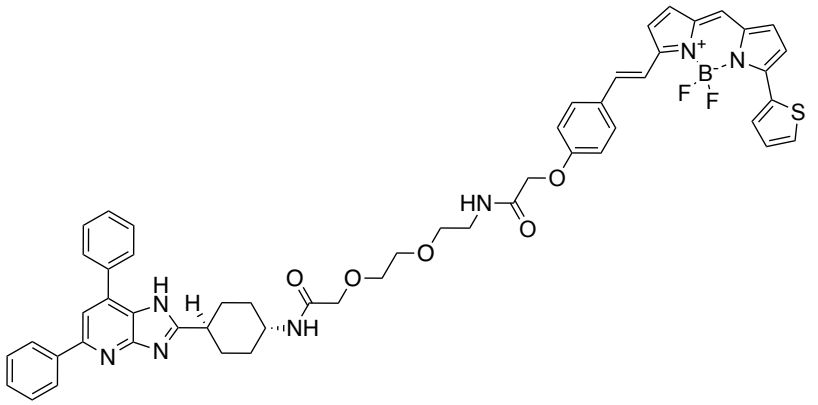
Analytical RP-HPLC t_R = 19.40 min, purity > 95% (Method C).



6-(2-(4-((*E*)-2-(5,5-Difluoro-7-(thiophen-2-yl)-5*H*-4*l*^{4},5*l*^{4}-dipyrrolo[1,2-*c*:2',1'-*f*][1,3,2]diazaborinin-3-yl)vinyl)phenoxy)acetamido)-*N*-(2-(2-(2-(((1*r*,4*r*)-4-(5,7-diphenyl-1*H*-imidazo[4,5-b]pyridin-2-yl)cyclohexyl)amino)-2-oxoethoxy)ethoxy)ethyl)hexanamide (**3.20a**)**.** Following general procedure D, amine congener **3.13** (0.8 mg, 1 μmoL, 1.1 equiv) was converted to the BODIPY 630/650-X conjugate **3.20a**. Purification by RP-HPLC (Method E) gave after lyophilisation the title compound as a blue solid (0.9 mg, 90%)

HRMS (TOF ES$^+$) calcd for $C_{59}H_{62}BF_2N_8O_6S$ $[MH]^+$: 1059.4574, found 1059.4666; calcd for $C_{59}H_{61}NaBF_2N_8O_6S$ $[MH]^+$: 1081.4447, found 1081.4447

Analytical RP-HPLC t_R = 21.20 min, purity > 99% (Method C).

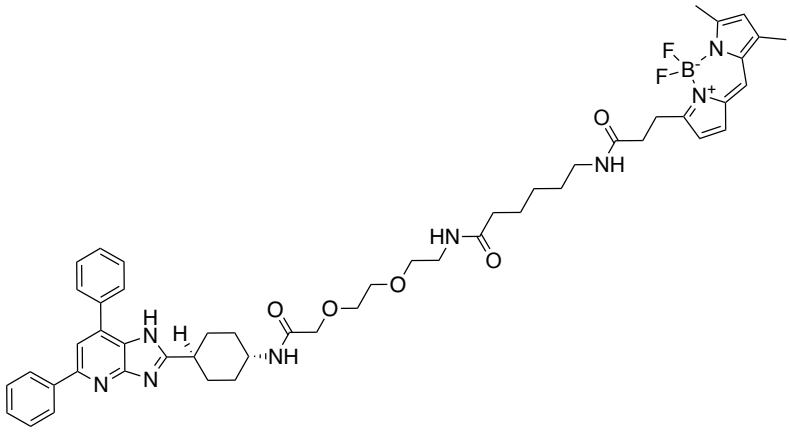


2-(4-((*E*)-2-(5,5-Difluoro-7-(thiophen-2-yl)-5*H*-4*l*^{4},5*l*^{4}-dipyrrolo[1,2-*c*:2',1'-

***f*][1,3,2]diazaborinin-3-yl)vinyl)phenoxy)-*N*-(2-(2-(2-(((1*r*,4*r*)-4-(5,7-diphenyl-1*H*-imidazo[4,5-*b*]pyridin-2-yl)cyclohexyl)amino)-2-oxoethoxy)ethoxy)ethyl)acetamide** (**3.20b**)**.** Following general procedure D, amine congener **3.13** (0.7 mg, 1.6 μmoL, 1.1 equiv) was converted to the BODIPY 630/650 conjugate **3.20b**, following pre activation of BODIPY 630/650 CO_2H (0.6 mg, 1.3 μmoL, 1 equiv) with HATU (0.6 mg, 1.6 μmoL, 1.2 equiv) in the presence of DIPEA (5 equiv). Purification by RP-HPLC (Method E) gave after lyophilisation the title compound as a blue solid (1 mg, 77%).

HRMS (TOF ES^+) calcd for $C_{53}H_{52}BF_2N_7O_5S$ $[MH]^+$: 946.3812, found 946.3711;

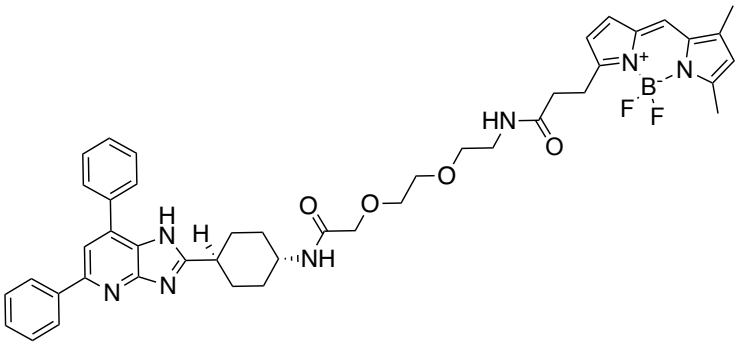
Analytical RP-HPLC t_R = 21.23 min, purity > 99% (Method C).



6-(3-(5,5-Difluoro-7,9-dimethyl-5*H*-4*l*^{4},5*l*^{4}-dipyrrolo[1,2-*c*:2',1'-*f*][1,3,2]diazaborinin-3-yl)propanamido)-*N*-(2-(2-(2-(((1*r*,4*r*)-4-(5,7-diphenyl-1*H*-imidazo[4,5-*b*]pyridin-2-yl)cyclohexyl)amino)-2-oxoethoxy)ethoxy)ethyl)hexanamide (**3.20c**)**.** Following general procedure D, amine congener **3.13** (1 mg, 1.9 μmoL, 1.1 equiv) was converted to the BODIPY FL-X conjugate X. Purification by RP-HPLC (Method E) gave after lyophilisation the title compound as a blue solid (1.6 mg, 91%)**.**

HRMS (TOF ES^+) calcd for $C_{50}H_{60}BF_2N_8O_5$ $[MH]^+$: 901.4742, found 901.4733; calcd for $C_{50}H_{59}NaBF_2N_8O_5$ $[MH]^+$: 923.4562, found 923.4566

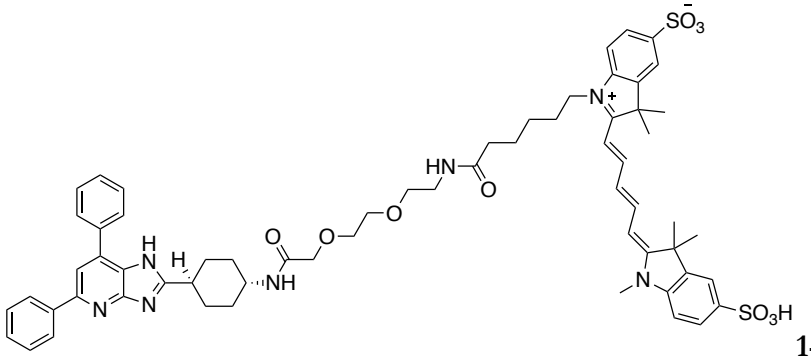
Analytical RP-HPLC t_R = 18.00 min, purity > 99% (Method C).



3-(5,5-Difluoro-7,9-dimethyl-5*H*-4λ^4,5λ^4-dipyrrolo[1,2-*c*:2',1'-*f*][1,3,2]diazaborinin-3-yl)-*N*-(2-(2-(2-(((1*r*,4*r*)-4-(5,7-diphenyl-1*H*-imidazo[4,5-*b*]pyridin-2-yl)cyclohexyl)amino)-2-oxoethoxy)ethoxy)ethyl)propenamide (**3.20d**)**.** Following general procedure D, amine congener **3.13** (0.8 mg, 1.7 μmoL, 1.1 equiv) was converted to the BODIPY FL conjugate X. Purification by RP-HPLC (Method E) gave after lyophilisation the title compound as a blue solid (1.1 mg, 92%).

HRMS (TOF ES$^+$) calcd for $C_{44}H_{49}BF_2N_7O_4$ $[MH]^+$: 788.3902, found 788.3930;

Analytical RP-HPLC t_R = 18.61 min, purity > 99% (Method C).



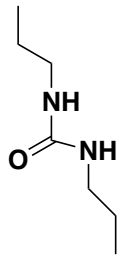
1-(6-((2-(2-(2-(((1*r*,4*r*)-4-(5,7-Diphenyl-1*H*-imidazo[4,5-*b*]pyridin-2-yl)cyclohexyl)amino)-2-oxoethoxy)ethoxy)ethyl)amino)-6-oxohexyl)-3,3-dimethyl-2-((1*E*,3*E*)-5-((*E*)-1,3,3-trimethyl-5-sulfoindolin-2-ylidene)penta-1,3-dien-1-yl)-3*H*-indol-1-ium-5-sulfonate (**3.20e**)**.**

Following general procedure D, amine congener **3.13** (0.7 mg, 1.3 μmoL, 1.1 equiv) was converted to the SulfoCy5 conjugate **3.20e**. Purification by RP-HPLC (Method E) gave after lyophilisation the title compound as a blue solid (1.4 mg, 93%).

HRMS (TOF ES^+) calcd for $C_{62}H_{72}N_7O_{10}S_2$ $[MH]^+$: 1138.4777, found 1138.4784;

Analytical RP-HPLC t_R = 18.68 min, purity > 97% (Method C).

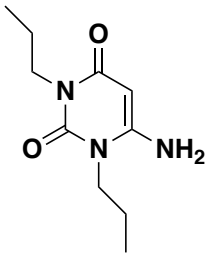
7.1.4 Methods Chapter 4



1,3-Dipropylurea (**1**). Propylamine (7.44 mL, 1.10 equiv.) was dissolved in anhydrous THF (20 mL) and the solution was cooled to 0 °C. Propyl isocyanate (7.63 mL, 1.0 equiv.) was added dropwise and the reaction was stirred at rt. After few seconds a white precipitate developed which was filtered off and dried to get the pure product as off-white solid (6.052 g, 97 %).

^{1}H NMR (DMSO-*d*6) δ 5.74 (t, J = 5.7 Hz, 2H, -NH), 2.92 (td, J = 7.1, 5.8 Hz, 4H, -CH_2-NH), 1.35 (h, J = 7.3 Hz, 4H, CH_3CH_2-), 0.82 (t, J = 7.4 Hz, 6H, CH_3).

^{13}C NMR (DMSO-*d*6) δ 158.1 (C=O), 41.1 05 (CH_2-NH), 23.2 (CH_2), 11.3 (CH_3).

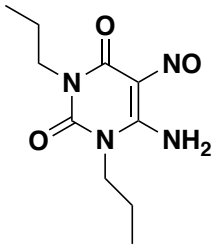


6-Amino-1,3-dipropylpyrimidine-2,4(1*H*,3*H*)-dione (**2**). 1,3-Diisopropylurea (0.100 g, 0.6 mmol, 1.0 equiv.) was dissolved in Ac_2O (2.5 mL). To the reaction mixture was added cyanoacetic acid (64.88 mg, 1.1 equiv.). The resulting mixture was stirred at 83 °C for 2 h. The solution was then concentrated to dryness (water bath set at 80 °C) to give the crude product as brown oil (HNMR of the crude product revealed that the 2-cyano-*N*-propyl-*N*-(propylcarbamoyl)acetamide intermediate was formed. ^{1}H NMR ($CDCl_3$) δ 3.78 (s, 2H), 3.64 – 3.57 (m, 2H), 3.28 – 3.21 (m, 2H), 1.68 – 1.51 (m, 5H), 0.98 – 0.89 (m, 7H)). H_2O (2 mL x2) was added and evaporated off to remove residual Ac_2O from the reaction mixture. The crude product was then dissolved in H_2O (4.5 mL) and the resulting solution was basified with 70% NaOH (three drops). A white precipitate developed which was subsequently filtered off and washed with H_2O. The precipitate was dried under vacuum overnight (73 mg, 50%).

LC-MS *m/z* calcd for $C_{10}H_{18}N_3O_2$ $[MH]^+$: 212.1, found 212.10 t_R = 3.07 min (Method B).

^{1}H NMR (DMSO-*d6*) δ 6.77 (br s, 2H, N$\underline{H}_2$), 4.64 (s, 1H, CO-a-$\underline{H}$), 3.73 (t, J = 8.0 Hz, 2H, -C$\underline{H}_2$-N), 3.66 (t, J = 7.3 Hz, 2H, -C$\underline{H}_2$-N), 1.58 – 1.40 (h, J = 7.2 Hz, 4H, CH_3-C$\underline{H}_2$-, two sextet partially overlapping)), 0.85 (t, J = 7.4 Hz, 3H, C$\underline{H}_3$), 0.80 (t, J = 7.5 Hz, 3H, C$\underline{H}_3$).

^{13}C NMR (DMSO-*d6*) δ 161.4 (C=O), 154.5 (C=O), 151.5 (C), 75.2 (C-H), 43.3 (CH_2), 41.4 (CH_2), 21.0 (CH_2), 11.4 (CH_3), 10.9 (CH_3).

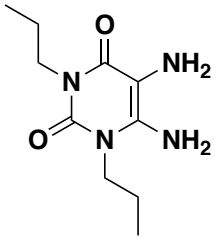


6-Amino-5-nitroso-1,3-dipropylpyrimidine-2,4(1*H*,3*H*)-dione (**3**)**.** 1,3-diisopropyl-6-amino uracil (70 mg, 1.0 equiv.) was dissolved in 50% acetic acid (1.5 mL) and the resulting solution was heated to 57 °C. To the mixture was added $NaNO_2$ (28 mg, 1.20 eq.) over 15 min. The solution from colourless turned pink and a pink precipitate formed. The reaction mixture was stirred at rt for 1h. The precipitate was collected, washed with cold water and dried to get the pure product as pink solid (51 mg, 64%).

LC-MS *m/z* calcd for $C_{10}H_{17}N_4O_3$ $[MH]^+$: 241.1, found 241.10 t_R = 3.10 min (Method B).

^{1}H NMR (DMSO-*d*6) δ 13.17 (s, 1H, OH), 9.12 (s, 1H, NH), 3.85 (t, J = 6.9 Hz, 2H, -CH_2-N), 3.78 (t, J = 7.3 Hz, 2H, -CH_2-N), 1.60 (h, J = 6.8 Hz, 2H, CH_3-CH_2-), 1.53 (h, J = 6.8 Hz, 2H, CH_3-CH_2-), 0.92 – 0.84 (m, 6H, CH_3).

^{3}C NMR (DMSO-*d*6) δ 159.9 (C=O), 149.1 (C=O), 145.4 (C), (one quaternary carbon not observed) 42.5 (CH_2), 42.4 (CH_2), 20.7 (CH_2), 19.7 (CH_2), 11.2 (CH_3), 10.7 (CH_3)



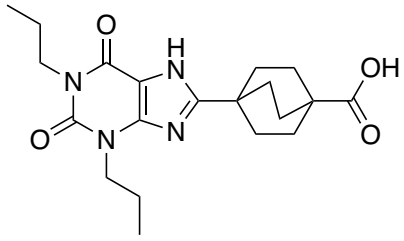
5,6-Diamino-1,3-dipropylpyrimidine-2,4(1H,3H)-dione (**4**). To a stirred solution of 6-amino-5-nitroso-1,3-diipropylpyrimidine-2,4(1*H*, 3*H*)-dione (**3**) in 12.5 % aqueous ammonium hydroxide solution (3 mL) at 60 °C was added sodium dithionite (5.7 equiv.) until a colourless solution had formed (30 min). After cooling to rt, the product was extracted with DCM (4x 20 mL). The combined organics were

dried over anhydrous Na_2SO_4, filtered and evaporated to dryness to give the title product as pale yellow solid (crystalline form) (39 mg, 87%).

LC-MS *m/z* calcd for $C_{10}H_{19}N_4O_2$ $[MH]^+$: 227.1, found 227.1, t_R = 2.70 min (Method B).

^{1}H NMR ($CDCl_3$) δ 5.01 (br s, 2H, $N\underline{H}_2$), 3.91 – 3.76 (m, 4H, -$C\underline{H}_2$-N), 2.32 (br s, 2H, $N\underline{H}_2$), 1.71 (h, J = 7.5 Hz, 2H, CH_3-$C\underline{H}_2$), 1.61 (h, J = 6.9 Hz, 2H, CH_3-$C\underline{H}_2$), 0.96 (t, J = 7.4 Hz, 3H, $C\underline{H}_3$), 0.90 (t, J = 7.5 Hz, 3H, $C\underline{H}_3$).

^{13}C NMR ($CDCl_3$) δ 161.7 ($\underline{C}$-NH_2), 150.4 ($\underline{C}$=O), 148.7($\underline{C}$=O), 95.7 ($\underline{C}$-NH_2), 44.8 ($\underline{C}H_2$), 43.2($\underline{C}H_2$), 21.8 ($\underline{C}H_2$), 21.3 ($\underline{C}H_2$), 11.4 ($\underline{C}H_3$), 11.3 ($\underline{C}H_3$).



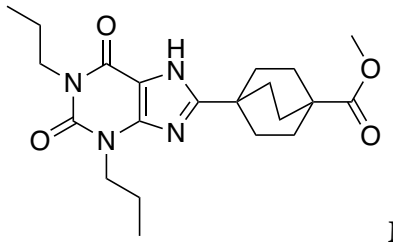
4-(2,6-Dioxo-1,3-dipropyl-2,3,6,9-tetrahydro-1H-purin-8-yl) bicyclo[2.2.2]octane-1-carboxylic acid (**6**)**.** To a solution of 5,6-Diamino-1,3-diisopropylpyrimidine-2,4(1*H*,3*H*)-dione (0.152 g, 1.10 equiv.) (**4**) in acetonitrile (5 mL) were added 4-(methoxycarbonyl) bicyclo [2.2.2] octane-1-carboxylic acid (0.128 g, 1.0 equiv.) and NEt_3 (0.16 mL, 2 equiv.) followed by HATU (0.250 g, 1.10 equiv.). The resulting mixture was stirred at rt for 1 h 30 min. The mixture was concentrated to dryness and the crude was taken up in EtOAc and washed with 10 % citric acid. The organics were collected washed with sat. $NaHCO_3$, brine, dried over $MgSO_4$, filtered and concentrated in vacuo to give methyl 4-((6-amino-2,4-dioxo-1,3-dipropyl-1,2,3,4-tetrahydropyrimidin-5-yl)carbamoyl)bicyclo[2.2.2]octane-1-carboxylate intermediate (**5**) which was used for the next step without any further purification . The residue was dissolved in a mixture of propan-2-ol and 1 M KOH (2.5 mL, 4 equiv.) and heated to reflux (91°C) for 2 h. The reaction mixture was then cooled to rt and the solvent concentrated to dryness. The yellow residue was taken up in 4 mL of water and extracted with DCM. The aqueous layer was collected and

acidified with conc HCl and a white precipitate formed which was collected by suction filtration and oven dried. (0.159 g, 68% over two steps).

LC-MS *m/z* calcd for $C_{20}H_{29}N_4O_4$ $[MH]^+$: 389.20, found 389.20 t_R = 3.44 min (Method B).

^{1}H NMR ($CDCl_3$) δ 12.62 (s, 1H, NH), 12.54 (br s, 1H, OH), 4.09 (t, J = 7.1 Hz, 2H, CH_2-N), 4.00 (t, J = 6.6 Hz, 2H, CH_2-N), 2.04 (s, 12H, bicycle [2.2.2]), 1.80 (h, J = 7.4 Hz, 2H, CH_3-CH_2-), 1.67 (h, J = 6.6 Hz, 2H, CH_3-CH_2-), 0.99 – 0.90 (m, 6H, CH_3).

^{13}C NMR ($CDCl_3$) δ 182.1 (HOC=O), 161.3 (C), 156.2 (C=O), 150.7 (C=O), 149.2 (C), 106.4 (C), 45.1 (C), 43.2 (C), 38.5 (CH_2), 33.6 (CH_2), 29.6 (CH_2), 27.9 (CH_2), 21.2 (CH_2), 21.1 (CH_2), 11.2 (CH_3), 11.0 (CH_3).

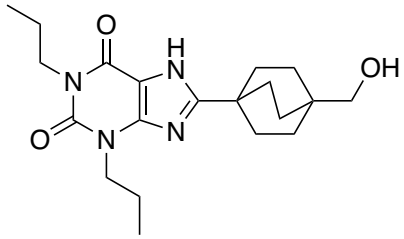


Methyl 4-(2,6-dioxo-1,3-dipropyl-2,3,6,9-tetrahydro-1H-purin-8-yl) bicyclo[2.2.2]octane-1-carboxylate. 4-(2,6-Dioxo-1,3-dipropyl-2,3,6,9-tetrahydro-1*H*-purin-8-yl) bicyclo[2.2.2]octane-1-carboxylic acid was diluted with 6 mL of MeOH and 3 drops of conc. H_2SO_4. The resulting mixture was refluxed until complete consumption of starting material. Once the reaction was completed, the resulting solution was neutralised with sat. $NaHCO_3$ (a couple of drops). The mixture was then concentrated to dryness and the residue was taken up in EtOAc and washed with sat. $NaHCO_3$ and brine. The resulting organic layer was dried over $MgSO_4$, filtered and concentrated to dryness to give the title compound as off-white solid (74 mg, 84%).

LC-MS *m/z* calcd for $C_{21}H_{31}N_4O_4$ $[MH]^+$: 403.20, found 403.20 t_R = 3.88 min (Method B).

^{1}H NMR ($CDCl_3$) δ 12.22 (s, 1H, N<u>H</u>), 4.09 (t, J = 7.1 Hz, 2H, C<u>H</u>$_2$-N), 4.03 (t, J = 6.6 Hz, 2H, C<u>H</u>$_2$-N), 3.67 (s, 3H, OC<u>H</u>$_3$), 2.08 – 2.03 (m, 6H, bicycle [2.2.2]), 1.96 – 1.90 (m, 6H, bicycle [2.2.2]), 1.80 (h, J = 7.4 Hz, 2H, CH_3-C<u>H</u>$_2$-), 1.71 (h, J = 6.6 Hz, 3H, CH_3-C<u>H</u>$_2$-), 1.00 – 0.93 (m, 6H, C<u>H</u>$_3$).

^{13}C NMR ($CDCl_3$) δ 177.9 (CH_3O<u>C</u>=O), 161.4 (<u>C</u>), 155.6 (<u>C</u>=O), 151.2 (<u>C</u>=O), 149.0 (<u>C</u>), 107.1 (<u>C</u>), 51.9 (O<u>C</u>H$_3$), 45.3 (<u>C</u>H$_2$), 43.3 (<u>C</u>H$_2$), 38.9 (<u>C</u>), 33.9 (<u>C</u>), 29.9 (<u>C</u>H$_2$), 28.2 (2x<u>C</u>H$_2$), 21.5 (<u>C</u>H$_2$), 11.6 (<u>C</u>H$_3$), 11.3 (<u>C</u>H$_3$).

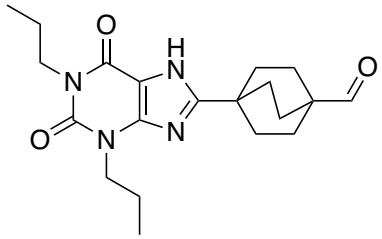


8-(4-(Hydroxymethyl)bicyclo[2.2.2]octan-1-yl)-1,3-dipropyl-3,9-dihydro-1H-purine-2,6-dione (**7**). Methyl 4-(2,6-dioxo-1,3-dipropyl-2,3,6,9-tetrahydro-1*H*-purin-8-yl) bicyclo[2.2.2]octane-1-carboxylate (74 mg, 184 μmol, 1 equiv.) was dissolved in dry THF and the resulting solution was evacuated and kept inert with cycles of vacuum and nitrogen. The solution was cooled to 0 °C and stirred for 10 min. At that point $LiAlH_4$ 1.0 M sol. In THF (0.28 mL, 276 μmol 1.50 equiv.) was slowly added dropwise (little effervescence developed). The resulting mixture was stirred at 0 °C for 1 h. Completion of the reaction was checked by TLC and LC-MS. After 1 h the solution was quenched by the dropwise addition of cold H_2O, followed by the addition of a saturated solution of Rochelle's reagent/salt (*circa* 7 mL added). The solution was stirred at rt for 1h. The reaction mixture was then extracted with EtOAc (3x20 mL). The organic layer was dried over $MgSO_4$, filtered and evaporated to dryness to yield the title compound as off-white/pale pink solid (66 mg, 97%).

LC-MS *m/z* calcd for $C_{20}H_{31}N_4O_3$ $[MH]^+$: 375.20, found 375.20 t_R = 3.45 min (Method B).

^{1}H NMR ($CDCl_3$) δ 12.08 (br s, 1H, N<u>H</u>), 4.10 (t, J = 6.5 Hz, 2H, C<u>H</u>$_2$-N), 4.02 (t, J = 6.9 Hz, 2H, C<u>H</u>$_2$-N), 3.35 (s, 2H, C<u>H</u>$_2$-OH), 2.06 – 1.99 (m, 6H, bicycle), 1.80 (h, J = 6.8 Hz, 2H, CH_3-C<u>H</u>$_2$-), 1.70 (h, J = 6.6 Hz, 2H, CH_3-C<u>H</u>$_2$-), 1.61 – 1.53 (m, 6H, bicycle), 1.00 – 0.91 (m, 6H, C<u>H</u>$_3$).

^{13}C NMR ($CDCl_3$) δ 161.9 (C), 155.6 (<u>C</u>=O), 151.3 (<u>C</u>=O), 149.1(<u>C</u>), 106.9 (<u>C</u>), 71.3 (CH_2OH), 45.3 (<u>C</u>H$_2$), 43.3 (<u>C</u>H$_2$), 34.4 (C), 33.4 (C), 30.3 (<u>C</u>H$_2$), 29.8 (C), 27.9 (<u>C</u>H$_2$), 21.5 (<u>C</u>H$_2$), 11.6 (<u>C</u>H$_3$), 11.3 (<u>C</u>H$_3$).

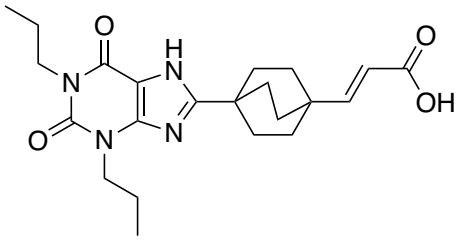


4-(2,6-Dioxo-1,3-dipropyl-2,3,6,9-tetrahydro-1H-purin-8-yl) bicyclo[2.2.2]octane-1-carbaldehyde. To a solution of 8-(4-(Hydroxymethyl) bicyclo[2.2.2]octan-1-yl)-1,3-dipropyl-3,9-dihydro-1*H*-purine-2,6-dione (66 mg, 184 μmol, 1 equiv.) (**7**) in DCM (4 mL) was added Dess -Martin periodinane (88 mg, 210 μmol, 1.20 equiv.). The reaction mixture was stirred at rt until the oxidation was complete (2 h). The mixture was subsequently filtered through a plug of basic alumina and the filtrated was washed with sat. $NaHCO_3$ (2x) and brine. The organics were collected, dried over $MgSO_4$ anhydrous, filtered and evaporated to dryness to get the product as off-white/pale pink solid (29 mg, 80%).

LC-MS *m/z* calcd for $C_{20}H_{29}N_4O_3$ $[MH]^+$: 373.20, found 373.20 t_R = 3.69 min (Method B).

^{1}H NMR ($CDCl_3$) δ 12.26 (s, 1H, N<u>H</u>), 9.52 (s, 1H, <u>H</u>-CO), 4.10 (t, J = 6.2, 2H, C<u>H</u>$_2$-N), 4.03 (t, J = 6.5 Hz, 2H, , C<u>H</u>$_2$-N), 2.14 – 2.06 (m, 6H, , bicycle), 1.83 – 1.76 (m, 8H, bicycle and CH_3-C<u>H</u>$_2$-), 1.73 (h, J = 7.3 Hz, 2H, CH_3-C<u>H</u>$_2$-), 1.00 – 0.93 (m, 6H, C<u>H</u>$_3$).

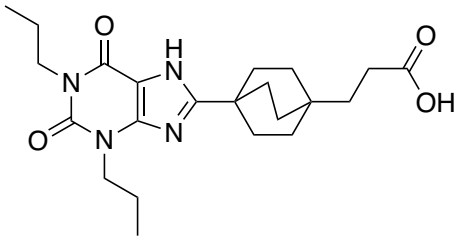
^{13}C NMR ($CDCl_3$) δ 205.3 (H<u>C</u>=O), 161.1 (C), 155.7(C=O), 151.2 (C=O), 149.1 (C), 107.1 (C), 45.4 (<u>C</u>H$_2$), 43.7 (<u>C</u>), 43.3 (<u>C</u>H$_2$), 34.7 (C), 29.8 (<u>C</u>H$_2$), 29.5 (<u>C</u>H$_2$), 25.6 (<u>C</u>H$_2$), 21.5 (<u>C</u>H$_2$), 11.7 (<u>C</u>H$_3$), 11.3 (<u>C</u>H$_3$).



(E)-3-(4-(2,6-dioxo-1,3-dipropyl-2,3,6,9-tetrahydro-1H-purin-8-yl) bicyclo[2.2.2]octan-1-yl)acrylic acid (**9**)**.** Triethylphosphono acetate (19 mg, 86 μmol, 1.10 equiv.) was dissolved in dry THF (5 mL) and cooled to 0°C. To the mixture was added dropwise potassium bid (trimethylsilyl)acetamide (KHDMS) 1.0 M sol. in THF (0.16 mL, 156 μmol, 2 equiv.). The resulting mixture was stirred 0 °C for 1h. After that time, 4-(2,6-dioxo-1,3-dipropyl-2,3,6,9-tetrahydro-1*H*-purin-8-yl)bicyclo[2.2.2]octane-1-carbaldehyde (29 mg, 78 μmol, 1.0 equiv.) previously dissolved in dry THF was added and the resulting mixture was stirred at rt for 1 h. Completion of the reaction was assessed by TLC and LCMS after 1 h. The reaction mixture was then concentrated to dryness. The resulting residue was diluted in EtOH and an aqueous solution of LiOH (10.0 equiv.) was added to the mixture which was stirred at rt for 4-5 h. The solution was concentrated to dryness and the residue was taken up in water and extracted twice with EtOAc. The aqueous layer was collected and acidified with conc. HCl, and the resulting precipitate was collected by suction filtration to give the title compound as off-white solid (14 mg, 30 %).

LC-MS ***m/z*** calcd for $C_{22}H_{31}N_4O_4$ $[MH]^+$: 415.20, found 415.20 t_R = 3.60min (Method B).

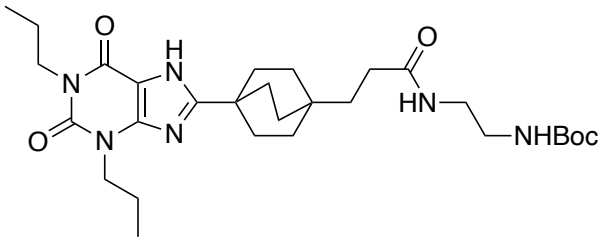
^{1}H NMR ($CDCl_3$) δ 12.34 (br s, 1H, NH), 7.00 (d, J = 15.9 Hz, 1H, CH), 5.83 (d, J = 15.9 Hz, 1H, CH), 4.09 (t, J = 6.3 Hz, 2H, CH_2-N), 4.00 (t, J = 6.7 Hz, 2H, CH_2-N), 2.08 – 2.00 (m, 6H, bicycle), 1.82 – 1.64 (m, 10H, bicycleand CH_3-CH_2-), 0.99 – 0.92 (m, 6H, CH_3).



3-(4-(2,6-Dioxo-1,3-dipropyl-2,3,6,9-tetrahydro-1H-purin-8-yl)bicyclo[2.2.2]octan-1-yl)propanoic acid *(Tonapofylline, BG9928*). (*E*)-3-(4-(2,6-dioxo-1,3-dipropyl-2,3,6,9-tetrahydro-1*H*-purin-8-yl) bicyclo[2.2.2]octan-1-yl)acrylic acid (120 mg, 290 μmol, 1.0 equiv.) was dissolved in MeOH and to the resulting mixture was added Pd/C 10% w/w while under a stream of N_2. The resulting mixture was evacuated with cycles of N_2 and vacuum (x3). Finally, the stream of N_2 was replaced with H_2 (balloon) and the mixture was allowed to stir at rt for 2 h. Upon completion of the reaction, the solution was filtered through Celite^{RT} and the pad was washed with DCM/MeOH. The filtrate was collected and evaporated to dryness, giving the title compound as off-white solid (120 mg, 100%).

LC-MS *m/z* calcd for $C_{22}H_{33}N_4O_4$ $[MH]^+$: 417.20, found 417.20 t_R = 3.60 min (Method B).

^{1}H NMR ($CDCl_3$) δ 11.99 (br s, 1H, NH), 4.08 (t, J = 6.9 Hz, 2H, CH_2-N), 3.98 (t, J = 6.5 Hz, 2H, CH_2-N), 2.37 (t, J = 7.7 Hz, 2H, CH_2-CO_2H), 2.00 – 1.91 (m, 6H, bicycle), 1.78 (h, J = 7.4 Hz, 2H, CH_3-CH_2-), 1.69 – 1.51 (m, 10H, bicycle, CH_3-CH_2-, bicycle-CH_2), 0.94 (t, J = 7.4 Hz, 6H, CH_3).



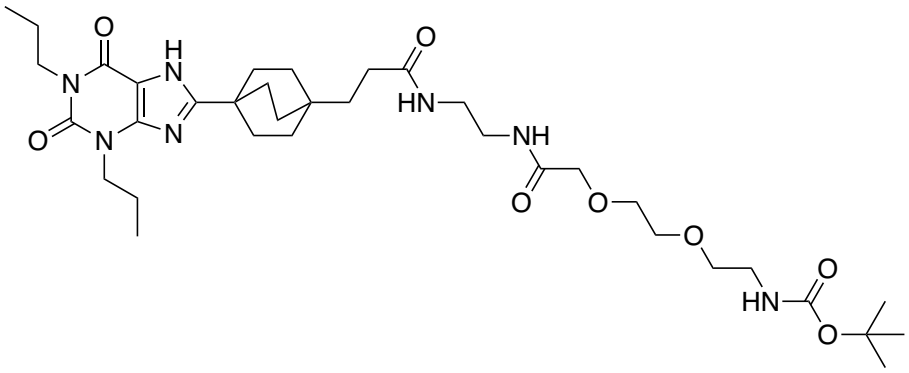
tert-Butyl(2-(3-(4-(2,6-dioxo-1,3-dipropyl-2,3,6,9-tetrahydro-1H-purin-8-yl) bicyclo[2.2.2]octan-1-yl)propanamido)ethyl)carbamate (**4.10**). Following general procedure A, to solution of 3-(4-(2,6-dioxo-1,3-dipropyl-2,3,6,9-tetrahydro-1*H*-purin-8-yl)bicyclo[2.2.2]octan-1-yl)propanoic acid,

Tonapofylline (120 mg, 288 μmol 1.0 equiv.) in DMF (1 mL) was added DIPEA (55 μL, 317 μmol, 1.10 equiv.) and COMU (136 mg, 317 μmol 1.10 equiv.) followed by a solution of *tert*-butyl (2-aminoethyl)carbamate (51 mg, 317 μmol 1.10 equiv.) in DMF (0.5 mL). Purification by flash column chromatography using a gradient of 97:3 to 94:6 DCM/MeOH gave the title compound as colourless oil (93 mg, 58%).

LC/MS *m/z* calcd for $C_{29}H_{47}N_6O_5$ $[MH]^+$: 559.20, found 559.20 t_R = 3.78 min (method B)

^{1}H NMR ($CDCl_3$) δ 12.13 (s, 1H, xanthine-NH), 6.33 (s, 1H, amide-NH), 5.03 (s, 1H, amide-NH), 4.08 (t, *J* = 7.0 Hz, 2H, CH_2-N), 4.00 (t, *J* = 7.3 Hz, 2H, CH_2-N), 3.35 (q, *J* = 5.4 Hz, 2H, -NHCH_2), 3.26 (q, *J* = 5.7 Hz, 2H, -NHCH_2), 2.16 – 2.08 (m, 2H, CH_2), 2.03 – 1.93 (m, 6H, bicycle), 1.79 (h, *J* = 7.4 Hz, 2H, CH_3-CH_2), 1.70 (h, *J* = 6.7, 6.0 Hz, 2H, CH_3-CH_2-), 1.54 – 1.38 (m, 17H, bicycle, Boc, bicycle-CH_2), 0.95 (t, *J* = 6.5 Hz, 6H, CH_3).

^{13}C NMR ($CDCl_3$) δ 174.2 (NHC=O), 161.9 (C), 157.2 (NHC=O), 155.5 (C=O), 151.2 (C=O), 148.9 (C), 106.9 (C), 79.8 (C), 45.3 (CH_2), 43.2 (CH_2), 41.1 (C), 40.3 (C), 36.8 (CH_2), 34.0 (CH_2), 31.5 (CH_2 bicycle), 30.6 (CH_2 bicycle), 30.6 (2xCH_2), 28.5 (Boc), 21.5 (2xCH_2), 11.7 (CH_3), 11.3 (CH_3).



tert-Butyl (15-(4-(2,6-dioxo-1,3-dipropyl-2,3,6,9-tetrahydro-1H-purin-8-yl)bicyclo[2.2.2]octan-1-yl)-8,13-dioxo-3,6-dioxa-9,12-diazapentadecyl)carbamate (**4.12**). Following general procedure C, Compound **4.11** (as HCl salt) was synthesized (75 mg, quantitative) and was used for the next steps without further purification.

LC/MS *m/z* calcd for $C_{24}H_{39}N_6O_3$ $[MH]^+$: 459.20, found 459.20 t_R = 3.07 min (method B).

Following general procedure A, to a solution of 2,2-dimethyl-4-oxo-3,8,11-trioxa-5-azatridecan-13-oic acid (linker **A**) (15 mg, 57 μmol, 1.0 equiv.) in DMF (0.5 mL) was added DIPEA (40 μL, 228 μmol, 4.0 equiv.), followed by COMU (26.84 mg, 63 μmol, 1.10 equiv.) and a solution of compound **4.11** (29 mg, 63 μmol , 1.10 equiv.) in DMF (0.5 mL). Purification by flash column chromatography using a gradient of 97:3 to 95:5 DCM/MeOH gave the title compound as colourless oil (15 mg, 38%).

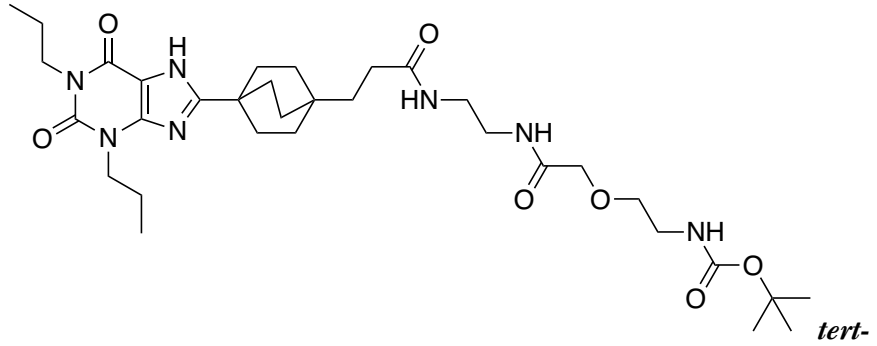
LC/MS *m/z* calcd for $C_{35}H_{56}N_7O_8$ $[MH]^-$: 702.20, found 702.20 t_R = 3.63 min (method B).

HRMS (TOF ES^+) calcd for $C_{35}H_{58}N_7O_8$ 704.4341, found 704.4356; calcd for $C_{35}H_{58}N_7O_8Na$ 726.4161, found 726.4178.

^{1}H NMR ($CDCl_3$) δ 11.86 (br s, 1H, NH), 7.33 (t, *J* = 5.7 Hz, 1H, amide-NH), 6.42 (s, 1H, amide-NH), 5.19 (s, 1H, amide-NH), 4.09 (t, *J* = 6.7 Hz, 2H, CH_2-N), 4.00 (m, 4H, CH_2-N-xanthine and CO-CH_2-O), 3.68 – 3.61 (m, 4H, NH-$(CH_2)_2$-NH), 3.57 (t, *J* = 5.3 Hz, 2H, CH_2), 3.47 – 3.38 (m, 4H, CH_2), 3.36 – 3.29 (m, 2H, CH_2), 2.15 – 2.07 (m, 2H, CH_2) 2.02 – 1.95 (m, 6H, bicycle), 1.79 (h, *J* = 7.4 Hz, 2H, CH_3-CH_2), 1.69 (h, *J* = 7.1 Hz, 2H, CH_3-CH_2), 1.54 – 1.46 (m, 8H, bicycle and -CH_2), 1.43 (s, 9H,Boc), 0.95 (t, *J* = 7.4 Hz, 6H, CH_3-CH_2-).

^{13}C NMR ($CDCl_3$) δ 174.2 (NHC=O), 161.7 (C), 156.3 (NHC=O), 155.1 (C=O), 151.3 (C=O), 148.8 (C), 106.9 (C), 71.2 (COCH_2O), 70.5 (CH_2O), 70.1(CH_2O), 45.3 (CH_2), 43.2 (CH_2), 40.6 (2xCH_2), 38.9 (C), 36.8 (C), 34.0 (CH_2), 31.5 (CH_2 bicycle), 30.6 (CH_2 bicycle), 30.6 (2xCH_2), 28.5 (Boc), 21.5 (CH_2), 21.5 (CH_2), 11.7 (CH_3), 11.3 (CH_3).

Analytical RP-HPLC t_R = 5.77 min, purity > 99% (method F).



***tert*-Butyl(2-(2-((2-(3-(4-(2,6-dioxo-1,3-dipropyl-2,3,6,9-tetrahydro-1H-purin-8-yl) bicyclo[2.2.2]octan-1-yl)propanamido)ethyl)amino)-2-oxoethoxy)ethyl)carbamate** (**4.13**). Following general procedure A, to a solution of 2-(2-((*tert*-butoxycarbonyl)amino)ethoxy)acetic acid (linker **B**) (12 mg, 55 μmol, 1.0 equiv.) in DMF (0.5 mL) was added DIPEA (38 μL, 219 μmol, 4.0 equiv.) and COMU (25.80 mg, 60 μmol, 1.10 equiv.), followed by a solution of **4.11** (28 mg, 60 μmol, 1.10 equiv.) in DMF (0.5 mL). Purification by flash column chromatography using a gradient of 96:4 to 94:6 DCM/MeOH gave the title compound as colourless oil (10 mg, 28%).

LC/MS ***m/z*** calcd for $C_{33}H_{52}N_7O_7$ $[MH]^-$: 658.20, found 658.40 t_R = 3.70 min (method A).

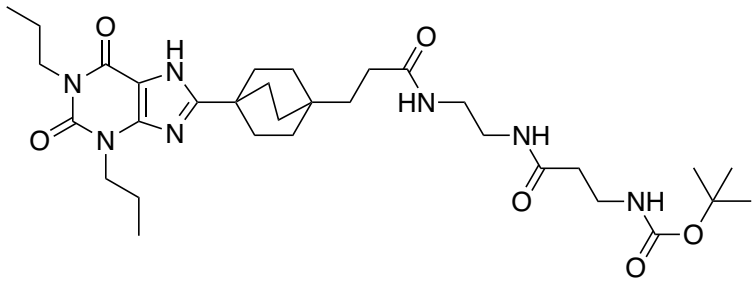
HRMS (TOF ES^+) calcd for $C_{33}H_{54}N_7O_7$ 660.4079, found 660.4096; calcd for $C_{33}H_{54}N_7O_7Na$ 682.3899, found 682.3917.

^{1}H NMR ($CDCl_3$) δ 7.43 (s, 1H, amide-NH), 6.44 (s, 1H, amide-NH), 5.57 (s, 1H, amide-NH), 4.09 (t, *J* = 6.9 Hz, 2H, CH_2-N), 4.00 (t, *J* = 6.9 Hz, 2H, CH_2-N), 3.95 (s, 2H, , CO-CH_2-O), 3.56 (t, *J* = 5.0 Hz, 2H, CH_2), 3.45 – 3.40 (m, 4H, CH_2), 3.40 – 3.33 (m, 2H, CH_2), 2.17 – 2.11 (m, 2H, CH_2), 2.02 – 1.95 (m, 6H, bicycle), 1.78 (h, *J* = 7.4 Hz, 2H, CH_3-CH_2-), 1.69 (h, *J* = 7.0 Hz, 2H, CH_3-CH_2-), 1.55 – 1.47 (m, 8H, bicycle and -CH_2), 1.44 (s, 9H, CH_3-Boc), 0.95 (t, *J* = 7.4 Hz, 6H, CH_3-CH_2-).

^{13}C NMR ($CDCl_3$) δ 174.9 (NHC=O), 170.8 (NHC=O), 161.7 (C), 156.5 (NHC=O), 155.4 (C=O), 151.2 (C=O), 148.8 (C), 106.8 (C), 79.4 (C), 71.3 ($COCH_2O$), 70.4 (CH_2O), 45.4 (CH_2), 43.2 (CH_2), 40.1(CH_2), 40.0 (C), 36.8

(C), 34.0 (CH_2), 31.5 (CH_2 bicycle), 30.6 (CH_2 bicycle), 30.6 (2xCH_2), 28.6 (Boc), 21.5 (CH_2), 21.5 (CH_2), 11.6 (CH_3), 11.3 (CH_3).

Analytical RP-HPLC t_R = 5.77 min, purity > 99% (method F).



tert-Butyl (3-((2-(3-(4-(2,6-dioxo-1,3-dipropyl-2,3,6,9-tetrahydro-1H-purin-8-yl)bicyclo[2.2.2]octan-1-yl)propanamido)ethyl)amino)-3-oxopropyl)carbamate (**4.14**). Following general procedure A, to a solution of 3-((*tert*-butoxycarbonyl)amino)propanoic acid (Boc-β-Ala-OH) (10 mg, 53 μmol, 1.0 equiv.) in DMF (0.5 mL) was added DIPEA (37 μL, 211 μmol, 4.0 equiv.) and COMU (25 mg, 58 μmol, 1.10 equiv.), followed by a solution of **4.11** (27 mg, 58 μmol, 1.10 equiv.) in DMF (0.5 mL). Purification by flash column chromatography using a gradient of 96:4 to 94:6 DCM/MeOH gave the title compound as an off-white solid (29 mg, 78%).

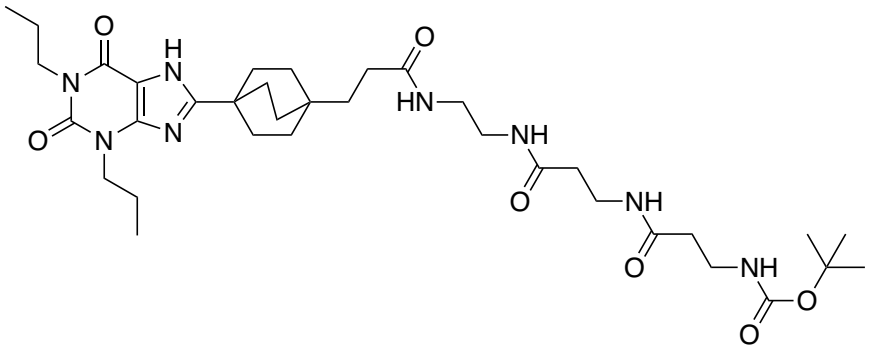
LC/MS ***m/z*** calcd for $C_{32}H_{52}N_7O_6$ $[MH]^+$: 630.20, found 630.40 t_R = 3.69 min (method B).

^{1}H NMR (CD_3OD) δ 4.07 (t, *J* = 6.3 Hz, 2H, CH_2-N), 3.95 (t, *J* = 6.8, 2H, CH_2-N), 3.29 (br s, 4H, NH-(CH_2)$_2$-NH), 2.37 (t, *J* = 6.8 Hz, 2H, CH_2), 2.20 – 2.14 (m, 2H, CH_2), 2.00 – 1.93 (m, 6H, bicycle), 1.78 (h, *J* = 6.8 Hz, 2H, CH_3-CH_2), 1.66 (h, *J* = 6.8 Hz, 2H, CH_3-CH_2), 1.59 – 1.48 (m, 8H, bicycle and CH_2), 1.45 (s, 9H, Boc), 0.95 (t, *J* = 7.5 Hz, 6H, CH_3).

^{13}C NMR (CD_3OD) δ 176.9 (2xNHC=O), 174.1 (NHC=O), 162.7 (C), 155.8 (C=O), 152.6 (C=O), 149.3 (C), 107.8 (C), 79.9 (C), 45.8 (CH_2), 43.6 (CH_2), 39.8 (2xCH_2), 37.9 (C), 37.3 (C), 34.9 (CH_2), 31.8 (CH_2), 31.4 (CH_2), 31.4 (CH_2

bicycle), 31.2 (CH$_2$ bicycle), 28.5 (Boc), 22.2 (CH$_2$), 22.1 (CH$_2$), 11.3 (CH$_3$), 11.1 (CH$_3$).

Analytical RP-HPLC t_R = 5.65 min, purity > 99% (method F).



***tert*-Butyl (3-((3-((2-(3-(4-(2,6-dioxo-1,3-dipropyl-2,3,6,9-tetrahydro-1H-purin-8-yl) bicyclo[2.2.2]octan-1-yl)propanamido)ethyl)amino)-3-oxopropyl)amino)-3-oxopropyl)carbamate** (**4.15**) Following general procedure C, compound **4.14** (27 mg, 1.0 equiv.) was reacted with 4 M HCl in dioxane (1 mL) and, after the removal of the solvent in vacuo, the resulting HCl salt was used for the subsequent step without further purification. The synthesis of **4.15** was carried out as described for xanthine **4.14**, following general procedure A, reacting a solution of 3-((2-(3-(4-(2,6-dioxo-1,3-dipropyl-2,3,6,7-tetrahydro-1*H*-purin-8-yl)bicyclo[2.2.2]octan-1-yl)propanamido)ethyl)amino)-3-oxopropan-1-aminium chloride intermediate (22 mg, 41 μmol, 1.10 equiv.) in DMF (0.5 mL) with a solution of 3-((*tert*-Butoxycarbonyl)amino)propanoic acid (Boc-β-Ala-OH) (7 mg, 37 μmol, 1.0 equiv.), DIPEA (32 μL, 185 μmol, 5eq.), COMU (17.43 mg, 41 μmol, 1.10 equiv.) in DMF (0.5 mL). Purification by flash column chromatography using a gradient of 96:4 to 93:7 DCM/MeOH gave the title compound as an off-white solid (12 mg, 46 %).

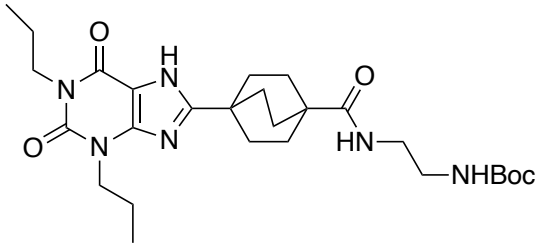
LC/MS ***m/z*** calcd for $C_{35}H_{57}N_8O_7$ $[MH]^+$: 701.20, found 701.40 t_R = 3.57 min (method B).

HRMS (TOF ES$^+$) calcd for $C_{35}H_{57}N_8O_7$ 701.4350, found 701.4360; calcd for $C_{35}H_{57}N_8O_7Na$ 723.4164, found 723.4184.

^{1}H NMR (CD_3OD) δ 4.07 (t, *J* = 6.3 Hz, 2H, C<u>H</u>$_2$-N), 3.95 (t, *J* = 6.3 Hz, 2H, C<u>H</u>$_2$-N), 3.45 (t, *J* = 6.8 Hz, 2H, C<u>H</u>$_2$), 3.33 – 3.31 (m, 2H, C<u>H</u>$_2$), 3.30 (br s, 4H, NH-(C<u>H</u>$_2$)$_2$-NH), 2.38 (dt, *J* = 9.0, 6.8 Hz, 4H, CH$_2$-C<u>H</u>$_2$-NH), 2.20 – 2.14 (m, 2H, C<u>H</u>$_2$), 2.00 – 1.92 (m, 6H, bicycle), 1.78 (h, *J* = 7.5 Hz, 2H, CH$_3$-C<u>H</u>$_2$-), 1.66 (h, *J* = 7.0 Hz, 2H, CH$_3$-C<u>H</u>$_2$-), 1.59 – 1.49 (m, 8H, bicycle and C<u>H</u>$_2$), 1.44 (s, 9H, Boc), 0.95 (t, *J* = 7.4, 6H, C<u>H</u>$_3$).

^{13}C NMR (CD_3OD) δ 177.1 (2xNHC=O), 174.1 (NHC=O), 162.7 (C), 158.3 (NHC=O), 156.0 (C=O), 152.9 (C=O), 149.5 (C), 108.0 (C), 80.1(C), 45.9 (<u>C</u>H$_2$), 43.8 (<u>C</u>H$_2$), 40.2 (<u>C</u>H$_2$), 40.0 (<u>C</u>H$_2$), 38.1 (<u>C</u>), 37.4 (<u>C</u>), 37.1 (<u>C</u>H$_2$), 36.9 (<u>C</u>H$_2$), 35.1 (<u>C</u>H$_2$), 32.1 (<u>C</u>H$_2$), 31.6 (2x<u>C</u>H$_2$, bicycle and <u>C</u>H$_2$), 31.4 (<u>C</u>H$_2$ bicycle), 28.8 (Boc), 22.4 (<u>C</u>H$_2$), 22.3 (<u>C</u>H$_2$), 11.5 (<u>C</u>H$_3$), 11.3 (<u>C</u>H$_3$).

Analytical RP-HPLC t_R = 5.52 min, purity > 99% (method F).

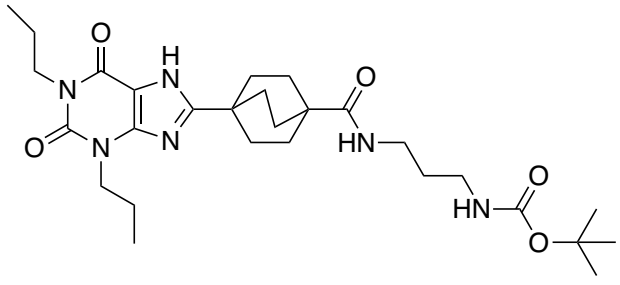


***tert*-Butyl(2-(4-(2,6-dioxo-1,3-dipropyl-2,3,6,9-tetrahydro-1H-purin-8-yl) bicyclo[2.2.2]octane-1-carboxamido)ethyl)carbamate** (**4.17a**). Following general procedure A , to a solution of (2,6-dioxo-1,3-dipropyl-2,3,6,9-tetrahydro-1H-purin-8-yl) bicyclo [2.2.2] octane-1-carboxylic acid (compound **16** from Kiesman et al.)[83] (80 mg, 206 mmol, 1.0 equiv.), *tert*-butyl (2-aminoethyl) carbamate (33 mg, 206 μmol, 1.0 equiv.), BOP (137 mg, 309 μmol ,1.50 equiv.) in dry DMF (2 mL) was added DIPEA (143 μL, 824 μmol, 4.0 equiv.). Purification by flash column chromatography using a gradient of 97:3 to 96:4 DCM/MeOH gave the title compound as off-white solid (85 mg, 78%).

LC/MS *m/z* calcd for $C_{27}H_{43}N_6O_5$ $[MH]^+$: 531.30, found 531.30 t_R = 3.61 min (method B).

^{1}H NMR ($CDCl_3$) δ 11.67 (br s, 1H, NH), 6.53 (br s, 1H, NH-amide), 4.90 (br s, 1H, NH-amide), 4.09 (t, *J* = 6.3 Hz, 2H, CH_2-N), 4.02 (t, *J* = 6.6 Hz, 2H, CH_2-N), 3.37 – 3.26 (m, 4H, NH-$(CH_2)_2$-NH), 2.08 – 2.01 (m, 6H, bicycle), 1.93 – 1.87 (m, 6H, bicycle), 1.80 (h, *J* = 6.5 Hz, 2H, CH_3-CH_2), 1.70 (h, *J* = 6.5 Hz, 2H, CH_3-CH_2), 1.45 (s, 9H, Boc), 0.96 (t, *J* = 7.5 Hz, 6H, CH_3).

^{13}C NMR ($CDCl_3$) δ 176.1 (NHC=O), 155.5 (C=O), 152.2 (C=O), 151.3 (C), 148.9 (C), 106.9 (C), 47.6 (CH_2), 45.3 (C), 44.9 (CH_2), 43.4(CH_2), 39.0 (C), 34.1(CH_2), 30.2 (CH_2 bicycle), 28.5 (CH_2 bicycle), 28.5 (Boc), 21.5 (2xCH_2), 11.6 (CH_3), 11.3 (CH_3).

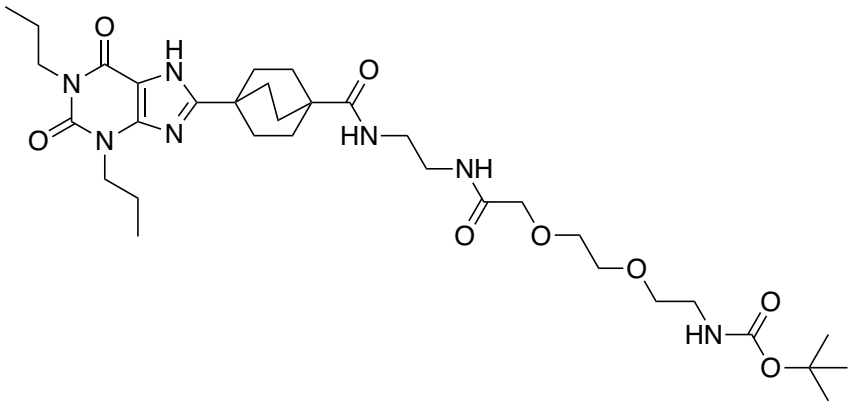


***tert*-Butyl (3-(4-(2,6-dioxo-1,3-dipropyl-2,3,6,9-tetrahydro-1H-purin-8-yl)bicyclo[2.2.2]octane-1-carboxamido)propyl)carbamate** (**4.17b**). The synthesis of the title compound **4.17b** was carried out as described for xanthine (**4.17a**), following general procedure A. To a stirred solution of (2,6-dioxo-1,3-dipropyl-2,3,6,9-tetrahydro-1*H*-purin-8-yl) bicyclo [2.2.2] octane-1-carboxylic acid (compound **16** from Kiesman et al.) (110 mg, 283 μmol, 1 equiv.), *tert*-butyl (3-aminopropyl) carbamate (49 mg, 283 μmol, 1.0 equiv.), BOP (188 mg, 425 μmol, 1.50 equiv.) in dry DMF (2 mL) was added DIPEA (197 μL, 1.13 μmol, 4.0 equiv.). Purification by flash column chromatography using a gradient of 97:3 to 96:4 DCM/MeOH gave the title pure compound as off-white solid (132 mg, 86%).

LC/MS *m/z* calcd for $C_{28}H_{45}N_6O_5$ $[MH]^+$: 545.30, found 545.40 t_R = 3.66 min (method B).

^{1}H NMR ($CDCl_3$) δ 12.20 (br s, 1H, NH), 6.55 (br s, 1H, NH-amide), 4.91 (br s, 1H, NH-amide), 4.08 (t, *J* = 6.9, Hz, 2H, CH_2-N), 4.02 (t, *J* = 6.2 Hz, 2H, CH_2-N), 3.30 (q, *J* = 4.6 Hz, 2H, NH-CH_2-CH_2), 3.16 (q, *J* = 4.6 Hz, 2H, CH_2-CH_2- NH), 2.10 – 2.04 (m, 6H, bicycle), 1.94 – 1.88 (m, 6H, bicycle), 1.78 (h, *J* = 6.5 Hz, 2H, CH_3-CH_2), 1.70 (h, *J* = 6.5 Hz, 2H, CH_3-CH_2), 1.62 – 1.54 (m, 2H, CH_2), 1.43 (s, 9H, Boc), 0.95 (t, *J* = 7.0 Hz, 6H, CH_3)).

^{13}C NMR ($CDCl_3$) δ 177.6 (NHC=O), 161.4 (C), 156.9 (NHC=O), 155.6 (C=O), 151.2 (C), 149.0 (C), 107.0 (C), 79.6 (C), 45.3 (CH_2), 43.2 (CH_2), 39.1 (C), 36.9 (CH_2), 35.6 (CH_2), 33.9 (C), 30.3 (CH_2), 30.2 (CH_2 bicycle), 28.6 (CH_2 bicycle), 28.5 (Boc), 21.5 (2xCH_2), 11.6 (CH_3), 11.3 (CH_3).



***tert*-Butyl (1-(4-(2,6-dioxo-1,3-dipropyl-2,3,6,9-tetrahydro-1H-purin-8-yl)bicyclo[2.2.2]octan-1-yl)-1,6-dioxo-8,11-dioxa-2,5-diazatridecan-13-yl)carbamate** (**4.19**). Following general procedure C, compound **4.17a** (85 mg, 206 μmol, 1.0 equiv.) was treated with 4 M HCl in dioxane (1 mL) to afford compound **4.18a** (68 mg, quantitative) as HCl salt, which was used in the next step without further purification.

LC/MS *m/z* calcd for $C_{22}H_{35}N_6O_3$ $[MH]^+$: 431.34, found 431.30 t_R = 3.10 min. Compound **4.19** was synthesized according to general procedure A, reacting a solution of compound **4.18a** (25 mg, 57 μmol, 1.1 equiv.) in DMF (0.5 mL) with 2,2-dimethyl-4-oxo-3,8,11-trioxa-5-azatridecan-13-oic acid (15 mg, 57 μmol, 1.0 equiv.), DIPEA (40 mL, 228 μmol, 4.0 equiv.) and BOP (38 mg, 85 μmol, 1.50 equiv.). Purification by flash column chromatography using a gradient of 98:2 to 96:4 DCM/MeOH gave the title compound as colourless oil (15 mg, 38%).

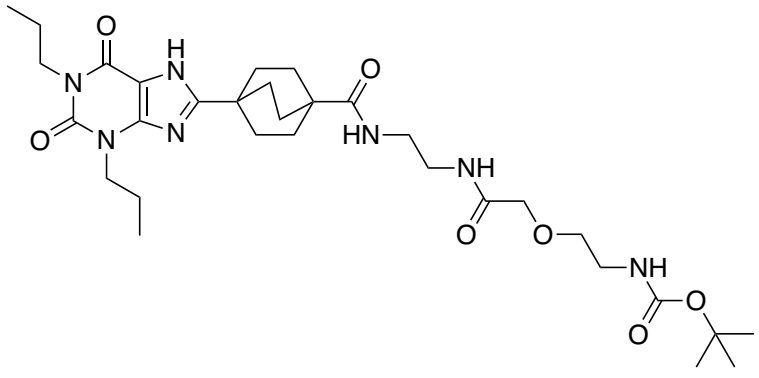
LC/MS ***m/z*** calcd for $C_{33}H_{54}N_7O_8$ $[MH]^+$: 676.20, found 676.40 t_R = 3.50 min (method B).

HRMS (TOF ES^+) calcd for $C_{33}H_{54}N_7O_8$ 676.4028, found 676.4045; calcd for $C_{33}H_{54}N_7O_8Na$ 698.3848, found 698.3869.

^{1}H NMR (CD_3OD) δ 4.07 (t, *J* = 6.9, Hz, 2H, C$\underline{H}_2$-N), 4.01 (s, 2H, CO-C$\underline{H}_2$-O-), 3.95 (t, *J* = 7.1 Hz, 2H, C$\underline{H}_2$-N), 3.72 – 3.66 (m, 4H, NH-(C$\underline{H}_2$)$_2$-NH), 3.56 (t, *J* = 5.7 Hz, 2H, O-C$\underline{H}_2$-CH_2-O), 3.41 – 3.37 (m, 2H, O- CH_2-C$\underline{H}_2$-O), 3.37 – 3.34 (m, 2H, O- C$\underline{H}_2$- CH_2), 3.27 (td, *J* = 5.7, 4.4 Hz, 2H, CH_2-C$\underline{H}_2$-NH), 2.05 – 1.98 (m, 6H, bicycle), 1.93 – 1.86 (m, 6H, bicycle), 1.79 (h, *J* = 7.3 Hz, 2H, CH_2-C$\underline{H}_2$-CH_3), 1.65 (h, *J* = 7.3 Hz, 2H, CH_2-C$\underline{H}_2$-CH_3), 1.44 (s, 9H, Boc), 0.96 (t, *J* = 7.4, 6.3 Hz, 6H, CH_2-C$\underline{H}_3$).

^{13}C NMR (CD_3OD) δ 180.5 (NHC=O), 173.3 (NHC=O), 160.9 (C), 156.0 (NHC=O), 152.9 (C=O), 151.6 (C=O), 149.5 (C), 108.2 (C), 80.1 (C), 72.0 (C$\underline{H}_2$), 71.3 (C$\underline{H}_2$), 71.2 (C$\underline{H}_2$), 71.1 (C$\underline{H}_2$), 49.6 (C$\underline{H}_2$), 45.9 (C$\underline{H}_2$), 43.8 (C$\underline{H}_2$), 41.3 (C$\underline{H}_2$), 40.5 (C$\underline{H}_2$), 40.5 (C$\underline{H}_2$), 40.1 (C$\underline{}$), 39.7 (C$\underline{H}_2$), 34.9 (C$\underline{}$), 31.0 (C$\underline{H}_2$ bicycle), 29.2 (C$\underline{H}_2$ bicycle), 28.8 (Boc), 22.4 (C$\underline{H}_2$), 22.3 (C$\underline{H}_2$), 11.5 (C$\underline{H}_3$), 11.4 (C$\underline{H}_3$).

Analytical RP-HPLC t_R = 5.85 min, purity >99% (method F).



***tert*-Butyl (2-(2-((2-(4-(2,6-dioxo-1,3-dipropyl-2,3,6,9-tetrahydro-1H-purin-8-yl) bicyclo[2.2.2]octane-1-carboxamido)ethyl)amino)-2-oxoethoxy)ethyl)carbamate** (**4.20**). The synthesis of **4.20** was carried out

as described for 8-bicyclo[2.2.2]octylxanthine **4.19**, following general procedure A. Compound **4.18a** (20 mg, 46 μmol, 1.1 equiv.) was added to a solution of 2-(2-((*tert*-butoxycarbonyl)amino)ethoxy)acetic acid (10 mg, 46 μmol, 1.0 equiv.), BOP (30 mg, 68 μmol, 1.50 equiv.) and DIPEA (32 mL, 182 μmol, 4.0 equiv.) in DMF (1 mL). Purification by flash column chromatography using a gradient of 97:3 to 96:4 DCM/MeOH gave the title compound as colourless oil which slightly solidified upon cooling (10 mg, 36%).

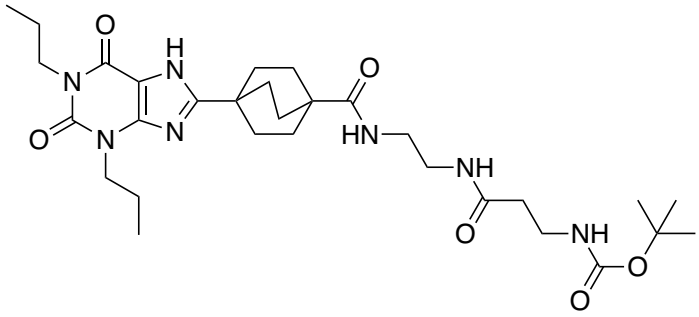
LC/MS ***m/z*** calcd for $C_{31}H_{50}N_7O_7$ $[MH]^+$: 632.20, found 632.40 t_R = 3.53 min (method B).

HRMS (TOF ES^+) calcd for $C_{31}H_{50}N_7O_7$ 632.3766, found 632.3781; calcd for $C_{31}H_{50}N_7O_7Na$ 654.3586, found 654.3601.

^{1}H NMR ($CDCl_3$) δ 11.86 (s, 1H, NH), 7.38 (s, 1H, NH-amide), 6.57 (s, 1H, NH-amide), 5.46 (s, 1H, NH-amide), 4.09 (t, *J* = 6.4 Hz, 2H, CH_2-N), 4.01 (t, *J* = 6.4 Hz, 2H, CH_2-N), 3.96 (s, 2H, CO-CH_2-O-), 3.57 (t, *J* = 5.0 Hz, 2H, O-CH_2-CH_2), 3.47 – 3.41 (m, 4H, NH-(CH_2)$_2$-NH), 3.40 – 3.33 (m, 2H, O-CH_2-CH_2-NH), 2.09 – 2.01 (m, 6H, bicycle), 1.92 – 1.85 (m, 6H, bicycle), 1.79 (h, *J* = 6.9 Hz, 2H, CH_2-CH_2-CH_3), 1.69 (h, *J* = 6.9 Hz, 2H, CH_2-CH_2-CH_3), 1.45 (s, 9H, Boc), 0.95 (t, *J* = 7.5 Hz, 6H, CH_2-CH_3).

^{13}C NMR ($CDCl_3$) δ 178.5 (NHC=O), 171.1 (NHC=O), 156.4 (NHC=O), 155.5 (C=O), 151.2 (C=O), 106.9 (C), 79.7 (C), 70.4 (CH_2), 69.5 (CH_2), 43.3 (CH_2) , 40.7 (2xCH_2), 39.9 (CH_2), 39.0 (C), 33.9 (C), 30.1 (CH_2 bicycle), 29.8 (CH_2), 28.6 (CH_2 bicycle), 28.5 (Boc), 21.5 (CH_2), 21.5 (CH_2), 11.6 (CH_3), 11.3 (CH_3).

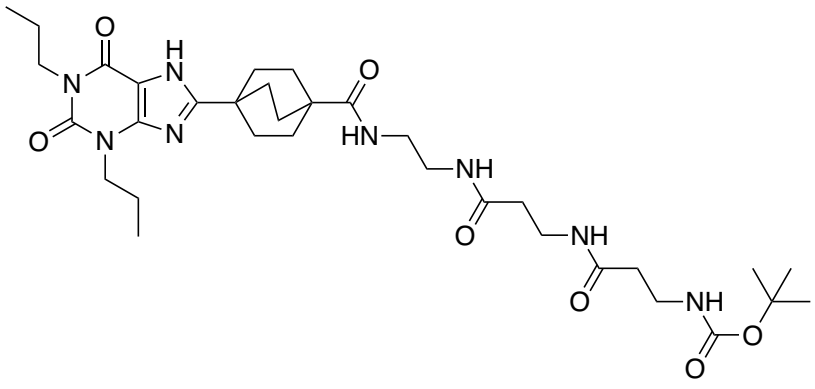
Analytical RP-HPLC t_R = 5.87 min, purity >97% (method F).



***tert*-Butyl (3-((2-(4-(2,6-dioxo-1,3-dipropyl-2,3,6,9-tetrahydro-1H-purin-8-yl)bicyclo[2.2.2]octane-1-carboxamido)ethyl)amino)-3-oxopropyl)carbamate** (**4.21**)**.** Compound **4.18a** (22 mg, 53 μmol, 1.0 equiv.) was reacted with Boc-β-Ala-OH (10 mg, 53 μmol ,1.0 equiv.) in the presence of BOP (35 mg, 79 μmol, 1.50 equiv.) and DIPEA (37 μl, 211 μmol, 4.0 equiv.) in DMF (2 mL) according to general procedure A. Purification by flash column chromatography uisng a gradient of 97:3 to 96:4 DCM/MeOH gave the title compound as colourless oil, which slightly solidified upon cooling (12 mg, 38%).

LC/MS *m/z* calcd for $C_{30}H_{48}N_7O_6$ $[MH]^+$: 602.20, found 602.40 t_R = 3.48 min (method B).

^{1}H NMR (CD_3OD) δ 4.07 (t, *J* = 6.9, 2H, C<u>H</u>$_2$N), 3.95 (t, *J* = 6.9, 2H, C<u>H</u>$_2$N), 3.32 (s, 2H, C<u>H</u>$_2$), 3.30 (s, 4H, NH-(C<u>H</u>$_2$)$_2$-NH), 2.37 (t, *J* = 6.8 Hz, 2H, C<u>H</u>$_2$), 2.05 – 1.98 (m, 6H, bicycle), 1.95 – 1.87 (m, 6H, bicycle), 1.77 (h, *J* = 7.5, 2H, CH_2-C<u>H</u>$_2$-CH_3), 1.66 (h, *J* = 7.5, 2H, CH_2-C<u>H</u>$_2$-CH_3), 1.45 (s, 9H, Boc), 0.96 (t, *J* = 7.4, 6H, C<u>H</u>$_3$).



***tert*-Butyl (3-((3-((2-(4-(2,6-dioxo-1,3-dipropyl-2,3,6,9-tetrahydro-1H-**

purin-8-yl)bicyclo[2.2.2]octane-1-carboxamido)ethyl)amino)-3-oxopropyl)amino)-3-oxopropyl)carbamate (**4.25a**). Compound **4.21** (12 mg, 1.0 equiv.) was treated with 4 M HCl in dioxane following general procedure B, to yield the corresponding 3-((2-(4-(2,6-dioxo-1,3-dipropyl-2,3,6,7-tetrahydro-1*H*-purin-8-yl)bicyclo[2.2.2]octane-1-carboxamido)ethyl)amino)-3-oxopropan-1-aminium chloride intermediate (9 mg, quantitative), which was used for the next step without any further purification. The synthesis of the title compound **4.25a** was carried out as described for 8-bicyclo[2.2.2]octylxanthine **4.21**, treating 3-((2-(4-(2,6-dioxo-1,3-dipropyl-2,3,6,7-tetrahydro-1*H*-purin-8-yl)bicyclo[2.2.2]octane-1-carboxamido)ethyl)amino)-3-oxopropan-1-aminium chloride intermediate (5 mg, 1.10 equiv.) with DIPEA (31 µl, 186 µmol, 10.0 equiv.), Boc-β-Ala-OH (4 mg, 19 µmol ,1.0 equiv.) and BOP (12 mg, 28 µmol, 1.50 equiv.) in DMF (1 mL). Purification by flash column chromatography using a gradient of 96:4 to 94:6 DCM/MeOH gave the title compound as colourless oil, which solidified upon cooling (8 mg, 67%).

LC/MS ***m/z*** calcd for $C_{33}H_{53}N_8O_7$ $[MH]^+$: 673.20, found 673.40 t_R = 3.42 min (method B).

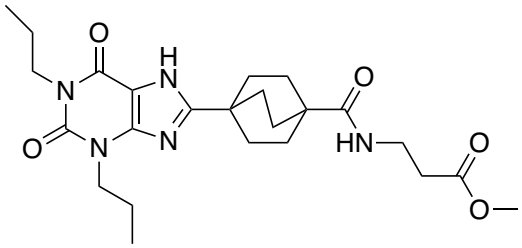
HRMS (TOF ES^+) calcd for $C_{33}H_{53}N_8O_7$ 673.4032, found 673.4043; calcd for $C_{33}H_{52}N_8O_7Na$ 695.3851, found 695.3866.

^{1}H NMR (CD_3OD) δ 4.07 (t, *J* = 6.3 Hz, 2H, C$\underline{H}_2$-N), 3.95 (t, *J* = 5.7 Hz, 2H, C$\underline{H}_2$-N), 3.45 (t, *J* = 6.8 Hz, 2H, C$\underline{H}_2$-NH-CO), 3.30 (s, 4H, NH-(C$\underline{H}_2$)$_2$-NH), 2.38 (t, *J* = 6.8 Hz, 4H, CO-C$\underline{H}_2$-CH_2), 2.04 – 1.98 (m, 6H, bicycle), 1.93 – 1.87 (m, 6H, bicycle), 1.77 (h, *J* = 7.4 Hz, 2H, CH_2-C$\underline{H}_2$-CH_3), 1.66 (h, *J* = 6.4 Hz, 2H, CH_2-C$\underline{H}_2$-CH_3), 1.43 (s, 9H, Boc), 0.96 (t, *J* = 7.2 Hz, 6H, CH_2-C$\underline{H}_3$).

^{13}C NMR (CD_3OD) δ 179.1(NHC=O), 172.9 (2xNHC=O), 161.5(C), 160.8 (C), 151.5 (2xC=O), 111.2 (C), 78.7 (C), 46.8 (C$\underline{H}_2$), 42.5 (C$\underline{H}_2$), 39.1 (C), 38.7(2xC$\underline{H}_2$), 35.7(C$\underline{H}_2$), 35.5(C$\underline{H}_2$), 33.6 (C$\underline{H}_2$), 33.6 (C), 33.3 (C$\underline{H}_2$), 29.6

($\underline{C}H_2$ bicycle), 27.8 ($\underline{C}H_2$ bicycle), 27.4 (Boc), 20.9 ($\underline{C}H_2$), 20.9 ($\underline{C}H_2$), 10.1 ($\underline{C}H_3$), 9.9 ($\underline{C}H_3$).

Analytical RP-HPLC t_R = 5.58 min, purity > 97% (method F).



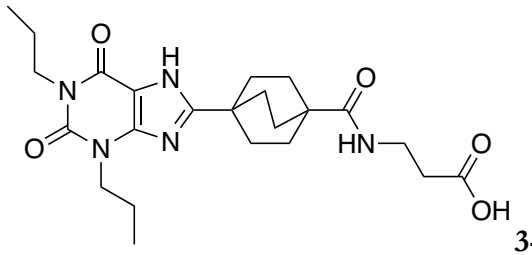
Methyl 3-(4-(2,6-dioxo-1,3-dipropyl-2,3,6,9-tetrahydro-1H-purin-8-yl) bicyclo[2.2.2]octane-1-carboxamido)propanoate (**4.26**)**.** To a solution of 4-(2,6-dioxo-1,3-dipropyl-2,3,6,9-tetrahydro-1*H*-purin-8-yl)bicyclo[2.2.2]octane-1-carboxylic acid (compound **16** from Kiesman et. al.) (80 mg, 206 μmol, 1.0 equiv.) in DMF (1 mL) was added DIPEA (0.143 mL, 824 μmol, 4.0 equiv.), β-Ala-methyl ester (29 mg, 206 μmol, 1.0 equiv.) and BOP (136 mg, 309 μmol, 1.50 equiv.). The resulting mixture was stirred at rt for 1 h. Upon completion of the reaction checked by TLC and LC/MS, DMF was evaporated to dryness and the resulting residue was taken up in water (20 mL) and extracted with EtOAc. The organic layer was collected and washed with 1 M HCl, sat. $NaHCO_3$ and brine. The organic layer was then dried over anhydrous Na_2SO_4, filtered and evaporated to dryness to give the crude as pale yellow oil. Purification by flash column chromatography using a gradient of 96:4 to 94:6 DCM/MeOH gave the title compound as off-white solid (76 mg, 56%).

LC/MS ***m/z*** calcd for $C_{24}H_{36}N_5O_5$ $[MH]^+$: 474.20, found 474.30 t_R = 3.57 min (Method B).

^{1}H NMR ($CDCl_3$) δ 12.25 (s, 1H, N$\underline{H}$), 6.33 (t, *J* = 6.0 Hz, 1H, N*H*-amide), 4.08 (t, *J* = 7.6, 6.1 Hz, 2H, C$\underline{H}_2$-N), 4.01 (t, *J* = 6.7 Hz, 2H, C$\underline{H}_2$-N), 3.69 (s, 3H, OC$\underline{H}_3$), 3.51 (q, *J* = 6.0 Hz, 2H, NH-C$\underline{H}_2$), 2.52 (t, *J* = 6.2 Hz, 2H, C$\underline{H}_2$-CO), 2.10 – 2.02 (m, 6H, bicycle), 1.87 (m, 6H, bicycle), 1.79 (h, *J* = 7.4 Hz,

2H, C<u>H</u>$_2$-CH$_3$), 1.74 – 1.64 (h, *J* = 7.4 Hz, 2H, C<u>H</u>$_2$-CH$_3$), 0.95 (t, *J* = 7.4 Hz, 6H, C<u>H</u>$_3$).

^{13}C NMR ($CDCl_3$) δ 177.1 (NHC=O), 173.5 (NHC=O), 161.2 (C), 155.5 (C=O), 151.2 (C=O), 149.0 (C), 107.1 (C), 51.9 (<u>C</u>H$_3$), 45.3 (<u>C</u>H$_2$), 43.3 (<u>C</u>H$_2$), 38.9 (C), 34.9 (<u>C</u>H$_2$), 33.9 (C), 33.7 (<u>C</u>H$_2$), 30.1 (<u>C</u>H$_2$ bicycle), 28.5 (<u>C</u>H$_2$ bicycle), 21.5 (2x<u>C</u>H$_2$), 11.6 (<u>C</u>H$_3$), 11.3 (<u>C</u>H$_3$).

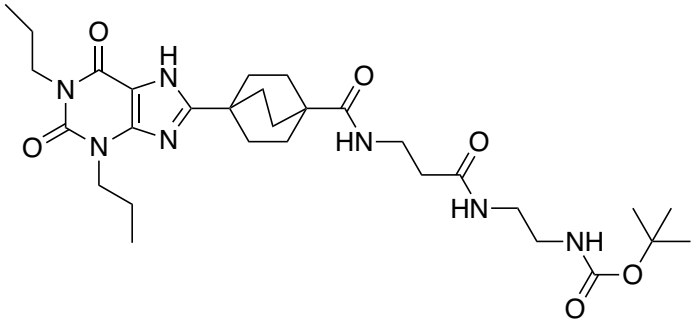


3-(4-(2,6-Dioxo-1,3-dipropyl-2,3,6,9-tetrahydro-1H-purin-8-yl)bicyclo[2.2.2]octane-1-carboxamido)propanoic acid (**4.27**). Methyl 3-(4-(2,6-dioxo-1,3-dipropyl-2,3,6,9-tetrahydro-1*H*-purin-8-yl)bicyclo[2.2.2]octane-1-carboxamido)propanoate (**4.26**) (76 mg, 160 μmol, 1.0 equiv.) was dissolved in MeOH (5 mL). To the mixture was added a solution of LiOH·H$_2$O (33.67 mg, 802 μmol, 5.0 equiv.) in water (5 mL). The resulting mixture was stirred at rt for 40 min. By that time, TLC and LC/MS showed the reaction was completed. MeOH was then removed under reduced pressure and the water layer was acidified with 2 M HCl to pH = 1. The water layer was extracted with EtOAc (2x20 mL). The organic layer was separated, dried over anhydrous $MgSO_4$, filtered and evaporated to dryness to give the title compound as off-white solid (61 mg, 84%).

^{1}H NMR ($CDCl_3$) δ 12.10 (s, 1H, N<u>H</u>), 6.45 (t, *J* = 6.0 Hz, 1H, N<u>H</u>-amide), 4.08 (t, *J* = 6.6 Hz, 2H, C<u>H</u>$_2$-N), 3.98 (t, *J* = 7.0 Hz, 2H, C<u>H</u>$_2$-N), 3.58 (q, *J* = 6.0 Hz, 2H, NH-C<u>H</u>$_2$), 2.66 (t, *J* = 4.9 Hz, 2H, C<u>H</u>$_2$), 2.07 – 2.00 (m, 6H, bicycle), 1.96 – 1.91 (m, 6H, bicyle), 1.78 (h, *J* = 7.0 Hz, 2H, C<u>H</u>$_2$-CH$_3$), 1.65 (h, *J* = 7.0 Hz, 2H, C<u>H</u>$_2$-CH$_3$), 0.94 (t, *J* = 7.4, 6H, C<u>H</u>$_3$-CH$_2$).

^{13}C NMR ($CDCl_3$) δ 178.2 (NHC=O), 176.6 (NHC=O), 161.4 (C), 156.4 (C=O), 150.8 (C=O), 149.7(C), 106.5 (C), 45.5 (<u>C</u>H$_2$), 43.6 (<u>C</u>H$_2$), 38.9 (C),

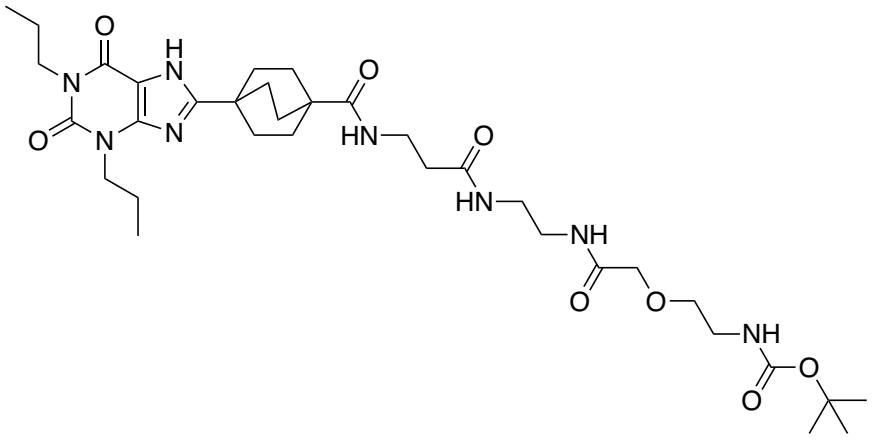
34.6 (<u>C</u>H$_2$), 33.8 (C), 30.2 (<u>C</u>H$_2$ bicycle), 28.5 (<u>C</u>H$_2$ bicycle), 21.4 (2x<u>C</u>H$_2$), 11.4 (<u>C</u>H$_3$), 11.3 (<u>C</u>H$_3$).



***tert*-Butyl (2-(3-(4-(2,6-dioxo-1,3-dipropyl-2,3,6,9-tetrahydro-1H-purin-8-yl)bicyclo[2.2.2]octane-1-carboxamido)propanamido)ethyl)carbamate** (**4.28**). Following general procedure A, to a solution of compound **4.27** (61.00 mg, 133 μmol, 1eq.) in DMF (1 mL) was added DIPEA (92 mL, 531 μmol, 4.0 equiv.), *tert*-butyl (2-aminoethyl)carbamate (21.27 mg, 133 μmol, 1.0 equiv.) and BOP (88 mg, 199 μmol, 1.50 equiv.). Purification by flash column chromatography using a gradient of 96:4 to 94:6 DCM/MeOH gave the title compound as off-white solid (62 mg, 70%).

LC/MS *m/z* calcd for $C_{30}H_{48}N_7O_6$ $[MH]^+$: 602.20, found 602.40 t_R = 3.62 min (Method B).

^{1}H NMR ($CDCl_3$) δ 6.86 (br s, 1H, N<u>H</u>-amide), 6.65 (br s, 1H, N<u>H</u>-amide), 5.02 (br s, 1H, N<u>H</u>-amide), 4.10 (t, *J* = 6.4 Hz, 2H, C<u>H</u>$_2$-N), 4.00 (t, *J* = 6.4 Hz, 2H, C<u>H</u>$_2$-N), 3.57-3.48 (m, 2H, C<u>H</u>$_2$), 3.39 – 3.32 (m, 2H, C<u>H</u>$_2$), 3.31 – 3.22 (m, 2H, C<u>H</u>$_2$), 2.46 – 2.37 (m, 2H, C<u>H</u>$_2$), 2.10 – 2.00 (m, 6H, bicycle), 1.95 – 1.85 (m, 6H, bicycle), 1.79 (h, *J* = 7.3 Hz, 2H, C<u>H</u>$_2$-CH$_3$), 1.68 (h, *J* = 7.4 Hz, 2H, C<u>H</u>$_2$-CH$_3$), 1.44 (s, 9H, Boc), 0.95 (t, *J* = 7.5 Hz, 6H, C<u>H</u>$_3$-CH$_2$).



***tert*-Butyl (1-(4-(2,6-dioxo-1,3-dipropyl-2,3,6,9-tetrahydro-1H-purin-8-yl)bicyclo[2.2.2]octan-1-yl)-1,5,10-trioxo-12-oxa-2,6,9-triazatetradecan-14-yl)carbamate** (**4.30**)**.** Following general procedure B, compound 2-(3-(4-(2,6-dioxo-1,3-dipropyl-2,3,6,9-tetrahydro-1H-purin-8-yl)bicyclo[2.2.2]octane-1-carboxamido)propanamido)ethan-1-aminium chloride (**4.29**) was synthesized reacting **4.28** (64 mg, 1.0 equiv.) with 4 M HCl in dioxane (1 mL). The resulting intermediate **4.29** was used for the subsequent step without further purification. The synthesis of the title compound **4.30** was carried out following general procedure A, reacting a solution of 2-(3-(4-(2,6-dioxo-1,3-dipropyl-2,3,6,9-tetrahydro-1H-purin-8-yl)bicyclo[2.2.2]octane-1-carboxamido)propanamido)ethan-1-aminium chloride (**4.29**) (54 mg, 100 μmol, 1.10 equiv.) in DMF (0.5 mL) with a solution of 2-(2-((*tert*-butoxycarbonyl)amino)ethoxy)acetic acid (20 mg, 91 μmol, 1.0 equiv.), DIPEA (64 μl, 365 μmol, 4.0 equiv.)and COMU (43 mg, 100 μmol, 1.10 equiv.) in DMF (0.5 mL). Purification by flash column chromatography using a gradient of 97:3 to 94:6 DCM/MeOH gave the title compound as an off-white solid (37 mg, 58%).

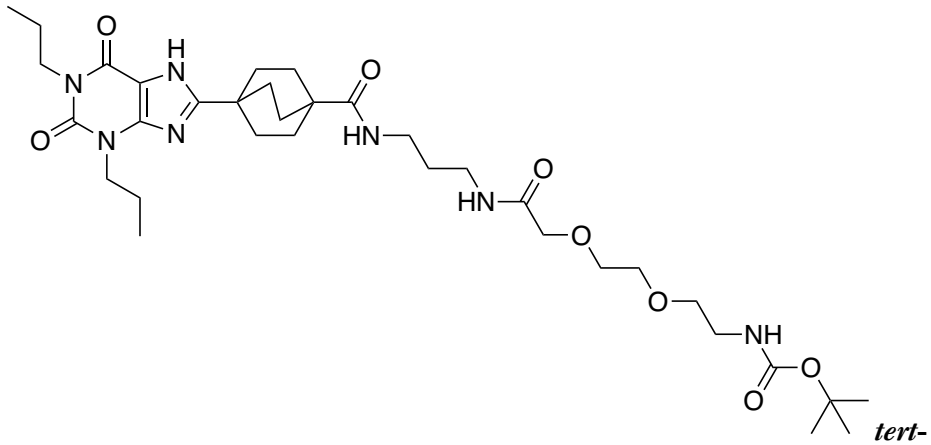
LC/MS ***m/z*** calcd for $C_{34}H_{55}N_8O_8$ $[MH]^+$: 703.20, found 703.40 t_R = 3.37 min (Method B).

HRMS (TOF ES^+) calcd for $C_{34}H_{55}N_8O_8$ 703.4137, found 703.4155; calcd for $C_{34}H_{55}N_8O_8Na$ 725.3957, found 725.3974.

^{1}H NMR ($CDCl_3$) δ 12.05 (s, 1H, NH), 7.57 (s, 1H, NH-amide), 7.10 (s, 1H, NH-amide), 6.71 (s, 1H, NH-amide), 5.62 (s, 1H, NH-amide), 4.07 (t, *J* = 6.1 Hz, 2H, CH_2-N), 4.01 – 3.93 (m, 4H, CO-CH_2-O- and CH_2-N-), 3.59 – 3.50 (m, 4H, CH_2), 3.43 – 3.38 (m, 4H, NH- $(CH_2)_2$-NH), 3.38 – 3.32 (m, 2H, CH_2), 2.56-2.42 (m, 2H, CH_2), 2.07 – 1.98 (m, 6H, bicycle), 1.90 – 1.82 (m, 6H, bicycle), 1.78 (h, *J* = 7.4 Hz, 2H, CH_2-CH_2-CH_3), 1.67 (h, *J* = 7.4 Hz, 2H, CH_2-CH_2-CH_3), 1.43 (s, 9H, Boc), 0.94 (t, *J* = 7.5 Hz, 6H, CH_2-CH_3).

^{13}C NMR ($CDCl_3$) δ 176.6 (NHC=O), 161.5 (C), 160.9 (NHC=O), 156.5 (C=O), 155.4 (NHC=O), 151.2 (C=O), 148.8 (C), 107.0 (C), 101.7 (NHC=O), 79.9 (C), 71.2 (CH_2), 70.5 (CH_2), 45.3 (2xCH_2), 43.2 (CH_2), 39.9 (CH_2), 39.0 (C), 35.9 (CH_2), 35.8 (CH_2), 33.9 (C), 30.1 (CH_2 bicycle), 28.6 (Boc), 28.4 (CH_2 bicycle), 21.5 (2xCH_2), 11.6 (CH_3), 11.3 (CH_3).

Analytical RP-HPLC t_R = 5.62 min, purity > 98% (Method F).



***tert*-Butyl (1-(4-(2,6-dioxo-1,3-dipropyl-2,3,6,9-tetrahydro-1H-purin-8-yl)bicyclo[2.2.2]octan-1-yl)-1,7-dioxo-9,12-dioxa-2,6-diazatetradecan-14-yl)carbamate** (**4.22**)**.** The title compound was synthesized as described for 8-bicyclo[2.2.2]octylxanthine **4.19**, following general procedure A: to a solution of 2,2-dimethyl-4-oxo-3,8,11-trioxa-5-azatridecan-13-oic acid (11 mg, 42 μmol, 1.0 equiv.) in DMF (0.7 mL) was added DIPEA (15 μL, 85 μmol, 4.0 equiv.) followed by COMU (20 mg, 46 μmol, 1.10 equiv.) and intermediate **4.18b** (21 mg, 46 μmol, 1.10 equiv.) previously dissolved in DMF (0.5 mL). Purification by flash column chromatography using a gradient

of 97:3 to 95:5 DCM/MeOH gave the title compound as colourless oil (15 mg, 39%).

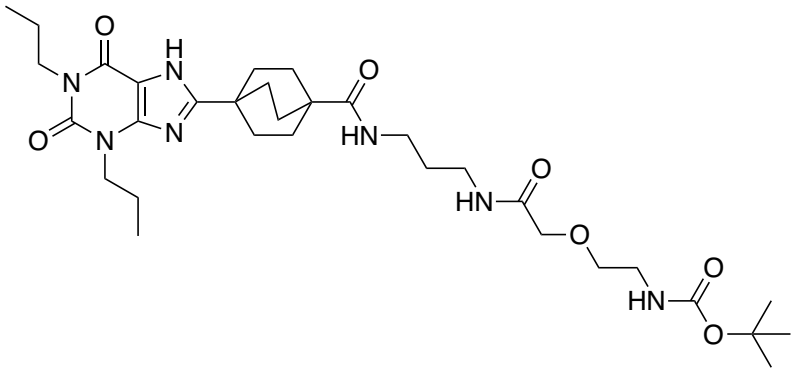
LC/MS ***m/z*** calcd for $C_{34}H_{56}N_7O_8$ $[MH]^+$: 690.20, found 690.40 t_R = 3.57 min (Method B).

HRMS (TOF ES^+) calcd for $C_{34}H_{56}N_7O_8$ 690.4185, found 690.4199; calcd for $C_{34}H_{56}N_7O_8$ Na 712.4004, found 712.4020.

^{1}H NMR ($CDCl_3$) δ 11.86 (s, 1H, NH), 7.17 (t, *J* = 6.6 Hz, 1H, NH-amide), 6.86 (t, *J* = 6.8 Hz, 1H, NH-amide), 4.92 (br s, 1H, NH-amide), 4.10 (t, *J* = 6.5 Hz, 2H, CH_2-N), 4.04 – 3.99 (m , 4H, CO-CH_2-O- and CH_2-N-), 3.71 – 3.66 (m, 2H, O-CH_2-CH_2-O), 3.66 – 3.63 (m, 2H, O- CH_2-CH_2-O), 3.57 (t, *J* = 5.3 Hz, 2H, O- CH_2- CH_2), 3.35 (dt, *J* = 10.5, 5.7 Hz, 4H, NH-$CH_2CH_2CH_2$-NH), 3.26 (q, *J* = 6.1 Hz, 2H, CH_2-CH_2-NH-CO), 2.10-2.03 (m, 6H, bicycle), 1.97-1.90 (m, 6H, bicycle), 1.79 (m, 2H, CH_2-CH_2-CH_3), 1.74 – 1.67 (m, 2H, CH_2-CH_2-CH_3), 1.67 – 1.60 (m, 2H, NH-$CH_2CH_2CH_2$-NH), 1.44 (s, 9H, Boc), 0.96 (t, *J* = 7.5 Hz, 6H, CH_2-CH_3).

^{13}C NMR ($CDCl_3$) δ 177.5 (NHC=O), 171.2 (NHC=O), 166.7 (NHC=O), 156.1(C), 155.5 (C=O), 151.2 (C=O), 148.7 (C), 106.9 (C), 75.4 (CH_2), 71.2 (CH_2), 70.5 (CH_2), 70.5 (CH_2), 70.5 (CH_2), 70.1 (CH_2), 43.3 (CH_2), 39.1 (C), 35.4 (CH_2), 35.3 (CH_2), 33.9 (C), 30.2 (CH_2), 29.7(CH_2 bicycle), 28.6 (CH_2 bicycle), 28.5 (Boc), 21.5 (CH_2), 21.5 (CH_2), 11.6 (CH_3), 11.3 (CH_3).

Analytical RP-HPLC t_R = 5.92 min, purity > 99% (Method F).



***tert*-Butyl (2-(2-((3-(4-(2,6-dioxo-1,3-dipropyl-2,3,6,9-tetrahydro-1H-purin-8-yl)bicyclo[2.2.2]octane-1-carboxamido)propyl)amino)-2-oxoethoxy)ethyl)carbamate** (**4.23**)**.** The synthesis of **4.23** was carried out as described for 8-bicyclo[2.2.2]octylxanthine **4.20**, following general procedure A: to a solution of 2-(2-((tert-butoxycarbonyl)amino)ethoxy)acetic acid (13 mg, 59.30 μmol, 1.0 equiv.) in DMF (0.7 mL) was added DIPEA (21 mL, 118.6 μmol, 4.0 equiv.), followed by COMU (27.93 mg, 65 μmmol, 1.10 equiv.) and intermediate **4.18b** (29 mg, 65.23 μmol, 1.10 equiv.) previously dissolved in DMF (0.5 mL). Purification by flash column chromatography using a gradient of 96:4 to 95:5 DCM/MeOH gave the title compound as colourless oil (14 mg, 37%).

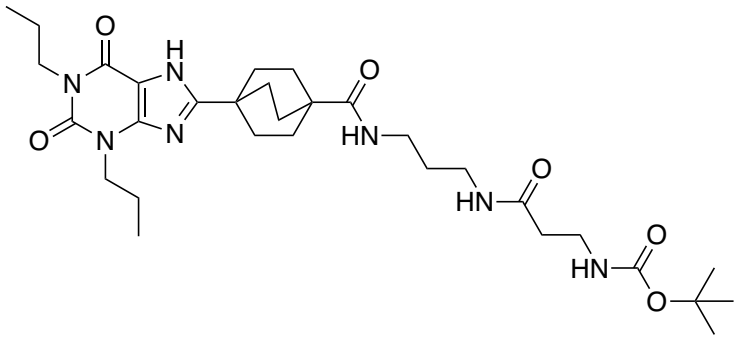
LC/MS *m/z* calcd for $C_{32}H_{52}N_7O_7$ $[MH]^+$: 646.20, found 646.40 t_R = 2.82 min (Method B).

HRMS (TOF ES^+) calcd for $C_{32}H_{52}N_7O_7$ 646.3923, found 646.3937; calcd for $C_{32}H_{52}N_7O_7$ Na 668.3742, found 668.3758.

^{1}H NMR ($CDCl_3$**)** δ 12.08 (s, 1H, NH)7.43 (br s, 1H, NH-amide), 6.52 (br s, 1H, NH-amide), 5.54 (br s, 1H, NH-amide), 4.09 (t, *J* = 6.0 Hz, 2H, CH_2-N), 4.01 (t, *J* = 6.3 Hz, 2H, CH_2-N), 3.98 (s, 2H, CO-CH_2-O), 3.58 (t, *J* = 5.0 Hz, 2H, O-CH_2-CH_2-NH), 3.40 – 3.35 (m, 2H, O-CH_2-CH_2-NH), 3.34 – 3.27 (m, 4H, NH-$CH_2CH_2CH_2$-NH), 2.11 – 2.04 (m, 6H, bicycle), 1.96 – 1.90 (m, 6H, bicycle), 1.79 (h, *J* = 6.5 Hz, 2H, CH_2-CH_2-CH_3), 1.71 (h, *J* = 6.5 Hz, 2H, CH_2-CH_2-CH_3), 1.66 – 1.57 (m, 2H, NH-$CH_2CH_2CH_2$-NH), 1.43 (s, 9H, Boc), 0.95 (t, *J* = 7.5 Hz, 6H, CH_2-CH_3).

^{13}C NMR ($CDCl_3$) δ 178.1 (NHC=O), 170.5 (NHC=O), 161.1(NHC=O), 156.4 (C), 155.5 (C=O), 151.2 (C=O), 148.8 (C), 106.9 (C), 79.4 (C), 71.4 ($\underline{C}H_2$), 70.5 ($\underline{C}H_2$), 45.4 ($\underline{C}H_2$), 43.3 ($\underline{C}H_2$), 40.7 ($\underline{C}H_2$), 39.2 (C), 35.4 ($\underline{C}H_2$), 34.9 ($\underline{C}H_2$), 33.9 (C), 30.2 ($\underline{C}H_2$), 29.7($\underline{C}H_2$ bicycle), 28.6 ($\underline{C}H_2$ bicycle and Boc), 21.5 ($\underline{C}H_2$), 21.5 ($\underline{C}H_2$), 11.6 ($\underline{C}H_3$), 11.3 ($\underline{C}H_3$).

Analytical RP-HPLC t_R = 5.95 min, purity > 99% (Method F).



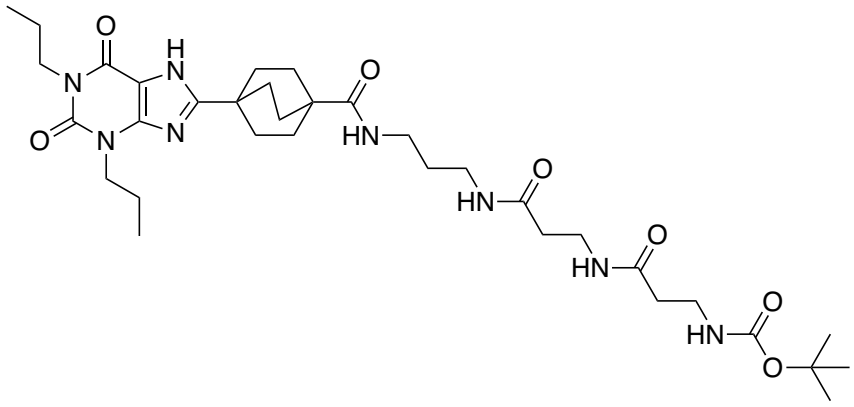
***tert*-Butyl (3-((3-(4-(2,6-dioxo-1,3-dipropyl-2,3,6,9-tetrahydro-1H-purin-8-yl)bicyclo[2.2.2]octane-1-carboxamido)propyl)amino)-3-oxopropyl)carbamate** (**4.24**). The synthesis of compound **4.24** was carried out as described for 8-bicyclo[2.2.2]octylxanthine **4.21**, following general procedure A: to a solution of Boc-β-Ala-OH (12 mg, 61 μmol, 1.0 equiv.) in DMF (0.5 mL) was added DIPEA (21 μL, 122 μmol, 2.0 equiv.) followed by COMU (29 mg, 67 μmol, 1.10 equiv.) and intermediate **4.18b** (30 mg, μmol, 1.10 equiv.) previously dissolved in DMF (0.5 mL). Purification by flash column chromatography using a gradient of 96:4 to 94:6 DCM/MeOH gave the title compound as an off-white solid (36 mg, 92%).

LC/MS *m/z* calcd for $C_{31}H_{50}N_7O_6$ $[MH]^+$: 616.37, found 616.40 t_R = 3.43 min (Method B).

^{1}H NMR ($CDCl_3$) δ 6.58 – 6.49 (m, 2H, N$\underline{H}$-amide), 5.20 (s, 1H, N$\underline{H}$-amide), 4.09 (t, *J* = 6.5 Hz, 2H, C$\underline{H}_2$-N-), 4.02 (t, *J* = 6.7 Hz, 2H, C$\underline{H}_2$-N-), 3.41 (t, *J* = 5.3 Hz, 2H, ,-COC$\underline{H}_2$CH$_2$), 3.31 – 3.23 (m, 4H, NH-C$\underline{H}_2$CH$_2$C$\underline{H}_2$-NH), 2.45 (t, *J* = 6.1 Hz, 2H, CH$_2$), 2.11 – 2.04 (m, 6H, bicycle), 1.96 – 1.89 (m, 6H, bicycle), 1.79 (h, *J* = 6.5 Hz, 2H, CH$_2$.C$\underline{H}_2$-CH$_3$), 1.70 (h, *J* = 6.4 Hz, 2H,

CH_2-C$\underline{H}_2$-CH_3), 1.65 – 1.56 (m, 2H, C$\underline{H}_2$), 1.42 (s, 9H, Boc), 0.96 (t, J = 7.4 Hz, 6H, -C$\underline{H}_3$).

^{13}C NMR ($CDCl_3$) δ 177.9 (NHC=O), 161.1 (C), 157.9 (NHC=O), 156.4 (NHC=O), 155.5 (C=O), 151.2 (C=O), 148.8 (C), 106.9 (C), 47.7 (C$\underline{H}_2$), 45.4 (C$\underline{H}_2$), 43.3 (C$\underline{H}_2$), 39.2 (C), 36.8 (C$\underline{H}_2$), 35.8 (C$\underline{H}_2$), 35.5 (C$\underline{H}_2$), 33.9 (C), 30.2 (C$\underline{H}_2$), 29.8 (C$\underline{H}_2$ bicycle), 28.6 (C$\underline{H}_2$ bicycle), 28.5 (Boc), 21.5 (C$\underline{H}_2$), 21.5 (C$\underline{H}_2$), 11.6 (C$\underline{H}_3$), 11.3 (C$\underline{H}_3$).



***tert*-Butyl (3-((3-((3-(4-(2,6-dioxo-1,3-dipropyl-2,3,6,9-tetrahydro-1H-purin-8-yl)bicyclo[2.2.2]octane-1-carboxamido)propyl)amino)-3-oxopropyl)amino)-3-oxopropyl)carbamate** (**4.25b**). Following general procedure C, the intermediate 3-((3-(4-(2,6-dioxo-1,3-dipropyl-2,3,6,7-tetrahydro-1*H*-purin-8-yl)bicyclo[2.2.2]octane-1-carboxamido)propyl)amino)-3-oxopropan-1-aminium chloride was synthesized and was used for the subsequent step without further purification. The synthesis of the title compound **4.25b** was carried out as described for xanthine **4.25a**, following general procedure A: to a solution of Boc-β-Ala-OH (11 mg, 58 μmol, 1.0 equiv.), DIPEA (41 μL, 233 μmol, 4.0 equiv.) and COMU (22 mg, 64 μmol, 1.10 equiv.) in DMF (0.5 mL) was added a solution of 3-((3-(4-(2,6-dioxo-1,3-dipropyl-2,3,6,7-tetrahydro-1*H*-purin-8-yl)bicyclo[2.2.2]octane-1-carboxamido)propyl)amino)-3-oxopropan-1-aminium chloride (33 mg, 64 μmol, 1.10 equiv.) in DMF (0.5 mL). Purification by flash column chromatography using a gradient of 96:4 to 93:7 DCM/MeOH gave the title compound as an off-white solid (12 mg, 31%).

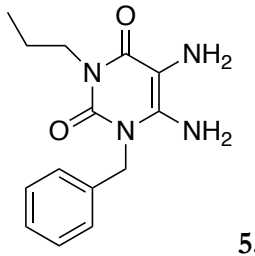
LC/MS ***m/z*** calcd for $C_{34}H_{55}N_8O_7$ $[MH]^+$: 687.20, found 687.40 t_R = 3.38 min (Method B).

HRMS (TOF ES^+) calcd for $C_{34}H_{55}N_8O_7$ 687.4188, found 687.4202; calcd for $C_{34}H_{55}N_8O_7$ Na 709.4008, found 709.4026.

^{1}H NMR (CD_3OD) δ 4.07 (t, *J* = 6.9 Hz, 2H, C<u>H</u>$_2$-N), 3.95 (t, *J* = 6.9 Hz, 2H, C<u>H</u>$_2$-N), 3.46 (t, *J* = 6.7 Hz, 2H, C<u>H</u>$_2$), 3.31 (s, 2H, C<u>H</u>$_2$), 3.22 (dt, *J* = 6.7, 4.2 Hz, 4H, C<u>H</u>$_2$), 2.39 (dt, *J* = 15.7, 6.8 Hz, 4H, C<u>H</u>$_2$), 2.06 – 1.99 (m, 6H, bicycle), 1.95 – 1.89 (m, 6H, bicycle), 1.78 (h, *J* = 6.9 Hz, 2H, CH_2-C<u>H</u>$_2$-CH_3), 1.72 – 1.61 (m, 4H, C<u>H</u>$_2$), 1.44 (s, 9H, Boc), 0.96 (t, *J* = 7.3 Hz, 6H, CH_2-C<u>H</u>$_3$).

^{13}C NMR (CD_3OD) δ 181.9 (NHC=O), 159.9 (C), 156.0 (NHC=O), 153.9 (NHC=O), 151.0 (C=O), 150.8(C=O), 143.9 (C), 109.1(C), 57.9 (<u>C</u>H$_2$), 47.4 (<u>C</u>H$_2$), 46.1 (<u>C</u>H$_2$), 43.3 (<u>C</u>H$_2$), 40.2 (C), 38.8 (<u>C</u>H$_2$), 36.9 (<u>C</u>H$_2$), 34.9 (C), 31.2 (<u>C</u>H$_2$), 31.0 (<u>C</u>H$_2$), 30.3 (<u>C</u>H$_2$ bicycle), 29.3 (<u>C</u>H$_2$ bicycle), 28.8 (Boc), 22.4 (<u>C</u>H$_2$), 22.3 (<u>C</u>H$_2$), 19.4(<u>C</u>H$_2$), 11.5 (<u>C</u>H$_3$), 11.3 (<u>C</u>H$_3$).

Analytical RP-HPLC t_R = 5.30 min, purity >99% (Method F).

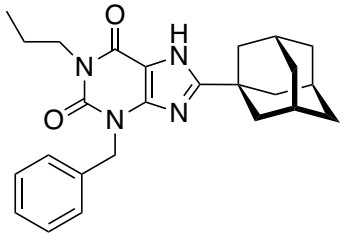


5,6-Diamino-1-benzyl-3-propylpyrimidine-2,4(1H,3H)-dione (**4.32**).[292] A solution of 6-amino-1-benzyl-5-nitroso-3-propylpyrimidine-2,4(1*H*,3*H*)-dione (**4.31**) (0.250 g, 0.87 mmol, 1 equiv.) in water (25 mL) and 30% NH_3OH (10 mL) was heated to 85 °C and sodium dithionite (3.0 equiv.) was added in small portions until the colour disappeared. The reaction was cooled to rt and the mixture was extracted with EtOAc. The organic phase was dried over anhydrous $MgSO_4$, filtered and evaporated to dryness to give the title compound as yellow solid (0.218 g, 92%).

LC/MS *m/z* calcd for $C_{14}H_{19}N_4O_2$ $[MH]^+$: 275.14, found 275.10 t_R = 2.90 min (Method B).

^{1}H NMR (DMSO-d_6) δ 7.36 – 7.30 (m, 2H, , Ar-H), 7.27 – 7.22 (m, 1H, , Ar-H), 7.21 – 7.15 (m, 2H, , Ar-H), 6.13 (s, 2H, -NH$_2$), 5.13 (s, 2H, -CH$_2$-Ar), 3.76 (t, *J* = 6.2 Hz, 2H, CH$_2$-CH$_2$-CH$_3$), 2.95 (br s, 2H, NH$_2$), 1.51 (h, *J* = 7.3 Hz, 2H, CH$_2$-CH$_2$-CH$_3$), 0.82 (t, *J* = 7.5 Hz, 3H, -CH$_3$).

^{13}C NMR (DMSO-d_6) δ 158.9 (C=O), 149.8 (C=O), 144.1(C), 136.9 (C), 128.4 (CH-Ar), 127.1 (CH-Ar), 126.4 (CH-Ar), 96.3 (C), 44.9(CH$_2$), 42.0 (CH$_2$), 20.9 (CH$_2$), 11.2 (CH$_3$).



8-((1*R*,3*R*,5*S*)-Adamantan-1-yl)-3-benzyl-1-propyl-3,7-dihydro-1*H*-purine-2,6-dione (**4.34**). To a solution of xanthine **4.32** (0.201 g, 0.73 mmol, 1.0 equiv.) in DMF (1 mL) was added DIPEA (0.13 mL, 0.73 mmol, 1.10 equiv.). The resulting mixture was added to a solution of 1-adamantane carboxylic acid (0.120 g, 0.67 mmol, 1 eq.) and COMU (0.314 g, 0.73 mmol, 1.10 equiv.) in DMF (1 mL). The resulting solution was stirred at rt for 15 min. Upon completion of the reaction (LC-MS) cold water was added to the reaction mixture and subsequent precipitation of a white solid occurred. The solid was filtrated, washed with cold water and dried. The title intermediate (1R,3R,5S)-N-(6-amino-1-benzyl-2,4-dioxo-3-propyl-1,2,3,4-tetrahydropyrimidin-5-yl)adamantane-1-carboxamide was obtained as off-white solid (0.254 g, 87%).[293]

LC/MS *m/z* calcd for $C_{25}H_{33}N_4O_4$ $[MH]^+$: 437.14, found 437.20 t_R = 2.99 min (Method B).

^{1}H NMR (DMSO-d_6) δ 7.83 (s, 1H, NH), 7.37 – 7.31 (m, 2H, Ar-H), 7.27-7.22 (m, 1H, Ar-H), 7.23 – 7.17 (m, 2H, Ar-H), 6.28 (s, 2H, -NH$_2$), 5.16 (s, 2H, -CH$_2$-Ar), 3.71 (t, *J* = 7.2, 2H, , CH$_2$-CH$_2$-CH$_3$), 2.00 – 1.92 (m, 3H,

adamantyl), 1.89-1.86 (m,5H, adamantyl), 1.71 – 1.60 (m, 6H, adamantyl), 1.49 (h, *J* = 7.3 Hz, 2H, -C<u>H</u>$_2$), 0.82 (t, *J* = 7.5 Hz, 3H, -C<u>H</u>$_3$).

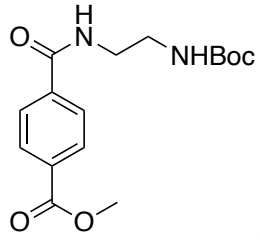
^{13}C NMR (DMSO-d_6)) δ 177.9 (NHC=O), 159.0 (C=O), 151.5 (C=O), 150.7, 136.6 (C), 128.6 (<u>C</u>H-Ar), 127.3 (<u>C</u>H-Ar), 126.4 (<u>C</u>H-Ar), 88.3 (C), 45.2 (<u>C</u>H$_2$), 42.1 (<u>C</u>H$_2$), 36.3(<u>C</u>H$_2$ adamantane), 27.8 (<u>C</u>H adamantane), 20.9 (<u>C</u>H$_2$), 11.3 (<u>C</u>H$_3$).

(1*R*,3*R*,5*S*)-*N*-(6-amino-1-benzyl-2,4-dioxo-3-propyl-1,2,3,4-tetrahydropyrimidin-5-yl)adamantane-1-carboxamide (0.254 g, 0.58 mmol, 1.0 equiv.) was dissolved in propan-2-ol (7 mL). To the resulting mixture was added 1 M KOH (7 mL) and the resulting solution was heated to reflux for 1 h. Upon completion of the reaction, the solvent was removed under reduced pressure and the residue was taken up in water and extracted with DCM (2 x 20 mL). The organic layers were combined, dried over anhydrous $MgSO_4$, filtered and evaporated to dryness to give the title compound as pale yellow solid. Subsequent recrystallization from hot ethanol and water gave the title compound as fluffy off-white solid (0.232 g, 95%).

LC/MS *m/z* calcd for $C_{25}H_{31}N_4O_2$ $[MH]^+$: 419.20, found 419.20 t_R = 4.73 min (Method B).

^{1}H NMR (CDCl3) δ 12.10 (s, 1H, -N<u>H</u>), 7.60 – 7.56 (m, 2H, Ar-<u>H</u>), 7.34 – 7.24 (m, 3H, Ar-<u>H</u>), 5.32 (s, 2H, C<u>H</u>$_2$-Ar), 4.04 (t, *J* = 6.3 Hz, 2H, C<u>H</u>$_2$-CH$_2$-CH$_3$), 2.19-2.09 (m, 9H, adamantyl), 1.90-1.77 (m, 6H, adamantyl), 1.69 (h, *J* = 6.5 Hz, 2H, CH$_2$-C<u>H</u>$_2$-CH$_3$), 0.94 (t, *J* = 7.4 Hz, 3H, C<u>H</u>$_3$).

^{13}C NMR ($CDCl_3$) δ 162.8 (C), 155.5 (C=O), 151.3 (C=O), 148.9 (C), 136.9 (C-Ar), 129.3 (<u>C</u>H-Ar), 128.5 (<u>C</u>H-Ar), 127.8 (<u>C</u>H-Ar), 106.7 (C), 46.9 (<u>C</u>H$_2$), 43.3 (<u>C</u>H$_2$), 41.0 (<u>C</u>H$_2$ adamantane), 36.6 (<u>C</u>H$_2$ adamantane), 35.9 (<u>C</u> adamantane), 28.3 (<u>C</u>H$_2$ adamantane) , 21.4 (<u>C</u>H$_2$), 11.4 (<u>C</u>H$_3$).

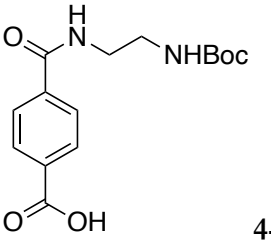


Methyl 4-((2-((tert-butoxycarbonyl)amino)ethyl)carbamoyl)benzoate (**4.37**). 4-(Methoxycarbonyl) benzoic acid **4.36** (0.200 g, 1.11 mmol, 1.0 eq.) was dissolved in DMF (2 mL). To the resulting solution was added DIPEA (0.21 mL, 1.22 mmol, 1.10 equiv.), COMU (0.523 g, 1.22 mmol, 1.10 equiv.) and *tert*-butyl (2-aminoethyl) carbamate (0.19 mL, 1.22 mmol, 1.10 equiv.). The reaction was stirred at rt for 20 min. Upon completion of reaction checked by LC-MS and TLC, cold water (7 mL) was added and a pale pink precipitate developed which was collected by suction filtration and washed with cold water. The title compound was obtained after air drying (0.270 g, 75 %).

LC/MS *m/z* calcd for $C_{16}H_{22}N_2O_5$ $[MH]^+$: 223.15, found 223.10 (-Boc); t_R = 2.69 min (Method B).

^{1}H NMR ($CDCl_3$)) δ 8.08 (d, *J* = 8.0 Hz, 2H, Ar-H), 7.89 (d, *J* = 7.3 Hz, 2H, Ar-H), 7.43 (br s, 1H, NH), 5.00 (br s, 1H, NH), 3.94 (s, 3H, -CH_3), 3.56 (dt, *J* = 6.5, 4.8 Hz, 2H, CH_2), 3.45 – 3.39 (m, 2H, CH_2), 1.43 (s, 9H, Boc).

^{13}C NMR ($CDCl_3$) δ 166.9 (NHC=O), 166.5 (NHC=O), 155.6 (NHC=O), 138.2 (C), 132.8 (C), 129.9 (CH-Ar), 127.2 (CH-Ar), 80.4 (C), 52.5 (CH_2), 28.5 (Boc).



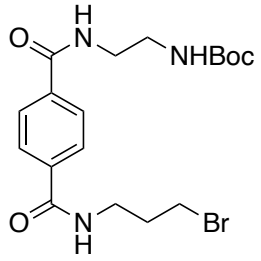
4-((2-((*tert*-Butoxycarbonyl)amino)ethyl)carbamoyl)benzoic acid (**4.38**). Methyl 4-((2-((*tert*-butoxycarbonyl)amino)ethyl)carbamoyl)benzoate (**4.37**) (0.260 g,

0.81 mmol, 1.0 equiv.) was dissolved in THF (10 mL). To the resulting mixture was added 1M NaOH (8 mL) and the solution was stirred at rt for 3 h. Upon completion of the reaction checked by TLC and LCMS, the organic layer was removed under reduced pressure. Dropwise addition of conc. HCl gave the title compound as white solid, which was obtained after suction filtration and vacuum drying (0.223, 90%).

LC/MS ***m/z*** calcd for $C_{15}H_{21}N_2O_5$ $[MH]^+$: 209.14, found 209.10 (-Boc); calcd for $C_{15}H_{21}N_2O_5Na$ $[MH]^+$ 331.14, found 331.10; t_R = 3.18 min. (Method B).

^{1}H NMR (CD_3OD) δ 8.08 (d, 2H, Ar-H), 7.89 (d, *J* = 8.3 Hz, 2H, Ar-H), 3.46 (t, *J* = 5.6 Hz, 2H, CH_2), 3.28 (t, *J* = 6.1 Hz, 2H, CH_2), 1.41 (s, 9H, Boc).

^{13}C NMR (CD_3OD) δ 169.0 (NHC=O), 158.8 (NHC=O), 139.6 (C-Ar), 134.8 (C-Ar), 130.8 (CH-Ar), 128.4 (CH-Ar), 80.2 (C), 41.5 (CH_2), 40.8 (CH_2), 28.7 (Boc).

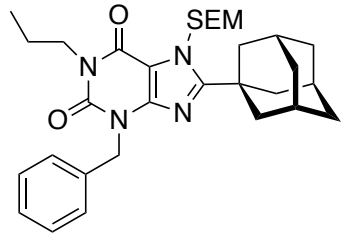


***tert*-Butyl (2-(4-((3-bromopropyl)carbamoyl)benzamido)ethyl)carbamate** (**4.39**). To a solution of 4-((2-((*tert*-Butoxycarbonyl) amino)ethyl)carbamoyl)benzoic acid **4.38** (0.100 g, 0.32 mmol, 1.0 equiv.) in DMF (2 mL) was added COMU (0.153 g, 0.36 mmol, 1.10 equiv.) and 3-bromopropyl amine hydrobromide (0.092 g, 0.42 mmol, 1.30 eq.). DIPEA (0.112 mL, 0.65 mmol, 2.0 equiv.) was subsequently added to the reaction mixture dropwise. The resulting mixture was stirred at rt for 15 min. Completion of the reaction was checked by TLC (R_f 0.35 in DCM/MeOH 95:5) and LCMS. The resulting mixture was diluted with water and extracted with EtOAc. The organic layer was subsequently washed with 1M HCl (10 mL), dried over $MgSO_4$, filtered and concentrated

to dryness to afford the crude product as orange oil. Purification by flash column chromatography on a gradient of 97:3 to 94:6 % DCM/MeOH afforded the title product as off-white solid (0.085 g, 61%).

^{1}H NMR (DMSO-d_6) δ 8.70 (t, J = 5.6 Hz, 1H, -NH), 8.55 (t, J = 5.3 Hz, 1H, -NH), 7.83 (s, 4H, Ar-H), 3.51 (t, J = 6.6 Hz, 2H, -CH_2-Br), 3.40 – 3.33 (m, 2H, , CH_2), 3.31-3.26 (m, 2H, , CH_2), 3.10 (t, J = 6.1 Hz, 2H, , CH_2), 2.05 (p, J = 6.7 Hz, 2H, , CH_2), 1.31 (s, 9H, Boc).

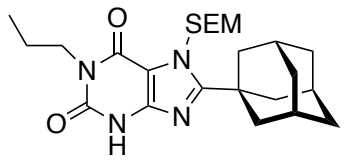
^{13}C NMR (DMSO-d_6) δ 167.6 (NHC=O), 155.1 (NHC=O), 129.9 (CH-Ar), 128.2 (CH-Ar), 36.8 (CH_2), 36.0 (CH_2), 34.3 (CH_2), 33.1 (2xCH_2), 28.8 (Boc) (two quaternary carbon not observed)



8-((1R,3R,5S)-Adamantan-1-yl)-3-benzyl-1-propyl-7-((2-(trimethylsilyl)ethoxy)methyl)-3,7-dihydro-1H-purine-2,6-dione (**4.34**). Potassium carbonate was added to a solution of xanthine **4.33** (0.232 g, 0.55 mmol, 1.0 equiv.) in DMF (3 mL) and the resulting mixture was stirred at rt for 2 h. (2-(Chloromethoxy)ethyl)trimethylsilane (0.110 g, 0.67 mmol, 1.20 equiv.) was the added dropwise and the solution was stirred at rt for additional 2 h. TLC showed complete consumption of the starting material. The reaction was then evaporated to dryness and the residue was adsorbed on isolute. Purification by flash column chromatography using a gradient of 100:0 to 80:20 PE/EtOAc gave the title compound as colourless oil which solidified upon cooling (0.200 g, 66%)

^{1}H NMR ($CDCl_3$) δ 7.61 – 7.56 (m, 2H, Ar-H), 7.34 – 7.24 (m, 3H, Ar-H), 5.91 (s, 2H, N-CH_2-O), 5.26 (s, 2H, CH_2-Ar), 3.94 (t, J = 6.9Hz, 2H, CH_2), 3.70 (t, J = 6.9 Hz, 2H, CH_2), 2.23 – 2.17 (m, 6H, adamantyl), 2.15 – 2.09 (m, 3H, adamantyl), 1.85 – 1.78 (m, 6H, adamantyl), 1.64 (h, J = 7.2 Hz, 2H, CH_2), 0.96 – 0.90 (m, 5H, CH_2(SEM) and CH_3), -0.02 (s, 9H, TMS).

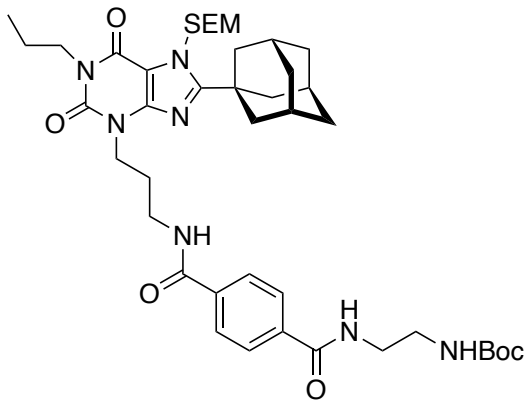
^{13}C NMR ($CDCl_3$) δ 161.6 (C), 155.3 (C=O), 151.3 (C=O), 147.0 (C), 137.0 (C-Ar), 129.5 (CH-Ar), 128.5 (CH-Ar), 127.9 (CH-Ar), 107.6 (C), 73.6 (CH_2), 66.5 (CH_2), 46.5 (CH_2), 43.1(CH_2), 40.9 (C adamantane), 37.9 (CH_2 adamantane), 36.6 (CH_2 adamantane), 28.5 (CH_2 adamantane), 21.5 (CH_2), 18.2 (CH_2), 11.5(CH_3), -1.3 (TMS).



8-((1R,3R,5S)-Adamantan-1-yl)-1-propyl-7-((2-(trimethylsilyl)ethoxy)methyl)-3,7-dihydro-1H-purine-2,6-dione (**4.35**).[360] Xanthine **4.34** (0.188 g, 0.34 mmol, 1.0 equiv.) was dissolved in methanol and to the solution was added 10% Pd/C (100 mg), followed by ammonium formate (3.53 mmol, 15 equiv.). The flask was equipped with a condenser with a balloon with N_2 at the top and heated to 140 °C for 9 h. The completion of the reaction was monitored by TLC. The reaction mixture was then cooled to rt and filtered through Celite™. The pad was washed with MeOH and DCM. The colourless solution was concentrated to dryness to give the title compound as off-white solid (0.105 g, 67%).

^{1}H NMR ($CDCl_3$) δ 5.93 (s, 2H, N-CH_2-O), 3.95 (t, J = 7.2, 5.4 Hz, 2H, CH_2), 3.71 (t, J = 7.2 Hz, 2H, CH_2), 2.19 (s, 6H, adamantyl), 2.09 (s, 3H, adamantyl), 1.78 (s, 6H, adamantyl), 1.66 (h, J = 7.6 Hz, 2H, CH_2), 0.98 – 0.89 (m, 5H, CH_2(SEM) and CH_3), -0.02 (s, 9H, TMS).

^{13}C NMR ($CDCl_3$) δ 162.1 (C), 155.9 (C=O), 107.7 (C), 73.6 (CH_2), 66.5 (CH_2), 42.5 (CH_2), 40.8 (CH_2), 37.9 (CH_2 adamantane), 36.5 (CH_2 adamantane), 28.4 (CH_2 adamantane), 21.5 (CH_2), 18.2 (CH_2), 11.5 (CH_3), -1.3 (TMS) (two quaternary carbon not observed)

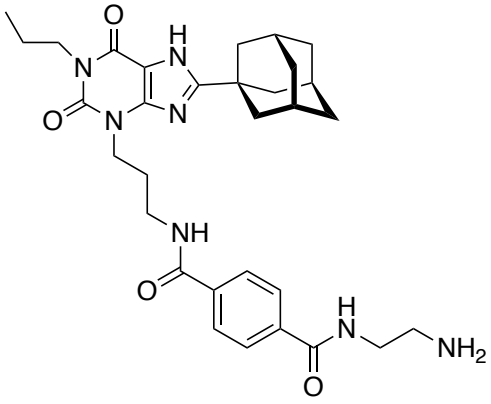


***tert*-Butyl (2-(4-((3-(8-((3R,5R,7R)-adamantan-1-yl)-2,6-dioxo-1-propyl-7-((2-(trimethylsilyl)ethoxy)methyl)-1,2,6,7-tetrahydro-3H-purin-3-yl)propyl)carbamoyl)benzamido)ethyl)carbamate** (**4.40**). To a solution of xanthine **4.35** (105 mg, 1.0 equiv.) in DMF (2 mL) was added K_2CO_3 (42 mg, 1.3 equiv.). The resulting mixture was stirred at rt for 1 h. After that time, a solution of *tert*-butyl (2-(4-((3-bromopropyl)carbamoyl)benzamido)ethyl)carbamate (**4.39**) (113 mg, 1.15 equiv.) in DMF (1 mL) was added to the reaction mixture, which was stirred at 40 °C for 23h. The reaction was subsequently filtered and concentrated to dryness. The crude material was adsorbed on isolute and purified by flash column chromatography using a gradient of 50:50 to 20:80 PE/EtOAc to give the title compound as off-white foam (90 mg, 49 %).

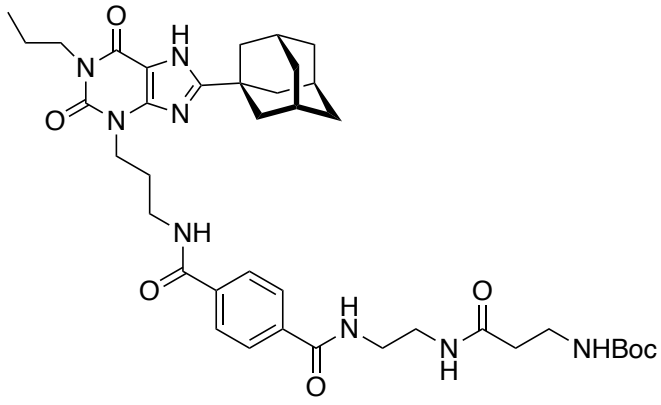
^{1}H NMR ($CDCl_3$) δ 7.90 (s, 4H, Ar-H), 7.78 (t, *J* = 6.1 Hz, 1H, -NH), 7.47 (s, 1H, -NH), 5.92 (s, 2H, , N-CH_2-O), 5.14 (br s, 1H, NH), 4.26 (t, *J* = 5.6 Hz, 2H, -CH_2-N3), 3.98 (t, *J* = 7.3 Hz, 2H, CH_2-N1), 3.71 (t, *J* = 8.0 Hz, 2H, -O-CH_2), 3.56 (q, *J* = 4.8 Hz, 2H, , CH_2-NHCO), 3.45 – 3.37 (m, 4H, -CH_2), 2.13 – 2.08 (m, 6H), 2.08 – 1.97 (m, 5H, adamantane + CH_2), 1.76 – 1.60 (m, 8H, adamantane + CH_2), 1.42 (s, 9H, Boc), 0.93 (m, 5H, CH_3 and CH_2), -0.03 (s, 9H, TMS).

^{13}C NMR ($CDCl_3$) δ 167.0 (NHC=O), 166.9 (NHC=O), 161.9 (C), 155.1 (C=O), 151.8 (C=O), 147.0 (C), 137.7 (C), 136.7 (C), 127.4 (CH-Ar), 127.4 (CH-Ar), 107.7 (C), 80.2 (C), 73.7 (OCH_2N), 66.6 (OCH_2), 43.1 (CH_2), 40.9 (CH_2 adamantane), 40.4 (CH_2), 37.9 (2xCH_2), 36.4 (CH_2 adamantane), 35.9

(CH_2), 28.5 (Boc), 28.3 (CH_2 adamantane), 28.2 (CH_2), 21.5 (CH_2), 18.2 (CH_2), 11.5 (CH_3), -1.3 (TMS).



N*^{1}-(3-(8-((3*R*,5*R*,7*R*)-Adamantan-1-yl)-2,6-dioxo-1-propyl-1,2,6,7-tetrahydro-3*H*-purin-3-yl)propyl)-*N*^{4}-(2-aminoethyl)terephthalamide** (**4.41**)**.** The synthesis of the title compound **4.41** was achieved following general procedure C. The title compound **4.41** was used for the subsequent step without any further purification (29 mg, quantitative). **LC-MS *m/z calcd for $C_{31}H_{42}N_7O_4$ $[MH]^+$: 576.20, found 576.40; t_R = 3.16 min (Method B).



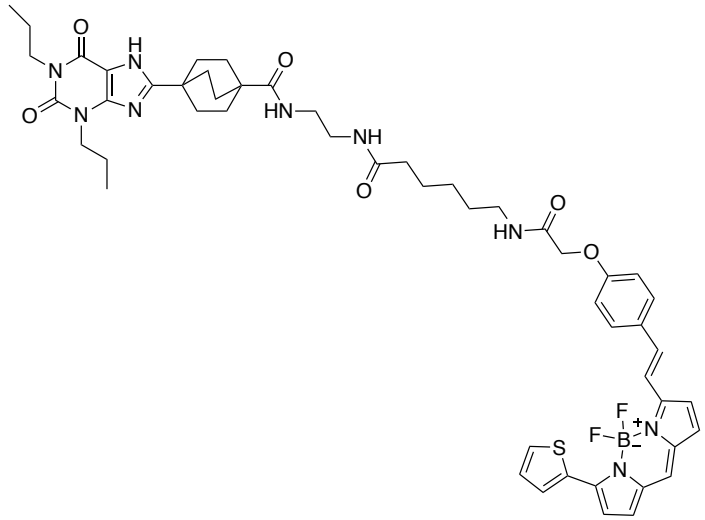
***tert*-Butyl (3-((2-(4-((3-(8-((3R,5R,7R)-adamantan-1-yl)-2,6-dioxo-1-propyl-1,2,6,7-tetrahydro-3H-purin-3-yl)propyl)carbamoyl)benzamido)ethyl)amino)-3-oxopropyl)carbamate** (**4.42**). The title compound **4.42** was synthesized following general procedure A, reacting a solution of Boc-β-Ala-OH (10 mg, 1.0 equiv.), DIPEA (18 μL, 2.0 equiv.) and COMU (24.90 mg, 1.10 equiv.) in DMF (0.5 mL) with a solution of N1-(3-(8-((1*R*,3*R*,5*S*)-adamantan-1-yl)-2,6-dioxo-1-propyl-1,2,6,7-tetrahydro-3*H*-purin-3-yl)propyl)-*N*-4-(2-

aminoethyl)terephthalamide (**4.41**) (34 mg, 1.10 equiv.) in DMF (0.5 mL). Purification by flash column chromatography using a gradient of 96:4 to 93:7 DCM/MeOH gave the title compound as an off-white solid (18 mg, 47%).

LC/MS ***m/z*** calcd for $C_{39}H_{55}N_8O_7$ $[MH]^+$: 747.40, found 747.40; t_R = 3.71 min (Method B).

^{1}H NMR (CD_3OD) δ 7.93 (s, 4H, Ar-H), 4.59 (s, 1H, NH), 4.26 (t, *J* = 6.6 Hz, 2H, CH_2), 3.95 (t, *J* = 6.3 Hz, 2H, CH_2), 3.52 (t, *J* = 5.8 Hz, 2H, CH_2), 3.48-3.39 (m, 4H, -NH(CH_2)$_2$NH), 3.36 (s, 2H, CH_2), 2.37 (t, *J* = 6.7 Hz, 2H, CH_2), 2.10 (q, *J* = 6.5 Hz, 2H, COCH_2), 2.02-1.96 (m, 9H, adamantane), 1.81 – 1.70 (m, 6H, adamantane), 1.69 – 1.62 (m, 2H, CH_2CH_3), 1.42 (s, 9H, Boc), 0.94 (t, *J* = 7.5 Hz, 3H, CH_3).

^{13}C NMR (CD_3OD) δ 187.4 (NHC=O), 181.9, 169.3 (NHC=O), 169.2 (NHC=O), 163.6 (C), 156.0 (C=O), 152.9 (C=O), 149.5 (C), 138.7 (C-Ar), 138.2 (C-Ar), 128.6 (CH-Ar), 128.5 (CH-Ar), 107.9 (C), 80.2 (C), 43.9(CH_2), 42.2 (CH_2), 41.9 (CH_2), 40.9 (CH_2 adamantane), 40.1 (CH_2), 38.0 (CH_2), 37.6 (CH_2), 37.4 (CH_2 adamantane), 36.9 (CH_2), 29.5 (CH_2 adamantane), 28.9 (CH_2), 28.7 (Boc), 22.3 (CH_2), 11.6 (CH_3).



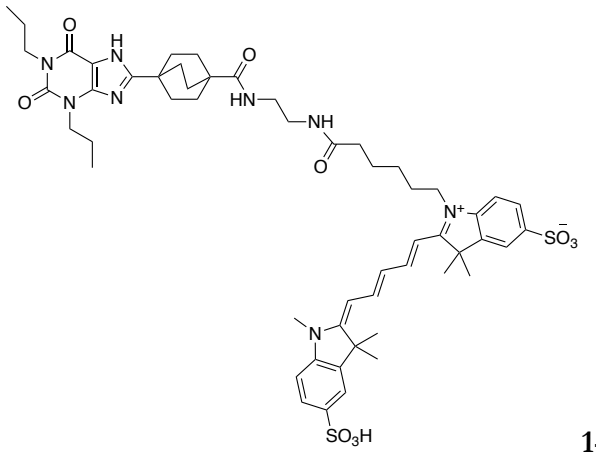
(*E*)-*N*-(2-(6-(2-(4-(2-(5,5-Difluoro-7-(thiophen-2-yl)-5*H*-4*l*^{4},5*l*^{4}-dipyrrolo[1,2-*c*:2',*1*'-*f*][1,3,2]diazaborinin-3-yl)vinyl)phenoxy)acetamido)hexanamido)ethyl)-4-(2,6-dioxo-1,3-

dipropyl-2,3,6,7-tetrahydro-1*H*-purin-8-yl)bicyclo[2.2.2]octane-1-carboxamide (**4.43a**). Following general procedure D, amine congener **4.18a** (0.5 mg, 1.10 equiv.) was converted to the BODIPY 630/650 conjugate. Purification by RP-HPLC (Method D) gave, after lyophilisation, the title compound as blue solid (0.4 mg, 39%)

LC/MS *m/z* calcd for $C_{51}H_{61}BF_2N_9O_6S$ $[MH]^+$: 976.30 found 976.30 t_R = 3.98 min (Method B).

HRMS (TOF ES^+) calcd for $C_{51}H_{61}BF_2N_9O_6S$ $[MH]^+$: 976.4530 found 976.4530; calcd for $C_{51}H_{61}BF_2N_9O_6SNa$ $[M+Na]^+$: 998.4349 found 998.4335.

Analytical RP-HPLC t_R = 6.86 min, purity > 99% (Method F).

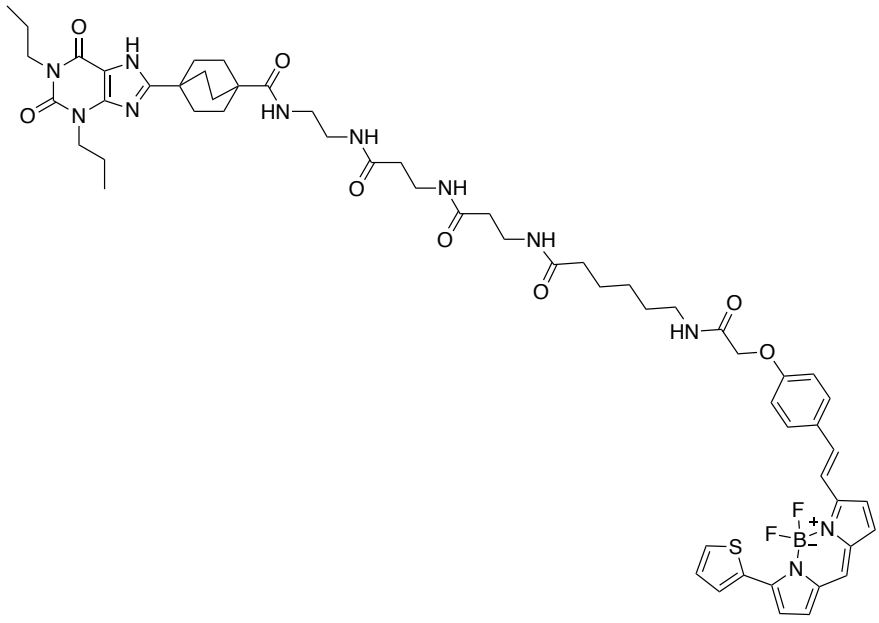


1-(6-((2-(4-(2,6-Dioxo-1,3-dipropyl-2,3,6,7-tetrahydro-1*H*-purin-8-yl)bicyclo[2.2.2]octane-1-carboxamido)ethyl)amino)-6-oxohexyl)-3,3-dimethyl-2-((1*E*,3*E*)-5-((*E*)-1,3,3-trimethyl-5-sulfoindolin-2-ylidene)penta-1,3-dien-1-yl)-3*H*-indol-1-ium-5-sulfonate (**4.43b**). Following general procedure D, amine congener **4.18a** (0.5 mg, 1.10 equiv.) was converted to the sulfo-Cyanine5 conjugate **4.43b**. Purification by RP-HPLC (Method D) gave after lyophilization the title compound as bright blue solid (0.5 mg, 56%).

LC/MS *m/z* calcd for $C_{54}H_{71}N_8O_{10}S_2$ $[MH]^+$: 1055.30 found 1055.30.; t_R = 3.09 min (Method B).

HRMS (TOF ES$^+$) calcd for $C_{54}H_{71}N_80_{10}S_2$ $[MH]^+$: 1055.4729 found 1055.4705; calcd for $C_{54}H_{71}N_80_{10}S_2Na$ $[M+Na]^+$: 1077.4549 found 1077.4527.

Analytical RP-HPLC t_R = 4.93 min, purity > 99% (Method F).



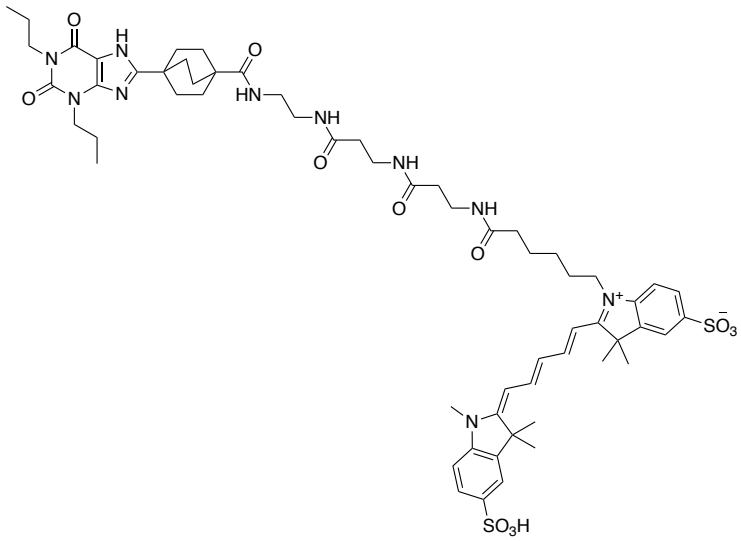
(*E*)-*N*-(20-(4-(2-(5,5-Difluoro-7-(thiophen-2-yl)-5*H*-4*l*^{4},5*l*^{4}-dipyrrolo[1,2-*c*:2',1'-*f*][1,3,2]diazaborinin-3-yl)vinyl)phenoxy)-4,8,12,19-tetraoxo-3,7,11,18-tetraazaicosyl)-4-(2,6-dioxo-1,3-dipropyl-2,3,6,9-tetrahydro-1*H*-purin-8-yl)bicyclo[2.2.2]octane-1-carboxamide (**4.44a**). Following general procedure C, compound **4.25a** (5 mg, 1.0 equiv.) was subjected to acidolysis and, after the removal of the solvent, the resulting intermediate (as HCl salt) was used for the next step without further purification (4 mg, quantitative). **LC-MS *m/z*** calcd for $C_{28}H_{45}N_8O_5$ $[MH]^+$: 573.34, found 573.30 t_R = 3.13 min. Following general procedure D, the resulting amine congener was converted to the BODIPY 630/650 conjugate. Purification by RP-HPLC (Method D) gave, after lyophilization, the title compound as blue solid (0.9 mg, 70%).

LC/MS *m/z* calcd for $C_{57}H_{71}BF_2N_{11}0_8S$ $[MH]^+$: 1118.30 found 1118.40 t_R = 3.78 min (Method B).

HRMS (TOF ES$^+$) calcd for $C_{57}H_{71}BF_2N_{11}0_8S$ $[MH]^+$: 1118.5273 found 1118.5252; calcd for $C_{57}H_{71}BF_2N_{11}0_8SNa$ $[M+Na]^+$: 1140.5092 found 1140.506.

Analytical RP-HPLC t_R = 6.73 min, purity > 99% (Method F)

.

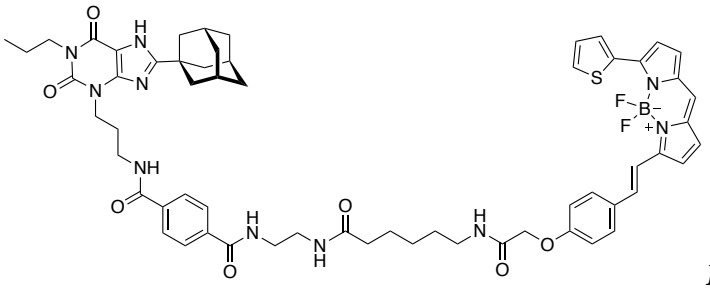


1-(1-(4-(2,6-Dioxo-1,3-dipropyl-2,3,6,7-tetrahydro-1*H*-purin-8-yl)bicyclo[2.2.2]octan-1-yl)-1,6,10,14-tetraoxo-2,5,9,13-tetraazanonadecan-19-yl)-3,3-dimethyl-2-((1*E*,3*E*)-5-((*E*)-1,3,3-trimethyl-5-sulfoindolin-2-ylidene)penta-1,3-dien-1-yl)-3*H*-indol-1-ium-5-sulfonate (**4.44b**). Following Boc-deprotection of **4.25a**, the resulting amine congener (0.5 mg, 1.10 equiv.) was converted to the sulfo-Cyanine5 conjugate **4.44b** following general procedure D. Purification by RP-HPLC (Method D) gave, after lyophilization, the title compound as bright blue solid (1.1 mg, quantitative).

LC/MS ***m/z*** calcd for $C_{60}H_{79}N_{10}0_{12}S_2$ $[MH]^-$: 1195.54 found 1195.60.; t_R = 3.05 min (Method B).

HRMS (TOF ES$^+$) calcd for $C_{60}H_{81}N_{10}0_{12}S_2$ $[MH]^+$: 1197.5471 found 1197.5450; calcd for $C_{60}H_{81}N_{10}0_{12}S_2Na$ $[M+Na]^+$: 1219.5291 found 1219.5255.

Analytical RP-HPLC t_R = 4.88 min, purity > 99% (Method F).

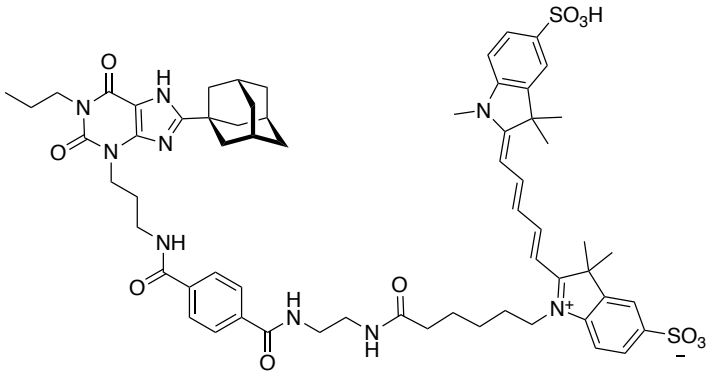


N^1-(3-(8-((3*R*,5*R*,7*R*)-Adamantan-1-yl)-2,6-dioxo-1-propyl-1,2,6,7-tetrahydro-3*H*-purin-3-yl)propyl)-N^4-(2-(6-(2-(4-((*E*)-2-(5,5-difluoro-7-(thiophen-2-yl)-5*H*-4λ^4,5λ^4-dipyrrolo[1,2-*c*:2',1'-*f*][1,3,2]diazaborinin-3-yl)vinyl)phenoxy)acetamido)hexanamido)ethyl)terephthalamide (**4.45a**). Following general procedure D, amine congener **4.41** (0.7 mg, 1.10 equiv.) was converted to the BODIPY 630/650 conjugate. Purification by RP-HPLC (Method D) gave after lyophilization the title compound as blue solid (0.7 mg, 59%).

LC/MS *m/z* calcd for $C_{60}H_{68}BF_2N_{10}O_7S$ $[MH]^+$: 1121.30 found 1121.30 t_R = 4.05 min (Method B).

HRMS (TOF ES^+) calcd for $C_{60}H_{68}BF_2N_{10}O_7S$ $[MH]^+$: 1121.5059 found 1121.5060; calcd for $C_{60}H_{68}BF_2N_{10}O_7SNa$ $[M+Na]^+$: 1143.4878 found 1143.4855.

Analytical RP-HPLC t_R = 7.00 min, purity > 99% (Method F).



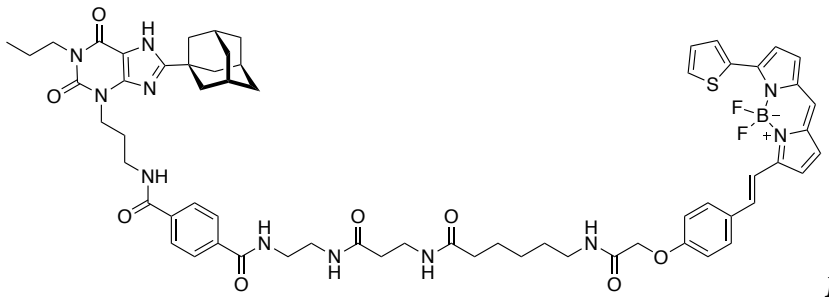
1-(6-((2-(4-((3-(8-((3*R*,5*R*,7*R*)-Adamantan-1-yl)-2,6-dioxo-1-propyl-1,2,6,7-tetrahydro-3*H*-purin-3-yl)propyl)carbamoyl)benzamido)ethyl)amino)-6-

oxohexyl)-3,3-dimethyl-2-((1*E*,3*E*)-5-((*E*)-1,3,3-trimethyl-5-sulfoindolin-2-ylidene)penta-1,3-dien-1-yl)-3*H*-indol-1-ium-5-sulfonate (**4.45b**). Following general procedure D, amine congener **4.41** (0.6 mg, 1.10 equiv.) was converted to the sulfo-Cyanine5 conjugate **4.45b**. Purification by RP-HPLC (Method D), followed by preparative TLC using 80:20 DCM/MeOH as eluent. After lyophilization, the title compound was obtained as bright blue solid (0.9 mg, 83%).

LC/MS *m/z* calcd for $C_{63}H_{78}N_9O_{11}S_2$ $[M-2]^+$: 600.76 found 600.8; t_R = 3.19 min (Method B).

HRMS (TOF ES^+) calcd for $C_{63}H_{78}N_9O_{11}S_2$ $[MH]^+$: 1200.5257 found 1200.5220; $[M-2]^+$:600.7665 found 600.7680.

Analytical RP-HPLC t_R = 5.19 min, purity > 99% (Method F).

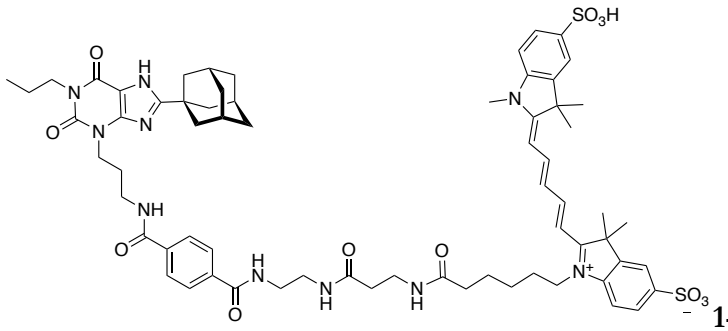


***N*1-(3-(8-((3*R*,5*R*,7*R*)-Adamantan-1-yl)-2,6-dioxo-1-propyl-1,2,6,7-tetrahydro-3*H*-purin-3-yl)propyl)-*N*4-(2-(3-(6-(2-(4-((*E*)-2-(5,5-difluoro-7-(thiophen-2-yl)-5*H*-4*l*4,5*l*4-dipyrrolo[1,2-*c*:2',1'-*f*][1,3,2]diazaborinin-3-yl)vinyl)phenoxy)acetamido)hexanamido)propanamido)ethyl)terephthalamide** (**4.46a**). Following general procedure C, compound **4.42** (5 mg, 1.0 equiv.) was converted to the corresponding HCl salt intermediate, which, after the removal of the solvent in vacuo, was used for the subsequent step without further purification. LC/MS *m/z* calcd for $C_{34}H_{47}N_8O_8$ $[MH]^+$: 647.34, found 647.40 t_R = 3.18 min. Following general procedure D, the resulting amine congener (0.7 mg, 1.10 equiv.) was converted to the BODIPY 630/650 conjugate. Purification by RP-HPLC (Method D) gave the title compound as blue solid (0.7 mg, 56%).

LC-MS *m/z* calcd for $C_{63}H_{73}BF_2N_{11}0_8S$ $[MH]^+$: 1192.40 found 1192.40 t_R = 3.95 min (Method B).

HRMS (TOF ES^+) calcd for $C_{63}H_{73}BF_2N_{11}0_8S$ $[MH]^+$: 1192.5430 found 1192.5433; calcd for $C_{63}H_{73}BF_2N_{11}0_8SNa$ $[M+Na]^+$: 1214.5250 found 1214.5229.

Analytical RP-HPLC t_R = 6.98 min, purity > 97% (Method F).



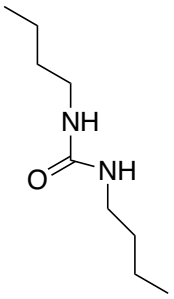
1-(6-((3-((2-(4-((3-(8-((3*R*,5*R*,7*R*)-Adamantan-1-yl)-2,6-dioxo-1-propyl-1,2,6,7-tetrahydro-3*H*-purin-3-yl)propyl)carbamoyl)benzamido)ethyl)amino)-3-oxopropyl)amino)-6-oxohexyl)-3,3-dimethyl-2-((1*E*,3*E*)-5-((*E*)-1,3,3-trimethyl-5-sulfoindolin-2-ylidene)penta-1,3-dien-1-yl)-3*H*-indol-1-ium-5-sulfonate (**4.46b**). Following general procedure D, amine congener (0.6 mg, 1.10 equiv.) was converted to the sulfo-Cyanine5 conjugate **4.46b**. Purification by RP-HPLC (Method B), followed by preparative TLC using 80:20 DCM/MeOH. After lyophilization, the title compound was isolated as bright blue solid (0.9 mg, 79%).

LC-MS *m/z* calcd for $C_{66}H_{83}N_{10}0_{12}S_2$ $[M-2]^+$: 636.3 found 636.3; t_R = 3.17 min (Method B).

HRMS (TOF ES^+) calcd for $C_{66}H_{83}N_{10}0_{12}S_2$ $[MH]^+$: 1271.5628 found 1271.5571; calcd for $C_{66}H_{83}N_{10}0_{12}S_2Na$ $[M+Na]^+$: 1293.5447 found 1293.5364; $[M-2]^+$:636.2850 found 636.2861.

Analytical RP-HPLC t_R = 5.25 min, purity > 99% (Method F).

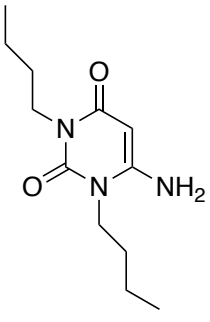
7.1.5 Methods Chapter 5



1,3-Dibutylurea (**5.13**) Butylamine (7.68 mL, 78 mmol, 1.10 equiv.) was dissolved in anhydrous THF (20 mL) and the solution was cooled to 0 °C. Butyl isocyanate (7.95 mL, 71 mmol 1.0 equiv.) was added dropwise and the reaction was stirred at rt. The resulting mixture was stirred at rt for 4h. Evaporation of the solvent in vacuo yielded the title product as off-white solid (12 g, quantitative).

^{1}H NMR (DMSO-d_6) δ 5.72 (t, J = 5.7 Hz, 2H, -NH), 2.95 (td, J = 6.8, 5.6 Hz, 4H, -C$\underline{H}_2$-NH), 1.37 – 1.19 (m, 8H, -C$\underline{H}_2$-), 0.85 (t, J = 7.2 Hz, 6H, -C$\underline{H}_3$).

^{13}C NMR (DMSO-d_6) δ 158.1 (C=O), 38.9(C$\underline{H}_2$-NH), 32.2(C$\underline{H}_2$), 19.5(C$\underline{H}_2$), 13.7 (C$\underline{H}_3$).



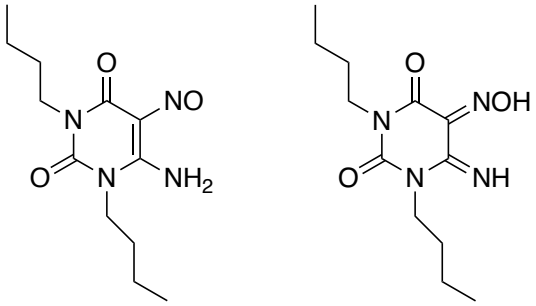
6-Amino-1,3-dibutylpyrimidine-2,4(1*H*,3*H*)-dione (**5.14**). 1,3-Dibutylurea (6 g, 35 mmol, 1 equiv) was reacted with cyanoacetic acid (3.26 g, 38 mmol, 1.10 equiv) in Ac_2O (20 mL). The resulting mixture was heated to 85 °C for 2 h. Afterwards, the solution was concentrated to dryness (water bath set to 80 °C) until brown syrup appeared. 3x4 mL of H_2O were added to remove excess of Ac_2O. 10 mL of H_2O were

added and the residue was basified with 70% NaOH (4 drops) to obtain a precipitate which was filtered off. The filtrate was collected and conentrated to dryness. The resulting residue was recrystallised from hot EtOH/H_2O to obtain fine pale yellow crystals (5.332 g, 64%)

LC-MS *m/z* calcd for $C_{12}H_{22}N_3O_2$ $[MH]^+$: 240.17, found 240.7 t_R = 2.65 min (Method A)

^{1}H NMR (DMSO-d_6) δ 6.75 (s, 2H, -N<u>H</u>$_2$), 4.64 (s, 1H, -C<u>H</u>, xanthine), 3.76 (t, J = 7.2 Hz, 2H, -C<u>H</u>$_2$-NH), 3.69 (t, J = 7.2 Hz, 2H, -C<u>H</u>$_2$-NH), 1.52 – 1.38 (m, 4H, -C<u>H</u>$_2$-), 1.25 (m, J = 20.6, 7.4 Hz, 4H, -C<u>H</u>$_2$-), 0.87 (q, J = 7.4 Hz, 6H, -C<u>H</u>$_3$).

^{13}C NMR (DMSO-d_6) δ 161. (C=O), 154.2 (C=O), 151.2 (<u>C</u>-NH$_2$), 75.1 (<u>C</u>H), 41.5 (<u>C</u>H$_2$), 29.7 (<u>C</u>H$_2$), 29.7 (<u>C</u>H$_2$), 19.6 (<u>C</u>H$_2$), 19.3 (<u>C</u>H$_2$), 13.7 (<u>C</u>H$_3$), 13.7 (<u>C</u>H$_3$).

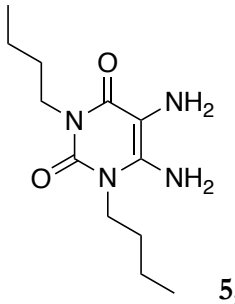


6-Amino-1,3-dibutyl-5-nitrosopyrimidine-2,4(1*H*,3*H*)-dione (**5.15**). 1,3-Dibuyl-6-amino uracil (3.577 g, 15 mmol, 1.0 equiv.) was dissolved in 50% acetic acid (50 mL) and the resulting solution was heated to 57 °C. To the mixture was added $NaNO_2$ (1.238 g, 18 mmol, 1.20 eq.) over 15 min. The solution from colourless turned pink and a pink precipitate formed. The reaction mixture was stirred at rt for 1h. The precipitate was collected, washed with cold water and dried to get the pure product as pink solid (1.625 g, 41%)

LC-MS *m/z* calcd for $C_{12}H_{21}N_4O_3$ $[MH]^+$: 269.16, found 269.10 t_R = 2.71 min (Method A)

^{1}H NMR (DMSO-d_6) δ 13.17 (s, 1H, =NOH), 9.10 (s, 1H, =NH), 3.89 (t, J = 7.3 Hz, 2H, -CH$_2$-NH), 3.81 (t, J = 7.7 Hz, 2H, -CH$_2$-NH), 1.61 – 1.52 (m, 2H, -CH$_2$-), 1.51 – 1.43 (m, 2H, -CH$_2$-), 1.38 – 1.26 (m, 4H, -CH$_2$-), 0.90 (dt, J = 11.4, 7.3 Hz, 6H, -CH$_3$).

^{13}C NMR (DMSO-d_6) δ 159.9 (C=O), 149.0 (C=O), 145.4(C=NH), 138.9(C=NOH), 41.0 (CH$_2$), 40.6 (CH$_2$), 29.5 (CH$_2$), 28.4 (CH$_2$), 19.6 (CH$_2$), 19.2 (CH$_2$), 13.7(CH$_3$), 13.6 (CH$_3$).

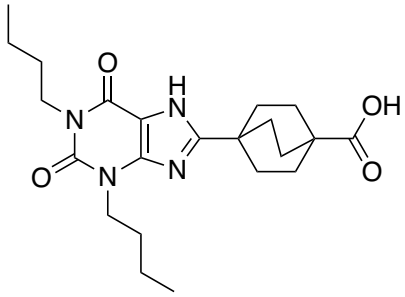


5,6-Diamino-1,3-dibutylpyrimidine-2,4(1*H*,3*H*)-dione (5.16). To a stirring solution of 6-amino-5-nitroso-1,3-diibutylpyrimidine-2,4(1*H*, 3*H*)-dione (0.700 g, 2.61 mmol, 1 equiv) in 12.5 % aqueous ammonium hydroxide solution (25 mL) at 60 °C was added sodium dithionite (3 equiv.) until a colourless solution had formed (30 min). After cooling to rt, the product was extracted with DCM (4x 20 mL). The combined organics were dried over anhydrous Na_2SO_4, filtered and evaporated to dryness to give the title product as pale yellow solid/wax (0.529 g, 80%)

LC-MS *m/z* calcd for $C_{12}H_{23}N_4O_2$ $[MH]^+$: 255.18, found 255.20 t_R = 2.20 min (Method A)

^{1}H NMR ($CDCl_3$) δ 5.16 (s, 2H, -NH$_2$), 3.91 (t, J = 7.4, 2H, -CH$_2$-NH), 3.87 (t, J = 8.4, 6.8 Hz, 2H, -CH$_2$-NH), 3.17 (s, 2H, -NH$_2$), 1.65 (p, J = 7.3, 2H), 1.58 (p, J = 7.3 Hz, 2H, -CH$_2$-), 1.41 (h, J = 7.1 Hz, 2H, -CH$_2$-), 1.35 (h, J = 7.1 Hz, 2H, -CH$_2$-), 0.94 (dt, J = 15.6, 7.3 Hz, 6H, -CH$_3$).

^{13}C NMR ($CDCl_3$) δ 161.5(<u>C</u>-NH_2), 150.4(<u>C</u>=O), 148.6(<u>C</u>=O), 94.7(<u>C</u>-NH_2), 43.2 (<u>C</u>H_2), 41.6 (<u>C</u>H_2), 30.5 (<u>C</u>H_2), 30.2 (<u>C</u>H_2), 20.4 (<u>C</u>H_2), 20.2 (<u>C</u>H_2), 14.0 (<u>C</u>H_3), 13.8 (<u>C</u>H_3).



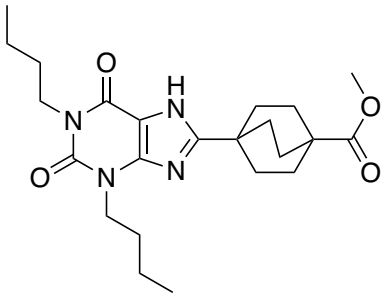
4-(1,3-Dibutyl-2,6-dioxo-2,3,6,7-tetrahydro-1*H*-purin-8-yl)bicyclo[2.2.2]octane-1-carboxylic acid (**5.17**)**.** To a solution of 5,6-Diamino-1,3-diisobutylpyrimidine-2,4(1*H*,3*H*)-dione (0.297 g, 1.10 mmol, 1.10 equiv.) (**5.16**) in DMF (5 mL) was added a solution of 4-(methoxycarbonyl) bicyclo [2.2.2] octane-1-carboxylic acid (0.225 g, 1.06 mmol, 1.0 equiv.), DIPEA (0.37 mL, 2 equiv.) and COMU (0.499 g, 1.10 mmol, 1.10 equiv.). The resulting mixture was stirred at rt for 15 min. The mixture was diluted with cold H_2O and extracted with EtOAc. The organic layer was separated and washed with 10 % citric acid. The organics were collected washed with sat. $NaHCO_3$, brine, dried over $MgSO_4$, filtered and concentrated in vacuo to give methyl 4-((6-amino-2,4-dioxo-1,3-dibutyl-1,2,3,4-tetrahydropyrimidin-5-yl)carbamoyl)bicyclo[2.2.2]octane-1-carboxylate intermediate, which was used for the next step without any further purification . The residue was dissolved in a mixture of propan-2-ol and 1 M KOH (2.5 mL, 4 equiv.) and heated to reflux (91°C) for 2 h. The reaction mixture was then cooled to rt and the solvent concentrated to dryness. The yellow residue was taken up in 4 mL of water and extracted with DCM. The aqueous layer was collected and acidified with conc HCl (until pH = 3-4) and a white precipitate formed which was collected by suction filtration and oven dried. (0.300 g, 68% over two steps)

LC-MS *m/z* calcd for $C_{22}H_{33}N_4O_4$ $[MH]^+$: 417.10, found 417.10 t_R = 3.08 min (Method A)

^{1}H NMR (DMSO-d_6) δ 12.73 (br s, 1H, -O<u>H</u>), 3.95 (t, *J* = 7.1 Hz, 2H, -C<u>H</u>$_2$-NH), 3.85 (t, *J* = 6.9 Hz, 2H, -C<u>H</u>$_2$-NH), 1.91 – 1.83 (m, 6H, bicycle), 1.79 –

1.72 (m, 6H, bicycle), 1.62 (p, *J* = 6.9 Hz, 2H, -C<u>H</u>$_2$-), 1.49 (p, *J* = 6.9 Hz, 2H, -C<u>H</u>$_2$-), 1.27 (h, *J* = 7.4 Hz, 4H, -C<u>H</u>$_2$-), 0.89 (dt, *J* = 7.3, 4.8 Hz, 6H, -C<u>H</u>$_3$).

^{13}C NMR (DMSO) δ 178.5 (HO<u>C</u>=O), 160.3 (<u>C</u>), 153.9 (C=O), 150.6 (C=O), 147.3 (C), 106.6 (<u>C</u>), 42.3 (<u>C</u>), 37.8 (<u>C</u>H$_2$), 33.2 (<u>C</u>H$_2$), 29.7 (<u>C</u>H$_2$), 29.6 (<u>C</u>H$_2$), 29.5 (<u>C</u>H$_2$), 27.7 (<u>C</u>H$_2$), 19.6 (<u>C</u>H$_2$), 19.3 (<u>C</u>H$_2$), 13.7 (<u>C</u>H$_3$), 13.6 (<u>C</u>H$_3$).

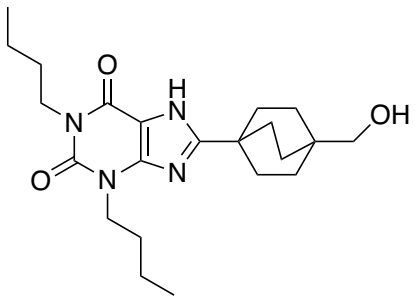


Methyl 4-(1,3-dibutyl-2,6-dioxo-2,3,6,7-tetrahydro-1*H*-purin-8-yl)bicyclo[2.2.2]octane-1-carboxylate (5.18). 4-(2,6-Dioxo-1,3-dibutyl-2,3,6,9-tetrahydro-1*H*-purin-8-yl) bicyclo[2.2.2]octane-1-carboxylic acid (**5.17**) (0.128 g, 0.31 mmol, 1 equiv) was diluted with 7 mL of MeOH and 3 drops of conc. H_2SO_4. The resulting mixture was refluxed until complete consumption of starting material. Once the reaction was completed, the resulting solution was neutralised with sat. $NaHCO_3$ (a couple of drops). The mixture was then concentrated to dryness and the residue was taken up in EtOAc and washed with sat. $NaHCO_3$ and brine. The resulting organic layer was dried over $MgSO_4$, filtered and concentrated to dryness to give the title compound as off-white solid (0.132 g, quantitative).

LC-MS *m/z* calcd for $C_{23}H_{35}N_4O_4$ $[MH]^+$: 431.27, found 431.30 t_R = 3.26 min (Method A)

^{1}H NMR ($CDCl_3$) δ 12.08 (s, 1H, -N<u>H</u>), 4.13 (t, *J* = 7.3 Hz, 2H, -C<u>H</u>$_2$-NH), 4.06 (t, *J* = 6.4 Hz, 2H, -C<u>H</u>$_2$-NH), 3.68 (s, 3H, OC<u>H</u>$_3$), 2.10-2.01 (m, 6H, bicycle), 1.97 – 1.89 (m, 6H, bicycle), 1.75 (p, *J* = 7.5 Hz, 2H, -C<u>H</u>$_2$-), 1.66 (p, *J* = 7.8 Hz, 2H, -C<u>H</u>$_2$-), 1.39 (hd, *J* = 7.3, 4.3 Hz, 4H), 0.96 (dt, *J* = 7.3, 4.8 Hz, 6H,-C<u>H</u>$_3$).

^{13}C NMR ($CDCl_3$) δ 177.9 ($CH_3O\underline{C}$=O), 161.3 (<u>C</u>), 155.6 (<u>C</u>=O), 151.2 (<u>C</u>=O), 149.0 (<u>C</u>), 107.1 (<u>C</u>), 52.0 (O<u>C</u>H_3), 43.6(<u>C</u>H_2), 41.7 (<u>C</u>H_2), 39.0 (<u>C</u>), 33.9 (<u>C</u>), 30.4 (<u>C</u>H_2), 30.2 (<u>C</u>H_2), 30.0 (<u>C</u>H_2), 28.2 (<u>C</u>H_2), 20.5 (<u>C</u>H_2), 20.1(<u>C</u>H_2), 14.0 (<u>C</u>H_3), 13.9 (<u>C</u>H_3).



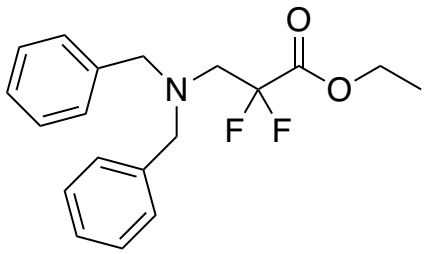
1,3-Dibutyl-8-(4-(hydroxymethyl)bicyclo[2.2.2]octan-1-yl)-3,7-dihydro-1*H*-purine-2,6-dione (5.19). Methyl 4-(2,6-dioxo-1,3-dibutyl-2,3,6,9-tetrahydro-1*H*-purin-8-yl) bicyclo[2.2.2]octane-1-carboxylate (**5.18**) (0.129 g, 0.3 mmol, 1 equiv.) was dissolved in dry THF and the resulting solution was evacuated and kept inert with cycles of vacuum and nitrogen. The solution was cooled to 0 °C and stirred for 10 min. At that point $LiAlH_4$ 1.0 M sol. In THF (0.449 mL, 0.450 mmol 1.50 equiv.) was slowly added dropwise (little effervescence developed). The resulting mixture was stirred at 0 °C for 1 h. Completion of the reaction was checked by TLC and LC-MS. After 1 h the solution was quenched by the dropwise addition of cold H_2O, followed by the addition of a saturated solution of Rochelle's reagent/salt (*circa* 7 mL added). The solution was stirred at rt for 1h. The reaction mixture was then extracted with EtOAc (3x20 mL). The organic layer was dried over $MgSO_4$, filtered and evaporated to dryness to yield the title compound as off-white/pale pink solid (0.103 g, 86%)

LC-MS *m/z* calcd for $C_{22}H_{35}N_4O_3$ $[MH]^+$: 403.27, found 403.30 t_R = 3.48 min (Method A)

^{1}H NMR ($CDCl_3$) δ 11.96 (s, 1H, -N<u>H</u>), 4.15 (t, *J* = 7.3 Hz, 2H, -C<u>H</u>$_2$-NH), 4.05 (t, *J* = 7.5 Hz, 2H, -C<u>H</u>$_2$-NH), 3.35 (s, 2H, -C<u>H</u>$_2$OH), 2.09 – 1.99 (m, 6H, bicycle), 1.75 (p, *J* = 7.6 Hz, 2H, -C<u>H</u>$_2$-), 1.66 (p, *J* = 7.7 Hz, 2H, -C<u>H</u>$_2$-

), 1.61 – 1.54 (m, 6H, bicycle), 1.39 (h, J = 7.4 Hz, 4H, -C<u>H</u>$_2$CH$_3$), 0.95 (q, J = 7.3 Hz, 6H, -C<u>H</u>$_3$).

^{13}C NMR ($CDCl_3$) δ 161.7(<u>C</u>), 155.5(<u>C</u>=O), 151.2(<u>C</u>=O), 148.7(<u>C</u>), 106.9(<u>C</u>), 71.3(-<u>C</u>H$_2$OH), 43.7(<u>C</u>H$_2$), 41.7(<u>C</u>H$_2$), 34.4 (<u>C</u>), 33.4 (<u>C</u>), 30.4(<u>C</u>H$_2$), 30.3(<u>C</u>H$_2$), 30.3(<u>C</u>H$_2$), 27.8(<u>C</u>H$_2$), 20.5(<u>C</u>H$_2$), 20.0(<u>C</u>H$_2$), 14.0 (<u>C</u>H$_3$), 13.9 (<u>C</u>H$_3$).

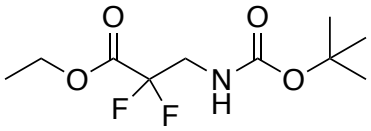


Ethyl 3-(dibenzylamino)-2,2-difluoropropanoate (5.10).[327] Zinc dust (99 mg, 1.53 mmol, 3.10 equiv) was added into a flame-dried round-bottom flask containing anhydrous THF (10 mL). To the resulting suspension, under N_2, was added chlorotrimethylsilane (TMSCl, 97 μL, 0.77 mmol, 1.56 equiv), followed, 10 min later, by ethyl bromodifluoroacetate (63 μL, 0.49 mmol, 1 equiv). After stirring for 10 min, a solution of 1-(benzylaminomethyl)benzotriazole in anhydrous THF (5 mL) was added to the reaction mixture and the resulting solution was stirred at rt for 3 h. After that time, the reaction mixture was diluted with 5 % $NaHCO_3$ (7 mL) and filtered through Celite. THF was evaporated and the resulting aqueous phase was extracted with EtOAc (3x 10 mL). The organic layers were combined, washed with 1 M HCl, dried over $MgSO_4$, filtered and concentrated to dryness. Purification by automated flash chromatography on a 12 g cartridge using a gradient of cyclohexane/EtOAc 99:1 to 95:5 and a flow rate of 20 mL/min, afforded the title compound as colourless oil (0.141 g, 86%)

LC-MS *m/z* calcd for $C_{19}H_{22}F_2NO_2$ $[MH]^+$: 334.20, found 334.20 t_R = 3.65 min (Method A)

^{1}H NMR ($CDCl_3$) δ 7.36 – 7.24 (m, 10H, Ar), 4.19 (q, *J* = 7.2 Hz, 2H, $C\underline{H}_2CH_3$), 3.71 (s, 4H, $C\underline{H}_2$-Ar), 3.17 (t, *J* = 13.1 Hz, 2H, $C\underline{H}_2CF_2$), 1.24 (t, *J* = 7.2 Hz, 3H, -$C\underline{H}_3$).

^{13}C NMR ($CDCl_3$) δ 163.9 (t, *J* = 31.8 Hz, $\underline{C}$=O), 138.2 (C), 129.3($\underline{C}$H-Ar), 128.4($\underline{C}$H-Ar), 127.5($\underline{C}$H-Ar), 116.3(t, *J* = 252.5 Hz, -$\underline{C}F_2$), 62.8(O$\underline{C}H_2$), 58.6($\underline{C}H_2$Ar), 55.3 (t, *J* = 26.4 Hz, $\underline{C}H_2CF_2$), 13.9($\underline{C}H_3$).

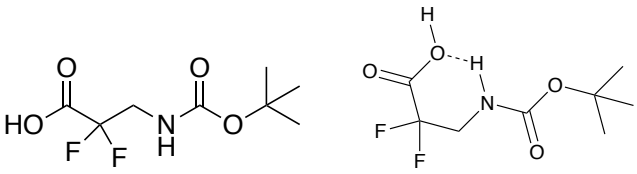


Ethyl 3-((*tert*-butoxycarbonyl)amino)-2,2-difluoropropanoate (5.11).[338] Under N_2, to a solution of ethyl 3-(dibenzylamino)-2,2-difluoropropanoate (**5.10**) (0.361 g, 1.08 mmol, 1 equiv) and Boc_2O (0.352 g, 1.64 mmol, 1.52 equiv) in EtOH was added Pd/C 10% w/w (37 mg). H_2 (balloon) was bubbled through while stirring vigoursly overnight. In the morning reaction was filtered through celite and the pad was washed with EtOH (3x). The clear filtrate was concentrated to dryness. Purification by automated flash chromatography on a 12 g cartridge using a gradient of cyclohexane/EtOAc 85:15 to 65:35 and a flow rate of 20 mL/min, afforded the title compound as colourless oil (0.257 g, 94%)

^{1}H NMR ($CDCl_3$) δ 4.85 (s, 1H, N$\underline{H}$), 4.32 (q, *J* = 7.1 Hz, 2H, O$\underline{C}H_2$), 3.75 (td, *J* = 13.4, 6.6 Hz, 2H, $C\underline{H}_2CF_2$), 1.43 (s, 9H, -Boc), 1.35 (t, *J* = 7.1 Hz, 3H, -$C\underline{H}_3$).

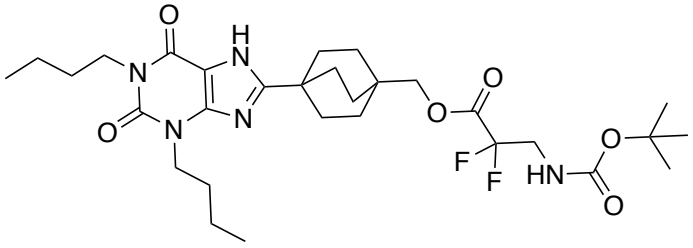
^{13}C NMR ($CDCl_3$) δ 163.2 (t, *J* = 31.7 Hz, $CF_2\underline{C}$=O), 155.4 (NH$\underline{C}$=O), 113.4 (t, *J* = 252.6 Hz, -$\underline{C}F_2$), 80.5 (C), 63.3 (O$\underline{C}H_2$), 43.6 (t, *J* = 28.2 Hz, $\underline{C}H_2CF_2$), 27.5 (-Boc), 14.0 ($\underline{C}H_3$).

^{19}F NMR (377 MHz, $CDCl_3$) δ -112.0.



(both rotamers observed by HNMR in $CDCl_3$) **3-((*tert*-Butoxycarbonyl)amino)-2,2-difluoropropanoic acid (5.12).**[361] To a solution of ethyl 3-((*tert*-butoxycarbonyl)amino)-2,2-difluoropropanoate (**5.11**) (63 mg, 0.25 mmol, 1 equiv) in THF (3 mL) was added a solution of LiOH (18 mg, 0.75 mmol, 3 equiv) in H_2O (3 mL). Reaction was stirred at rt for 10 min and, upon completion of the reaction checked by TLC, the organic layer was evaporated in vacuo. The resulting aqueous layer was extracted with EtOAc (2x 5 mL), separated and acidified with M HCl until pH = 3-4. The aqueous layer was then extracted with EtOAc (3 x5 mL). The organic layers were combined, dried over anhydrous $MgSO_4$, filtered and concentrated to dryness to give the title compound as colourless oil (42 mg, 75%).

^{1}H NMR ($CDCl_3$) δ 8.21 (s, 3H), 6.52 (d, *J* = 7.8 Hz, 1H), 5.07 (s, 1H), 3.74 (td, 4H), 1.46 (d, *J* = 19.3 Hz, 18H).



(4-(1,3-Dibutyl-2,6-dioxo-2,3,6,7-tetrahydro-1*H*-purin-8-yl)bicyclo[2.2.2]octan-1-yl)methyl 3-((tert-butoxycarbonyl)amino)-2,2-difluoropropanoate (5.20). 3-((*tert*-Butoxycarbonyl)amino)-2,2-difluoropropanoic acid (**5.12**) (6 mg, 29 μmol, 1 equiv) was dissolved in anhydrous DCM and cooled to 0 °C in an ice-bath. To the resulting mixture was added 1,3-dibutyl-8-(4-(hydroxymethyl)bicyclo[2.2.2]octan-1-yl)-3,7-dihydro-1*H*-purine-2,6-dione (**5.19**) (10 mg, 29 μmol, 1 equiv), DCC (5.13 mg, 29 μmol, 1 equiv) and DMAP (2.43 mg, 20 μmol, 0.8 equiv) and the resulting mixture was stirred overnight. Purification by preparative thin layer

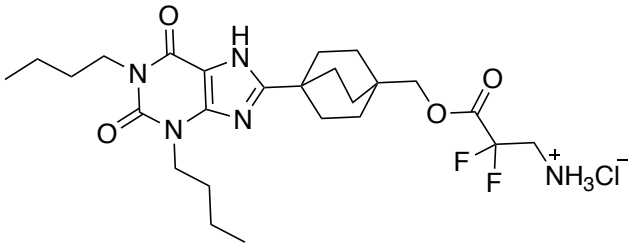
chromatography (TLC) with DCM/MeOH 98:2 afforded the title product as white foam (5 mg, 33%).

LC-MS *m/z* calcd for $C_{30}H_{46}F_2N_5O_6$ $[MH]^+$: 610.20, found 610.20 t_R = 3.86 min (Method A)

^{1}H NMR ($CDCl_3$) δ 11.85 (br s, 1H, -NH), 4.83 (s, 1H, -NH), 4.14 (t, *J* = 7.4 Hz, 2H, -CH_2-NH), 4.05 (t, *J* = 7.5 Hz, 2H, -CH_2-NH), 3.99 (s, 2H, -CH_2OH), 3.77 (td, *J* = 13.4, 6.5 Hz, 2H, -CF_2CH_2-), 2.09-2.00 (m, 6H, bicycle), 1.75 (p, *J* = 7.5 Hz, 2H, -CH_2-), 1.69-1.59 (m, 8H, bicyle +-CH_2-), 1.44 (s, 9H, -Boc), 1.42 – 1.34 (m, 4H,-CH_2-), 0.96 (q, *J* = 7.6 Hz, 6H, -CH_3).

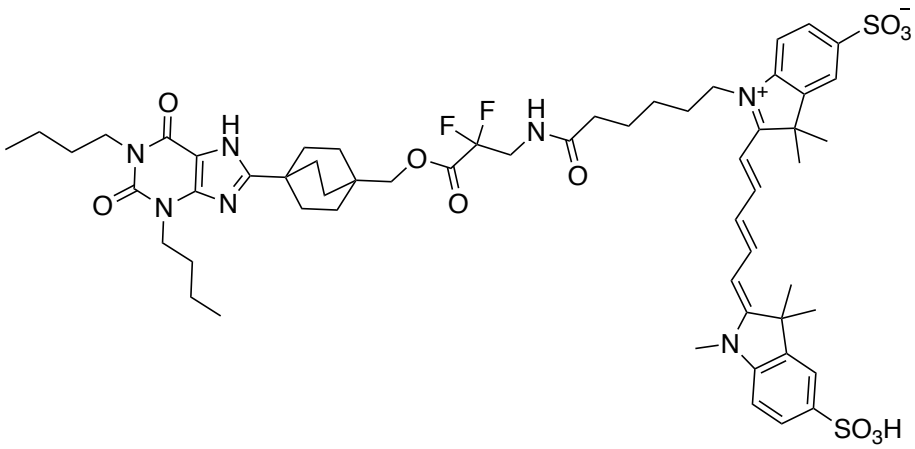
^{13}C NMR ($CDCl_3$) δ 163.2 (CH_2OC=O), 161.2(C), 155.5(HNC=O), 155.4(C=O), 151.2(C=O), 148.8(C), 113.5(-CF_2-), 106.9(C), 80.6(C), 74.1(-CH_2OH), 43.7(2xC), 41.7(CH_2), 34.1(-CH_2NH), 32.1(CH_2), 30.4(CH_2), 30.3(CH_2), 30.0(CH_2), 28.4(-(CH_3)$_3$), 27.9(CH_2), 20.5(CH_2), 20.0(CH_2), 14.0(CH_3), 13.9(CH_3).

^{19}F NMR (377 MHz, $CDCl_3$) δ -111.6.



3-((4-(1,3-Dibutyl-2,6-dioxo-2,3,6,7-tetrahydro-1*H*-purin-8-yl)bicyclo[2.2.2]octan-1-yl)methoxy)-2,2-difluoro-3-oxopropan-1-aminium chloride (5.21). A solution of (4-(1,3-dibutyl-2,6-dioxo-2,3,6,7-tetrahydro-1*H*-purin-8-yl)bicyclo[2.2.2]octan-1-yl)methyl 3-((tert-butoxycarbonyl)amino)-2,2-difluoropropanoate (**5.20**) (3 mg, 5 μmol, 1 equiv) in anhydrous DCM (200 μL) was treated with 4 M HCl in dioxane (200 μL). Upon completion of the reaction (20 min), solvent was removed under reduced pressure (water bath set < 32 ^{O}C) and the resulting amine salt was used for the next step without further purification (quantitative).

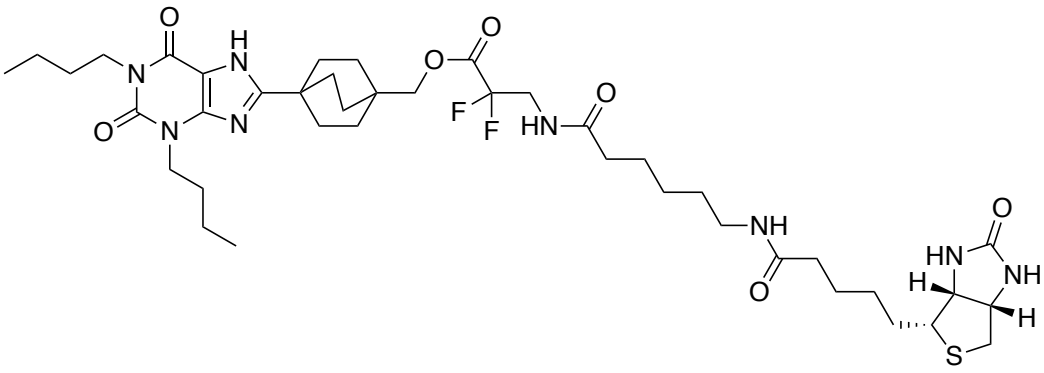
LC-MS ***m/z*** calcd for $C_{25}H_{38}F_2N_5O_4$ $[MH]^+$: 510.20, found 510.20 t_R = 2.83 min (Method A)



1-(6-((3-((4-(1,3-Dibutyl-2,6-dioxo-2,3,6,7-tetrahydro-1*H*-purin-8-yl)bicyclo[2.2.2]octan-1-yl)methoxy)-2,2-difluoro-3-oxopropyl)amino)-6-oxohexyl)-3,3-dimethyl-2-((1*E*,3*E*)-5-((*E*)-1,3,3-trimethyl-5-sulfoindolin-2-ylidene)penta-1,3-dien-1-yl)-3*H*-indol-1-ium-5-sulfonate (5.22a). A solution of Sulfo-Cy5 CO_2H (1 mg, 1.5 μmol, 1 equiv) in anhydrous DMF (0.25 mL) was reacted with DIPEA (10 mg) and BEP (0.4 mg, 1.5 μmol, 1 equiv) for 15 min. Afterwards, this mixture was added to a solution of amine (**5.21**) (0.8 mg, 1.5 μmol, 1 equiv) in anhydrous DMF (0.5 mL) and the resulting reaction mixture was stirred overnight. The solvent was evaporated with high vacuum and the residue dissolved in 1:1 CH_3CN/H_2O. Purification by RP-HPLC on a linear gradient 35 % to 95% CH_3CN/H_2O afforded, after lyophilization, the title product as bright blue solid (0.7 mg, 42%).

HRMS (TOF ES^-) calcd for $C_{57}H_{72}F_2N_7O_{11}S_2$ $[MH]^-$: 1132.4705, found 1132.4671

Analytical RP-HPLC t_R = 17.12 min, purity > 98% (Method E).

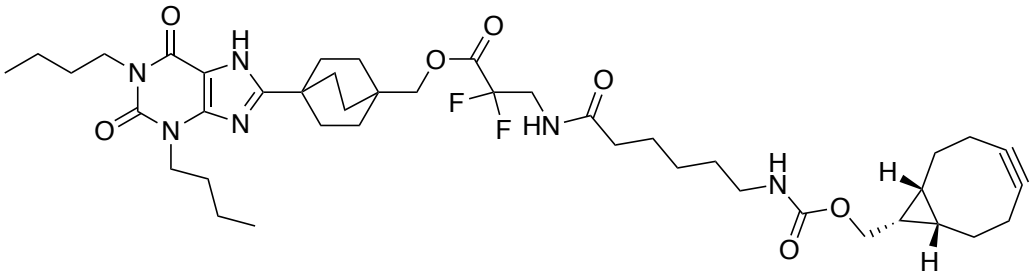


(4-(1,3-Dibutyl-2,6-dioxo-2,3,6,7-tetrahydro-1*H*-purin-8-yl)bicyclo[2.2.2]octan-1-yl)methyl 2,2-difluoro-3-(6-(5-((3*aR*,4*R*,6*aS*)-2-oxohexahydro-1*H*-thieno[3,4-*d*]imidazol-4-yl)pentanamido)hexanamido)propanoate (5.22b). A solution of *N*-(+)-Biotinyl-6-aminohexanoic acid (0.7 mg, 1.9 μmol, 1 equiv) in anhydrous DMF (0.25 mL) was reacted with DIPEA (10 mg) and BEP (0.5 mg, 1.9 μmol, 1 equiv) for 15 min. Afterwards, this mixture was added to a solution of Amine (**5.21**) (1 mg, 1.9 μmol, 1 equiv) in anhydrous DMF (0.5 mL) and the resulting reaction mixture was stirred overnight. The solvent was evaporated with high vacuum and the residue dissolved in 1:1 CH_3CN/H_2O. Purification by RP-HPLC on a linear gradient 35 % to 95% CH_3CN/H_2O afforded, after lyophilization, the title product as bright blue solid (0.7 mg, 41%).

LC-MS ***m/z*** calcd for $C_{41}H_{63}F_2N_8O_7S$ $[MH]^+$: 849.50, found 849.50 t_R = 3.30 min (Method A)

HRMS (TOF ES^+) calcd for $C_{41}H_{63}F_2N_8O_7S$ $[MH]^+$: 849.4503, found 849.4489; calcd for $C_{41}H_{62}F_2N_8NaO_7S$ $[M+Na]^+$: 871.4322, found 871.4327.

Analytical RP-HPLC t_R = 16.94 min, purity > 98% (Method E).

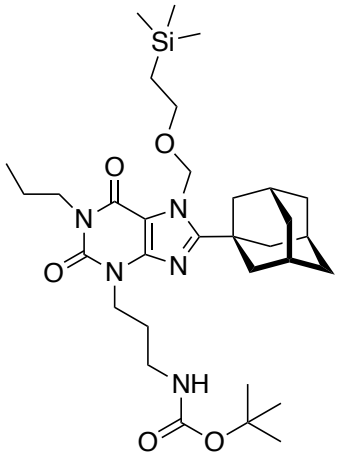


(4-(1,3-Dibutyl-2,6-dioxo-2,3,6,7-tetrahydro-1*H*-purin-8-yl)bicyclo[2.2.2]octan-1-yl)methyl 3-(6-(((((1*R*,8*S*,9*s*)-bicyclo[6.1.0]non-4-yn-9-yl)methoxy)carbonyl)amino)hexanamido)-2,2-difluoropropanoate (5.22c). A solution of 6-(((((1*R*,8*S*,9*s*)-bicyclo[6.1.0]non-4-yn-9-yl)methoxy)carbonyl)amino)hexanoic acid (1.8 mg, 5.7 μmol, 1 equiv) in anhydrous DMF (0.300 mL) was reacted with DIPEA (10 mg) and BEP (1.6 mg, 5.7 μmol, 1 equiv) for 15 min. Afterwards, this mixture was added to a solution of amine (**5.21**) (2.90 mg, 5.7 μmol, 1 equiv) in anhydrous DMF (0.5 mL) and the resulting reaction mixture was stirred overnight. The solvent was evaporated with high vacuum and the residue dissolved in 1:1 CH_3CN/H_2O. Purification by RP-HPLC on a linear gradient 45 % to 95% CH_3CN/H_2O afforded, after lyophilization, the title product as bright blue solid (0.75 mg, 17%).

LC-MS *m/z* calcd for $C_{42}H_{61}F_2N_6O_7$ $[MH]^+$: 799.50, found 799.50 t_R = 8.30 min (Method A)

HRMS (TOF ES^+) calcd for $C_{42}H_{61}F_2N_6O_7$ $[MH]^+$: 799.4564, found 799.4553; calcd for $C_{42}H_{60}F_2N_6NaO_7$ $[M+Na]^+$: 821.4384, found 821.4378.

Analytical RP-HPLC t_R = 20.34 min, purity > 98% (Method E).

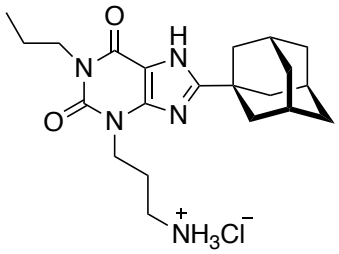


***tert*-Butyl (3-(8-((3*r*,5*r*,7*r*)-adamantan-1-yl)-2,6-dioxo-1-propyl-7-((2-(trimethylsilyl)ethoxy)methyl)-1,2,6,7-tetrahydro-3*H*-purin-3-yl)propyl)carbamate (5.1a).** To a solution of **4.35** (SEM-protected xanthine) (0.223 g, 486 μmol, 1 equiv.) in DMF (4 mL) was added K_2CO_3 (87 mg, 632 μmol, 1.50 equiv.). The resulting solution was stirred at rt for 2 h. Then 3-(Boc-amino) propylbromide (0.127 g, 534 μmol, 1.10 equiv.) was added and the resulting solution was stirred at rt for 9 h. Upon completion of the reaction monitored by TLC and LCMS, the solution was diluted with H_2O (10 mL) and extracted with EtOAc (2x15 mL). The organic layer was washed with sat. $NaHCO_3$ and brine. The combined organic extracts were dried over anhydrous $MgSO_4$, filtered and evaporated to dryness. The resulting crude material was purified by flash column chromatography with PE/EtOAc 8:2 to yield the title compound as white foam (0.165 g, 55%).

LC-MS *m/z* calcd for $C_{32}H_{54}N_5O_5Si$ $[MH]^+$: 616.40, found 616.40 t_R = 5.69 min (Method B)

^{1}H NMR ($CDCl_3$) δ 6.05 (br s, 1H), 5.91 (s, 2H, N-C$\underline{H}_2$-O), 4.20 – 4.14 (t, *J* = 5.4 Hz, 2H, OC$\underline{H}_2$-), 3.98 – 3.90 (t, *J* = 7.4 Hz, 2H, -NC$\underline{H}_2$-), 3.74 – 3.65 (t, *J* = 7.4 Hz, 2H, NC$\underline{H}_2$-), 3.02 (q, *J* = 5.7 Hz, 2H, NHC$\underline{H}_2$-), 2.20-2.14 (m, 6H, adamantane), 2.13-2.07 (m, 3H, adamantane), 1.94-1.84 (m, 2H), 1.82-1.76 (m, 6H, adamantane), 1.63 (h, *J* = 7.4 Hz, 2H, -C$\underline{H}_2$CH$_3$), 1.43 (s, 9H, -Boc), 0.96 – 0.89 (m, 5H, -C$\underline{H}_2$- + C$\underline{H}_3$), -0.04 (s, 9H, -SEM).

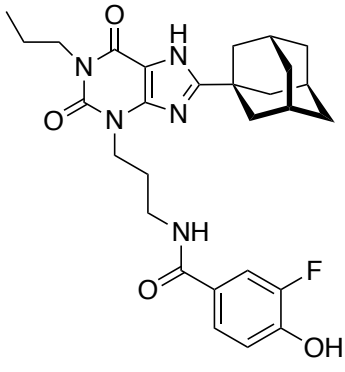
^{13}C NMR ($CDCl_3$) δ 161.7(C), 156.1(NH<u>C</u>=O), 155.3(C=O), 151.2(C=O), 147.3(C), 107.4(C), 78.9(C-Boc), 73.7(N<u>C</u>H_2O), 66.5 (O<u>C</u>H_2), 43.0(<u>C</u>H_2), 40.8(<u>C</u>H_2 adamantane), 40.4(<u>C</u>H_2), 37.9 (<u>C</u> adamantane), 36.5(<u>C</u>H adamantane), 28.6(<u>C</u>H_2 adamantane), 28.4(Boc), 21.4(<u>C</u>H_2), 18.2(<u>C</u>H_2), 11.4(<u>C</u>H_3), -1.3 (SEM).



3-(8-((3*r*,5*r*,7*r*)-Adamantan-1-yl)-2,6-dioxo-1-propyl-1,2,6,7-tetrahydro-3*H*-purin-3-yl)propan-1-aminium chloride (5.2a). To *tert*-butyl (3-(8-((1r,3R,5S)-adamantan-1-yl)-2,6-dioxo-1-propyl-7-((2-(trimethylsilyl)ethoxy)methyl)-1,2,6,7-tetrahydro-3H-purin-3-yl)propyl)carbamate (**5.1a**) (0.162 g, 263 μmol, 1 equiv.) was added 4 M HCl in dioxane (1.50 mL). The resulting solution was stirred at rt for 1 h. After that time a white precipitate developed and the reaction was completed. The solvent was evaporated to dryness and the product was used for the subsequent step without further purification.

LC-MS *m/z* calcd for $C_{21}H_{32}N_5O_2$ $[MH]^+$: 386.30, found 386.30 t_R = 3.22 min (Method B)

Analytical RP-HPLC t_R = 4.64 min, purity > 99% (Method F).



***N*-(3-(8-((3*r*,5*r*,7*r*)-Adamantan-1-yl)-2,6-dioxo-1-propyl-1,2,6,7-tetrahydro-3*H*-purin-3-yl)propyl)-3-fluoro-4-hydroxybenzamide (5.3).** 3-Fluoro-4-hydroxybenzoic acid (20 mg, 131 μmol 1.01 equiv.) was dissolved in DMF (0.5 mL) and reacted with COMU (67 mg, 156 μmol, 1.10 equiv.) in the presence of DIPEA (67 μL, 389 μmol,

3 equiv.). To the resulting mixture was added a solution of 3-(8-((1r,3R,5S)-adamantan-1-yl)-2,6-dioxo-1-propyl-1,2,6,7-tetrahydro-3H-purin-3-yl)propan-1-aminium chloride(**5.2a**) (50 mg, 39 μmol, 1.10 equiv.) in DMF (0.5 mL). The resulting solution was stirred at 90 °C for 1 h. Upon completion of the reaction monitored by LCMS, the solvent was removed under reduced pressure and the resulting residue was dissolved in EtOAc and washed with water (2x10 mL). The organics were collected, dried over $MgS0_4$ anhydrous, filtered and evaporated to dryness. The resulting residue was purified by flash column chromatography with DCM/MeOH on a gradient of 100: 0 % to 97: 3 %. The title compound was obtained as off-white solid (32 mg, 47%).

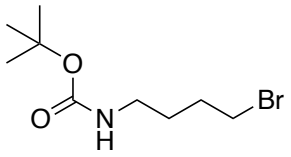
LC-MS *m/z* calcd for $C_{28}H_{35}FN_5O_4$ $[MH]^+$: 524.30, found 524.30 t_R = 3.69 min (Method B)

^{1}H NMR ($CDCl_3$) δ 11.40 (br s, 1H, NH xanthine), 7.87 (t, *J* = 5.4 Hz, 1H, NH), 7.69 (dd, *J* = 9.9, 2.2 Hz, 1H, Ar), 7.62 (dd, *J* = 8.5 Hz, 1H, Ar), 7.05 (t, *J* = 8.4 Hz, 1H, Ar), 6.65 (br s, 1H, OH), 4.28 (t, *J* = 5.7 Hz, 2H, CH_2), 4.05 (t, *J* = 6.8 Hz, 2H, CH_2), 3.39 (q, *J* = 6.1 Hz, 2H, CH_2), 2.05 – 1.99 (m, 9H, Adamantane), 1.81 – 1.68 (m, 10H, adamantane + 2xCH_2), 0.96 (t, *J* = 7.4 Hz, 3H, CH_3).

^{13}C NMR (MeOD) δ 168.7(NHC=O), 163.2 (C), 155.9(C=O), 152.90(C=O), 152.4 (d, *J* = 241.7 Hz, CF), 149.7 (d, *J* = 13.1 Hz, Ar), 149.1(C), 127.2 (d, *J* = 5.3 Hz, Ar), 125.1 (d, *J* = 3.1 Hz, Ar), 118.4 (d, *J* = 2.9 Hz, Ar), 116.3 (d, *J* = 20.0 Hz, Ar), 107.9 (C), 43.9(C adamantane), 42.3(CH_2), 41.8 (CH_2 adamantane), 37.8(CH_2), 37.4(CH_2 adamantane), 36.9(CH_2), 29.5(CH_2 adamantane), 29.0 (CH_2), 22.3(CH_2), 11.5 (CH_3).

HRMS (TOF ES^+) calcd for $C_{28}H_{35}FN_5O_4$ $[MH]^+$: 524.2668, found 524.2688; calcd for $C_{28}H_{34}FN_5O_4Na$ $[M+Na]^+$: 546.2487, found 546.2512

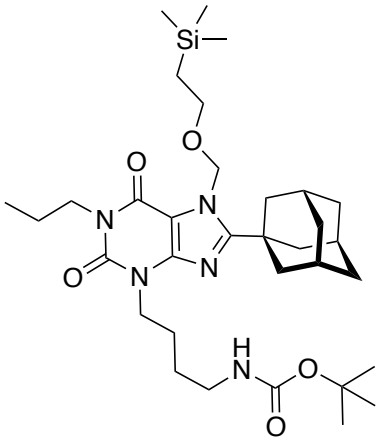
Analytical RP-HPLC t_R = 5.59 min, purity > 99% (Method F).



***tert*-Butyl (4-bromobutyl)carbamate (5.9).** To a solution of tert-butyl(4-hydroxybutyl)carbamate (0.700g, 3.70 mmol, 1 equiv.) in dry THF (20 mL) was added PPh_3 (1.46 g, 5.55 mmol, 1.50 equiv.), followed by CBr_4 (1.84 g, 5.55 mmol, 1.50 equiv.). The resulting solution was stirred at rt for 3 h. Upon completion of the reaction monitored by TLC, the solvent was removed under reduced pressure and the resulting solid was adsorbed on isolute and purified by flash column chromatography using PE/EtOAc 3:1 to give the title compound as colourless oil which solidified upon cooling (0.846 g, 91%).

^{1}H NMR ($CDCl_3$) δ 4.57 (s, 1H, NH), 3.40 (t, *J* = 6.7 Hz, 2H, CH_2), 3.13 (t, *J* = 7.1 Hz, 2H, CH_2), 1.87 (p, *J* = 6.6 Hz, 2H, CH_2), 1.62 (p, *J* = 6.6 Hz, 2H, CH_2), 1.42 (s, 9H, Boc).

^{13}C NMR ($CDCl_3$) δ 156.1(NHC=O), 79.4 (C), 39.8 (CH_2), 33.4 (CH_2), 30.0 (CH_2), 28.9 (CH_2), 28.5 (Boc).



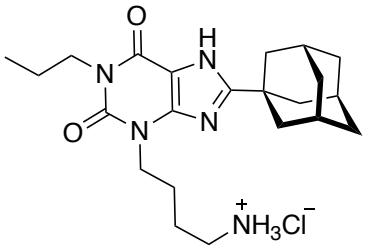
***tert*-Butyl (4-(8-((3*r*,5*r*,7*r*)-adamantan-1-yl)-2,6-dioxo-1-propyl-7-((2-(trimethylsilyl)ethoxy)methyl)-1,2,6,7-tetrahydro-3*H*-purin-3-yl)butyl)carbamate (5.1b).** To a solution of **4.35** (0.200 g, 0.43 mmol, 1 equiv.) in DMF (4 mL) was added K_2CO_3 (90 mg, 654 μmol, 1.50 equiv.). The resulting solution was stirred at rt for 2 h. Then 4-(Boc-amino) butyl bromide (**5.9**) (0.120 g, 480 μmol, 1.10 equiv.) was added and the resulting

solution was stirred at rt for 9 h. Upon completion of the reaction monitored by TLC and LCMS, the solution was diluted with H_2O (10 mL) and extracted with EtOAc (2x15 mL). The organic layer was washed with sat. $NaHCO_3$ and brine. The combined organic extracts were dried over anhydrous $MgSO_4$, filtered and evaporated to dryness. The resulting crude material was purified by flash column chromatography with PE/EtOAc 8:2 to yield the title compound as white foam (0.186 g, 68%).

LC-MS *m/z* calcd for $C_{33}H_{56}N_5O_5Si$ $[MH]^+$: 630.40, found 630.40 t_R = 6.15 min (Method B).

^{1}H NMR ($CDCl_3$) δ 5.91 (s, 2H, N-C<u>H</u>$_2$-O), 4.74 (s, 1H, N<u>H</u>), 4.11 (t, *J* = 7.2 Hz, 2H, C<u>H</u>$_2$), 3.95 (t, *J* = 6.6 Hz, 2H, C<u>H</u>$_2$), 3.71 (t, *J* = 7.8 Hz, 2H, C<u>H</u>$_2$), 3.18 (q, *J* = 6.1 Hz, 2H, C<u>H</u>$_2$), 2.20-2.14 (m, 6H, adamantane), 2.13 – 2.06 (m, 3H, adamantane), 1.82-1.75 (m, 8H, adamantane + C<u>H</u>$_2$), 1.64 (h, *J* = 7.6 Hz 2H, C<u>H</u>$_2$), 1.54 (h, *J* = 5.8 Hz 2H, C<u>H</u>$_2$), 1.42 (s, 9H), 0.93 (td, *J* = 8.2, 2.9 Hz, 5H, C<u>H</u>$_2$ + C<u>H</u>$_3$).

^{13}C NMR ($CDCl_3$) δ 161.7 (C), 156.1(NH<u>C</u>=O), 155.4(C=O), 151.2 (C=O), 147.1 (C), 107.6 (C), 79.2 (C-Boc), 73.6(N<u>C</u>H$_2$O), 66.4(O<u>C</u>H$_2$), 43.0 (<u>C</u>H$_2$), 42.7 (<u>C</u>H$_2$), 40.9(<u>C</u>H$_2$ adamantane), 37.8 (<u>C</u> adamantane), 36.6(<u>C</u>H$_2$ adamantane), 28.60 (<u>C</u>H adamantane)28.4(Boc), 27.1(<u>C</u>H$_2$), 25.6(<u>C</u>H$_2$), 21.5(<u>C</u>H$_2$), 18.2(<u>C</u>H$_2$), 11.5 (<u>C</u>H$_3$), -1.3 (-SEM).

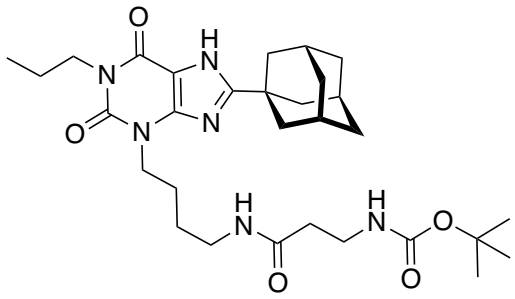


4-(8-((3*r*,5*r*,7*r*)-Adamantan-1-yl)-2,6-dioxo-1-propyl-1,2,6,7-tetrahydro-3*H*-purin-3-yl)butan-1-aminium chloride (5.2b). To *tert*-Butyl (4-(8-((3r,5r,7r)-adamantan-1-yl)-2,6-dioxo-1-propyl-7-((2-(trimethylsilyl)ethoxy)methyl)-1,2,6,7-tetrahydro-3H-purin-3-yl)butyl)carbamate (**5.1b**) (0.145 g, 230 μmol, 1 equiv.) was added 4 M HCl in dioxane (1.50 mL). The resulting solution was stirred at rt for 2 h. AT that

time a white precipitate developed and the reaction was completed. The solvent was evaporated to dryness and the product was used for the subsequent step without further purification.

LC-MS *m/z* calcd for $C_{22}H_{34}N_5O_2$ $[MH]^+$: 400.30, found 400.30 t_R = 3.36 min (Method B).

Analytical RP-HPLC t_R = 4.73 min, purity > 99% (Method F).

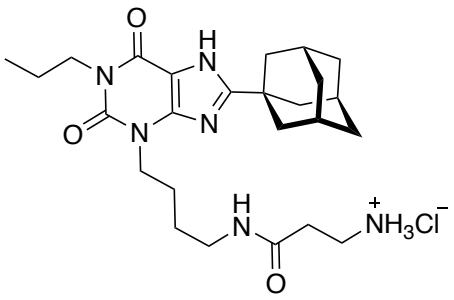


***tert*-Butyl (3-((4-(8-((3*r*,5*r*,7*r*)-adamantan-1-yl)-2,6-dioxo-1-propyl-1,2,6,7-tetrahydro-3*H*-purin-3-yl)butyl)amino)-3-oxopropyl)carbamate (5.5).** To a solution of Boc-β alanine (40 mg, 211 μmol, 1 equiv.) in DMF (0.5 mL) was added DIPEA (110 μL, 634 μmol, 3 equiv.) followed by COMU (107 mg, 253 μmol, 1.20equiv.). To the resulting mixture was added a solution of 4-(8-((1r,3R,5S)-adamantan-1-yl)-2,6-dioxo-1-propyl-1,2,6,7-tetrahydro-3H-purin-3-yl)butan-1-aminium chloride (**5.2b**) (100 mg, 232 μmol, 1.10 equiv.) in DMF (0.5 mL). The resulting solution was stirred at rt for 9 h. Upon completion of the reaction monitored by TLC and LCMS, the solution was diluted with H_2O and extracted with EtOAc (20 mL). The organic layer was subsequently washed with 1 M HCl (15 mL), sat $NaHCO_3$ (15 mL) and brine (15 mL). The combined organic extracts were collected, dried over anhydrous $MgSO_4$, filtered and evaporated to dryness. The crude was purified by flash column chromatography with DCM/MeOH 99:1 to 96:4. The title compound was obtained as colourless oil (93 mg, 77%).

LC-MS *m/z* calcd for $C_{30}H_{47}N_6O_5$ $[MH]^+$: 571.40, found 571.40 t_R = 3.93 min (Method B).

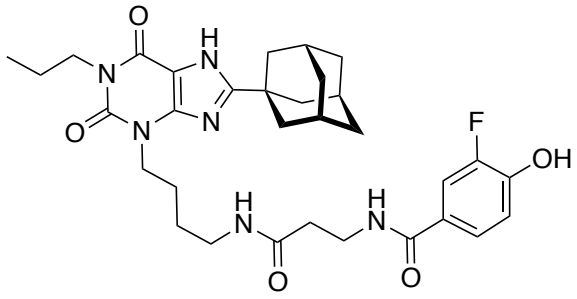
^{1}H NMR ($CDCl_3$) δ 12.05 (s, 1H, NH xanthine), 6.35 – 6.24 (m, 1H, NH), 5.37 (s, 1H, NH), 4.14 (t, *J* = 7.2 Hz, 2H, CH_2), 4.01 (t, *J* = 6.6, 4.8 Hz, 2H, CH_2), 3.36 (dq, *J* = 19.5, 6.2 Hz, 4H, 2xCH_2), 2.39 (t, *J* = 6.1 Hz, 2H, CH_2), 2.13 – 2.06 (m, 9H, adamantane), 1.85 – 1.73 (m, 8H, adamantane + CH_2), 1.66 (h, *J* = 6.6 Hz, 2H, CH_2), 1.58 (h, *J* = 6.9 Hz, 2H, CH_2), 1.38 (s, 9H, Boc), 0.91 (t, *J* = 7.5 Hz, 3H CH_3).

^{13}C NMR ($CDCl_3$) δ 171.6 (NHC=O), 162.8 (C), 156.3 (NHC=O), 155.4 (C=O), 151.3(C=O), 148.8 (C), 106.7(C), 79.2(C-Boc), 43.2 (CH_2), 42.9 (CH_2), 41.0 (CH_2 adamantane), 39.1(CH_2), 36.9(C adamantane), 36.5(CH adamantane), 35.9 (CH_2), 28.5(CH_2 adamantane), 28.2(Boc), 26.2 (CH_2), 25.6 (CH_2), 21.4 (CH_2), 11.4(CH_3).



3-((4-(8-((3*r*,5*r*,7*r*)-Adamantan-1-yl)-2,6-dioxo-1-propyl-1,2,6,7-tetrahydro-3*H*-purin-3-yl)butyl)amino)-3-oxopropan-1-aminium chloride (5.6). To *tert*-butyl (3-((4-(8-((3*r*,5*r*,7*r*)-adamantan-1-yl)-2,6-dioxo-1-propyl-1,2,6,7-tetrahydro-3*H*-purin-3-yl)butyl)amino)-3-oxopropyl)carbamate (**5.5**) (93 g, 163 μmol, 1 equiv.) was added 4 M HCl in dioxane (1.50 mL). The resulting solution was stirred at rt for 2 h. AT that time a white precipitate developed and the reaction was completed. The solvent was evaporated to dryness and the product was used for the subsequent step without further purification

LC-MS *m/z* calcd for $C_{25}H_{39}N_6O_3$ $[MH]^+$: 471.30, found 541.40 t_R = 3.24 min (Method B).



***N*-(3-((4-(8-((3*r*,5*r*,7*r*)-Adamantan-1-yl)-2,6-dioxo-1-propyl-1,2,6,7-tetrahydro-3*H*-purin-3-yl)butyl)amino)-3-oxopropyl)-3-fluoro-4-hydroxybenzamide (5.7).** 3-Fluoro-4-hydroxybenzoic acid (23 mg, 147 μmol 1.01 equiv.) was dissolved in DMF (0.5 mL) and reacted with COMU (69 mg, 162 μmol, 1.10 equiv.) in the presence of DIPEA (51 μL, 295 μmol, 3 equiv.). To the resulting mixture was added a solution of 3-((4-(8-((1r,3R,5S)-adamantan-1-yl)-2,6-dioxo-1-propyl-1,2,6,7-tetrahydro-3H-purin-3-yl)butyl)amino)-3-oxopropan-1-aminium chloride (**5.6**) (76 mg, 162 μmol, 1.10 equiv.) in DMF (0.5 mL). The resulting solution was stirred at 90 °C for 1 h. Upon completion of the reaction monitored by LCMS, the solvent was removed under reduced pressure and the resulting residue was dissolved in EtOAc and washed with water (2x10 mL). The organics were collected, dried over anhydrous $MgSO_4$, filtered and evaporated to dryness. The resulting residue was purified by flash column chromatography with DCM/MeOH on a gradient of 99:1 % to 96:4 %. The title compound was obtained as off-white solid (32 mg, 36%).

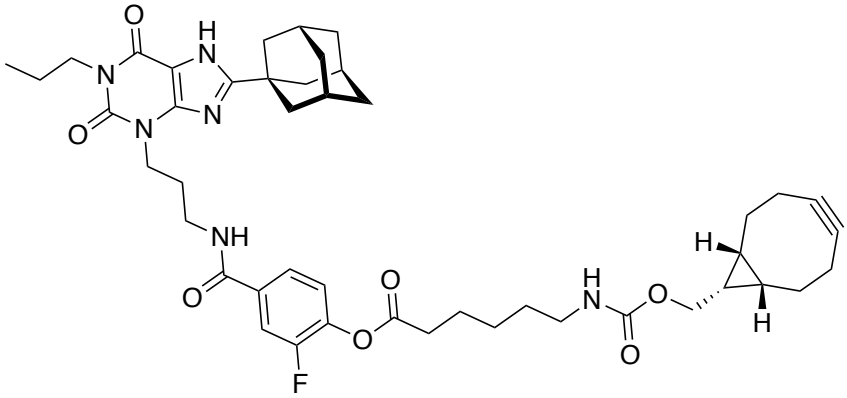
LC-MS *m/z* calcd for $C_{32}H_{42}FN_6O_3$ $[MH]^+$: 609.30, found 609.30 t_R = 3.57 min (Method B).

^{1}H NMR (DMSO-d_6) δ 10.42 (s, 1H, NH xanthine), 8.34 (t, J = 5.6 Hz, 1H, NH), 7.85 (t, J = 5.6 Hz, 1H, NH), 7.60 (dd, J = 12.4, 2.1 Hz, 1H, Ar-H), 7.52 (dd, J = 8.4, 2.1 Hz, 1H, Ar-H), 6.96 (t, J = 8.6 Hz, 1H, Ar-H), 3.96 (t, J = 6.9 Hz, 2H, CH_2-N), 3.82 (t, J = 5.9 Hz, 2H, CH_2-N), 3.43 – 3.36 (m, 2H, CH_2), 3.11 – 3.04 (m, 2H, CH_2), 2.31 (t, J = 7.3 Hz, 2H, CH_2), 2.04 – 1.99 (m, 3H, adamantane), 1.98 – 1.94 (m, 6H, adamantane), 1.74-1.67 (m, 6H, adamantane), 1.64 (h, J = 7.2 Hz, 2H, CH_2), 1.54 (h, J = 7.1 Hz, 2H, CH_2), 1.42 – 1.33 (m, 2H, CH_2), 0.84 (t, J = 7.4 Hz, 3H, CH_3).

^{13}C NMR (DMSO-d_6) δ 170.2 (NHC=O), 164.8 (ArNHC=O), 158.5 (C), 153.9 (C=O), 150.8 (C=O), 148.2 (d, J = 182.2 Hz, CF), 147.8 (C), 125.7 (d, J = 4.6 Hz, ArCH), 124.1 (d, J = 2.7 Hz, ArCH), 117.1 (d, J = 3.1 Hz, ArCH), 115.1 (d, J = 19.03 Hz, ArCHCF) 106.1 (C), 42.4(CH_2), 42.0 (CH_2), 38.1(CH_2), 36.2 (C adamantane), 35.9 (CH_2), 35.5(CH_2), 35.1(CH_2 adamantane), 27.6 (CH adamantane), 26.3 (CH_2), 25.1 (CH_2), 20.9 (CH_2), 11.2 (CH_3).

HRMS (TOF ES$^+$) calcd for $C_{32}H_{42}FN_6O_5$ $[MH]^+$: 609.3195, found 609.3218; calcd for $C_{32}H_{42}FN_6O_5Na$ $[M+Na]^+$: 631.3015, found 631.3038

Analytical RP-HPLC t_R = 5.34 min, purity > 99% (Method F).

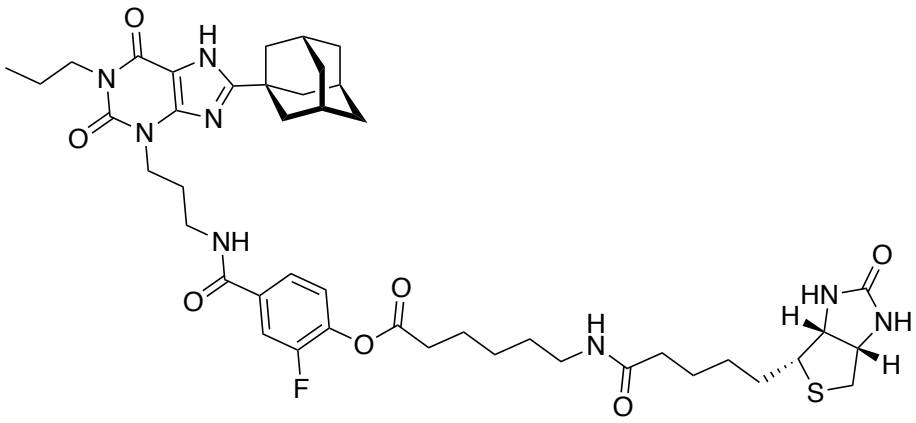


4-((3-(8-((3*r*,5*r*,7*r*)-Adamantan-1-yl)-2,6-dioxo-1-propyl-1,2,6,7-tetrahydro-3*H*-purin-3-yl)propyl)carbamoyl)-2-fluorophenyl 6-(((((1*R*,8*S*,9*s*)-bicyclo[6.1.0]non-4-yn-9-yl)methoxy)carbonyl)amino)hexanoate (5.4c). Following general procedure B, phenol **5.3** (1 mg, 2 μmol, 1 equiv) was converted to the BCN analogue **5.4c**. Purification by RP-HPLC (Method C) gave after lyophilization the title compound as an off-white solid (0.34 mg, 23%).

LC-MS ***m/z*** calcd for $C_{45}H_{58}FN_6O_7$ $[MH]^+$: 813.50, found 813.50 t_R = 3.23 min (Method A)

HRMS (TOF ES$^+$) calcd for $C_{45}H_{58}FN_6O_7$ $[MH]^+$: 813.4346, found 813.4350; calcd for $C_{45}H_{57}FN_6NaO_7$ $[M+Na]^+$: 835.4165, found 835.4146.

Analytical RP-HPLC t_R = 20.41 min, purity > 97% (Method E).

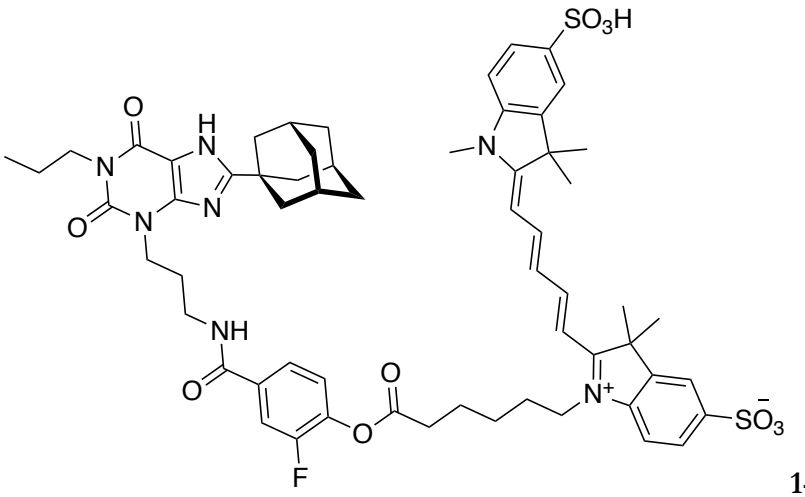


4-((3-(8-((3*r*,5*r*,7*r*)-Adamantan-1-yl)-2,6-dioxo-1-propyl-1,2,6,7-tetrahydro-3*H*-purin-3-yl)propyl)carbamoyl)-2-fluorophenyl 6-(5-((3*aR*,4*R*,6*aS*)-2-oxohexahydro-1*H*-thieno[3,4-*d*]imidazol-4-yl)pentanamido)hexanoate (5.4b). Following general procedure B, phenol **5.3** (1.5 mg, 2.8 μmol, 1 equiv) was converted to the Biotin analogue **5.4b**. Purification by RP-HPLC (method C) gave after lyophilization the title compound as an off-white solid (0.34 mg, 23%).

LC-MS ***m/z*** calcd for $C_{44}H_{60}FN_8O_7S$ $[MH]^+$: 863.20, found 863.20 t_R = 3.23 min (Method A)

HRMS (TOF ES^+) calcd for $C_{44}H_{60}FN_8O_7S$ $[MH]^+$: 863.4284, found 863.4274; calcd for $C_{44}H_{59}FN_8NaO_7S$ $[M+Na]^+$: 885.4104, found 885.4116.

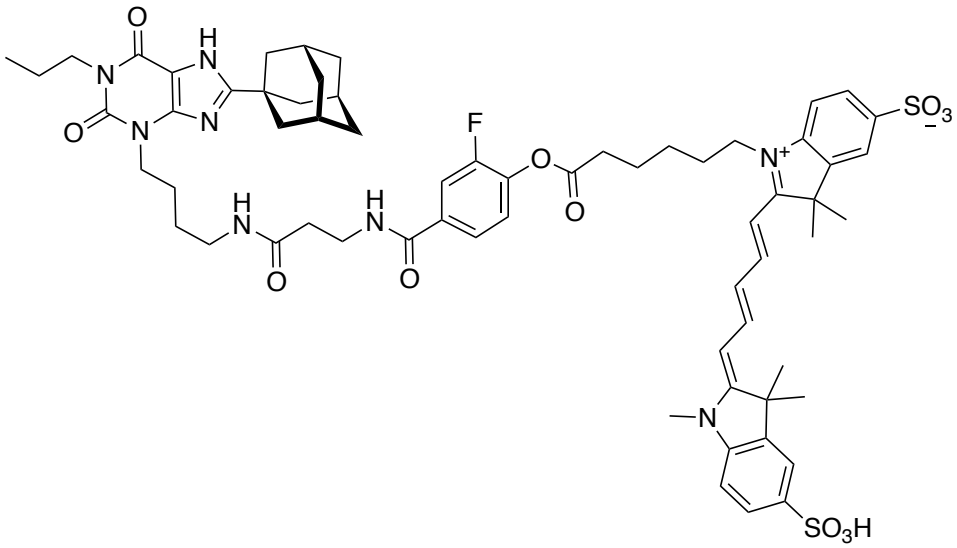
Analytical RP-HPLC t_R = 16.91 min, purity > 99% (Method E).



1-(6-(4-((3-(8-((3*r*,5*r*,7*r*)-Adamantan-1-yl)-2,6-dioxo-1-propyl-1,2,6,7-tetrahydro-3*H*-purin-3-yl)propyl)carbamoyl)-2-fluorophenoxy)-6-oxohexyl)-3,3-dimethyl-2-((1*E*,3*E*)-5-((*E*)-1,3,3-trimethyl-5-sulfoindolin-2-ylidene)penta-1,3-dien-1-yl)-3*H*-indol-1-ium-5-sulfonate (5.4a). Following general procedure (B), 3-fluoro-4-hydroxybenzamido congener (**5.3**) (1 mg, 1.17 μmol, 1 equiv) was converted to the SulfoCy5 conjugate **5.4a**. Purification by RP-HPLC (Method C) gave, after lyophilization, the title compound as a bright blue solid (1 mg, 74%).

HRMS (TOF ES$^-$) calcd for $C_{60}H_{69}FN_7O_{11}S_2$ [MH]$^-$: 1146.4486, found 1146.4452

Analytical RP-HPLC t_R = 17.28 min, purity > 98% (Method E).

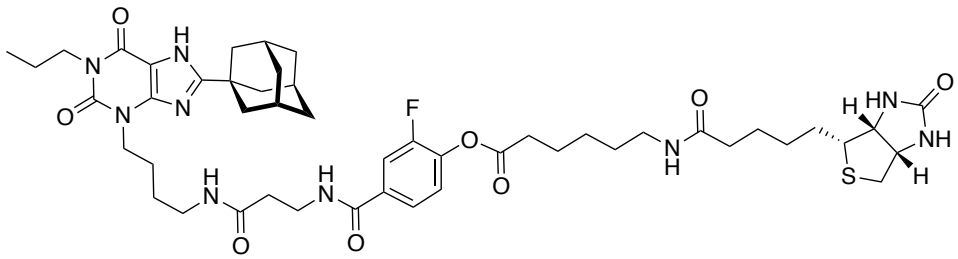


1-(6-(4-((3-((4-(8-((3*r*,5*r*,7*r*)-Adamantan-1-yl)-2,6-dioxo-1-propyl-

1,2,6,7-tetrahydro-3*H*-purin-3-yl)butyl)amino)-3-oxopropyl)carbamoyl)-2-fluorophenoxy)-6-oxohexyl)-3,3-dimethyl-2-((1*E*,3*E*)-5-((*E*)-1,3,3-trimethyl-5-sulfoindolin-2-ylidene)penta-1,3-dien-1-yl)-3*H*-indol-1-ium-5-sulfonate (5.8a). Following general procedure B, phenol **5.7** (0.7 mg, 1.2 μmol, 1 equiv) was converted to the SulfoCy5 analogue **5.8a**. Purification by RP-HPLC (Method C) gave after lyophilization the title compound as an off-white solid (0.47 mg, 37%).

HRMS (TOF ES$^-$) calcd for $C_{64}H_{76}FN_8O_{12}S_2$ [MH]$^-$: 1231.5014, found 1231.4988

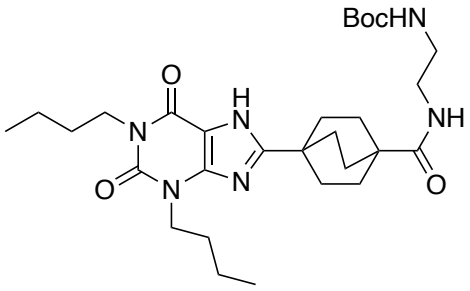
Analytical RP-HPLC t_R = 16.78 min, purity > 98% (Method E).



4-((3-((4-(8-((3*r*,5*r*,7*r*)-Adamantan-1-yl)-2,6-dioxo-1-propyl-1,2,6,7-tetrahydro-3*H*-purin-3-yl)butyl)amino)-3-oxopropyl)carbamoyl)-2-fluorophenyl 6-(5-((3*aR*,4*R*,6*aS*)-2-oxohexahydro-1*H*-thieno[3,4-d]imidazol-4-yl)pentanamido)hexanoate (5.8b). Following general procedure B, phenol **5.7** (1.70 mg, 2 μmol, 1 equiv) was converted to the Biotin analogue **5.8b**. Purification by RP-HPLC (Method C) gave after lyophilization the title compound as an off-white solid (0.80 mg, 30%).

HRMS (TOF ES$^+$) calcd for $C_{48}H_{67}FN_9O_8S$ [MH]$^+$: 948.4812, found 948.4810; calcd for $C_{48}H_{66}FN_9NaO_8S$ [M+Na]$^+$: 970.4631, found 970.4633.

Analytical RP-HPLC t_R = 15.89 min, purity > 97% (Method E).

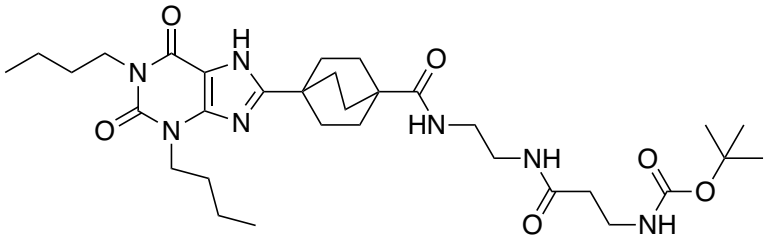


***tert*-Butyl (2-(4-(1,3-dibutyl-2,6-dioxo-2,3,6,7-tetrahydro-1*H*-purin-8-yl)bicyclo[2.2.2]octane-1-carboxamido)ethyl)carbamate (5.27).** Following general procedure A, to a stirring solution of (2,6-dioxo-1,3-dibutyl-2,3,6,9-tetrahydro-1H- purin-8-yl) bicyclo [2.2.2] octane-1-carboxylic acid (**5.17**) (300 mg, 720 µmol, 1 equiv), DIPEA (138 µL, 792 µmol, 1.10 equiv) and COMU (339 mg, 792 µmol, 1.10 equiv) and DMF (1.5 mL) was added tert-butyl (2- aminoethyl) carbamate (0.125 mL, 792 µmol, 1.10 equiv). Purification by automated flash column chromatography using a gradient of 98:2 to 90:10 DCM/MeOH gave the title pure compound as an off-white solid (284 mg, 71%).

LC-MS *m/z* calcd for $C_{29}H_{47}N_6O_5$ $[MH]^+$: 599.30, found 599.30 t_R = 3.22 min (Method A)

^{1}H NMR (MeOD) δ 4.12 (t, *J* = 7.3 Hz, 2H, C$\underline{H}_2$-N), 3.99 (t, *J* = 7.3 Hz, 2H, C$\underline{H}_2$-N), 3.26 (t, *J* = 5.8 Hz, 2H, C$\underline{H}_2$-NH), 3.19 (t, *J* = 6.0 Hz, 2H C$\underline{H}_2$-NH), 2.05 – 1.98 (m, 6H, bicycle), 1.94 – 1.86 (m, 6H, bicycle), 1.75 (p, *J* = 6.4 Hz, 2H -C$\underline{H}_2$-), 1.62 (p, *J* = 6.6 Hz, 2H, -C$\underline{H}_2$-), 1.47 (s, 9H, Boc), 1.39 (hd, *J* = 7.3, 3.6 Hz, 4H, -C$\underline{H}_2$CH$_3$), 0.99 (dt, *J* = 7.3, 7.3 Hz, 6H, -C$\underline{H}_3$).

^{13}C NMR (MeOD) δ 180.4 (NHC=O), 162.1(C), 158.8 (NHC=O), 156.0 (C=O), 152.8 (C=O), 149.4 (C), 108.2 (C), 80.2 (C), 44.2 (C$\underline{H}_2$), 42.1 (C$\underline{H}_2$), 41.3 (C), 40.7 (C), 40.1(C$\underline{H}_2$), 34.9 (C$\underline{H}_2$), 31.2(C$\underline{H}_2$), 31.0 (C$\underline{H}_2$ bicycle), 29.2(C$\underline{H}_2$ bicycle), 28.8 (Boc), 21.1 (C$\underline{H}_2$), 20.8 (C$\underline{H}_2$) , 14.2 (C$\underline{H}_3$), 14.1 (C$\underline{H}_3$).



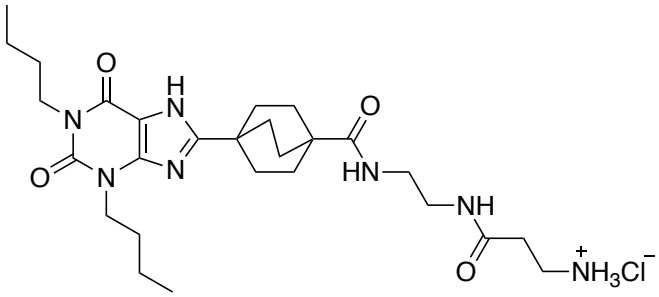
***tert*-Butyl (3-((2-(4-(1,3-dibutyl-2,6-dioxo-2,3,6,7-tetrahydro-1*H*-purin-8-yl)bicyclo[2.2.2]octane-1-carboxamido)ethyl)amino)-3-oxopropyl)carbamate (5.29).** Compound **5.27** (274 mg, 1.0 equiv) was treated with 4 M HCl in dioxane (1 mL) following general procedure C to yield the corresponding 3-((2-(4-(2,6-dioxo- 1,3-dibutyl-2,3,6,7-tetrahydro-1H-purin-8-yl)bicyclo[2.2.2]octane-1- carboxamido)ethyl)amino)-3-oxopropan-1-aminium chloride intermediate (**5.28**) (quantitative), which was used for the next step without any further purification. Following general procedure A, 3-((2-(4-(2,6-dioxo-1,3-dibutyl-2,3,6,7-tetrahydro-1H- purin-8-yl)bicyclo[2.2.2]octane-1-carboxamido)ethyl)amino)-3-oxo- propan-1-aminium chloride intermediate (**5.28**) (225 mg, 1.0 equiv) was treated with with DIPEA (234 μL, 1.4 mmol, 10.0 equiv) and reacted with a solution of Boc-β-Ala-OH (85 mg, 449 μmol, 1.0 equiv), COMU (211 mg, 494 μmol, 1.10 equiv) in DMF (1 mL). Purification by automated flash column chromatography using a gradient of 97:3 to 90:10 DCM/MeOH gave the title compound as off-white solid (250 mg, 88%).

LC-MS *m/z* calcd for $C_{32}H_{52}N_7O_6$ $[MH]^+$: 630.30, found 630.30 t_R = 3.13 min (Method A)

^{1}H NMR (MeOD) δ 4.11 (t, *J* = 7.3 Hz, 2H, C$\underline{H}_2$-N), 3.99 (t, *J* = 6.1 Hz, 2H, C$\underline{H}_2$-N), 3.30 (s, 4H (C$\underline{H}_2$)$_2$NH), 2.37 (t, *J* = 6.7 Hz, 2H C$\underline{H}_2$NH), 2.05 – 1.98 (m, 6H, bicycle), 1.94 – 1.87 (m, 6H, bicycle), 1.74 (p, *J* = 5.4 Hz, 2H, -C$\underline{H}_2$-), 1.62 (p, *J* = 4.9 Hz, 2H, -C$\underline{H}_2$-), 1.45 (s, 9H, Boc), 1.38 (hd, *J* = 7.4, 2.5 Hz, 4H, -C$\underline{H}_2$CH$_3$), 0.98 (q, *J* = 7.2 Hz, 6H, , -C$\underline{H}_3$).

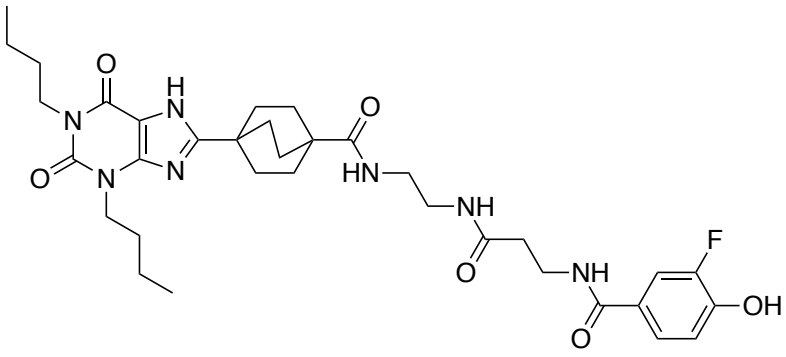
^{13}C NMR (MeOD) δ 179.1 (NHC=O), 173.1 (NHC=O), 160.8 (C), 157.0 (NHC=O), 154.6 (C=O), 151.4 (C=O), 148.1(C), 106.8 (C), 78.8 (C), 42.8 (C$\underline{H}_2$), 40.7 (C$\underline{H}_2$), 39.2 (C$\underline{H}_2$), 38.7 (C$\underline{H}_2$), 38.6 (C$\underline{H}_2$), 36.7 (C$\underline{H}_2$), 36.2 (C$\underline{H}_2$), 33.5

($\underline{C}H_2$), 29.8 ($\underline{C}H_2$), 29.8 ($\underline{C}H_2$), 29.6 ($\underline{C}H_2$ bicycle), 27.8 ($\underline{C}H_2$ bicycle), 27.4 (Boc), 19.8($\underline{C}H_2$), 19.4($\underline{C}H_2$), 12.8 ($\underline{C}H_3$), 12.7 ($\underline{C}H_3$).



3-((2-(4-(1,3-Dibutyl-2,6-dioxo-2,3,6,7-tetrahydro-1*H*-purin-8-yl)bicyclo[2.2.2]octane-1-carboxamido)ethyl)amino)-3-oxopropan-1-aminium chloride (5.30). Compound **5.29** (70 mg, 0.11 mmol, 1.0 equiv) was treated with 4 M HCl in dioxane (1 mL) following general procedure C to yield the title intermediate as HCl salt (quantitative), which was used for the next step without any further purification.

LC-MS *m/z* calcd for $C_{27}H_{44}N_7O_4$ $[MH]^+$: 530.30, found 530.30 t_R = 2.47 min (Method A)



4-(1,3-Dibutyl-2,6-dioxo-2,3,6,7-tetrahydro-1*H*-purin-8-yl)-*N*-(2-(3-(3-fluoro-4-hydroxybenzamido)propanamido)ethyl)bicyclo[2.2.2]octane-1-carboxamide (5.31). 3-fluoro-4-hydroxybenzoic acid (16 mg, 102 μmol 1.01 equiv.) was dissolved in DMF (0.5 mL) and reacted with COMU (53 mg, 123 μmol, 1.10 equiv.) in the presence of DIPEA (54 μL, 307 μmol, 3 equiv.). To the resulting mixture was added a solution of dibutyl-2,6-dioxo-2,3,6,7-tetrahydro-1*H*-purin-8-yl)bicyclo[2.2.2]octane-1-carboxamido)ethyl)amino)-3-oxopropan-1-aminium chloride (**5.30**) (59 mg,

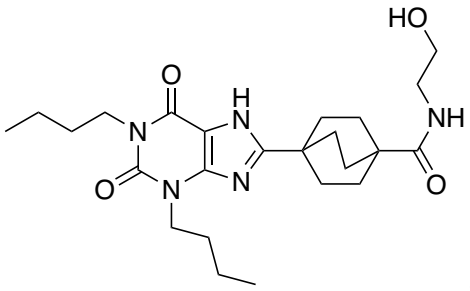
111 μmol, 1.0 equiv.) in DMF (0.5 mL). The resulting solution was stirred at 90 °C for 1 h. Upon completion of the reaction monitored by LCMS, the solvent was removed under reduced pressure and the resulting residue was dissolved in EtOAc and washed with water (2x10 mL). The organics were collected, dried over anhydrous $MgSO_4$, filtered and evaporated to dryness. The resulting residue was purified by automated flash column chromatography with DCM/MeOH on a gradient of 94: 6 % to 90: 10 %. The title compound was obtained as off-white solid (39 mg, 53%).

LC-MS *m/z* calcd for $C_{34}H_{47}FN_7O_6$ $[MH]^+$: 668.30, found 668.30 t_R = 2.96 min, purity > 99% (Method A)

^{1}H NMR (MeOD) δ 7.58 (dd, *J* = 11.9, 2.1 Hz, 1H, Ar-H), 7.53 (dd, *J* = 8.4, 2.2 Hz, 1H, Ar-H), 6.95 (t, *J* = 8.5 Hz, 1H, Ar-H), 4.10 (t, *J* = 7.3 Hz, 2H, C$\underline{H}_2$-N), 3.97 (t, *J* = 6.9 Hz, 2H, C$\underline{H}_2$-N), 3.62 (t, *J* = 6.7 Hz, 2H, -C$\underline{H}_2$), 3.30 (s, 4H, (C$\underline{H}_2$)$_2$NH), 2.50 (t, *J* = 6.7 Hz, 2H, -C$\underline{H}_2$), 2.01 – 1.93 (m, 6H, bicycle), 1.89 – 1.82 (m, 6H, bicycle), 1.73 (p, *J* = 6.8 Hz, 2H, -C$\underline{H}_2$), 1.60 (p, *J* = 6.2 Hz, 2H, -C$\underline{H}_2$), 1.37 (hd, *J* = 7.4, 3.3 Hz, 4H, -C$\underline{H}_2$), 0.97 (q, *J* = 7.3 Hz, 6H-C$\underline{H}_3$).

^{13}C NMR (MeOD) δ 180.5 (NHC=O), 174.5 (NHC=O), 168.73 (d, *J* = 2.2 Hz, NHC=OAr), 162.1(C), 156.0 (C=O), 152.8 (C=O), 152.4 (d, *J* = 241.5 Hz, $\underline{C}$F), 149.86 (d, *J* = 13.0 Hz, $\underline{C}$OH), 149.4 (C), 126.88 (d, *J* = 5.4 Hz, CO$\underline{C}$-Ar), 125.15 (d, *J* = 3.1 Hz, $\underline{C}$H-Ar), 118.43 (d, *J* = 3.0 Hz, $\underline{C}$H-Ar), 116.32 (d, *J* = 20.1 Hz, $\underline{C}$H-Ar), 108.2 (C), 79.5, 44.2 ($\underline{C}$H$_2$), 42.1 ($\underline{C}$H$_2$), 40.6($\underline{C}$ bicycle), 40.1($\underline{C}$H$_2$), 37.7 ($\underline{C}$H$_2$), 36.9 ($\underline{C}$H$_2$), 34.9 ($\underline{C}$ bicycle), 31.2 ($\underline{C}$H$_2$), 31.2 ($\underline{C}$H$_2$), 31.0 ($\underline{C}$H$_2$ bicycle), 29.2 ($\underline{C}$H$_2$ bicycle), 21.2 ($\underline{C}$H$_2$), 20.8 ($\underline{C}$H$_2$), 14.2 ($\underline{C}$H$_3$), 14.1 ($\underline{C}$H$_3$).

^{19}F NMR (377 MHz, MeOD) δ -138.6.

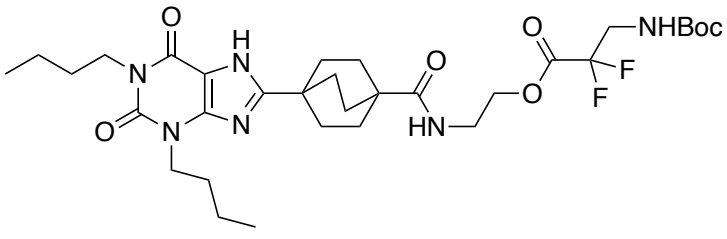


4-(1,3-Dibutyl-2,6-dioxo-2,3,6,7-tetrahydro-1*H*-purin-8-yl)-*N*-(2-hydroxyethyl)bicyclo[2.2.2]octane-1-carboxamide (5.23). Following general procedure A, to a stirring solution of (2,6-dioxo-1,3-dibutyl-2,3,6,9-tetrahydro-1H- purin-8-yl) bicyclo [2.2.2] octane-1-carboxylic acid (**5.17**) (100 mg, 240 μmol, 1 equiv), DIPEA (50 μL, 288 μmol, 1.20 equiv) and COMU (113 mg, 264 μmol, 1.10 equiv) and DMF (1.5 mL) was added ethanolamine (29 μL, 480 μmol, 2 equiv). Purification by automated flash column chromatography using a gradient of 96:4 to 90:10 DCM/MeOH gave the title pure compound as an off-white solid (58 mg, 53%).

LC-MS *m/z* calcd for $C_{24}H_{38}N_5O_4$ $[MH]^+$: 460.30, found 460.30 t_R = 2.94 min (Method A)

^{1}H NMR ($CDCl_3$) δ 6.19 (t, *J* = 6.1 Hz, 1H, NH), 4.12 (t, *J* = 7.4 Hz, 2H, CH_2-N), 4.04 (t, *J* = 7.4 Hz, 2H, CH_2-N), 3.73 (t, *J* = 5.0 Hz, 2H, CH_2), 3.46 (dt, *J* = 5.2 Hz, 2H, CH_2), 2.13 – 2.02 (m, 6H, bicycle), 1.96 – 1.86 (m, 6H, bicycle), 1.73 (p, *J* = 6.7 Hz, 2H, CH_2), 1.64 (p, *J* = 6.7 Hz, 2H, CH_2), 1.37 (h, *J* = 7.4 Hz, 4H, CH_2), 0.94 (dt, *J* = 9.3, 7.4 Hz, 6H, CH_3).

^{13}C NMR ($CDCl_3$) δ 178.3 (NHC=O), 160.8 (C), 155.4 (C=O), 151.0 (C=O), 148.6 (C), 106.9 (C), 62.3 (CH_2), 43.6 (C), 42.4 (CH_2), 41.6 (C), 39.0 (CH_2), 33.8 (CH_2), 30.2 (CH_2), 30.1 (CH_2), 29.9 (CH_2 bicycle), 28.4 (CH_2 bicycle), 20.4 (CH_2), 19.9 (CH_2), 13.9 (CH_3), 13.8 (CH_3).



2-(4-(1,3-Dibutyl-2,6-dioxo-2,3,6,7-tetrahydro-1*H*-purin-8-

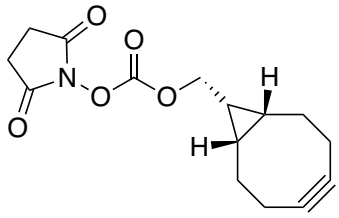
yl)bicyclo[2.2.2]octane-1-carboxamido)ethyl 3-((tert-butoxycarbonyl)amino)-2,2-difluoropropanoate (5.24). Under N_2, to a solution of 4-(1,3-Dibutyl-2,6-dioxo-2,3,6,7-tetrahydro-1*H*-purin-8-yl)-*N*-(2-hydroxyethyl)bicyclo[2.2.2]octane-1-carboxamide (**5.23**) (58 mg, 126 µmol, 1.0 equiv) in anhydrous DCM (3 mL) were added in sequence, 3-((*tert*-butoxycarbonyl)amino)-2,2-difluoropropanoic acid (**5.12**) (31 mg, 189 µmol, 1.5 equiv), DCC (52 mg, 256 µmol, 2.0 equiv) and DMAP (4.6 mg, 39 µmol, 0.3 equiv). The resulting mixture was stirred at rt overnight. Purification by automated flash column chromatography on a linear gradient of 98:2 to 96:4 DCM/MeOH afforded the title compound as colourless resin (60 mg, 71%).

LC-MS *m/z* calcd for $C_{32}H_{49}F_2N_6O_7$ $[MH]^+$: 667.30, found 667.30 t_R = 3.30 min (Method A)

^{1}H NMR ($CDCl_3$) δ 12.07 (br s, 1H, NH xanthine), 6.89 (t, *J* = 5.8 Hz, 1H, -N<u>H</u>), 5.18 (t, *J* = 6.9 Hz, 1H, -N<u>H</u>), 4.36 (t, *J* = 5.5 Hz, 2H, C<u>H</u>$_2$O), 4.12 (t, *J* = 6.4 Hz, 2H, C<u>H</u>$_2$ C<u>H</u>$_2$-N), 4.04 (t, *J* = 7.4 Hz, 2H C<u>H</u>$_2$-N), 3.76 (td, *J* = 11.9, 6.9 Hz, 2H, CF_2C<u>H</u>$_2$-N), 3.52 (q, *J* = 5.1 Hz, 2H, C<u>H</u>$_2$), 2.10 – 2.02 (m, 6H, bicycle), 1.96 – 1.88 (m, 6H, bicycle), 1.74 (p, *J* = 6.1 Hz, 2H, C<u>H</u>$_2$), 1.65 (p, *J* = 6.6 Hz, 2H, C<u>H</u>$_2$), 1.41 (s, 9H, Boc), 1.36 (hd, *J* = 11.7, 4.4 Hz, 4H, C<u>H</u>$_2$), 0.94 (dt, *J* = 10.8, 7.3 Hz, 6H C<u>H</u>$_3$).

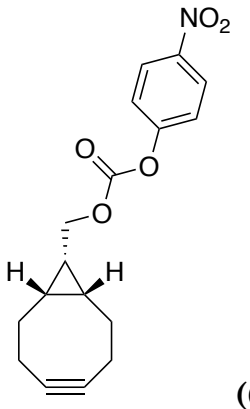
^{13}C NMR ($CDCl_3$) δ 177.8 (NHC=O), 162.81 (t, *J* = 32.5 Hz, CF_2<u>C</u>=O), 161.2 (C), 156.0 (NHC=O), 155.5 (C=O), 151.2(C), 148.9(C), 113.16 (t, *J* = 252.1 Hz, <u>C</u>F_2), 107.0(C), 81.1 (C), 66.4(<u>C</u>H$_2$O), 43.94 (t, *J* = 29.9 Hz, CF_2<u>C</u>H$_2$), 43.6 (<u>C</u>H$_2$), 41.6 (<u>C</u>H$_2$), 39.0 (<u>C</u>), 38.3(<u>C</u>H$_2$), 33.9 (C), 30.4 (<u>C</u>H$_2$), 30.2 (<u>C</u>H$_2$), 30.2 (<u>C</u>H$_2$ bicycle), 28.4(<u>C</u>H$_2$ bicycle), 28.3 (Boc), 20.4 (<u>C</u>H$_2$), 20.0 (<u>C</u>H$_2$), 14.0 (<u>C</u>H$_3$), 13.9 (<u>C</u>H$_3$).

^{19}F NMR (377 MHz, $CDCl_3$) δ -111.5.



((1*R*,8*S*,9*s*)-Bicyclo[6.1.0]non-4-yn-9-yl)methyl (2,5-dioxopyrrolidin-1-yl) carbonate.[362] (1*R*,8*S*,9*s*)-bicyclo[6.1.0]non-4-yn-9-ylmethanol (BCN-OH) (32 mg, 213µmol, 1.0 equiv) was dissolved in anhydrous CH_3CN (1 mL). To the resulting mixture was added DIPEA (15 µL, 850 µmol, 4.0 equiv) and the solution was cooled to 0 ^{O}C under N_2 (balloon). To the mixture was added *N*,*N*-disuccinimidyl carbonate (82 mg, 320 µmol, 1.50 equiv) and the resulting solution was stirred at rt for 6 h. Purification by automated flash column chromatography on a linear gradient of cyclohexane/(3:1 EtoAC/IPA) 90:10 to 80:20afforded the title product as off-white resin (10 mg, 16%).

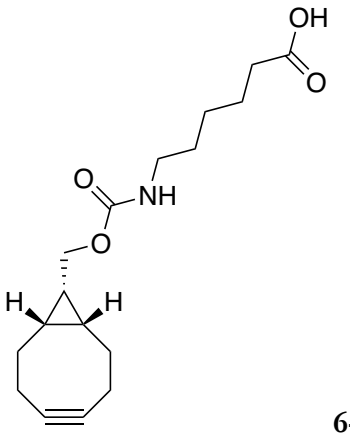
^{1}H NMR ($CDCl_3$) δ 4.45 (d, *J* = 8.3 Hz, 2H, C$\underline{H}_2$O), 2.84 (s, 4H, (C$\underline{H}_2$)$_2$CO), 2.36 – 2.18 (m, 6H, cyclooctine- C$\underline{H}_2$), 1.62 – 1.53 (m, 2H, cyclooctine- C$\underline{H}_2$), 1.49 (p, *J* = 8.2 Hz, 1H, CH_2C$\underline{H}$), 1.10 – 1.00 (m, 2H, C$\underline{H}$).



((1*R*,8*S*,9*s*)-Bicyclo[6.1.0]non-4-yn-9-yl)methyl (4-nitrophenyl) carbonate.[363] (1*R*,8*S*,9*s*)-bicyclo[6.1.0]non-4-yn-9-ylmethanol (BCN-OH) (50 mg, 333 µmol, 1.0 equiv) was dissolved in anhydrous DCM (1 mL). While under N_2 (balloon), to the resulting mixture was added pyridine (67 µL, 832 µmol, 2.5 equiv), followed by 4-nitrophenyl chloroformate (84 mg, 416 µmol, 1.25 equiv). Upon completion of the reaction (25 min), the reaction mixture was quenched with sat. NH_4Cl (5 mL) and the resulting aqueous layer was extracted with DCM (3x 5 mL). Organic layer was separated, dried over anhydrous $MgSO_4$, filtered and

concentrated to dryness. Purification by automated column chromatography on a linear gradient of cyclohexane/EtoAC 100:0 to 80:20 afforded the title product as colourless resin (61 mg, 58%).

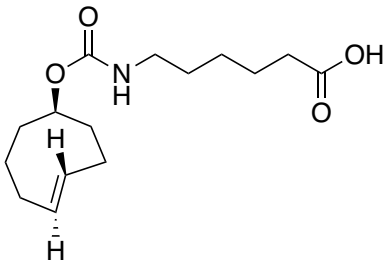
^{1}H NMR ($CDCl_3$) δ 8.26 (d, *J* = 8.9 Hz, 2H, Ar-H), 7.37 (d, *J* = 8.9 Hz, 2H, Ar-H), 4.39 (d, *J* = 8.3 Hz, 2H, CH_2O), 2.37 – 2.17 (m, 6H, cyclooctine-CH_2), 1.65 – 1.53 (m, 2H, cyclooctine- CH_2), 1.49 (p, *J* = 8.1 Hz, 1H, CH_2CH), 1.09 – 0.99 (m, 2H, CH).



6-(((((1*R*,8*S*,9*s*)-Bicyclo[6.1.0]non-4-yn-9-yl)methoxy)carbonyl)amino)hexanoic acid.[363] ((1*R*,8*S*,9*s*)-Bicyclo[6.1.0]non-4-yn-9-yl)methyl (4-nitrophenyl) carbonate (x) (61 mg, 193 μmol, 1.0 equiv) was added into a flame-dried RBF and was diluted with anhydrous DMF (0.7 mL) while under a stream of N_2. To the solution was added NEt_3 (108 μL, 774 μmol, 4 equiv), followed by 6-aminohexanoic acid (46 mg, 348 μmol, 1.80 equiv) added in one portion. The flask was wrapped in foil and stirred under N_2 at rt for 20 h. After that time the solution was diluted with H_2O and extracted with EtOAc (2x5 mL). The aqueous layer was acidified with 6% acetic acid (until pH = 3-4) and extracted with DCM (3x 7 mL). The organic layers were combined and concentrated to dryness. Purification by automated column chromatography using a linear gradient of cyclohexane/(3:1 EtoAC/IPA) 80:20 to 50:50 afforded the title product as colourless oil (35 mg, 59%).

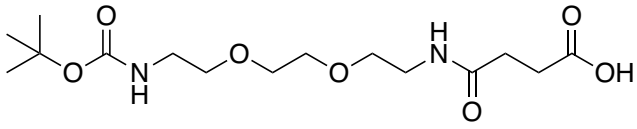
^{1}H NMR ($CDCl_3$) δ 4.75 (t, *J* = 5.8 Hz, 1H, NH), 4.13 (d, *J* = 8.0 Hz, 2H, CH_2O), 3.16 (q, *J* = 6.8 Hz, 2H, $NHCH_2$), 2.34 (t, *J* = 7.4 Hz, 2H, CH_2CO), 2.30 – 2.14 (m, 6H, cyclooctine- CH_2), 1.70 – 1.46 (m, 6H, cyclooctine- CH_2+

C<u>H</u>$_2$ linker), 1.39 – 1.29 (m, 3H, CH$_2$C<u>H</u> + C<u>H</u>$_2$ linker), 0.93 (t, *J* = 9.9 Hz, 2H, C<u>H</u> cyclopropyl).



(*R*,*E*)-6-(((Cyclooct-4-en-1-yloxy)carbonyl)amino)hexanoic acid (5.38).[341] *trans*-Cyclooctene-NHS (TCO-NHS) (13 mg, 49 μmol, 1.0 equiv) was added into a flame-dried RBF and was diluted with anhydrous DMF (0.7 mL) while under a stream of N_2. To the solution was added NEt_3 (27 μL, 195 μmol, 4 equiv), followed by 6-aminohexanoic acid (12 mg, 88 μmol, 1.80 equiv) added in one portion. The flask was wrapped in foil and stirred under N_2 at rt for 20 h. After that time the solution was diluted with H_2O and extracted with EtOAc (2x5 mL). The aqueous layer was acidified with 6% acetic acid (until pH = 3-4) and extracted with DCM (3x 7 mL). The organic layers were combined and concentrated to dryness. Purification by automated column chromatography using a linear gradient of cyclohexane/(3:1 EtoAC/IPA) 60:40 to 20:80 afforded the title product as colourless oil (10 mg, 16%).

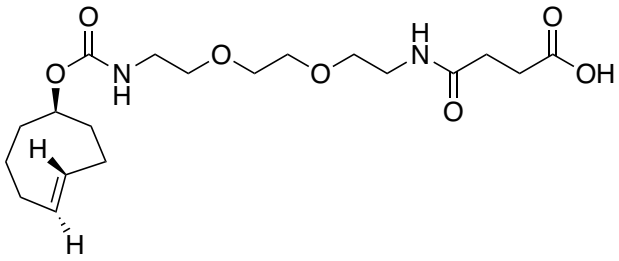
^{1}H NMR (MeOD) δ 5.59 (ddd, *J* = 21.9, 7.5, 1.8 Hz, 1H, alkene-H), 5.47 (ddd, *J* = 16.0, 10.7, 3.5 Hz, 1H, alkene-H), 4.29 (dt, *J* = 9.1, 4.4 Hz, 1H, OC<u>H</u>), 3.06 (t, *J* = 6.9 Hz, 2H, C<u>H</u>$_2$NH), 2.34 (m, 3H, cyclooctene-C<u>H</u>$_2$), 2.28 (t, *J* = 7.4 Hz, 2H, C<u>H</u>$_2$CO), 2.01 – 1.88 (m, 4H, cyclooctene-C<u>H</u>$_2$), 1.77 – 1.66 (m, 2H, cyclooctene-C<u>H</u>$_2$), 1.60 (m, 3H, C<u>H</u>$_2$+ cyclooctene-C<u>H</u>), 1.52 – 1.44 (m, 2H, C<u>H</u>$_2$), 1.39 – 1.32 (m, 2H, C<u>H</u>$_2$).



2,2-Dimethyl-4,15-dioxo-3,8,11-trioxa-5,14-diazaoctadecan-18-oic acid (5.33). At 0 ^{O}C, to the mono protected amine (0.200 g, 0.8 mmol, 1 equiv) in chloroform (7 mL) was added succinic anhydride (81 mg, 1 equiv). The resulting solution was warmed to rt and stirred for 12 h. The solvent was removed under

reduced pressure to afford the crude product as pale yellow oil. Purification by automated flash column chromatography using a linear gradient of cyclohexane/(3:1 EtoAC/IPA) 65:35 to 25:75 afforded the title product as colourless oil (120 mg, 43%).

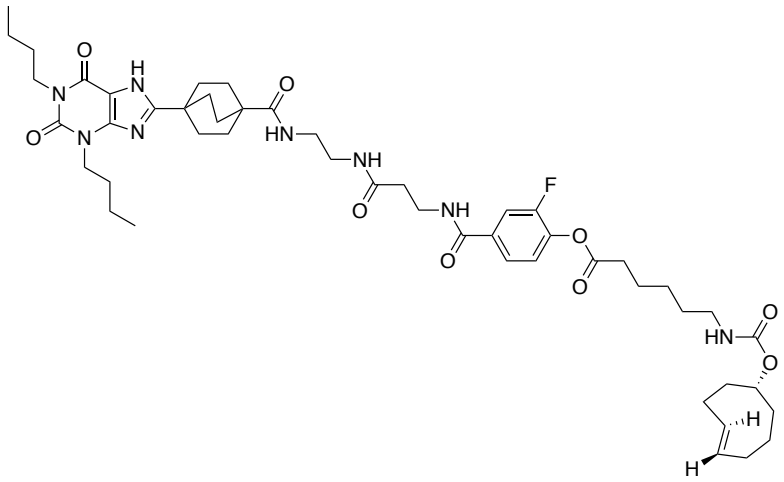
^{1}H NMR ($CDCl_3$) δ 7.45 (s, 1H, -NH), 6.90 (s, 1H, -NH), 3.61 (s, 4H, $O(CH_2)_2O$), 3.54 (q, *J* = 5.1 Hz, 4H, OCH_2), 3.44 (q, *J* = 5.1 Hz, 2H, CH_2), 3.32 (t, *J* = 5.1 Hz, 2H, CH_2), 2.70 – 2.63 (t, *J* = 5 Hz, 2H, CH_2), 2.50 (t, *J* = 4.5 Hz, 2H, CH_2), 1.45 (s, 9H, Boc).



(*R*,*E*)-1-(Cyclooct-4-en-1-yloxy)-1,12-dioxo-5,8-dioxa-2,11-diazapentadecan-15-oic acid (5.36). 2,2-Dimethyl-4,15-dioxo-3,8,11-trioxa-5,14-diazaoctadecan-18-oic acid (**5.33**) was treated with 4 M HCl in dioxane (1 mL) at rt for 1 h. Removal of the solvent with high vacuum, followed by three cycles of Et_2O evaporation, afforded the title amine as its HCl salt, which was used for the subsequent step without further purification. Following the method described for compound (**5.38**), *trans*-Cyclooctene-NHS (TCO-NHS) (11 mg, 47 μmol, 1.0 equiv) was reacted with 2-(2-(2-(3-carboxypropanamido)ethoxy)ethoxy)ethan-1-aminium chloride (**5.34**) (30 mg, 1.10 equiv) in the presence of NEt_3 (8 equiv). Purification by automated column chromatography using a linear gradient of cyclohexane/(3:1 EtoAC/IPA) 60:40 to 15:85 afforded the title product as colourless oil (6 mg, 36%).

^{1}H NMR (MeOD) δ 5.62 (ddd, *J* = 16.7, 10.0, 4.7 Hz, 1H, alkene-H), 5.49 (ddd, *J* = 16.4, 7.9, 3.2 Hz, 1H, alkene-H), 4.38 – 4.29 (m, 1H, OCH), 3.65 – 3.60 (m, 4H, $O(CH_2)_2O$), 3.57 – 3.51 (m, 4H, OCH_2), 3.37 (t, *J* = 5.5 Hz, 2H, CH_2), 3.27 (q, *J* = 5.1 Hz, 2H, CH_2), 2.60 (t, *J* = 6.8 Hz, 2H, $COCH_2$), 2.49 (t, *J* = 6.9 Hz, 2H, $COCH_2$), 2.35 (dq, *J* = 9.7, 4.9 Hz, 3H, cyclooctene-CH_2),

2.04 – 1.88 (m, 4H, cyclooctene-C$\underline{H}_2$), 1.80 – 1.68 (m, 2H, cyclooctene-C$\underline{H}_2$), 1.66 – 1.55 (m, 1H, cyclooctene-C$\underline{H}_2$).



4-((3-((2-(4-(1,3-Dibutyl-2,6-dioxo-2,3,6,7-tetrahydro-1*H*-purin-8-yl)bicyclo[2.2.2]octane-1-carboxamido)ethyl)amino)-3-oxopropyl)carbamoyl)-2-fluorophenyl (*R*,*E*)-6-(((cyclooct-4-en-1-yloxy)carbonyl)amino)hexanoate (5.32c). Following general procedure B, 3-fluoro-4-hydroxybenzamido congener (**5.31**) (2.24 mg, 3.32 μmol, 1 equiv) was converted to the TCO conjugate **5.32c**. Purification by RP-HPLC (Method C) gave, after lyophilization, the title compound as a off-white solid (1 mg, 32%).

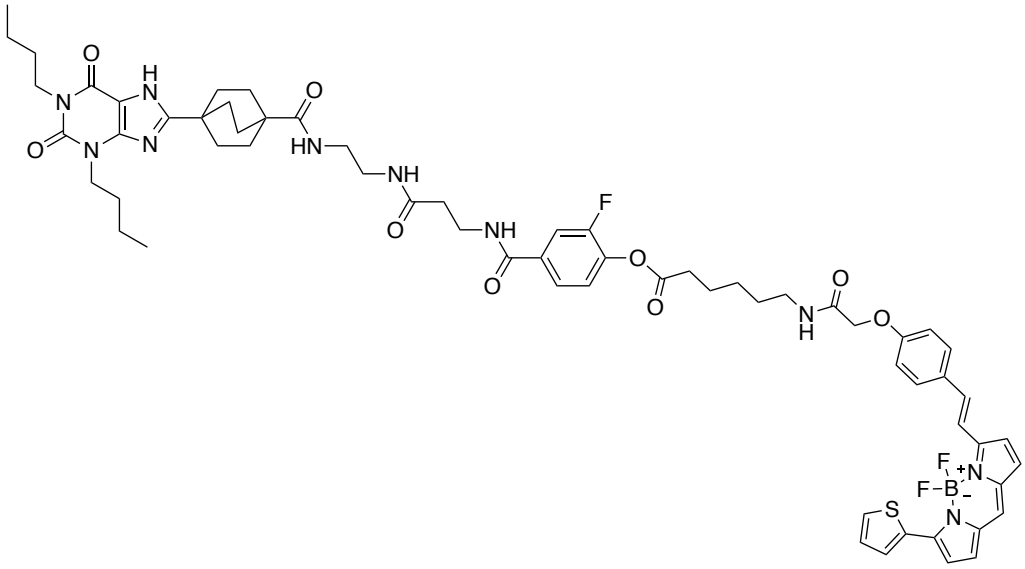
LC-MS *m/z* calcd for $C_{49}H_{70}FN_8O_9$ $[MH]^+$: 933.50, found 933.50 t_R = 3.31 min (Method A)

^{1}H NMR ($CDCl_3$) δ 7.68 (d, *J* = 9.7 Hz, 1H, Ar-H) , 7.63 (d, *J* = 8 Hz, 1H, Ar-H), 7.53 (d, *J* = 10.4 Hz, 1H, Ar-H), 7.17 (t, *J* = 7.9 Hz, 1H, N$\underline{H}$CO), 6.54 (br s, 1H, N$\underline{H}$CO), 6.34 (br s, 1H, N$\underline{H}$CO), 5.57 (ddd, *J* = 21.8, 15.1, 6.6 Hz, 1H, alkene-H), 5.48 (ddd, *J* = 15.6, 9.0, 2.8 Hz, 1H, alkene-H), 4.65 (s, 1H, N$\underline{H}$CO), 4.38-4.30 (m, 1H, OC$\underline{H}$), 4.10 (t, *J* = 7.3 Hz, 2H, C$\underline{H}_2$-N), 4.01 (t, *J* = 7.3 Hz, 2H, C$\underline{H}_2$N), 3.72 (q, *J* = 5.7 Hz, 2H C$\underline{H}_2$NH), 3.46 – 3.37 (m, 4H, (C$\underline{H}_2$)$_2$NH), 3.21-3.13 (m, 2H, C$\underline{H}_2$NH), 2.64 (t, *J* = 7.3 Hz, 2H, COC$\underline{H}_2$), 2.52 (t, *J* = 5.7 Hz, 2H, COC$\underline{H}_2$), 2.37-2.31 (m, 2H, cyclooctene-C$\underline{H}_2$), 1.97 – 1.90 (m, 8H, bicycle + cyclooctene-C$\underline{H}_2$), 1.85 – 1.79 (m, 6H, bicycle), 1.77 – 1.60 (m, 12H cyclooctene-C$\underline{H}_2$ + linker C$\underline{H}_2$), 1.58 – 1.51 (m,

2H, C<u>H</u>$_2$), 1.48 – 1.42 (m, 2H, C<u>H</u>$_2$), 1.37 (qd, *J* = 7.3, 4.4 Hz, 4H, C<u>H</u>$_2$), 0.94 (dt, *J* = 10.4, 7.3 Hz, 6H, C<u>H</u>$_3$).

HRMS (TOF ES$^+$) calcd for $C_{49}H_{70}FN_8O_9$ $[MH]^+$: 933.5244, found 933.5226; calcd for $C_{49}H_{69}FN_8NaO_9$ $[M+Na]^+$: 955.5064, found 955.5037.

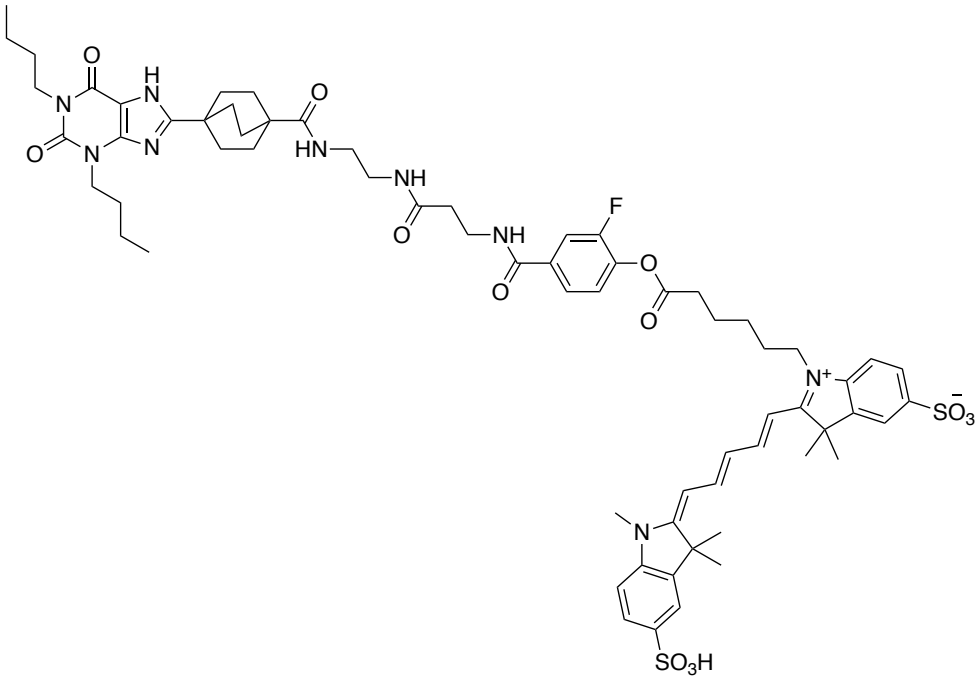
Analytical RP-HPLC t_R = 19.04 min, purity > 99% (Method E).



4-((3-((2-(4-(1,3-Dibutyl-2,6-dioxo-2,3,6,7-tetrahydro-1*H*-purin-8-yl)bicyclo[2.2.2]octane-1-carboxamido)ethyl)amino)-3-oxopropyl)carbamoyl)-2-fluorophenyl (*E*)-6-(2-(4-(2-(5,5-difluoro-7-(thiophen-2-yl)-5*H*-4*l*^{4},5*l*^{4}-dipyrrolo[1,2-c:2',1'-*f*][1,3,2]diazaborinin-3-yl)vinyl)phenoxy)acetamido)hexanoate (5.32a). Following general procedure B, 3-fluoro-4-hydroxybenzamido congener (5.31) (2.06 mg, 3.09 μmol, 1 equiv) was converted to the BODIPY 630/650-X conjugate **5.32a**. Purification by RP-HPLC (Method C) gave, after lyophilization, the title compound as a off-white solid (0.7 mg, 19%).

HRMS (TOF ES$^+$) calcd for $C_{63}H_{73}BF_3N_{10}O_9S$ $[MH]^+$: 1213.5322, found 1213.5263;

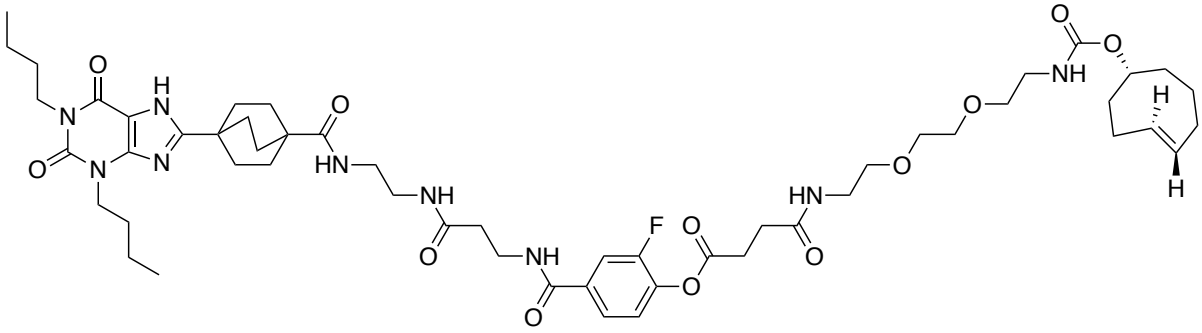
Analytical RP-HPLC t_R = 20.24 min, purity > 98% (Method E).



1-(6-(4-((3-((2-(4-(1,3-Dibutyl-2,6-dioxo-2,3,6,7-tetrahydro-1*H*-purin-8-yl)bicyclo[2.2.2]octane-1-carboxamido)ethyl)amino)-3-oxopropyl)carbamoyl)-2-fluorophenoxy)-6-oxohexyl)-3,3-dimethyl-2-((1*E*,3*E*)-5-((*E*)-1,3,3-trimethyl-5-sulfoindolin-2-ylidene)penta-1,3-dien-1-yl)-3*H*-indol-1-ium-5-sulfonate (5.32b). Following general procedure B, 3-fluoro-4-hydroxybenzamido congener (**5.31**) (0.98 mg, 1.47 μmol, 1 equiv) was converted to the SulfoCy5 conjugate **5.32b**. Purification by RP-HPLC (Method C) gave, after lyophilization, the title compound as an off-white solid (1.42 mg, 75%).

HRMS (TOF ES$^-$) calcd for $C_{66}H_{81}FN_9O_{13}S_2$ $[MH]^-$: 1290.5385, found 1290.5345

Analytical RP-HPLC t_R = 15.72 min, purity > 98% (Method E).



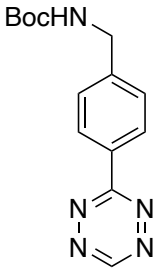
4-((3-((2-(4-(1,3-Dibutyl-2,6-dioxo-2,3,6,7-tetrahydro-1*H*-purin-8-yl)bicyclo[2.2.2]octane-1-carboxamido)ethyl)amino)-3-oxopropyl)carbamoyl)-2-fluorophenyl (*R*,*E*)-1-(cyclooct-4-en-1-yloxy)-1,12-dioxo-5,8-dioxa-2,11-diazapentadecan-15-oate (5.32d). Following general procedure B, 3-fluoro-4-hydroxybenzamido congener (**5.31**) (6.67 mg, 9.99 μmol, 1 equiv) was converted to the PEG-TCO conjugate **5.32d**. Purification by RP-HPLC (Method C) gave, after lyophilization, the title compound as an off-white solid (3.02 mg, 29%).

LC-MS *m/z* calcd for $C_{53}H_{77}FN_9O_{12}$ $[MH]^+$: 1050.57, found 1050.80 t_R = 3.12 min (Method A)

^{1}H NMR (400 MHz, $CDCl_3$) δ 7.68 (d, *J* = 2.0 Hz, 1H, Ar-H), 7.61 (d, *J* = 8.6 Hz, 1H, Ar-H), 7.54 (t, *J* = 6.0 Hz, 1H, Ar-H), 7.21 (t, *J* = 7.4 Hz, 1H, NHCO), 6.67 (br s, 1H, NHCO), 6.52 (br s, 1H, NHCO), 6.32 (br s, 1H, NHCO), 5.58 (ddd, *J* = 17.7, 8.5, 4.2 Hz, 1H, alkene-H), 5.48 (ddd, *J* = 15.6, 9.6, 3.3 Hz, 1H, alkene-H), 5.12 (br s, 1H, NHCO), 4.33 (br s, 1H, NHCO), 4.09 (t, *J* = 7.3 Hz, 2H, CH_2-N), 4.00 (t, *J* = 7.5 Hz, 2H, CH_2-N), 3.73 (q, *J* = 5.8 Hz, 2H, CH_2NH), 3.61 – 3.49 (m, 7H, CH_2), 3.48 – 3.39 (m, 6H, CH_2), 3.35 – 3.27 (m, 2H, CH_2), 3.04 – 2.94 (m, 2H, CH_2), 2.65 (t, *J* = 6.7 Hz, 2H, CH_2), 2.51 (t, *J* = 5.8 Hz, 2H, CH_2), 2.38 – 2.29 (m, 2H, cyclooctene-CH_2), 2.03 – 1.94 (m, 2H, cyclooctene-CH_2), 1.93 – 1.81 (m, 8H, bicycle + cyclooctene-CH_2), 1.77 – 1.71 (m, 8H, bicycle + cyclooctene-CH_2), 1.67 – 1.57 (m, 10H, cyclooctene-CH_2 + 2xCH_2 butyl, over integrating for 4H due to the presence of water peak at 1.66 ppm following freeze drying), 1.37 (hd, *J* = 7.4, 2.7 Hz, 4H, CH_2), 0.95 (dt, *J* = 9.4, 7.3 Hz, 6H, CH_3).

HRMS (TOF ES$^+$) calcd for $C_{53}H_{77}FN_9O_{12}$ $[MH]^+$: 1050.5670, found 1050.5656; calcd for $C_{53}H_{76}FN_9NaO_{12}$ $[MH]^+$: 1072.5490, found 1072.5491

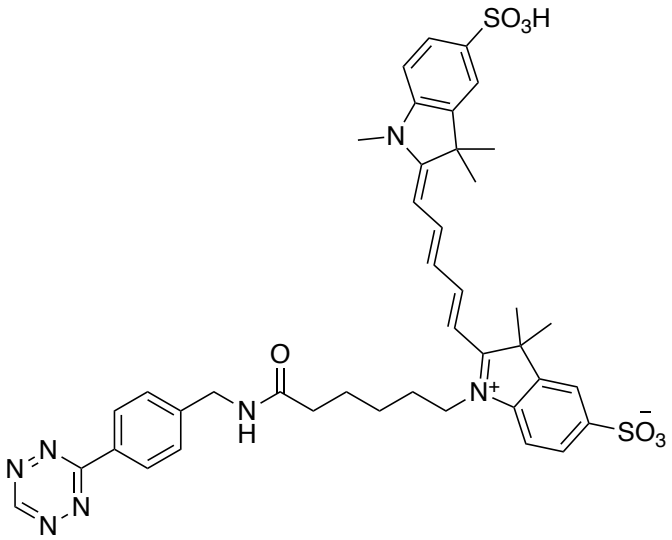
Analytical RP-HPLC t_R = 17.24 min, purity > 98% (Method E).



***tert*-Butyl (4-(1,2,4,5-tetrazin-3-yl)benzyl)carbamate.**[364] In a sealed vessel**,** hydrazine monohydrate (1.024 mL) was added to a stirring suspension of *tert*-butyl (4-cyanobenzyl)carbamate (98 mg, 0.42 mmol, 1 equiv), formamidine acetate (0.421 g, 4.05 mmol, 9.60 equiv) and $Zn(OTf)_2$ (77 mg, 0.5 equiv) in dioxane at rt. The resulting suspension was heated to 60 ^{O}C in a sealed vessel for 3 days. After that time the reaction mixture was cooled to rt and the vessel was gently evacuated. The reaction mixture was diluted with EtOAc (10 mL) and washed with 1 M HCl (10 mL). The organic phase was dried over $MgSO_4$, filtered and concentrated to dryness. The resulting crude was dissolved in a mixture of DCM/AcOH (1:1, 5 mL) and $NaNO_2$ (0.582 g, 8.44 mmol) was added slowly over a period of 15 min during which time the reaction turned bright red. The nitrous fumes were chased with active air purge and the reaction was then diluted with DCM (25 mL). The mixture was washed with $NaHCO_3$ (25 mL) and the aqueous phase extracted with DCM (2x 10 mL). The organic phase was concentrated to dryness and purified by automated column chromatography with 20 % EtOAc in cyclohexane. Title compound was obtained as pink solid (11 mg, 9%).

LC-MS *m/z* calcd for $C_{14}H_{18}N_5O_2$ $[MH]^+$: 288.50, found 288.50 t_R = 2.97 min (Method A)

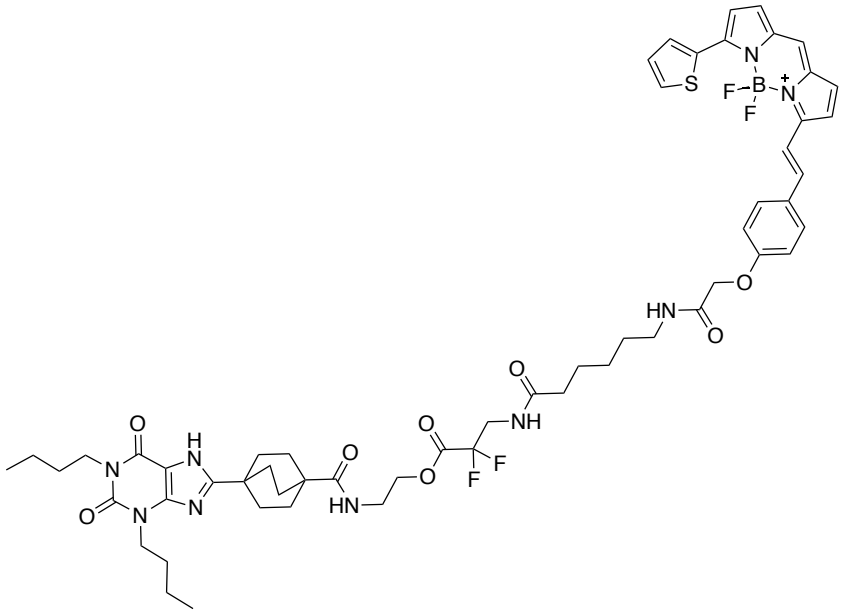
^{1}H NMR ($CDCl_3$) δ 10.23 (s, 1H C<u>H</u>-Tz), 8.62 (d, *J* = 7.4 Hz, 2H, Ar-<u>H</u>), 7.55 (d, *J* = 8.3 Hz, 2H, Ar-<u>H</u>), 5.01 (br s, 1H NH), 4.47 (d, *J* = 6.0 Hz, 2H, C<u>H</u>$_2$-Ar), 1.49 (s, 9H, Boc).



1-(6-((4-(1,2,4,5-Tetrazin-3-yl)benzyl)amino)-6-oxohexyl)-3,3-dimethyl-2-((1*E*,3*E*)-5-((*E*)-1,3,3-trimethyl-5-sulfoindolin-2-ylidene)penta-1,3-dien-1-yl)-3*H*-indol-1-ium-5-sulfonate. *tert*-Butyl (4-(1,2,4,5-tetrazin-3-yl)benzyl)carbamate (x) was treated with 4 M HCl in dioxane (1 mL) for 1 h, at rt. After that time, the reaction was completed and the solvent was evaporated to dryness to afford the title deprotected amine (x) as its HCl salt, which was used for the subsequent step without further purification. Following general procedure D, (4-(1,2,4,5-tetrazin-3-yl)phenyl)methanaminium chloride (x) was converted to the corresponding SulfoCy5 tetrazine (x). Purification by RP-HPLC (Method C) gave, after lyophilization, the title compound as a bright blue solid (0.7 mg, 33%).

HRMS (TOF ES$^-$) calcd for $C_{41}H_{44}N_7O_7S_2$ $[MH]^-$: 810.2749, found 810.2715

Analytical RP-HPLC t_R = 12.32 min, purity > 99% (Method E).



2-(4-(1,3-Dibutyl-2,6-dioxo-2,3,6,7-tetrahydro-1*H*-purin-8-yl)bicyclo[2.2.2]octane-1-carboxamido)ethyl (*E*)-3-(6-(2-(4-(2-(5,5-difluoro-7-(thiophen-2-yl)-5*H*-4*l*^{4},5*l*^{4}-dipyrrolo[1,2-*c*:2',1'-*f*][1,3,2]diazaborinin-3-yl)vinyl)phenoxy)acetamido)hexanamido)-2,2-difluoropropanoate (5.26a). 2-(4-(1,3-Dibutyl-2,6-dioxo-2,3,6,7-tetrahydro-1*H*-purin-8-yl)bicyclo[2.2.2]octane-1-carboxamido)ethyl 3-((tert-butoxycarbonyl)amino)-2,2-difluoropropanoate (**5.24**) (2.50 mg, 3.75 μmol, 1 equiv) was dissolved in anhydrous DCM (0.5 mL) and treated with 4 M HCl in dioxane (0.5 mL). The resulting mixture was stirred at rt until completion of the reaction (20 min). Solvent was removed in vacuo and the resulting residue was dissolved in anhydrous DMF (0.25 mL). To the mixture was added a previously reacted solution of BODIPY 630/650-X-CO_2H (1 mg, 1.77 μmol, 1 equiv), DIPEA (10 mg) and BEP (0.49 mg, 1.77 μmol, 1 equiv) in anhydrous DMF (0.3 mL). The resulting reaction mixture was stirred under the exclusion of light overnight at rt. Solvent was removed with high vacuum and residue was dissolved in 1:1 CH_3CN/H_2O. Purification by RP-HPLC (Method C), followed by lyophilization, afforded the pure product as blue solid (0.5 mg, 25 %).

HRMS (TOF ES$^+$) calcd for $C_{56}H_{67}BF_4N_9O_8S$ $[MH]^+$: 1112.4857, found 1112.4823; calcd for $C_{56}H_{66}BF_4N_9NaO_8S$ $[MH]^+$: 1134.4676, found 1134.4657

Analytical RP-HPLC t_R = 20.55 min, purity > 98% (Method E).

7.1.6 Molecular modelling studies

For studies performed in chapter 2, docking of preladenant to the high resolution $hA_{2A}AR$ crystal structure was performed using Schrodinger software suite (release 2018-3) and the 1.8 angstrom resolution $hA_{2A}AR$ crystal structure was imported from the Protein Data Bank (PDB = 4EIY) and was prepared with the Protein Preparation Wizard program. This involved removal of water molecules, co-crystalized head groups, with the exclusion of the co-crystalized ligand ZM241385, and the addition of hydrogen atoms. For studies performed in chapter 3, molecular docking simulation of Tonapofylline (BG9928) and **16** to the 3.2 Å resolution A_1AR crystal structure was performed using Schrödinger software suite (release 2019-2). The 3.2 Å A_1AR crystal structure in complex with the irreversible ligand DU172 was retrieved from the Protein Data Bank (PDB 5UEN) depository and was firstly prepared in PyMOL (2.2.0) as follows: one copy of the A_1AR-dimer crystal structure was removed and the covalent bond between the Y271 and the irreversible antagonist DU172 was broken to facilitate the definition of docking site during the Grid generation step. This structure was subsequently imported on Maestro and was prepared with the Protein Preparation Wizard tool. Hydrogen atoms were added. For all studies, the H-bonding network was optimized using PROPKA at pH= 7.0. The structures of the proteins were energy minimized using OPLS3 force field. The docking site was defined using Glide Grid generation with the barycenter of the co-crystallized ZM241385 or DU172 representing the centre of the grid. Preladenant, Tonapofylline, **16** and congener **4.42** were prepared for docking using LigPrep tool. Molecular docking of these ligands was performed using Glide with XP (extra precision) mode and flexible ligand sampling with no restriction applied. For all ligands the highest docking scoring pose was selected and depicted with PyMOL to include key binding interactions and distance measurements.

7.2 Pharmacology

Cell culture reagent were purchased from Sigma Chemicals (Pool, Dorset, UK) except Fetal Calf Serum (FCS) which was provided by PAA Laboratories (Teddington, Middlesex, UK). G418 and Optimem were obtained from Life Technologies (Paisley, UK). SNAP-Lumi4-Tb was obtained by Cisbio Bioassays (Bagnols-sur-Cèze, France). All plates were obtained from Corning Costar (Corning Incorporated, Corning, NY, USA) unless otherwise stated. FuGENE® transfection reagent and furimazine were purchased from Promega (Southampton, UK). Adenosine deaminase (ADA) and Hygromycin B were purchased from Roche Diagnostics (Mannheim, Germany) Ultima Gold™ scintillation cocktail, [^{3}H] DPCPX (8-cyclopentyl-1,3-dipropylxanthine, [dipropyl-2,3-^{3}H(N)], specific activity 137 Ci/mmol), and LANCE® cAMP kit were purchased from PerkinElmer Life Sciences (Glen Waverley, Australia). Adenosine receptor ligands, 8-(4-(4-(4-chlorophenyl)piperazide-1-sulfonyl)phenyl)-1-propylxanthine (PSB-603), *N*-[9-chloro-2-(2-furanyl)[1,2,4]-triazolo[1,5-*c*]quinazolin-5-yl]benzene acetamide (MRS1220), 4-(2-[7-Amino-2-(2-furyl)[1,2,4]triazolo[2,3-*a*][1,3,5]triazin-5-ylamino]ethyl)phenol (ZM241385), and *trans*-4-((2-phenyl-7*H*-pyrrolo[2,3-d]pyrimidin-4-yl)amino)cyclohexanol (SLV320) were purchased from Tocris Bioscience (Bristol, UK). 8-Cyclopentyl-1,3-dipropylxanthine (DPCPX), 5'-(*N*-ethylcarboxamido)adenosine (NECA) and all other reagents were purchased from Sigma-Aldrich (UK or Castel Hill, Australia) and were of analytical quality.

7.2.1 General Cell culture

7.2.1.1 Passaging of Cells

The cell lines were split once they had grown 80% confluency in a 75cm^2 tissue culture flask. Medium was aspirated with vacuum and the flask was washed with Dulbecco's Phosphate Buffered Saline (PBS) (2-3 mL) to remove residual FBS, which deactivates trypsin. PBS was removed and cells

were detached from the flask by employing trypsin/EDTA (1 mL). Trypsin is a serine protease which allows cell detachment from culture flask, as it hydrolyses proteins involved in cell adherence. Once detached fresh medium (10 mL) was added to the flask and the resulting mixture was collected, added to a universal vial (30 mL) and spun at 1000 rpm for five minutes. The medium was then removed and the pellet of cells was re-suspended in fresh medium (10 mL) in a universal flask and passaged into a new 75cm^2 flask containing 20 mL of fresh medium. All cell colonies were incubated at 37 °C, 5% CO_2 and the tissue culture procedures were performed in a class II laminar flow hood using sterile conditions. For experiments, 100 µL cell suspension was placed onto a haemocytometer and the number of cells, within a 1 mm^2 area, was counted (25x0.04mm^2 squares). The average number of cells was multiplied by 10000 to determine the number of cells present in 1 mL. This cell suspension was subsequently resuspended in an appropriate amount of media to give the cell density required for the experiment. For studies using HEK293 cells, plates were pre-coated with poly-D-lysine (10 µg/mL in PBS, filter sterilised using 0.2 µm filter and a 20mL syringe). Poly-D-lysine was left for 30min and washed with DMEM before seeding the cells or PBS for plate storage.

7.2.1.2 Cell Freezing

Cell from confluent T-75 flask were treated with trypsin and centrifuged as described previously. Finally, the pellet of cells was re-suspended in freezing mix composed of FCS containing 10% DMSO (filter sterilised using 0.2 µm filter and a 20mL syringe). DMSO was added to prevent the formation of big ice crystals. Consequently, 1 mL of the resulted suspension was transferred to a cryovial (Nalgene, Rochester, NY, USA) and cooled in an isopropanol-filled freezing chamber (Mr Frosty) to reduce the temperature at slow rate for 24 h. The next day, cryovials were transferred to the -80°C freezer and eventually to liquid nitrogen for long term storage.

7.2.1.3 Defrosting Cells

Cryovials containing the cells were moved from -80°C freezer to the hood and they were allowed to warm at 37°C. The cells were suspended in 10mL of fresh complete media and then spun at 1000 rpm for five minutes. The medium was removed and the pellet of cells was re-suspended in 1 mL of fresh complete medium and transferred to a T75 flask containing 20 mL of medium.

7.2.1.4 Cell lines used in the experiments

Transfection is the process of introducing DNA into a recipient eukaryotic cell and, for stable transfection, the integration of this DNA into the genome of the host cell. A CHO cell line stably expressing cAMP response element-secreted placental alkaline phosphatase (CRE-SPAP) reporter gene and the human A_2AR were generated as previously described.[127] CHO A_{2A} CRE-SPAP cell lines were cultured in Dulbecco's modified Eagle's medium (DMEM-F12) nutrient mix supported by 10% heat-inactivated FCS and 2mM L-glutamine. HEK293 cells stably expressing Nluc-A_1 and Nluc-A_3 were as described previously.[165] To generate cells stably expressing the Nluc-A_{2B} HEK293 cells were stably transfected with pcDNA-Nluc-A_{2B} using FUGENE® reagent, following the manufacturer's instructions, using 2:1 reagent:DNA ratio. Transfected cells were selected using 1 μg/mL G418. Cells were cultured in DMEM supplemented with 10% FCS. A SNAP-tagged HEK293 cell line stably expressing the human SNAP-A_2AR was generated by Dr. Laura Kilpatrick who performed the transfection, dilution cloning and isolation of a stable clone line. HEK293 cells expressing the GloSensor cAMP bionsensor (HEK293G) were obtained from Promega (Madison, United States). The HEK293 cell lines were maintained in DMEM containing 10% FCS and 2 mM L-glutamine and were grown to 70-80% confluency in 75 cm^2 tissue culture flask before splitting.

Transient Transfection of NanoLuc-tagged human A_2AR in HEK293G cell line was carried out as follows: 72 h prior the experiment cells were removed from a confluent T75 flask and centrifuged. The pellet of cells was re-suspended in 10 mL of fresh complete DMEM. Afterwards, each

CORNING® 10mmx20mm style dish was seeded with a density of $3x10^6$ cells per dish in 10 mL complete DMEM. 48 h prior the experiment transfection of the NanoLuc-tagged human A_2AR in HEK 293G cell line was carried out using a mixture of 6 µg DNA and 12 µL FuGENE®(1:2 ratio) in 880 µl OptiMEM, followed by 5 min incubation at room temperature to allow the DNA: FuGENE complex to form. After that time, the entire mixture was carefully added to the CORNING® dish and incubated at 37°C, 5%CO_2 overnight. 24h prior the experiment day cells were removed from a confluent dish and centrifuged. The pellet of cells was re-suspended in 10 mL of fresh DMEM and the resulting NanoLuc-tagged *h*A_2AR HEK293G cells were seeded in white Thermo Scientific 96-well plates at a density of 32000 cells/well and grown in normal growth medium.

Terbium labelling of SNAP-tagged $A_{2A}AR$ cells. To terbium label the SNAP-HEK293-$A_{2A}AR$ cells, cell culture media was removed from confluent SNAP-HEK293-$A_{2A}AR$ cells contained in T175 cm^2 flasks, washed once in DPBS and then incubated with 100 nM of SNAP-Lumi4-Tb in 1xLabMed buffer for 1h at 37°C, 5%CO_2. Then the terbium labelling reagent was removed and cells were washed once with ice cold 15 mL PBS. The cells were then removed from the wall of the flask by scraping and centrifuged at 2000 rpm for 10 min and the resulting cells pellets were stored at -80°C.

Membrane preparations of Terbium-labelled *SNAP-HEK293-$A_{2A}AR$ cells*. The following described steps were conducted at 4 °C to prevent receptor degradation. Thawed pellets of cells were resuspended in PBS and homogenized using an electronical homogenizer, 10x2 sec bursts. Homogenized solution of cells was centrifuged at 1500 rpm for 20 min to remove unbroken cells and nuclei. The supernatant was subsequently centrifuged at 41,415 g for 30 min. The resulting pellet was resuspended in 4 mL PBS and fully homogenized. Protein concentration was determined using a BCA protein assay and membranes were stored at -80°C until required. Before their use, frozen membranes were thawed and suspended in HBSS buffer

7.2.2 Cell culture chapter 4

Chinese Hamster Ovary FlpIn (FlpIn-CHO) cells stably expressing the human A_1AR were generated as described previously. [365] A_1AR-FlpIn-CHO cell lines were cultured in DMEM, supplemented with 10% (v/v) FBS and the selection antibiotic hygromycin B (500 μg/mL) to maintain adenosine receptor expression. Non transfected HEK293 adherent (HEK293A) cells were cultured in DMEM, supplemented with 10% (v/v) FBS. All cells were cultured at 37°C in a humidified incubator containing 5% CO_2, grown to confluence, and then seeded into 96-well culture plates at assay-specific densities. Transfection of NanoLuc-tagged human A_1AR, A_{2A}AR, A_{2B}AR and A_3AR and SNAP-tagged-hA_1AR in HEK293A cells was performed using polyethylamine (PEI) at 4:1 ratio of PEI:DNA. Cells were transfected with 3 μg DNA in 10 mm x 20 mm style dishes at a density of 5 x 10^6 cells per dish, and used 48 h following transfection.

7.2.3 Experiments

7.2.3.1 *NanoBRET-based* binding assays

All NanoBRET experiments were performed in white flat bottomed 96-well Greiner plates (Bio One, UK) precoated with Poly-D-Lysine and were read on a PheraSTAR FS plate reader (BMG Labtech) at room temperature or at 37 °C for kinetic binding experiments. The filter light emissions were read at 420nm (80 nm bandpass; donor NanoLuc emission) and 535 nm (60nm-bandpass; fluorescent ligand emission) for BYFL-labelled ligands and at 420 nm (80 nm-bandpass) and > 610 nm (longapass; fluorescent ligand emission) for the BY630/Cy5/AF647-labelled ligands. The raw BRET ratio was calculated by dividing the > 610 nm emission or 533 nm emission by the 420 nm emission. The term "raw BRET ratio" refers to the unprocessed data as no background ratio has been subtracted. In all NanoBRET binding experiments, non-specific binding was determined in the presence of 10 μM competitive antagonist selective for the adenosine receptor under investigation.

For studies described in **chapter 2**, HEK 293G cells were transiently transfected to express Nluc-A_{2A}AR. For experiments described in chapter 2, 3, 5, HEK293 cells stably/transiently expressing Nluc-AR were seeded in white 96-well plates Greiner plates (Bio One, UK) at 32000 cells/well and grown 24 h prior the day of the experiment in normal growth medium. Before the experiment, DMEM was replaced with warm HBSS. For saturation and competition assays the required concentration of fluorescent ligands and competing ligand was added at the same time. Thereafter, plates were incubated for 2 h at 37 °C. After 2 h, 10 μM furimazine (1:400 dilution; Promega) was added to each well and plates were incubated for further 5 min at 37 °C. For dissociation kinetic experiments described in chapter 5, stable NanoLuc-hA_1AR HEK293 cells were incubated with compounds for 5 h or 2 h for CA200645 (CA-XAC) at 37 °C in 96-well plates. After that time, 10 μM furimazine was added to each well and incubated at 37°C for 15 min in the dark to allow the luminescence signal to reach equilibrium. Basal BRET readings were acquired on the PheraSTAR every 30 s for 5 min. Then, 10 μM DPCPX was added manually in a 1:10 ratio and BRET readings were taken every 30 s for 60 min at 37°C. Bioluminescence emission at two different wavelengths was measured using a PHERAstar FS plate reader (BMG Labtech) at room temperature (saturation and competition binding experiments) or at 37°C (association and dissociation kinetic binding experiments).

For studies described in **chapter 4**, HEK293A cells were transiently transfected to express either the NanoLuc-tagged human A_1AR, A_{2A}AR, A_{2B}AR and A_3AR. 24 h following transfection, cells were seeded into 96-well poly-D-lysine solid white bottom plates at 40,000 cells/well and incubated overnight in serum-free DMEM. Before the experiment, DMEM was replaced with HBSS. For saturation and competition assays the required concentration of fluorescent ligand, and competing ligands, was added at the same time and the plates were then incubated at 37°C for 1 h. After 50 min incubation, 1 μM furimazine was added to each well and plates were incubated for additional 10 min (1 h total) at 37°C. For association kinetic

experiments, 1 μM furimazine was added to each well and incubated at 37°C for 15 min in the dark. The required concentration of fluorescent ligand in the presence or absence of 1 μM SLV320 (to define non-specific binding) was added simultaneously. The plates were then read immediately, with each well read once every 30 s for 60 min. Bioluminescence emission at two different wavelengths was measured at room temperature (for saturation and competition binding experiments) or at 37°C (for kinetic binding assays) using a PheraSTAR Omega plate reader (BMG Labtech).

7.2.3.2 NanoBRET Saturation Assay to Investigate A_1-A_{2A} Interactions (Chapter 4).

HEK293T cells were seeded into poly-D-lysine coated white flat bottom 96-well plates and incubated for 24 h at 37 ^{O}C, 5% CO_2. At 70-80% confluency, cells were transiently transfected with a fixed concentration of donor N-terminal tagged NanoLuc-hA_{2A}AR (0.050 μg/well) and increasing concentrations of N-terminal tagged acceptor SNAP-hA_1AR (0.0005-0.100 μg/well). All transfections were performed using FuGENE HD in Opti-MEM at 3:1 ratio of reagent to cDNA, following manufacturer's protocol. Empty p3.1zeo was used when necessary to ensure total concentration of cDNA were maintained consistent across all wells. Cells were incubated for further 24 h at 37 ^{O}C, 5% CO_2. 24 h post transfection, cells were incubated at 37 ^{O}C, 5% CO_2 for 30 min with 0.2 μM SNAP-AF488 prepared in DMEM/10%FCS. Following incubation, cells were washed 3x with pre-warmed HBSS and incubated with HBSS for 1 h at 37 ^{O}C. After this time, 10 μM furimazine (1:400 dilution) was added in each well and plates were left for 5 min in the dark at room temperature. Sequential emission measurements were taken using a PHERAStar FS plate reader using 460nm (80nm bandpass; donor NanoLuc emission) and 535nm (60nm bandpass; SNAP-Tag emission) filters. Raw BRET ratios were calculated by dividing the 535nm emission (acceptor) by the 460nm emission (donor).

7.2.3.3 *CRE-SPAP* gene transcription functional assay (performed in Chapter 2)

48 h prior the experiment day CHO CRE-SPAP A_2AR cells were seeded into clear 96-well plates and subsequently serum starved 24 h before the experiment employing DMEM-12 supplemented with 2 mM L-glutamine (serum-free media). On the day of the assay serum-free media was added to the cells and the fluorescent compounds under investigation were further added to the appropriate well at three concentrations (10 nM, 100 nM, 1000 nM), and the plates were incubated for 30 min at 37 °C, 5% CO_2. After 30 min NECA was added at increasing concentrations and the plates were incubated for further 5h at 37 °C/5% CO_2. Following 5h incubation the media was removed and replaced with 40 μL of serum-free media. The plates were further incubated for 1h at 37 °C/5% CO_2. Following 1h incubation the plates were moved to an oven at 65 °C for 30 min to degrade endogenous alkaline phosphatases. The plates were then allowed to cool to room temperature and 100 μL of 5 mM of 4-*p*-nitrophenyl phosphate in DEA buffer (100 mM Diethanolamine; 280 mM NaCl; 0.5 mM $MgCl_2.6H_2O$, pH=9.85) were added in each well and the plates incubated at 37°C for 15 min. Once the yellow colour had developed, the plates were read on the Dynex MRX plate reader which measured the absorbance at 405 nm.

7.2.3.4 HTRF Binding Kinetic of BODIPY-630/650-X conjugate *2.12* (performed in Chapter 2)

To determine the binding kinetics of fluorescent conjugate **2.12,** HEK293 SNAP-$hA_{2A}AR$ cell membranes were diluted to the required concentration (10 μg/well) in HBSS buffer containing saponin (1 mg/mL) and added to white Thermo Scientific 96-well microplates. Fluorescent conjugate **2.12** was added simultaneously at four different concentrations in the presence and absence of 10 μM ZM241385 to define non-specific binding. The plates were read immediately: each well was read every 30 s for 60 min. TR-FRET signals were acquired in a PHERAstarFS plate reader (BMG Labtech) equipped with a Homogeneous Time Resolved Fluorescence

module with excitation at 337 nm and emission 620 nm and 655 nm. HTRF ratios were calculated by dividing the acceptor signal (655 nm) by the donor signal (620 nm).

7.2.3.5 *[^{3}H] DPCPX* Radioligand binding assay (performed in Chapter 4)

A_1AR-FlpIn-CHO cells were seeded into white 96-well isoplates at 40,000 cells/well and incubated overnight. Before the experiment, DMEM was replaced with binding buffer (10 mM HEPES, 10 mM D-glucose, 145 mM NaCl, 5 mM KCl, 1 mM $MgSO_4$, 1.5 mM $NaHCO_3$, 2 mM $CaCl_2$, 1U/mL adenosine deaminase (ADA), pH 7.4) and cells were incubated with increasing concentrations of competing ligands, followed by addition of 1 nM [^{3}H] DPCPX (precise concentration in each experiments was determined by β-counting). The cells were incubated for 4 h in binding buffer at 37°C. Buffer was removed and cells were washed three times with ice-cold phosphate buffer saline (PBS, 10 mM Na_2HPO_4, 1.8 mM KH_2PO_4, 137 mM NaCl, 2.7 mM KCl), and then dissolved in Ultima Gold scintillation liquid (100 μL/well). Isoplates were sealed and allowed to incubate at RT for 1 h before radioactivity was determined by β-counting using a MicroBeta 2 LumiJET microplate counter (PerkinElmer). In all radioligand binding experiments, non-specific binding was determined in the presence of 1 μM SLV320.

7.2.3.6 cAMP functional assay

A_1AR-FlpIn-CHO cells were seeded into 96-well culture plates at 20,000 cells/well and incubated overnight. The $G_{i/o}$ protein mediated inhibition of cAMP accumulation was determined as described previously.[39] Briefly, media was removed and cells were incubated with stimulation buffer (140 mM NaCl, 5.4 mM KCl, 0.8 μM $MgSO_4$, 0.2 mM Na_2HPO_4, 0.44 mM KH_2PO_4, 1.3 mM $CaCl_2$, 5.6 mM D-glucose, 5 mM HEPES, 0.1% bovine serum albumin (BSA), 0.1 U/mL ADA, and 10 μM rolipram, pH 7.4) and incubated at 37 °C for 30 min. Inhibition of cAMP was assessed by preincubation with increasing concentrations of

antagonists for 10 min. NECA concentration response curves were performed by subsequent incubation of increasing concentrations of NECA in the presence of 3 μM forskolin for additional 30 min at 37 °C. The reactions were terminated by the addition of 50 μL ice-cold 100% ethanol. The lysis buffer (0.1% BSA, 0.3% tween-20, 5 mM HEPES, pH 7.4) was added to the cells after ethanol evaporation. Level of cAMP was detected using LANCE cAMP 384 kits (PerkinElmer) following the manufacturer's protocol and fluorescence was measured with EnVision® plate reader (PerkinElmer). Ligand concentration-response curves were normalized to the response mediated by 3 μM forskolin (0%) or buffer (100%) alone. All experiments were performed in duplicate.

7.2.3.7 Confocal Imaging studies using Zeiss LSM710

Confocal microscopy using LSM710 was performed on cells grown to 70-80 % confluence on 8-well LabteK chambered coverglass (Nunc Nalgene) pre-coated with poly-D-lysine. On the day of the experiment medium was removed and the cells were labelled for 30 min at 37 °C with 0.2 μM SNAP AF488 or AF647 as required in fresh HBSS [HEPES Balanced Salt Solution (HBSS), 25 mM HEPES, 10 mM glucose, 145 mM NaCl, 5 mM KCl, 1 mM $MgSO_4$, 2 mM sodium pyruvate, 1.3 mM $CaCl_2$ at pH 7.4]. After washing twice with HBSS the cells were treated with or without 10 μM AR competitive antagonist (DPCPX for studies with A_1 or ZM241385 for studies with A_{2A}) for 30 min at 37 °C. Following the incubation step the fluorescent ligands under investigation were added to the appropriate wells at the required concentrations.

For the experiments discussed in **Chapter 5**, HEK293T cells were seeded in 8-well plates (Nunc Lab-Tek, Thermo Fischer Scientific), pre-coated with Poly -D-Lysine, at 12, 000 cells per well in DMEM/10% FCS. 24 h post seeding, cells were transiently transfected with human SNAP-A_1. Transient transfections were carried out following manufacturer's protocol: used FuGENE HD at 3:1 ratio of reagent to cDNA with a total of 300 ng

cDNA per well. Transfection solutions were made up in Gibco Opti-MEM (Thermo Fischer Scientific), incubated at rt for 5 min and added as 11 µL per well. Cells were incubated for additional 24 h at 37 ^{O}C, 5% CO_2.
On the day of the experiment medium was removed and the cells were labelled for 30 min at 37 °C with 0.2 µM SNAP AF488 in SFM. After washing twice with SMF the cells were treated with or without 10 µM AR competitive antagonist (DPCPX for A_1, ZM241385 for $A_{2A,}$ PSB603 for A_{2B} and MRS1220 for A_3) for 30 min at 37 °C. Following the incubation step the ligand-directed probe under investigation (SulfoCy5 or TCO) (**5.32b** or **5.32d**) was added to the appropriate wells at the required concentrations and incubated for 2 h. After that time, cells were washed 4x with warm HBSS, followed by the addition of 300 µL warm HBSS and imaged. For click-chemistry reactions, after washing 4x with warm HBSS, cells pre-labelled with the corresponding *trans*-cyclooctene-conjugated ligand (TCO-**5.32d**) were subsequently treated with 1.5 µM Methyl-TetrazineSulfoCy5 (Lumiprobe, Germany) for 10 min at RT in the dark. Cells were washed 2x with warm HBSS and imaged. When required, 10 µM DPCPX was added after 2 h and cells were incubated for and additional 1 h before imaging.

For all the experiments, Live cell imaging was performed at 37 °C using a Zeiss LSM 710 laser scanning confocal microscope fitted with a Zeiss Plan-Neofluar 40 × 1.2 NA water immersion objective. A 633 nm HeNe laser was used for the excitation of BY630/650, Cy5 or AF647 respective fluorophores, and a 488/561/633 dichroic, and the emission was detected between 634 and 755 nm (laser power 5 %, laser power 7.5 % with Met-TetrSulfoCy5). A 488 nm HeNe laser was used to excite SNAP-AF488 and the emission was detected between 493 and 586 nm (laser power 5 %). The pinhole diameter (1 Airy Unit; 1.1 µm optical slice), laser power and gained remained constant in all the experiments. Images were acquired as 16-bit depth, 1024x1024 pixel resolution with a line averaging of 8 and a pixel dwell time 6.30 µs (set to 5). Imges were either processed in Zeiss ZEN 2 (blue edition) or FIJI (ImageJ) version 2.0.0 software, and linear adjustments to the brightness and contrast have been applied equally across

all the images. To obtain membrane intensity values, regions of interest were drawn by hand around the cell membranes in FIJI (ImageJ) version 2.0.0 software.

7.2.3.8 Confocal Imaging studies using Leica TCS SP8X (Chapter 4)

Transiently transfected SNAP-tagged human A_1AR HEK293 cells were grown to 80-90% confluence in a μ-Slide 8 well chambered coverslip (Ibidi GmbH, Gräfelfing, Germany) precoated with poly-D-lysine. On the day of the experiment culture media was removed and the cells were labelled for 30 min at 37 ºC with 0.2 μM SNAP AlexaFluor488 label as required in binding buffer (10 mM HEPES, 10 mM D-glucose, 145 mM NaCl, 5 mM KCl, 1 mM $MgSO_4$, 1.5 mM $NaHCO_3$, 2 mM $CaCl_2$, 1U/mL ADA, pH 7.4). After washing twice with buffer, the cells were treated with or without 10 μM SLV320 for 30 min at 37 ºC. After that time, the cells were treated with the required concentration of fluorescent ligand under investigation. Live cell imaging was performed at 37 ºC on a Leica TCS SP8 X confocal running system fitted with a HC PL APO CS2 40x/1.1 NA water immersion objective. A diode 633 laser was used for the excitation of BODIPY-630/650 and SulfoCy5 fluorophores and a beam splitter TD 488/552/638 and the emission was collected using a Hybrid Detector (HyD) (emission filter range 642-782 nm). A 488 Optically Pumped Semiconductor Laser (OPLS) was used for the excitation of the SNAP AF488 label and the emission was detected using a Hybrid Detector (HyD) (emission filter range 493-572 nm). The pinhole diameter (1 Airy Unit; 1.1 μm optical slice), laser power and gain remained constant in all the experiments. The images were captured using 1024x1024 pixel resolution, 16-bit depth, scan speed of 200 Hz with line averaging of 6. Images were processed in FIJI (ImageJ)[366] version 2.0.0 software and linear adjustments to the brightness and contrast have been applied equally across all the images.

7.2.3.9 Total Internal Reflection Fluorescence Microscopy *(TIRF-M,* Chapter 4*).*

HEK293A cells were seeded into 10 mm x 20 mm style dishes at a density of 5 x 10^6 cells per dish in complete DMEM. After 12 h, cells were transiently transfected with 2 μg cDNA of SNAP-hA_1AR using 1:4 ratio of DNA/PEI to achieve lower receptor expression levels. After 12 h, transiently transfected SNAP-hA_1AR HEK293 cells were seeded onto a poly-D-lysine-pre-coated FluoroDish™ (35 mm, 23 mm well) to 70-80 % confluency. On the day of the experiment (24 h following transfection), DMEM was removed and the cells were incubated with 0.2 μM BG-AF488 in binding buffer (10 mM HEPES, 10 mM D-glucose, 145 mM NaCl, 5 mM KCl, 1 mM $MgSO_4$, 1.5 mM $NaHCO_3$, 2 mM $CaCl_2$, 1U/mL ADA, pH 7.4) for 30 min at 37 °C. Buffer was removed and the cells were washed twice with warm binding buffer to remove any unbound BG-AF488. Subsequently, the cells were treated with or without 10 μM SLV320 for 30 min at 37 °C. After that time, the cells were treated with the required concentration of fluorescent ligand under investigation.

TIRF Imaging was performed by Mr. Cameron Nowell (Drug Discovery Biology research theme within the Monash Institute of Pharmaceutical Sciences, Australia). Images were captured on a Leica DMI6000 3D GSD TIRF microscope running LAS X version 1.9 using a HC Plan Apo 100x NA 1.43 TIRF Objective. Excitation was provided from a 633 nm laser for the BODIPY-630/650 and SulfoCy5 fluorophores. Detection was through either a 540-620 nm emission filter or 640-700nm emission filter. The TIRF field penetration depth was kept at 80 nm for all wavelengths and samples. Images were captured with an Andor iXon3 897 Ultra EM-CCD camera with exposure times and gain settings being consistent across all images. ***TIRF Image Analysis***. Analysis of TIRF images were carried out using a custom macro written in the Fiji distribution of ImageJ (Schindelin et al., 2012). In brief, the user was asked to manually outline the cell of interest. Both image channel were then filtered to remove noise (Gaussian filter-Sigma = 1) and discrete spots were extracted from the red channel using the find maxima command (prominence = 3) and displaying the same as single binary points. The extracted binary points were

used to measure the intensity in both the red and far red channel for each discrete spot.

7.2.3.10 Data Analysis

All data are represented as mean ± SEM of *n* experiments performed either in duplicate or triplicate. The *n* refers to the number of separate experiments. A separate experiment required a separate flask of cells and a separate drug dilution used throughout the experiment. The data were presented and analysed using Prism software (GraphPad Prism 7.0, 8.0, 9.0, San Diego, CA) and Excel.

Reporter Gene SPAP Assay: Antagonism by unlabeled and labelled (fluorescent) ligands of the CRE-reporter gene response (SPAP, secreted placental alkaline phosphatase) to NECA in CHO cells expressing the human A_{2A} AR was analysed. For each concentration of the antagonists, the ratio (DR, dose ratio) of NECA concentrations required to produce the same sized response in the presence and absence of the antagonist was determined. The antagonist dissociation constant (K_B) was determined by globally fitting the data to the Schild equation:

Schild : $\quad \text{Log (DR-1)} = \text{Log([B])} - \text{Log}K_B$

Where DR (dose ratio) is the ratio of the agonist concentration required to stimulate an identical response in the presence or absence of antagonist, [B]. K_B represents the equilibrium dissociation constant of the antagonist.

NanoBRET saturation binding assay. Total and nonspecific saturation binding curves were fit simultaneously using the following equation:

$$BRET\ ratio = \frac{B_{max}[B]}{B + (K_D)} + M(B) + C$$

Where B_{max} is the maximal specific binding, [B] is the concentration of fluorescent ligand in nM, K_D is the equilibrium dissociation constant in nM, M is the slope of the nonspecific binding component, C is the intercept with the y axis.

[^{3}H] DPCPX binding assay and NanoBRET competition binding assays. The competition binding curves were fit to the following equation:

$$Uninhibited\ specific\ binding = 100 - \frac{100\ x\ [A]}{[A] + (IC_{50})}$$

Where [A] is the concentration of competing drug and the IC_{50} is the molar concentration of ligand required to inhibit 50% of the specific binding of specified concentrations of fluorescent ligands or 1 nM [^{3}H] DPCPX.

The Cheng-Prusoff equation was used to correct fitted IC_{50} values to K_i values:

$$K_i = \frac{IC_{50}}{1+\frac{L}{K_D}}$$

Where L is the concentration of fluorescent ligand or [^{3}H] DPCPX in nM and K_D is the dissociation constant of fluorescent ligand or [^{3}H] DPCPX in nM. The K_D values used were calculated from the saturation binding experiments. The concentration in the assay of [^{3}H] DPCPX was directly determined by measuring DPM counts with a scintillation counter using the following equation:

$$[l] = \frac{DPM}{\frac{SA\ x\ 2.2\ x\ 10^6}{volume}}$$

Where SA is the specific activity of the radioligand in Ci/mmol and volume is the final volume of the assay in litre.

NanoBRET and HTRF kinetic binding assay. For association binding kinetics, nonspecific binding was determined at each concentration of the fluorescent ligands at each time point by adding 1 μM SLV320 for A_1AR or 10 μM ZM241385 for A_{2A}AR studies, respectively. This was subtracted from total binding to obtain specific binding measurements. The association rate (k_{on}) in M^{-1} min^{-1} and dissociation rate (k_{off}) min^{-1} constants were calculated from specific binding using the following equation:

$$k_{on} = \frac{k_{obs} - k_{off}}{[L]}$$

Where [L] is the concentration of the fluorescent conjugate in M and k_{obs} is calculated from the global fitting of the data to the following exponential association function:

$$Y = Y_{max}(1 - e^{-k_{obs}t})$$

Where Y is the specific binding at time t, Y_{max} represents the specific binding at infinite time (t) and k_{obs} is the rate constant for the observed rate of association.

The kinetic equilibrium dissociation constant (K_D) was determined from the data using the following equation:

$$K_D = \frac{k_{off}}{k_{on}}$$

cAMP Assay. Antagonism by fluorescent ligands of the NECA-induced inhibition of cAMP accumulation in FlpIn-CHO cells expressing the human A_1AR was analysed. For each concentration of the antagonists, the ratio (DR, dose ratio) of NECA concentrations required to produce the same magnitude of response in the presence and absence of the antagonist was determined. To estimate antagonist affinity values, functional interaction studies between NECA and single concentration of each antagonist in the cAMP assays were fitted to the following form of Schild regression analysis:

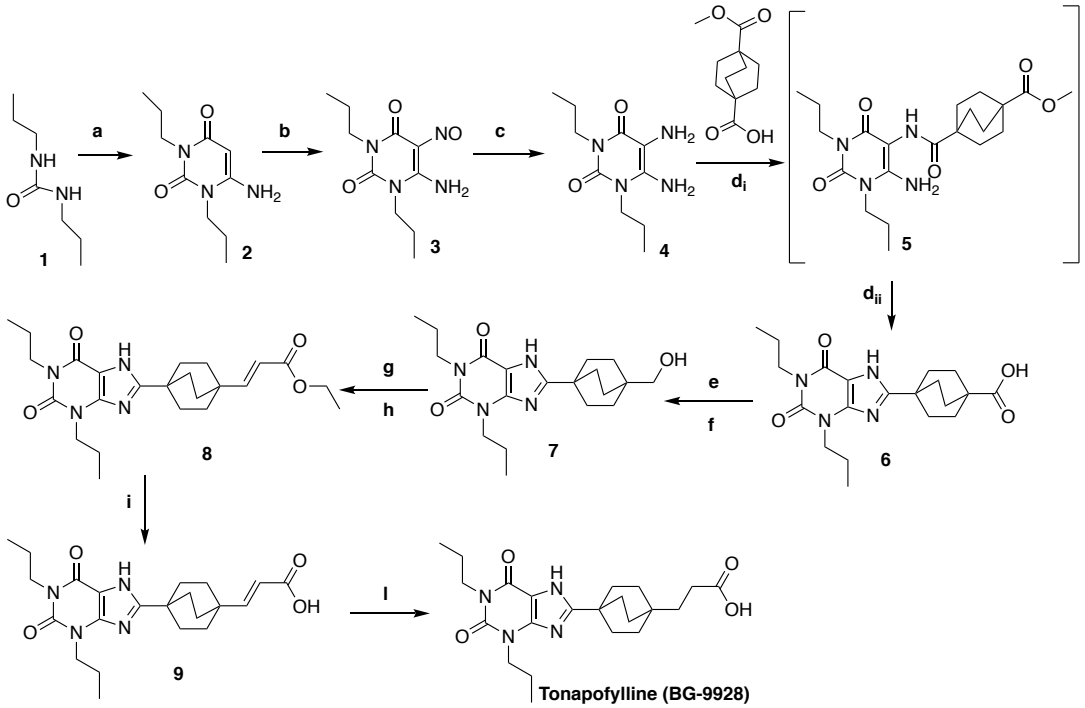
$$Response = Bottom + \frac{(\mathrm{E_{max}} - bottom)}{1 + \left(\frac{10^{-\mathrm{pEC_{50}}} \left[1 + \left[\frac{[\mathrm{B}]}{10^{-\mathrm{pA_2}}} \right]^{\mathrm{S}} \right]}{[\mathrm{A}]} \right)^{\mathrm{HillSlope}}}$$

Where pEC_{50} is the negative logarithm of the EC_{50} of NECA (A) in the absence of antagonist (B). HillSlope is the slope of the agonist curve, S is the Schild slope, pA_2 is the negative logarithm of the molar concentration of antagonist necessary to shift the agonist EC_{50} by a factor of two. The Schild slope parameter, S, was constrained to 1 and therefore the estimated pA_2 values for each antagonist are equal to the pK_B (negative logarithm of the antagonist equilibrium dissociation constant).

Appendix I

▪Supplementary Material Chapter 4

Scheme 1. Synthesis of Tonapofylline (BG9928)[a]



[a] Reagents and conditions: a) i. Cyanoacetic acid, Ac_2O, 83 °C, 2 h, ii. H_2O, 70% NaOH, rt, 50%; b) $NaNO_2$, 50% AcOH, rt, 1 h, 64%; c) $Na_2S_2O_4$, 12.5% NH_4OH, 60 °C, 30 min, 87%; d_i) 4-(methoxycarbonyl)bicyle [2.2.2] octane-1-carboxylic acid, NEt_3, HATU, CH_3CN, rt, 90 min. d_{ii}) 1.0 M KOH, propan-2-ol, reflux, 2 h, 68% (over two steps); e) MeOH, conc. H_2SO_4, reflux, 84%; f) $LiAlH_4$ (1 M in THF), anhydrous THF, 0 °C, 1 h, 97%; g) Dess-Martin periodinane, DCM, rt, 2 h, 80%; h) Triethylphosphono acetate, 1. 0 M potassium bid (trimethylsilyl)acetamide (KHDMS) in THF, anhydrous THF, 0 °C, 1 h; i) aq. LiOH, EtOH, reflux, 5 h, 30% (over two steps); l) H_2, Pd/C 10% w/w, MeOH, rt, 2 h, quantitative.

Chemistry Methods.

1,3-Dipropylurea (**1**). Propylamine (7.44 mL, 1.10 equiv.) was dissolved in anhydrous THF (20 mL) and the solution was cooled to 0 °C. Propyl isocyanate (7.63 mL, 1.0 equiv.) was added dropwise and the reaction was stirred at rt. After few seconds a white precipitate developed which was filtered off and dried to get the pure product as off-white solid (6.052 g, 97

%). ^{1}H NMR (DMSO-*d*6) δ 5.74 (t, J = 5.7 Hz, 2H), 2.92 (td, J = 7.1, 5.8 Hz, 4H), 1.35 (h, J = 7.3 Hz, 4H), 0.82 (t, J = 7.4 Hz, 6H). ^{13}C NMR (DMSO-*d*6) δ 158.1, 41.1, 23.2, 11.3.

6-Amino-1,3-dipropylpyrimidine-2,4(1H,3H)-dione (**2**). 1,3-Diisopropylurea (0.100 g, 0.6 mmol, 1.0 equiv.) was dissolved in Ac_2O (2.5 mL). To the reaction mixture was added cyanoacetic acid (64.88 mg, 1.1 equiv.). The resulting mixture was stirred at 83 °C for 2 h. The solution was then concentrated to dryness (water bath set at 80 °C) to give the crude product as brown oil (HNMR of the crude product revealed that the 2-cyano-*N*-propyl-*N*-(propylcarbamoyl)acetamide intermediate was formed. ^{1}H NMR ($CDCl_3$) δ 3.78 (s, 2H), 3.64 – 3.57 (m, 2H), 3.28 – 3.21 (m, 2H), 1.68 – 1.51 (m, 5H), 0.98 – 0.89 (m, 7H)). H_2O (2 mL x2) was added and evaporated off to remove residual Ac_2O from the reaction mixture. The crude product was then dissolved in H_2O (4.5 mL) and the resulting solution was basified with 70% NaOH (three drops). A white precipitate developed which was subsequently filtered off and washed with H_2O. The precipitate was dried under vacuum overnight (73 mg, 50%). LC-MS *m/z* calcd for $C_{10}H_{18}N_3O_2$ $[MH]^+$: 212.1, found 212.10 t_R = 3.07 min (Method A). ^{1}H NMR (DMSO-*d*6) δ 6.77 (br s, 2H), 4.64 (s, 1H), 3.73 (t, J = 8.0 Hz, 2H), 3.66 (t, J = 7.3 Hz, 2H), 1.58 – 1.40 (h, J = 7.2 Hz, 4H), 0.85 (t, J = 7.4 Hz, 3H), 0.80 (t, J = 7.5 Hz, 3H). ^{13}C NMR (DMSO-*d*6) δ 161.4, 154.5, 151.5, 75.2, 43.3, 41.4, 21.0, 11.4, 10.9.

6-Amino-5-nitroso-1,3-dipropylpyrimidine-2,4(1H,3H)-dione ***(3).*** 1,3-diisopropyl-6-amino uracil (70 mg, 1.0 equiv.) was dissolved in 50% acetic acid (1.5 mL) and the resulting solution was heated to 57 °C. To the mixture was added $NaNO_2$ (28 mg, 1.20 eq.) over 15 min. The solution from colourless turned pink and a pink precipitate formed. The reaction mixture was stirred at rt for 1h. The precipitate was collected, washed with cold water and dried to get the pure product as pink solid (51 mg, 64%). LC-MS *m/z* calcd for $C_{10}H_{17}N_4O_3$ $[MH]^+$: 241.1, found 241.10 t_R = 3.10 min (Method A). ^{1}H NMR (DMSO-*d*6) δ 13.17 (s, 1H), 9.12 (s, 1H), 3.85 (t, J = 6.9 Hz, 2H), 3.78 (t, J = 7.3 Hz, 2H), 1.60 (h, J = 6.8 Hz, 2H), 1.53 (h, J = 6.8 Hz, 2H), 0.92 – 0.84 (m, 6H). ^{3}C NMR (DMSO-*d*6) δ 159.9, 149.1, 145.4, 42.5, 42.4, 20.7, 19.7, 11.2, 10.7, (one quaternary carbon not observed),

5,6-Diamino-1,3-dipropylpyrimidine-2,4(1H,3H)-dione (***4***). To a stirred solution of 6-amino-5-nitroso-1,3-diipropylpyrimidine-2,4(1*H*, 3*H*)-dione in 12.5 % aqueous ammonium hydroxide solution (3 mL) at 60 °C was added sodium dithionite (5.7 equiv.) until a colourless solution had formed (30 min). After cooling to rt, the product was extracted with DCM (4x 20 mL). The combined organics were dried over anhydrous Na_2SO_4, filtered and evaporated to dryness to give the title product as pale yellow solid (crystalline form) (39 mg, 87%). LC-MS *m/z* calcd for $C_{10}H_{19}N_4O_2$ $[MH]^+$: 227.1, found 227.10 t_R = 2.70 min (Method A). ^{1}H NMR ($CDCl_3$) δ 5.01 (br s, 2H), 3.91 – 3.76 (m, 4H), 2.32 (br s, 2H), 1.71 (h, J = 7.5 Hz, 2H), 1.61 (h, J = 6.9 Hz, 2H), 0.96 (t, J = 7.4 Hz, 3H), 0.90 (t, J = 7.5 Hz, 3H). ^{13}C NMR ($CDCl_3$) δ 161.7, 150.4, 148.7, 95.7, 44.8, 43.2, 21.8, 21.3, 11.4, 11.3.

4-(2,6-Dioxo-1,3-dipropyl-2,3,6,9-tetrahydro-1H-purin-8-yl) bicyclo[2.2.2]octane-1-carboxylic acid (***6***)**.** To a solution of 5,6-Diamino-1,3-diisopropylpyrimidine-2,4(1*H*,3*H*)-dione (0.152 g, 1.10 equiv.) in acetonitrile (5 mL) were added 4-(methoxycarbonyl) bicyclo [2.2.2] octane-1-carboxylic acid (0.128 g, 1.0 equiv.) and NEt_3 (0.16 mL, 2 equiv.) followed by HATU (0.250 g, 1.10 equiv.). The resulting mixture was stirred at rt for 1 h 30 min. The mixture was concentrated to dryness and the crude was taken up in EtOAc and washed with 10 % citric acid. The organics were collected washed with sat. $NaHCO_3$, brine, dried over $MgSO_4$, filtered and concentrated in vacuo to give methyl 4-((6-amino-2,4-dioxo-1,3-dipropyl-1,2,3,4-tetrahydropyrimidin-5-yl)carbamoyl)bicyclo[2.2.2]octane-1-carboxylate intermediate **5** which was used for the next step without any further purification . The residue was dissolved in a mixture of propan-2-ol and 1 M KOH (2.5 mL, 4 equiv.) and heated to reflux (91°C) for 2 h. The reaction mixture was then cooled to rt and the solvent concentrated to dryness. The yellow residue was taken up in 4 mL of water and extracted with DCM. The aqueous layer was collected and acidified with conc HCl and a white precipitate formed which was collected by suction filtration and oven dried. (0.159 g, 68% over two steps). LC-MS *m/z* calcd for $C_{20}H_{29}N_4O_4$ $[MH]^+$: 389.20, found 389.20 t_R = 3.44 min (Method A). ^{1}H NMR ($CDCl_3$) δ 12.62 (s, 1H), 12.54 (br s, 1H), 4.09 (t, J = 7.1 Hz, 2H), 4.00 (t, J = 6.6 Hz, 2H), 2.04 (s, 12H), 1.80 (h, J = 7.4 Hz, 2H), 1.67 (h, J = 6.6 Hz, 2H), 0.99 – 0.90

(m, 6H). ^{13}C NMR ($CDCl_3$) δ 182.1, 161.3, 156.2, 150.7, 149.2, 106.4, 77.2, 76.8, 76.5, 45.1, 43.2, 38.5, 33.6, 29.6, 27.9, 21.2, 21.1, 11.2, 11.0.

Methyl 4-(2,6-dioxo-1,3-dipropyl-2,3,6,9-tetrahydro-1H-purin-8-yl) bicyclo[2.2.2]octane-1-carboxylate. 4-(2,6-Dioxo-1,3-dipropyl-2,3,6,9-tetrahydro-1*H*-purin-8-yl) bicyclo[2.2.2]octane-1-carboxylic acid was diluted with 6 mL of MeOH and 3 drops of conc. H_2SO_4. The resulting mixture was refluxed until complete consumption of starting material. Once the reaction was completed, the resulting solution was neutralised with sat. $NaHCO_3$ (a couple of drops). The mixture was then concentrated to dryness and the residue was taken up in EtOAc and washed with sat. $NaHCO_3$ and brine. The resulting organic layer was dried over $MgSO_4$, filtered and concentrated to dryness to give the title compound as off-white solid (74 mg, 84%). LC-MS *m/z* calcd for $C_{21}H_{31}N_4O_4$ $[MH]^+$: 403.20, found 403.20 t_R = 3.88 min (Method A). ^{1}H NMR ($CDCl_3$) δ 12.22 (s, 1H), 4.09 (t, J = 7.1 Hz, 2H), 4.03 (t, J = 6.6 Hz, 2H), 3.67 (s, 3H), 2.08 – 2.03 (m, 6H), 1.96 – 1.90 (m, 6H), 1.80 (h, J = 7.4 Hz, 2H), 1.71 (h, J = 6.6 Hz, 3H), 1.00 – 0.93 (m, 6H). ^{13}C NMR ($CDCl_3$) δ 177.9, 161.4, 155.6, 151.2, 149.0, 107.1, 51.9, 45.3, 43.3, 38.9, 33.9, 29.9, 28.2, 21.5, 11.6, 11.3.

8-(4-(Hydroxymethyl)bicyclo[2.2.2]octan-1-yl)-1,3-dipropyl-3,9-dihydro-1H-purine-2,6-dione (7). Methyl 4-(2,6-dioxo-1,3-dipropyl-2,3,6,9-tetrahydro-1*H*-purin-8-yl) bicyclo[2.2.2]octane-1-carboxylate (74 mg, 184 mmol, 1 equiv.) was dissolved in dry THF and the resulting solution was evacuated and kept inert with cycles of vacuum and nitrogen. The solution was cooled to 0 °C and stirred for 10 min. At that point $LiAlH_4$ 1.0 M sol. In THF (0.28 mL, 276 mmol 1.50 equiv.) was slowly added dropwise (little effervescence developed). The resulting mixture was stirred at 0 °C for 1 h. Completion of the reaction was checked by TLC and LC-MS. After 1 h the solution was quenched by the dropwise addition of cold H_2O, followed by the addition of a saturated solution of Rochelle's reagent/salt (*circa* 7 mL added). The solution was stirred at rt for 1h. The reaction mixture was then extracted with EtOAc (3x20 mL). The organic layer was dried over $MgSO_4$, filtered and evaporated to dryness to yield the title compound as off-white/pale pink solid (66 mg, 97%). LC-MS *m/z* calcd for $C_{20}H_{31}N_4O_3$ $[MH]^+$: 375.20, found 375.20 t_R = 3.45 min (Method A). ^{1}H NMR ($CDCl_3$) δ 12.08 (br s, 1H), 4.10 (t, J =

6.5 Hz, 2H), 4.02 (t, J = 6.9 Hz, 2H), 3.35 (s, 2H), 2.06 – 1.99 (m, 6H), 1.80 (h, J = 6.8 Hz, 2H), 1.70 (h, J = 6.6 Hz, 2H), 1.61 – 1.53 (m, 6H), 1.00 – 0.91 (m, 6H). ^{13}C NMR ($CDCl_3$) δ 161.9, 155.6, 151.3, 149.1, 106.9, 71.3, 45.3, 43.3, 34.4, 33.4, 30.3, 27.9, 21.5, 11.6, 11.3.

*4-(2,6-Dioxo-1,3-dipropyl-2,3,6,9-tetrahydro-1H-purin-8-yl) bicyclo[2.2.2]octane-1-carbaldehyde***.** To a solution of 8-(4-(Hydroxymethyl) bicyclo[2.2.2]octan-1-yl)-1,3-dipropyl-3,9-dihydro-1*H*-purine-2,6-dione (66 mg, 184 mmol, 1 equiv.) in DCM (4 mL) was added Dess -Martin periodinane (88 mg, 210 mmol, 1.20 equiv.). The reaction mixture was stirred at rt until the oxidation was complete (2 h). The mixture was subsequently filtered through a plug of basic alumina and the filtrated was washed with sat. $NaHCO_3$ (2x) and brine. The organics were collected, dried over $MgSO_4$ anhydrous, filtered and evaporated to dryness to get the product as off-white/pale pink solid (29 mg, 80%). LC-MS *m/z* calcd for $C_{20}H_{29}N_4O_3$ $[MH]^+$: 373.20, found 373.20 t_R = 3.69 min (Method A). ^{1}H NMR ($CDCl_3$) δ 12.26 (s, 1H), 9.52 (s, 1H), 4.10 (t, J = 6.2, 2H), 4.03 (t, J = 6.5 Hz, 2H), 2.14 – 2.06 (m, 6H), 1.83 – 1.76 (m, 8H), 1.73 (h, J = 7.3 Hz, 2H), 1.00 – 0.93 (m, 6H). ^{13}C NMR ($CDCl_3$) δ 205.3, 161.1, 155.7, 151.2, 149.1, 107.1, 45.4, 43.7, 43.3, 34.7, 29.5, 25.6, 21.5, 11.7, 11.3.

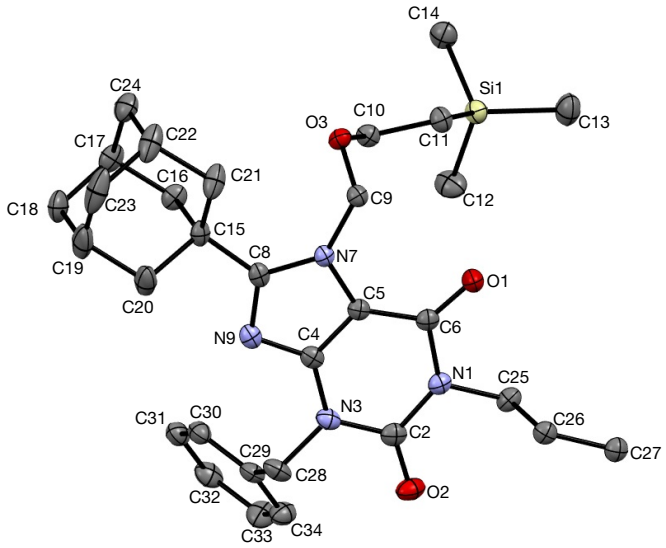
*(E)-3-(4-(2,6-dioxo-1,3-dipropyl-2,3,6,9-tetrahydro-1H-purin-8-yl) bicyclo[2.2.2]octan-1-yl)acrylic acid***.** Triethylphosphono acetate (19 mg, 86 mmol, 1.10 equiv.) was dissolved in dry THF (5 mL) and cooled to 0ºC. To the mixture was added dropwise potassium bid (trimethylsilyl)acetamide (KHDMS) 1.0 M sol. in THF (0.16 mL, 156 mmol, 2 equiv.). The resulting mixture was stirred 0 ºC for 1h. After that time, 4-(2,6-dioxo-1,3-dipropyl-2,3,6,9-tetrahydro-1*H*-purin-8-yl)bicyclo[2.2.2]octane-1-carbaldehyde (29 mg, 78 mmol, 1.0 equiv.) previously dissolved in dry THF was added and the resulting mixture was stirred at rt for 1 h. Completion of the reaction was assessed by TLC and LCMS after 1 h. The reaction mixture was then concentrated to dryness. The resulting residue was diluted in EtOH and an aqueous solution of LiOH (10.0 equiv.) was added to the mixture which was stirred at rt for 4-5 h. The solution was concentrated to dryness and the residue was taken up in water and extracted twice with EtOAc. The aqueous layer was collected and acidified with conc. HCl, and the resulting precipitate

was collected by suction filtration to give the title compound as off-white solid (14 mg, 30 %). LC-MS m/z calcd for $C_{22}H_{31}N_4O_4$ $[MH]^+$: 415.20, found 415.20 t_R = 3.60 min (Method A). ^{1}H NMR ($CDCl_3$) δ 12.34 (br s, 1H), 7.00 (d, J = 15.9 Hz, 1H), 5.83 (d, J = 15.9 Hz, 1H), 4.09 (t, J = 6.3 Hz, 2H), 4.00 (t, J = 6.7 Hz, 2H), 2.08 – 2.00 (m, 6H), 1.82 – 1.64 (m, 10H), 0.99 – 0.92 (m, 6H).

*3-(4-(2,6-Dioxo-1,3-dipropyl-2,3,6,9-tetrahydro-1H-purin-8-yl)bicyclo[2.2.2]octan-1-yl)propanoic acid (**Tonapofylline, BG9928**).* (*E*)-3-(4-(2,6-dioxo-1,3-dipropyl-2,3,6,9-tetrahydro-1*H*-purin-8-yl) bicyclo[2.2.2]octan-1-yl)acrylic acid (120 mg, 290 mmol, 1.0 equiv.) was dissolved in MeOH and to the resulting mixture was added Pd/C 10% w/w while under a stream of N_2. The resulting mixture was evacuated with cycles of N_2 and vacuum (x3). Finally, the stream of N_2 was replaced with H_2 (balloon) and the mixture was allowed to stir at rt for 2 h. Upon completion of the reaction, the solution was filtered through Celite^{RT} and the pad was washed with DCM/MeOH. The filtrate was collected and evaporated to dryness, giving the title compound as off-white solid (120 mg, 100%). LC-MS m/z calcd for $C_{22}H_{33}N_4O_4$ $[MH]^+$: 417.20, found 417.20 t_R = 3.60 min (Method A). ^{1}H NMR ($CDCl_3$) δ 11.99 (br s, 1H), 4.08 (t, J = 6.9 Hz, 2H), 3.98 (t, J = 6.5 Hz, 2H), 2.37 (t, J = 7.7 Hz, 2H), 2.00 – 1.91 (m, 6H), 1.78 (h, J = 7.4 Hz, 2H), 1.69 – 1.51 (m, 10H), 0.94 (t, J = 7.4 Hz, 6H).

Crystallography[4]

Intensity data for **4.34** was collected on a Rigaku XtalLAB Synergy at 100.0(1) K. The temperature was maintained using an Oxford Cryostream cooling device. The structures were solved by direct methods and difference Fourier synthesis.[1] The thermal ellipsoid plot was generated using the program Mercury[2] integrated within the WINGX[3] suite of programs.



Crystal data for **4.34**. $C_{31}H_{44}N_4O_3Si$, M = 548.79, T = 100.0 K, λ = 1.54184 Å, Monoclinic, space group $P2_1/c$, a = 16.3125(2) b = 13.8503(2), c =13.9346(2) *Å*, β = 109.184(1)° V = 2973.46(7) *Å*^{3}, Z = 4, D_c = 1.226 mg M^{-3} μ(Cu-Kα) 0.994 mm^{-1}, F(000) = 1184 crystal size 0.40 x 0.10 x 0.05 mm^3, 21537 reflections measured θ_{max} = 77.2°, 6133 independent reflections [R(int) = 0.0432], the final R was 0.0402 [I > 2sym(I), 5424 data] and wR(F^2) was 0.1066 (all data), GOF 1.068.

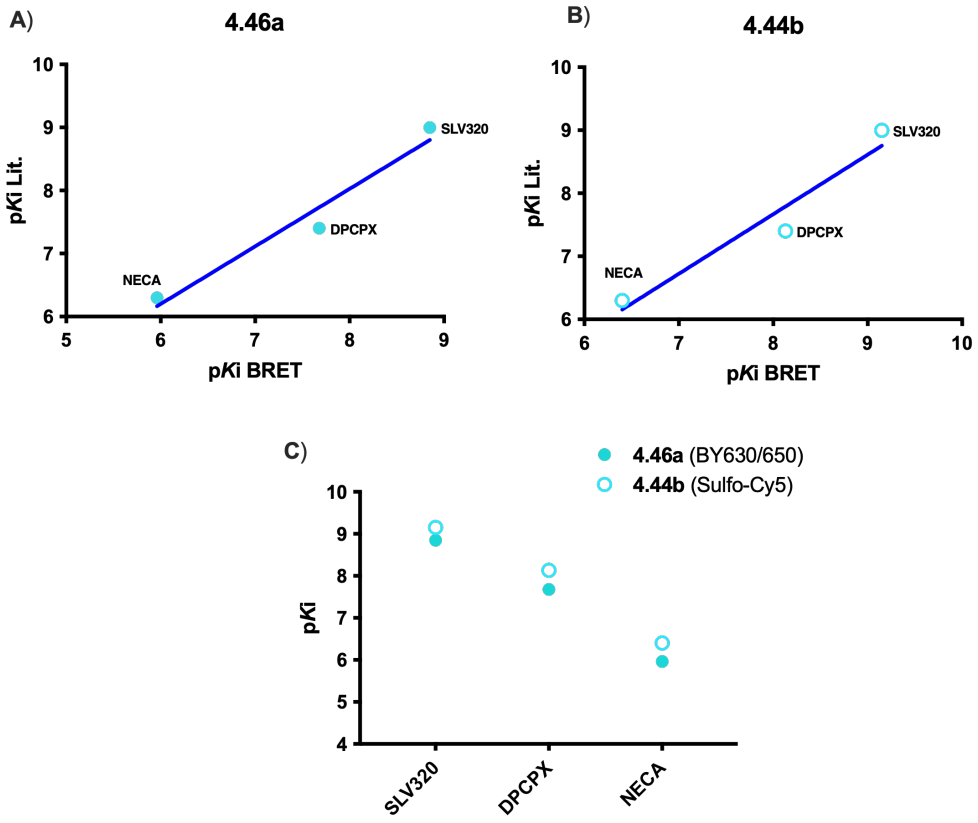


Figure S1 Regression plots comparing the p*K*i of competing ligands SLV320, DPCPX and NECA reported in the Literature to p*K*i measured in the NanoBRET competition ligand binding assay using **4.46a** (**A**) ($R^2 = 0.95$) or **4.44b** (**B**) ($R^2 = 0.94$) as fluorescent tracers. **C**) A comparison of the p*K*i values measured at the NanoLuc-hA_1AR using the two fluorescent ligands **4.46a** and **4.44b**. The values were taken from Table 6. in the main article body.

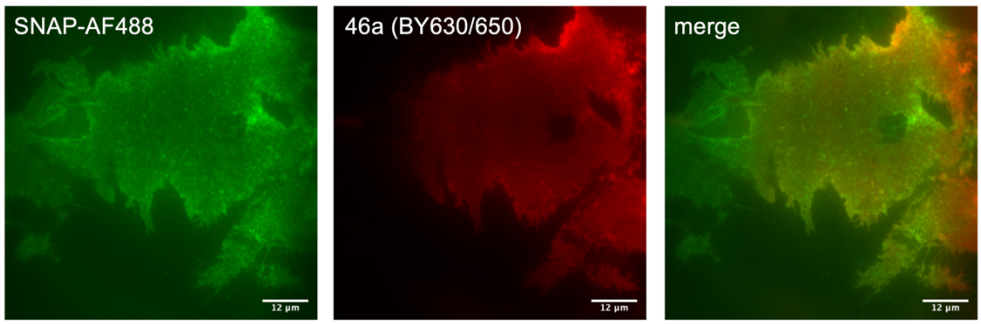


Figure S2 Total Internal Reflection Fluorescence Microscopy (TIRF-M) studies of probe **4.46a** (10 nM) performed in living HEK293 cells transiently expressing the SNAP-tagged-hA_1AR (2 μg) 24 h prior imaging to achieve low expression levels, suitable for TIRF-M studies. The frames show one individual cell. The cells were treated with 0.2 μM BG-Alexa Fluor 488 dye for 30 min at 37 °C (left frame), followed by treatment with fluorescent ligand **4.46a** (BY630/650-X) (middle frame). The right frame represents the overlay of both green and red channels.

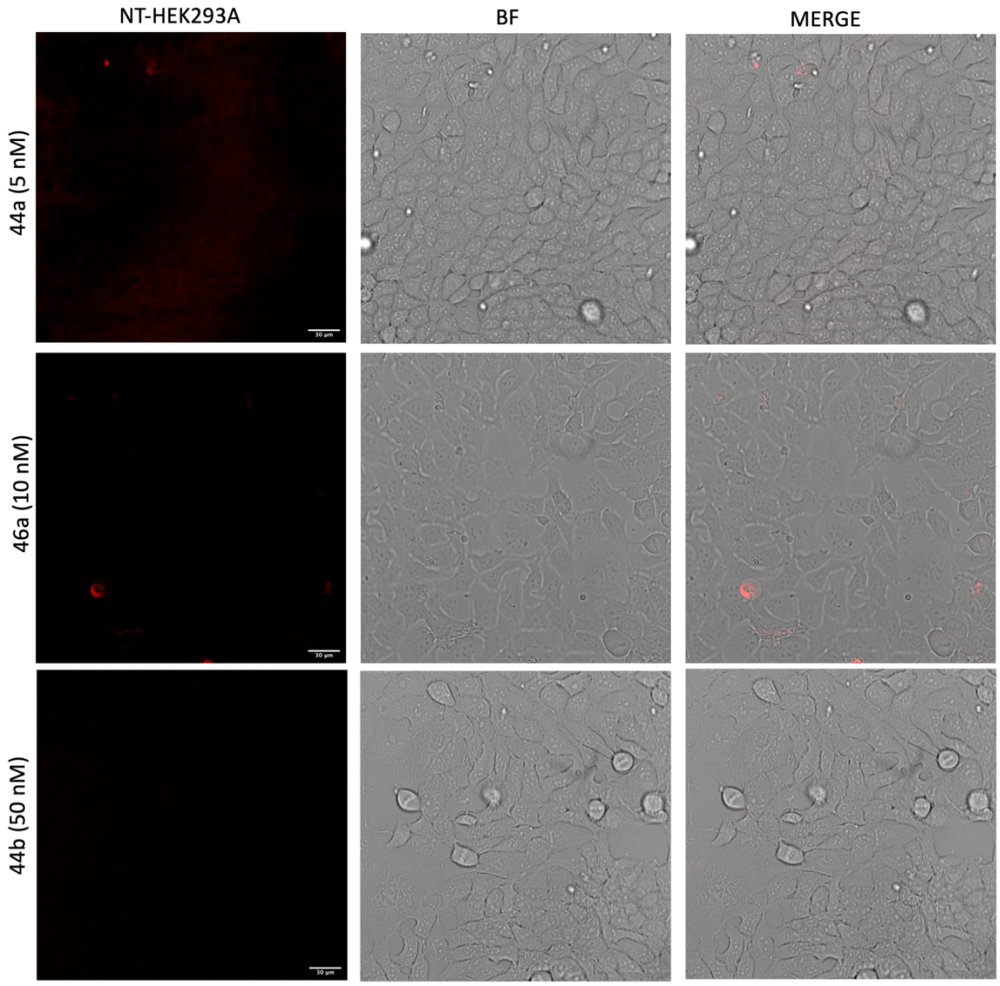


Figure S3. Live cell confocal imaging studies of probes **4.44a** (5 nM), **4.46a** (10 nM), and **4.44b** (50 nM), performed in Non-Transfected (NT) HEK293 cells at given concentrations at 37 °C. Left frames represent the far-red channel for imaging the red-shifted probes. Middle frames show the brightfield (BF) channel for the visualization of the whole cell population under focus. Right frames represent merge of the two channels. The images presented here are representative of images captured in two independent experiments. Scale bar = 30 μm

References Appendix I

[1] G. Sheldrick, *Acta Crystallogr. Section C*, **2015**, **71**, 3-8.

[2] C.F. Macrae, I.J. Bruno, J.A. Chisholm, P.R. Edgington, P. McCabe, E. Pidcock, L. Rodriguez-Monge, R. Taylor, J. van de Streek, P.A. Wood, *J. Appl. Cryst.* **2008**, *41*, 466–470.

[3] Farrugia, L. J.; *J. Appl. Cryst.* **1999**, *32*, 837-838.

[4] X-Ray crystallography was performed by Professor Jonathan M. White at the Bio21 Institute, University of Melbourne.

References

(1) Venkatakrishnan, A. J.; Deupi, X.; Lebon, G.; Tate, C. G.; Schertler, G. F.; Madan Babu, M. Molecular Signatures of G-Protein-Coupled Receptors. *Nature* **2013**, *494*, 185–194. https://doi.org/10.1038/nature11896.

(2) Sriram, K.; Insel, P. A. G Protein-Coupled Receptors as Targets for Approved Drugs: How Many Targets and How Many Drugs? *Mol. Pharmacol.* **2018**, *93* (4), 251–258. https://doi.org/10.1124/mol.117.111062.

(3) Alexander, S. P. H.; Christopoulos, A.; Davenport, A. P.; Kelly, E.; Marrion, N. V; Peters, J. A.; Faccenda, E.; Harding, S. D.; Pawson, A. J.; Sharman, J. L.; et al. The Concise Guide To Pharmacology 2017 / 18 : G Protein-Coupled Receptors. *Br. J. Pharmacol.* **2017**, *174*, S17–S129.

(4) Lagerström, M. C.; Schiöth, H. B. Structural Diversity of G Protein-Coupled Receptors and Significance for Drug Discovery. *Nat. Rev. Drug Discov.* **2008**, *7* (4), 339–357. https://doi.org/10.1038/nrd2518.

(5) Alexander, S. P. H.; Christopoulos, A.; Davenport, A. P.; Kelly, E.; Mathie, A.; Peters, J. A.; Veale, E. L.; Armstrong, J. F.; Faccenda, E.; Harding, S. D.; et al. THE CONCISE GUIDE TO PHARMACOLOGY 2019 / 20 : G Protein-Coupled Receptors. *Br. J. Pharmacol.* **2019**, *176*, S21-2141.

(6) Wootten, D.; Christopoulos, A.; Marti-Solano, M.; Babu, M. M.; Sexton, P. M. Mechanisms of Signalling and Biased Agonism in G Protein-Coupled Receptors. *Nat. Rev. Mol. Cell Biol.* **2018**, *19* (10), 638–653. https://doi.org/10.1038/s41580-018-0049-3.

(7) Hilger, D.; Masureel, M.; Kobilka, B. K. Structure and Dynamics of GPCR Signaling Complexes. *Nat. Struct. Mol. Biol.* **2018**, *25*, 4–12.

(8) Hauser, A. S.; Attwood, M. M.; Rask-Andersen, M.; Schiöth, H. B.; Gloriam, D. E. Trends in GPCR Drug Discovery: New Agents, Targets and Indications. *Nat. Rev. Drug Discov.* **2017**, *16* (12), 829–842. https://doi.org/10.1038/nrd.2017.178.

(9) Congreve, M.; de Graaf, C.; Swain, N. A.; Tate, C. G. Impact of GPCR Structures on Drug Discovery. *Cell* **2020**, *181* (1), 81–91.

https://doi.org/10.1016/j.cell.2020.03.003.

(10) Szent-Györgyi, A. N. D. A. The Physiological Activity of Adenine Compounds with Especial Reference to Their Action upon the Mammalian Heart1. *J. Physiol.* **1929**, *68* (3), 213–217. https://doi.org/https://doi.org/10.1113/jphysiol.1929.sp002608.

(11) Taisija De Gubareff and William Sleator. Effects of Caffeine On Mammalian Atrial Muscle And Its Interaction With Adexosine and Calcium. *J. Pharmacol. Exp. Ther.* **1965**, *148* (2), 202–214.

(12) SATTIN, A.; RALL, T. W. The Effect of Adenosine and Adenine Nucleotides on the Cyclic Adenosine 3', 5'-Phosphate Content of Guinea Pig Cerebral Cortex Slices. *Mol. Pharmacol.* **1970**, *6* (1), 13– 23.

(13) Fredholm, B. B. Are Methylxanthine Effects Due to Antagonism of Endogenous Adenosine? *Trends Pharmacol. Sci.* **1979**, *1*, 129–132. https://doi.org/https://doi.org/10.1016/0165-6147(79)90046-4.

(14) Fredholm, B. B.; Abbracchio, M. P. .; Burnstock, G. .; Daly, J. W.; Harden;, K.; Jacobson, K. A. .; Leff, P.; Williams, M. Nomenclature and Classification of Purinoceptors. *Pharmacol. Rev.* **1994**, *46* (2), 143–156.

(15) Fredholm, B. B.; IJzerman, A. P.; Jacobson, K.; Klotz, K. N.; Linden, J. International Union of Pharmacology. XXV. Nomenclature and Classification of Adenosine Receptors. *Pharmacol. Rev.* **2001**, *53* (4), 527–552. https://doi.org/10.1124/pr.110.003285.1.

(16) Calker, D. van; Müller, M.; Hamprecht, B. Adenosine Regulates Via Two Different Types of Receptors, the Accumulation of Cyclic Amp in Cultured Brain Cells. *J. Neurochem.* **1979**, *33* (5), 999–1005. https://doi.org/10.1111/j.1471-4159.1979.tb05236.x.

(17) Daly, J. W.; Butts-Lamb, P.; Padgett, W. L. Subclasses of Adenosine Receptors in the Central Nervous System" Interaction with Caffeine and Related Methylxanthines. *Cell. Mol. Neurobiol.* **1983**, *3* (1), 69–80.

(18) Schulte, G.; Fredholm, B. B. Human Adenosine A(1), A(2A), A(2B), and A(3) Receptors Expressed in Chinese Hamster Ovary Cells All Mediate the Phosphorylation of Extracellular-Regulated Kinase 1/2. *Mol. Pharmacol.* **2000**, *58* (3), 477–482. https://doi.org/10.1124/mol.58.3.477.

(19) Verzijl, D.; IJzerman, A. P. Functional Selectivity of Adenosine Receptor Ligands. *Purinergic Signal.* **2011**, *7* (2), 171–192. https://doi.org/10.1007/s11302-011-9232-0.

(20) Borea, P. A.; Gessi, S.; Merighi, S.; Vincenzi, F.; Varani, K. Pharmacology of Adenosine Receptors: The State of the Art. *Physiol. Rev.* **2018**, *98* (3), 1591–1625. https://doi.org/10.1152/physrev.00049.2017.

(21) Jacobson, K. A. and Gao, Z.-G. Adenosine Receptors as Therapeutic Targets. *Nat. Rev. Drug Discov.* **2006**, *49* (5), 247–264. https://doi.org/10.1038/nrd1983.

(22) Schulte, G.; Fredholm, B. B. Signalling from Adenosine Receptors to Mitogen-Activated Protein Kinases. *Cell. Signal.* **2003**, *15* (9), 813–827. https://doi.org/10.1016/S0898-6568(03)00058-5.

(23) Linden, J. Adenosine in Tissue Protection and Tissue Regeneration. *Mol. Pharmacol.* **2005**, *67* (5), 1385–1387. https://doi.org/10.1124/mol.105.011783.

(24) Borea, P. A.; Gessi, S.; Merighi, S.; Varani, K. Adenosine as a Multi-Signalling Guardian Angel in Human Diseases: When, Where and How Does It Exert Its Protective Effects? *Trends Pharmacol. Sci.* **2016**, *37* (6), 419–434. https://doi.org/10.1016/j.tips.2016.02.006.

(25) Antonioli, L.; Csóka, B.; Fornai, M.; Colucci, R.; Kókai, E.; Blandizzi, C.; Haskó, G. Adenosine and Inflammation: What's New on the Horizon? *Drug Discov. Today* **2014**, *19* (8), 1051–1068. https://doi.org/10.1016/j.drudis.2014.02.010.

(26) Palczewski, K.; Kumasaka, T.; Hori, T.; Behnke, C. A.; Motoshima, H.; Fox, B. A.; Le Trong, I.; Teller, D. C.; Okada, T.; Stenkamp, R. E.; et al. Crystal Structure of Rhodopsin: A G Protein-Coupled Receptor. *Science,* **2000**, *289*, 739–745. https://doi.org/10.1126/science.289.5480.739.

(27) Rasmussen, S. G. F.; Choi, H. J.; Rosenbaum, D. M.; Kobilka, T. S.; Thian, F. S.; Edwards, P. C.; Burghammer, M.; Ratnala, V. R. P.; Sanishvili, R.; Fischetti, R. F.; et al. Crystal Structure of the Human B2 Adrenergic G-Protein-Coupled Receptor. *Nature* **2007**, *450*, 383–387. https://doi.org/10.1038/nature06325.

(28) Rasmussen, S. G. F.; Devree, B. T.; Zou, Y.; Kruse, A. C.; Chung, K. Y.; Kobilka, T. S.; Thian, F. S.; Chae, P. S.; Pardon, E.; Calinski, D.; et al. Crystal Structure of the β 2 Adrenergic Receptor-Gs Protein Complex. *Nature* **2011**, *477*, 549–557. https://doi.org/10.1038/nature10361.

(29) Jaakola VP, Griffith MT, Hanson MA, Cherezov V, Chien EY, Lane JR, Ijzerman AP, S. R. The 2.6 Angstrom Crystal Structure of a Human A_{2A} Adenosine Receptor Bound to an Antagonist. *Science,* **2008**, *322* (2), 1211–1218. https://doi.org/10.1126/science.1164772.

(30) Xu, F.; Wu, H.; Katritch, V.; Han, G. W.; Jacobson, K. A.; Gao, Z. G.; Cherezov, V.; Stevens, R. C. Structure of an Agonist-Bound Human A_{2A} Adenosine Receptor. *Science,* **2011**, *332* (6027), 322–327. https://doi.org/10.1126/science.1202793.

(31) Gutiérrez-De-Terán, H.; Massink, A.; Rodríguez, D.; Liu, W.; Han, G. W.; Joseph, J. S.; Katritch, I.; Heitman, L. H.; Xia, L.; Ijzerman, A. P.; et al. The Role of a Sodium Ion Binding Site in the Allosteric Modulation of the A_{2A} adenosine G Protein-Coupled Receptor. *Structure* **2013**, *21* (12), 2175–2185. https://doi.org/10.1016/j.str.2013.09.020.

(32) Carpenter, B.; Nehmé, R.; Warne, T.; Leslie, A. G. W.; Tate, C. G. Structure of the Adenosine A_{2A} Receptor Bound to an Engineered G Protein. *Nature* **2016**, *536*, 104–107. https://doi.org/10.1038/nature18966.

(33) García-Nafría, J.; Lee, Y.; Bai, X.; Carpenter, B.; Tate, C. G. Cryo-EM Structure of the Adenosine A_{2A} Receptor Coupled to an Engineered Heterotrimeric G Protein. *Elife* **2018**, *7*, 1–19. https://doi.org/10.7554/eLife.35946.001.

(34) Draper-joyce, C. J.; Khoshouei, M.; Thal, D. M.; Liang, Y.; Nguyen, A. T. N.; Furness, S. G. B.; Venugopal, H.; Baltos, J.; Plitzko, J. M.; Danev, R.; et al. Structure of the Adenosine-Bound Human Adenosine A_1 Receptor – G i Complex. *Nature* **2018**, *558*, 559–563. https://doi.org/10.1038/s41586-018-0236-6.

(35) Draper-Joyce;, C. J.; Bhola, R.; Wang;, J.; Bhattarai;, A.; Nguyen;, A. T. N.; Cowie-Kent;, I.; O'Sullivan;, K.; Chia;, L. Y.; Venugopal;, H.;

Valant;, C.; et al. Positive Allosteric Mechanisms of Adenosine A_1 Receptor-Mediated Analgesia. *Nature* **2021**, 1–6.

(36) Glukhova, A.; Thal, D. M.; Nguyen, A. T.; May, L. T.; Sexton, P. M.; Christopoulos, A.; Scammells, P. J. Structure of the Adenosine A 1 Receptor Reveals the Basis for Subtype Selectivity. *Cell* **2017**, *168*, 867–877. https://doi.org/10.1016/j.cell.2017.01.042.

(37) Cheng, R. K. Y.; Segala, E.; Robertson, N.; Marshall, F. H.; Cooke, R. M.; Errey, J. C.; Marshall, F. H.; Cooke, R. M. Structures of Human A_1 and A_{2A} Adenosine Receptors with Xanthines Reveal Determinants of Selectivity. *Structure* **2017**, *25*, 1275–1285. https://doi.org/10.1016/j.str.2017.06.012.

(38) Jespers, W.; Schiedel, A. C.; Heitman, L. H.; Cooke, R. M.; Kleene, L.; van Westen, G. J. P.; Gloriam, D. E.; Müller, C. E.; Sotelo, E.; Gutiérrez-de-Terán, H. Structural Mapping of Adenosine Receptor Mutations: Ligand Binding and Signaling Mechanisms. *Trends Pharmacol. Sci.* **2018**, *39* (1), 75–89. https://doi.org/10.1016/j.tips.2017.11.001.

(39) Nguyen, A. T. N.; Baltos, J. A.; Thomas, T.; Nguyen, T. D.; Muñoz, L. L.; Gregory, K. J.; White, P. J.; Sexton, P. M.; Christopoulos, A.; May, L. T. Extracellular Loop 2 of the Adenosine A1 Receptor Has a Key Role in Orthosteric Ligand Affinity and Agonist Efficacy. *Mol. Pharmacol.* **2016**, *90* (6), 703–714. https://doi.org/10.1124/mol.116.105007.

(40) Ciancetta, A.; Jacobson, K. A. Breakthrough in GPCR Crystallography and Its Impact on Computer-Aided Drug Design. In *Computational Methods for GPCR Drug Discovery*; (eds), H. A., Ed.; Humana Press, New York, NY, 2018; Vol. 1705, pp 45–72.

(41) Mason, J. S.; Bortolato, A.; Weiss, D. R.; Deflorian, F.; Tehan, B.; Marshall, F. H. High End GPCR Design: Crafted Ligand Design and Druggability Analysis Using Protein Structure, Lipophilic Hotspots and Explicit Water Networks. *Silico Pharmacol.* **2013**, *1* (1), 1–12. https://doi.org/10.1186/2193-9616-1-23.

(42) Baraldi, S.; Baraldi, P. G.; Oliva, P.; Toti, K. S.; Ciancetta, A.; Jacobson, K. A. A 2a Adenosine Receptor: Structures, Modeling, and

Medicinal Chemistry. *Receptors* **2018**, *34*, 91–136. https://doi.org/10.1007/978-3-319-90808-3_5.

(43) Gao, Z. G.; Tosh, D. K.; Jain, S.; Yu, J.; Suresh, R. R.; Jacobson, K. A. A_1 Adenosine Receptor Agonists, Antagonists, and Allosteric Modulators. *Receptors* **2018**, *34*, 59–89. https://doi.org/10.1007/978-3-319-90808-3_4.

(44) Müller, C. E.; Jacobson, K. A. Recent Developments in Adenosine Receptor Ligands and Their Potential as Novel Drugs. *Biochim. Biophys. Acta - Biomembr.* **2011**, *1808* (5), 1290–1308. https://doi.org/10.1016/j.bbamem.2010.12.017.

(45) Liu, W.; Chun, E.; Thompson, A. A.; Chubukov, P.; Xu, F.; Han, G. W.; Roth, C. B.; Heitman, L. H.; Ijzerman, A. P.; Cherezov, V.; et al. Structural Basis for Allosteric Regulation of GGPCRs by Sodium Ions. *Science,* **2013**, *337* (6091), 232–236. https://doi.org/10.1126/science.1219218.Structural.

(46) Piirainen, H.; Ashok, Y.; Nanekar, R. T.; Jaakola, V. P. Structural Features of Adenosine Receptors: From Crystal to Function. *Biochim. Biophys. Acta - Biomembr.* **2011**, *1808* (5), 1233–1244. https://doi.org/10.1016/j.bbamem.2010.05.021.

(47) Ballesteros, J. A.; Weinstein, H. Integrated Methods for the Construction of Three-Dimensional Models and Computational Probing of Structure-Function Relations in G Protein-Coupled Receptors. *Methods Neurosci.* **1995**, *25*, 366–428. https://doi.org/10.1016/S1043-9471(05)80049-7.

(48) Tucker, A. L.; Robeva, A. S.; Taylor, H. E.; Holeton, D.; Bockner, M.; Lynch, K. R.; Linden, J. A_1 Adenosine Receptors. Two Amino Acids Are Responsible for Species Differences in Ligand Recognition. *J. Biol. Chem.* **1994**, *269* (45), 27900–27906.

(49) Cooper, S. L.; Soave, M.; Jörg, M.; Scammells, P. J.; Woolard, J.; Hill, S. J. Probe Dependence of Allosteric Enhancers on the Binding Affinity of Adenosine A 1 -Receptor Agonists at Rat and Human A 1 -Receptors Measured Using NanoBRET. *Br. J. Pharmacol.* **2019**, 864–878. https://doi.org/10.1111/bph.14575.

(50) Mattedi, G.; Deflorian, F.; Mason, J. S.; de Graaf, C.; Gervasio, F. L.

Understanding Ligand Binding Selectivity in a Prototypical GPCR Family. *J. Chem. Inf. Model.* **2019**, 59, 2830-2836. https://doi.org/10.1021/acs.jcim.9b00298.

(51) Segala, E.; Guo, D.; Cheng, R. K. Y.; Bortolato, A.; Deflorian, F.; Doré, A. S.; Errey, J. C.; Heitman, L. H.; Ijzerman, A. P.; Marshall, F. H.; et al. Controlling the Dissociation of Ligands from the Adenosine A_{2A} Receptor through Modulation of Salt Bridge Strength. *J. Med. Chem.* **2016**, *59* (13), 6470–6479. https://doi.org/10.1021/acs.jmedchem.6b00653.

(52) Mason, J. S.; Bortolato, A.; Congreve, M.; Marshall, F. H. New Insights from Structural Biology into the Druggability of G Protein-Coupled Receptors. *Trends Pharmacol. Sci.* **2012**, *33* (5), 249–260. https://doi.org/10.1016/j.tips.2012.02.005.

(53) Ralevic, V.; Burnstock, G. Receptors for Purines and Pyrimidines. *Pharmacol. Rev.* **1998**, *50* (3), 413–492. https://doi.org/10.1007/978-3-642-28863-0_5.

(54) Ruiz, M. D. L.; Lim, Y.; Zheng, J. Adenosine A_{2A} Receptor as a Drug Discovery Target. *J. Med. Chem.* **2014**, *57*, 3623–3650. https://doi.org/10.1021/jm4011669.

(55) Fredholm, B. B.; IJzerman, A. P.; Jacobson, K. A.; Linden, J.; Müller, C. E.; AP, I. J.; Jacobson, K. A.; Klotz, K. N.; Linden, J. International Union of Pharmacology. XXV. Nomenclature and Classification of Adenosine Receptors-An Update. *Pharmacol Rev* **2011**, *63* (4), 527–552. https://doi.org/10.1124/pr.110.003285.1.

(56) Fredholm, B. B.; Arslan, G.; Halldner, L.; Kull, B.; Schulte, G.; Wasserman, W. Structure and Function of Adenosine Receptors and Their Genes. *Naunyn. Schmiedebergs. Arch. Pharmacol.* **2000**, *362*, 364–374. https://doi.org/10.1007/s002100000313.

(57) Kull, B.; Svenningsson, P.; Fredholm, B. B. Adenosine A(2A) Receptors Are Colocalized with and Activate g(Olf) in Rat Striatum. *Mol. Pharmacol.* **2000**, *58* (4), 771–777. https://doi.org/10.1124/mol.58.4.771.

(58) Ramlackhansingh, A. F.; Bose, S. K.; Ahmed, I.; Turkheimer, F. E.; Pavese, N.; Brooks, D. J. Adenosine A_{2A} Receptor Availability in

Dyskinetic and Nondyskinetic Patients with Parkinson Disease. *Neurology* **2011**, *76* (21), 1811–1816. https://doi.org/10.1212/WNL.0b013e31821ccce4.

(59) Fredholm, B. B. Adenosine Receptors as Drug Targets. *Exp. Cell Res.* **2010**, *316* (8), 1284–1288. https://doi.org/10.1016/j.yexcr.2010.02.004.

(60) Zhou, Z.; Rajamani, U.; Labazi, H.; Tilley, S. L.; Ledent, C.; Teng, B.; Mustafa, S. J. Involvement of NADPH Oxidase in A_{2A} Adenosine Receptor-Mediated Increase in Coronary Flow in Isolated Mouse Hearts. *Purinergic Signal.* **2015**, *11* (2), 263–273. https://doi.org/10.1007/s11302-015-9451-x.

(61) Al Jaroudi, W.; Iskandrian, A. E. Regadenoson: A New Myocardial Stress Agent. *J. Am. Coll. Cardiol.* **2009**, *54* (13), 1123–1130. https://doi.org/10.1016/j.jacc.2009.04.089.

(62) Canals, M.; Marcellino, D.; Fanelli, F.; Ciruela, F.; De Benedetti, P.; Goldberg, S. R.; Neve, K.; Fuxe, K.; Agnati, L. F.; Woods, A. S.; et al. Adenosine A_{2A}-Dopamine D_2 Receptor-Receptor Heteromerization: Qualitative and Quantitative Assessment by Fluorescence and Bioluminescence Energy Transfer. *J. Biol. Chem.* **2003**, *278* (47), 46741–46749. https://doi.org/10.1074/jbc.M306451200.

(63) Fuxe, K.; Ferre, S.; Canals, M.; Torvinen, M.; Terasmaa, A.; Marcellino, D.; Goldberg, S. R.; Staines, W.; Jacobsen, K. X.; Lluis, C.; et al. Adenosine A_{2A} and Dopamine D_2 Heteromeric Receptor Complexes and Their Function. *J. Mol. Neurosci.* **2005**, *26*, 209–217. https://doi.org/10.1385/JMN/26.

(64) Borroto-Escuela, D. O.; Fuxe, K. Adenosine Heteroreceptor Complexes in the Basal Ganglia Are Implicated in Parkinson's Disease and Its Treatment. *J. Neural Transm.* **2019**, *126* (4), 455–471. https://doi.org/10.1007/s00702-019-01969-2.

(65) Administration, U. S. F. and D. FDA approves new add-on drug to treat off episodes in adults with Parkinson's disease https://www.fda.gov/news-events/press-announcements/fda-approves-new-add-drug-treat-episodes-adults-parkinsons-disease.

(66) Gessi, S.; Merighi, S.; Varani, K.; Borea, P. A. *Adenosine Receptors in*

Health and Disease, 1st ed.; Elsevier Inc., 2011; Vol. 61. https://doi.org/10.1016/B978-0-12-385526-8.00002-3.

(67) Fuxe, K.; Ferré, S.; Genedani, S.; Franco, R.; Agnati, L. F. Adenosine Receptor-Dopamine Receptor Interactions in the Basal Ganglia and Their Relevance for Brain Function. *Physiol. Behav.* **2007**, *92*, 210–217. https://doi.org/10.1016/j.physbeh.2007.05.034.

(68) Bartoli, F.; Burnstock, G.; Crocamo, C.; Carrà, G. Purinergic Signaling and Related Biomarkers in Depression. *Brain Sci.* **2020**, *10* (3), 1–12. https://doi.org/10.3390/brainsci10030160.

(69) Burnstock, G. Purinergic Signalling and Disorders of the Central Nervous System. *Nat. Rev. Drug Discov.* **2008**, *7*, 575–590. https://doi.org/10.1038/nrd2605.

(70) Ohta, A.; Sitkovsky, M. Role of G-Protein-Coupled Adenosine Receptors in Downregulation of Inflammation and Protection from Tissue Damage. *Nature* **2001**, *414*, 916–920. https://doi.org/10.1038/414916a.

(71) Ohta, A.; Gorelik, E.; Prasad, S. J.; Ronchese, F.; Lukashev, D.; Wong, M. K. K.; Huang, X.; Caldwell, S.; Liu, K.; Smith, P.; et al. A2A Adenosine Receptor Protects Tumors from Antitumor T Cells. *Proc. Natl. Acad. Sci.* **2006**, *103* (35), 13132–13137. https://doi.org/10.1073/pnas.0605251103.

(72) Beavis, P. A.; Paget, C.; Devaud, C.; John, L. B.; Dwyer, K.; Divisekera, U.; Stagg, J.; Chow, M. T.; Darcy, P. K.; Smyth, M. J. Blockade of A 2A Receptors Potently Suppresses the Metastasis of CD73 + Tumors . *Proc. Natl. Acad. Sci.* **2013**, *110* (36), 14711–14716. https://doi.org/10.1073/pnas.1308209110.

(73) Yu, F.; Zhu, C.; Xie, Q.; Wang, Y. Adenosine A 2A Receptor Antagonists for Cancer Immunotherapy. *J. Med. Chem.* **2020**, *63*, 12196–12212.

(74) Jacobson, K. A.; Gao, Z. G.; Matricon, P.; Eddy, M. T.; Carlsson, J. Adenosine A_{2A} Receptor Antagonists: From Caffeine to Selective Non-Xanthines. *Br. J. Pharmacol.* **2020**,1-16. https://doi.org/10.1111/bph.15103.

(75) Congreve, M.; Andrews, S. P.; Doré, A. S.; Hollenstein, K.; Hurrell,

E.; Langmead, C. J.; Mason, J. S.; Ng, I. W.; Tehan, B.; Zhukov, A.; et al. Discovery of 1,2,4-Triazine Derivatives as Adenosine A_{2A} antagonists Using Structure Based Drug Design. *J. Med. Chem.* **2012**, *55* (5), 1898–1903. https://doi.org/10.1021/jm201376w.

(76) Borodovsky, A.; Barbon, C. M.; Wang, Y.; Ye, M.; Prickett, L.; Chandra, D.; Shaw, J.; Deng, N.; Sachsenmeier, K.; Clarke, J. D.; et al. Small Molecule AZD4635 Inhibitor of A2AR Signaling Rescues Immune Cell Function Including CD103+ Dendritic Cells Enhancing Anti-Tumor Immunity. *J. Immunother. cancer* **2020**, *8* (2). https://doi.org/10.1136/jitc-2019-000417.

(77) Borodovsky, A.; Minwei Ye, Y. W.; Shaw, J. C.; Sachsenmeier, K. F.; Deng, N.; DelSignore, K. J.; Fretland, A. J.; Clarke, J. D.; Goodwin, R. J.; Strittmatter, N.; et al. Preclinical Pharmacodynamics and Antitumor Activity of AZD4635, a Novel Adenosine A_{2A} Receptor Inhibitor That Reverses Adenosine Mediated T Cell Suppression. In *Preclinical pharmacodynamics and antitumor activity of AZD4635, a novel adenosine 2A receptor inhibitor that reverses adenosine mediated T cell suppression [abstract]*.; 2017. https://doi.org/doi:10.1158/1538-7445.AM2017-5580.

(78) Mediavilla-Varela, M.; Castro, J.; Chiappori, A.; Noyes, D.; Hernandez, D. C.; Allard, B.; Stagg, J.; Antonia, S. J. A Novel Antagonist of the Immune Checkpoint Protein Adenosine A2a Receptor Restores Tumor-Infiltrating Lymphocyte Activity in the Context of the Tumor Microenvironment. *Neoplasia (United States)* **2017**, *19* (7), 530–536. https://doi.org/10.1016/j.neo.2017.02.004.

(79) Mittal, D.; Sinha, D.; Barkauskas, D.; Young, A.; Kalimutho, M.; Stannard, K.; Caramia, F.; Haibe-Kains, B.; Stagg, J.; Khanna, K. K.; et al. Adenosine 2B Receptor Expression on Cancer Cells Promotes Metastasis. *Cancer Res.* **2016**, *76* (15), 4372–4382. https://doi.org/10.1158/0008-5472.CAN-16-0544.

(80) Gao, Z.-G.; Jacobson, K. A. A_{2B} Adenosine Receptor and Cancer. *Int. J. Mol. Sci.* **2019**, *1*, 1–18.

(81) Seitz, L. C.; Ashok, D.; Leleti, M.; Powers, J.; Rosen, B.; Miles, D.; Sharif, E.; Jin, L.; Park, A.; Young, S.; et al. Final Results of the Phase

I Study in Healthy Volunteers of AB928, a Dual Antagonist of the $A_{2A}R$ and $A_{2B}R$ Adenosine Receptors Being Studied as an Activator of Anti-Tumor Immune Response. *Ann. Oncol.* **2018**, *29*, 649. https://doi.org/10.1093/annonc/mdy303.

(82) DiRenzo, D. M.; Narasappa, N.; Piovesan, D.; Ashok, D.; Adam, P.; Jeffrey, J. L.; Leleti, M. R.; Tan, J. B. L.; Seitz, L.; Young, S. W.; et al. Abstract A10: The Dual A2a/A2b R Antagonist AB928 Reverses Adenosine-Mediated Immune Suppression and Inhibits Tumor Growth in Vivo. *Cancer Immunol. Res.* **2020**, *8*, A10 LP-A10. https://doi.org/10.1158/2326-6074.TUMIMM18-A10.

(83) Kiesman, W. F.; Zhao, J.; Conlon, P. R.; Dowling, J. E.; Petter, R. C.; Lutterodt, F.; Jin, X.; Smits, G.; Fure, M.; Jayaraj, A.; et al. Potent and Orally Bioavailable 8-Bicyclo[2.2.2]Octylxanthines as Adenosine A1 Receptor Antagonists. *J. Med. Chem.* **2006**, *49* (24), 7119–7131. https://doi.org/10.1021/jm0605381.

(84) Vu, C. B.; Kiesman, W. F.; Conlon, P. R.; Lin, K. C.; Tam, M.; Petter, R. C.; Smits, G.; Lutterodt, F.; Jin, X.; Chen, L.; et al. Tricyclic Imidazoline Derivatives as Potent and Selective Adenosine A_1 Receptor Antagonists. *J. Med. Chem.* **2006**, *49* (24), 7132–7139. https://doi.org/10.1021/jm060539t.

(85) Gottlieb, S. S.; Brater, D. C.; Thomas, I.; Havranek, E.; Bourge, R.; Goldman, S.; Dyer, F.; Gomez, M.; Bennett, D.; Ticho, B.; et al. BG9719 (CVT-124), an A1 Adenosine Receptor Antagonist, Protects against the Decline in Renal Function Observed with Diuretic Therapy. *Circulation* **2002**, *105* (11), 1348–1353. https://doi.org/10.1161/hc1102.105264.

(86) Dennissen, F. J. A.; Anglada-Huguet, M.; Sydow, A.; Mandelkow, E.; Mandelkow, E. M. Adenosine A_1 Receptor Antagonist Rolofylline Alleviates Axonopathy Caused by Human Tau ΔK280. *Proc. Natl. Acad. Sci. U. S. A.* **2016**, *113* (41), 11597–11602. https://doi.org/10.1073/pnas.1603119113.

(87) Massie, B. M.; O'Connor, C. M.; Metra, M.; Ponikowski, P.; Teerlink, J. R.; Cotter, G.; Weatherley, B. D.; Cleland, J. G. F.; Givertz, M. M.; Voors, A.; et al. Rolofylline, an Adenosine A1-Receptor Antagonist,

in Acute Heart Failure. *N. Engl. J. Med.* **2010**, *363* (15), 1419–1428. https://doi.org/10.1056/NEJMoa0912613.

(88) Ensor, C. R.; Russell, S. D. Tonapofylline: A Selective Adenosine-1 Receptor Antagonist for the Treatment of Heart Failure. *Expert Opin. Pharmacother.* **2010**, *11* (14), 2405–2415. https://doi.org/10.1517/14656566.2010.514605.

(89) Baltos, J. A.; Gregory, K. J.; White, P. J.; Sexton, P. M.; Christopoulos, A.; May, L. T. Quantification of Adenosine A1 Receptor Biased Agonism: Implications for Drug Discovery. *Biochem. Pharmacol.* **2016**, *99*, 101–112. https://doi.org/10.1016/j.bcp.2015.11.013.

(90) Smith, J. S.; Lefkowitz, R. J.; Rajagopal, S. Biased Signalling: From Simple Switches to Allosteric Microprocessors. *Nat. Rev. Drug Discov.* **2018**, *17* (4), 243–260. https://doi.org/10.1038/nrd.2017.229.

(91) Valant, C.; May, L. T.; Aurelio, L.; Chuo, C. H.; White, P. J.; Baltos, J.-A.; Sexton, P. M.; Scammells, P. J.; Christopoulos, A. Separation of On-Target Efficacy from Adverse Effects through Rational Design of a Bitopic Adenosine Receptor Agonist. *Proc. Natl. Acad. Sci.* **2014**, *111* (12), 4614–4619. https://doi.org/10.1073/pnas.1320962111.

(92) Knight, A.; Hemmings, J. L.; Winfield, I.; Leuenberger, M.; Frattini, E.; Frenguelli, B. G.; Dowell, S. J.; Lochner, M.; Ladds, G. Discovery of Novel Adenosine Receptor Agonists That Exhibit Subtype Selectivity. *J. Med. Chem.* **2016**, *59* (3), 947–964. https://doi.org/10.1021/acs.jmedchem.5b01402.

(93) Wall, M. J.; Hill, E.; Huckstepp, R.; Deganutti, G.; Leuenberger, M.; Preti, B.; Barkan, K.; Winfield, I.; Wei, H.; Imlach, W.; et al. A Biased Adenosine A1R Agonist Elicits Analgesia without Cardiorespiratory Depression. *BiorXiv* **2020**.

(94) Wootten, D.; Christopoulos, A.; Sexton, P. M. Emerging Paradigms in GPCR Allostery: Implications for Drug Discovery. *Nat. Rev. Drug Discov.* **2013**, *12* (8), 630–644. https://doi.org/10.1038/nrd4052.

(95) Kenakin, T. P. Allosteric Drug Effects. *Pharmacol. Drug Discov. Dev.* **2017**, 101–129. https://doi.org/10.1016/b978-0-12-803752-2.00005-3.

(96) Hill, S. J.; May, L. T.; Kellam, B.; Woolard, J. Allosteric Interactions at Adenosine A1 and A3 Receptors: New Insights into the Role of Small Molecules and Receptor Dimerization. *Br. J. Pharmacol.* **2014**, *171* (5), 1102–1113. https://doi.org/10.1111/bph.12345.

(97) May, L. T. .; Leach, K.; Sexton, P. M. .; Christopoulos, A. Allosteric Modulation of G-Protein Coupled Receptors. *Annu. Rev. Pharmacol. Toxicol.* **2007**, *47*, 1–51. https://doi.org/10.1016/j.ejps.2003.11.007.

(98) Wold, E. A.; Chen, J.; Cunningham, K. A.; Zhou, J. Allosteric Modulation of Class A GPCRs: Targets, Agents, and Emerging Concepts. *J. Med. Chem.* **2019**, *62* (1), 88–127. https://doi.org/10.1021/acs.jmedchem.8b00875.

(99) Bruns, R. F.; Fergus, J. H. Allosteric Enhancement of Adenosine A_1 Receptor Binding and Function by 2-Amino-3-Benzoylthiophenes. *Mol. Pharmacol.* **1990**, *38* (6), 939–949.

(100) Bruns, R. F.; Fergus, J. H.; Coughenour, L. L.; Courtland, G. G.; Pugsley, T. A.; Dodd, J. H.; Tinney, F. J. Structure-Activity Relationships for Enhancement of Adenosine A_1 Receptor Binding by 2-Amino-3-Benzoylthiophenes. *Mol. Pharmacol.* **1990**, *38* (6), 950–958.

(101) Valant, C.; Aurelio, L.; Devine, S. M.; Ashton, T. D.; White, J. M.; Sexton, P. M.; Christopoulos, A.; Scammells, P. J. Synthesis and Characterization of Novel 2-Amino-3-Benzoylthiophene Derivatives as Biased Allosteric Agonists and Modulators of the Adenosine A 1 Receptor. *J. Med. Chem.* **2012**, *55* (5), 2367–2375. https://doi.org/10.1021/jm201600e.

(102) Aurelio, L.; Valant, C.; Flynn, B. L.; Sexton, P. M.; Christopoulos, A.; Scammells, P. J. Allosteric Modulators of the Adenosine A1 Receptor: Synthesis and Pharmacological Evaluation of 4-Substituted 2-Amino-3-Benzoylthiophenes. *J. Med. Chem.* **2009**, *52* (14), 4543–4547. https://doi.org/10.1021/jm9002582.

(103) Vincenzi, F.; Targa, M.; Romagnoli, R.; Merighi, S.; Gessi, S.; Baraldi, P. G.; Borea, P. A.; Varani, K. TRR469, a Potent A1 Adenosine Receptor Allosteric Modulator, Exhibits Anti-Nociceptive Properties in Acute and Neuropathic Pain Models in Mice. *Neuropharmacology*

2014, *81*, 6–14. https://doi.org/10.1016/j.neuropharm.2014.01.028.

(104) Göblyös, A.; De Vries, H.; Brussee, J.; Ijzerman, A. P. Synthesis and Biological Evaluation of a New Series of 2,3,5-Substituted [1,2,4]-Thiadiazoles as Modulators of Adenosine A1 Receptors and Their Molecular Mechanism of Action. *J. Med. Chem.* **2005**, *48* (4), 1145–1151. https://doi.org/10.1021/jm049337s.

(105) Imlach, W. L.; Bhola, R. F.; May, L. T.; Christopoulos, A.; Christie, M. J. A Positive Allosteric Modulator of the Adenosine A1 Receptor Selectively Inhibits Primary Afferent Synaptic Transmission in a Neuropathic Pain Model. *Mol. Pharmacol.* **2015**, *88* (3), 460–468. https://doi.org/10.1124/mol.115.099499.

(106) Romagnoli, R.; Baraldi, P. G.; Carrion, M. D.; Cara, C. L.; Cruz-Lopez, O.; Kimatrai Salvador, M.; Preti, D.; Tabrizi, M. A.; Moorman, A. R. .; Vincenzi, F.; et al. Synthesis and Biological Evaluation of 2-Amino-3-(4-Chlorobenzoyl)- 4-[(4-Arylpiperazin-1-Yl)Methyl]-5-Substituted-Thiophenes. Effect of the 5-Modification on Allosteric Enhancer Activity at the A1 Adenosine. *J. Med. Chem.* **2012**, *55* (9), 7719–7735. https://doi.org/10.1017/CBO9781107415324.004.

(107) Li, X.; Conklin, D.; Pan, H. L.; Eisenach, J. C. Allosteric Adenosine Receptor Modulation Reduces Hypersensitivity Following Peripheral Inflammation by a Central Mechanism. *J. Pharmacol. Exp. Ther.* **2003**, *305* (3), 950–955. https://doi.org/10.1124/jpet.102.047951.

(108) Giorgi, I.; Nieri, P. Adenosine A1 Modulators: A Patent Update (2008 to Present). *Expert Opin. Ther. Pat.* **2013**, *23* (9), 1109–1121. https://doi.org/10.1517/13543776.2013.799142.

(109) Jacobson, K. A.; Tosh, D. K.; Jain, S.; Gao, Z. G. Historical and Current Adenosine Receptor Agonists in Preclinical and Clinical Development. *Front. Cell. Neurosci.* **2019**, *13*, 1–17. https://doi.org/10.3389/fncel.2019.00124.

(110) Meibom, D.; Albrecht-Küpper, B.; Diedrichs, N.; Hübsch, W.; Kast, R.; Krämer, T.; Krenz, U.; Lerchen, H. G.; Mittendorf, J.; Nell, P. G.; et al. Neladenoson Bialanate Hydrochloride: A Prodrug of a Partial Adenosine A1 Receptor Agonist for the Chronic Treatment of Heart Diseases. *ChemMedChem* **2017**, *12* (10), 728–737.

https://doi.org/10.1002/cmdc.201700151.

(111) Voors, A. A.; Bax, J. J.; Hernandez, A. F.; Wirtz, A. B.; Pap, A. F.; Ferreira, A. C.; Senni, M.; van der Laan, M.; Butler, J. Safety and Efficacy of the Partial Adenosine A1 Receptor Agonist Neladenoson Bialanate in Patients with Chronic Heart Failure with Reduced Ejection Fraction: A Phase IIb, Randomized, Double-Blind, Placebo-Controlled Trial. *Eur. J. Heart Fail.* **2019**, *21* (11), 1426–1433. https://doi.org/10.1002/ejhf.1591.

(112) Fogel, D. B. Factors Associated with Clinical Trials That Fail and Opportunities for Improving the Likelihood of Success: A Review. *Contemp. Clin. Trials Commun.* **2018**, *11*, 156–164. https://doi.org/10.1016/j.conctc.2018.08.001.

(113) Jucker, M. The Benefits and Limitations of Animal Models for Translational Research in Neurodegenerative Diseases. *Nat. Med.* **2010**, *16* (11), 1210–1214. https://doi.org/10.1038/nm.2224.

(114) Steven R. Houser , Kenneth B. Margulies , Anne M. Murphy , Francis G. Spinale , Gary S. Francis , Sumanth D. Prabhu , Howard A. Rockman , David A. Kass , Jeffery D. Molkentin , Mark A. Sussman, and W. J. K. Animal Models of Heart Failure. *Circ. Res.* **2012**, *111*, 131–150. https://doi.org/10.1161/res.0b013e3182582523.

(115) Alnouri, M. W.; Jepards, S.; Casari, A.; Schiedel, A. C.; Hinz, S.; Müller, C. E. Selectivity Is Species-Dependent: Characterization of Standard Agonists and Antagonists at Human, Rat, and Mouse Adenosine Receptors. *Purinergic Signal.* **2015**, *11* (3), 389–407. https://doi.org/10.1007/s11302-015-9460-9.

(116) Rueda, P.; Merlin, J.; Chimenti, S.; Feletou, M.; Paysant, J.; White, P. J.; Christopoulos, A.; Sexton, P. M.; Summers, R. J.; Charman, W. N.; et al. Pharmacological Insights Into Safety and Efficacy Determinants for the Development of Adenosine Receptor Biased Agonists in the Treatment of Heart Failure. *Front. Pharmacol.* **2021**, *12*, 1–15. https://doi.org/10.3389/fphar.2021.628060.

(117) McNeill, S. M.; Baltos, J. A.; White, P. J.; May, L. T. Biased Agonism at Adenosine Receptors. *Cell. Signal.* **2021**, *82*. https://doi.org/10.1016/j.cellsig.2021.109954.

(118) Simon, G. M.; Niphakis, M. J.; Cravatt, B. F. Determining Target Engagement in Living Systems. *Nat. Chem. Biol.* **2013**, *9* (4), 200–205. https://doi.org/10.1038/nchembio.1211.

(119) Tyler, D. S.; Vappiani, J.; Cañeque, T.; Lam, E. Y. N.; Ward, A.; Gilan, O.; Chan, Y. C.; Hienzsch, A.; Rutkowska, A.; Werner, T.; et al. Click Chemistry Enables Preclinical Evaluation of Targeted Epigenetic Therapies. *Science.* **2017**, *356*, 1397–1401. https://doi.org/10.1126/science.aal2066.

(120) Bathe-Peters, M.; Gmach, P.; Boltz, H. H.; Einsiedel, J.; Gotthardt, M.; Hübner, H.; Gmeiner, P.; Lohse, M. J.; Annibale, P. Visualization of β-Adrenergic Receptor Dynamics and Differential Localization in Cardiomyocytes. *Proc. Natl. Acad. Sci.* USA. **2021**, *118* (23), 1–10. https://doi.org/10.1073/PNAS.2101119118.

(121) Halls, M. L.; Yeatman, H. R.; Nowell, C. J.; Thompson, G. L.; Gondin, A. B.; Civciristov, S.; Bunnett, N. W.; Lambert, N. A.; Poole, D. P.; Canals, M. Plasma Membrane Localization of the μ-Opioid Receptor Controls Spatiotemporal Signaling. *Sci. Signal.* **2016**, *9* (414), 1–14. https://doi.org/10.1126/scisignal.aac9177.

(122) van Waarde, A. ; Dierckx, R. J. O. .; Zhou, X. ; Khanapur, S. ; Tsukada, H.; Ishiwata, K.; Luurtsema, G.; de Vries, E. F. J. ;; Elsinga, P. H. Potential Therapeutic Applications of Adenosine A_{2A} Receptor Ligands and Opportunities for A_{2A} Receptor Imaging. *Med. Res. Rev.* **2018**, *1* (38), 5–56. https://doi.org/10.1002/med.

(123) Yang, X.; Heitman, L. H.; IJzerman, A. P.; van der Es, D. Molecular Probes for the Human Adenosine Receptors. *Purinergic Signal.* **2021**, *17* (1), 85–108. https://doi.org/10.1007/s11302-020-09753-8.

(124) Stoddart, L. A.; White, C. W.; Nguyen, K.; Hill, S. J.; Pfleger, K. D. G. Fluorescence- and Bioluminescence-Based Approaches to Study GPCR Ligand Binding. *Br. J. Pharmacol.* **2016**, *173* (20), 3028–3037. https://doi.org/10.1111/bph.13316.

(125) Hazari, P. P.; Pandey, A.; Chaturvedi, S.; Mishra, A. K. New Trends and Current Status of Positron-Emission Tomography and Single-Photon-Emission Computerized Tomography Radioligands for Neuronal Serotonin Receptors and Serotonin Transporter. *Bioconjug.*

Chem. **2017**, *28* (11), 2647–2672. https://doi.org/10.1021/acs.bioconjchem.7b00243.

(126) Soave, M.; Briddon, S. J.; Hill, S. J.; Stoddart, L. A. Fluorescent Ligands: Bringing Light to Emerging G Protein-coupled Receptor Paradigms. *Br. J. Pharmacol.* **2019**, 1–14. https://doi.org/10.1111/bph.14953.

(127) Stoddart, L. A.; Kilpatrick, L. E.; Briddon, S. J.; Hill, S. J. Probing the Pharmacology of G Protein-Coupled Receptors with Fluorescent Ligands. *Neuropharmacology* **2015**, *98*, 48–57. https://doi.org/10.1016/j.neuropharm.2015.04.033.

(128) Kozma, E.; Suresh Jayasekara, P.; Squarcialupi, L.; Paoletta, S.; Moro, S.; Federico, S.; Spalluto, G.; Jacobson, K. A. Fluorescent Ligands for Adenosine Receptors. *Bioorganic Med. Chem. Lett.* **2013**, *23* (1), 26–36. https://doi.org/10.1016/j.bmcl.2012.10.112.

(129) Valeur, B. Molecular Fluorescence: Principles and Applications; Wiley-VCH Verlag GmbH, 2001; pp 3–19.

(130) Briddon, S. J.; Kilpatrick, L. E.; Hill, S. J. Studying GPCR Pharmacology in Membrane Microdomains: Fluorescence Correlation Spectroscopy Comes of Age. *Trends Pharmacol. Sci.* **2018**, *39* (2), 158–174. https://doi.org/10.1016/j.tips.2017.11.004.

(131) Kecskés, M.; Kumar, T. S.; Yoo, L.; Gao, Z. G.; Jacobson, K. A. Novel Alexa Fluor-488 Labeled Antagonist of the A2A Adenosine Receptor: Application to a Fluorescence Polarization-Based Receptor Binding Assay. *Biochem. Pharmacol.* **2010**, *80* (4), 506–511. https://doi.org/10.1016/j.bcp.2010.04.027.

(132) Soethoudt, M.; Stolze, S. C.; Westphal, M. V.; Van Stralen, L.; Martella, A.; Van Rooden, E. J.; Guba, W.; Varga, Z. V.; Deng, H.; Van Kasteren, S. I.; et al. Selective Photoaffinity Probe That Enables Assessment of Cannabinoid CB 2 Receptor Expression and Ligand Engagement in Human Cells. *J. Am. Chem. Soc.* **2018**, *140* (19), 6067–6075. https://doi.org/10.1021/jacs.7b11281.

(133) Cottet, M.; Faklaris, O.; Zwier, J. M.; Trinquet, E.; Pin, J. P.; Durroux, T. Original Fluorescent Ligand-Based Assays Open New Perspectives in G-Protein Coupled Receptor Drug Screening. *Pharmaceuticals* **2011**,

4 (1), 202–214. https://doi.org/10.3390/ph4010202.

(134) Cottet, M.; Faklaris, O.; Falco, A.; Trinquet, E.; Pin, J. P.; Mouillac, B.; Durroux, T. Fluorescent Ligands to Investigate GPCR Binding Properties and Oligomerization. *Biochem. Soc. Trans.* **2013**, *41* (1), 148–153. https://doi.org/10.1042/BST20120237.

(135) Hell, S. W. Toward Fluorescence Nanoscopy. *Nat. Biotechnol.* **2003**, *21* (11), 1347–1355. https://doi.org/10.1038/nbt895.

(136) Sydor, A. M.; Czymmek, K. J.; Puchner, E. M.; Mennella, V. Super-Resolution Microscopy: From Single Molecules to Supramolecular Assemblies. *Trends Cell Biol.* **2015**, *25* (12), 730–748. https://doi.org/10.1016/j.tcb.2015.10.004.

(137) Shaner, N. C.; Steinbach, P. A.; Tsien, R. Y. A Guide to Choosing Fluorescent Proteins. *Nat. Methods* **2005**, *2* (12), 905–909. https://doi.org/10.1038/nmeth819.

(138) Michel, M. C.; Wieland, T.; Tsujimoto, G. How Reliable Are G-Protein-Coupled Receptor Antibodies? *Naunyn. Schmiedebergs. Arch. Pharmacol.* **2009**, *379* (4), 385–388. https://doi.org/10.1007/s00210-009-0395-y.

(139) Tian, H.; Furstenberg, A.; Huber, T. Labeling and Single-Molecule Methods to Monitor G Proteincoupled Receptor Dynamics. *Chem. Rev.* **2017**, *117* (1), 186–245. https://doi.org/10.1021/acs.chemrev.6b00084.

(140) Soave, M.; Stoddart, L. A.; White, C. W.; Kilpatrick, L. E.; Goulding, J.; Briddon, S. J.; Hill, S. J. Detection of Genome-Edited and Endogenously Expressed G Protein-Coupled Receptors. *FEBS J.* **2021**, *288*, 2585–2601. https://doi.org/10.1111/febs.15729.

(141) Goulding, J.; Mistry, S. J.; Soave, M.; Woolard, J.; Briddon, S. J.; White, C. W.; Kellam, B.; Hill, S. J. Subtype Selective Fluorescent Ligands Based on ICI 118,551 to Study the Human B2-Adrenoceptor in CRISPR/Cas9 Genome-Edited HEK293T Cells at Low Expression Levels. *Pharmacol. Res. Perspect.* **2021**, *9* (3), 1–13. https://doi.org/10.1002/prp2.779.

(142) Sridharan, R.; Zuber, J.; Connelly, S. M.; Mathew, E.; Dumont, M. E. Fluorescent Approaches for Understanding Interactions of Ligands

with G Protein Coupled Receptors. *Biochim. Biophys. Acta - Biomembr.* **2014**, *1838*, 15–33. https://doi.org/10.1016/j.bbamem.2013.09.005.

(143) Jazayeri, A.; Andrews, S. P.; Marshall, F. H. Structurally Enabled Discovery of Adenosine A2a Receptor Antagonists. *Chem. Rev.* **2017**, *117* (1), 21–37. https://doi.org/10.1021/acs.chemrev.6b00119.

(144) Baker, J. G.; Middleton, R.; Adams, L.; May, L. T.; Briddon, S. J.; Kellam, B.; Hill, S. J. Influence of Fluorophore and Linker Composition on the Pharmacology of Fluorescent Adenosine A_1 Receptor Ligands: Themed Section: Imaging in Pharmacology Research Paper. *Br. J. Pharmacol.* **2010**, *159* (4), 772–786. https://doi.org/10.1111/j.1476-5381.2009.00488.x.

(145) Briddon, S. J.; Kellam, B.; Hill, S. J. Design and Use of Fluorescent Ligands to Study Ligand–Receptor Interactions in Single Living Cells. *Recept. Signal Transduct. Protoc.* **2011**, *746*, 211–236. https://doi.org/10.1007/978-1-61779-126-0.

(146) Vernall, A. J.; Hill, S. J.; Kellam, B. The Evolving Small-Molecule Fluorescent-Conjugate Toolbox for Class A GPCRs. *Br. J. Pharmacol.* **2014**, *171* (5), 1073–1084. https://doi.org/10.1111/bph.12265.

(147) Alcobia, D. C.; Ziegler, A. I.; Kondrashov, A.; Comeo, E.; Mistry, S.; Kellam, B.; Chang, A.; Woolard, J.; Hill, S. J.; Sloan, E. K. Visualising Ligand-Binding to a GPCR in Vivo Using NanoBRET. *iScience* **2018**, *6*, 280–288. https://doi.org/10.1016/j.isci.2018.08.006.

(148) Middleton, R. J.; Briddon, S. J.; Cordeaux, Y.; Yates, A. S.; Dale, C. L.; George, M. W.; Baker, J. G.; Hill, S. J.; Kellam, B. New Fluorescent Adenosine A 1 -Receptor Agonists That Allow Quantification of Ligand - Receptor Interactions in Microdomains of Single Living Cells. *J. Med. Chem.* **2007**, *50* (4), 782–793.

(149) Vernall, A. J.; Stoddart, L. A.; Briddon, S. J.; Ng, H. W.; Laughton, C. A.; Doughty, S. W.; Hill, S. J.; Kellam, B. Conversion of a Non-Selective Adenosine Receptor Antagonist into A_3-Selective High Affinity Fluorescent Probes Using Peptide-Based Linkers. *Org. Biomol. Chem.* **2013**, *11* (34), 5673–5682. https://doi.org/10.1039/c3ob41221k.

(150) Vernall, A. J.; Stoddart, L. A.; Briddon, S. J.; Hill, S. J.; Kellam, B.

Highly Potent and Selective Fluorescent Antagonists of the Human Adenosine A3 Receptor Based on the 1,2,4-Triazolo[4,3-a]Quinoxalin-1-One Scaffold. *J. Med. Chem.* **2012**, *55* (4), 1771–1782. https://doi.org/10.1021/jm201722y.

(151) Lavis, L. D.; Raines, R. T. Bright Building Blocks for Chemical Biology. *ACS Chem. Biol.* **2014**, *9* (4), 855–866. https://doi.org/10.1021/cb500078u.

(152) Lavis, L. D.; Raines, R. T. Bright Ideas for Chemical Biology. *ACS Chem. Biol.* **2008**, *3* (3), 142–155. https://doi.org/10.1021/cb700248m.

(153) Hirabayashi, K.; Hanaoka, K.; Takayanagi, T.; Toki, Y.; Egawa, T.; Kamiya, M.; Komatsu, T.; Ueno, T.; Terai, T.; Yoshida, K.; et al. Analysis of Chemical Equilibrium of Silicon-Substituted Fluorescein and Its Application to Develop a Scaffold for Red Fluorescent Probes. *Anal. Chem.* **2015**, *87* (17), 9061–9069. https://doi.org/10.1021/acs.analchem.5b02331.

(154) Grimm, J. B.; Muthusamy, A. K.; Liang, Y.; Brown, T. A.; Lemon, W. C.; Patel, R.; Lu, R.; Macklin, J. J.; Keller, P. J.; Ji, N.; et al. A General Method to Fine-Tune Fluorophores for Live-Cell and in Vivo Imaging. *Nat. Methods* **2017**, *14* (10), 987–994. https://doi.org/10.1038/nmeth.4403.

(155) Grimm, J. B.; English, B. P.; Chen, J.; Slaughter, J. P.; Zhang, Z.; Revyakin, A.; Patel, R.; Macklin, J. J.; Normanno, D.; Singer, R. H.; et al. A General Method to Improve Fluorophores for Live-Cell and Single-Molecule Microscopy. *Nat. Methods* **2015**, *12* (3), 244–250. https://doi.org/10.1038/nmeth.3256.

(156) Pansare, V. J.; Hejazi, S.; Faenza, W. J.; Prud'homme, R. K. Review of Long-Wavelength Optical and NIR Imaging Materials. *Chem. Mater.* **2012**, *24*, 812–827.

(157) Ma, Z.; Lin, Y.; Cheng, Y.; Wu, W.; Cai, R.; Chen, S.; Shi, B.; Han, B.; Shi, X.; Zhou, Y.; et al. Discovery of the First Environment-Sensitive Near-Infrared (NIR) Fluorogenic Ligand for A1-Adrenergic Receptors Imaging in Vivo. *J. Med. Chem.* **2016**, *59* (5), 2151–2162. https://doi.org/10.1021/acs.jmedchem.5b01843.

(158) Esteoulle, L.; Daubeuf, F.; Collot, M.; Riché, S.; Durroux, T.; Brasse, D.; Marchand, P.; Karpenko, I. A.; Klymchenko, A. S.; Bonnet, D. A Near-Infrared Fluorogenic Dimer Enables Background-Free Imaging of Endogenous GPCRs in Living Mice. *Chem. Sci.* **2020**, *11* (26), 6824–6829. https://doi.org/10.1039/d0sc01018a.

(159) Loudet, A.; Burgess, K. BODIPY Dyes and Their Derivatives: Syntheses and Spectroscopic Properties. *Chem. Rev.* **2007**, *107* (11), 4891–4932. https://doi.org/10.1021/cr078381n.

(160) Karolin, J.; Johansson, L. B. A.; Strandberg, L.; Ny, T. Fluorescence and Absorption Spectroscopic Properties of Dipyrromethene boron Difluoride (BODIPY) Derivatives in Liquids, Lipid Membranes, and Proteins. *J. Am. Chem. Soc.* **1994**, *116* (17), 7801–7806. https://doi.org/10.1021/ja00096a042.

(161) Ulrich, G.; Ziessel, R.; Harriman, A. The Chemistry of Fluorescent Bodipy Dyes: Versatility Unsurpassed. *Angew. Chemie - Int. Ed.* **2008**, *47* (7), 1184–1201. https://doi.org/10.1002/anie.200702070.

(162) Stoddart, L. A.; Vernall, A. J.; Denman, J. L.; Briddon, S. J.; Kellam, B.; Hill, S. J. Fragment Screening at Adenosine-A_3 Receptors in Living Cells Using a Fluorescence-Based Binding Assay. *Chem. Biol.* **2012**, *19* (9), 1105–1115. https://doi.org/10.1016/j.chembiol.2012.07.014.

(163) Hall, M. P.; Unch, J.; Binkowski, B. F.; Valley, M. P.; Butler, B. L.; Wood, M. G.; Otto, P.; Zimmerman, K.; Vidugiris, G.; MacHleidt, T.; et al. Engineered Luciferase Reporter from a Deep Sea Shrimp Utilizing a Novel Imidazopyrazinone Substrate. *ACS Chem. Biol.* **2012**, *7* (11), 1848–1857. https://doi.org/10.1021/cb3002478.

(164) Machleidt, T.; Woodroofe, C. C.; Schwinn, M. K.; Méndez, J.; Robers, M. B.; Zimmerman, K.; Otto, P.; Daniels, D. L.; Kirkland, T. A.; Wood, K. V. NanoBRET-A Novel BRET Platform for the Analysis of Protein-Protein Interactions. *ACS Chem. Biol.* **2015**, *10* (8), 1797–1804. https://doi.org/10.1021/acschembio.5b00143.

(165) Stoddart, L. A.; Johnstone, E. K. M.; Wheal, A. J.; Goulding, J.; Robers, M. B.; MacHleidt, T.; Wood, K. V.; Hill, S. J.; Pfleger, K. D. G. Application of BRET to Monitor Ligand Binding to GPCRs. *Nat. Methods* **2015**, *12* (7), 661–663. https://doi.org/10.1038/nmeth.3398.

(166) May, L. T.; Bridge, L. J.; Stoddart, L. A.; Briddon, S. J.; Hill, S. J. Allosteric Interactions across Native Adenosine-A_3 Receptor Homodimers: Quantification Using Single-Cell Ligand-Binding Kinetics . *FASEB J.* **2011**, *25* (10), 3465–3476. https://doi.org/10.1096/fj.11-186296.

(167) Albizu, L.; Cottet, M.; Kralikova, M.; Stoev, S.; Seyer, R.; Brabet, I.; Roux, T.; Bazin, H.; Bourrier, E.; Lamarque, L.; et al. Time-Resolved FRET between GPCR Ligands Reveals Oligomers in Native Tissues. *Nat. Chem. Biol.* **2010**, *6* (8), 587–594. https://doi.org/10.1038/nchembio.396.

(168) Fernandez-Duenas, V.; Taura, J. J.; Cottet, M.; Gomez-Soler, M.; Lopez-Cano, M.; Ledent, C.; Watanabe, M.; Trinquet, E.; Pin, J.-P.; Lujan, R.; et al. Untangling Dopamine-Adenosine Receptor-Receptor Assembly in Experimental Parkinsonism in Rats. *Dis. Model. Mech.* **2015**, *8* (1), 57–63. https://doi.org/10.1242/dmm.018143.

(169) Ciruela, F.; Fernández-Dueñas, V.; Jacobson, K. A. Lighting up G Protein-Coupled Purinergic Receptors with Engineered Fluorescent Ligands. *Neuropharmacology* **2015**, *98*, 58–67. https://doi.org/10.1016/j.neuropharm.2015.04.001.

(170) White, C. W.; Vanyai, H. K.; See, H. B.; Johnstone, E. K. M.; Pfleger, K. D. G. Using NanoBRET and CRISPR/Cas9 to Monitor Proximity to a Genome-Edited Protein in Real-Time. *Sci. Rep.* **2017**, *7* (1), 1–14. https://doi.org/10.1038/s41598-017-03486-2.

(171) Doudna, J. A.; Charpentier, E. The New Frontier of Genome Engineering with CRISPR-Cas9. *Science,* **2014**, *346*. https://doi.org/10.1126/science.1258096.

(172) White, C. W.; Johnstone, E. K. M.; See, H. B.; Pfleger, K. D. G. NanoBRET Ligand Binding at a GPCR under Endogenous Promotion Facilitated by CRISPR/Cas9 Genome Editing. *Cell. Signal.* **2019**, *54*, 27–34. https://doi.org/10.1016/j.cellsig.2018.11.018.

(173) White, C. W.; Caspar, B.; Vanyai, H. K.; Pfleger, K. D. G.; Hill, S. J. CRISPR-Mediated Protein Tagging with Nanoluciferase to Investigate Native Chemokine Receptor Function and Conformational Changes. *Cell Chem. Biol.* **2020**, 1–12.

https://doi.org/10.1016/j.chembiol.2020.01.010.

(174) Godbole, A.; Lyga, S.; Lohse, M. J.; Calebiro, D. Internalized TSH Receptors En Route to the TGN Induce Local Gs-Protein Signaling and Gene Transcription. *Nat. Commun.* **2017**, *8* (1). https://doi.org/10.1038/s41467-017-00357-2.

(175) Federico, S.; Lassiani, L.; Spalluto, G. Chemical Probes for the Adenosine Receptors. *Pharmaceuticals* **2019**, *12* (4). https://doi.org/10.3390/ph12040168.

(176) Ma, Z.; Du, L.; Li, M. Toward Fluorescent Probes for G-Protein-Coupled Receptors (GPCRs). *J. Med. Chem.* **2014**, *57* (20), 8187–8203. https://doi.org/10.1021/jm401823z.

(177) Brand, F.; Klutz, A. M.; Jacobson, K. A.; Fredholm, B. B.; Schulte, G. Adenosine A_{2A} Receptor Dynamics Studied with the Novel Fluorescent Agonist Alexa488-APEC. *Eur. J. Pharmacol.* **2008**, *590*, 36–42. https://doi.org/10.1016/j.ejphar.2008.05.036.

(178) Fernández-Dueñas, V.; Gõmez-Soler, M.; Jacobson, K. A.; Kumar, S. T.; Fuxe, K.; Borroto-Escuela, D. O.; Ciruela, F. Molecular Determinants of A_{2A}R-D_2R Allosterism: Role of the Intracellular Loop 3 of the D 2R. *J. Neurochem.* **2012**, *123* (3), 373–384. https://doi.org/10.1111/j.1471-4159.2012.07956.x.

(179) Duroux, R.; Ciancetta, A.; Mannes, P.; Yu, J.; Boyapati, S.; Gizewski, E.; Yous, S.; Ciruela, F.; Auchampach, J. A.; Gao, Z.-G.; et al. Bitopic Fluorescent Antagonists of the A $_{2A}$ Adenosine Receptor Based on Pyrazolo[4,3-e][1,2,4]Triazolo[1,5-c]Pyrimidin-5-Amine Functionalized Congeners. *Med. Chem. Commun.* **2017**, *8* (8), 1659–1667. https://doi.org/10.1039/C7MD00247E.

(180) May, L. T.; Self, T. J.; Briddon, S. J.; Hill, S. J. The Effect of Allosteric Modulators on the Kinetics of Agonist-G Protein-Coupled Receptor Interactions in Single Living Cells. *Mol. Pharmacol.* **2010**, *78* (3), 511–523. https://doi.org/10.1124/mol.110.064493.

(181) Stoddart, L. A.; Vernall, A. J.; Briddon, S. J.; Kellam, B.; Hill, S. J. Direct Visualisation of Internalization of the Adenosine A_3 Receptor and Localization with Arrestin3 Using a Fluorescent Agonist. *Neuropharmacology* **2015**, *98*, 68–77.

https://doi.org/10.1016/j.neuropharm.2015.04.013.

(182) Cordeaux, Y.; Briddon, S. J.; Alexander, S. P. H.; Kellam, B.; Hill, S. J. Agonist-Occupied A3 Adenosine Receptors Exist within Heterogeneous Complexes in Membrane Microdomains of Individual Living Cells. *FASEB J.* **2007**, *22* (3), 850–860. https://doi.org/10.1096/fj.07-8180com.

(183) Jacobson, K. A.; Kirk, K. L.; Padgett, W. L.; Daly, J. W. Functionalized Congeners of Adenosine: Preparation of Analogues with High Affinity for ArAdenosine Receptors. *J. Med. Chem.* **1985**, *28* (9), 1341–1346.

(184) McCabe, T. T.; Skonick, P.; Jacobson, K. A. FITC-APEC: A Fluorescent Ligand For A2a -Adenosine Receptors. *J. Fluoresc.* **1992**, *2* (4), 217–223.

(185) Jacobson, K. A.; Ukena, D.; Padgett, W.; Daly, J. W.; Kirk, K. L. Xanthine Functionalized Congeners as Potent Ligands at A2-Adenosine Receptors. *J. Med. Chem.* **1987**, *30* (1), 211–214. https://doi.org/10.1021/jm00384a037.

(186) Jacobson, K. A.; Ukena, D.; Padgett, W.; Kirk, K. L.; Daly, J. W. Molecular Probes for Extracellular Adenosine Receptors. *Biochem. Pharmacol.* **1987**, *36* (10), 1697–1707. https://doi.org/10.1016/0006-2952(87)90056-6.

(187) McNeely, P. M.; Naranjo, A. N.; Forsten-Williams, K.; Robinson, A. S. A_{2A}R Binding Kinetics in the Ligand Depletion Regime. *SLAS Discov.* **2017**, *22* (2), 166–175. https://doi.org/10.1177/1087057116667256.

(188) Kumar, T. S.; Mishra, S.; Deflorian, F.; Yoo, L. S.; Phan, K.; Kecskés, M.; Szabo, A.; Shinkre, B.; Gao, Z. G.; Trenkle, W.; et al. Molecular Probes for the A2Aadenosine Receptor Based on a Pyrazolo[4,3-e][1,2,4]Triazolo[1,5-c]Pyrimidin-5-Amine Scaffold. *Bioorganic Med. Chem. Lett.* **2011**, *21* (9), 2740–2745. https://doi.org/10.1016/j.bmcl.2010.11.082.

(189) Gao, Z.; Toti, K. S.; Campbell, R.; Suresh, R. R.; Yang, H.; Jacobson, K. A. Allosteric Antagonism of the A 2A Adenosine Receptor by a Series of Bitopic Ligands. *Cells* **2020**, *9*, 1–23.

https://doi.org/10.3390/cells9051200.

(190) Macchia, M.; Salvetti, F.; Barontini, S.; Calvani, F.; Gesi, M.; Hamdan, M.; Lucacchini, A.; Pellegrini, A.; Soldani, P.; Martini, C. Fluorescent Probes for Adenosine Receptors: Synthesis and Biology of N6-Dansylaminoalkyl-Substituted Neca Derivatives. *Bioorg. Med. Chem. Lett.* **1998**, *8*, 3223–3228.

(191) Briddon, S. J.; Middleton, R. J.; Cordeaux, Y.; Flavin, F. M.; Weinstein, J. A.; George, M. W.; Kellam, B.; Hill, S. J. Quantitative Analysis of the Formation and Diffusion of A 1 -Adenosine Receptor – Antagonist Complexes in Single Living Cells. *PNAS* **2004**, *101* (13), 4673–4678.

(192) Corriden, R.; Kilpatrick, L. E.; Kellam, B.; Briddon, S. J.; Hill, S. J. Kinetic Analysis of Antagonist-Occupied Adenosine-A3 Receptors within Membrane Microdomains of Individual Cells Provides Evidence of Receptor Dimerization and Allosterism. *FASEB J.* **2014**, *28* (10), 4211–4222. https://doi.org/10.1096/fj.13-247270.

(193) Briddon, S. J.; Middleton, R. J.; Yates, A. S.; George, M. W.; Kellam, B.; Hill, S. J. Application of Fluorescence Correlation Spectroscopy to the Measurement of Agonist Binding to a G-Protein Coupled Receptor at the Single Cell Level. *Faraday Discuss.* **2004**, *126* (1), 197–207. https://doi.org/10.1039/b307407b.

(194) Macchia, M.; Salvetti, F.; Bertini, S.; Di Bussolo, V.; Gattuso, L.; Gesi, M.; Hamdan, M.; Klotz, K. N.; Laragione, T.; Lucacchini, A.; et al. 7-Nitrobenzofurazan (NBD) Derivatives of 5'-N-Ethylcarboxamidoadenosine (NECA) as New Fluorescent Probes for Human A3 Adenosine Receptors. *Bioorganic Med. Chem. Lett.* **2001**, *11* (23), 3023–3026. https://doi.org/10.1016/S0960-894X(01)00610-2.

(195) Rose, R. H.; Briddon, S. J.; Hill, S. J. A Novel Fluorescent Histamine H(1) Receptor Antagonist Demonstrates the Advantage of Using Fluorescence Correlation Spectroscopy to Study the Binding of Lipophilic Ligands. *Br. J. Pharmacol.* **2012**, *165* (6), 1789–1800. https://doi.org/10.1111/j.1476-5381.2011.01640.x.

(196) Tsukiji, S.; Miyagawa, M.; Takaoka, Y.; Tamura, T.; Hamachi, I. Ligand-Directed Tosyl Chemistry for Protein Labeling in Vivo. *Nat.*

Chem. Biol. **2009**, *5* (5), 341–343. https://doi.org/10.1038/nchembio.157.

(197) Fujishima, S. H.; Yasui, R.; Miki, T.; Ojida, A.; Hamachi, I. Ligand-Directed Acyl Imidazole Chemistry for Labeling of Membrane-Bound Proteins on Live Cells. *J. Am. Chem. Soc.* **2012**, *134* (9), 3961–3964. https://doi.org/10.1021/ja2108855.

(198) Hayashi, T.; Hamachi, I. Traceless Affinity Labeling of Endogenous Proteins for Functional Analysis in Living Cells. *Acc. Chem. Res.* **2012**, *45* (9), 1460–1469. https://doi.org/10.1021/ar200334r.

(199) Shiraiwa, K.; Cheng, R.; Nonaka, H.; Tamura, T.; Hamachi, I. Chemical Tools for Endogenous Protein Labeling and Profiling. *Cell Chem. Biol.* **2020**, *27* (8), 970–985. https://doi.org/10.1016/j.chembiol.2020.06.016.

(200) Tamura, T.; Hamachi, I. Chemistry for Covalent Modification of Endogenous/Native Proteins: From Test Tubes to Complex Biological Systems. *J. Am. Chem. Soc.* **2019**, *141*, 2782–2799. https://doi.org/10.1021/jacs.8b11747.

(201) Tamura, T.; Ueda, T.; Goto, T.; Tsukidate, T.; Shapira, Y.; Nishikawa, Y.; Fujisawa, A.; Hamachi, I. Rapid Labelling and Covalent Inhibition of Intracellular Native Proteins Using Ligand-Directed N-Acyl-N-Alkyl Sulfonamide. *Nat. Commun.* **2018**, *9* (1). https://doi.org/10.1038/s41467-018-04343-0.

(202) Tamura, T.; Tsukiji, S.; Hamachi, I. Native FKBP12 Engineering by Ligand-Directed Tosyl Chemistry: Labeling Properties and Application to Photo-Cross-Linking of Protein Complexes in Vitro and in Living Cells. *J. Am. Chem. Soc.* **2012**, *134* (4), 2216–2226. https://doi.org/10.1021/ja209641t.

(203) Yamaura, K.; Kiyonaka, S.; Numata, T.; Inoue, R.; Hamachi, I. Discovery of Allosteric Modulators for GABA A Receptors by Ligand-Directed Chemistry. *Nat. Chem. Biol.* **2016**, *12* (10), 822–830. https://doi.org/10.1038/nchembio.2150.

(204) Miki, T.; Fujishima, S. H.; Komatsu, K.; Kuwata, K.; Kiyonaka, S.; Hamachi, I. LDAI-Based Chemical Labeling of Intact Membrane Proteins and Its Pulse-Chase Analysis under Live Cell Conditions.

Chem. Biol. **2014**, *21* (8), 1013–1022. https://doi.org/10.1016/j.chembiol.2014.07.013.

(205) Wakayama, S.; Kiyonaka, S.; Arai, I.; Kakegawa, W.; Matsuda, S.; Ibata, K.; Nemoto, Y. L.; Kusumi, A.; Yuzaki, M.; Hamachi, I. Chemical Labelling for Visualizing Native AMPA Receptors in Live Neurons. *Nat. Commun.* **2017**, *8*. https://doi.org/10.1038/ncomms14850.

(206) Ojima, K.; Shiraiwa, K.; Soga, K.; Doura, T.; Takato, M.; Komatsu, K.; Yuzaki, M.; Hamachi, I.; Kiyonaka, S. Ligand-Directed Two-Step Labeling to Quantify Neuronal Glutamate Receptor Trafficking. *Nat. Commun.* **2021**, *12* (1). https://doi.org/10.1038/s41467-021-21082-x.

(207) Gehringer, M.; Laufer, S. A. Emerging and Re-Emerging Warheads for Targeted Covalent Inhibitors: Applications in Medicinal Chemistry and Chemical Biology. *J. Med. Chem.* **2019**, *62* (12), 5673–5724. https://doi.org/10.1021/acs.jmedchem.8b01153.

(208) Mino, T.; Sakamoto, S.; Hamachi, I. Recent Applications of N-Acyl Imidazole Chemistry in Chemical Biology. *Biosci. Biotechnol. Biochem.* **2021**, *85* (1), 53–60. https://doi.org/10.1093/bbb/zbaa026.

(209) Takaoka, Y.; Nishikawa, Y.; Hashimoto, Y.; Sasaki, K.; Hamachi, I. Ligand-Directed Dibromophenyl Benzoate Chemistry for Rapid and Selective Acylation of Intracellular Natural Proteins. *Chem. Sci.* **2015**, *6* (5), 3217–3224. https://doi.org/10.1039/c5sc00190k.

(210) Matsuo, K.; Nishikawa, Y.; Masuda, M.; Hamachi, I. Live-Cell Protein Sulfonylation Based on Proximity-Driven N-Sulfonyl Pyridone Chemistry. *Angew. Chemie - Int. Ed.* **2018**, *57* (3), 659–662. https://doi.org/10.1002/anie.201707972.

(211) Lang, K.; Chin, J. W. Cellular Incorporation of Unnatural Amino Acids and Bioorthogonal Labeling of Proteins. *Chem. Rev.* **2014**, *114* (9), 4764–4806. https://doi.org/10.1021/cr400355w.

(212) Arttamangkul, S.; Plazek, A.; Platt, E. J.; Jin, H.; Murray, T. F.; Birdsong, W. T.; Rice, K. C.; Farrens, D. L.; Williams, J. T. Visualizing Endogenous Opioid Receptors in Living Neurons Using Ligand-Directed Chemistry. *Elife* **2019**, *8*, 1–25. https://doi.org/10.7554/eLife.49319.

(213) Stoddart, L. A.; Kindon, N. D.; Otun, O.; Harwood, C. R.; Patera, F.; Veprintsev, D. B.; Woolard, J.; Briddon, S. J.; Franks, H. A.; Hill, S. J.; et al. Ligand-Directed Covalent Labelling of a GPCR with a Fluorescent Tag in Live Cells. *Commun. Biol.* **2020**, *3* (1), 1–9. https://doi.org/10.1038/s42003-020-01451-w.

(214) Moss, S. M.; Jayasekara, P. S.; Paoletta, S.; Gao, Z. G.; Jacobson, K. A. Structure-Based Design of Reactive Nucleosides for Site-Specific Modification of the A2A Adenosine Receptor. *ACS Med. Chem. Lett.* **2014**, *5* (9), 1043–1048. https://doi.org/10.1021/ml5002486.

(215) Stoddart, L. A.; Kilpatrick, L. E.; Hill, S. J. NanoBRET Approaches to Study Ligand Binding to GPCRs and RTKs. *Trends Pharmacol. Sci.* **2018**, *39* (2), 136–147. https://doi.org/10.1016/j.tips.2017.10.006.

(216) Chen, J. F.; Eltzschig, H. K.; Fredholm, B. B. Adenosine Receptors as Drug Targets-What Are the Challenges? *Nat. Rev. Drug Discov.* **2013**, *12* (4), 265–286. https://doi.org/10.1038/nrd3955.

(217) Kooistra, A. J.; Mordalski, S.; Pándy-Szekeres, G.; Esguerra, M.; Mamyrbekov, A.; Munk, C.; Keserű, G. M.; Gloriam, D. E. GPCRdb in 2021: Integrating GPCR Sequence, Structure and Function. *Nucleic Acids Res.* **2021**, *49*, D335–D343. https://doi.org/10.1093/nar/gkaa1080.

(218) Doré, A. S.; Robertson, N.; Errey, J. C.; Ng, I.; Hollenstein, K.; Tehan, B.; Hurrell, E.; Bennett, K.; Congreve, M.; Magnani, F.; et al. Structure of the Adenosine A 2A Receptor in Complex with ZM241385 and the Xanthines XAC and Caffeine. *Structure* **2011**, *19* (9), 1283–1293. https://doi.org/10.1016/j.str.2011.06.014.

(219) Sun, B.; Bachhawat, P.; Chu, M. L.-H.; Wood, M.; Ceska, T.; Sands, Z. A.; Mercier, J.; Lebon, F.; Kobilka, T. S.; Kobilka, B. K. Crystal Structure of the Adenosine A $_{2A}$ Receptor Bound to an Antagonist Reveals a Potential Allosteric Pocket. *Proc. Natl. Acad. Sci.* **2017**, *114* (8), 2066–2071. https://doi.org/10.1073/pnas.1621423114.

(220) Jacobson, K. A.; IJzerman, A. P.; Müller, C. E. Medicinal Chemistry of P2 and Adenosine Receptors: Common Scaffolds Adapted for Multiple Targets. *Biochem. Pharmacol.* **2020**, *187*. https://doi.org/10.1016/j.bcp.2020.114311.

(221) Guerrero, A. A_{2A} Adenosine Receptor Agonists and Their Potential Therapeutic Applications. An Update. *Curr. Med. Chem.* **2018**, *25* (30), 3597–3612. https://doi.org/10.2174/0929867325666180313110254.

(222) Merighi, S.; Battistello, E.; Giacomelli, L.; Varani, K.; Vincenzi, F.; Borea, P. A.; Gessi, S. Targeting A_3 and A_{2A} Adenosine Receptors in the Fight against Cancer. *Expert Opin. Ther. Targets* **2019**, *23* (8), 669–678. https://doi.org/10.1080/14728222.2019.1630380.

(223) Waickman, A. T.; Alme, A.; Senaldi, L.; Zarek, P. E.; Horton, M.; Powell, J. D. Enhancement of Tumor Immunotherapy by Deletion of the A_{2A} Adenosine Receptor. *Cancer Immunol. Immunother.* **2012**, *61* (6), 917–926. https://doi.org/10.1007/s00262-011-1155-7.

(224) Jenner, P.; Mori, A.; Aradi, S. D.; Hauser, R. A. Istradefylline–a First Generation Adenosine A_{2A} Antagonist for the Treatment of Parkinson's Disease. *Expert Rev. Neurother.* **2021**, *21* (3), 317–333. https://doi.org/10.1080/14737175.2021.1880896.

(225) Dungo, R.; Deeks, E. D. Istradefylline: First Global Approval. *Drugs* **2013**, *73* (8), 875–882. https://doi.org/10.1007/s40265-013-0066-7.

(226) Arruda, M. A.; Stoddart, L. A.; Gherbi, K.; Briddon, S. J.; Kellam, B.; Hill, S. J. A Non-Imaging High Throughput Approach to Chemical Library Screening at the Unmodified Adenosine-A_3 Receptor in Living Cells. *Front. Pharmacol.* **2017**, *8*, 1–13. https://doi.org/10.3389/fphar.2017.00908.

(227) Todde, S.; Moresco, R. M.; Simonelli, P.; Baraldi, P. G.; Cacciari, B.; Spalluto;, G.; Varani, K.; Monopoli, A.; Matarrese, M.; Carpinelli, A.; et al. Design, Radiosynthesis, and Biodistribution of a New Potent and Selective Ligand for in Vivo Imaging of the Adenosine A_{2A} Receptor System Using Positron Emission Tomography. *J. Med. Chem.* **2000**, No. 43, 4359–4362.

(228) Neustadt, B. R.; Hao, J.; Lindo, N.; Greenlee, W. J.; Stamford, A. W.; Tulshian, D.; Ongini, E.; Hunter, J.; Monopoli, A.; Bertorelli, R.; et al. Potent, Selective, and Orally Active Adenosine A_{2A} receptor Antagonists: Arylpiperazine Derivatives of Pyrazolo[4,3-e]-1,2,4-Triazolo[1,5-c]Pyrimidines. *Bioorganic Med. Chem. Lett.* **2007**, *17* (5), 1376–1380. https://doi.org/10.1016/j.bmcl.2006.11.083.

(229) Hauser, R. A.; Stocchi, F.; Rascol, O.; Huyck, S. B.; Capece, R.; Ho, T. W.; Sklar, P.; Lines, C.; Michelson, D.; Hewitt, D. Preladenant as an Adjunctive Therapy with Levodopa in Parkinson Disease: Two Randomized Clinical Trials and Lessons Learned. *JAMA Neurol.* **2015**, *72* (12), 1491–1500. https://doi.org/10.1001/jamaneurol.2015.2268.

(230) Stocchi, F.; Rascol, O.; Hauser, R. A.; Huyck, S.; Tzontcheva, A.; Capece, R.; Ho, T. W.; Sklar, P.; Lines, C.; Michelson, D.; et al. Randomized Trial of Preladenant, given as Monotherapy, in Patients with Early Parkinson Disease. *Neurology* **2017**, *88* (23), 2198–2206. https://doi.org/10.1212/WNL.0000000000004003.

(231) Yuan, G.; Jankins, T. C.; Patrick, C. G.; Philbrook, P.; Sears, O.; Hatfield, S.; Sitkovsky, M.; Vasdev, N.; Liang, S. H.; Ondrechen, M. J.; et al. Fluorinated Adenosine A_{2A} Receptor Antagonists Inspired by Preladenant as Potential Cancer Immunotherapeutics . *Int. J. Med. Chem.* **2017**, *2017*, 1–8. https://doi.org/10.1155/2017/4852537.

(232) Baraldi, P. G.; Tabrizi, M. A.; Gessi, S.; Borea, P. A. Adenosine Receptor Antagonists : Translating Medicinal Chemistry and Pharmacology into Clinical Utility. *Chem. Rev.* **2008**, *108*, 238–263.

(233) Shinkre, B. A.; Kumar, T. S.; Gao, Z. G.; Deflorian, F.; Jacobson, K. A.; Trenkle, W. C. Synthesis and Evaluation of 1,2,4-Triazolo[1,5-c]Pyrimidine Derivatives as A_{2A} Receptor-Selective Antagonists. *Bioorganic Med. Chem. Lett.* **2010**, *20* (19), 5690–5694. https://doi.org/10.1016/j.bmcl.2010.08.021.

(234) Basu, S.; Barawkar, D. A.; Ramdas, V.; Naykodi, M.; Shejul, Y. D.; Patel, M.; Thorat, S.; Panmand, A.; Kashinath, K.; Bonagiri, R.; et al. Discovery of Potent and Selective A_{2A} Antagonists with Efficacy in Animal Models of Parkinson's Disease and Depression. *ACS Med. Chem. Lett.* **2017**, *8* (8), 835–840. https://doi.org/10.1021/acsmedchemlett.7b00175.

(235) Carlsson, J.; Yoo, L.; Gao, Z.-G.; Irwin, J. J.; Shoichet, B. K.; Jacobson, K. A. Structure-Based Discovery of A_{2A} Adenosine Receptor Ligands. *J. Med. Chem.* **2010**, *53* (9), 3748–3755. https://doi.org/10.1021/jm100240h.

(236) Iliopoulos-Tsoutsouvas, C.; Kulkarni, R. N.; Makriyannis, A.; Nikas,

S. P. Fluorescent Probes for G-Protein-Coupled Receptor Drug Discovery. *Expert Opinion on Drug Discovery*. 2018, 933–947. https://doi.org/10.1080/17460441.2018.1518975.

(237) Stoddart, L. A.; Vernall, A. J.; Bouzo-Lorenzo, M.; Bosma, R.; Kooistra, A. J.; De Graaf, C.; Vischer, H. F.; Leurs, R.; Briddon, S. J.; Kellam, B.; et al. Development of Novel Fluorescent Histamine H1-Receptor Antagonists to Study Ligand-Binding Kinetics in Living Cells. *Sci. Rep.* **2018**, *8* (1), 1–19. https://doi.org/10.1038/s41598-018-19714-2.

(238) Schembri, L. S.; Stoddart, L. A.; Briddon, S. J.; Kellam, B.; Canals, M.; Graham, B.; Scammells, P. J. Synthesis, Biological Evaluation, and Utility of Fluorescent Ligands Targeting the μ-Opioid Receptor. *J. Med. Chem.* **2015**, *58* (24), 9754–9767. https://doi.org/10.1021/acs.jmedchem.5b01664.

(239) Conroy, S.; Kindon, N. D.; Glenn, J.; Stoddart, L. A.; Lewis, R. J.; Hill, S. J.; Kellam, B.; Stocks, M. J. Synthesis and Evaluation of the First Fluorescent Antagonists of the Human $P2Y_2$ Receptor Based on AR-C118925. *J. Med. Chem.* **2018**, *61* (7), 3089–3113. https://doi.org/10.1021/acs.jmedchem.8b00139.

(240) Kuo, Shen-Chun; Tran, Thanh; Zhang, P. Process For Preparing Substituted 5-Amino-Pyrazolo-[4,3-e]- 1,2,4-triaz0l0[1,5-c]pyrimidine. US007235659B2, 2007. https://doi.org/10.1197/jamia.M1139.Adar.

(241) Klötzer, W; Herberz, M. Chlorierende Formylierungsreaktionen an Pyrimidinen Die Reaktion Des Formylierungsreagens Mit Einer Am Pyrimidinkern. *Monatshefte für Chemie* **1965**, *96* (5), 1567–1572.

(242) Ashry, E. S. H. E. L.; Rashed, Y. E. L. K. N.; Assafir, H. Dimroth Rearrangement : Translocation of Heteroatoms in Heterocyclic Rings and Its Role in Ring Transformations of Heterocycles. *Adv. Heterocycl. Chem.* **1999**, *75*, 79–165.

(243) Dale, C. L.; Hill, S. J.; Kellam, B. New Potent, Short-Linker BODIPY-630/650™ Labelled Fluorescent Adenosine Receptor Agonists. *Medchemcomm* **2012**, *3* (3), 333–338. https://doi.org/10.1039/c2md00247g.

(244) Hill, S. J.; Baker, J. G.; Rees, S. Reporter-Gene Systems for the Study

of G-Protein-Coupled Receptors. *Curr. Opin. Pharmacol.* **2001**, *1* (5), 526–532. https://doi.org/10.1016/S1471-4892(01)00091-1.

(245) Christopoulos, A. .; Kenakin, T. G Protein-Coupled Receptor Allosterism and Complexing. *Pharmacol. Rev.* **2002**, *54* (2), 323–374. https://doi.org/10.1124/pr.54.2.323.

(246) Sykes, D. A.; Stoddart, L. A.; Kilpatrick, L. E.; Hill, S. J. Binding Kinetics of Ligands Acting at GPCRs. *Mol. Cell. Endocrinol.* **2019**, *485*, 9–19. https://doi.org/10.1016/j.mce.2019.01.018.

(247) Copeland, R. A.; Pompliano, D. L.; Meek, T. D. Drug-Target Residence Time and Its Implications for Lead Optimization. *Nat. Rev. Drug Discov.* **2006**, *5* (9), 730–739. https://doi.org/10.1038/nrd2082.

(248) van der Velden, W. J. C.; Heitman, L. H.; Rosenkilde, M. M. Implications of Ligand-Receptor Binding Kinetics for Therapeutic Targeting of G Protein-Coupled Receptors. *ACS Pharmacol. Transl. Sci.* **2020**, acsptsci.0c00012. https://doi.org/10.1021/acsptsci.0c00012.

(249) Guo, D.; Heitman, L. H.; Ijzerman, A. P. Kinetic Aspects of the Interaction between Ligand and g Proteincoupled Receptor: The Case of the Adenosine Receptors. *Chem. Rev.* **2017**, *117* (1), 38–66. https://doi.org/10.1021/acs.chemrev.6b00025.

(250) Cottet, M.; Faklaris, O.; Maurel, D.; Scholler, P.; Doumazane, E.; Trinquet, E.; Pin, J. P.; Durroux, T. BRET and Time-Resolved FRET Strategy to Study GPCR Oligomerization: From Cell Lines toward Native Tissues. *Front. Endocrinol.* **2012**, *3*, 1–14. https://doi.org/10.3389/fendo.2012.00092.

(251) Ongini, E.; Dionisotti, S.; Gessi, S.; Irenius, E.; Fredholm, B. B. Comparison of CGS 15943, ZM 241385 and SCH 58261 as Antagonists at Human Adenosine Receptors. *Naunyn. Schmiedebergs. Arch. Pharmacol.* **1999**, *359* (1), 7–10. https://doi.org/10.1007/PL00005326.

(252) Antonioli, L.; Fornai, M.; Blandizzi, C.; Pacher, P.; Haskó, G. Adenosine Signaling and the Immune System: When a Lot Could Be Too Much. *Immunol. Lett.* **2019**, *205*, 9–15. https://doi.org/10.1016/j.imlet.2018.04.006.

(253) Kilpatrick, L. E.; Hill, S. J. The Use of Fluorescence Correlation

Spectroscopy to Characterize the Molecular Mobility of Fluorescently Labelled G Protein-Coupled Receptors. *Biochem. Soc. Trans.* **2021**, *49*, 1547–1554. https://doi.org/10.1042/BST20150285.

(254) Ast, J.; Arvaniti, A.; Fine, N. H. F.; Nasteska, D.; Ashford, F. B.; Stamataki, Z.; Koszegi, Z.; Bacon, A.; Jones, B. J.; Lucey, M. A.; et al. Super-Resolution Microscopy Compatible Fluorescent Probes Reveal Endogenous Glucagon- like Peptide-1 Receptor Distribution and Dynamics. *Nat. Commun.* **2020**, *11* (467), 1–18.

(255) Daly, C. J.; Ross, R. A.; Whyte, J.; Henstridge, C. M.; Irving, A. J.; McGrath, J. C. Fluorescent Ligand Binding Reveals Heterogeneous Distribution of Adrenoceptors and 'cannabinoid-like' Receptors in Small Arteries. *Br. J. Pharmacol.* **2010**, *159* (4), 787–796. https://doi.org/10.1111/j.1476-5381.2009.00608.x.

(256) Kroll, T.; Odyvanova, L.; Clement, J.; Platzer, C.; Naumann, A.; Marr, N.; Höffken, K.; Wölfl, S. Molecular Characterization of Breast Cancer Cell Lines by Expression Profiling. *J. Cancer Res. Clin. Oncol.* **2002**, *128* (3), 125–134. https://doi.org/10.1007/s00432-001-0308-z.

(257) Goulding, J.; Kondrashov, A.; Mistry, S. J.; Melarangi, T.; Vo, N. T. N.; Hoang, D. M.; White, C. W.; Denning, C.; Briddon, S. J.; Hill, S. J. The Use of Fluorescence Correlation Spectroscopy to Monitor Cell Surface B2-Adrenoceptors at Low Expression Levels in Human Embryonic Stem Cell-Derived Cardiomyocytes and Fibroblasts. *FASEB J.* **2021**, *35* (4), 1–20. https://doi.org/10.1096/fj.202002268R.

(258) Bunnage, M. E.; Chekler, E. L. P.; Jones, L. H. Target Validation Using Chemical Probes. *Nat. Chem. Biol.* **2013**, *9* (4), 195–199. https://doi.org/10.1038/nchembio.1197.

(259) Faudone, G.; Arifi, S.; Merk, D. The Medicinal Chemistry of Caffeine. *Journal of Medicinal Chemistry*. **2021**, 7156–7178. https://doi.org/10.1021/acs.jmedchem.1c00261.

(260) Mendiola-Precoma, J.; Padilla, K.; Rodríguez-Cruz, A.; Berumen, L. C.; Miledi, R.; García-Alcocer, G. Theobromine-Induced Changes in A1 Purinergic Receptor Gene Expression and Distribution in a Rat Brain Alzheimer's Disease Model. *J. Alzheimer's Dis.* **2017**, *55* (3),

1273–1283. https://doi.org/10.3233/JAD-160569.

(261) Kiesman, W. F.; Ensinger, Carol, L. .; Petter, R. C. .; Dowling, J. E. .; Kumaravel, G.; Chang, H.; Lin, K. C. ADENOSINE RECEPTOR ANATGONISTS AND METHODS OF MAKING AND USING THE SAME. 2003.

(262) Gao, Z. G.; Jacobson, K. A. Purinergic Signaling in Mast Cell Degranulation and Asthma. *Front. Pharmacol.* **2017**, *8*, 1–14. https://doi.org/10.3389/fphar.2017.00947.

(263) Müller, C. E.; Jacobson, K. A. *Xanthines as Adenosine Receptor Antagonists*; 2011; Vol. 200. https://doi.org/10.1007/978-3-642-13443-2_6.

(264) Soave, M.; Goulding, J.; Markus, R.; Hill, S. J.; Stoddart, L. A. Application of Fluorescent Purinoceptor Antagonists for Bioluminescence Resonance Energy Transfer Assays and Fluorescent Microscopy. In *Purinergic Signalling:Methods and Protocols*; 2020; Vol. 2041, 163–181.

(265) Chang, L. C. W.; Von Frijtag Drabbe Künzel, J. K.; Mulder-Krieger, T.; Westerhout, J.; Spangenberg, T.; Brussee, J.; Ijzerman, A. P. 2,6,8-Trisubstituted 1-Deazapurines as Adenosine Receptor Antagonists. *J. Med. Chem.* **2007**, *50* (4), 828–834. https://doi.org/10.1021/jm0607956.

(266) Chang, L. C. W.; Spanjersberg, R. F.; Frijtag, J. K. Von; Ku, D.; Mulder-krieger, T.; Brussee, J.; Ijzerman, A. P. 2,6-Disubstituted and 2,6,8-Trisubstituted Purines as Adenosine Receptor Antagonists Lisa. *J. Med. Chem.* **2006**, *49*, 2861–2867. https://doi.org/10.1021/jm050640i.

(267) Young, R. C.; Jones, M.; Milliner, K. J.; Rana, K. K.; Ward, J. G. Purine Derivatives as Competitive Inhibitors of Human Erythrocyte Membrane Phosphatidylinositol 4-Kinase. *J. Med. Chem.* **1990**, *33* (8), 2073–2080. https://doi.org/10.1021/jm00170a005.

(268) Scammells, P. J.; Baker, S. P. .; Belardinelli, L.; Olsson, R. A. . Irreversible Antagonists of Adenosine Receptors. *J. Med. Chem.* **1994**, 2704–2712.

(269) Basu, S.; Barawkar, D. A.; Thorat, S.; Shejul, Y. D.; Patel, M.;

Naykodi, M.; Jain, V.; Salve, Y.; Prasad, V.; Chaudhary, S.; et al. Design, Synthesis of Novel, Potent, Selective, Orally Bioavailable Adenosine A2A Receptor Antagonists and Their Biological Evaluation. *J. Med. Chem.* **2017**, *60* (2), 681–694. https://doi.org/10.1021/acs.jmedchem.6b01584.

(270) Basu, S.; Barawkar, D. A.; Ramdas, V.; Patel, M.; Waman, Y.; Panmand, A.; Kumar, S.; Thorat, S.; Naykodi, M.; Goswami, A.; et al. Design and Synthesis of Novel Xanthine Derivatives as Potent and Selective A2B Adenosine Receptor Antagonists for the Treatment of Chronic Inflammatory Airway Diseases. *Eur. J. Med. Chem.* **2017**, *134*, 218–229. https://doi.org/10.1016/j.ejmech.2017.04.014.

(271) Beutner, G. L.; Young, I. S.; Davies, M. L.; Hickey, M. R.; Park, H.; Stevens, J. M.; Ye, Q. TCFH-NMI: Direct Access to N-Acyl Imidazoliums for Challenging Amide Bond Formations. *Org. Lett.* **2018**, *20* (14), 4218–4222. https://doi.org/10.1021/acs.orglett.8b01591.

(272) Singh, S.; Cooper, S. L.; Glenn, J. R.; Beresford, J.; Percival, L. R.; Tyndall, J. D. A.; Hill, S. J.; Kilpatrick, L. E.; Vernall, A. J. Synthesis of Novel (Benzimidazolyl)Isoquinolinols and Evaluation as Adenosine A1 Receptor Tools. *RSC Adv.* **2018**, *8* (29), 16362–16369. https://doi.org/10.1039/c7ra13148h.

(273) Soave, M.; Kellam, B.; Woolard, J.; Briddon, S. J.; Hill, S. J. NanoBiT Complementation to Monitor Agonist-Induced Adenosine A_1 Receptor Internalization. *SLAS Discov.* **2020**, *25* (2), 186–194. https://doi.org/10.1177/2472555219880475.

(274) De Ligt, R. A. F.; Rivkees, S. A.; Lorenzen, A.; Leurs, R.; Ijzerman, A. P. A 'Locked-on,' Constitutively Active Mutant of the Adenosine A1 Receptor. *Eur. J. Pharmacol.* **2005**, *510* (1–2), 1–8. https://doi.org/10.1016/j.ejphar.2005.01.007.

(275) Iredale, P. A.; Alexander, S. P. H.; Hill, S. J. Coupling of a Transfected Human Brain A1 Adenosine Receptor in CHO-K1 Cells to Calcium Mobilisation via a Pertussis Toxin-sensitive Mechanism. *Br. J. Pharmacol.* **1994**, *111* (4), 1252–1256. https://doi.org/10.1111/j.1476-5381.1994.tb14880.x.

(276) Weyler, S.; Fülle, F.; Diekmann, M.; Schumacher, B.; Hinz, S.; Klotz, K. N.; Müller, C. E. Improving Potency, Selectivity, and Water Solubility of Adenosine A 1 Receptor Antagonists: Xanthines Modified at Position 3 and Related Pyrimido[1,2,3-Cd]Purinediones. *ChemMedChem* **2006**, *1* (8), 891–902. https://doi.org/10.1002/cmdc.200600066.

(277) Baker, J. G.; Hill, S. J. A Comparison of the Antagonist Affinities for the Gi- and Gs- Coupled States of the Human Adenosine A_1-Receptor. *J. Pharmacol. Exp. Ther.* **2007**, *320* (1), 218–228. https://doi.org/10.1124/jpet.106.113589.recent.

(278) Bouzo-Lorenzo, M.; Stoddart, L. A.; Xia, L.; IJzerman, A. P.; Heitman, L. H.; Briddon, S. J.; Hill, S. J. A Live Cell NanoBRET Binding Assay Allows the Study of Ligand-Binding Kinetics to the Adenosine A_3 Receptor. *Purinergic Signal.* **2019**, *15* (2), 139–153. https://doi.org/10.1007/s11302-019-09650-9.

(279) Muijlwijk-Koezen, J. E. van; Timmerman, H.; Goot, H. van der; Menge, W. M. P. B.; Künzel, J. F. von D.; de Groote, M.; IJzerman;, A. P. Isoquinoline and Quinazoline Urea Analogues as Antagonists for the Human Adenosine A_3 Receptor. *J. Med. Chem.* **2000**, 11, 2227–2238.

(280) Müller, C. E.; Thorand, M.; Qurishi, R.; Diekmann, M.; Jacobson, K. A. .; Padgett, W. L.; Daly, J. W. Imidazo[2,1-i]Purin-5-One s and Re Lated Tricyc Lic Water-Soluble Purine Derivatives: Potent A2A-and A3-Adenos Ine Receptor Antagonists. *J. Med. Chem.* **2002**, *45*, 3440–3450.

(281) Yates, A. S.; Doughty, S. W.; Kendall, D. A.; Kellam, B. Chemical Modification of the Naphthoyl 3-Position of JWH-015: In Search of a Fluorescent Probe to the Cannabinoid CB2 Receptor. *Bioorganic Med. Chem. Lett.* **2005**, *15* (16), 3758–3762. https://doi.org/10.1016/j.bmcl.2005.05.049.

(282) Haskó, G.; Linden, J.; Cronstein, B.; Pacher, P. Adenosine Receptors: Therapeutic Aspects for Inflammatory and Immune Diseases. *Nat. Rev. Drug Discov.* **2008**, *7* (9), 759–770. https://doi.org/10.1038/nrd2638.

(283) Deb, P. K.; Deka, S.; Borah, P.; Abed, S. N.; Klotz, K.-N. Medicinal Chemistry and Therapeutic Potential of Agonists, Antagonists and Allosteric Modulators of A_1 Adenosine Receptor: Current Status and Perspectives. *Curr. Pharm. Des.* **2019**, *25* (25), 2697–2715. https://doi.org/10.2174/1381612825666190716100509.

(284) Delacretaz, E. Supraventricular Tachycardia. *N. Engl. J. Med.* **2006**, *28* (1), 109–111. https://doi.org/10.1378/chest.28.1.109.

(285) Aurelio, L.; Baltos, J. A.; Ford, L.; Nguyen, A. T. N.; Jörg, M.; Devine, S. M.; Valant, C.; White, P. J.; Christopoulos, A.; May, L. T.; et al. A Structure-Activity Relationship Study of Bitopic N6-Substituted Adenosine Derivatives as Biased Adenosine A_1Receptor Agonists. *J. Med. Chem.* **2018**, *61* (5), 2087–2103. https://doi.org/10.1021/acs.jmedchem.8b00047.

(286) Peakman, M. -C; Hill, S. J. Adenosine A1 Receptor-mediated Changes in Basal and Histamine-stimulated Levels of Intracellular Calcium in Primary Rat Astrocytes. *Br. J. Pharmacol.* **1995**, *115* (5), 801–810. https://doi.org/10.1111/j.1476-5381.1995.tb15004.x.

(287) Ginés, S.; Ciruela, F.; Burgueño, J.; Casadó, V.; Canela, E. I.; Mallol, J.; Lluís, C.; Franco, R. Involvement of Caveolin in Ligand-Induced Recruitment and Internalization of A1 Adenosine Receptor and Adenosine Deaminase in an Epithelial Cell Line. *Mol. Pharmacol.* **2001**, *59* (5), 1314–1323. https://doi.org/10.1124/mol.59.5.1314.

(288) Beauglehole, A.; Baker, S.; Scammells, P. Fluorosulfonyl-Substituted Xanthines as Selective Irreversible Antagonists for the A1-Adenosine Receptor. *J. Med. Chem.* **2000**, *43*, 4973–4980.

(289) Dale, C. L.; Hill, S. J.; Kellam, B. Supp_info_New Potent, Short-Linker BODIPY-630/650[Trade Mark Sign] Labelled Fluorescent Adenosine Receptor Agonists. *Med. Chem. Commun.* **2012**, *3* (3), 333–338. https://doi.org/10.1039/C2MD00247G.

(290) Müller, C. E. Synthesis of 3-Substituted 6-Aminouracils. *Tetrahedron Lett.* **1991**, *32* (45), 6539–6540.

(291) Müller, C. E.; Sandoval-Ramirez, J. A New Versatile Synthesis of Xanthines with Variable Substituents in the 1-, 3-, 7- and 8-Positions. *Synthesis (Stuttg).* **1995**, *10*, 1295–1299.

(292) Baraldi, P. G.; Borea, P. A.; Preti, D.; Tabrizi, M. A. NOVEL ADENOSINE A3 RECEPTOR MODULATORS. US 2006/0178385 A1, 2006.

(293) Marx, D.; Wingen, L. M.; Schnakenburg, G.; Müller, C. E.; Scholz, M. S. Fast, Efficient, and Versatile Synthesis of 6-Amino-5-Carboxamidouracils as Precursors for 8-Substituted Xanthines. *Front. Chem.* **2019**, *7*, 1–15. https://doi.org/10.3389/fchem.2019.00056.

(294) Olsson, Ray, A. .; Holschbach, M. H. .; Schrader, J. ADENOSINE RECEPTO ANTAGONISTS WITH IMPROVED BIOACTIVITY. WO 99/31101, 1999.

(295) Comeo, E.; Kindon, N. D.; Soave, M.; Stoddart, L. A.; Kilpatrick, L. E.; Scammells, P. J.; Hill, S. J.; Kellam, B. Subtype-Selective Fluorescent Ligands as Pharmacological Research Tools for the Human Adenosine A_{2A} Receptor. *J. Med. Chem.* **2020**, *63* (5), 2656–2672. https://doi.org/10.1021/acs.jmedchem.9b01856.

(296) Bolcato, G.; Bissaro, M.; Deganutti, G.; Sturlese, M.; Moro, S. New Insights into Key Determinants for Adenosine 1 Receptor Antagonists Selectivity Using Supervised Molecular Dynamics Simulations. *Biomolecules* **2020**, *10* (5), 1–11. https://doi.org/10.3390/biom10050732.

(297) Mercier, J. F.; Salahpour, A.; Angers, S.; Breit, A.; Bouvier, M. Quantitative Assessment of B1- and B2-Adrenergic Receptor Homo- and Heterodimerization by Bioluminescence Resonance Energy Transfer. *J. Biol. Chem.* **2002**, *277* (47), 44925–44931. https://doi.org/10.1074/jbc.M205767200.

(298) Marullo, S.; Bouvier, M. Resonance Energy Transfer Approaches in Molecular Pharmacology and Beyond. *Trends Pharmacol. Sci.* **2007**, *28* (8), 362–365. https://doi.org/10.1016/j.tips.2007.06.007.

(299) Pfleger, K. D. G.; Eidne, K. A. Illuminating Insights into Protein-Protein Interactions Using Bioluminescence Resonance Energy Transfer (BRET). *Nat. Methods* **2006**, *3* (3), 165–174. https://doi.org/10.1038/nmeth841.

(300) Uhlén, M.; Fagerberg, L.; Hallström, B. M.; Lindskog, C.; Oksvold, P.; Mardinoglu, A.; Sivertsson, Å.; Kampf, C.; Sjöstedt, E.; Asplund, A.;

et al. Tissue-Based Map of the Human Proteome. *Science.* **2015**, *347*. https://doi.org/10.1126/science.1260419.

(301) The Human Protein Atlas https://www.proteinatlas.org/ENSG00000163485-ADORA1/cell.

(302) Ciruela, F.; Casadó, V.; Rodrigues, R. J.; Luján, R.; Burgueño, J.; Canals, M.; Borycz, J.; Rebola, N.; Goldberg, S. R.; Mallol, J.; et al. Presynaptic Control of Striatal Glutamatergic Neurotransmission by Adenosine A_1-A_{2A} Receptor Heteromers. *J. Neurosci.* **2006**, *26* (7), 2080–2087. https://doi.org/10.1523/JNEUROSCI.3574-05.2006.

(303) Briddon, S. J.; Gandía, J.; Amaral, O. B.; Ferré, S.; Lluís, C.; Franco, R.; Hill, S. J.; Ciruela, F. Plasma Membrane Diffusion of g Protein-Coupled Receptor Oligomers. *Biochim. Biophys. Acta - Mol. Cell Res.* **2008**, *1783* (12), 2262–2268. https://doi.org/10.1016/j.bbamcr.2008.07.006.

(304) O.Borroto-Escuela;, D.; Flajolet;, M.; F.Agnati;, L.; Greengard;, P.; Kjell, F. Bioluminescence Resonance Energy Transfer Methods to Study G Protein-Coupled Receptor–Receptor Tyrosine Kinase Heteroreceptor Complexes. *Methods Cell Biol. 117*, 141–164.

(305) Kilpatrick, L. E.; Alcobia, D. C.; White, C. W.; Peach, C. J.; Glenn, J. R.; Zimmerman, K.; Kondrashov, A.; Pfleger, K. D. G.; Ohana, R. F.; Robers, M. B.; et al. Complex Formation between VEGFR2 and the B2-Adrenoceptor. *Cell Chem. Biol.* **2019**, 1–12. https://doi.org/10.1016/j.chembiol.2019.02.014.

(306) Schwehm, C.; Kellam, B.; Garces, A. E.; Hill, P. S. J.; Kindon, N. D.; Tracey, D.; Li, J.; Macdonald, S. J. F.; Rowedder, J. E.; Stoddart, L. A.; et al. Design and Elaboration of a Tractable Tricyclic Scaffold to Synthesize Drug-like Inhibitors of Dipeptidyl Peptidase-4 (DPP-4), Antagonists of the C-C Chemokine Receptor Type 5 (CCR5), and Highly Potent and Selective Phospho- Inositol-3 Kinase δ (PI3K. **2017**, 60, 1534-1554. https://doi.org/10.1021/acs.jmedchem.6b01801.

(307) Hoffmann, C.; Castro, M.; Rinken, A.; Leurs, R.; Hill, S. J.; Vischer, H. F. Ligand Residence Time at G-Protein-Coupled Receptors - Why We Should Take Our Time to Study It. *Mol. Pharmacol.* **2015**, *88* (3),

552–560. https://doi.org/10.1124/mol.115.099671.

(308) Sykes, D. A.; Parry, C.; Reilly, J.; Wright, P.; Fairhurst, R. A.; Charlton, S. J. Observed Drug-Receptor Association Rates Are Governed by Membrane Affinity: The Importance of Establishing 'Micro-Pharmacokinetic/Pharmacodynamic Relationships' at the B2-Adrenoceptor. *Mol. Pharmacol.* **2014**, *85* (4), 608–617. https://doi.org/10.1124/mol.113.090209.

(309) Kalk, P.; Eggert, B.; Relle, K.; Godes, M.; Heiden, S.; Sharkovska, Y.; Fischer, Y.; Ziegler, D.; Bielenberg, G. W.; Hocher, B. The Adenosine A 1 Receptor Antagonist SLV320 Reduces Myocardial Fibrosis in Rats with 5/6 Nephrectomy without Affecting Blood Pressure. *Br. J. Pharmacol.* **2007**, *151* (7), 1025–1032. https://doi.org/10.1038/sj.bjp.0707319.

(310) Townsend-Nicholson, A.; Schofield, P. B. A Threonine Residue in the Seventh Transmembrane Domain of the Human A1 Adenosine Receptor Mediates Specific Agonist Binding. *J. Biol. Chem.* **1994**, *269* (4), 2373–2376.

(311) Rivkees, S. A.; Barbhaiya, H.; IJzerman, A. P. Identification of the Adenine Binding Site of the Human A1 Adenosine Receptor. *J. Biol. Chem.* **1999**, *274* (6), 3617–3621. https://doi.org/10.1074/jbc.274.6.3617.

(312) Gao, Z. G.; Mamedova, L. K.; Chen, P.; Jacobson, K. A. 2-Substituted Adenosine Derivatives: Affinity and Efficacy at Four Subtypes of Human Adenosine Receptors. *Biochem. Pharmacol.* **2004**, *68* (10), 1985–1993. https://doi.org/10.1016/j.bcp.2004.06.011.

(313) Steyer, J. A.; Almers, W. A Real-Time View of Life within 100 nm of the Plasma Membrane. *Nat. Rev. Mol. Cell Biol.* **2001**, *2* (4), 268–275. https://doi.org/10.1038/35067069.

(314) Calebiro, D.; Rieken, F.; Wagner, J.; Sungkaworn, T.; Zabel, U.; Borzi, A.; Cocucci, E.; Zürn, A.; Lohse, M. J. Single-Molecule Analysis of Fluorescently Labeled G-Protein-Coupled Receptors Reveals Complexes with Distinct Dynamics and Organization. *Proc. Natl. Acad. Sci. U. S. A.* **2013**, *110* (2), 743–748. https://doi.org/10.1073/pnas.1205798110.

(315) Schulte, G.; Robertson, B.; Fredholm, B. B.; Delander, G. E.; Shortland, P.; Molander, C. Distribution of Antinociceptive Adenosine A1 Receptors in the Spinal Cord Dorsal Horn, and Relationship to Primary Afferents and Neuronal Subpopulations. *Neuroscience* **2003**, *121* (4), 907–916. https://doi.org/10.1016/S0306-4522(03)00480-9.

(316) King, A. Analgesia without Opiods. *Nature* **2019**, *573*, S4–S6. https://doi.org/10.7551/mitpress/8605.003.0011.

(317) Sletten, E. M.; Bertozzi, C. R. Bioorthogonal Chemistry: Fishing for Selectivity in a Sea of Functionality. *Angew. Chemie - Int. Ed.* **2009**, *48* (38), 6974–6998. https://doi.org/10.1002/anie.200900942.

(318) Comeo, E.; Trinh, P.; Nguyen, A. T.; Nowell, C. J.; Kindon, N. D.; Soave, M.; Stoddart, L. A.; White, J. M.; Hill, S. J.; Kellam, B.; et al. Development and Application of Subtype-Selective Fluorescent Antagonists for the Study of the Human Adenosine A_1 Receptor in Living Cells. *J. Med. Chem.* **2021**, *64*, 6670–6695. https://doi.org/10.1021/acs.jmedchem.0c02067.

(319) Jacobson, K. A.; Barone, S.; Kammula, U. .; Stiles, G. Electrophilic Derivatives of Purines Irreversible Inhibitors of A_1 Adenosine Receptors. *J. Med. Chem.* **1989**, *32*, 1043–1051.

(320) Stiles, G. L.; Jacobson, K. A. High Affinity Acylating Antagonists for the A1 Adenosine Receptor: Identification of Binding Subunit. *Mol. Pharmacol.* **1988**, *34* (6), 724–728.

(321) Sakamoto, S.; Hamachi, I. Recent Progress in Chemical Modification of Proteins. *Anal. Sci.* **2019**, *35* (1), 5–27. https://doi.org/10.2116/analsci.18R003.

(322) Meng, H.; Kumar, K. Antimicrobial Activity and Protease Stability of Peptides Containing Fluorinated Amino Acids. *J. Am. Chem. Soc.* **2007**, *129* (50), 15615–15622. https://doi.org/10.1021/ja075373f.

(323) Mei, H.; Han, J.; Klika, K. D.; Izawa, K.; Sato, T.; Meanwell, N. A.; Soloshonok, V. A. Applications of Fluorine-Containing Amino Acids for Drug Design. *Eur. J. Med. Chem.* **2020**, *186*. https://doi.org/10.1016/j.ejmech.2019.111826.

(324) Gillis, E. P.; Eastman, K. J.; Hill, M. D.; Donnelly, D. J.; Meanwell, N.

A. Applications of Fluorine in Medicinal Chemistry. *J. Med. Chem.* **2015**, *58* (21), 8315–8359. https://doi.org/10.1021/acs.jmedchem.5b00258.

(325) Cheguillaume, A.; Gillart, J.; Labar, D.; Grégoire, V.; Marchand-Brynaert, J. Perfluorinated Markers for Hypoxia Detection: Synthesis of Sulfur-Containing Precursors and [18F]-Labelling. *Bioorganic Med. Chem.* **2005**, *13* (4), 1357–1367. https://doi.org/10.1016/j.bmc.2004.11.010.

(326) Uchimaru, T.; Kutsuna, S.; Chandra, A. K.; Sugie, M.; Sekiya, A. Effect of Fluorine Substitution on the Rate for Ester Hydrolysis: Estimation of the Hydrolysis Rate of Perfluoroalkyl Esters. *J. Mol. Struct. THEOCHEM* **2003**, *635*, 83–89. https://doi.org/10.1016/S0166-1280(03)00404-4.

(327) Cheguillaume, A.; Lacroix, S.; Marchand-Brynaert, J. A Practical Synthesis of 2,2-Difluoro-3-Amino-Propanoic Acid (α,α-Difluoro-β-Alanine). *Tetrahedron Lett.* **2003**, *44* (11), 2375–2377. https://doi.org/10.1016/S0040-4039(03)00243-0.

(328) Vidal, A.; Nefzi, A.; Houghten, R. A. Solid-Phase Synthesis of α,α-Difluoro-β-Amino Acids via the Reformatsky Reaction. *J. Org. Chem.* **2001**, 8268–8272.

(329) Nakayama, K.; Kawato, H. C. .; Inagaki, H.; Nakajima, R.; Kitamura, A.; Someya, K.; Ohta, T. Synthesis and Antifungal Activity of Rhodopeptin Analogues . 2 . Modification of the West Amino Acid Moiety. *Org. Lett.* **2000**, *2* (7), 977–980.

(330) Blackman, M. L.; Royzen, M.; Fox, J. M. Tetrazine Ligation: Fast Bioconjugation Based on Inverse-Electron-Demand Diels-Alder Reactivity. *J. Am. Chem. Soc.* **2008**, *130* (41), 13518–13519. https://doi.org/10.1021/ja8053805.

(331) Oliveira, B. L.; Guo, Z.; Bernardes, G. J. L. Inverse Electron Demand Diels-Alder Reactions in Chemical Biology. *Chem. Soc. Rev.* **2017**, *46* (16), 4895–4950. https://doi.org/10.1039/c7cs00184c.

(332) Appel, R. Tertiary Phosphane/Tetrachloromethane, a Versatile Reagent for Chlorination, Dehydration, and P-N Linkage. *Angew. Chemie - Int. Ed.* **1975**, *14* (2), 801–811.

(333) Papesch, V.; Schroeder, E. F. SYNTHESIS OF 1-MONO- AND 1,3-DI-SUBSTITUTED 6-AMINO- URACILS. DIURETIC ACTIVITY1. *J. Org. Chem.* **1951**, *16* (12), 1879–1890.

(334) Jörg, M.; Shonberg, J.; Mak, F. S.; Miller, N. D.; Yuriev, E.; Scammells, P. J.; Capuano, B. Novel Adenosine A_{2A} Receptor Ligands: A Synthetic, Functional and Computational Investigation of Selected Literature Adenosine A_{2A} Receptor Antagonists for Extending into Extracellular Space. *Bioorganic Med. Chem. Lett.* **2013**, *23* (11), 3427–3433. https://doi.org/10.1016/j.bmcl.2013.03.070.

(335) Hockemeyer, J.; Burbiel, J. C. .; Müller, C. E. Multigram-Scale Synthe Se s , Stabi Lity, and Photoreactions of A2A Adenos Ine Receptor Antagon Is Ts w Ith 8-Styrylxanth Ine Structure : Potential Drugs for Parkinson's Disease. *J. Org. Chem.* **2004**, *69*, 3308–3318.

(336) Fischer, E.; Speier, A. Darstellung Der Ester. *Berichte der Dtsch. Chem. Gesellschaft* **1895**, *28* (3), 3252–3258. https://doi.org/10.1002/cber.189502803176.

(337) Katritzky, A. R.; Nichols, D. A.; Qi, M. Benzotriazole Mediated Syntheses of α-Fluoro-β-Amino Esters. *Tetrahedron Lett.* **1998**, *39* (39), 7063–7066. https://doi.org/10.1016/S0040-4039(98)01520-2.

(338) Nadon, J. F.; Rochon, K.; Grastilleur, S.; Langlois, G.; Dao, T. T. H.; Blais, V.; Guérin, B.; Gendron, L.; Dory, Y. L. Synthesis of Gly-ψ[(Z)CF□ CH]-Phe, a Fluoroalkene Dipeptide Isostere, and Its Incorporation into a Leu-Enkephalin Peptidomimetic. *ACS Chem. Neurosci.* **2017**, *8* (1), 40–49. https://doi.org/10.1021/acschemneuro.6b00163.

(339) Neises, B.; Steglich, W. Simple Method for the Esterification of Carboxylic Acids. *Angew. Chemie Int. Ed. English* **1978**, *17* (7), 522–524. https://doi.org/10.1002/anie.197805221.

(340) Nikić, I.; Plass, T.; Schraidt, O.; Szymański, J.; Briggs, J. A. G.; Schultz, C.; Lemke, E. A. Minimal Tags for Rapid Dual-Color Live-Cell Labeling and Super-Resolution Microscopy. *Angew. Chemie - Int. Ed.* **2014**, *53* (8), 2245–2249. https://doi.org/10.1002/anie.201309847.

(341) Liu, D. S.; Tangpeerachaikul, A.; Selvaraj, R.; Taylor, M. T.; Fox, J.

M.; Ting, A. Y. Diels-Alder Cycloaddition for Fluorophore Targeting to Specific Proteins inside Living Cells. *J. Am. Chem. Soc.* **2012**, *134* (2), 792–795. https://doi.org/10.1021/ja209325n.

(342) Serfling, R.; Seidel, L.; Bock, A.; Lohse, M. J.; Annibale, P.; Coin, I. Quantitative Single-Residue Bioorthogonal Labeling of G Protein-Coupled Receptors in Live Cells. *ACS Chem. Biol.* **2019**, *14* (6), 1141–1149. https://doi.org/10.1021/acschembio.8b01115.

(343) Işbilir, A.; Serfling, R.; Möller, J.; Thomas, R.; De Faveri, C.; Zabel, U.; Scarselli, M.; Beck-Sickinger, A. G.; Bock, A.; Coin, I.; et al. Determination of G-Protein–Coupled Receptor Oligomerization by Molecular Brightness Analyses in Single Cells. *Nat. Protoc.* **2021**, *16* (3), 1419–1451. https://doi.org/10.1038/s41596-020-00458-1.

(344) Rahim, M. K.; Kota, R.; Haun, J. B. Enhancing Reactivity for Bioorthogonal Pretargeting by Unmasking Antibody-Conjugated Trans -Cyclooctenes. *Bioconjug. Chem.* **2015**, *26* (2), 352–360. https://doi.org/10.1021/bc500605g.

(345) Ramil, C. P.; Dong, M.; An, P.; Lewandowski, T. M.; Yu, Z.; Miller, L. J.; Lin, Q. Spirohexene-Tetrazine Ligation Enables Bioorthogonal Labeling of Class B G Protein-Coupled Receptors in Live Cells. *J. Am. Chem. Soc.* **2017**, *139* (38), 13376–13386. https://doi.org/10.1021/jacs.7b05674.

(346) Koshi, Y.; Nakata, E.; Miyagawa, M.; Tsukiji, S.; Ogawa, T.; Hamachi, I. Target-Specific Chemical Acylation of Lectins by Ligand-Tethered DMAP Catalysts. *J. Am. Chem. Soc.* **2008**, *130* (1), 245–251. https://doi.org/10.1021/ja075684q.

(347) Boring, D. L.; Ji, X. D.; Zimmet, J.; Taylor, K. E.; Stiles, G. L.; Jacobson, K. A. Trifunctional Agents as a Design Strategy for Tailoring Ligand Properties: Irreversible Inhibitors of A_1 Adenosine Receptors. *Bioconjug. Chem.* **1991**, *2* (2), 77–88. https://doi.org/10.1021/bc00008a002.

(348) Zheng, J.; Zhan, Q.; Jiang, L.; Xing, D.; Zhang, T.; Wong, K. L. A Bioorthogonal Time-Resolved Luminogenic Probe for Metabolic Labelling and Imaging of Glycans. *Inorg. Chem. Front.* **2020**, *7* (21), 4062–4069. https://doi.org/10.1039/d0qi00728e.

(349) Briddon, S. J.; Hill, S. J. Pharmacology under the Microscope: The Use of Fluorescence Correlation Spectroscopy to Determine the Properties of Ligand-Receptor Complexes. *Trends Pharmacol. Sci.* **2007**, *28* (12), 637–645. https://doi.org/10.1016/j.tips.2007.09.008.

(350) Jamwal, S.; Mittal, A.; Kumar, P.; Alhayani, D. M.; Al-Aboudi, A. Therapeutic Potential of Agonists and Antagonists of A1, A2a, A2b and A3 Adenosine Receptors. *Curr. Pharm. Des.* **2019**, *25* (26), 2892–2905. https://doi.org/10.2174/1381612825666190716112319.

(351) Garnock-Jones, K. P.; Curran, M. P. Regadenoson. *Am. J. Cardiovasc. Drugs* **2010**, *10* (1), 65–71. https://doi.org/10.2165/10489040-000000000-00000.

(352) Chen, J. F.; Cunha, R. A. The Belated US FDA Approval of the Adenosine A_{2A} Receptor Antagonist Istradefylline for Treatment of Parkinson's Disease. *Purinergic Signal.* **2020**, *16* (2), 167–174. https://doi.org/10.1007/s11302-020-09694-2.

(353) Peleli, M.; Fredholm, B. B.; Sobrevia, L.; Carlström, M. Pharmacological Targeting of Adenosine Receptor Signaling. *Mol. Aspects Med.* **2017**, *55*, 4–8. https://doi.org/10.1016/j.mam.2016.12.002.

(354) Vanderheyden, P. M. L.; Benachour, N. Influence of the Cellular Environment on Ligand Binding Kinetics at Membrane-Bound Targets. *Bioorganic Med. Chem. Lett.* **2017**, *27* (16), 3621–3628. https://doi.org/10.1016/j.bmcl.2017.06.051.

(355) Ellisdon, A. M.; Halls, M. L. Compartmentalization of GPCR Signalling Controls Unique Cellular Responses. *Biochem. Soc. Trans.* **2016**, *44* (2), 562–567. https://doi.org/10.1042/BST20150236.

(356) Wang, W.; Qiao, Y.; Li, Z. New Insights into Modes of GPCR Activation. *Trends Pharmacol. Sci.* **2018**, *39* (4), 367–386. https://doi.org/10.1016/j.tips.2018.01.001.

(357) Boursier, M. E.; Levin, S.; Zimmerman, K.; MacHleidt, T.; Hurst, R.; Butler, B. L.; Eggers, C. T.; Kirkland, T. A.; Wood, K. V.; Ohana, R. F. The Luminescent HiBiT Peptide Enables Selective Quantitation of G Protein-Coupled Receptor Ligand Engagement and Internalization in Living Cells. *J. Biol. Chem.* **2020**, *295* (15), 5124–5135.

https://doi.org/10.1074/jbc.RA119.011952.

(358) Altenbach, R. J.; Adair, R. M.; Bettencourt, B. M.; Black, L. A.; Fix-Stenzel, S. R.; Gopalakrishnan, S. M.; Hsieh, G. C.; Liu, H.; Marsh, K. C.; McPherson, M. J.; et al. Structure-Activity Studies on a Series of a 2-Aminopyrimidine-Containing Histamine H4 Receptor Ligands. *J Med Chem* **2008**, *51* (20), 6571–6580. https://doi.org/10.1021/jm8005959.

(359) Zhang, L.; Bu, T.; Bao, X.; Liang, T.; Ge, Y.; Xu, Y.; Zhu, Q. Design, Synthesis and Biological Evaluation of Novel 3H-Imidazole [4,5-b] Pyridine Derivatives as Selective MTOR Inhibitors. *Bioorganic Med. Chem. Lett.* **2017**, *27* (15), 3395–3398. https://doi.org/10.1016/j.bmcl.2017.06.010.

(360) Lin, K.-C.; Vu, C. Condensed Purine Derivatived as A_1 Adenosine Receptor Antagonists. WO 02/44182 A1, 2002.

(361) Sprott, K.; Marineau, J.J.; Schmidt, D.; Bradley, M.; Ciblat, S.; Sidiqui, M.; Kabro, A.; Leblanc, M.; Leger, S.; Roy, S.; Winter, D. K.; Miller, T Inhibitors of Cyclin-Dependent Kinase (CDK7), WO 2015/154039 A2, Oct 8, 2015.

(362) Fiala, T.; Wang, J.; Dunn, M.; Šebej, P.; Choi, S. J.; Nwadibia, E. C.; Fialova, E.; Martinez, D. M.; Cheetham, C. E.; Fogle, K. J.; et al. Chemical Targeting of Voltage Sensitive Dyes to Specific Cells and Molecules in the Brain. *J. Am. Chem. Soc.* **2020**, *142* (20), 9285–9301. https://doi.org/10.1021/jacs.0c00861.

(363) Baalmann, M.; Neises, L.; Bitsch, S.; Schneider, H.; Deweid, L.; Ilkenhans, N.; Wolfring, M.; Ziegler, M. J.; Werther, P.; Wilhelm, J.; et al. A Bioorthogonal Click Chemistry Toolbox for Targeted Synthesis of Branched and Well-Defined Protein-Protein Conjugates. *Angew. Chemie - Int. Ed.* **2019**, *59*, 12885–12893. https://doi.org/10.26434/chemrxiv.10743344.v1.

(364) Lang, K.; Davis, L.; Wallace, S.; Mahesh, M.; Cox, D. J.; Blackman, M. L.; Fox, J. M.; Chin, J. W. Supp_Info_Genetic Encoding of Bicyclononynes and Trans-Cyclooctenes for Site-Specific Protein Labeling in Vitro and in Live Mammalian Cells via Rapid Fluorogenic Diels-Alder Reactions. *J. Am. Chem. Soc.* **2012**, *134* (25), 10317–10320.

https://doi.org/10.1021/ja302832g.

(365) Stewart, G. D.; Valant, C.; Dowell, S. J.; Mijaljica, D.; Devenish, R. J.; Scammells, P. J.; Sexton, P. M.; Christopoulos, A. Determination of Adenosine A_1 Receptor Agonist and Antagonist Pharmacology Using Saccharomyces Cerevisiae: Implications for Ligand Screening and Functional Selectivity. *J. Pharmacol. Exp. Ther.* **2009**, *331* (1), 277–286. https://doi.org/10.1124/jpet.109.158667.

(366) Schindelin, J.; Arganda-Carreras, I.; Frise, E.; Kaynig, V.; Longair, M.; Pietzsch, T.; Preibisch, S.; Rueden, C.; Saalfeld, S.; Schmid, B.; et al. Fiji: An Open-Source Platform for Biological-Image Analysis. *Nat. Methods* **2012**, *9* (7), 676–682. https://doi.org/10.1038/nmeth.2019.